



HAL
open science

Phosphorylation of prebiotic precursors on the early Earth

Anastasiia Shvetsova

► **To cite this version:**

Anastasiia Shvetsova. Phosphorylation of prebiotic precursors on the early Earth. Chemical Sciences. Université Claude Bernard - Lyon I, 2023. English. NNT : 2023LYO10237 . tel-04880935

HAL Id: tel-04880935

<https://theses.hal.science/tel-04880935v1>

Submitted on 11 Jan 2025

HAL is a multi-disciplinary open access archive for the deposit and dissemination of scientific research documents, whether they are published or not. The documents may come from teaching and research institutions in France or abroad, or from public or private research centers.

L'archive ouverte pluridisciplinaire **HAL**, est destinée au dépôt et à la diffusion de documents scientifiques de niveau recherche, publiés ou non, émanant des établissements d'enseignement et de recherche français ou étrangers, des laboratoires publics ou privés.



THESE de DOCTORAT DE L'UNIVERSITE CLAUDE BERNARD LYON 1

**Ecole Doctorale N° 52
Physique et astrophysique**

Discipline : Chimie

Soutenue publiquement le 17/11/2023, par :
Anastasiia Shvetsova

Phosphorylation of prebiotic precursors on the early Earth

Devant le jury composé de :

Farizon, Michel	Professeur, Université Claude Bernard Lyon 1	Président
Jaber, Maguy	Professeure, Sorbonne Université	Rapporteuse
Moran, Joseph	Professeur, Université de Strasbourg	Rapporteur
Danger, Grégoire	Professeur, Aix-Marseille Université	Examineur
Daniel, Isabelle	Professeure, Université Claude Bernard Lyon 1	Directrice de thèse
Strazewski, Pierre	Professeur, Université Claude Bernard Lyon 1	Co-Directeur de thèse
Fiore, Michele	Maître de Conférences, Université Claude Bernard Lyon 1	Invité
Grossi, Vincent	Directeur de Recherche, Université Claude Bernard Lyon 1	Invité
Vinogradoff, Vassilissa	Chargée de Recherche, Aix-Marseille Université	Invitée

Acknowledgements

I would like to express my gratitude to all those who have been involved in this journey named PhD, this great work of three years that could not have been completed by only myself.

To begin with, I thank the jury members for accepting the invitation to evaluate my work and for giving a professional and independent opinion on my research.

First of all, my dear and marvellous supervisors, Isabelle Daniel, Pierre Strazewski, and Michele Fiore, I am immensely grateful for everything you have done for me and the project over these years. Thank you for all the guidance and experience you have passed on to me. For all the time you have devoted and the knowledge I have been able to learn from you. These three years have been challenging and your advice and feedback have always been a guiding light on this path. Thank you for introducing me to fascinating astrobiology research, an engaging and inspiring field.

Dear Isabelle, communicating and engaging in intellectual exchange with you has constantly generated fruitful outcomes with a significant impact on my work. Thank you for always finding the right words and perfect solutions at the moments of need. Peter, working with you has been an incredibly beneficial experience. Thanks to you, I have learned and exposed myself to many new disciplines and analytical approaches. I have literally outgrown myself every day under your encouragement. This has helped me mature tremendously, both professionally and personally. Michele, it has been an honour and a pleasure to work with you in the lab and learn new skills and techniques from you. Thank you for your kind words helped me to always stay creative and reasonable about my work.

I am also grateful to the other professors and researchers who collaborated on my project. I would like to thank Jean-Philippe Perrillat, Sylvie Le Floch, Hervé Cardon and Gilles Montagnac for the laboratory and scientific support with the high-pressure experiments and Marc Vedrenne from Université Paul Sabatier for help with obtaining best quality NMR spectra. I express my gratitude to all members of the CCRMN and CCSM groups for your very outstanding and attentive approach to the experimental analyses and your collaboration in their processing. A special mention of thanks to Elodie Fromentin, who introduced me to the world of MS and has become my friend.

I would like to express my gratitude to all the members of the research team LGL and LCO2 for always being ready to give advice and have productive discussions, David Gueyrard, Thierry Granjon and especially Peter Goekjian who introduced me to the University of Lyon and to my supervisors. I am grateful to my former supervisor, Elena Shinkar', who encouraged me to pursue my interest and curiosity in science.

All current and former PhD students, LGL Elena, Anastasis, Marine, Elettra, Matilda and Anaïs, LCO2 Caroline, Augustin, Fanny, Bastian, Andrea, Anna, Layth thank you guys for sharing the adventures of PhD life with me and for always having kind words and friendly advice.

Many thanks to my family and friends for their support and understanding. I am very grateful to my grandmother, Valentina, who believed in her granddaughter's scientific career more than anyone else. And of course, the biggest credit goes to my dear husband, Mathieu, who always believes in me more than I believe in myself. Thank you, my love, for always being on my side. Without your strength, love, care and support I would never have made it so far.

It has been a great journey full of growth and overcoming, and I am grateful to all those who have supported me and been there during this time. Thank you! Merci! Спасибо!

Abstract (in English)

One key step in the emergence of life is the spontaneous phosphorylation of prebiotic precursors that are central to the integrity, heredity and metabolism of living cells. Assuming favourable conditions for the formation of complex biopolymers on the early Earth about four billion years ago, the main source of phosphorus could have been delivered by meteorites in the form of minerals such as merrillite or schreibersite, among others. If not already, they would have subsequently oxidised at the surface of the early Earth, mostly into inorganic orthophosphate (P_i) and some condensed phosphates (P_{ni}). Phosphorylation reactions from P_i are thermodynamically unfavourable in the presence of water and require mediation by a condensing agent, for instance, non-volatile and hydrolysable reduced-nitrogen compounds such as cyanamide, urea, etc. On the early Earth, this could have happened during wet-dry cycles on the emerged land (tidal zone) or in hydrothermal seafloor vents and geysers.

In this work, we studied alcohol phosphorylation reactions using glycerol and its derivatives and nucleosides under arid conditions at 75 or 115 °C in a dry state (liquid-solid mixtures with only traces of water), atmospheric pressure and high pressure-high temperature (115 °C, <1 GPa).

We confirmed the need for a condensing agent to achieve phosphorylation and identified alternatives to the classically used urea, such as carboxamides and sodium N-cyanofornamide. In parallel, we varied the source of phosphorus, including inorganic orthophosphate, thiophosphate, condensed cyclic metaphosphate and natural P-bearing minerals (struvite, vivianite and canaphite). We also investigated different molar excesses of the condensing agents and their effect on the reaction yield. The reaction products were identified and quantified by NMR (nuclear magnetic resonance spectroscopy), MS (mass spectrometry) and HPLC methods (high-performance liquid chromatography).

In summary, we conclude that phosphorylation of prebiotic precursors is achievable with relatively high yields even under the harsh and dry conditions of early Earth. The presence of a condensing agent is mandatory in reactions with single-long-carbon-chain glyceryl derivatives such as MPG and nucleosides, and an excess of the condensing agent increases reaction yields. The suggested approach to these phosphorylated products under prebiotic conditions opens the prospect for further oligomerization of nucleotides into oligonucleotides to give RNA or DNA and phosphorylated glyceryl derivatives into phospholipids for vesicles or cell membranes.

Abstract (En Français)

L'une des étapes clés de l'émergence de la vie est la phosphorylation spontanée de précurseurs prébiotiques qui sont essentiels à l'intégrité, à l'hérédité et au métabolisme des cellules vivantes. Dans l'hypothèse de conditions favorables à la formation de biopolymères complexes sur la Terre primitive, il y a environ quatre milliards d'années, la principale source de phosphore aurait pu être apportée par des météorites sous la forme de minéraux tels que la merrillite ou la schreibersite, entre autres. S'ils ne l'étaient pas déjà, ils se seraient ensuite oxydés à la surface de la Terre primitive, principalement en orthophosphate inorganique (P_i) et en phosphates condensés (P_{ni}). Les réactions de phosphorylation à partir de P_i sont thermodynamiquement défavorables en présence d'eau et nécessitent la médiation d'un agent de condensation, par exemple des composés d'azote réduits non volatils et hydrolysables tels que le cyanamide, l'urée, etc. Sur la Terre primitive, cela aurait pu se produire lors de cycles humides et secs sur les terres émergées (zone tidale) ou dans les sources hydrothermales océanique ou continentales.

Dans ce travail, nous avons étudié les réactions de phosphorylation d'alcools à partir du glycérol et de ses dérivés et de nucléosides dans des conditions arides à 75 ou 115 °C à l'état sec (mélanges liquide-solide avec seulement des traces d'eau), à la pression atmosphérique et à haute pression-haute température (115 °C, <1 GPa).

Nous avons confirmé la nécessité d'un agent de condensation pour réaliser la phosphorylation et identifié des alternatives à l'urée généralement utilisée, telles que les carboxamides et le N-cyanoformamide de sodium. Parallèlement, nous avons varié la source de phosphore (l'orthophosphate inorganique, le thiophosphate ou le métaphosphate cyclique condensé) et les minéraux naturels contenant du P (struvite, vivianite et canaphite). Nous avons également étudié différents excès molaires des agents de condensation et leur effet sur le rendement de la réaction. Les produits de réaction ont été identifiés et quantifiés par RMN (spectroscopie de résonance magnétique nucléaire), MS (spectrométrie de masse) et CLHP (chromatographie liquide à haute performance).

En résumé, nous concluons que la phosphorylation des précurseurs prébiotiques est possible avec des rendements relativement élevés, même dans les conditions difficiles et sèches de la Terre primitive. La présence d'un agent condensant est indispensable dans les réactions avec les dérivés glycériques à longue chaîne de carbone comme le MPG et les nucléosides. De plus, un excès d'agent condensant augmente les rendements de la réaction. L'approche proposée pour ces produits phosphorylés dans des conditions prébiotiques ouvre la perspective d'une oligomérisation plus poussée des nucléotides en oligonucléotides pour donner de l'ARN ou de l'ADN et des dérivés glycérinés phosphorylés en phospholipides pour les vésicules ou les membranes cellulaires.

Table of contents

Introduction	16
List of abbreviations	19
I State of the art	20
1. Phosphorous role in the origin of life.....	21
2. Geochemical settings at the late Hadean.....	23
3. Availability of the key precursors for phosphorylation reactions and the mechanisms involved in their production on the early Earth.....	27
3.1. Inventories of organic molecules and their transformation into prebiotic precursors... 27	
3.1.1. Nucleosides as RNA and DNA precursors.....	28
3.1.1.1. <i>Nucleobases (purines and pyrimidines)</i>	28
3.1.1.2. <i>Sugars (ribose/2-deoxyribose)</i>	29
3.1.1.3. <i>Nucleosides (purines and pyrimidines)</i>	30
3.1.2. Lipids and membrane precursors.....	33
3.1.3. Synthesis of pyruvic acid.....	34
3.2. Natural sources of phosphorus on the early Earth and prebiotically plausible phosphorus-containing minerals	36
4. Modern approaches for abiotic synthesis of phosphorylated prebiotic precursors	41
4.1. Role of urea as a condensing agent under prebiotic conditions	41
4.1.1. Phosphorylation of nucleosides	43
4.1.1.1. <i>Phosphorylation in the absence of a condensing agent</i>	43
4.1.1.2. <i>Cyanamide, cyanate and cyanogen or their derivatives as a condensing agent</i> ...	46
4.1.1.3. <i>Urea as an effective prebiotic condensing agent</i>	48
4.1.1.4. <i>Mechanism of urea-assisted phosphorylation</i>	53
4.1.1.5. <i>Formamide as a solvent, liquidiser and condensing agent</i>	54
4.1.2. Phosphorylation of glycerol, fatty acids and their derivatives	55
4.1.2.1. <i>Phosphorylation of long-chain alcohols including decanol and geraniol</i>	57
4.1.2.2. <i>Production of phospholipids and their polymerisation</i>	59
4.1.3. Synthesis of PEP (phosphoenol-pyruvate)	61
4.2. Phosphorylation of glycerol and adenosine in hydrothermal conditions	61
5. Overview and aims of the thesis	64
II Materials and Methods	66
1. Chemical materials.....	67
2. Analytical methods	72
2.1. NMR spectroscopy methods	72

2.1.1.	<i>Sample preparation for NMR spectroscopic analysis</i>	72
2.2.	MS and LC-MS methods.....	73
2.2.1.	<i>Sample preparation for MS analysis (LC-MS, LRMS, HRMS) of the crude reaction mixtures</i>	74
2.3.	HPLC method for the analysis of mono-palmitoylglycerol (MPG) phosphorylation...	74
2.4.	Raman spectroscopy.....	74
3.	Syntheses methods	76
3.1.	Synthesis and characterization of racemic mono-palmitoylglycerol (MPG, 6)	76
3.2.	Synthesis and characterization of racemic <i>bis</i> -tridecanoyl and dioleoyl glycerol	78
3.2.1.	<i>Synthesis of TBDMS-rac-BTG (18)</i>	78
3.2.2.	<i>Synthesis of rac-BTG (7)</i>	80
3.3.	Synthesis of NaH ₂ P[¹⁸ O ₄] ([¹⁸ O ₄]P _i)	83
3.3.1.	H ₃ P[¹⁸ O ₄]	83
3.3.2.	NaH ₂ P[¹⁸ O ₄].....	84
4.	Design of experiments	86
4.1.	Carousel™ reactions	86
4.2.	Experimental set-up for tracing stable isotopes in urea-assisted phosphorylation reactions of glycerol and racemic monopalmitoylglycerol	86
4.2.1.	Sample preparation for MS analysis (LC-MS, LRMS, HRMS) of Trap 1 and Trap 2 contents.....	88
4.3.	High pressure experiments	88
III	Results and discussion.....	89
1.	Identification and quantification of main reaction products	89
	Introduction	90
1.1.	Urea assisted glycerol phosphorylation.....	91
1.1.1.	Identification of the main reaction products.....	91
1.1.2.	Two persistent organic phosphorylated and carbonylated minor reaction products .	96
1.1.3.	Proton-decoupled heteronuclear multiple-bond correlation and J-modulation ¹³ C nuclear magnetic resonance spectroscopies	101
1.1.4.	High-resolution mass spectrometry and hydrophilic ion liquid chromatography ...	105
1.2.	Urea-assisted phosphorylation of MPG	110
1.2.1.	¹ H and ³¹ P NMR and ¹ H- ³¹ P HMBC spectroscopies	110
1.2.2.	Reversed-phase high-performance liquid chromatography coupled to high-resolution mass spectrometry (RPHPLC-HRMS).....	113
	Conclusions to the Section 1	115
2.	Study of the mechanism and kinetic of urea-assisted alcohol phosphorylation	116

2.1. Associative vs. dissociative mechanism.....	117
2.2. Tracing stable isotopes in volatiles evaporating from ‘dry’ phosphorylation reactions	118
2.2.1. Trap 1: Gaseous nucleophiles (ammonia, water) trapped as benzamide and benzoic acid	121
2.2.2. Trap 2: CO ₂ trapped as benzoic acid (benzamide from trapping HNCO not found by LC-MS)	124
2.3. Inorganic cyanate (NCO ⁻) and carbamoyl phosphate (CP _i).....	127
2.4. Kinetic study of urea-assisted phosphorylation reactions	132
2.4.1. Phosphorylation of glycerol.....	132
2.4.1.1. Degradation of urea.....	132
2.4.1.2. Glycerol phosphorylation mixtures containing [¹⁵ N ₂]urea	136
2.4.2. Phosphorylation of racemic monopalmitoylglycerol	146
Conclusions to the Section 2	157
3. A scope of phosphorylation reactions of glycerol and its derivatives	158
3.1. Dependence on condensing agent in phosphorylation of glycerol and MPG	159
3.1.1. Effect of the molar excess of the condensing agent (catalyst, liquidiser) of phosphorylation of MPG (6)	162
3.2. Dependence of phosphorylation of glycerol and MPG on phosphorous source	165
3.2.1. Effect of protonation degree of sodium orthophosphate on phosphorylation of glycerol (5)	165
3.2.2. Experiments with cyclic trimetaphosphate (cTMP)	167
3.2.3. Experiments with sodium thiophosphate (SP _i).....	171
3.2.3.1. Competition of SP _i and [¹⁸ O ₄]P _i in urea-assisted phosphorylation of glycerol and MPG	179
3.2.4. Involving natural minerals and their analogues in phosphorylation of glycerol and MPG	183
3.3. Phosphorylation of 2,3-bis-(tridecanoyl)glycerol: BTG (7)	185
3.4. Phosphorylation of 2,3-dioleoylglycerol: DOG (8)	189
Conclusions to the Section 3	191
4. Phosphorylation other prebiotic alcohols.....	193
4.1. Phosphorylation of dodecan-1-ol	194
4.2. Phosphorylation of geraniol (10).....	202
4.3. Phosphorylation of pyruvic acid (16a)	207
Conclusions to the Section 4	215
5. Phosphorylation of nucleosides	216
5.1. Phosphorylation of adenosine in the presence of water or formamide	217

5.2. Experiments with different condensing agents (cyanamide 1 and urea 2a)	219
5.2.1. Temperature dependence of urea- and cyanamide-assisted adenosine phosphorylation	230
5.2.2. Effect of urea excess on phosphorylation of nucleosides	231
5.3. Experiments with cTMP and prebiotic minerals as a phosphorous source	240
Conclusions to the Section 5	242
6. ‘Messy’ Chemistry	243
6.1. Urea-assisted phosphorylation of equimolar ‘dry’ mixtures of all ribonucleosides ...	244
6.1.1. HPLC-HRMS analysis of urea-assisted phosphorylation of a dry equimolar mixture of all ribonucleosides	246
6.1.2. Urea-assisted phosphorylation of a mixture of ribonucleosides in the presence of valine	253
6.2. One-pot experiment with urea as a condensing agent	256
6.2.1. NMR analyses of products	256
6.2.2. MS analyses of products	262
Conclusions to the Section 6	269
7. High pressure induced experiments	271
7.1. High pressure induced phosphorylation of glycerol	272
7.1.1. Assignment of the starting molecules Raman spectra	272
7.1.1.1. Glycerol	272
7.1.1.2. Urea	274
7.1.1.3. Monosodium dihydrogen phosphate NaH_2PO_4 (P_1)	275
7.1.1.4. Glyceryl phosphate	276
7.1.2. Experiments on glycerol phosphorylation under pressure	277
7.2. Sodium N-formylcyanamide as a new potential condensing agent	284
7.2.1. Characterisation of starting molecule	286
7.2.2. High pressure experiment with NCF at ambient temperature	290
7.2.3. High-pressure high-temperature experiment with NCF	296
7.2.4. NCF in prebiotic synthesis of phosphate esters	300
Conclusions to the section 7	308
Final conclusions and future prospective	309
Appendix A1 Tracing stable isotopes in urea-assisted phosphorylation reactions	312
List of citations	337

Introduction

Phosphorus is one of the key elements for all existing life on Earth, with a few femtograms of P per cell. Essential parts of any living cell contain phosphate groups in their structure; ribonucleic acid (RNA) and deoxyribonucleic acid (DNA) store and transfer genetic information. Adenosine -triphosphate, -diphosphate, -monophosphate (ATP-ADP-AMP) and their intermediates, such as phosphoenolpyruvate (PEP) or phosphocreatine, are central to the biochemical energy cycle of the cell. Phospholipids constitute the cellular barrier as a bilayer membrane. Those complex structures are based on the stability of phosphate diesters. The presence of a triple negative charge of the PO_4 group between building blocks in large molecules stabilises them, which allows the existence and long-term preservation of biopolymers such as DNA and RNA. Another important feature is its buffering capacity, which helps sustain the pH level of the environment at the same level, and its hydrophilicity, which ensures the stability of the cell membrane. This makes phosphate biopolymers resistant and reactive in the primitive conditions of the early Earth.

Phosphorus, as the other elements that built the Earth, came from smaller bodies that have accreted to grow the planet. The cosmochemistry of phosphorous can be investigated in the meteorites that are the testimony of the early stages of the solar system and planetary formation. In chondrites or iron meteorites, phosphorus was found in the form of phosphides (P^{-3}) as in schreibersite $(\text{Fe,Ni})_3\text{P}$ (see Pasek 2007, for instance).¹ In rocky meteorites like basaltic achondrites and shergottite-nakhlite-Chassigny (SNC) meteorites, phosphorus is in the form of phosphates (P^{+5}), mainly in apatite and whitlockite minerals. At the surface or subsurface of the Earth, the number of phosphorus-bearing minerals is much larger, reaching a few hundreds of mineral species. In the presence of seawater together with reduced N species, such as urea or cyanide, hydroxyapatite is known to spontaneously form struvite ($\text{NH}_4\text{MgPO}_4 \cdot 6\text{H}_2\text{O}$) which is a reactive source of phosphate that was tested in this work.

The emergence of life could have happened as early as 4.3 billion years ago, when Earth became habitable although the oldest most certain fossils are probably only 3.4 Ga old, located in stromatolitic deposits of the Strelley Pool Formation of the Pilbara Craton (Western Australia). Our understanding of early Earth environments is still not mature, and the late Hadean Earth environments that witnessed the emergence of life may never be fully constrained due to the very low preservation of rocks. What has been established and most agreed among the geoscience community is the presence of an ocean, a mild surface temperature able to sustain liquid water and a stable condensation-evaporation cycle, a few emerged lands and a variety of available organic molecules. This thesis focuses on one class of reactions that is ubiquitous in the three domains of life, and central to the cell machinery, that is phosphorylation. The phosphorylation of prebiotic organics is a mandatory step prior to life emergence.

Among the geoscience and astrobiology communities, there are two settings that are considered the most favourable to the emergence of life and that guided the experimental and analytical work performed in the thesis. One hereafter named prebiotic focuses on the evaporative environments that occurred at the transition between the ocean and the few emerged lands, where dry-wet cycles are favourable to phosphorylation and polymerisation of the known building blocks of life, such as nucleotides or amino acids. The other favours hydrothermal conditions, at marine vents or hot springs where water-rock interactions supply microbes with thermal and chemical energy and concentrate prebiotic reactants. It is important to emphasise that at the current stage, one does not exclude the other. In this work, phosphorylation has been investigated in both conditions, though with different levels of detail.

To model the phosphorylation reactions, we chose (1) some prebiotically plausible alcohols such as glycerol and glyceryl derivatives mono- and disubstituted with fatty acid chains, geraniol and dodecanol, as precursors for the cell membrane; (2) nucleosides, adenosine, guanosine, cytidine, uridine and thymidine, which by phosphorylation become the monomers at the foundation of the genetic code in the form of DNA and RNA, or the most energetic carrier in the cells in the form of ATP, or pyruvic acid, as a PEP precursor, which is one of the keys to the energy cycle of the cell.

The plausibility of those prebiotic precursors for phosphorylation reactions is covered in the state-of-the-art section. There are several approaches suggested for their synthesis on the Earth's surface (nucleosides, glycerol, geraniol and sugars) and in hydrothermal vents (lipids, nucleobases and sugars). Another source of organic material could be from impact bombardment. Some of the small organic molecules, such as formaldehyde, methanol, simple amino acids (glycine, alanine and aspartic acid), sugars (glycolaldehyde and glyceraldehyde), pyrimidine and purine bases, and other molecules, were found in the interstellar medium or in comets and meteorites. Those materials could also potentially contribute to the organic precursor inventory on the early Earth.

The challenges of phosphorylation reactions are the low solubility of phosphate-containing minerals in water and their relatively low reactivity towards the formation of phosphoesters. Phosphorylation is thermodynamically unfavourable in water and thus needs some driving force for the initiation of the reaction. For example, the transformation of ADP to ATP ($\text{ADP} + \text{P}_i \rightarrow \text{ATP} + \text{H}_2\text{O}$) is a strongly endergonic reaction that requires +30.5 kJ/mol, which in living cells is assisted by the exergonic hydrolysis of phosphoenol pyruvate ($\text{PEP} + \text{H}_2\text{O} \rightarrow \text{pyruvate} + \text{P}_i$, $\Delta G = -61.9$ kJ/mol) that compensates for the phosphorylation of ADP ($\text{PEP} + \text{ADP} \rightarrow \text{pyruvate} + \text{ATP}$, $\Delta G = -31.4$ kJ/mol).²

One approach for overcoming thermodynamic constraints and initiating the reaction is the presence of a “condensing” agent. If such a molecule is added to the alcohol and phosphate mixture, it provides a thermodynamic driving force for the phosphorylation reaction by irreversibly eliminating water. In this work, we studied different “condensing” agents that could be non-volatile reduced nitrogen compounds such as urea or cyanamide. The mechanism and kinetics of urea-promoted phosphorylation were studied in detail in the thesis. We confirmed the dissociative mechanism that is going through phosphate activation (urea-promoted) and phosphate substitution (alcoholysis) steps. The urea-promoted phosphate activation, called

"dissociative" due to the dissociation of urea to cyanate and ammonium, is promoted by inorganic phosphate. Ammonium cyanate was not observed; however, it linked covalently to phosphate, giving an intermediate ammonium carbamoyl phosphate, which constitutes the mentioned phosphate activation.

We also explored other potential condensing agents, such as carboxamides and N-cyanoformamide. In the hydrothermal scenario, the driving force is pressure and/or temperature, which may act similarly as a condensing agent. To simulate these conditions, experiments were performed at high pressure in a diamond anvil cell and analysis was done by in-situ Raman spectroscopy.

All experiments were conducted in the absence of solvent in a constant dry state, with yields much higher than previously achieved. High phosphorylation yields were obtained (up to 95%), which proved that phosphorylation of prebiotic precursors could have taken place even in such a hostile place as the early Earth. A negative control test confirmed the necessity of a condensing agent for the majority of alcohols. The complex experimental product mixtures were analysed and quantified by nuclear magnetic resonance spectroscopy (NMR), mass spectrometry (MS), Raman spectroscopy and high-performance liquid chromatography (HPLC) methods. The abiotic production of phosphate diesters achieved in this thesis opens perspectives for further polymerisation.

List of abbreviations

- A** – adenosine (nucleoside)
ACN – acetonitrile
AcOH – acetic acid
Ade – adenine (nucleobase)
AMP, ADP, ATP – adenosine mono-, di- and triphosphate (nucleotide)
BTG – *rac*-1,2-*bis*-Tridecanoyl glycerol
C – cytidine (nucleoside)
CDCl₃ – deuterated chloroform
CMP, CDP, CTP – cytidine mono-, di- and triphosphate (nucleotide)
CP_i – dilithium carbamoylphosphate hydrate
cTMP – cyclic trimetaphosphate
Cy – cyclohexane
Cyt – cytosine (nucleobase)
DAC – diamond anvil cell
DAP – diamidophosphate
DCM – dichloromethane
DES – deep eutectic solvent
DMAP – 4-dimethylaminopyridine
DMSO-*d*₆ – deuterated dimethyl sulfoxide
DNA – deoxyribonucleic acid
DOG – *rac*-1,2-dioleoylglycerol
EDC-HCl – N-(3-Dimethylaminopropyl)-N'-ethylcarbodiimide hydrochloride
EDTA – ethylenedinitrilotetraacetic acid disodium salt
ELSD – evaporative light scattering detection
ESI – electrospray ionization source
Et₂O – diethyl ether
Et₃N·HF – triethylamine *tris*-hydrofluoride
EtOAc – ethyl acetate
EtOH – ethanol
G – guanosine (nucleoside)
GMP, GDP, GTP – guanosine mono-, di- and triphosphate (nucleotide)
Gua – guanine (nucleobase)
HILIC – hydrophilic ion liquid chromatography column
HPLC – high-performance liquid chromatography
 - **UHPLC** – Ultra-High-Performance Liquid Chromatography
 - **RP-UHPLC** – reversed-phase ultrahigh-performance chromatography**MeOH** – methanol
MS – mass spectrometry
 - **HRMS** – High Resolution Mass Spectrometry
 - **LRMS** – Low Resolution Mass Spectrometry
 - **LC-MS** – liquid chromatography-mass spectrometry**NMR** – nuclear magnetic resonance spectroscopy
 - **JMOD** – J-Modulated Spin-Echo
 - **HMBC** – Heteronuclear Multiple Bond Correlation
 - **QCI** – Quadruple Resonance CryoProbe**MDCs** – metal-doped-clays
MPG – *rac*-mono-palmitoylglycerol
MPGP – monopalmitoyl glyceryl phosphate
MTG – *rac*-mono-tridecanoyl glycerol
MW – molecular weight
NCF – N-cyanofornamide
PEP – phosphoenolpyruvate
PhMgBr – phenyl magnesium bromide (1.6 M in cyclopentyl methyl ether)
P_i – **orthophosphate** PO₄³⁻
rt – room temperature
SP_i – trisodium thiophosphate (Na₃SPO₃)
Q-TOF – hybrid Quadrupole Time-of-Flight mass spectrometer
RNA – ribonucleic acid
SP_i – Sodium thiophosphate
T – thymidine (nucleoside)
TBDMS-*rac*-BTG – *rac*-(2,2-Dimethyl-1,3-ioxolan-4-yl)methyl palmitate
THF – tetrahydrofuran
Thy – thymine (nucleobase)
TLC – thin-layer chromatography
TMP, TDP, TTP – thymidine mono-, di- and triphosphate (nucleotide)
U – uridine (nucleoside)
UAFW – urea:ammonium formate:water eutectic
UMP, UDP, UTP – uridine mono-, di- and triphosphate (nucleotide)
Ura – uracil (nucleobase)
UV – ultra-violet

I State of the art

1. Phosphorous role in the origin of life

One of the biggest mysteries fascinating mankind is the origin of life. What was there before us? Where did we come from? What is life? These and other existential questions belong not only to philosophical discussions but are also investigated by science.

The origin of life study presents many challenging and, at the same time, fascinating questions.

- What was the origin of the first organic molecules?
- How did relatively simple molecules self-arrange into complex biopolymers?
- At what point did these biopolymers develop self-replication and become proto-cells?

At the moment, there is no definitive answer to these questions and there may not be a unique answer. One of the missing pieces is designated as the "phosphorus problem." Life as we know it now contains large amounts of phosphorus in the most essential parts of every cell (**Figure 1**).

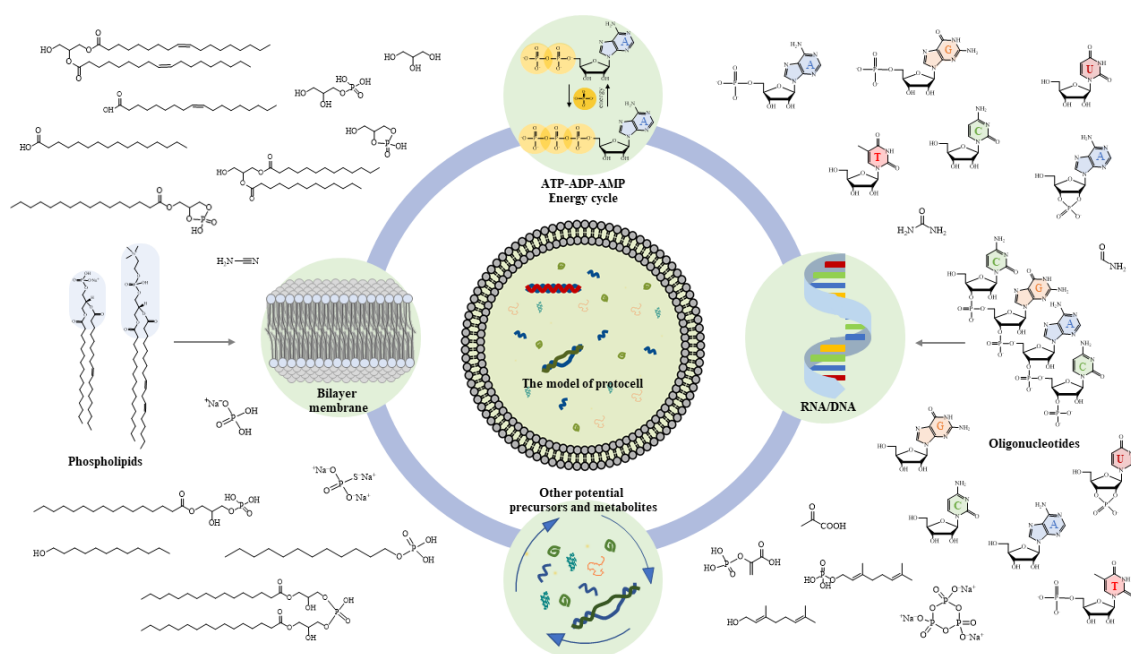


Figure 1. Schematics of the cell machineries highlighting phosphorus-bearing molecules and their potential prebiotic precursors.

The phosphorus used by life is in the form of phosphates ($\text{P}^{+5}\text{O}_4^{3-}$). The phosphate group plays a structural role in cells due to its hydrophilic features, which ensure, for example, the stability of the cell membrane. This is possible because of the low pK_a value ($\text{pK}_a = 2.2, 7.2, 12.3$) of its charge-neutral form at a normal pH, typical for life.³ The buffering capacity of phosphate is assumed to be an important feature for the origin of life because it could have helped to create a stable environment for the formation of the first cells. When the pH of the environment changes, phosphate can either release or absorb hydrogen ions, helping to keep the pH constant. This is important because many of the reactions that are thought to be involved in the formation of life are sensitive to pH.

Phosphate group enables the existence of RNA and DNA because of its ionic structure. The negative charge between two phosphodiester bonds stabilises the polymer chain and also protects it from nucleophilic attacks (hydrolysis, alcoholysis, aminolysis, etc.).⁴ Thus, phosphates are kinetically stable and, at the same time, chemically active due to the presence of a charge in the cellular environment. Those features make these biopolymers reliably water-soluble, with remarkable polymer lengths, as an example, any type of nucleotide chain is soluble in water. Phosphates are mandatory in many biochemical reactions and are an essential part of energy metabolism.

It is still enigmatic that life relies so much on phosphorus-bearing molecules, whereas phosphorus is a relatively rare element in the Earth's crust and is highly diluted in the ocean, with a concentration in the range of $2 \mu\text{mol kg}^{-1}$ in the global ocean.^{5,6} Despite those considerations, we assume that all the precursors needed for phosphorylation were accessible on the young Earth about 4 billion years ago, during the Late Hadean.^{7,8} Taking into consideration the intense bombardment by meteorites, phosphorus may have been available on Earth. The iron and nickel phosphides in the meteorite material were converted to phosphorus-bearing minerals on land or in the oceans by being heated, oxidised and corroded by the atmosphere.^{9,10} Another source of phosphorus may have resulted from the active volcanic activity in the late Hadean. Under the influence of elevated temperatures and pressure, phosphorus could possibly accumulate and be accessible for dissolution in the ocean. It should also be mentioned that phosphorus-bearing minerals (especially phosphates) are rather stable and cannot be easily involved in organic synthesis.

Thus, we are approaching the main challenges of the "phosphorus problem," to which we have attempted to find a solution:

- What was a possible source of phosphorus-containing minerals on the early Earth? Which minerals could be available?
- In which early Earth environments could the phosphorylation reactions have happened? For instance, was it on the land surface or the ocean floor?
- What was the driving force and the pathway for phosphorylation reactions under the aforementioned conditions?
- Could phosphorylation and oligomerisation (polymerisation) occur under the same conditions?

This represents a complex problem and one of the mysteries of the origin of life. To answer the questions, I have looked at the big picture of the early Earth, including the multiple sources of phosphorus and the ways they have been formed. I have considered both prebiotic conditions at the surface of the Earth^{11,12,13} and hydrothermal conditions at the sea floor,^{14,15,16} where phosphorylation could have occurred. I examined the possible factors affecting the phosphorylation rate of organic prebiotic molecules, such as temperature, pressure, the presence of condensing agents, and their concentration.

2. Geochemical settings at the late Hadean

It is necessary to consider the geological setting of the Hadean (4.5–4.0 Ga) for a better understanding of the conditions that gave rise to the organic phosphorylated precursors from which life could possibly developed as one of the approaches. The formation of all the essential molecular ingredients for life must have occurred after the large Moon-forming impact^{17,18} and the relatively rapid cooling of the Earth's crust (between hundreds of thousands or millions of years).¹⁹ The estimation of magma's ocean lifetime depends on viscosities, compositions, thermal boundary layer thicknesses and initial core temperatures.²⁰

The oldest records of Earth's history are enclosed in ancient mineral grains, namely zircons, that are often called “deep-time capsules”. Zircons provide evidence of plate tectonics about 4.3 Ga ago²¹ that gives us an idea about the regime of mantle convection and tectonics on the early Earth. Zircons also suggest the presence of a continental crust at 4.37 Ga ago.^{22,23} At that time, the continental crust was formed and quickly recycled into the mantle. It consisted of cooled mantle rocks interacting with the atmosphere and ocean, influenced by both bombardment and geological processes. Crust-mantle-atmosphere evolution models predict a relatively fast growth of the continental crust, reaching about 80 % of its modern volume by the early Archean.^{24,25} This fact enables the presence of different landforms, hydrothermal vents, the circulation of energy and nutrients from the Earth's mantle to the surface environments and likely the creation of the right conditions for self-replicating molecules to form.



Figure 2. My artistic representation of late Hadean Earth \approx 4 Ga ago, created with the AI software “Midjourney”

However, there is no yet conclusive agreement about the composition and volume of the oceanic and continental crust on the very early Earth due to the significantly limited residual evidence from Hadean history, by definition. The primitive crust was most likely formed of basalts, possibly mixed with some felsic and ultramafic rocks.^{21,26,27} It sets the geochemical conditions for the emergence of life.²⁸ In the future, we might acquire more information about Earth's early history from nearby "models" such as the Moon, Mars, and other extraterrestrial bodies that, in the absence of tectonic activity, preserved older rocks that were recycled on our planet.

During Hadean, the Moon was much closer to the Earth compared to present day.^{29,30} This induced stronger tidal effects, which had a broad and significant influence on the Earth's settings.³¹ First, it could contribute to dry-wet cycling of high amplitude in coastal environments. The frequent flooding and draining of tidal zones would create a dynamic environment with alternating periods of wetness and dryness. This would have helped to concentrate chemicals, which could be highly beneficial to the formation of biomolecules. The mixing of seawater and freshwater during tides would cause fluctuations and gradients in pH. Additionally, dynamic tidal effects could also provide a source of energy for biochemical reactions and early life forms. The mixing of seawater and freshwater might also create currents and vortices that generate energy. Strong tidal currents would transport organic molecules and could therefore provide a constant supply of nutrients to the cradles of life.

The presence of immense volumes of liquid water on the Hadean Earth was confirmed by the isotopic analyses of oxygen isotopes in zircons.^{21,32,33} The Sun was significantly fainter (about 70 % of today) and much more XUV-active than at present day.³⁴ This creates the so-called "Faint Young Sun Problem", i.e., an apparent contradiction between the presence of liquid water on the early Earth and a solar activity too low to support moderate temperatures. This paradox is solved when considering different characteristics of the early Earth. The composition of the late Hadean atmosphere,^{35,36,37} which was probably rich in the green-house gas carbon dioxide that thereby heated^{38,39,40} the atmosphere together with CH₄.⁴¹ Additional heat may have arisen from volcanic emissions and tidal warming³¹. Clouds with lower albedo, a low land-to-ocean ratio of the Earth's surface and other factors have likely contributed to increasing the greenhouse effect in the early atmosphere.^{34,42} Perhaps forthcoming missions to Venus, Titan, and other satellites of the giant planets with heavy atmospheres will help to understand the environment of the early Earth.^{43,44}

Understanding the atmospheric composition is equally important for deciphering the life elements cycle of the Hadean oxygen-free world. There is currently no unified scientific consensus about the composition of the early Earth's atmosphere. It is commonly considered to consist of large quantities of N₂/CO₂/H₂O^{45,46} and be devoid of O₂. Atmospheric records during this time period confirm the presence of established evaporation and condensation cycles of water^{47,48}. The quantity of atmospheric nitrogen is still debated, and most probably it was higher than the present-day level.^{45,49,50} Oxygen and hydrogen were present in much lower quantities as well. H₂ is a very volatile gas and it was slowly escaping from the atmosphere.⁴⁹ Free O₂ began to appear in the atmosphere much later, after the development of oxygenic photosynthesis and the great oxygenation events.^{51,52}

The early Earth's atmosphere and ocean were anoxic. Additionally, meteorite impacts may have converted water to hydrogen and carbon dioxide to methane.^{53,54} In the absence of free oxygen in the atmosphere, the oceans were not only anoxic but also slightly acidic.^{55,56} This allowed for the existence of large amounts of reactive Fe^{2+} , which could potentially prompt a variety of prebiotic reactions.⁵⁷ The processes of oxidation, corrosion, and weathering of phosphorus-bearing minerals on the Earth's surface may have concentrated enough phosphate and other microelements for the emergence of life.^{58,59} The presence of ferrous phosphorus-containing minerals might have an important role in phosphorylation reactions.⁷

Under such reducing conditions, atmospheric chemistry may have facilitated the production of nitrogen-reduced compounds, such as hydrogen cyanide $\text{H}-\text{C}\equiv\text{N}$ and cyanoacetylene $\text{H}-\text{C}\equiv\text{C}-\text{C}\equiv\text{N}$, which may have accumulated and concentrated in lakes or closed pools.⁶⁰ Those highly reactive molecules are prone to produce abiotically complex molecules such as nucleobases.^{12,61} They are also part of the diverse chemical inventory of the organics found in the primitive bodies of the solar system, e.g., meteorites, comets, and beyond the solar system in dust clouds. Those prebiotic precursors could have been brought to the early Earth by impact bombardment.^{62,63} Amino acids,^{64,65,66} nucleobases,^{67,68,69} sugar-related compounds,⁷⁰ short aliphatic molecules⁷¹ and macromolecular materials,⁷² have been found on carbonaceous meteorites.⁷³ In carbonaceous meteorites, many of the organic molecules are found as complexes of insoluble organic matter,⁷⁴ which, under hydrothermal alteration or UV-irradiation, produce primary chemical reagents such as ammonium.⁷⁵ High-velocity impact shocks might also have brought an additional energy source for the synthesis of several amino acids.^{62,76} Phosphate might have accumulated on the Earth surface because of intense impact bombardment,^{77,78} and is part of the mandatory chemicals for life in lipids, metabolism coenzymes, RNA and DNA.^{3,8,12} However, there is not yet a consensus on the relative amount and chemical diversity of extraterrestrial organics delivered to Earth and their implications for the origin of life. Upcoming missions to extra-terrestrial bodies such as OSIRIS-Rex (NASA's mission to asteroid Bennu) or Hayabusa2 (Japan's mission to Ryugu and other asteroids) and analysis of samples in space and after return should provide deeper insights on the nature of organic molecules present on meteorites and comets.

Among the prebiotic environments favourable to the origin of life, I shall mention hydrothermal vents, in particular at mid-ocean ridges.⁷⁹⁻⁸⁰ An interesting example is represented by the Lost City system,^{81,82} which may resemble the early Earth with reactive gases, dissolved elements, and thermal and chemical gradients. Altogether, it comprises a chemically reactive environment favourable to prebiotic synthesis.^{83,84,85} The hot water-rock interactions occurring in hydrothermal flows under pressure may have been a "bridge" between the abiotic and biotic chemistry of primitive life.^{86,87}

From the flourishing literature on the origin of life and the environmental conditions that may have witnessed it on the early Earth, I conclude that there are two major settings that have the preference of the origin of life community. The first setting is dry land or shallow-water reservoirs. There, the main building blocks of life result from organic synthesis from small molecules available on the surface or brought in by meteorite impacts. Reactions proceed with the energy brought by UV irradiation, temperature, the presence of minerals, interaction

with atmospheric gases, or active organic agents (urea, formamide). The second setting, at hydrothermal vents, places prebiotic reactions on geyser field or the sea floor. The driving forces are pressure, temperature, concentration and pH, and their gradients, together with the porous surface of chimneys, work as catalysts for chemical reactions. Thus, numerous chemicals such as formamide, sugars, amino acids and others become available due to the constant flow of material from the vent and other molecules dissolved in water.

There is no conclusive answer to what exactly early Earth conditions were most favourable for life self-assembly. It is also not known in what precise order prebiotic precursors were introduced into biosynthesis or if there were other possible forms of proto-life and their diversity. Thus, we take into consideration all known prebiotically plausible chemical reactions that could fit into the conditions of the early Earth described above. We assume that there are several alternative pathways to the synthesis of prebiotic precursors under different conditions, and each of them could contribute to the origin of life.

3. Availability of the key precursors for phosphorylation reactions and the mechanisms involved in their production on the early Earth

In the current work, the main efforts focus on studying and understanding the phosphorylation reaction in early Earth environments, as described above. Before moving forward, in particular with phosphorylation, there are several questions that need to be discussed. A better understanding of these challenges could provide us with a better vision of the modern approach to phosphorylation reactions on the Early Earth.

- First, as a result of which processes, small organic molecules such as nucleic acids, fatty acids, sugars, and others become available? The main pathways and availability are the among debatable questions. In section **3.1**, I discuss the main approaches to their formation and synthesis.

- Second, one crucial point regarding phosphorylation is the actual source of phosphorus. In which environments could phosphorus be available on Hadean Earth? In section **3.2**, I discuss the main sources of phosphorus and the pathways of its transformation into phosphate-containing minerals.

3.1. Inventories of organic molecules and their transformation into prebiotic precursors

Starting with Miller-Urey's famous experiments in the 1950s', prebiotic synthesis became an exciting research field. It has been greatly advanced, and new approaches have been found to synthesise the essential parts that constitute life. As mentioned before, the primary sources of organic molecules on the Early Earth could be extraterrestrial delivery, hydrothermal vents, the atmosphere processed by surface chemistry, or reactions induced by ultraviolet (UV) radiation or lightning strikes, etc.

As there are only a limited number of hypotheses that can be tested during a PhD thesis, the hypothesis here is that (i) the prebiotic alcohols used in phosphorylation reactions were already present on the early Earth, and (ii) they self-assembled from simpler molecules to make the main building blocks (nucleosides, glyceryl and its derivatives, long-chain alcohols and others) available for phosphorylation.⁸⁸ In the following section, I investigate the possible prebiotic pathways for the synthesis of nucleosides (nucleobases, sugars, nucleosides), glycerol-based lipids (glycerol, fatty acids) and other prebiotic alcohols (geraniol, pyruvic acid, dodecanol-1).

3.1.1. Nucleosides as RNA and DNA precursors

3.1.1.1. Nucleobases (purines and pyrimidines)

Any living system requires genetic information. It controls the main biological processes of cells, such as the production of proteins, and, in general, life's functioning. In life as we know it, the bar code relies on deoxyribonucleic acid (DNA) and ribonucleic acid (RNA) chains connected by the complementarity principle, which is essential for self-replication.⁸⁹ Each piece of the code is made of four canonical nucleotides made of the phosphorylated nucleosides adenosine (**A**), cytidine (**C**), guanosine (**G**) and thymidine (**T**) in the case of DNA, **T** being replaced by uridine (**U**) in the case of RNA, and are connected by phosphate groups. Each nucleoside contains a nucleobase, either purine (cytosine (**Cyt**), thymine (**Thy**), uracil (**Ura**)) or pyrimidine (adenine (**Ade**), guanine (**Gua**)) and pentose sugars, deoxyribose (DNA) or ribose (RNA) (**Figure 3**).

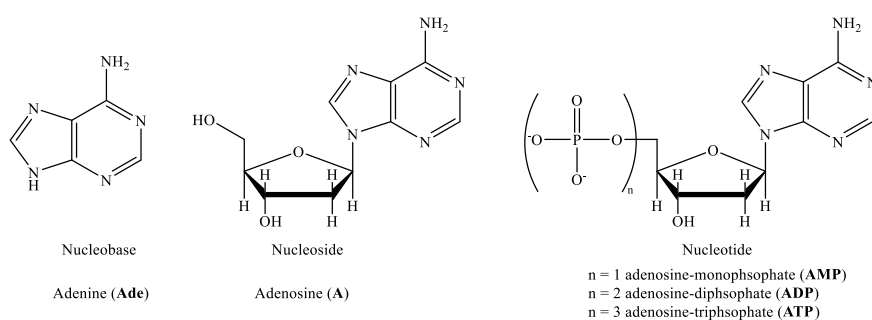


Figure 3. Schematics and abbreviations of nucleic acid monomers, with the example of adenosine

The prebiotic synthesis of the canonical nucleobases adenine (**Ade**), cytosine (**Cyt**), guanine (**Gua**), thymine (**Thy**), and uracil (**Ura**) started with Oró's experiment.⁹⁰ A mix of purines, including a small amount of **Ade**, was produced by heating at 100 °C a concentrated ammonium cyanide solution. Later improved,^{91,92} its relevance to the origin of life was questioned considering the prebiotically unrealistic concentration of HCN, its complex polymerisation⁹³ and its variable stability depending on pH and temperature.⁹⁴ Miller and co-workers carried this experiment further and explored different temperatures and conditions, including keeping HCN and NH₃ frozen at -78 °C for 27 years.^{95,96} After hydrolysis, a mix of organics was identified, including the canonical nucleobases **Ade**, **Cyt**, **Gua**, and **Ura** (**Figure 4**).

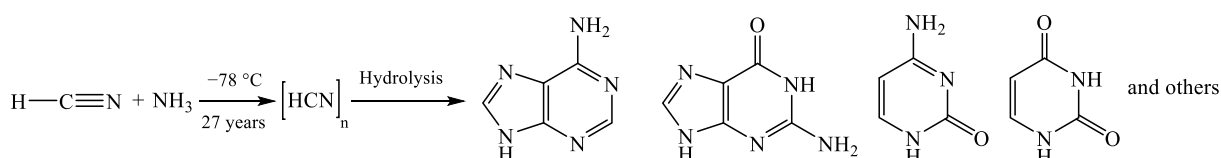


Figure 4. HCN polymerisation from Miyakawa and others^{95,96}

One of the other early approaches was synthesis through a Fischer-Tropsch-type reaction. Gas mixtures of CO and H₂;⁹⁷ NH₃, CH₄, H₂ and water;⁹⁸ CO, N₂ and water⁹⁹ were activated by electric discharge or proton irradiation and produced purines and pyrimidines.

However, those approaches are highly debated due to the upcoming research data about the composition of the primitive atmosphere, for example, predominance of CO₂ rather than CO and relatively low levels of H₂ and NH₃.^{40,41}

A potential starting molecule with prebiotic interest could be cyanoacetylene H–C≡C–C≡N. Starting from the spark discharge of CH₄ and N₂ gas mix heated with urea and potassium cyanate at 100 °C for 1 day, it produces about 5 % **Cyt**.¹⁰⁰ Pyrimidines can be produced by heating at 55 °C for a day cyanoacetylene with ammonium sulphide dissolved in dimethylamine solution and repeating the same experiment with *N*-methyl-*N*-nitrosourea.¹⁰¹

Urea and formamide could be possible building blocks for prebiotic precursors. Heating formamide at 170–190 °C for 28 hours produces high yields of purine from formamide consumption (more than 70 %).¹⁰² Saladino and DiMauro explored the effect of inorganic metal oxides such as silica, alumina, kaolin, and zeolite¹⁰³, TiO₂.^{104,105} Formamide and metal oxides were heated at 160 °C for 48 h, resulting in purines **Ade** and **Cyt**. If titanium oxide or montmorillonite clay were used, it also produced acylated purines and pyrimidines. The same team confirmed that the presence of minerals also helps the formation of canonical nucleobases under similar conditions (160 °C for 48 hours). Various phosphate minerals (turquoise, childrenite, ludlamite, vivianite, etc.) facilitated the production of **Ade**, purine, hypoxanthine, **Cyt**, **Ura**, and 5,6-dihydrouracil.¹⁰⁶ Iron/copper sulfur minerals (pyrrhotine, pyrite, chalcopyrite, bornite, etc.) heated with formamide led to the formation of **Ade**, purine, iso**Cyt**, urea and other organics.¹⁰⁷ Irradiation of formamide HCONH₂ with high-energy protons in the presence of meteorite mineral material,¹⁰⁸ UV-irradiation¹⁰⁹ or conducting experiments on the surface of photocatalysts (TiO₂) in hydrothermal conditions¹¹⁰ produced nucleobases along with other biologically relevant chemicals such as acids and sugars. Following the idea that urea could be a prebiotic precursor, it was combined with β-alanine and formed **Ura**¹¹¹ and¹¹² **Thy** by the photodehydrogenation reaction.

Research about the interstellar formation of nucleobases led to the study of freeze-thaw cycles of aqueous urea solution.¹¹³ Using spark discharges as the energy source of the reaction led to the formation of **Cyt**, **Ura**, **Ade** and others. Pyrimidines (**Cyt**, **Ura**, and **Thy**) and purines (**Ade**, xanthine, and hypoxanthine) were detected in laboratory-simulated interstellar ice analogues (mixtures of water, carbon monoxide, ammonia and methanol) under irradiation with ultraviolet photons.¹¹⁴

3.1.1.2. Sugars (ribose/2-deoxyribose)

The most common method of synthesis of sugars is the Butlerow¹¹⁵ formose reaction, described in detail by Breslow¹¹⁶. It proceeds through aldol and aldose-ketose isomerisation and is principally a polymerisation of formaldehyde (**Figure 5**). Adding glycolaldehyde (one of the products) increases the yield of the chemical reaction. The formose reaction is a self-catalysed reaction that can be looped into an autocatalytic cycle.

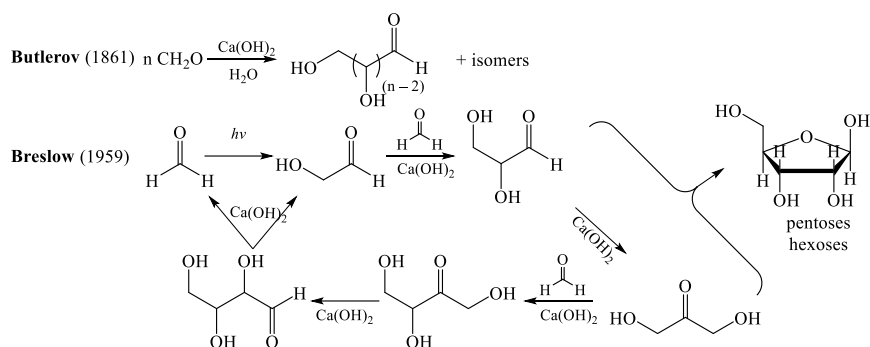


Figure 5. Principal scheme of the formose reaction^{115,116}

However, some constraints question the prebiotic plausibility of the formose reaction.^{117,118,119} The resulting mixture is rather complex, and the reaction time is a crucial factor in its composition. A major issue is that ribose is a very minor product, with a yield of only about 1%. A number of methods have been reported that control the formose reaction. The presence of lead ions increases the pentose yield.¹²⁰ Borate,^{121,122} silicate,^{123,124} schreibersite¹²⁵ and hydroxyapatite¹²⁶ minerals stabilise the reaction and direct it towards pentose production. Ribose is also selectively enriched on metal-doped-clays (MDCs) from a complex formose mixture.¹²⁷ Additional computational studies help to elucidate the unique stability of the ribose-MDC complex and promote further 5-phosphorylation of nucleosides with greater yield and selectivity.¹²⁷

It is also possible to conduct the formose reaction under hydrothermal conditions¹²⁸ or in presence of 2-aminooxazole¹²⁹ or glycolaldehyde phosphate¹³⁰ to enhance the yield. In fact, the self-condensation of glycolaldehyde-2-phosphate produces a mixture of phosphorylated sugars that are more stable and less likely to further inhibit polymerisation.¹³¹ Another suggested approach is to use glyoxylate and dihydroxyfumarate as reactants, which result in linear ketoses and sugar-acids.¹³²

A particular case is the synthesis of 2-deoxyribose. There is no clear understanding of whether it was part of abiotic synthesis or appeared later during the evolution of protocells. One way to produce 2-deoxyribose prebiotically is by heating formaldehyde or glyceraldehyde and acetaldehyde with $\text{Ca}(\text{OH})_2$ in water, with a yield of about 3%.¹³³ Other approaches obtained deoxyribose using either enantioselective aldol reactions of formaldehyde and glycolaldehyde;¹³⁴ or photoreduction of cyanohydrins by hydrogen sulfide in the presence of copper(I) cyanide;¹³⁵ or hydrolysis of 2-thio-deoxyuridine through phosphorylation of the 2-thiouridine nucleoside.¹³⁶ The method of Xu et al.¹³⁶ using principles of system chemistry, produced not only sugars but also other chemicals such as nucleobases or nucleotides all together in prebiotic conditions.

3.1.1.3. Nucleosides (purines and pyrimidines)

Moving towards nucleotide formation, it is straightforward to assume that two obvious building blocks, ribofuranose and one of the nucleobases, were just “glued” together. The first

approach is to find a path connecting them and, later, to phosphorylate the resulting nucleosides into nucleotides. An alternative pathway would be to add a nucleobase to phosphorylated ribofuranose. However, the latter does not appear to be easy and raises “the nucleosidation problem”.

The reactions forming sugars and nucleobases seem to be rather different and could hardly happen in the same environment. For example, an extreme condition that is needed for nucleobases might lead to uncontrolled formose polymerisation. Otherwise, if sugars and nucleobases were synthesised separately, some mechanism should be introduced for bringing them together.

Another point is that the majority of building blocks are synthesised in complex mixtures and do not appear as the main product. Aside from improbable chemical or physical purification under prebiotic conditions, it is worth focusing on the fact that other reaction products may also participate in reactions leading to a multitude of non-selective, unavoidable results. An additional challenge is the chiral asymmetry of nucleosides, with life using only D-ribose and D-deoxyribose. This is still an open question.

Mixing pure nucleobases and sugars does not lead to high yields of the canonical nucleosides due to the numerous possible structural isomers of ribose and nucleobases.¹³⁷ In water, the hydrolysis of bonds between ribose and the nucleobases is more favourable thermodynamically rather than their formation. The first attempts at directly coupling ribose and a nucleobase were made on a dry mixture of purine nucleosides and ribose heated in the absence or presence of certain salts and minerals. The products included ribosylaminopurines (ribose can also react with the primary amine group of nucleobases, like adenine or guanosine) and several structural isomers of the nucleosides, with a low fraction of canonical ones.^{138,139} Also, reactions with pyrimidine do not work as well as for purines. The possible reason for this is a kinetic barrier due to the delocalization of the lone pair on N(1) of the pyrimidine bases.^{140,141} Following the direct approach, alternative nucleobases as precursors to pyrimidine nucleoside, such as urazole¹⁴¹ or 2-pyrimidinone¹⁴² were proposed and succeeded in assembling into nucleosides.

Peering into the natural processes of modern living organisms, we see the process of nucleotide assembly starting with phosphoribosyl pyrophosphate. The presence of a phosphate group makes sugar molecules more reactive. Following this idea, Benner and his colleagues used 1,2-cyclic phosphate and succeeded in producing adenosine-2'-phosphate.¹⁴³ The reaction was carried out in a dry state in the presence of divalent metal ions such as calcium or magnesium and heated at 85 °C for 18 hours. Although the yields were relatively small, the reaction was stereoselective towards the β -anomer of nucleotides. This approach was improved using higher temperatures and concentrations, and all canonical nucleotides were synthesised, although still with low yields (<8%).¹⁴⁴

A system approach was applied by Carell and colleagues, who investigated the complex pathways to both purines and pyrimidine nucleosides.¹⁴⁵ Starting from simple molecules like HCN, NH₃ and formic acid derivatives, they found a prebiotic pathway to nucleosides. The key idea was to use *N*-formamidopyrimidines (suggested earlier by Eschenmoser¹⁴⁶) to overcome

purines and stereoselectivity problems. High yields up to 60 % and good regioselectivity towards N-9 purine and both α - and β -anomers were reported. Later, the same group investigated the merged pathway to nucleotides, including dry-wet cycles, the influence of metals (Zn, Fe and others), the involvement of other small organic molecules (urea, isocyanate, formic acid, etc.) and suggested a complete scheme of parallel synthesis of canonical RNA-nucleosides.^{147,148} The suggested synthesis is efficient only in a sequential way, excluding cross-reactions of other isomers of pentoses in place of ribose in the nucleosidation step.

Zhao & Wang discovered that metal-doped clays have a distinctive ability to selectively retain and stabilise ribose within the complex formose mixture.¹²⁷ Also, the direct ribosylation of uracil, which was not previously feasible, became possible in the presence of metal cations and clay minerals.¹⁴⁹ Later, in particular, a Ti-catalysed regioselective ribosylation method for the synthesis of purine and pyrimidine ribonucleosides was reported.¹⁵⁰ The authors suggested that Ti minerals enhanced the selectivity of N9 purine nucleosides compared to exocyclic NC6 isomers. For example, N9-ribosylated adenines yielded 14% with high regioselectivity (N9:NC6 up to 13:1). Even better results were demonstrated for β -guanosine, with the best yields and selectivity. Without affecting the nucleoside products, acidified titanium minerals enabled an equilibrium between the fast ribosylated primary amino group and the more favourable endocyclic ribosyl amino group. There is no such pathway previously described in the literature.

The complex method of pyrimidine ribonucleotide synthesis was demonstrated by Powner and others.¹² Instead of the direct approach using nucleosides and ribose, they produced phosphorylated uridine and cytidine from arabinose amino-oxazoline and anhydronucleoside. This idea was first introduced by Sanchez & Orgel, without inorganic phosphate, and consequently with low yields.¹⁵¹ Powner¹² suggested that the synthesis of those intermediates is possible from small prebiotic molecules such as cyanamide, cyanoacetylene, glycolaldehyde and glyceraldehyde together with inorganic phosphate.

Recently, the possibility of the mutual synthesis of both purine and pyrimidine nucleosides was studied based on the amino-oxazoline approach.¹⁵² A potential common precursor of pentose, oxazolidinone thione was used, which is derived from glycolaldehyde and thiocyanic acid. It reacted with ammonia or hydrogen cyanide trimer and produced purine or pyrimidine precursors, respectively. The obtained molecules could be phosphorylated and produce nucleotides with the proper sugar β -stereochemistry. Patel and others proposed an entire reaction network for producing nucleotides, sugars, amino acids and lipids from HCN and hydrogen sulphide driven by ultraviolet light and Cu(I)–Cu(II) photoredox cycling.¹⁵³

There have also been some successes in deoxyribonucleoside synthesis. Aside from arguing its abiotic or evolutionary origin, the first “direct” approach was tested on a solution of adenine and 2-deoxyribose in the presence of NaCN and $\text{NH}_4\text{H}_2\text{PO}_4$ under UV-light and produced deoxyadenosine with a 7% yield.¹⁵⁴ Another pathway for 2-deoxyadenosine synthesis was suggested through the phosphorylation of 2-thiouridine¹³⁶ (could be produced as the result of prebiotic RNA synthesis¹⁵³). The latter formed 2'-deoxy-2-thiouridine reacted with adenine in the dry state (100 °C, 31 hours) to produce 2'-deoxyadenosine. This pathway could be a

prebiotic “bridge” between RNA and DNA formation. Later, the same team suggested thioanhydropurines and derivatives as key intermediates for the synthesis of deoxyribonucleosides.¹⁵⁵ The authors demonstrated a high-yielding, stereo- and regioselective prebiotic pathway for the production of deoxyadenosine and deoxyinosine. The work demonstrated that deoxyadenosine, deoxyinosine, cytidine and uridine can be obtained within the same chemical network, which led to the idea that deoxyribonucleosides and ribonucleosides could co-exist in the same environment.

3.1.2. Lipids and membrane precursors

Life as we know it is in the form of a cell. The wall separating the living from the non-living is a membrane. It helps to maintain a self-sufficient system and protect it from hostile environments. All membranes are composed of two layers of amphiphilic phospholipids connected by a hydrophobic part. Each molecule has a hydrophilic headgroup and two hydrophobic nonpolar lipid tails. Both parts are variable and depend on living species. Despite the variability, the principal structure systematically includes two fatty acids connected by phosphorylated glycerol with various groups attached to them (-H, -ethanolamine, -choline, and others).¹⁵⁶

One of the methods for the prebiotic formation of glycerol has already been reviewed in the previous sub-section (3.1.1.2) as part of the UV-irradiated formose-type reaction.^{119,153,157} Another approach is glycerol synthesis in space, on interstellar bodies. Photolysis of mixture CO, NH₃ in H₂O at 12 K;¹⁵⁸ ice film of NH₃, CH₃OH, HCN in H₂O at 15 K;¹⁵⁹ CO, NH₃, and H₂O gas mixture on Al block at 10K;¹⁶⁰ ice grains of H₂O, CH₃OH, and NH₃;¹⁶¹ led to the formation of a mixture of chemicals, including a minor fraction of glycerol (up to 5% yield).

This seems to be in contrast with the formation of long-chain fatty acids that are suggested to form in hydrothermal conditions during the Fisher-Tropsch reaction at elevated temperatures.⁷⁹ For example, a mixture of *n*-alkanols, *n*-alkanoic acids, *n*-alkenes, *n*-alkanes and *n*-alkanones (C₂ to C₃₅) was obtained from formic or oxalic acid after heating at 175 °C for 2-3 days.¹⁶² The formation of long-chain fatty acids was demonstrated by the thermal decomposition of iron oxalate (FeC₂O₄·2H₂O) at 400°C.¹⁶³ Similar experiments with a solution of oxalic acid carried out at 150–250 °C for two days, resulted in the formation of C₁₂-C₃₃ lipids (*n*-alkanols, *n*-alkanoic acids, *n*-alkyl formates, *n*-alkanals, *n*-alkanones, *n*-alkanes, and *n*-alkenes).¹⁶⁴

UV-irradiation is also a good way to obtain *n*-decanoic and *n*-hexadecanoic alcohols from corresponding *n*-alkanes (*n*-RH) with 1-naphthol.¹⁶⁵ Some quantities of monocarboxylic acids were produced in classical Miller-Urey experiments induced by spark discharge (C₂-C₇)¹⁶⁶ and semi-corona discharge (C₂-C₁₂)¹⁶⁷ from simple molecules such as methane, ammonia, hydrogen and water. Another possibility for long-chain fatty acids formation is a Fisher-Tropsch-type reaction on carbonaceous chondrites. It was explored in experiments promoted by meteoritic iron, iron ore and nickel-iron alloy.¹⁶⁸ As an example, fatty acids were

produced along with alkanes, alkenes (C₁-C₂₅), aromatic hydrocarbons and others after heating deuterium with carbon monoxide at 200-370 °C for 6-480 hours

The further step is acylation, which brings together fatty acids and glycerol. This is a dehydration-type chemical reaction that takes water away, again. One way to accomplish it is by using a “condensing” agent, i.e., a molecule that will help to take H₂O away. One example is cyanamide which was studied by Oró and colleagues.¹⁶⁹ The presence of cyanamide helps to produce acylglycerols from mono-, di-, and tri-palmitoyl glycerol derivatives at 60–100 °C. Rushdi & Simoneit¹⁶⁴ demonstrated lipids formation, as discussed before, and continued work on lipids acylation in hydrothermal conditions.¹⁷⁰ Mono- and diacylglycerols were obtained after heating n-heptanoic acid with glycerol at 100 to 250 °C. In similar conditions, alkanolic acids (C₇- C₁₆) and glycerol in aqueous media produced mono-, di- and triacylglycerols.¹⁷¹ Lipids formation is also favourable in the presence of silicic acid and kaolin solution from glycerol and C₁₂ fatty acids after incubation for several days at 65 °C (≈ 3 %).¹⁷²

Other interesting precursors in terms of membranogenic compounds are dodecanol-1 or geraniol. The formation of dodecanol-1 as one of the long-chain alcohol molecules could be possible in accordance with other methods for lipid precursors synthesis described above.

Membranes of Archaea, which are among the oldest microorganisms, are formed of terpenoids such as geraniol, which make them more resistant to temperature. It is possible that primitive or proto-cells also had such a molecule in their membrane, for which geraniol could be a potential prebiotic precursor.^{173,174} One approach is to synthesise geraniol by C₅ monoprenol condensation in the presence of montmorillonite K-10 at room temperature after 9 days.¹⁷⁴ Other pathways to produce similar molecules, such as squalene¹⁷⁵ from farnesol in the presence of a redox system H₂S/FeS or as polyprenols¹⁷⁶ from five-carbon homologation of regular prenyl halides are assisted by two regio- and stereospecific routes to compounds of the polyprenol (dolichol) series. The information regarding this area of research is very limited. One of the few published suggestions is by Ritson & Sutherland,²⁶¹ who used a prebiotic pathway leading to a monoprenol or even the isoprenoid (terpenoid) carbon skeleton.

Although lipid formation is central to the origin of cellular life, there are only a limited number of dedicated research papers, mostly focusing on nucleoside formation and phosphorylation. Thus, my work focused on lipid synthesis is an important accomplishment for the origin of life research.

3.1.3. Synthesis of pyruvic acid

Another key prebiotic molecule is pyruvic acid, which is used for phosphorylation reactions aside from RNA (DNA) and membranogenic precursors. Pyruvic acid is an important molecule for lipid synthesis through acetyl-CoA and is an oxidant in amino acids production. Moreover, pyruvic acid is a precursor to phosphoenol-pyruvate (PEP), an intermediate in biochemistry with a high-energy phosphate group. It is involved in the glycolysis and gluconeogenesis processes.^{2,177,178}

There are several methods proposed for the prebiotic synthesis of pyruvic acid. One of them is based on the reduction of CO₂ to acetate and pyruvate in water with the participation of transition metals (Fe⁰, Ni⁰, Co⁰).¹⁷⁹ The CO₂ gas is under pressure 1-40 bar and heated to 30-100 °C over hours to days to achieve the production of acetate and pyruvate as important precursors to acetyl-CoA. Recently, a similar approach was used for the synthesis of formate, acetate, and pyruvate under mild hydrothermal conditions from CO₂ and water in the presence of Ni-Fe nanoparticles.¹⁸⁰ In another work, pyruvic acid was obtained from hydantoin with good yields (>20%).¹⁷⁸ The amount of the product depends on the pH of the solution (7-14), buffer (bicarbonate and phosphate), temperature (60-80 °C) and concentration of the starting molecule. The maximum yield of pyruvic acid was achieved at neutral pH after 96 hours at 80 °C. Pyruvic acid was also detected as one of the products of sugar formation from formaldehyde and glycolaldehyde based on ammonia and amines (including amino acids) at pH 5.5 and 50 °C.¹⁸¹

Another way is the oxidation of lactate into pyruvate via photooxidation in the presence of ZnS;¹⁸² or under the redox-system FeS/S/FeS(2) at a temperature of about 113 °C.¹⁸³ Small amounts of pyruvic acid (below 1%) were obtained in simulated hydrothermal vent conditions (50–200 MPa, 250 °C).¹⁸⁴ It was synthesised from FeS, alkyl(nonyl) thiols and formamide through the formation of methyl thiol as an intermediate. Alternatively, pyruvic acid could be formed in interstellar conditions on carbonaceous meteorites at low temperature.¹⁸⁵

The multiple approaches and methods of synthesis of prebiotic precursors are a nourishing ground for the advancement of science. However, in order to correlate all the data and place it in a common reaction network, a system approach is mandatory. A great example is the study of Sutherland and colleagues¹⁵³, who demonstrated the synthesis of most of the molecules listed above in a single reaction network. Starting from the simplest molecules of hydrogen cyanide, ammonia and others, the authors achieved the production of nucleotides, amino acids, membrane precursors, etc. Indeed, in nature, there is no synthesis of particular molecules for each reaction steps, but all the available inventory in a certain environment is used.

Summarising the section, I conclude that the organic precursors needed as building blocks for life could have been available for further phosphorylation on the early Earth. Diverse approaches confirm the possible presence of prebiotic alcohols such as nucleosides, fatty acids and others in various environments, such as emerged lands or shallow water reservoirs, hydrothermal vents and even astrochemical reactions on meteorites or comets. What remains indeed a challenge is the estimation of the amounts of available organic material in each environment. There is no final answer yet, but all the data should be taken into consideration when placing the phosphorylation process in the bigger picture of an origin of life study.

In the context of this work, it is clear that phosphorus plays an essential role in the formation of RNA, DNA, membranogenic compounds and other precursors. Additionally, the presence of phosphorus minerals promotes the formation of many complex molecules and participates in phosphorylation reactions. This field is fast-developing and raises a lot of interest in the scientific community.

3.2. Natural sources of phosphorus on the early Earth and prebiotically plausible phosphorus-containing minerals

In this section, I review the origin of phosphorus and phosphorus-containing minerals on the early Earth. The Hadean Earth was a completely different place than it is now, which provides particular conditions for the plausibility of P-containing minerals. In the introduction and in section 2, I mentioned the importance of intense impact bombardment and volcanic activity, different plate tectonics, an anoxic atmosphere that favoured the presence of Fe^{2+} rather than Fe^{3+} , and other factors affecting mineral formation. There are two principal sources: the delivery by impact meteorites and the crystallisation from magmatic processes within the Earth.

Several forms of phosphorus could have been present on the Hadean Earth (**Figure 6**), such as phosphides (P^{-2}), orthophosphate (PO_4^{3-}), pyrophosphate ($\text{P}_2\text{O}_7^{4-}$), polyphosphate (condensed phosphates), thiophosphates (HPSO_3^{2-}) and phosphites (HPO_3^{2-}). Most of them have very limited solubility and are rather unreactive in standard conditions. Therefore, difficulties arise not only in predicting the plausibility of certain minerals but also in how to make them reactive in chemical synthesis as well as in estimating their available quantities.^{5,6} In this section, I review prebiotically plausible P-containing minerals, their possible occurrence on Earth, and potential ways for their involvement in prebiotic reactions.

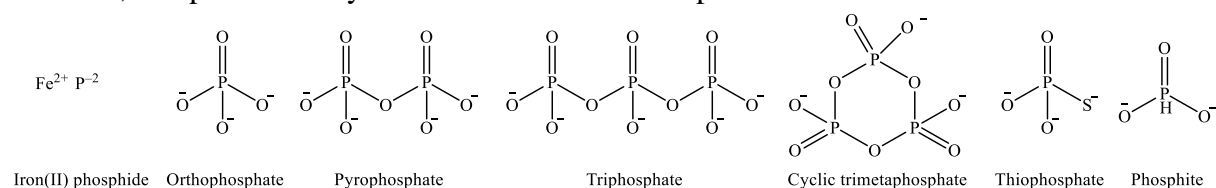


Figure 6. Variety of inorganic P-bearing molecules on the early Earth

Any P atom in the Universe was created inside the stars and, after its explosion, became part of protoplanetary disk formation. Cooling down over time, along with other processes, it condensed to form $(\text{Fe},\text{Ni})_3\text{P}$ (schreibersite), that is the main interstellar source of phosphorus in meteorites.^{186,187,188} Aside from metal phosphide, phosphate minerals are rare inclusions in meteorites and several species have been described in the literature., Chlorapatite $[\text{Ca}_5(\text{PO}_4)_3\text{Cl}]$ and whitlockite $[\text{Ca}_9\text{Mg}(\text{PO}_4)_6(\text{PO}_3\text{OH})]$ were found in chondrite and achondrite;¹⁸⁹ beusite $[(\text{Mn}^{2+}\text{Fe}^{2+}_2(\text{PO}_4)_2)]$, galileiite $[\text{NaFe}^{2+}_4(\text{PO}_4)_3]$, grafftonite $[(\text{Fe}^{2+},\text{Mn}^{2+},\text{Ca})_3(\text{PO}_4)_2]$, were detected in iron meteorites (**Figure 7**).¹⁹⁰

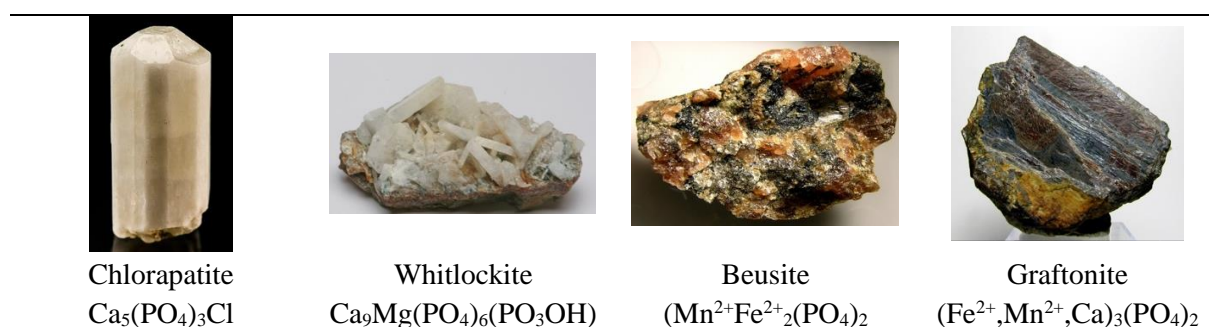


Figure 7. Pictures of modern phosphate minerals similar to inclusions in meteorites (from mindat.org)

After the Earth's accretion, meteorites were eventually still falling down on the surface. It could contribute important amounts of phosphorus-containing materials.⁹ Taking into consideration the geological timescale of millions to hundreds of millions of years, even slow processes such as corrosion or weathering could have contributed to the availability of inorganic phosphates. The reducing conditions of the early Earth, being affected by temperature, atmosphere, water, and the presence of organics (ethanol, acetic acid), could possibly help transform meteorite material into other P-forms and possibly make it accessible for involvement in prebiotic reactions.

For instance, Pasek & Lauretta suggested a pathway for involving schreibersite in interactions with organic molecules.¹⁰ As a result of experiments on iron/nickel phosphide corrosion, they produced a mixture of mixed-valence P-containing ions, including phosphate and phosphite. These represent the most abundant forms of P in minerals. In another series of experiments, successful phosphorylation of adenosine and uridine was achieved in aqueous conditions at 80 °C directly by analogues of schreibersite.¹⁹¹ The same team suggested that reduced P-minerals and, in particular, phosphites could play an important role in prebiotic chemistry.^{192,193} Those relatively more soluble and reactive species could be part of the early Earth's bioprocesses.

P is the 11th most abundant element on Earth, with a concentration of 0.07 wt% or 1 ppm, in the bulk Earth, with most of the phosphorus stored in the Earth core. A comprehensive list of prebiotically plausible minerals from the Hadean aeon has been published by Hazen.¹⁹⁴ Due to immature plate tectonics and the absence of stable continents 4 billion years ago, the diversity of phosphorus-bearing minerals was a lot smaller than in modern times and the concentration in the ocean was very low.^{58,194} In the Earth's crust, P is mostly located in the hardly soluble apatite [$\text{Ca}_5(\text{PO}_4)_3(\text{OH},\text{Cl},\text{F})$], whose alteration controls the concentration of P in the modern ocean.^{6,195} There are several alternative approaches to addressing this issue, such as using high temperatures, changing pH and, most importantly in the given context, the involvement of organic molecules.

Generally, phosphate minerals are most soluble at high and low pH. In iron-rich contexts, the solubility of iron-phosphates increases significantly at lower pH; however, it is buffered at higher pH by the solubility of iron oxides (depending on redox conditions).¹⁹⁶ It is the opposite for calcium phosphates, which are more soluble at higher pH. For example, an increase of pH in carbonate-rich lakes limits the precipitation of phosphates, which may help phosphorylation.¹⁹⁷ Thus, the most favourable conditions for phosphate mineral solubilisation are below pH 3 and above pH 9.¹⁹⁶

It is possible to transform apatite, in the presence of highly concentrated small organic molecules such as urea or formamide, into other minerals that are more reactive and prebiotically relevant.^{198,199} Menor-Salván and colleagues suggested that due to the steady evaporation-condensation cycles of water, urea or cyanide could be accumulated over time in small lakes. They observed that struvite ($\text{MgNH}_4\text{PO}_4 \cdot 6\text{H}_2\text{O}$), newberyite ($\text{MgHPO}_4 \cdot 3\text{H}_2\text{O}$), and brushite ($\text{CaHPO}_4 \cdot 2\text{H}_2\text{O}$) could form from hydroxyapatites in urea-rich environments that contain Mg^{2+} and Ca^{2+} in early Earth conditions. In similar conditions under anoxia and in the

presence of Fe^{2+} , vivianite $[\text{Fe}^{2+}_3(\text{PO}_4)_2 \cdot 8\text{H}_2\text{O}]$ could form.²⁰⁰ Other phosphate minerals such as biphosphammite $[\text{NH}_4(\text{H}_2\text{PO}_4)]$, archerite $[(\text{K},\text{NH}_4)(\text{H}_2\text{PO}_4)]$, gengenbachite $[\text{KFe}^{3+}_3(\text{PO}_3\text{OH})_4[\text{PO}_2(\text{OH})_2]_2 \cdot 6\text{H}_2\text{O}]$ and others could likely be formed in various prebiotic environments (**Figure 8**).^{8,58}

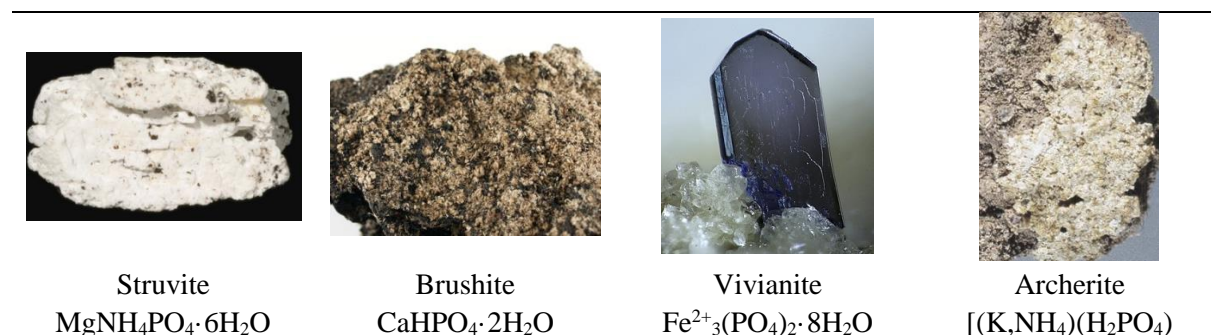


Figure 8. Images of modern minerals analogous to potential prebiotic minerals of the early Earth (from mindat.org)

Inorganic phosphate was most likely a component of the acidic Hadean ocean. There are variable estimates about its concentration depending on the pH and the composition of the ocean, from sub-micromolar to mM based on early Archean data.^{5,7,201,202} One of the plausible sources of phosphorus on the early Earth could be hydrothermal vents, with concentrations on the order of a few micromolars. The mineral surfaces of chimney chambers may perhaps represent a potentially good starting point for proto-organisms due to the constant flux of energy and nutrients. Through water-rock chemistry, phosphate could be released from apatite in the presence of iron sulphide structures in hot springs.^{203,204,205} Along with it, hydrothermal vents may also be a potential source of pyrophosphates and polyphosphates.^{206,207}

Condensed phosphates such as pyrophosphate ($\text{P}_2\text{O}_7^{4-}$), triphosphate ($\text{P}_3\text{O}_{10}^{5-}$) or polyphosphates have high prebiotic relevance. Polyphosphates in general are more soluble and, in the case of cyclic phosphates, more reactive compared to apatite. They could be formed by dehydration at high temperatures as a result of volcanic activity.^{208,209} Dry heating of orthophosphates at elevated temperatures leads to the formation of 5-50 % pyro- and triphosphates, depending on the starting molecule.²¹⁰ An example of a pyrophosphate mineral is canaphite $[\text{Na}_2\text{Ca}(\text{P}_2\text{O}_7) \cdot 4\text{H}_2\text{O}]$.⁵⁸

Some of the prebiotic molecules, such as urea or cyanamide, can actually facilitate the condensation of phosphates in water.²¹¹ In the presence of Ca^{2+} or Mg^{2+} ions, the production of pyro- and condensed phosphates from orthophosphate is stimulated at mild temperatures (37-80°C).²¹² At room temperature, pyrophosphates can also be formed from hydroxyapatite in the presence of cyanate.^{213,214} The authors suggested a possible reaction mechanism through the formation of carbamoyl phosphate as an intermediate of the reaction (**Figure 9**).

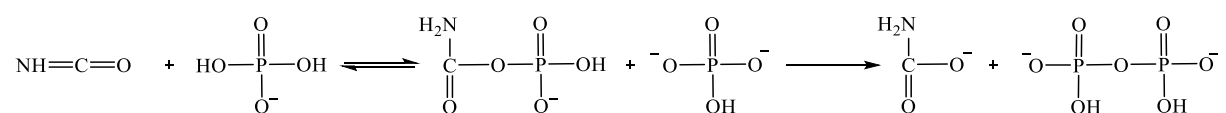


Figure 9. Pyrophosphate synthesis, as suggested by Miller & Parris²¹³

Other potential condensing agents for pyrophosphates are thioesters. Weber demonstrated the synthesis of condensed phosphates (2.5% to 11.4%, depending on pH) at ambient temperature from hydroxyapatite in water.²¹⁵ In another series of experiments, 7 % of pyro- and triphosphates were obtained in dry conditions after heating at 50 °C for 6 days with thioesters (or N, S-diacetylcysteamine).²¹⁶

Pasek et al. suggested another route to condensed phosphates.²¹⁷ They explored the possibility of obtaining pyro-, tri- and cyclic phosphates by oxidation reactions of HPO_3^{2-} and H_2PO_2^- . Cyclic trimetaphosphate ($\text{P}_3\text{O}_9^{3-}$), which is a synthetic compound widely used in prebiotic chemistry, though remains a highly debatable phosphorous source. It does not correspond to any known modern minerals; however, it is assumed to be available in the early Earth conditions. Even though the results seemed promising with 34 % yields of condensed products, the authors mentioned that the studied conditions (mimicking prebiotic oxidation by the Fenton reactor at room temperature) related more to plausible early Precambrian (3.0 billion years ago) than late Hadean conditions.

In summary, pyrophosphates might be available for the phosphorylation of other molecules such as nucleotides (ADP, ATP) and also to store or provide energy for primitive metabolisms. However, it remains a highly debated subject due to the specific conditions for their formation. Condensed phosphates are currently relatively rare in nature, and due to their high chemical activity, they could be unstable in the harsh conditions of the early Earth. Additionally, it is assumed that the Hadean atmosphere was mostly anoxic, which would have also made it difficult for these molecules to form.

Another potentially interesting group of P-bearing minerals in prebiotic chemistry is thiophosphate. Thiophosphate is known as the only alternative to the phosphate group in the DNA of certain bacterial species.²¹⁸ The formation of thiophosphates can happen during the corrosion of P-bearing minerals in the presence of H_2S as a result of volcanic activity.^{219,220} Ritson et al. suggested a mechanism for the photochemical synthesis of orthophosphate, including thiophosphate formation (**Figure 10**).²²¹

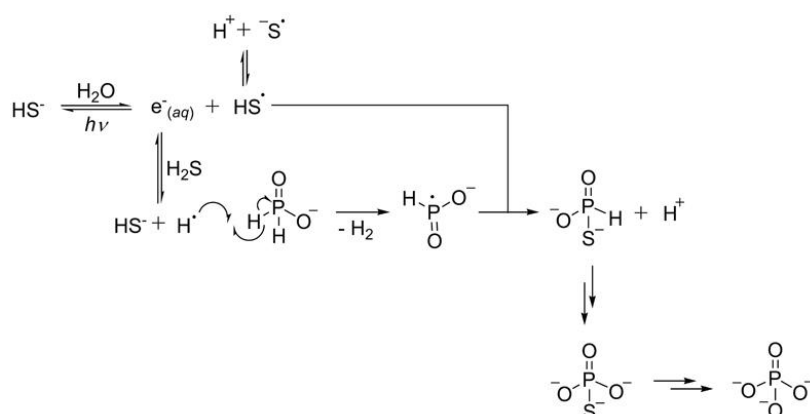


Figure 10. Thiophosphate synthesis, as suggested by Ritson et al.²²¹

Also, sulphides are known as a part of the (Fe,Ni)P inclusions in the meteorites, which could also contribute to the formation of thiophosphates.²²² Alternatively, it could be formed

from P-containing minerals affected by FeS in hydrothermal vents' environments.¹⁸³ Thiophosphate has a strong chemical advantage over orthophosphate in the phosphorylation reaction, as H₂S can play a role in leaving a group that induces phosphorylation at lower temperatures.

A recent review from Walton et al.²²³ reconsiders the amount and availability of phosphorus on the early Earth. In general, phosphorus is assumed to be one of the limiting factors in prebiotic chemistry due to its low solubility and other challenges mentioned above. The authors described models of extraterrestrial P flux, cumulative P mineral diversity, apatite weathering rate, total possible P recycling, average ocean P concentration and the presence of atmospheric oxygen from 4.5 billion years ago to modern time. Taking into consideration all the listed factors, they concluded that subaerial closed-system basins or microscale environments could have achieved concentrations of inorganic phosphates as high as a few 100 mM. Those concentrations are assumed to be sufficient for the rise of Org-P sinks and to drive a range of prebiotic chemical pathways.

It is challenging to definitively assess the minerals that were present on the Hadean Earth. However, by gathering data from numerous sources, we can summarise that substantial amounts of phosphorus have probably been present at the time. Contributed by various sources, from extraterrestrial impact to volcanic and hydrothermal activity, phosphorus-bearing minerals should have been available. A number of approaches exist to their involvement in organic synthesis, such as heating, corrosion, weathering, reacting with soluble organic chemical agents, and, in general, their interaction with all of the above over long periods of time. Thus, we come to the following section on the actual prebiotically plausible phosphorylation reactions on the early Earth.

4. Modern approaches for abiotic synthesis of phosphorylated prebiotic precursors

As discussed in previous sections, phosphorylation reactions are one of the keys to the origin of life. All the organic molecules reviewed here as life's building blocks (sugars, nucleosides, glycerol, lipids, pyruvic acid) can be considered alcohols due to the presence of an OH-group in the molecule structure. Following this way of thinking, the P-bearing minerals can be considered complex phosphorus oxides. Thus, we formulate the main subject of the next section as a prebiotically plausible reaction of alcohol phosphorylation.

Approaches for the synthesis of the main organic precursors for phosphorylation reactions and sources of phosphorus have been discussed in previous sections. Hereafter, I review the existing methods of phosphorylation of these molecules under possible prebiotic conditions. This process has several fundamental challenges and some possible answers to them.

- Under what conditions could phosphorylation reactions occur? There are two main directions: evaporitic and hydrothermal environments. The contributions of each do not exclude and, perhaps, complement each other.
- Did the reactions take place in water or in another medium, which might actually be more favourable for the phosphorylation of alcohols?
- What is the source of the chemical energy mandatory for phosphorylation? Phosphorylation is an energy-intensive reaction, and it is not clear how this energy could have been provided on the early Earth. Possible sources could be temperature, UV radiation, chemical agents, or prebiotic minerals.
- How were stereo- and regioselectivity achieved? This question is especially relevant for polyols. For example, the phosphorylation of nucleosides in nature is at the 5' and 3' positions, and not 2'. Another point is that synthesis often results in a complex reaction mixture with many different by-products that may compete with the main objective of the synthesis.
- What is the potential contribution of the proposed reaction in terms of subsequent oligomerisation and polymerisation? The next step after phosphorylation is the spontaneous self-organisation of the products into complex biomolecules such as vesicles or polynucleotide chains.

Answering these questions at the end of the present bibliographic review will help to formulate the objectives and expected results of this thesis.

4.1. Role of urea as a condensing agent under prebiotic conditions

Taking into consideration the data suggested in state of the arts section 2, we can place phosphorylation reactions in the context of prebiotic environments on the early Earth. There are some factors that are favourable for phosphorylation and, more generally, for prebiotic

chemistry on the Earth's surface. First, the water cycles create a dynamic condition on the Earth's surface, changing landscapes and transferring resources. The main idea is that the limited presence of water in the evaporitic environments or coastal regions of the early Earth could help the dehydration reaction and avoid the chemical inventories being diluted, which provides the availability of abundant molecules of prebiotic precursors. Diverse energy sources and varied mineral surfaces could have helped prebiotic reactions. A reducing atmosphere would have been more favourable for the formation of organic molecules. The advantage and, at the same time, disadvantage of intense UV radiation, is that it can help start some syntheses while damaging biomolecules.

Since life is impossible without water and it is also a universal solvent for many biological reactions, it is assumed that prebiotic reactions had to happen in water.^{11,213} However, looking at the principal reaction of alcohol's phosphorylation (**Figure 11**), we instantly see thermodynamic constraints. In the presence of water, hydrolysis is preferred to the formation of phosphoesters. Thus, it was suggested that hot, dry and/or evaporative conditions are more favourable for phosphorylation.

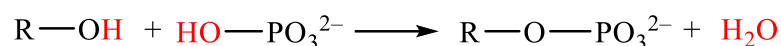


Figure 11. Principle scheme of alcohol's phosphorylation

There are several pathways to overcome the water problem. One of them is the assistance of a "condensing" agent. If those molecules are co-localised with alcohol and phosphate sources, it provides a thermodynamic driving force for the phosphorylation reaction by irreversibly eliminating water, thus acting as an efficient condensing agent. Earlier, I reviewed the involvement of those agents in the section 3.1 for lipid and nucleotide formation and in section 3.2 for minerals such as struvite. The molecules known as good condensing agents are cyanate, cyanamide, urea and formamide (**Figure 12**).

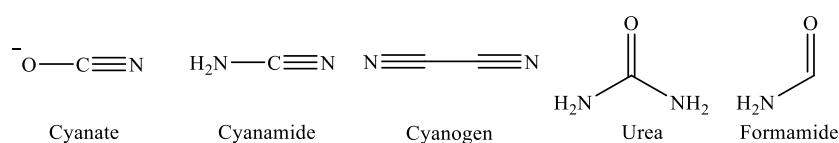


Figure 12. Molecular structures of potential prebiotic condensing agents

Condensing agents have value not only in phosphorylation but also in many other prebiotic syntheses, an example of a comprehensive summary for cyanamide was suggested by Fiore and Strazewski (**Figure 13**).²²⁴

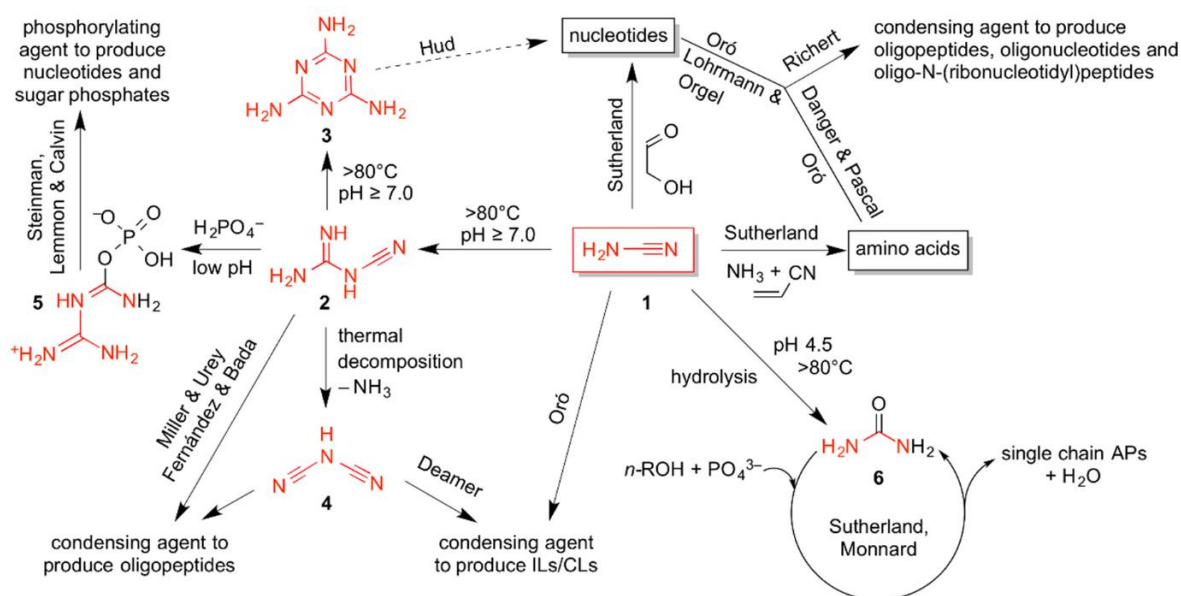


Figure 13. Representation of chemical transformations of cyanamide (from Fiore and Strazewski)²²⁴

Adding a condensing agent is sufficient when the energy of the molecule's hydrolysis matches the energy requirement for phosphorylation. Pasek demonstrated an example of urea-assisted phosphorylation of a nucleoside, where urea hydrolysis (-14.8 kJ/mol) is close to nucleoside phosphorylation ($+14.2$ kJ/mol).¹⁹⁶ Therefore, the overcoming of the thermodynamic barrier is possible by producing reaction intermediates between the condensing agent and other reactants. Thus, effective phosphorylation can be achieved in prebiotic environments.

4.1.1. Phosphorylation of nucleosides

4.1.1.1. Phosphorylation in the absence of a condensing agent

The very first experiments on nucleoside phosphorylation were attempted by Ponnamperna et al.²²⁵ Several water solutions of nucleobases with sugars, nucleotides and adenosine mono- and diphosphates with phosphoric acid (or ethyl metaphosphate) were UV-irradiated. After one hour, minor amounts of related phosphorylated products ($< 3\%$) were identified by paper chromatography. Although phosphoric acid was not in particular a plausible prebiotic molecule, this work was one of the first steps in understanding phosphorylation reactions.

The same team performed a similar experiment in dry conditions (absence of water), treating lyophilised mixture of various nucleosides with dihydrogen orthophosphate. Depending on temperature and heating time, they obtained mixtures of 2'-, 3'- and 5'-mono-phosphates with a minority of 2'3'-cyclic phosphate and dinucleotides.²²⁶ Yields obtained for

monophosphates reached 3-20 %, depending on the conditions (**Figure 14**). The highest yield was achieved for uridine phosphorylation after two hours at 80 °C.

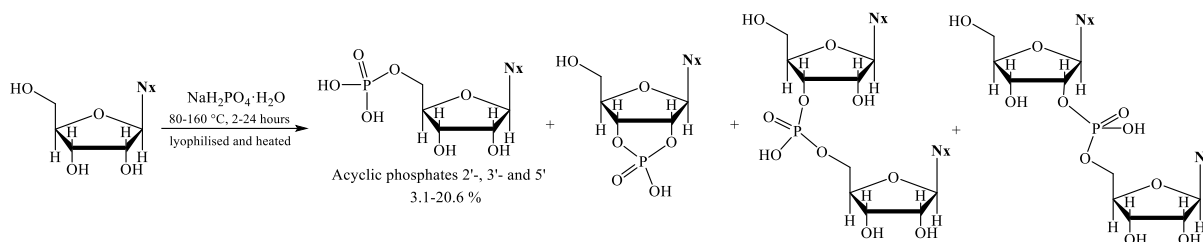


Figure 14. Reaction of nucleoside phosphorylation (adapted from Ponnampereuma et al).²²⁶

Beck et al.²²⁷ obtained nucleotides in a series of long-term dry-state experiments at moderate temperatures. They heated uridine and inorganic phosphate salts at 65-85 °C for 6-9 months. As a result, they obtained UMP (11.3 %) with small quantities of UDP (3.3 %) in the experiments with $\text{Ca}(\text{H}_2\text{PO}_4)_2$. Other tested salts Na_2HPO_4 , KH_2PO_4 , CaHPO_4 , $(\text{NH}_4)_2\text{HPO}_4$ and $\text{Mg}(\text{NH}_4)\text{PO}_4$ generated negative outcomes.

These studies performed in dry conditions in the absence of a condensing agent produced relatively small amounts of phosphorylated products (nucleotides) and are insufficient for further polymerisation even over a long time.

Gibard et al. tested the phosphorylation of nucleosides and corresponding monophosphates in both dry and wet-evaporative conditions (water initially is present in the reaction mixture but evaporates eventually during heating).²²⁸ Diamidophosphate was used as a phosphate source and also played the role of a condensing agent. The authors succeeded in achieving not only phosphorylation of cyclic and acyclic mon-, di-, and tri-phosphates but also oligomerisation. Very high conversion of starting molecules into phosphorylated products was achieved (up to 90 %) at mild temperatures $\text{rt}-45$ °C. This makes diamidophosphate an interesting potential phosphate source, especially in terms of further polymerisation of nucleotides in water. The latter authors suggest that diamidophosphate could be formed prebiotically from condensed phosphates and facilitate intramolecular phosphorylation by nucleophilic attack of the NH_2 -group in the absence of an additional condensing agent (**Figure 15**).²²⁹

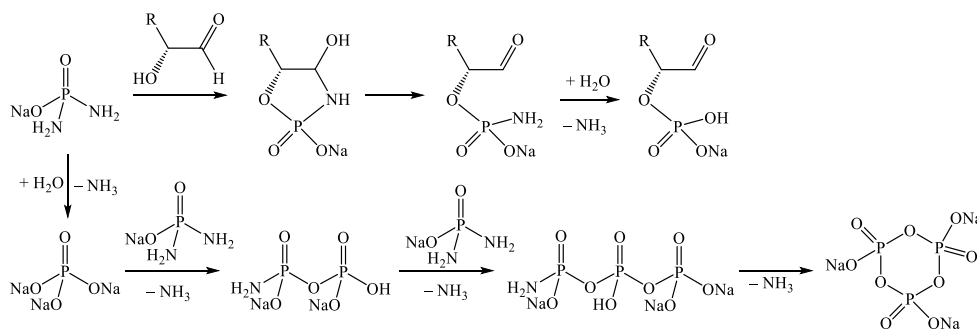


Figure 15. Formation of DAP from cTMP and phosphorylation of sugars by DAP, as adapted from Krishnamurthy and colleagues^{228,229}

Even though diamidophosphate seems to be an effective phosphorylation agent, it would take a lot of volatile ammonia to develop in a prebiotic environment, which is unlikely in the late Hadean. There is still no clear approach for the synthesis of DAP on the early Earth, even though it was detected in the interstellar medium.²³⁰

Another way to overcome the water and phosphate problem is by involving condensed (cyclic) or polyphosphates in the phosphorylation reactions. For example, cyclic trimetaphosphate (cTMP) has the capacity to initiate a phosphorylation reaction by ring-opening energy release. Thus, it plays the role of both a phosphorus source and a condensing agent at the same time.

Therefore, adenosine was mixed with polyphosphate ($\text{Na}_4\text{P}_2\text{PO}_7$, $\text{Na}_5\text{P}_3\text{O}_9$, $[\text{NaPO}_3]_6$) and dissolved in water under heating.²³¹ After 4-6 hours, the main products, AMP, ADP and ATP, were identified by thin-layer chromatography. Both reactions of triphosphate and hexametaphosphate gave yields 54-57 (AMP), 17-18 (ADP) and 26-28 % (ATP). Pyrophosphate gave a negative result. The authors showed that low pH and a long reaction duration are more favourable for the product's formation, meaning that there is a kinetic aspect to be considered in such a reaction. However, it was not studied in detail.

An interesting experiment on the phosphorylation of adenosine and deoxyadenosine was carried out by Schwartz.²³² A solution of nucleoside in NaOH was mixed with cyclic trimetaphosphate (cTMP) and heated for 4-5 hours. After the synthesis, 31 % of the total yield was obtained for adenosine-monophosphates and only 3 % for deoxyadenosine-monophosphate. Another intriguing finding is adenosine's preference for 2'- and 3'-phosphates during phosphorylation. The author suggested that it was directly connected to a specific interaction of cTMP ion with the cis-vicinal configuration of the nucleoside. It was also shown that the presence of Mg^{2+} ions in the solution of adenosine and cTMP is favourable for the production of 2',3'-cyclic nucleoside phosphates, leading to the following reaction mechanism (**Figure 16**).²³³ The role of magnesium ions is to accelerate the reaction by approximately a hundred times, probably due to the formation of a Mg^{2+} chelating complex of 2,3-diol group and phosphate salt that helps phosphorylation.

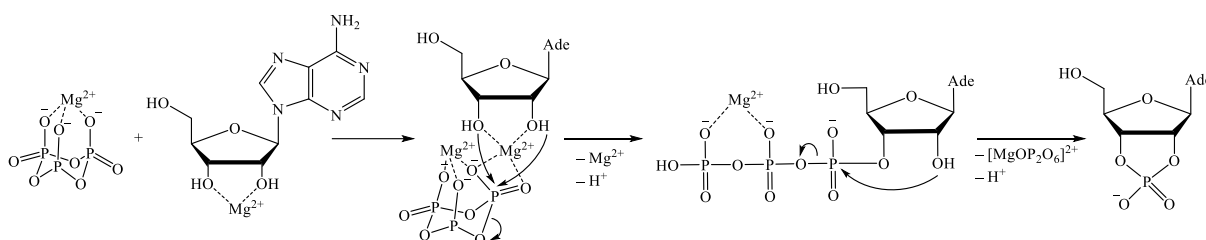


Figure 16. Phosphorylation reaction of adenosine in the presence of trimetaphosphate and Mg^{2+} ions, suggested by Yamagata et al.²³³

Another example is the production of sugar phosphates and ribonucleosides in aqueous microdroplets. Such an environment might have existed on the early Earth as part of clouds and aerosols in the atmosphere or as a result of breaking ocean waves. Nam et al.²³⁴ used electro-spray ionisation on a water solution of sugar (D-ribose, L-ribose, D-glucose, D-galactose, or D-

fructose) and 5 mM H₃PO₄. They obtained a phosphorylation yield of 6-13 % depending on the starting molecule (sugar-1-phosphates being the majority*). In the case of the ionisation of a mixture containing D-ribose, phosphoric acid, and uracil, they observed the presence of uridine, although it was not detected in the absence of phosphoric acid. This pathway suggests a prebiotic way of phosphorylating sugars, directly creating nucleosides from ribose and a pyrimidine nucleobase at room temperature and atmospheric pressure. Using the same approach and nano-ESI (electro-spray ionisation), Hu et al.²³⁵ achieved stereoselective phosphorylation of ribose and ribonucleosides towards the 5'-position. The reaction was promoted by the formation of an anionic complex between ribose and Na₂H₂P₂O₇ induced by nano-ESI.

Even though phosphorylation of nucleosides demonstrated the presence of cyclic and acyclic phosphorylation products, it still had a relatively low yield in the presence of orthophosphate, or involved prebiotically debatable phosphate sources (cTMP or DAP), or appeared in very local and particular reaction conditions, such as aqueous microdroplets.

4.1.1.2. *Cyanamide, cyanate and cyanogen or their derivatives as a condensing agent*

The previous section outlined relatively efficient methods for the phosphorylation of nucleosides and sugars in the absence of additional organic activators. Their presence decreases the activation energy of phosphorylation and increases the yield of the reaction. Among the best-known condensing agents is cyanamide and the variety of its precursors and derivatives. Many papers describe the origin of cyanamide on Earth, for example, by UV irradiation of cyanide solutions or electron irradiation of CH₄, NH₃ and H₂O mixtures.²³⁶

Steinman et al.²³⁷ tested cyanamide and orthophosphoric acid (NH₂CN:H₃PO₄ 6:1) with adenosine dissolved in water. They detected the formation of adenosine-5'-phosphate after 4.5 hours at room temperature. The authors state that the reaction occurred slowly at pH 2 and did not happen at all at pH 7. They suggest amidinium phosphate is responsible for the dehydration reaction as an additional intermediate between cyanoguanidine (“dicyandiamide” a dimer of cyanamide) and phosphoric acid (**Figure 17**).

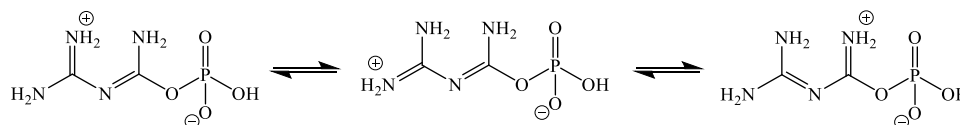


Figure 17. Principal resonance forms of amidinium phosphate, as suggested by Steinman et al.²³⁷

* Comment of Peter Strazewski, 20/08/2023, from a private communication: “The authors repeatedly presume that the phosphate group is attached uniquely to the 1-position of any sugar they tested. This cannot be correct due to the fact that the 1-position applies only to aldoses, that is, sugars that are an aldehyde in their (very rare) ring-opened tautomeric form. The 1-position of fructose, for example, can never be phosphorylated that way, simply because only the anomeric centre of an ose sugar can be phosphorylated without chemical activation of phosphate (by urea, for example). The anomeric centre of fructose, being a ketose, is the 2-position, so the correct product structure is that of D-fructose-2-phosphate, as rightly shown in Figure S4D (SI), giving rise to fragment 2 in the corresponding CID MS. This proves the authors are mistaken when writing about D-fructose-1-phosphate and drawing it in Figure S1D.”

Another series of experiments in aqueous solutions were performed by Lohrmann & Orgel¹¹ on U and T. They tested condensing agents (cyanogen, cyanofornamide, cyanate, cyanamide and others) in reaction with inorganic phosphate. The solutions were heated for hours and resulted in cyclic and acyclic monophosphates, with yields depending on pH, temperature and duration. One of the most valuable results is the synthesis of 5-membered ring uridine-2',3-cyclic phosphate in reaction with cyanogen, with a 94 % yield (**Figure 18**). The take-home message from this paper is that cyanogen and the products of its hydrolysis seem to be promising condensing agents in reactions of nucleoside phosphorylation.

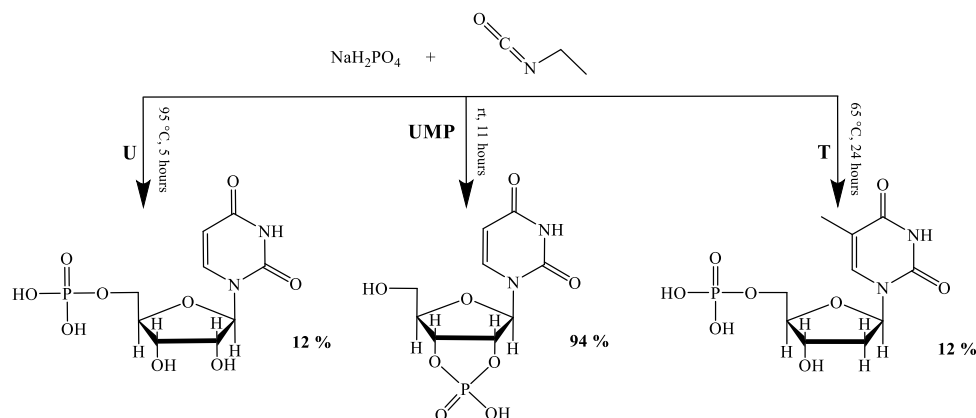


Figure 18. Reaction of phosphorylation (adapted from Lohrmann & Orgel).¹¹

The conversion of AMP to ADP and ATP was studied by Yamagata²³⁸ in the presence of cyanate in an aqueous solution of calcium phosphate. Previously, in section 3.2, we already discussed a plausible pathway for hydroxyapatite condensation into pyrophosphates in similar conditions.^{213,214} $\text{CaCl}_2 \cdot 2\text{H}_2\text{O}$ powder (or other calcium phosphate salt) was added to a solution of AMP (ADP), KH_2PO_4 with NaOCN excess. The solution was shaken and left incubating at room temperature for hours or days, with regular pH adjustments to 5. As a result, ADP and ATP were formed with yields of up to 25% and 20%, respectively. Calcium phosphate salts ($\text{Ca}_3(\text{PO}_4)_2$, $\text{CaHPO}_4 \cdot 2\text{H}_2\text{O}$ and $\text{Ca}(\text{H}_2\text{PO}_4)_2$) did not show significant improvement in yields, with only the first two relatively efficient towards ATP production. The authors also mentioned that the addition of Mg^{2+} to the solution significantly reduced the yield. As a reason, they suggest that the presence of Mg^{2+} pushes the equilibrium of the reaction towards the formation of insoluble apatites rather than helping their solubility.

Phosphorylation of ribose was studied by Halmann et al.²³⁹ They heated a solution of D-ribose, orthophosphate, and cyanamide (or cyanogen) at neutral pH at 65°C for 7 days and produced ribose phosphate. The yield of the main products depended on the reaction duration and concentration of the condensing agent, and did not exceed 27 % (**Figure 19**).

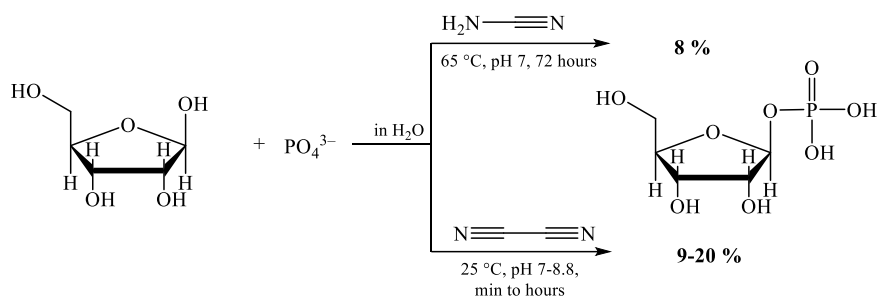


Figure 19. Reaction of phosphorylation, adapted from Halmann et al.²³⁹

Another way to overcome the water problem in the phosphorylation of nucleosides was suggested by Tsanakopoulou et al.²⁴⁰ The authors applied the idea of catalysts in activation chemistry in order to simulate conditions in which the production of cyclic nucleotides is faster than their hydrolysis. In the control experiment, cyanamide in an aqueous solution of adenosine-3'-phosphate yielded 1 % of cyclic adenosine-phosphate at rt. In the presence of metal ions (Mg^{2+} or Ca^{2+}) and an excess of glyoxylic acid at 40 °C, the yield increased up to 95 %. The authors suggested a mechanism with *O*-acylisourea as a key intermediate involved in phosphate activation (**Figure 20**). It was formed by the cyclisation of the carbonyl adduct of cyanamide and glyoxylate association. Thus, the authors propose an effective approach to cyclisation of AMP.

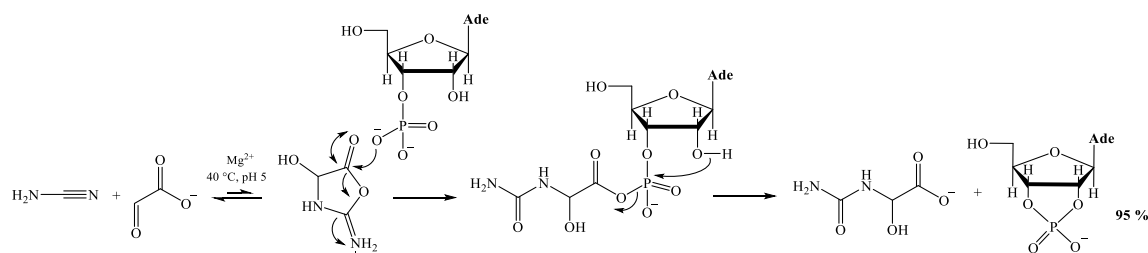


Figure 20. Reaction of phosphorylation, adapted from Tsanakopoulou et al.²⁴⁰

Thus, literature suggests that the presence of condensing agents enhances yields of phosphorylation reactions under relatively mild conditions. The condensing agent not only assists in the interaction of phosphate and alcohol, but in excess, it also promotes the formation of cyclic organic products of phosphorylation. Cyclic phosphates are potentially interesting compounds for the further oligomerisation of nucleotides. And their presence proves the effect of condensing agents on phosphorylation.

4.1.1.3. Urea as an effective prebiotic condensing agent

In water, cyanamide expectably produces urea, which is its first hydration derivative. Several publications confirm the plausibility of urea on the early Earth.^{241, 242, 243} It is assumed that such a molecule could be available in the prebiotic environments described above, such as dry land or evaporative lakes.

One of the first scientific teams to investigate urea as a condensing agent was Lohrmann and Orgel.²⁴⁴ Following the idea that urea facilitates condensation of ammonium phosphates at high temperatures, they tested it in reactions with aqueous solutions of nucleosides. A solution containing nucleosides, Na_2HPO_4 , NH_4HCO_3 and NH_4Cl in excess of urea was dried and heated at 100 °C for several hours. As a result, they produced the corresponding cyclic and acyclic nucleotides, their carbamylated forms, and small quantities of dinucleotides. The authors obtained relatively high yields. For example, in reaction with uridine, 24 % of UMP and 9 % of cyclic uridine-2',3'-phosphate were produced. The authors also mention that in similar conditions, in the absence of urea, phosphorylation was very limited. Later, the same team succeeded in phosphorylating thymidine, as a result of heating urea, NH_4Cl , thymidine and Na_2HPO_4 .²⁴⁵ They produced thymidine cyclic and acyclic phosphates with up to 45 % yield, depending on the ratio of starting products and reaction time. Thus, they described an effective, fast, and prebiotically plausible method of nucleoside phosphorylation in the presence of urea.

Another successful experiment of the conversion of 5'-monophosphate into di- and triphosphate nucleotides by reaction with struvite was reported.²⁴⁶ The authors demonstrated that the presence of Mg^{2+} in a solution of $(\text{NH}_4)_2\text{HPO}_4$, urea and nucleoside 5'-phosphates after heating at 65-100 °C produces organic and inorganic pyrophosphates. The yields increased at elevated temperatures and reached, on the example of UMP, 14.3 % uridine (results of hydrolysis), 47.8 % mix of 5'-, 3-, or 2'-UMP, 18.4 % UDP, 16.6 % diuridine pyrophosphate (UppU) and 2.8 % uridine 5',2'(3')-diphosphate. The authors confirm that no phosphorylation occurred in the absence of urea.

A similar experiment, but in dry conditions, was performed by Österberg et al..²⁴⁷ They showed that if the amount of nucleoside exceeded the amount of phosphate, it was possible to achieve higher yields of polynucleotides with a majority 3'-5' linked oligomers (**Figure 21**). Excess of inorganic phosphate led to the formation of organic and inorganic pyro- and polyphosphates.

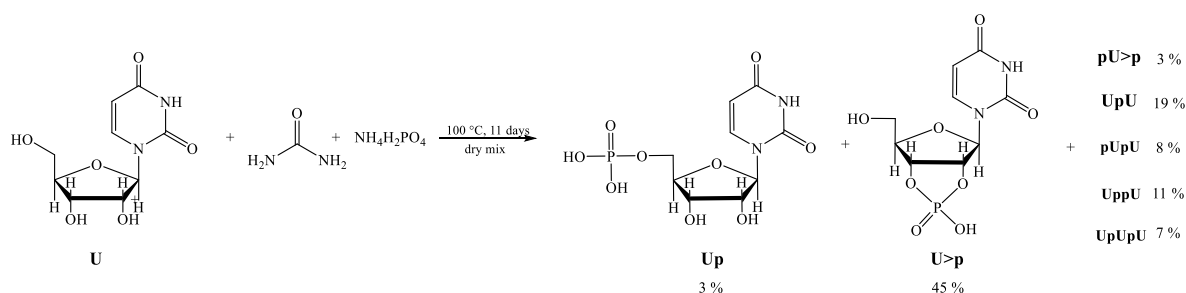


Figure 21. Reaction of phosphorylation of uridine in excess of nucleoside over phosphate after 11 days, adapted from Österberg et al..²⁴⁷ with the author's products abbreviations

Reimann and Zubay²⁴⁸ expanded the main Lohrmann experiment²⁴⁴. They tested the same starting materials, nucleosides, condensing agent and inorganic phosphate, but at different molar ratios, temperatures, solvents, reaction durations and pH. As a result, they demonstrated optimised conditions for nucleotide formation in dry conditions. First of all, they confirmed that there is no phosphorylation in the absence of a condensing agent. Second, among ammonium formate, diaminomaleonitrile, arginine, asparagine, 2-methyl imidazole, imidazole,

formamide and urea, the last two are the most efficient in phosphorylation of nucleosides. Third, they demonstrated that the phosphorylation reaction is sensitive to the pH of the mixture; a higher pH (above 7.4) led to the formation of a smaller number of phosphorylated products. Fourth, the most influential ratio affecting yield is urea/nucleoside. When there is more urea and less nucleoside, more phosphorylated products are made, especially 5-membered ring nucleoside phosphates. The highest yields were achieved at 95 °C after 6 hours, at 85 °C after 18 hours and at 75 °C after 60 hours. At lower temperatures, the yields of the same products were significantly lower. The authors explained it by reaction speed and mentioned the presence of the key products, nucleoside-2',3'-cyclic phosphates, only at temperatures above 85 °C. Their kinetic study suggests that the first step of the reaction is the synthesis of acyclic phosphates, and the second is the formation of cyclic derivatives. This extensive and thorough study of phosphorylation reactions gives us a clearer picture of favourable conditions for further experiments. However, due to the chosen analytical method, paper chromatography, these data are difficult to compare numerically with each other.

In the research of Schwartz,²⁴⁹ different approaches were taken. First, they used oxalate, which is supposed to help release the phosphate group from calcium minerals (such as apatite). In another set of tests, the amount of phosphorylation in the presence of urea or cyanamide was compared to the amount of phosphorylation in a solution of cyanogen, which is a precursor to their hydrolysis.²⁵⁰ In both scenarios, evaporative conditions were used at elevated temperatures. As a result, monophosphates were obtained, and the presence of condensing agents (urea, cyanamide and others) increased yields greatly.

Another experiment¹⁹¹ proving that the presence of water slows down the phosphorylation of nucleosides was conducted with schreibersite analogues (Fe₃P and Fe₂NiP) in water. The presence of a condensing agent (urea) or additional salts (MgSO₄, K₂CO₃, NH₄OH) did not facilitate the production of nucleotides by more than 7% after heating the solution for 14 days at 80 °C. However, this pathway can still be considered for the production of inorganic phosphate and phosphites (more in section 3.2).

One issue with arid reactions is the low interaction between solid chemicals. For experiments with urea, nucleosides, and phosphates, which are solid crystals at rt, it is necessary to have some medium, a so-called liquidiser, to make them react together.

Formamide as a liquidiser has been suggested in a more complex approach for nucleotide synthesis by Powner et al.¹² It was briefly discussed in section 3.1.1.3, in light of nucleoside synthesis. The suggested reaction scheme is shown in **Figure 22**.

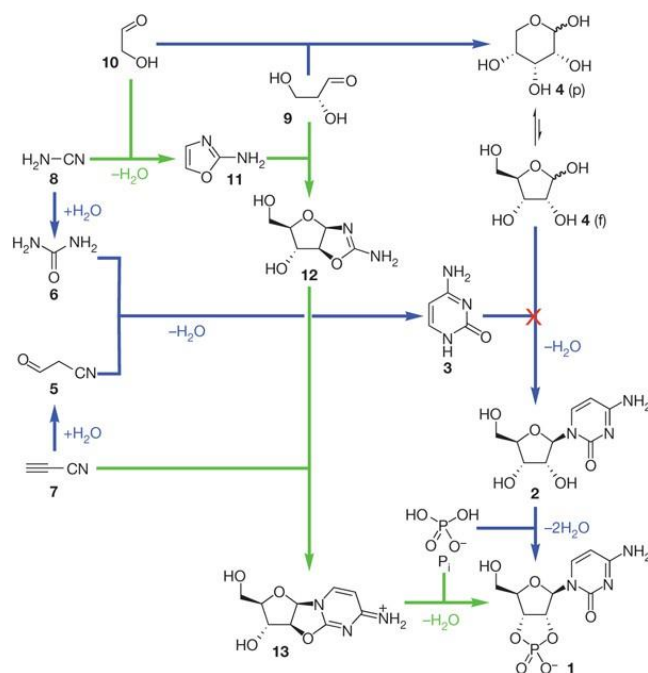


Figure 22. Scheme of prebiotic pathways for nucleotide synthesis developed by Powner et al.¹²

In two series of experiments, they used urea as a condensing agent and water and formamide as liquidiser. In the first protocol, the authors used a solution of urea with 2,2'-anhydronucleotide (**13** on **Figure 22**) and tetrasodium pyrophosphate that was mixed, dried at 40 °C for 2 hours, and then heated at 100 °C for 24 hours. In the second, formamide was used as a liquidiser, and the mixture of **13** and NH₄H₂PO₄ with urea was suspended in formamide and heated at 100 °C for 72 h. In both experiments, β-ribofuranose-2',3'-cyclic phosphate (**1** on **Figure 22**) was the major product with yields of 32 and 46 %, respectively. Among others, phosphorylated products such as 5'-phosphates derivatives of **13** and **1**, and β-arabinofuranose-5'-phosphate were identified.

The conclusion is that formamide is a better liquidiser for phosphorylation reactions, and the absence of water favours the process. Another point is that condensing agents are not only exceptional as chemical activators of the phosphorylation reaction but can also provide connections between dry chemicals in a mixture. It cannot be excluded that formamide can also play a role as a condensing agent by itself and participate in the reaction; its contribution should not be excluded.

Among the approaches employed to overcome water and low interaction problems, an option is the use of a deep eutectic solvent (DES) such as choline chloride:urea 1:2 as a medium and condensing agent at the same time.²⁵¹ The authors considered that those experiments could take place in some microenvironments where conditions for concentrated DES were possible; however, they could not be globally applicable on the early Earth. Along with other alcohols, they successfully phosphorylated adenosine and uridine up to 10-99 %, depending on the phosphorus source (NaH₂PO₄, struvite, monetite [Ca(PO₃OH)]) and its solubility. Their suggested mechanism of phosphate activation is demonstrated in **Figure 23**. Despite the high yields, it is worth saying that the prebiotic plausibility of choline eutectics is debatable, and it is by itself competing with alcohols for being phosphorylated.

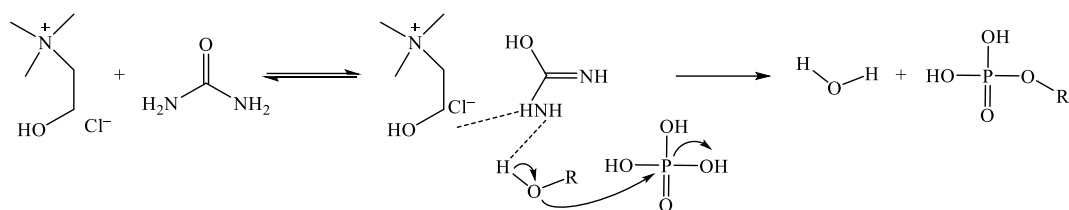


Figure 23. Phosphate activation scheme proposed by Gull and colleagues²⁵¹ for the phosphorylation of alcohols in a deep eutectic solvent (choline chloride:urea 1:2)

As an alternative, Menor-Salvan and colleagues^{198,199} suggested using urea:ammonium formate:water (UAFW) eutectic (molar ratio of 1:2:4). Those studies were reviewed in section 3.2 as a potential prebiotic environment for the formation of minerals such as struvite, newberyite and brushite. In a series of experiments,¹⁹⁸ adenosine and uridine were phosphorylated by Na_2HPO_4 and hydroxyapatite $\text{Ca}(\text{PO}_4)_3\text{OH}$ in DES. Comparing the results to the same experiment in a water-urea system, there was a noticeable increase in the production of phosphorylated products after several days: from 7 to 58 % at 65 °C and from 27 to 34 % at 85 °C. The authors identified the main products of the reaction as cyclic and acyclic phosphates. Also, longer reaction time favoured the production of more cyclic product and oligomers (di- and trinucleotides). Comparing the phosphorylation degree to the phosphate source in reaction with adenosine, the authors demonstrated that struvite and newberyite are the most proficient ($\approx 25\%$) phosphorus sources. In later work,¹⁹⁹ the same research group tested identical DES in anaerobic conditions in the presence of iron phosphates. In a new scenario, they considered the potential presence of cyanides that could facilitate metal complexation and contribute to phosphate release in evaporative pools (**Figure 24**).

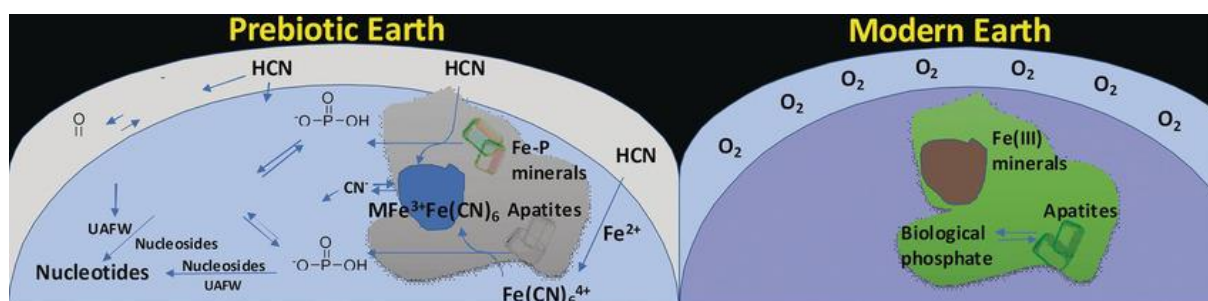


Figure 24. Schematics of a prebiotic scenario from Menor-Salvan and colleagues.¹⁹⁹ The key step is the complexification of Fe-minerals by cyanide, which promotes phosphorylation reactions

They observed that the reaction with ferrous minerals in the presence of NaCN increased the degree of phosphorylation. After 9 days of reaction of vivianite with adenosine, yields reached 15 % of phosphorylated products as compared to the non-NaCN experiment, which yielded 5 %. The presence of NaCN slightly facilitated the reaction with hydroxylapatite (a 5 % increase) and did not help in the experiment with sodium phosphate. Though iron phosphates were expected to be abundant in the Hadean aeon, they are rather insoluble in water. The presence of cyanides, suggestively synthesised in evaporative DES conditions, could serve as a solution to this problem. Although good yields of phosphorylated products were achieved in mild conditions, urea:ammonium formate:water seems to be more prebiotically plausible than choline chloride:urea eutectic solvent.

4.1.1.4. Mechanism of urea-assisted phosphorylation

To the best of my knowledge, there has been no in-depth research on the urea-inorganic phosphate mechanism of alcohol phosphorylation. There are currently two opposite approaches to urea-assisted phosphorylation. Both require the activation of inorganic orthophosphate, first through association with urea (the associative phosphate activation mechanism) and second through urea degradation (the dissociative phosphate activation mechanism).

Lohrmann and Orgel²⁵² proposed an associative mechanism and the catalytic role of urea. They suggested that the reaction is going through a hydrogen-bonded pentacovalent intermediate created when the carbamoyl oxygen of urea attacks the phosphate group (**Figure 25**). This hypothesis is indirectly confirmed by the fact that the activity of amides and asymmetric dialkylureas in the phosphorylation of nucleosides is higher compared to the inactivity of symmetric dialkylureas²⁴⁵ mentioned in section 4.1.1.3.

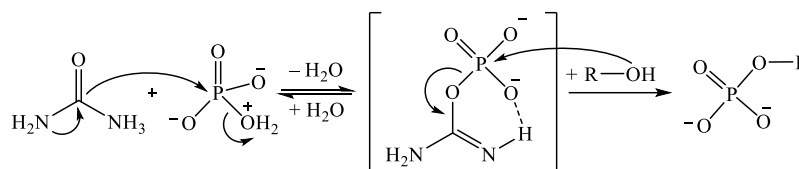


Figure 25. Urea-catalysed phosphate activation associative mechanism proposed by Powner and Sutherland²⁶⁶ with pentacovalent intermediate suggested by Lohrmann & Orgel²⁵²

Later, Powner and Sutherland²⁶⁶ rationalised the mechanism of urea-catalysed phosphate activation and placed it in the context of systems chemistry nucleotide synthesis.¹² According to them, the carbonyl group's lone pair initiates an attack on a less common tautomer of the phosphate mono-anion, leading to the displacement of water and the formation of the imidoyl compound (**Figure 25**). The authors note that even if phosphate mono-anion is a minor part, it is very reactive in nucleophilic substitution; thus, water is a good leaving group for the replacement with alcohol. Although the phosphorylation mechanism of alcohols has been extensively studied, there is still no final consensus for the proposed associative reaction mechanism.

Alternatively, phosphorylation can be induced by urea dissociation into carbon dioxide and ammonia. The first step of the reaction was studied almost 70 years ago; Shaw and Bordeaux²⁵³ demonstrated urea degradation in water solutions induced by temperature and acidic environments. They suggested that this process occurs through the formation of ammonium cyanate ($\text{NH}_4^+\text{CNO}^-$) that decomposes into isocyanic acid and ammonia. This mechanism was later confirmed by Callahan et al. in the context of urease hydrolysis.²⁵⁴ The next piece of the puzzle is the formation and degradation of carbamoyl phosphate, which was introduced by Seel and Schinnerling.²⁵⁵ They studied the formation and decomposition of carbamoyl phosphate in water in the presence of alkaline-earth metals. It was synthesised from cyanate and phosphate salts, and its degradation led to the formation of ammonia, carbon dioxide, and phosphate.

The mechanism suggested by Strazewski and colleagues[†] is in agreement with studies on the degradation of urea in water and the phosphorylation of alcohols with urea and phosphate, whereby urea eliminates ammonia to give isocyanic acid, which is trapped by P_i , to provide carbamoyl phosphate as the phosphorylating agent (**Figure 26**). This mechanism is awaiting confirmation.

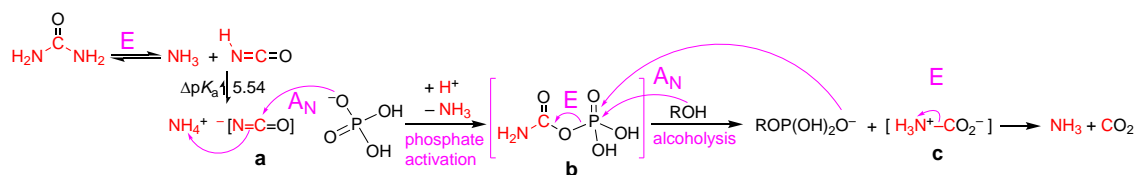


Figure 26. Urea-assisted dissociative mechanism of alcohol phosphorylation, as suggested by Strazewski and colleagues[†]

4.1.1.5. Formamide as a solvent, liquidiser and condensing agent

The advantage of formamide over urea is that it is liquid even at elevated temperatures. One of the first studies of phosphorylation in formamide was carried out by Schoffstall.²⁵⁶ Equimolar solutions of nucleosides and dihydrogen phosphate were heated in formamide. After carrying out the reaction for 15 days at 70 °C, a sum of phosphorylated product yield above 50% was achieved. The author also tested condensed phosphates ($(NH_4)_4P_2O_7$, $Na_5P_3O_{10}$ and $Na_3P_3O_9$) in light of obtaining di- and polynucleotides. However, 95 % of them consisted of 2',5'-internucleotides that are unusual in nature.

Xu and colleagues²⁵⁷ further developed the idea of Schoffstall using formamide as a solvent and applied it to the synthesis of nucleotides through the intermediate 2-thiouridine nucleoside.¹³⁶ The phosphorylation reaction was studied in the context of a bigger system approach to nucleotide synthesis starting from glyceraldehyde and 2-aminoxazole. Cyclic cytosine-2',3'-phosphate was obtained by direct phosphorylation of β -2-thioribocytidine in the presence of urea. In analogy to the unproven aforementioned associative phosphate activation mechanism, the reaction of Xu is going through the generation of an active intermediate, formidoyl phosphate (**Figure 27**).

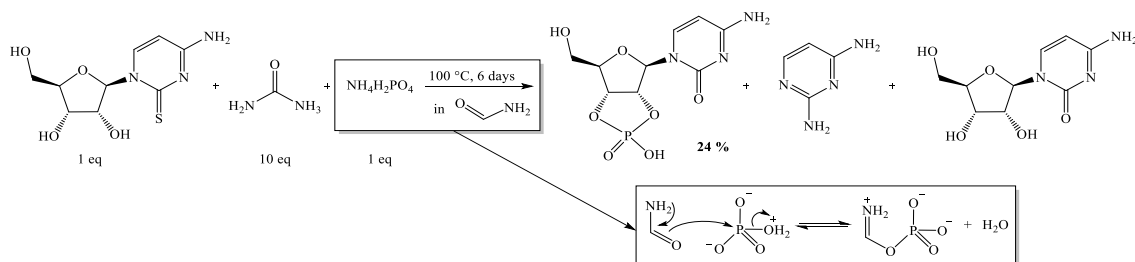


Figure 27. Phosphorylation step of an alternative route to the ribonucleoside with a mechanism of phosphate activation, adapted from Xu and colleges²⁵⁷

[†] Unpublished results

Benner and colleagues demonstrated that the presence of borate led to the phosphorylation of adenosine by inorganic phosphates in formamide towards adenosine-5'-phosphate.²⁵⁸ A study of the variation of prebiotic minerals was tested in the phosphorylation of adenosine (cytidine) using formamide as a solvent.²⁵⁹ Minerals were presolubilised in formamide and then joined with the nucleoside's solution. An experiment carried out at 90 °C showed that the maximum conversion of adenosine was 16 % into 5'-, 2'- and 3'-AMP, 2',3'-cyclic AMP and adenine. A kinetic study demonstrated that the formation of reaction products reached a plateau after 50 hours. Out of 12 tested prebiotic minerals, the most active ones were: libethenite $\text{Cu}^{2+}_2(\text{PO}_4)(\text{OH})$, ludjibaite $\text{Cu}^{2+}_5(\text{PO}_4)_2(\text{OH})_4$, reichenbachite $\text{Cu}^{2+}_5(\text{PO}_4)_2(\text{OH})_4$, cornetite $\text{Cu}^{2+}_3(\text{PO}_4)(\text{OH})_3$ and hydroxylapatite $\text{Ca}_5(\text{PO}_4)_3\text{OH}$.

In summary, we see that there are several pathways to the phosphorylation of nucleosides. The solutions for the water problem suggest using excess urea in water or its complete replacement by a deep eutectic mixture or another condensing agent, such as formamide. However, the most effective in terms of phosphorylated products and the production of oligomers is evaporative heating or dry state experiments. Both are prebiotically more plausible, and were not explored completely, and still lack a detailed understanding of the phosphorylation mechanism.

4.1.2. Phosphorylation of glycerol, fatty acids and their derivatives

Glycerol plays a functional role as the structural backbone of lipid molecules. It is an essential part for lipids precursors of both acylglycerols (simple lipids) and phospholipids (complex lipids). The formation of cell membranes depends on both lipid precursors and phosphorylated glycerol derivatives. Phosphorylation of glycerol is more effective under many relatively prebiotic conditions due to its stability, solubility, reactivity and liquid state at the "temperature window" (25-160 °C) of prebiotic chemistry.

A straightforward experimental procedure for glycerol phosphorylation was demonstrated by Pasek et al.¹⁹² They heated a water solution of schreibersite with glycerol at 65 °C in anoxic conditions. The possibility of phosphite production in water, a potentially more reactive phosphorus molecule, was described in section 3.2. As a result of heating, the major products were inorganic phosphate and, as mentioned above, phosphite, along with a minority of glyceryl-phosphates (2.5 %). This experiment proved not only that P-sources suitable for phosphorylation may come from meteorites, but also that alcohol can be phosphorylated under the same conditions in water at a mild temperature without a condensing agent.

Another prebiotic mineral, struvite, was tested in a water solution with glycerol.²⁶⁰ The reaction mixture was heated at 75 °C for 7-8 days. As a result, glyceryl-phosphates were formed in yields of about 28 % and 5% for the primary and secondary positions, respectively (**Figure 28**). Phosphorylation of nucleosides with monetite, as a phosphorus source, did not produce any organic phosphates.

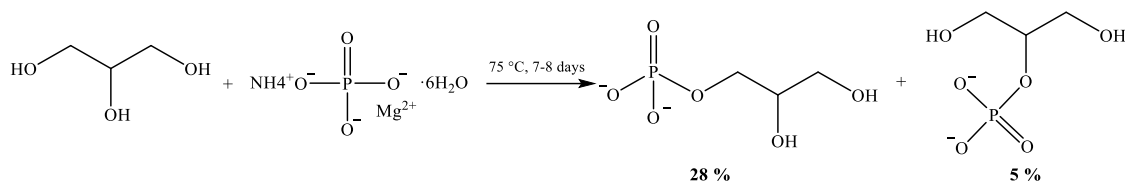


Figure 28. Reaction of glycerol phosphorylation, adapted from Gull et al.²⁶⁰

Recently, Ritson and Sutherland²⁶¹ demonstrated an entire reaction network connecting the formation of sugars (tetroses and pentoses), terpenoids and glyceryl phosphate based on reactions with inorganic sulfur species and hydrogen cyanide. One reaction includes glycerol phosphorylation by thiophosphates in formamide. PSO_3^{3-} by itself is an effective phosphorylation product with yields of glyceryl monophosphates of about 35 % after heating for 10 hours at 75 °C. Even lower temperatures are favourable for phosphorylation in the presence of a chemical activator. Phosphorylation with the addition of acrylonitrile or iron cyanate reveals similar yields, but at rt. UV irradiation induces phosphorylation with comparable yields at 40 °C. The effectiveness of thiophosphate can be explained by good leaving group formation through the reaction of H₂S that facilitates phosphorylation.

As urea is an effective condensing agent in reactions with alcohols, Epps et al. studied the phosphorylation of glycerol by ammonium dihydrogen phosphate in the presence of urea or cyanamide.²⁶² A water solution of glycerol, condensing agent and NH₄H₂PO₄ was evaporated and heated at 85 °C for 16 hours. As a result, glyceryl-1 (and 2) phosphates along with cyclic glyceryl phosphate were obtained. The maximum yield of phosphorylated products was 33 % in the reaction with cyanamide. A comparable result in the urea-assisted reaction was achieved only with the addition of NH₄Cl.

Phosphorylation of glycerol in eutectic urea/ammonium formate/water¹⁹⁸ or choline chloride/urea,²⁵¹ as described in section 4.1.1.3, follows the same trend as nucleoside reactions. The experiment in eutectic urea/ammonium formate/water solution¹⁹⁸ of glycerol with Na₂HPO₄ at 65 °C after 22 days resulted in cyclic and acyclic glycerol monophosphate, diglycerol mono- and diphosphates, along with several carbamoylated glyceryl derivatives. Unlike nucleosides, lower temperatures were more favourable for phosphorylation of glycerol. In the absence of urea, reactions were not effective, even at higher temperatures or in the presence of different phosphates.

Phosphorylation in a choline chloride/urea²⁵¹ eutectic solution was studied for glycerol phosphorylation. The yields of phosphorylated products (the majority are acyclic glyceryl phosphates) relative to nucleosides were higher in reaction with inorganic phosphate (65 %), struvite (65 %) and phosphite (52 %) after 7 days of heating at 65 °C. Later, the same research group proposed glycerol as a starting molecule and, at the same time, as a part of the eutectic solution glycerol and choline chloride (2.5:1) to compare it with formamide.²⁶³ The total yields of organic phosphorylated products for all tested phosphates were low: 0, 15 and 15 % for NaH₂PO₄, cTMP and struvite, respectively; the reaction in formamide was more efficient, resulting in 16, 37 and 35 %, respectively. Another factor explored by the authors was the effect of kaolinite and quartz on the reaction intensity. Their presence in both solvents greatly

increased the production of phosphorylated products, up to a maximum of, for example, 87-90 % in the reaction of struvite in formamide. The authors do not give a definitive answer but suggest an explanation based on the mineral reactivity or catalytic activity of kaolinite and quartz that promotes the reaction.

However, despite the success of this approach, the same problems identified in reactions with nucleotides remained. In particular, the small probability of the presence of such a large concentration of used substances and competition with choline in the phosphorylation reaction.

4.1.2.1. Phosphorylation of long-chain alcohols including decanol and geraniol

Albertsen et al. reported the formation of *n*-decyl phosphate.²⁶⁴ It was synthesised from *n*-decanol in a phosphorylation reaction with urea and $\text{NH}_4(\text{H}_2\text{PO}_4)$ at 100 °C. Later, the authors demonstrated the formation of vesicles from the obtained crude mixtures as well as from pure *n*-decyl phosphate.

There are several approaches for vesicle formation from single-chain alkyl phosphates and their derivatives in prebiotic conditions. Walde et al.²⁶⁵ reported the aggregation properties of different linear, single-chain alkyl phosphates and phosphonates in water. In particular, spontaneous vesicle formation was observed for *n*-dodecyl phosphoric acid, *n*-decyl phosphonic acid, and *n*-dodecyl phosphonic acid at rt and other examples at elevated temperatures.

Powner and Sutherland²⁶⁶ performed competitive phosphorylation of mixed-length alkanols under the same conditions that they had suggested for nucleotide synthesis¹² (**Figure 22**, sections **3.1.1.3**, **4.1.1.3**). A mixture of ethanol, hexanol, decanol, urea and ammonium dihydrogen phosphate were dissolved in water, dried at 40 °C and heated for 24 hours at 100 °C. The reaction was chemoselective towards decyl- over hexyl-phosphate, with a complete absence of ethyl phosphate (7:3:0, respectively). The authors explained it by the reversibility of phosphorylation and the progressively lower volatility of ethanol, hexanol and decanol (**Figure 29**).

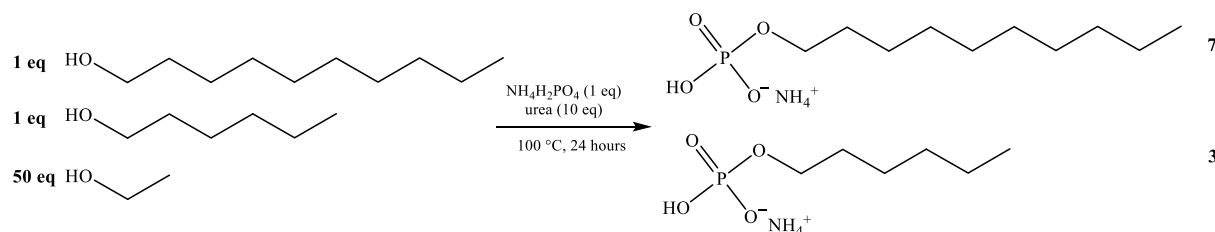


Figure 29. Phosphorylation reaction of alkanols, adapted from Powner and Sutherland²⁶⁶

Archean lipids, hopanoids, carotenoids, sterols, dolichols, ubiquinones are only a few examples of the incredibly diverse and pervasive terpenoid components found in biological membranes. Research in particular about **geraniol** phosphorylation is an active field of research

and its direct phosphorylation and prebiotic plausibility are debated. However, there are several approaches to it.

A theoretical approach by Ourisson²⁶⁷ envisaged that phosphorylation of polyprenyl alcohols would work in the same way as other prebiotic alcohols and, on the next step, form vesicles.

Lira et al.²⁶⁸ suggested one-pot phosphorylation of alcohols, including geraniol and other starting molecules. They used a direct approach and achieved a 66 % yield of geranyl monophosphate in reaction with tetrabutylammonium dihydrogenphosphate, which is used as the phosphate donor in combination with trichloroacetonitrile as a condensing agent. The reaction mechanism is similar to the phosphorylation by cyanamide described before (**Figure 30**).

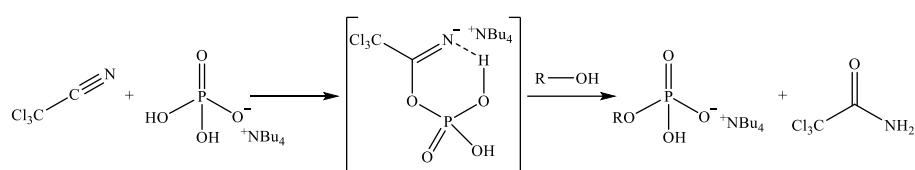


Figure 30. Mechanism of alcohol phosphorylation, as suggested by Lira et al.²⁶⁸

Using the same method of phosphorylation, Pozzi et al.²⁶⁹ produced monopolyprenyl mono- and diphosphates from geraniol, farnesol, geranylgeraniol, dodecanol and others. As a result, stable vesicles were produced only from the last two alcohols. The failure of geraniol can be explained by its complete solubility in water under the studied conditions. At the same time, stable vesicles detected by optical microscopy were formed from a crude mixture of dodecanol phosphates.

There are several fast and effective approaches for phosphorylating various polyprenols. First, the reaction of trichloroacetonitrile with tetra-*n*-butylammonium dihydrogen phosphate solubilised in chloroform or acetonitrile,²⁷⁰ has a yield towards phosphorylated product of 27-87 %, depending on the starting molecule. To accomplish effective phosphorylation, at least 3 mol of phosphate per mol of prenol is required. The method proved to be relevant to a broad variety of α -unsaturated polyprenols; polyprenyl phosphates that can be phosphorylated with medium to high yields.

Second is the approach suggested by Keller and Thompson for the preparation of isoprenol diphosphates.²⁷¹ The authors present a concise methodology for the efficient synthesis of isoprenoid diphosphates with carbon chain lengths ranging from C₅ to C₂₀. The phosphorylating reagent employed in this process consists of bis-triethylammonium phosphate dissolved in trichloroacetonitrile. The reaction occurs in 15 minutes, with final yields of phosphorylated product after isolation of 17-35 %.

Nakatani et al. suggested a hypothetical approach to the formation of vesicles from polyprenols and glycerol.²⁷² Phosphorylation of glycerol could be approached by amido-

triphosphate or other sources in the presence of Mg^{2+} . Suggested methods for phosphorylation of polyprenyl were described above (**Figure 31**).

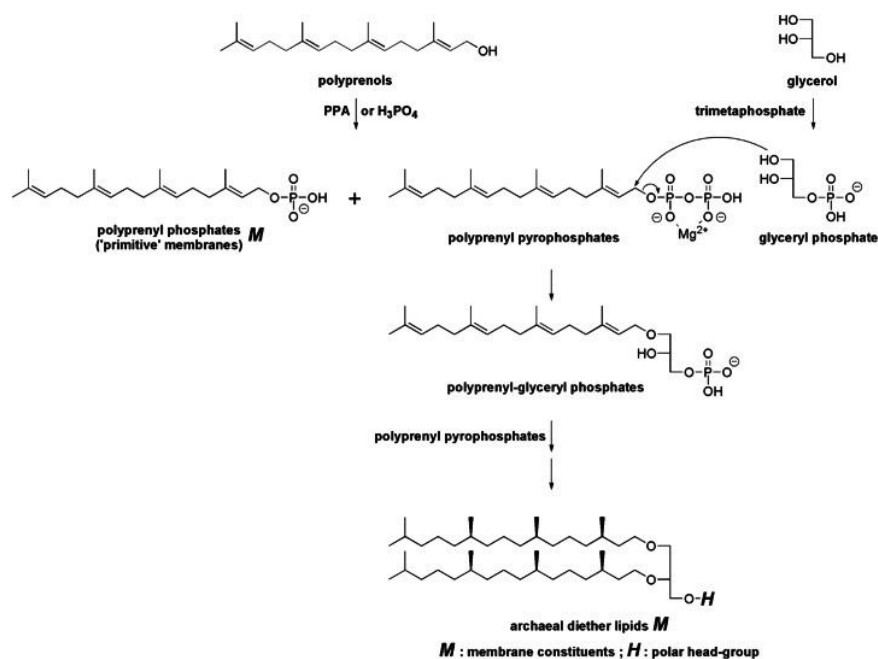


Figure 31. Hypothetical pathways for vesicle formation from polyprenols and glycerol, from Nakatani et al.²⁷²

Similar to the biosynthesis of geranylgeranyl-glycerol phosphate from geranylgeraniol and glyceryl phosphate, the nucleophilic attack of glyceryl phosphate on polyprenyl pyrophosphate could generate polyprenyl-glycerol phosphates. Polyprenyl-glycerol phosphates have the potential to form vesicles as well, perhaps when paired with enough quantities of polyprenols. However, the potential for vesicle formation may be limited by the hydrophobic/hydrophilic equilibrium inside the polyprenyl-glycerol phosphate structure.

4.1.2.2. Production of phospholipids and their polymerisation

Acylated glycerol molecules obtained during the condensation reaction induced by silicic acid and kaolin (section 3.1.2) can be phosphorylated under the same conditions.¹⁷² Glycerol, dodecanoate, phosphate and dicyanamide were incubated together for 12 hours at 65 °C, resulting in the formation of <1 % of phospholipids. Even from such a small purified fraction, the authors managed to produce stable vesicles.

The pathway towards the successful phosphorylation of nucleosides and nucleotides by diamidophosphate was discussed before (section 4.1.1.1).²²⁸ The authors also tested the phosphorylation and polymerisation of glycerol and fatty acids under the same conditions. Synthesis of glycerol-1,2-cyclophosphate (12%) at rt and diglycerol-phosphodiester at 55 °C was achieved. In the next step, the synthesis of phospholipids was attempted. A one-pot experiment of glycerol and nonanoic acid in the presence of diamidophosphate and imidazole led to the formation of a cyclophospholipid after several days at rt (**Figure 32**).

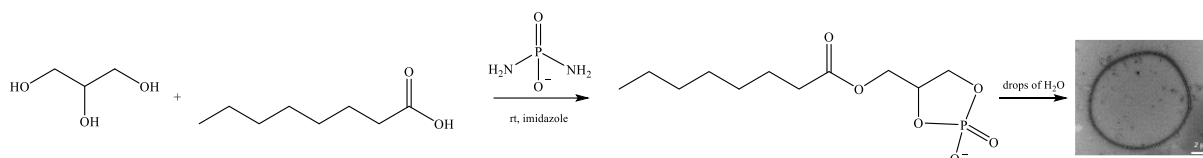


Figure 32. Reaction of one-pot phosphorylation and esterification of glycerol and its vesiculation, adapted from Gibard et al.²²⁸

Fayolle et al. demonstrated the phosphorylation and further vesiculation of racemic dioleoylglycerol.²⁷³ It was mixed with cyanamide (or urea) and $\text{NH}_4\text{H}_2\text{PO}_4$ for 24-48 hours at 80 °C in dry or wet-evaporative conditions. As a result, the main product, racemic dioleoylglyceryl phosphate, was obtained with the by-products mono-oleoyl glycerol, mono-oleoylglyceryl phosphate and oleic acid.

Phospholipids can be produced not only by phosphorylating acylated glycerol derivatives directly but also by glycerol phosphates reacting with fatty acids. Such an approach to the synthesis of phospholipids was suggested by Epps et al.²⁷⁴ In the reaction of glycerol-1(3)-phosphate with ammonium palmitate and cyanamide were synthesised monopalmitoylglycerophosphate (MPGP), dipalmitoylglycerophosphate (DPGP) and monopalmitoyl cyclic glycerophosphate (cMPGP) with a maximal conversion of glycerol phosphate of 45 % after heating at 60-90 °C for several hours (**Figure 33**). The average ratio of products is 60% MPGP, 27% DPGP and 13% cMPGP.

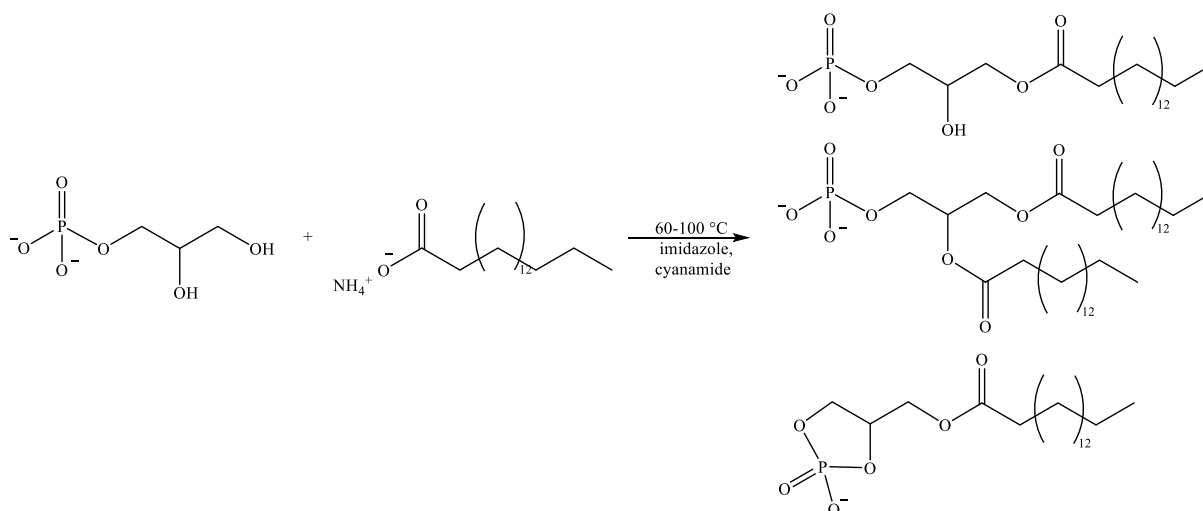


Figure 33. Reaction of glycerol phosphate acylation in the presence of cyanamide, adapted from Epps et al.²⁷⁴

Bonfio et al.²⁷⁵ suggested a pathway through heating the acyl imidazolides of fatty acids (C_4 , C_6 , C_8 , C_9 , and C_{10} acyl chains) at 50 °C in water or water-formamide solutions. As a result, libraries of different chain-length mono- and bis-acylated products were produced. Stable membranes were formed only on the basis of C_8 – C_{10} acylglycerol-2-phosphates.

In short, there is a prebiotically plausible pathway for lipid phosphorylation and their further spontaneous self-organisation into vesicles.

4.1.3. Synthesis of PEP (phosphoenol-pyruvate)

The phosphorylation of pyruvic acid is an important step in many cellular processes. Understanding the challenges of this process will bring science one step closer to solving the origin of life. Pyruvic acid is hard to phosphorylate because it is a negatively charged molecule. As is well known, at this stage of the manuscript, phosphorylation is the process of adding a phosphate group to a molecule, and this process requires a high-energy molecule, such as ATP. There are a few enzymes that help phosphorylate pyruvic acid. For example, pyruvate kinase uses ATP to produce phosphoenolpyruvate (PEP). PEP is a high-energy molecule that can be used for other cellular processes, such as glycolysis. There are very few prebiotic methods of direct phosphorylation of pyruvate under prebiotic conditions.

Coggins et al.²⁷⁶ demonstrated an indirect approach for PEP synthesis. A rapid dehydration of glyceraldehyde 2-phosphate would produce phosphoenol pyruvaldehyde and the next step through oxidation would result in PEP under prebiotically plausible conditions (**Figure 34**).

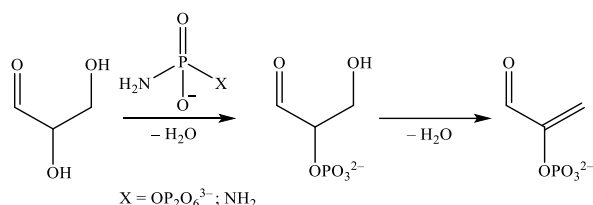


Figure 34. Prebiotic pathway for phosphoenol pyruvate synthesis, adapted from Coggins et al.²⁷⁶

In the first step, aldehyde was phosphorylated by diamidophosphate. The mixture was dissolved in phosphate buffer and incubated at rt; it resulted in glyceraldehyde 2-phosphate (96%) as the main product. In the next step, it was mixed with pentaerythritol and dissolved in phosphate buffer. A maximum yield of 74 % of phosphoenol pyruvaldehyde was obtained after 23 hours of incubation at 65 °C. The last step was the oxidation of the obtained product with hydrogen peroxide in the presence of ferrous chloride in phosphate buffer. The solution was stirred while hydrogen peroxide was added. After warming up and centrifugation, up to 30-93 % potassium phosphoenolpyruvate was isolated, depending on the oxidant and additive. Thus, an effective approach to PEP formation in prebiotic conditions was demonstrated. Aside from this product, the authors suggested that the entire reaction network of the triose glycolysis in mild conditions is controlled by α -phosphorylation.

4.2. Phosphorylation of glycerol and adenosine in hydrothermal conditions

Hydrothermal settings are also suggested as plausible environments for the origin of life. They are characterized by distinctive features that could be favourable for the formation of life.

The first is abundant energy: hydrothermal vents release heat from the Earth's interior, which can provide energy for the formation of molecules necessary for life. The second is the intense supply of chemicals that are released together with heat from hydrothermal vents. It can be a possible source of precursors for the formation of biomolecules, the many different minerals could also participate in and induce chemical reactions. The obvious feature is the presence of water as a universal solvent and essential factor of life, but at the same time, it could hydrolyse and degrade synthesised molecules and make their presence negligible compared to ocean volume. Another feature is presence of gradients of temperature, pH and redox that form a kind of chemical reactor for the production of a prebiotic inventory. An advantage and a disadvantage, as mentioned in the prebiotic conditions section, is protection from UV radiation. On one side, the deep ocean depths could preserve biomolecules from UV radiation; on the other, it limits UV-radiated chemistry (prebiotic photooxidation) that makes some of life's precursors available.

One of the very first experiments on alcohol phosphorylation in hydrothermal conditions was reported by Gull et al.²⁷⁷ As a result of glycerol phosphorylation, glycerol-2-phosphate and glycerol-3-phosphate were obtained (**Figure 35**).

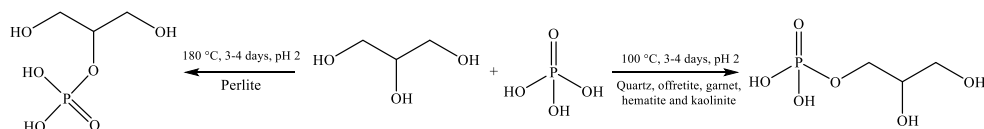


Figure 35. Scheme of glycerol phosphorylation reaction suggested by Gull et al.²⁷⁷

The experiment mixture, which contained phosphoric acid, glycerol and the studied minerals (quartz, offretite, garnet, perlite, hematite, and kaolinite), was loaded in steel alloy autoclaves (Fe-Cr-Ni, alloy GB1220-92) with water. It was heated at 100-200 °C for 3-4 days at pH 2. The total yields of phosphorylated molecules did not exceed 1%; however, some important discoveries were revealed after analysing the results. First, glyceryl phosphates were detected even after conducting the experiment at 200 °C. Second, most of the minerals produced detectable amounts of primary phosphate, but in the reaction with perlite, only secondary phosphate was identified (**Figure 35**). However, these results about the relative amounts of products should be taken with caution due to the very low amounts produced. It is important to mention that the reaction was carried out in water in the absence of a condensing agent and produced phosphorylated glycerol.

The same team²⁷⁸ successfully phosphorylated glucose into mono-phosphates (total yield of both isomers) and glucose-di-phosphate. The soup-like mixture of glucose, phosphoric acid and prebiotically plausible clay minerals (montmorillonite and kaolinite) was heated at 100-160 °C and under pressure of 0.8–1.8 MPa for 4 days. A maximal phosphorylation degree of 2 % mono- and 0.3% di-phosphate was obtained in the range of 100-130 °C and 1.5-1.8 MPa. Product yields were relatively low in the absence of montmorillonite and kaolinite, below detection limits. The authors suggested that clay minerals in hydrothermal environments have two functions: to catalyse and stabilise organic products at higher temperatures.

Ozawa et al. reported the phosphorylation of adenosine monophosphate in hydrothermal conditions.²⁷⁹ A flow-through reactor with two connected chambers, one cold (0 °C) and the

other one hot (100 °C), operating at 15 MPa and recycling fluid, was used as a model of a hydrothermal vent in contact with cold deep seawater. A solution of 5'-AMP, trimetaphosphate and magnesium chloride was maintained in the reactor for 3 hours per run. Samples taken between runs provided dynamic information about the production of the main products ADP and ATP, along with the by-products adenosine and adenine. The yields of the principal components were 0.03% and 0.09% for ADP and ATP, respectively. The authors discovered that the presence of magnesium chloride and a neutral pH are favourable for phosphorylation and the yields increased significantly. At pH 7, in the presence of MgCl₂, yields of ADP grow if the temperature of the hot chamber increases, whereas the opposite holds true for ATP.

There are very few studies on hydrothermal phosphorylation. However, there are many reports discussed in different parts of section **3.1**, where, under such conditions, a variety of organic precursors were synthesised. This field seems to have a broad perspective in terms of condensation and polymerisation reactions. High temperatures and elevated pressure could be favourable conditions for alcohol phosphorylation in particular and the origin of life study in general.

5. Overview and aims of the thesis

In this chapter reviewing the state of the art, the role of phosphorus in living organisms and its prebiotic importance for the emergence of life on Earth were examined. The basic geological parameters of the late Hadean eon and the availability of organic and mineral materials for phosphorylation reactions have been discussed. And, of course, the reactions themselves and modern methods of involving phosphates in reactions with organic alcohols were reviewed.

This review of the literature demonstrates that even though many different experiments on alcohol phosphorylation have been performed over the last 70 years, there are still subjects that are awaiting exploration. Well-studied nucleotide synthesis contrasts with the limited number of papers describing the formation and phosphorylation of lipids; although this process is central to the origin of cellular life. Phosphorylation of some of the potential prebiotic molecules, such as pyruvic acid or geraniol, has raised limited interest; sometimes only theoretical or indirect approaches have been suggested. Urea is one of the most widely used and well-known condensing agents, but a clear and detailed reaction mechanism explaining the principal phosphorylation reaction has not yet been described, with only tentative suggestions. There is no common prebiotically plausible chemical system involving nucleosides, glycerol and fatty acids together. There are only a few works studying the phosphorylation reaction in hydrothermal conditions, even though this approach could provide all the necessary requirements for prebiotic reactions. Those explorations form a superficial reaction network that does not always go deep or look for connections. Here we tried to cover some of the "blind" spots and expand our understanding of the phosphorylation reactions of prebiotic precursors.

The First aim of the thesis is to understand the conditions that are most favourable for the phosphorylation of organic precursors on the early Earth. We conducted comparative experiments on the phosphorylation of organic precursors in both conditions. It is difficult to determine under which conditions phosphorylation reactions could occur more efficiently, prebiotic or hydrothermal; it is possible that each contributed to the different processes. To obtain comprehensive results, we tested one of the reactions under both conditions. As far as I know, there is no report on exploring both scenarios and comparing results, although it is extremely important for understanding prebiotic phosphorylation processes. The prebiotic molecules chosen for experimental study were glycerol and some of its long-carbon-chain derivatives, as well as nucleosides, pyruvic acid, dodecanol and geraniol.

The Second aim of the thesis is to explore plausible prebiotic conditions, agents that could be involved, and factors that could possibly affect phosphorylation reactions. Although there are many results about some chemicals and reaction conditions influencing phosphorylation, there is no work that would summarise the scope of different factors compared to each other. The main inorganic sources of phosphorus, including orthophosphate, thiophosphate and condensed phosphate, were investigated and their comparative characterisation was conducted. Along with inorganic models, the most promising natural minerals from the prebiotic chemistry point of view, such as vivianite, struvite, canaphite and others, were investigated. Given the results of the previous study, dry or wet-evaporative

conditions were chosen as the prebiotic conditions of the study. An open atmosphere could provide interaction with the air's residual water; disregarding modern oxygen level. The reaction conditions are under atmospheric pressure and a temperature 75-115 °C to test harsher and milder prebiotic conditions for 1-5 days. The influence of temperature, pH, concentration of condensing agent and other factors was investigated.

The Third aim of the thesis is to confirm the mechanism of urea-assisted phosphorylation of prebiotic alcohols, which could give a key to understanding the role of the condensing agent and explain its necessity. Even though condensing agents have been used in prebiotic chemistry since the early days, there is no conclusive proof of the reaction mechanism. The presence of a condensing agent in phosphorylation reactions was therefore studied in detail. In addition to the standard and well-known urea and cyanamide, non-volatile, liquid carboxamides were investigated and a completely new agent, N-cyanofornamide, was proposed. The experimental proof of the dissociative mechanism of phosphorylation in reaction with glycerol and diphosphate was a milestone of the current research. The kinetic of this reaction was also studied in detail.

The Forth aim of the thesis is to place in a united, challenging environment all pieces of the explored reaction, such as precursors of membrane and RNA, to discover their competition and interaction in the reaction network. Aside from the separated reactions of each precursor, we performed system chemistry experiments. They were carried out with different starting molecules (glycerol, fatty acids and nucleosides) that were mixed with orthophosphate together with a condensing agent in the same pot to study competitive alcohol phosphorylation and phosphorylated products.

Therefore, the overall goal of this study is to address the phosphorylation problem in a multifaceted way, to deepen the understanding of the details of the phosphorylation mechanism, at the same time as broadening the possible reaction agents and phosphorylation conditions.

II Materials and Methods

1. Chemical materials

1-Dodecanol (98 %), urea (99.5 %), formamide (99 %), benzoyl chloride (99 %), acetic acid (≥ 99 %), 4-dimethylaminopyridine (DMAP) (99 %), phenyl magnesium bromide (1.6 M PhMgBr in cyclopentyl methyl ether), tetrahydrofuran (99.5 %), toluene (99.85 %), cytidine (99.5 %), uridine (99.5 %) and 4-dimethylaminopyridine (99 %) were purchased from *ACROS Organics (Thermo-Fisher Scientific Inc.)*.

Geraniol (97 %), sodium cyclic trimetaphosphate (≥ 99 %) and adenosine (99 %) were purchased from *Alfa Caesar*. Palmitoyl chloride (98 %), guanosine (≥ 98 %), thymidine (99 %) and triethylamine *tris*-hydrofluoride (37% HF) were purchased from *Fluka BioChemika (Honeywell International Inc.)*.

Labelled [^{13}C]Urea (98 %), [^{15}N]formamide (≥ 98 %) and [^{15}N]acetamide (≥ 98 %) were purchased from *Cambridge Isotope Laboratories Inc. (CIL)*. [^{15}N] $_2$ Urea (≥ 98 %) was purchased from *CIL* and *Sigma-Aldrich*.

Sodium dihydrogen phosphate (≥ 99 %), sodium thiophosphate tribasic hydrate (≥ 90 %), sodium phosphate dibasic (≥ 99 %), sodium phosphate tribasic dodecahydrate (≥ 98 %), N-methylacetamide (≥ 99 %), N-methylformamide (99 %), cyanamide (99 %), pyruvic acid (98 %), glycerol (≥ 99.5 %), acetamide (99 %), adenosine 5'-diphosphate sodium salt (≥ 95 %), L-Valine (≥ 99 %), D-Valine (≥ 98 %), cyclohexylammonium phosphoenolpyruvate (≥ 97 %) and dilithium carbamoylphosphate hydrate (≥ 85 %) were purchased from *Sigma-Aldrich (Sigma Aldrich Chimie S.a.r.l., Merck KGaA)*.

Adenosine 5'-monophosphate disodium salt ($\geq 98\%$), adenosine 5'-triphosphate disodium salt hydrate (≥ 97 %), guanosine 5'-monophosphate disodium salt (≥ 98 %), uridine 5'-monophosphate disodium salt (≥ 98 %) and cytidine 5'-monophosphate disodium salt (≥ 95 %) were purchased from *Carbosynth (Biosynth Carbosynth Ltd)*.

Palmitic acid (> 99.5 %), oleic acid (> 85.0 %), oleoyl chloride (> 80.0 %) and N-(3-dimethylaminopropyl)-N'-ethylcarbodiimide hydrochloride (> 98.0 %) were purchased from *Tokyo Chemical Industry Co., Ltd. (formerly Tokyo Kasei Kogyo Co., Ltd.)*. Tridecanoic acid (95.0 %) and DL-1,2-isopropylidenglycerol (98 %) were purchased from *Fluorochem (Fluorochem Ltd.)*.

Sodium N-cyanofornamide (95 %) was made on demand by *ChemSpace (SIA "ChemSpace")*.

A crystalline mixture of 1- and 2-glyceryl phosphate ($\approx 6:4$ mol/mol) was produced by *Prolabo, Rhône-Poulenc*.

Anhydrous toluene, dichloromethane ($\text{CH}_2\text{Cl}_2 = \text{DCM}$) and tetrahydrofuran (THF) were produced using a solvent drying apparatus (*Innovative Technology Ltd, China*) and the needed volumes of solvents were collected under a constant argon flow. All deuterated solvents were purchased from *Eurisotop (Saint-Aubin, France)*. HPLC solvents were purchased from

Thermo-Fischer Scientific (mass spectrometry grade). Thin-layer chromatography (TLC) was carried out on aluminium sheets coated with silica gel 60 F254 (*Merck*). TLC plates were inspected by UV light ($\lambda = 254$ nm) and developed by treatment with a mixture of 10 % H₂SO₄ in EtOH/H₂O (1:1 v/v) followed by heating. Melting points were measured in a capillary in heated oil on a *Büchi 510* apparatus.

Table 1-1. Chemicals used in this work. Reduced-nitrogen compounds **1-4c**, alcohols **5-16a** (pyruvic acid, **16a**, can react as enol tautomer), phosphoenol pyruvate (PEP, **16b** = reference compound), mono-palmitoylglyceryl phosphate (MPGP, **17**), amino acids, phosphate sources, reference compounds (nucleoside phosphates) and chemical reagents.

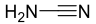
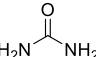
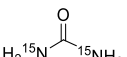
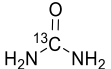
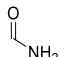
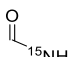
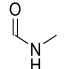
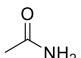
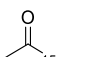
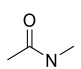
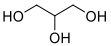
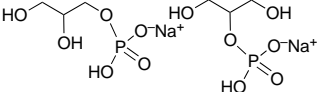
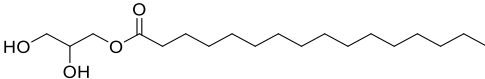
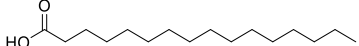
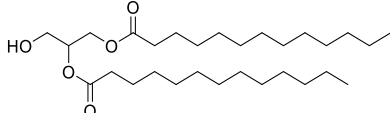
Compound number	Compound name	Structure	Molecular weight [g/mol]	Mono-isotopic molecular mass* [Da]
1	Cyanamide		42.04	42.0218
2a	Urea		60.06	60.0324
2b	[¹⁵ N ₂]Urea		62.04	62.0264
2c	[¹³ C]Urea		61.05	63.0357
3a	Formamide		45.04	45.0215
3b	[¹⁵ N]Formamide		46.03	46.0185
3c	N-Methylformamide		59.07	59.0371
4a	Acetamide		59.07	59.0371
4b	[¹⁵ N]Acetamide		60.06	60.0341
4c	N-Methylacetamide		73.09	73.0528
5	Glycerol		92.09	92.0473
5a	Sodium glyceryl phosphate		194.05	171.0064
6	<i>rac</i> -mono-Palmitoylglycerol (MPG)		330.51	330.2770
6a	Palmitic acid		256.43	256.2402
7	<i>rac</i> -1,2-bis-Tridecanoyl glycerol (BTG)		484.76	484.4128

Table 1-2. Chemicals used in this work

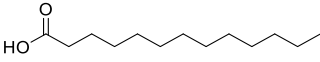
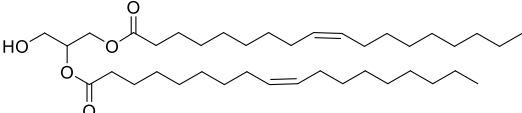
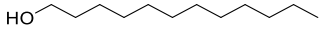
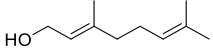
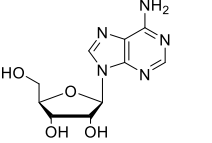
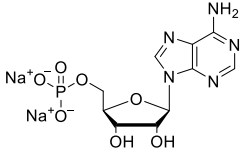
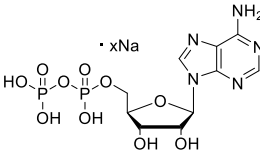
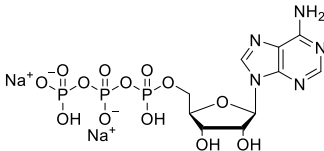
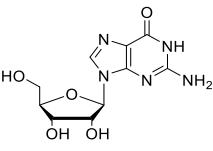
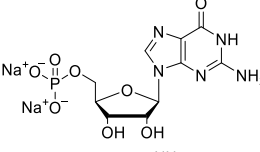
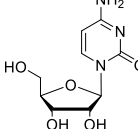
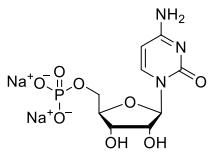
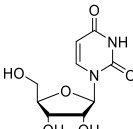
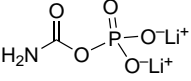
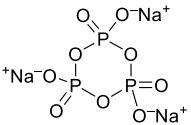
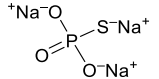
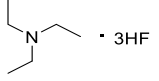
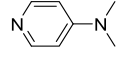
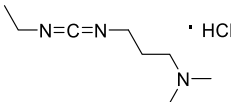
Compound number	Compound name	Structure	Molecular weight [g/mol]	Mono-isotopic molecular mass* [Da]
7a	Tridecanoic acid		214.35	214.1933
8	<i>rac</i> -1,2-Dioleoylglycerol (DOG)		621.00	620.5380
9	Dodecan-1-ol		186.34	186.1984
10	Geraniol		154.25	154.1358
11	Adenosine		267.25	267.0968
11a	Adenosine 5'-monophosphate disodium salt		391.19	345.0485
11b	Adenosine 5'-diphosphate sodium salt		427.20	424.0076
11c	Adenosine 5'-triphosphate disodium salt hydrate		551.14	502.9666
12	Guanosine		283.24	283.0917
12a	Guanosine 5'-monophosphate disodium salt		407.18	361.0434
13	Cytidine		243.22	243.0855
13a	Cytidine 5'-monophosphate disodium salt		367.16	321.0373
14	Uridine		244.20	244.0695

Table 1-3. Chemicals used in this work

Compound number	Compound name	Structure	Molecular weight [g/mol]	Mono-isotopic molecular mass* [Da]
14a	Uridine 5'-monophosphate disodium		368.15	322.0213
15	Thymidine		242.23	242.0903
16a	Pyruvic acid		88.06	88.0160
16b	Cyclohexyl ammonium phosphoenolpyruvate		267.22	166.9751
17	α,β -Isopropylidene-DL-glycerol		132.16	132.0786
18	<i>rac</i> -(2,2-Dimethyl-1,3-ioxolan-4-yl)methyl palmitate		370.57	370.3083
19	<i>tert</i> -Butyldimethylsilyl-glycerol		221.39	221.1573
20	<i>tert</i> -Butyldimethylsilyl- <i>rac</i> -1,2-bis-tridecanoyl glycerol		614.06	613.5227
21	<i>tert</i> -Butyldimethylsilyl- <i>rac</i> -1,2-dioleoylglycerol		750.30	749.6479
22a	L-Valine		117.15	117.0790
22b	D-Valine		117.15	117.0790
P _i	NaH ₂ PO ₄		119.98	94.9551
[¹⁸ O ₄]P _i	NaH ₂ P[¹⁸ O ₄] [§]		127.98	102.9720
P _i (dibasic)	Na ₂ HPO ₄		141.96	94.9551
P _i (tribasic)	Na ₃ PO ₄ · 12 H ₂ O		163.94 (anhydrous)	94.9551

Table 1-4. Chemicals used in this work

Compound number	Compound number	Compound number	Compound number	Compound number
CP_i (dibasic lithium hydrate)	Dilithium carbamoylphosphate hydrate		152.88 (anhydrous)	138.9682
cTMP	Trisodium cyclic trimetaphosphate		305.89	236.8772
SP_i	Na ₃ SPO ₃ · H ₂ O		180.01 (anhydrous)	110.9322
Et₃N·HF	Triethylamine <i>tris</i> -hydrofluoride	 · 3HF	161.21	102.2005 (Et ₃ NH ⁺)
DMAP	4-Dimethylamino pyridine		122.17	122.0844
EDC-HCl	N-(3-Dimethylaminopropyl)-N'-ethylcarbodiimide hydrochloride	 · HCl	191.70	156.1495 (C ₈ H ₁₈ N ₃ ⁺)

* for salts: of the larger ion demonstrated here

2. Analytical methods

2.1. NMR spectroscopy methods

Nuclear Magnetic Resonance spectra were recorded in CDCl₃, fully deuterated dimethyl sulfoxide (DMSO-*d*₆), D₂O on *Bruker Avance 300, 400 and 500* spectrometers equipped with a standard BBFO probe. ¹H spectra were recorded with a 2 s relaxation time and excitation sculpting when pre-saturation was needed. ³¹P spectra were performed using inverse gated decoupling with 90-degree pulses and 60 s relaxation time to ensure quantitative measurement. ³¹P-¹H Heteronuclear Multiple Bond Correlation (HMBC) spectra were run with the standard pulse program from *Bruker*, using 512 increments with 100 ppm spectral width in F1, 4 scans and 1.6 s relaxation delay, giving a 1 h measurement time. ¹⁵N experiments on enriched products were run using a 90-degree single pulse, with 30 s relaxation delay.

Additional ³¹P{¹³C,¹H}, ¹³C{³¹P,¹H}, J-Modulated Spin-Echo (JMOD) NMR, together with ³¹P-¹³C, and ³¹P-¹⁵N HMBC spectra, were taken on a *Bruker Avance NEO 600* MHz spectrometer equipped with a QCI ¹H, ¹³C, ³¹P, ¹⁵N probe (*Institut de Chimie de Toulouse, Université Paul Sabatier*).

Chemical shifts of solvents (CDCl₃: δ_H = 7.26 and δ_C = 77.23 ppm; DMSO-*d*₆: δ_H = 2.50 ppm (quintet, J_{H,D} = 1.9 Hz) and δ_C = 40.0 ppm (septet, J_{C,D} = 32 Hz); D₂O: δ_H = 4.65) served as internal references. Signal shapes and multiplicities are abbreviated as br (broad), s (singlet), d (doublet), t (triplet), q (quartet), quint (quintet) and m (multiplet). Where possible, a scalar coupling constant J is given in Hertz (Hz). ³¹P NMR chemical shifts were referenced to NaH₂PO₄ (δ_P = 0.00 ppm). Although ¹³C NMR chemical shifts were usually referenced to DMSO (δ_C = 40.0 ppm), in the case of spectra taken in H₂O/D₂O the signal of urea (**2a**) at δ_C = 160.50 ppm was considered an internal reference.

2.1.1. Sample preparation for NMR spectroscopic analysis

The NMR sample preparation for the crude mixtures depended on the starting alcohol that was used in the reaction. In cases where the initial phosphorylated alcohol was liquid (glycerol, geraniol, dodecanol and DOG) and the crude mixture had low heterogeneity, fewer preparation steps were needed rather than for MPG and BTG, which were hardly soluble even in DMSO-*d*₆. In the case of nucleosides, the only solvent used is D₂O.

Work-up of the crude reaction mixtures obtained using **5**, **8-10** and **16a** as a starting molecule: the whole reaction mixture (≈50-100 mg) was dissolved in 1000 μL DMSO-*d*₆, vortexed at a medium rate for 20-30 seconds and centrifuged for 120 seconds at 5000 rpm. The final extract was filtered off and then placed in an NMR tube for analysis.

Work-up of the crude reaction mixtures obtained using compounds **6** and **7** as a starting molecule: about 50 mg of the reaction mixture were added 1000 μL DMSO-*d*₆, the mixture was sonicated for 60 seconds, vortexed at a medium rate for 20-30 seconds and centrifuged for 120

seconds at 5000 rpm. The final extract was filtered off and then placed in an NMR tube for analysis.

Work-up of the crude reaction mixtures obtained using compounds **11-15** as a starting molecule: about 50 mg of the reaction mixture were added 1000 μ l D₂O, the mixture was sonicated for 60 seconds, vortexed at a medium rate for 20-30 seconds and centrifuged for 120 seconds at 5000 rpm. The final extract was filtered off and placed in an NMR tube for analysis.

2.2. MS and LC-MS methods

For mass-spectrometry (MS) or liquid chromatography-mass spectrometry (LC-MS), I used MS-quality ultra-pure water (*Elga*®), acetonitrile \geq 99.9 % *Optima* LC-MS grade, methanol \geq 99.9 % *Optima* LC-MS grade, formic acid 99.0 % *Optima* LC-MS grade, DCM $>$ 99.8 % for HPLC stabilised with amylene. All these chemicals were obtained from *Fisher Chemicals*.

For direct injection analyses, samples were diluted 100 times in a solvent mixture (46.1 % MeOH, 38.4 % DCM, 15.4 % ultra-pure water and 0.1 % formic acid) and injected at 10 μ L/min using a syringe pump. The low-resolution mass spectrometry (LRMS) analyses were performed using an ion trap (*AmaZon SL, Bruker*) equipped with an electrospray ion source (ESI) operated in positive or negative ion mode. The capillary voltage was set to \pm 4500 V, the nebulizer gas was set to 3.4-4.8 bar (50-70 psi), the dry heater was set to 200 °C and the dry gas was set to 4-9 L/min, m/z range 50-1000 Da. The data were processed by the *DataAnalysis 5.2* software from Bruker. The high-resolution mass spectrometry (HRMS) analyses were performed using a high-resolution hybrid quadrupole-time of flight mass spectrometer (*Impact II, Bruker*) also equipped with an electrospray ionisation source (ESI). The source parameters and the processing software were the same. The calibration of high-resolution data was performed with a sodium formate solution.

The liquid chromatography-high resolution mass spectrometry (LC-HRMS) analyses were performed by a UHPLC system (*Ultimate 3000, Thermo Scientific*) coupled with the hybrid Quadrupole – Time-of-Flight (Q-TOF) mass spectrometer (*Impact II, Bruker*). The samples were not diluted before injection. The injection volume was adjusted to the concentration of the sample and was, in general, 0.5 μ L. The columns, eluents and gradients used were:

(1) reversed-phase ultrahigh-performance chromatography (RP-UHPLC) for mixtures containing **5**: *Luna Omega Polar C18* – 50 x 2.1 mm (1.6 μ m), solvent A = 0.1 % formic acid in ultra-pure water, solvent B = 0.1 % formic acid in acetonitrile/methanol (ACN/MeOH) 1:1, ambient temp., flow rate 0.5 ml/min, 0-5 min 0 % B, 5-10 min 0-100 % B, 10-12 min 100 % B, 12.0-12.2 min 100-0 % B, 12.2-15 min 0 % B;

(2) RP-HPLC for mixtures containing nucleosides and nucleotides (**11-14a**): *Luna Omega Gemini C18* – 250 x 4.6 mm (5 μ m), solvent A = 5 mM ammonium acetate pH 8.0,

solvent B = ACN/A 95:5, ambient temp., flow rate 1 ml/min, 0-2 min 2 % B, 2-29 min 2-20 % B, 29-30 min 20-80 % B, 30-34.5 min 80 % B, 34.5-35 min 98-2 % B, 35-45 min 2 % B;

(3) hydrophilic ion liquid chromatography (HILIC) for mixtures containing glycerol (**5**) and glyceryl phosphates: *Luna Omega Sugar*—100 x 2.1 mm (3 μ m), solvent A = 8 mM ammonium acetate in ultra-pure water, solvent B = ACN, isocratic elution A/B = 55:45, ambient temp., flow rate 0.5 ml/min.

2.2.1. Sample preparation for MS analysis (LC-MS, LRMS, HRMS) of the crude reaction mixtures

Similar to NMR analyses, the solvent for sample preparation for MS analyses depended on the initial starting alcohol molecule. The crude extracts obtained from reactions with **5** to **16**: about 1-2 mg of the solid reaction mixture was dissolved in methanol or water (**11-15** in water); sonicated for 60 seconds, centrifuged at 5000 rpm for 120 seconds; if necessary, filtered through an organic filter *Millipore* 0.45 μ m PTFE (hydrophobic) and the final extract was collected for analysis.

2.3. HPLC method for the analysis of mono-palmitoylglycerol (MPG) phosphorylation

All analyses were performed with a High-Performance Liquid Chromatography (HPLC) using reversed-phase elution on a LC20 system from *Shimadzu* (high-pressure mixing double-pump system; max flow rate 20 ml/min for each pump). The system was equipped with a DGU-20A3R degasser (*Shimadzu*, up to 10 ml/min per line), separate analytical and preparative capillary lines, two separate injectors from *Rheodyne* (100 μ L and 2 ml loops). For each analysis, 5 μ L were commonly injected. The eluted compounds were observed by ultraviolet (UV) detection using two wavelengths at a time (SPD-20A, *Shimadzu*), fluorescence detection (RF-20A XS, *Shimadzu*) and by laser-driven evaporative light scattering detection (ELSD, *Sedex 90 LT*,TM *Sedere*®). The three detectors could be used separately, pairwise, or all together in the order mentioned in the previous sentence.

Crude mixtures produced in phosphorylation reactions, such as lipids, were analysed using a Phenyl-Hexyl column (*Kinetex*TM, 2.6 μ m, 100 x 3 mm, *Phenomenex*®). The lipids were detected by ELSD on a device operating at 40°C with a gain of 10 or 11. Phases A (0.1% formic acid in H₂O) and B (0.1% HCOOH in acetonitrile (CH₃CN)) were used in a linear binary gradient from A/B 50:50 to 100% B at 0.8 ml/min in 10 min at 25°C.

2.4. Raman spectroscopy

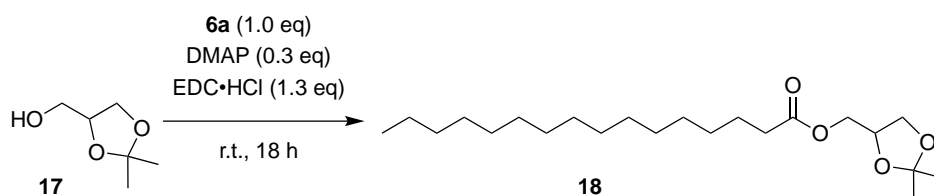
We used the LabRAM HR800 confocal spectrometer optimised for microscopic measurements. The set-up at the ENS de Lyon is dedicated to the *in-situ* analysis of high-

pressure, high-temperature experiments in the diamond anvil cell. Measurements were done up to 13 GPa and to 130 °C. The characteristics of the setup are the following: Confocal - Czerny-Turner configuration, a grating of 1800 tr/mm, a Quantum Torus 400 laser source (YAG doubled) at 532.14 nm (500 mW). The spectrometer is surrounded by an experimental environment optimised for diamond anvil cells (micro-positioning, automatic pressure regulation, temperature regulation, etc.). Depending on the experiment, I used super long-working distance Mitutoyo® objectives x50 or x20 slwd; the laser power was adjusted to 25-100 %; the entrance slit of the spectrometer that defines the spectral resolution was adjusted to 100-200 μm ; the confocal hole was kept open to 500 μm and ensured a comfortable signal/noise ratio; the acquisition time was usually adjusted to 3-15 accumulations of 2-30 s.

3. Syntheses methods

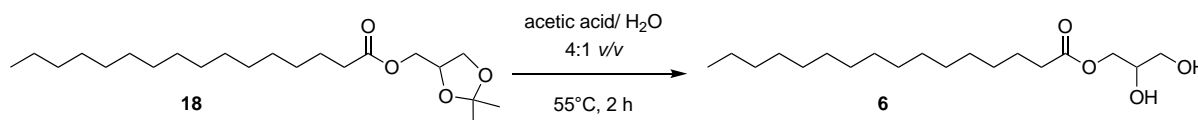
3.1. Synthesis and characterization of racemic mono-palmitoylglycerol²⁸⁰ (MPG, **6**)

1) *rac*-(2,2-dimethyl-1,3-dioxolan-4-yl)methyl palmitate (**18**):

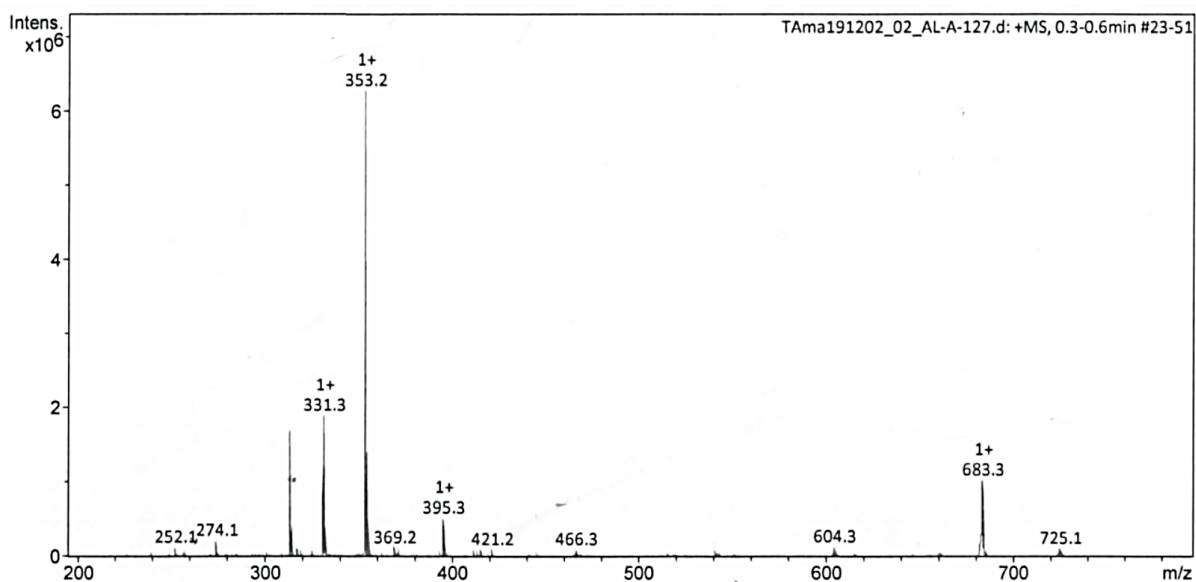
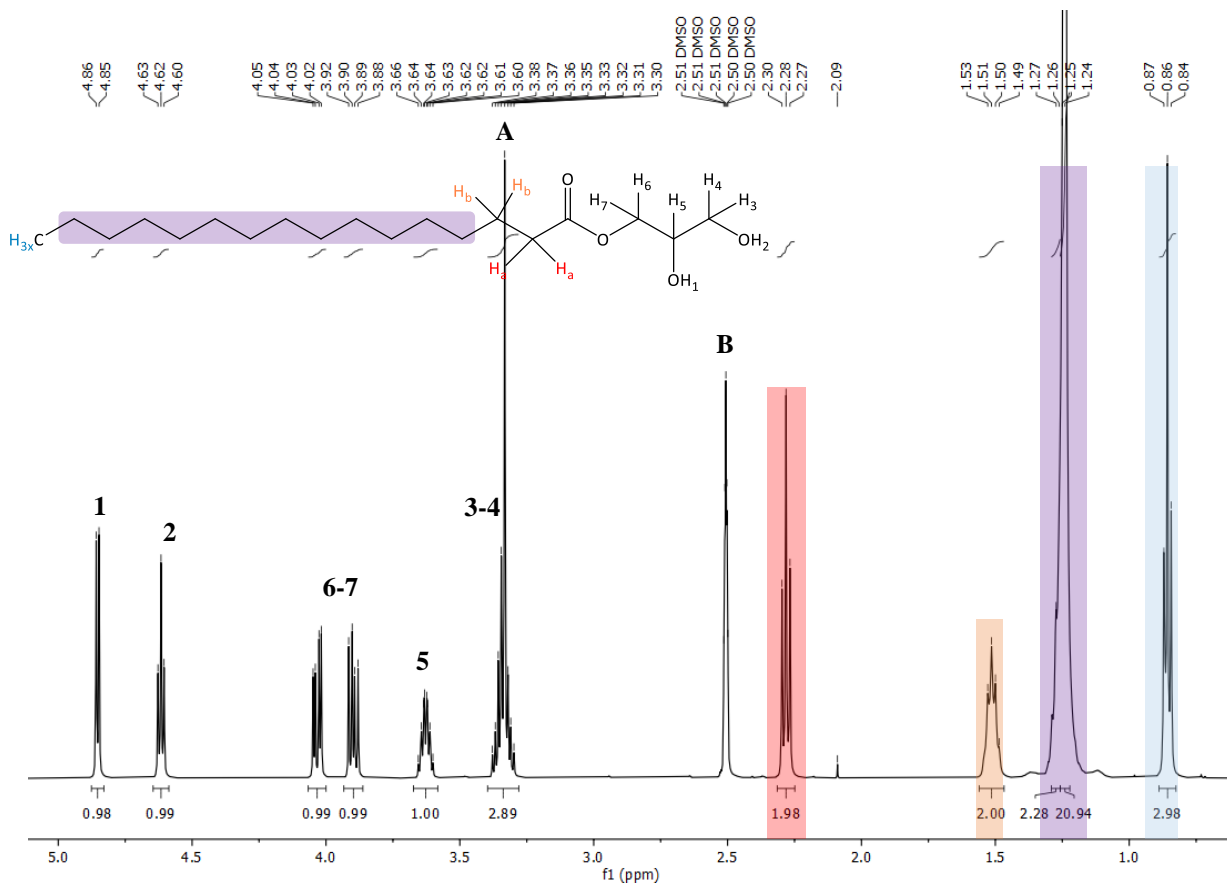


3.7 g α,β -isopropylidene-DL-glycerol (28.6 mmol, **17**) were dissolved in dry DCM (75 ml) and 7.3 g palmitic acid (28.6 mmol) were added. The solution was cooled to 0 °C using an ice bath, DMAP (1.0 g, 8.6 mmol) and EDC·HCl (7.1 g, 37.2 mmol) were added together. The resulting solution was left under vigorous stirring at rt for 18 h. A quantity of 150 ml of saturated NaHCO₃ was added to quench the reaction. The product was extracted with DCM (2 x 100 ml), the combined organic phases were dried over anhydrous MgSO₄ and the crude material obtained after evaporation of the solvent was chromatographed over SiO₂ with petrol ether-ethyl acetate (PE:EtOAc 99:1 to 85:15 v/v) yielding **18** as a white powder (9.99 g, 94 %).

2) Procedure for the synthesis of *rac*-1-palmitoyl-glycerol (**6**):



Racemic 2,2-dimethyl-1,3-dioxolan-4-yl)methyl palmitate (9.99 g, 26.9 mmol, **18**) was dissolved in a mixture of AcOH/H₂O (100:25 ml) and kept under vigorous stirring at 55 °C for 2 h. The solution was cooled to rt and 150 ml of saturated NaHCO₃ were added dropwise until the solution was neutralized. The product was then extracted with EtOAc (2 x 100 ml). The combined organic phases were washed with brine (100 ml) and dried over anhydrous MgSO₄. The resulting solution was evaporated, yielding MPG as a white powder (8.90 g, 99 %, **6**), mp. 65-68 °C. The product was characterised by ¹H NMR spectroscopy and LRMS (**Figure 36-Figure 37**).



3.2. Synthesis and characterization of racemic *bis*-tridecanoyl and dioleoyl glycerol

rac-1,2-*bis*-Tridecanoyl glycerol (BTG, **7**) was prepared after Altamura et al.²⁸⁰ as shown in **Figure 38**, and *rac*-1,2-Dioleoylglycerol (DOG, **8**) after Fayolle et al.²⁸¹

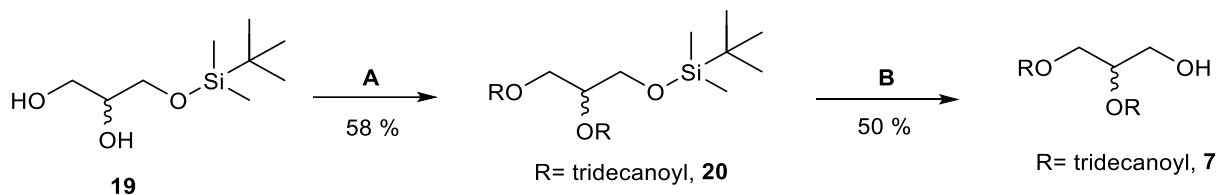


Figure 38. Synthesis of **7**. **A** – **19** (1 eq), tridecanoic acid (2.1 eq), DMAP (2eq), EDC-HCl (2.2 eq); **B** – Et₃N·HF (5 eq).

3.2.1. Synthesis of TBDMS-*rac*-BTG (**18**)

TBDMS-*rac*-BTG was synthesised as follows. In a 250 ml argon-flushed round bottom flask containing (**19**, 3 g, 0.013 mol) and tridecanoic acid (7 g, 0.03 mol) in dry DCM (50 ml) were added DMAP (0.4 g, 0.03 mol) and EDC·HCl (5 g, 0.04 mol) at 0 °C. The solution, once reached rt, was stirred for 16 h after which TLC (Et₂O: Cy, 8:1 v/v) showed complete consumption of **19**. 75 ml of distilled water were added and the organic phase was extracted twice. The organic phases were dried over dry Na₂SO₄ and the solvent was evaporated. Product **20** was isolated through flash chromatography (Et₂O: Cy 1:9 v/v to 3:7) and characterised by polarimetry, $[\alpha]_D^{25} = 0.00$ (c 0.1, CHCl₃), ¹H and ¹³C NMR spectroscopies (**Figure 39-Figure 40**).

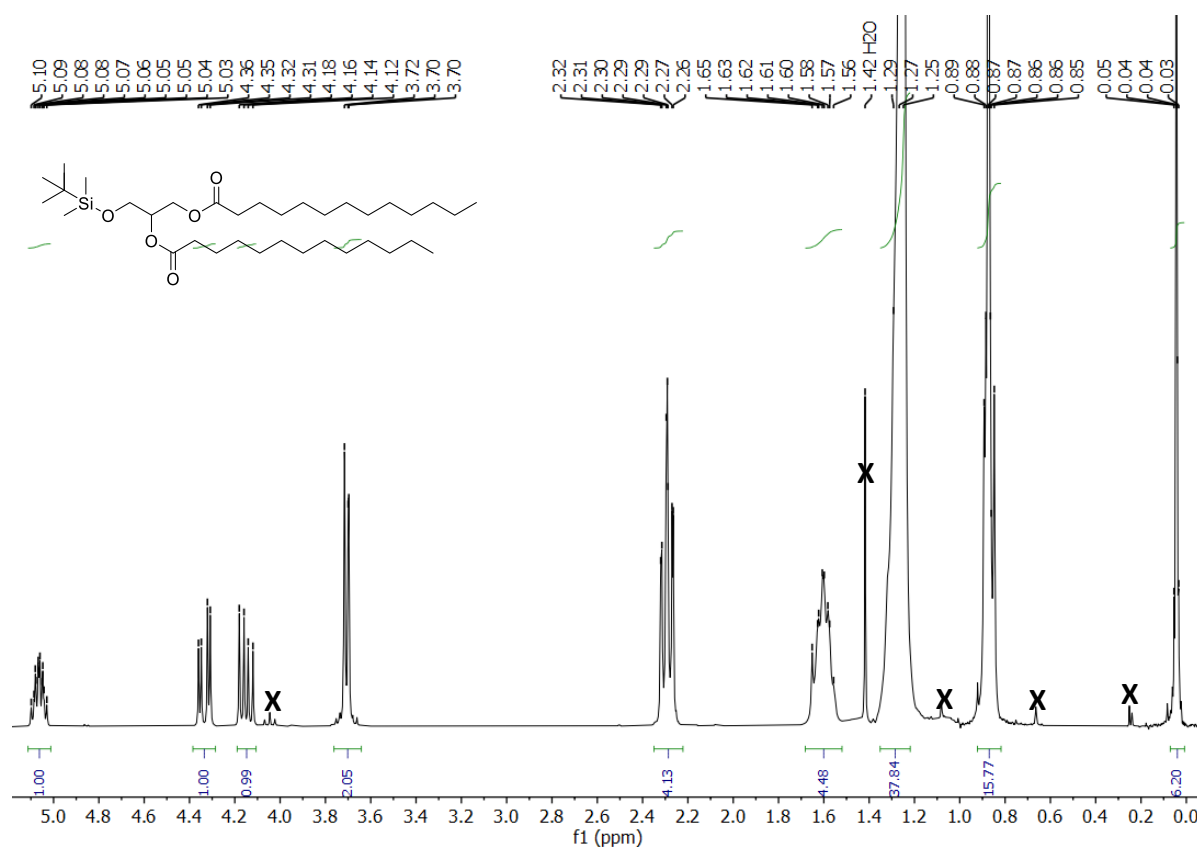


Figure 39. ^1H NMR (300 MHz, CDCl_3) TBDMS-*rac*-BTG (**20**): $\delta_{\text{H}} = 5.05\text{--}4.29$ (*m*, 1H, C(2)H); 4.31 (*dd*, $J = 10.2, 5.6$ Hz, 1H, C(3)H_b), 4.11 (*dd*, $J = 10.2, 4.6$ Hz, 1 H, C(3)H_a), 3.66 (*d*, $J = 5.7$ Hz, 2 H, C(1)H₂), 2.20-2.30 (2 *t*, $J = 7.6$ Hz, $\Delta\delta_{\text{H}} = 1.6$ Hz, 4 H, 2 x CH_2COOR), 1.65-1.68 (*m*, 4 H, 2 x $\text{CH}_2\text{CH}_2\text{COOR}$), 1.20-1.35 (*m*, 36 H, 18 x CH_2), 0.85-0.89 (*m*, 15 H, 5 x CH_3 *t*Bu-Si, Me-Si), 0.04 (*m*, 6 H, 2 x $\text{CH}_3(\text{CH}_2)_{11}$). **X** = impurities.

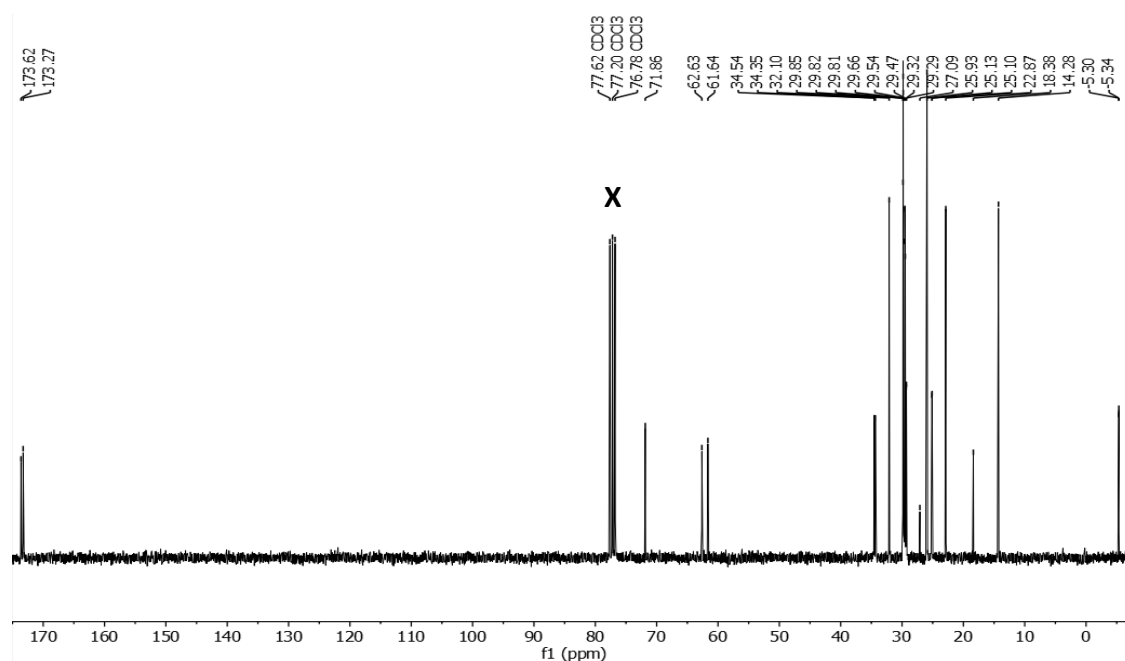


Figure 40. ^{13}C NMR (75.5 MHz, CDCl_3) TBDMS-*rac*-BTG (**20**): $\delta_{\text{C}} = -5.34, -5.30$ (MeSi), 14.1 (CH_3), 18.2 (Cq *t*BuSi), 22.7 (CH_2), 25.0 (CH_2), 25.7 (3 x CH_3), 29.1-29.7 (series of CH_2), 32.0 (CH_2), 34.1 (CH_2), 34.4 (CH_2), 61.5 (C(1)H₂), 62.4 (C(2)H), 71.7 (C(3)H₂), 173.1 (C=O), 173.3 (C=O). **X** = CDCl_3 .

3.2.2. Synthesis of *rac*-BTG (7)

rac-1,2-bis-Tridecanoyl glycerol was synthesised as follows. In a 250 ml argon-flushed round bottom flask containing 3.3 g **20** (0.01 mol) dry THF/ACN (50 ml, 1:1 *v/v*) were slowly added 2 ml (5 eq) of Et₃N·HF. The obtained pale-yellow solution was stirred overnight. TLC (Cy/AcOEt 2:1) showed complete consumption of the starting material. A saturated sodium bicarbonate solution (160 ml) was added together with 50 ml of DCM. The organic phase was extracted twice and the water phases were washed with more DCM. The combined organic phases were dried over anhydrous Na₂SO₄ and the solvent was evaporated. Flash chromatography (AcOEt/Cy 1:9 to 3:7 *v/v*) furnished a mixture of 3.4 g 92 %-pure **7** (70 % yield) and 0.3 g Et₃NHF (according to ¹H NMR, 22 mol% with respect to pure **7**) as a white solid, mp. 50-55 °C. A small fraction (60 mg) contained racemic mono-tridecanoyl glycerol (MTG) together with BTG. The main fraction of product **7** was characterised by polarimetry, [α]_D²⁵ = 0.00 (c 0.1, CHCl₃), ¹H, ¹³C NMR spectroscopies and LRMS (**Figure 41-Figure 43**).

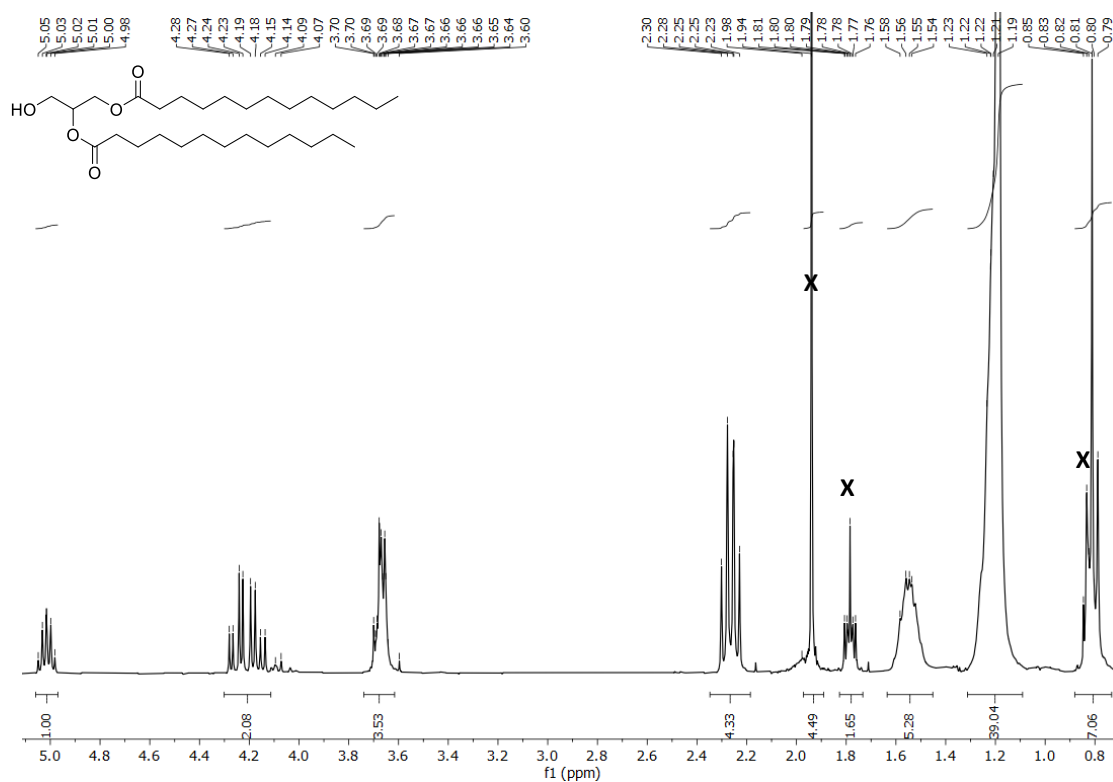


Figure 41. ¹H NMR (300 MHz, CDCl₃) BTG (**7**): δ_H= 5.06-4.95 (*m*, 1H, C(2)H), 4.21 (*ddd*, 2 H, J = 17.6, 11.9, 5.1 Hz, C(1)H₂), 3.62-3.72 (*m*, 2 H, C(3)H₂), 2.26 (*dd*, J = 14.7, 7.1 Hz, 4 H, 2 x CH₂COOR), 1.63-1.48 (*m*, 4 H, CH₂CH₂COOR), 1.19 (*m*, 36 H, 18 x CH₂), 0.81 (2 *t*, J = 6.7 Hz, 6 H, 2 x CH₃), **X** – 1.94 (Et₃NHF), 1.78 ((CH₃CH₂)₃NHF), 0.83 (CH₃CH₂)₃NHF.

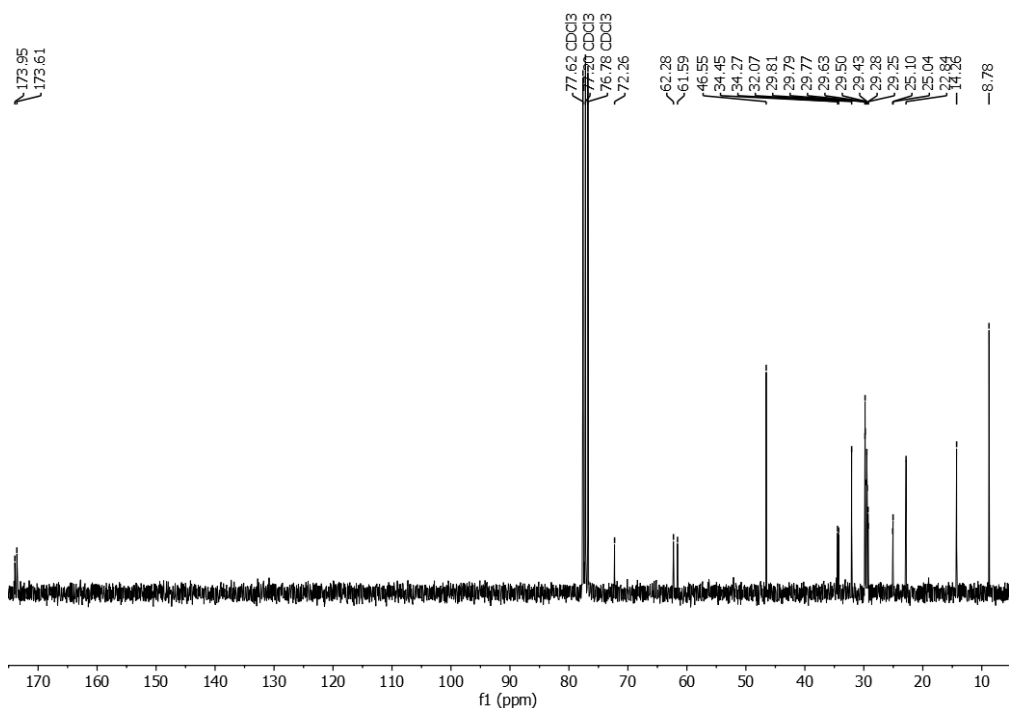
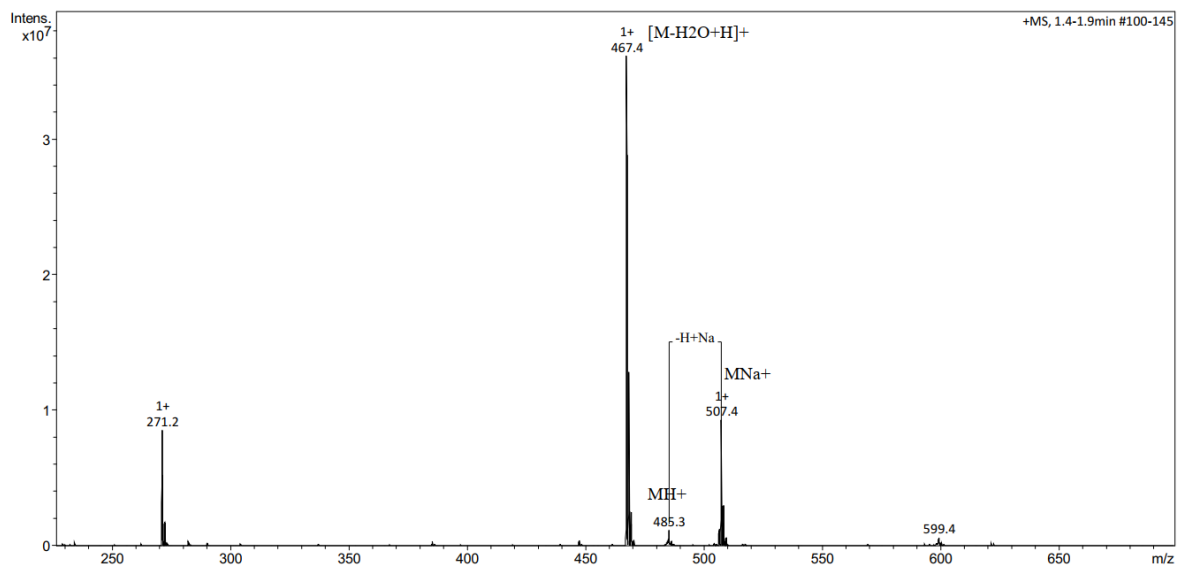


Figure 42. ^{13}C NMR (75.5 MHz, CDCl_3) BTG (**7**): $\delta_{\text{C}} = 14.2$ (CH_3), 22.5 (CH_2), 27.0 (CH_2), 29.2 (CH_2), 29.2-29.8 (series of CH_2), 32.0 (CH_2), 34.2 (CH_2), 61.4 (C_1), 62.0 (C_2), 72.1 (C_3), 173.5 and 173.8 ($\text{C}=\text{O}$).



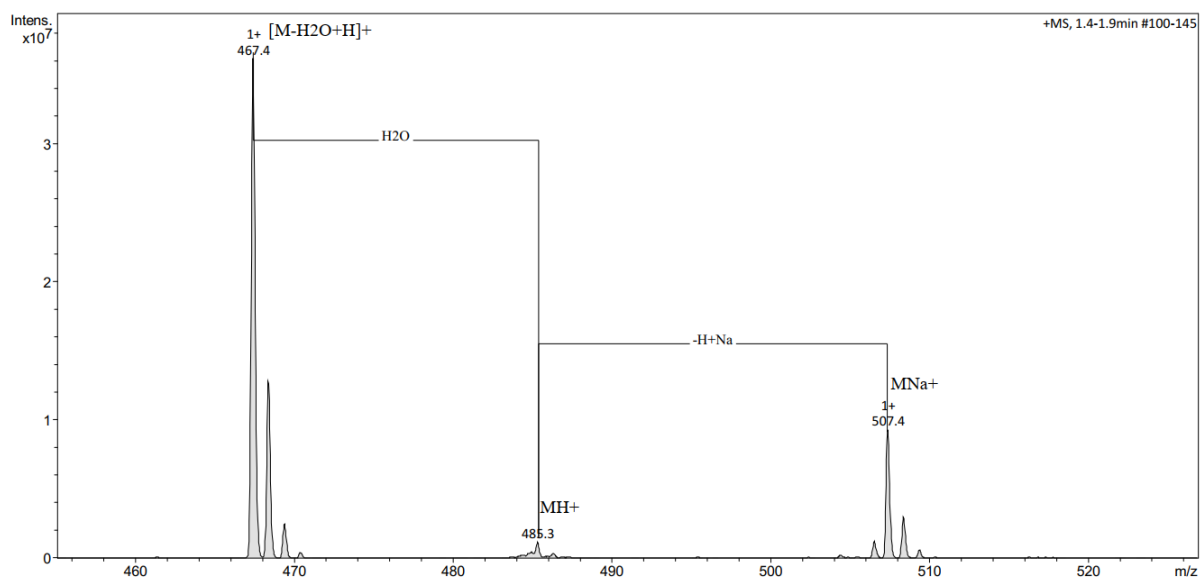


Figure 43. Low-resolution positive-ion mode mass spectrum of BTG (**7**). m/z 458.3 $[M+H]^+$, 467.4 $[M-H_2O+H]^+$, 507.4 $[M+Na]^+$, 599.4 $[2M+Na]^+$. m/z 271.2 $[MTG]^+$ (*rac*-mono-tridecanoyl glycerol).

3.3. Synthesis of NaH₂P[¹⁸O₄] ([¹⁸O₄]P_i)

Unlike BTG and MPG, the synthesis of the first batch of NaH₂P[¹⁸O₄] was performed before the beginning of my thesis. However, I assisted my supervisor, Michele Fiore, in the preparation of the second batch following the procedure invented by Michele Fiore and Pierre Strazewski.

3.3.1. H₃P[¹⁸O₄]

H₃P[¹⁸O₄] was synthesized from 5.00 g of normalized water 97 %-enriched in ¹⁸O {H₂[¹⁶O] exact mass = 18.0106 g/mol; H₂[¹⁸O] exact mass = 20.0148 g/mol; average MW (0.03 x 18.0106 + 0.97 x 20.0148) = 19.9575 g/mol}, hence (5.00 g =) 250.5324 mmol water were placed in a thick-walled tube-shaped glassware flask (24 cm long x 4 cm diameter) equipped with a small magnetic stirrer (tare: 241.6 g). To this stirred water, 10.4043 g PCl₅ (1/5 equiv., 49.90 mmol, MW = 208.24 g/mol) were added portion-wise (approximately 250 mg per portion). During the addition, HCl fog developed in the flask, which was periodically blown away with a short gentle argon stream. Care was taken that the upper half of the glassware remained at ambient temperature and that the portions were added slower during the second half (towards the end) of the PCl₅ addition, since the hydrolysis became more and more violent and HCl, perhaps Cl₂ and water (vapour, droplets) developed. Once all the PCl₅ was added (after 25 minutes), the resulting colourless solution was weighed (220.4 g total weight of the flask corresponding to 5.8 g of the solution) and, after 45 min at rt (since the beginning of PCl₅ addition), the liquid was heated to 70 °C (reached at 90 min total time). HCl bubbles developed continuously even when stirring was stopped for a moment. After 90 min at 70 °C the flask was cooled and weighed (total time 135 min) and the net weight was 4.928 g (expected 5.238 g = 100 %).

The solution was cooled down and sampled (50 μL + 1ml ACN) for ESI-HRMS. According to the negative-ion mode MS it contained residual amounts of H₂P[¹⁸O₂]Cl₂ (as *m/z* P[¹⁸O₂]Cl₂⁻) that could be ignored, since the neutralisation to NaH₂P[¹⁸O₄] was made 16 hours later, during which the rest could hydrolyse to H₃P[¹⁸O₄]. Isotopes relative abundances are summarised in **Table 2** and ESI-HRMS spectra are shown in **Figure 44**.

Table 2. Isotopolog ratio of phosphoric acid in two batches. Both products were used in the series of experiments.

Isotopolog	Ratio in a first batch, %	Ratio in a second batch, %
H ₃ P[¹⁸ O ₄]	93.8	81.5
H ₃ P[¹⁶ O ¹⁸ O ₃]	6.0	15.8
H ₃ P[¹⁶ O ₂ ¹⁸ O ₂]	0.2	15.8

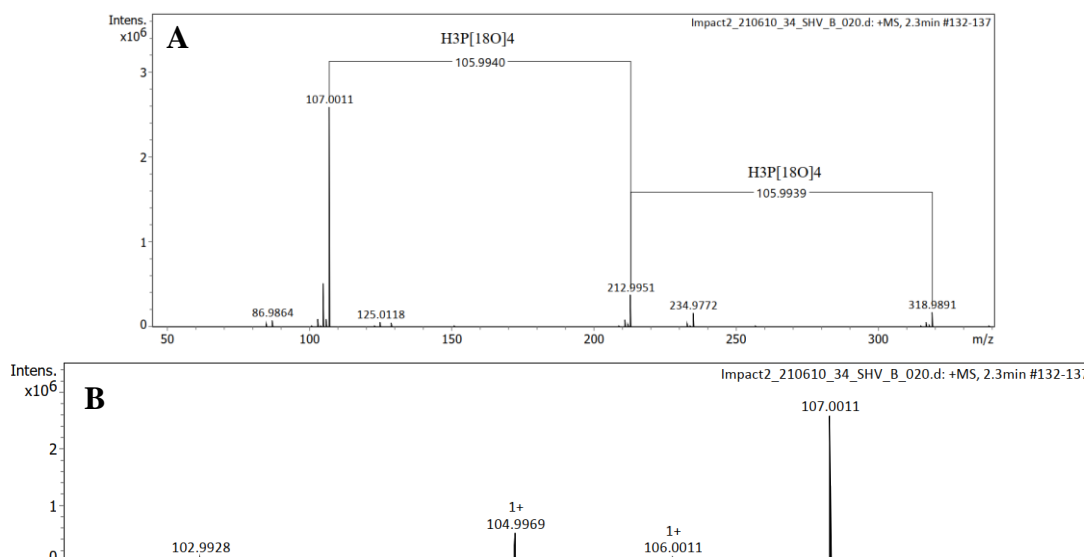


Figure 44. High-resolution positive-ion mode mass spectrum of H₃P[¹⁸O₄] (second batch). **A** – total ion spectrum: phosphoric acid monomer, dimer and trimer (gas phase adducts). **B** – zoom into the main signal cluster from which the isotopolog ratios were determined (**Table 2**): *m/z* 107.001 [H₄P¹⁸O₄]⁺, 104.9969 [H₄P¹⁶O¹⁸O₃]⁺, 102.9928 [H₄P¹⁶O₂¹⁸O₂]⁺, 212.9951 [2M+H]⁺, 318.9891 [3M+H]⁺.

3.3.2. NaH₂P[¹⁸O₄]

For the synthesis of NaH₂P[¹⁸O₄], a solution prepared by suspending 2.60 gr (24.0 mmol) of Na₂CO₃ in 8 ml of water (natural isotope abundance) was placed in a double-neck 25 ml round-bottom flask equipped with a magnetic stirrer and a calibrated pH meter. The solution was placed in a thermostatic bath. The full amount H₃P[¹⁸O₄], prepared as described above, was transferred in a plastic syringe and was then slowly added (~50 μl/min) to the well-stirred Na₂CO₃ suspension. The initial pH of the suspension was 11.03. The pH was continuously monitored. The pH-change from basic to moderately acidic, provoked changes in the physical appearance of the solution/suspension, from milky to transparent until showing a new precipitation, probably of a mixture of Na₃PO₄, Na₂HPO₄ and/or NaH₂PO₄ that re-dissolved almost completely upon further addition of H₃PO₄. Once all the content of the syringe was added, the measured pH was 2.91 (= the pH value of a saturated commercial NaH₂PO₄ solution).

The obtained solution was evaporated under reduced pressure and the obtained residue was dried at 70°C for 2 hours (weight loss 2 gr), at 105-150°C for 4 hours, at 105 °C for 2 hours after which another weight loss of 1.9 % was detected. After the transfer of the salt to another vial, 4.998 g highly enriched NaH₂P[¹⁸O₄] could be used for further experimentation. A dry sample was analysed by ESI-HRMS to determine the isotope abundancies (**Table 3, Figure 45**).

Table 3. Isotopolog ratio of $\text{NaH}_2\text{P}^{18}\text{O}_4$ of two batches. Both products were used in the series of experiments.

Isotopolog	Ratio in a first batch, %	Ratio in a second batch, %
$\text{NaH}_2\text{P}^{18}\text{O}_4$	93.7	90.0
$\text{NaH}_2\text{P}^{16}\text{O}^{18}\text{O}_3$	6.1	9.2
$\text{NaH}_2\text{P}^{16}\text{O}_2^{18}\text{O}_2$	0.2	0.8

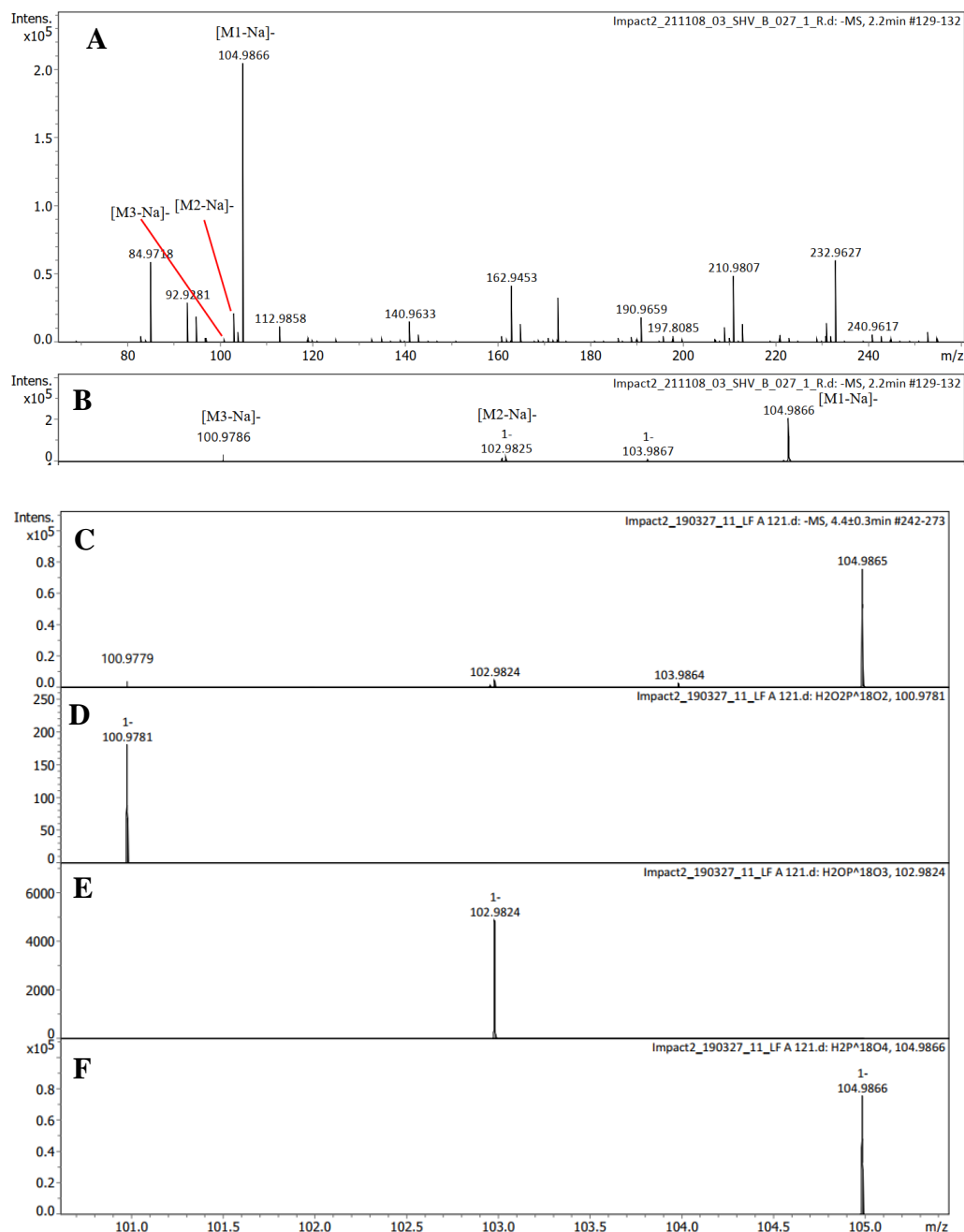


Figure 45. High-resolution negative-ion mode mass spectra of $\text{NaH}_2\text{P}^{18}\text{O}_4$. **A** – total ion spectrum (second batch). **B** – zoom into the main signal (second batch) from which the isotopolog ratios were determined (**Table 3**), m/z 104.9866 $[\text{H}_2\text{P}^{18}\text{O}_4]^-$, 102.9825 $[\text{H}_2\text{P}^{16}\text{O}_1^{18}\text{O}_3]^-$, 100.9786 $[\text{H}_2\text{P}^{16}\text{O}_2^{18}\text{O}_2]^-$. **C** – zoom into the main signal (first batch) from which the isotopolog ratios were determined (**Table 3**), m/z 104.9865 $[\text{H}_2\text{P}^{18}\text{O}_4]^-$, 102.9824 $[\text{H}_2\text{P}^{16}\text{O}_1^{18}\text{O}_3]^-$, 100.9779 $[\text{H}_2\text{P}^{16}\text{O}_2^{18}\text{O}_2]^-$. **D-F** – simulated mono-isotopic mass spectra of $[\text{H}_2\text{P}^{16}\text{O}_2^{18}\text{O}_2]^-$, $[\text{H}_2\text{P}^{16}\text{O}_1^{18}\text{O}_3]^-$ and $[\text{H}_2\text{P}^{18}\text{O}_4]^-$

4. Design of experiments

4.1. Carousel™ reactions

“Carousel™ reactions” on a scale of 0.5–1 mmol alcohol were carried out using a *Carousel 12 Plus* Reaction Station (R. B. Radley & Co Ltd) depicted in **Figure 46**. Reactions were carried out at 60, 75, and 115 °C without a reflux head or inert atmosphere, on a time scale from 0.25 to 120 hrs. The final reaction temperature was reached incrementally with a constant, moderate interdiffusion of the contents using a magnetic stirrer. All phosphorylation reactions and control experiments were carried out in 50, 100, 250 ml round-bottom flasks or in carousel glass tubes. All phosphorylation reactions under ‘dry’ (neat) conditions were in a solid or mixed solid-liquid state throughout the experiment. Control reactions under ‘wet and evaporating’ (first solubilized) conditions were initially clear aqueous solutions that eventually evaporated to reach a solid state. Stirring or swaying visibly worked only during the first 1-2 days and halted eventually owing to the mechanical resistance of the formed solid-state mixtures.



Figure 46. Radleys *Carousel 12 Plus* Reaction Station for studying the scope of prebiotic reactions

4.2. Experimental set-up for tracing stable isotopes in urea-assisted phosphorylation reactions of glycerol and racemic monopalmitoylglycerol

In order to study the mechanism of urea-assisted phosphorylation reactions of glycerol and racemic monopalmitoyl glycerol, the experimental set-up was used as shown in **Figure 47**. The installation contained the reaction mixture in a round bottom flask placed in an oil bath on an electric heating plate under steady, slow stirring. The reactor was connected to two traps by pipes under a slow argon flow (initially 1-2 bubbles every 10 seconds). Trap 1 was filled with 0.1 mM solution of benzyl chloride in dry toluene at rt. Trap 2 contained 0.1 mM solution phenyl magnesium bromide, made of a 1.6 M (PhMgBr) stock solution in cyclopentyl methyl ether and diluted with anhydrous tetrahydrofuran (THF). Trap 2 was placed in a *KGW Isotherm™* Dewar bottle with an aluminum jacket filled with acetone and dry ice at temperature between –75 and –50 °C. The Dewar was refilled every 12-16 hours with fresh dry ice. Such a condition was needed to slow down the formation of by-products from the reaction of PhMgBr with THF as well as the phenylation of benzoate to benzophenone and trityl alcohol. The argon flow allowed to push forward gases that were produced in the phosphorylation reaction. Depending on the experiment, the traps (solution and precipitate) were sampled every 1-2 days for further analyses by mass spectrometry.

Glycerol and MPG were also submitted to the same phosphorylation conditions as in the Carousel but using this time ¹³C-labeled urea and ¹⁸O-labeled sodium dihydrogen phosphate (3 to 6 mmoles of each reactant in equimolar ratio). The open reactor was connected

to a gas flow system that allowed to free the reaction mixture from all generated gases through a gentle stream of argon. The gases would bubble through a first ‘Trap 1’, containing benzoyl chloride in anhydrous toluene, to efficiently trap any nucleophiles (NH_3 , H_2O). Therein, gaseous, acidic electrophiles (CO_2 , HNCO) could perhaps reside for some time but would eventually continue to be transported to electrophiles ‘Trap 2’ containing phenyl magnesium bromide in anhydrous tetrahydrofuran always cooled to between -78 and -50 °C. All products in the reactor, Trap 1 and Trap 2 have been analysed by electrospray-ionisation (low- or high-resolution) mass spectrometry (ESI-MS) and HPLC-UV or UHPLC-ESI-MS. Extracts of the crude reaction mixtures were additionally analysed by ^1H and ^{31}P NMR spectroscopy, i.e., proton-coupled, proton-decoupled $^{31}\text{P}\{^1\text{H}\}$ and $^{31}\text{P}\text{-}^1\text{H}$ HMBC.

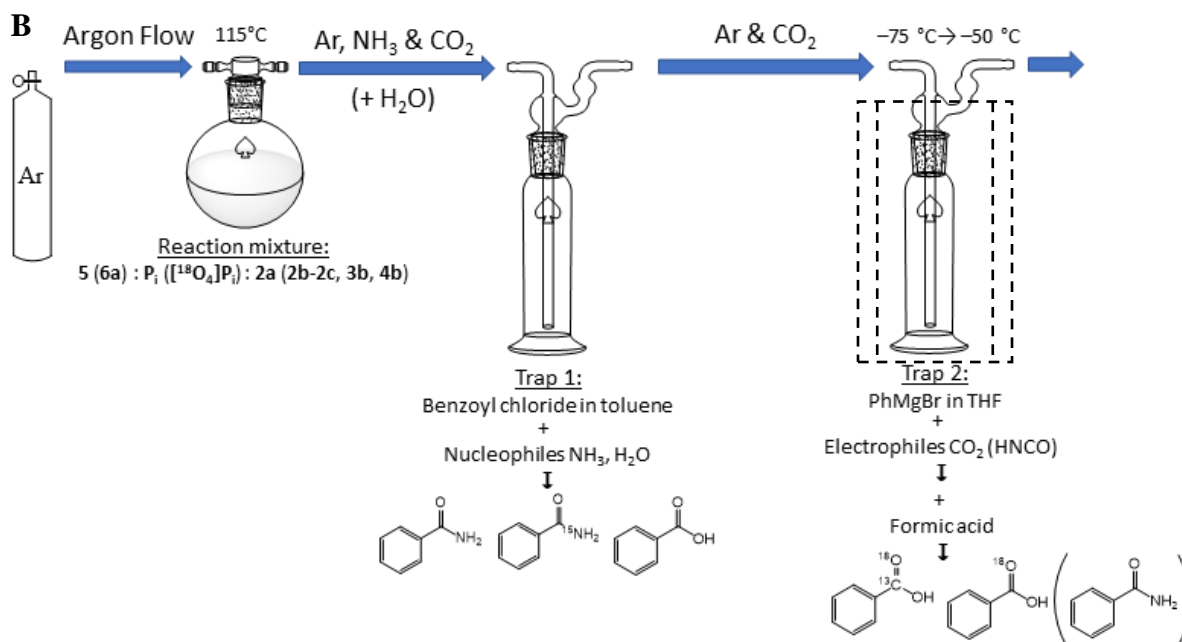


Figure 47. Experimental set-up for tracing stable isotopes in volatiles produced in prebiotic reactions. **A** – photograph of the laboratory installation. **B** – schematized set-up and expected reactions in Traps 1 and 2, in parentheses: molecules found in very low amounts (H_2O trapped as benzoic acid in Trap 1) or not at all (HNCO trapped as benzamide in Trap 2).

4.2.1. Sample preparation for MS analysis (LC-MS, LRMS, HRMS) of Trap 1 and Trap 2 contents

Analysis of Trap 1 (**Figure 47**) consisted of studying separately the solution and precipitate that accumulated by the end of the reaction. In order to collect the precipitate, all the content of trap 1 was filtered under vacuum through a fritted glass (porosity 4) and dried for at least 24 h. A fraction of the powder (1-2 mg) was dissolved in methanol (1 ml), filtered off and placed in a vial for MS analysis. Samples of the separated solution (2-3 ml filtrate) was evaporated and the residue was dissolved in methanol (1 ml) filtered off and placed in a vial for MS analysis.

For analysing the content of Trap 2 (**Figure 47**), a 1-2 ml sample was taken, usually shortly before the end of the experiment, while applying an enhanced argon flow in order to avoid CO₂ contamination from the air. The first step was to quench unreacted PhMgBr and protonate benzoate and other organic salts with an excess formic acid (1-2 ml). Then, the solution was evaporated and the residue was dissolved in MS-grade methanol (1 ml), filtered off and placed in a vial for MS analysis.

4.3. High pressure experiments

Pressure experiments were carried out in a diamond anvil cell (DAC). Tests at room temperature were conducted in a mechanically pressurised DAC (Almax-Boelher DAC) equipped with ultra-low fluorescence 600 μ m-culets anvils. For high-pressure-high temperature experiments at 115 °C, I used a gas-driven membrane DAC, to which a resistive heating ring was added. The ambient temperature was read from the thermometer placed in the experimental room. When resistive heating was applied, temperature was controlled in the external heating device, and was read on a K-type thermocouple placed at contact with the diamond anvil of the DAC cylinder. Pressure was calculated as a function of the red-shift of the R1 fluorescence line of the ruby, after temperature correction for the high temperature experiment^{282,283}.

To scale up the volume of the pressurised sample, we used a tabletop Paris-Edinburgh press.²⁸⁴ Two samples of N-cyanofornamide were pressurised to 7 GPa, at room temperature and 130 °C. The mass of the samples was about 3-5 mg and was suitable for NMR and MS analysis.

III Results and discussion

1. Identification and quantification of main reaction products

Introduction

As presented at the end of chapter **I**, there are several topics that are missing from the modern approaches to the phosphorylation reaction in the context of the origin of life study. In the experimental part of the thesis, we:

- describe the main products of alcohol phosphorylation using the example of glycerol;
- study the kinetics and mechanism of urea-assisted phosphorylation on the example of glycerol and MPG;
- explore possible varieties of phosphorylation reactions such as temperature, pressure, excess of the condensing agent urea and its possible replacements, and different phosphorus sources;
- attempt phosphorylation of other prebiotically plausible alcohols (nucleosides, pyruvic acid, dodecanol, geraniol);
- test a competitive environment of "messy" chemistry where glycerol, fatty acids and nucleosides were mixed with a condensing agent (urea or the CaNCN-methyl formate couple).

In the state-of-the-art section **3.1.2**, glycerol and its long-chain fatty acid derivatives were suggested as prebiotically plausible precursors that could be available building blocks for membrane precursors. And unlike nucleoside phosphorylation reactions, the products of the mixture of glycerol and its derivatives were not described in many details. One goal of this work is to expand our knowledge about possible phosphorylation reactions on the early Earth and glycerol or MPG phosphorylation is one of the missing pieces.

As a starting point, we chose to test phosphorylation reactions of glycerol (**5**) and racemic monopalmitoylglycerol (**6**). As a triol, we expected glycerol to be a very reactive molecule that could suggest the possibility of phosphorylation under certain conditions. The next step is a glycerol derivative MPG, more specifically, a diol containing an additional long chain of palmitic acid instead of a third OH group. This further introduces some challenges.

Given the state of the art, we chose dry and dry-evaporative conditions at an elevated temperature of 115 °C as the best avenue. For the modelling experiments described in this section, we used the carousel reactor described in section Materials and Methods **4.1**.

1.1. Urea assisted glycerol phosphorylation

Starting from the principal reaction of this work, glycerol (**5**):urea (**2a**): NaH_2PO_4 (**P_i**), we describe here the diversity and nature of the phosphorylated products of the reaction. In order to understand the main processes going on during the reaction, we chose the molar ratio of the starting molecules **5:2a:P_i** as 1:1:1, respectively. After heating these molecules for 120 hours at 115 °C we obtained a complex mixture of organic products. It was analysed by NMR spectroscopic and MS methods. For a deeper understanding of the product structures and later illuminating the reaction mechanism, we used labelled [$^{15}\text{N}_2$]urea (**2b**), [^{13}C]urea (**2c**) and $\text{NaH}_2\text{P}[^{18}\text{O}_4]$ (**[$^{18}\text{O}_4$]**P_i**) and tracked the fate of the enriched stable ^{15}N , ^{13}C and ^{18}O isotopes in some of the products. It started as a simple main signal assignment, and over three years of detailed and perceptive work with Peter Strazewski, we succeeded in presenting here one of the most advanced descriptions of phosphorylated products from a complex product mixture.**

1.1.1. Identification of the main reaction products

^1H and ^{31}P NMR and their modes are very useful tools for identifying and quantifying products. Looking at the ^1H NMR spectrum (**Figure 48**), we immediately see that there is a mixture of products present that are different from pure glycerol or urea spectra.

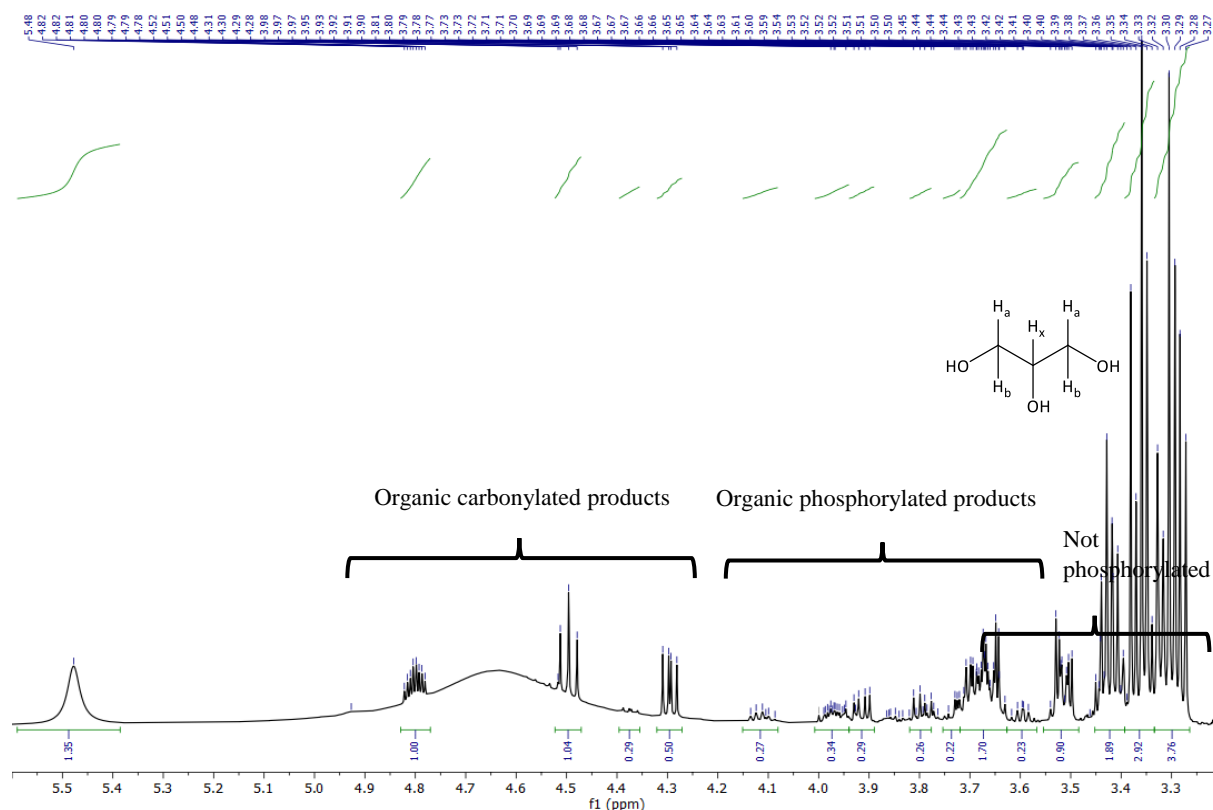


Figure 48. ^1H NMR spectrum (500 MHz) of the $\text{DMSO-}d_6$ extract of a mixture of glycerol (**5**), natural isotope abundance-urea (**2a**) and NaH_2PO_4 (**P_i**) (1:1:1, 0.5 mmol each) after heating it neat for 120 h at 115 °C.

Comparing the data of **Figure 48** with 2D spectral analyses (**Figure 50**, **Figure 52**), we conclude that ^1H signals at $\delta_{\text{H}} = 3.25\text{-}3.45$ ppm (dd δ_{Hx} , dd δ_{Hb} , dd δ_{Ha}) are protons from unreacted glycerol, $\delta_{\text{H}} = 3.60\text{-}4.20$ ppm are glyceryl protons from phosphorylated organic products and $\delta_{\text{H}} = 4.30\text{-}4.95$ ppm are protons from organic carbonylated products (carbamate or cyclic carbonate) and the intense AB part at $\delta_{\text{H}} = 3.51$ and 3.66 ppm (2 dd) is from carbonylated but not phosphorylated products (Ha' , Hb' cf. **Figure 49**).

In the spectrum **Figure 48**, the baseline between $\delta_{\text{H}} = 4.10$ and 5.20 ppm is elevated due to the NH_2 groups of urea and carbamates. The broad signal at $\delta_{\text{H}} = 5.48$ might be from OH groups. Using the MNova tool *Global Spectral Deconvolution*, we were able to extract the broad signal of the NH_2 groups of urea and glyceryl carbamates to generate spectra with a corrected baseline for the C-H signal area, which could be more reliably integrated (**Figure 49**). Comparing the (upper) ^1H NMR spectrum with the one obtained in experiments using $[^{13}\text{C}]$ urea we note in the latter a doubling of multiplicity of the signals in the range of organic carbonylated products (lower **Figure 49**). The ^1H NMR spectrum after using $[^{15}\text{N}_2]$ urea (not shown) shows the same multiplicities in this region as those of the unlabeled mixture. This confirms the presence of one ^{13}C carbonyl atom next to these protons.

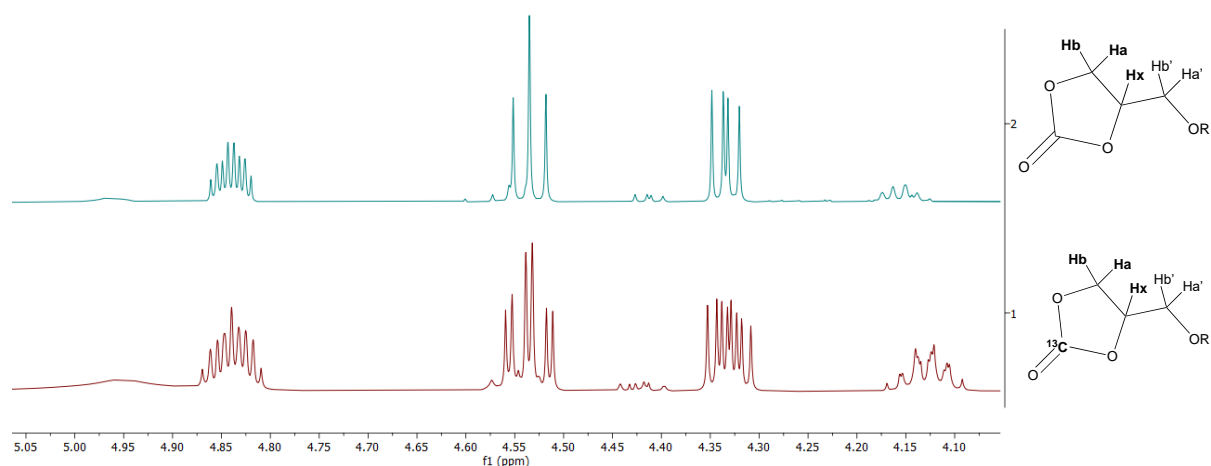


Figure 49. Zoom on baseline-flattened ^1H NMR spectra (*Global Spectra Deconvolution*, MNova) of DMSO- d_6 extracts of two 0.5 mmol scale equimolar ‘dry’ (neat) mixtures of glycerol (**5**), natural isotope abundance-urea (**2a**) or $[^{13}\text{C}]$ urea (**2c**) and NaH_2PO_4 (**P_i**) after heating at 115 °C for 120 hours. **Blue** (**5:2a:P_i** 1:1:1, **Figure 48**, 500 MHz): $\delta_{\text{H}} = 4.83$ (ddd , $J = 8.8, 6.0, 3.1$ Hz, 1H, H_x), 4.55 (t , $J = 8.4$ Hz, 1H_b), 4.33 (dd , $J = 8.1, 6.1$ Hz, 1H, H_a), 4.17-4.07 (m , 1H, H_a). **Red** (**5:2c:P_i** 1:1:1, 400 MHz): $\delta_{\text{H}} = 4.83$ (apparent tt ($dddd$), $J = 9.1, 3.1$ Hz, 1H, H_b), 4.55 (td , $J = 8.3, 2.6$ Hz, 1H, H_b), 4.33 (ddd , $J = 8.1, 5.8, 3.8$ Hz, 1H, H_a). R = H or PO_2OH .

From the COSY (**Figure 50**) we conclude that the main signals $\delta_{\text{H}} = 4.83, 4.55, 4.33, 3.51$ and 3.66 ppm belong to glyceryl-1,2-cyclic carbonate, where the resonances for H_x, H_b and H_b take 10.7 % of the total area integral in the baseline-flattened ^1H NMR spectrum, which means that this compound (H_x, H_b, H_a, H_{b'}, H_{a'}) is present in almost 18 %.

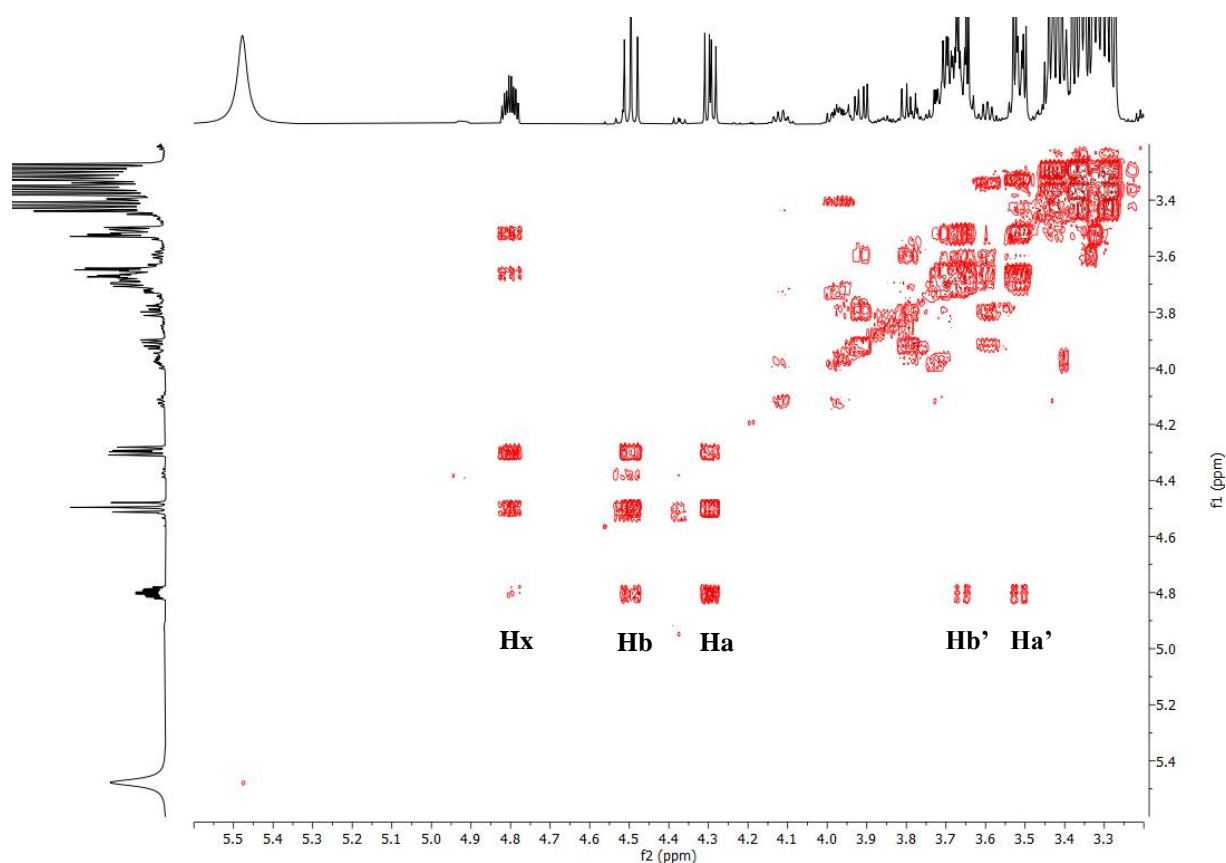


Figure 50. ^1H - ^1H COSY (500 MHz) of the DMSO- d_6 extract of a mixture of glycerol (**5**), natural isotope abundance-urea (**2a**) and NaH_2PO_4 (**P_i**) (1:1:1, 0.5 mmol each) after heating it neat for 120 h of at 115 $^\circ\text{C}$.

Although ^1H NMR can provide immense amounts of information, the most practical tool for the immediate identification and quantification of products is ^{31}P NMR. In this work; we used proton-coupled (^{31}P NMR) and proton-decoupled spectra ($^{31}\text{P}\{^1\text{H}\}$ NMR) as well as ^1H - ^{31}P HMBC. Thus, we could determine the main phosphorylated products that would be used as a standard throughout this thesis.

We studied in detail the multiplicity of the ^1H -coupled ^{31}P NMR resonances to confirm the immediate through-bond neighborships of the ^{31}P atoms. Proton-coupled triplets indicate acyclic primary phosphate esters $\text{RCH}_2\text{OP}(\text{O})_3^{-2}$, doublets indicate secondary phosphate esters $\text{R}_2\text{CHOP}(\text{O})_3^{-2}$ (**Figure 53 C**) and singlets originate from inorganic ortho- and pyrophosphates. Cyclic phosphate esters produce ^1H - ^{31}P couplings to give either a *ddd* ^{31}P multiplicity for five-membered rings or a *tt(d)* ^{31}P multiplicity for symmetrical 6-membered rings, provided that the long-range doublet can be resolved (**Figure 53 A and B**).

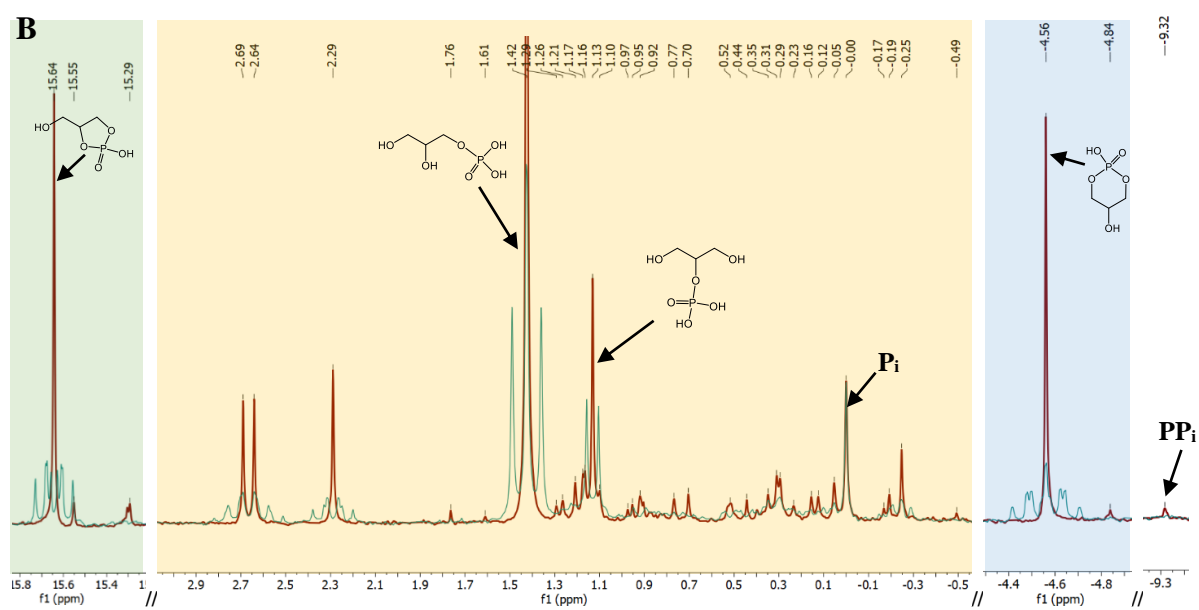
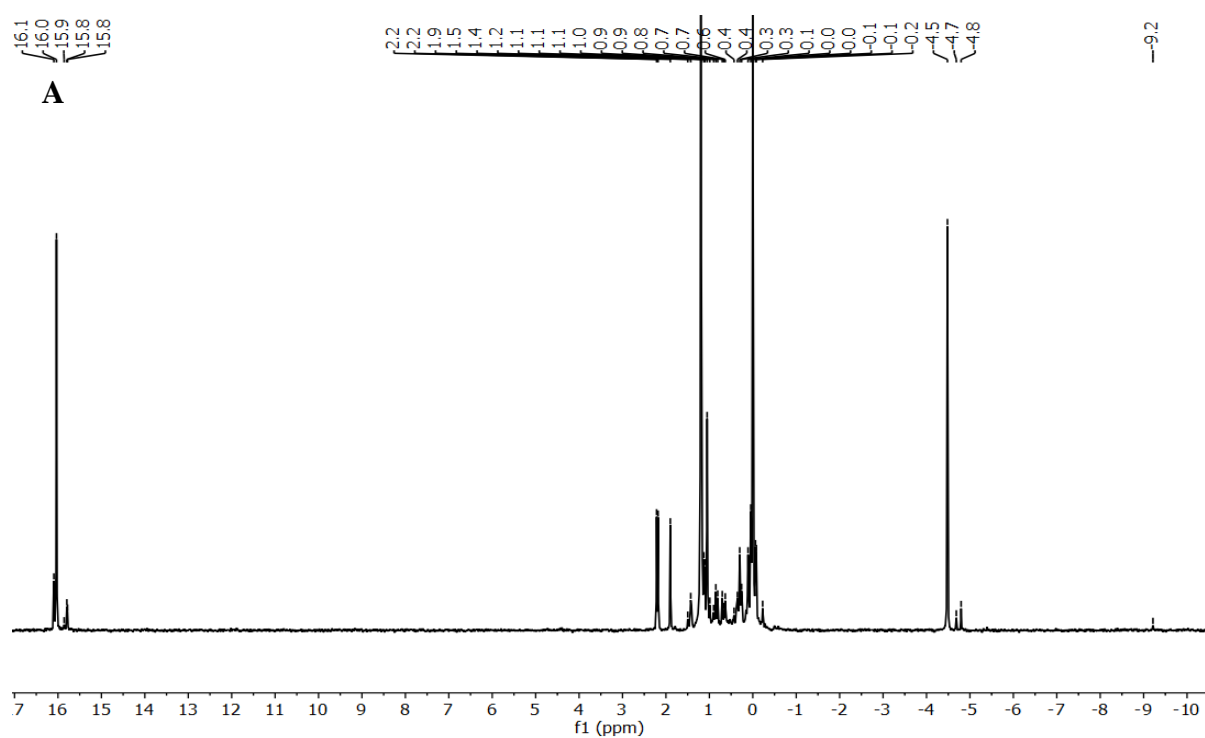


Figure 51. **A** – $^{31}\text{P}\{^1\text{H}\}$ NMR (202.5 MHz, $\text{DMSO-}d_6$) of the extract of a neat 0.5 mmol scale mixture of glycerol (**5**), natural isotope abundance-urea (**2a**) and NaH_2PO_4 (**P_i**) (1:1:1) after 120 h of heating at 115 °C. **B** – excerpts of **A** (red) superimposed with ^1H -coupled ^{31}P NMR spectrum (turquoise blue) of the same mixture. Pale green, ochre and pale blue zones as in **Figure 52**.

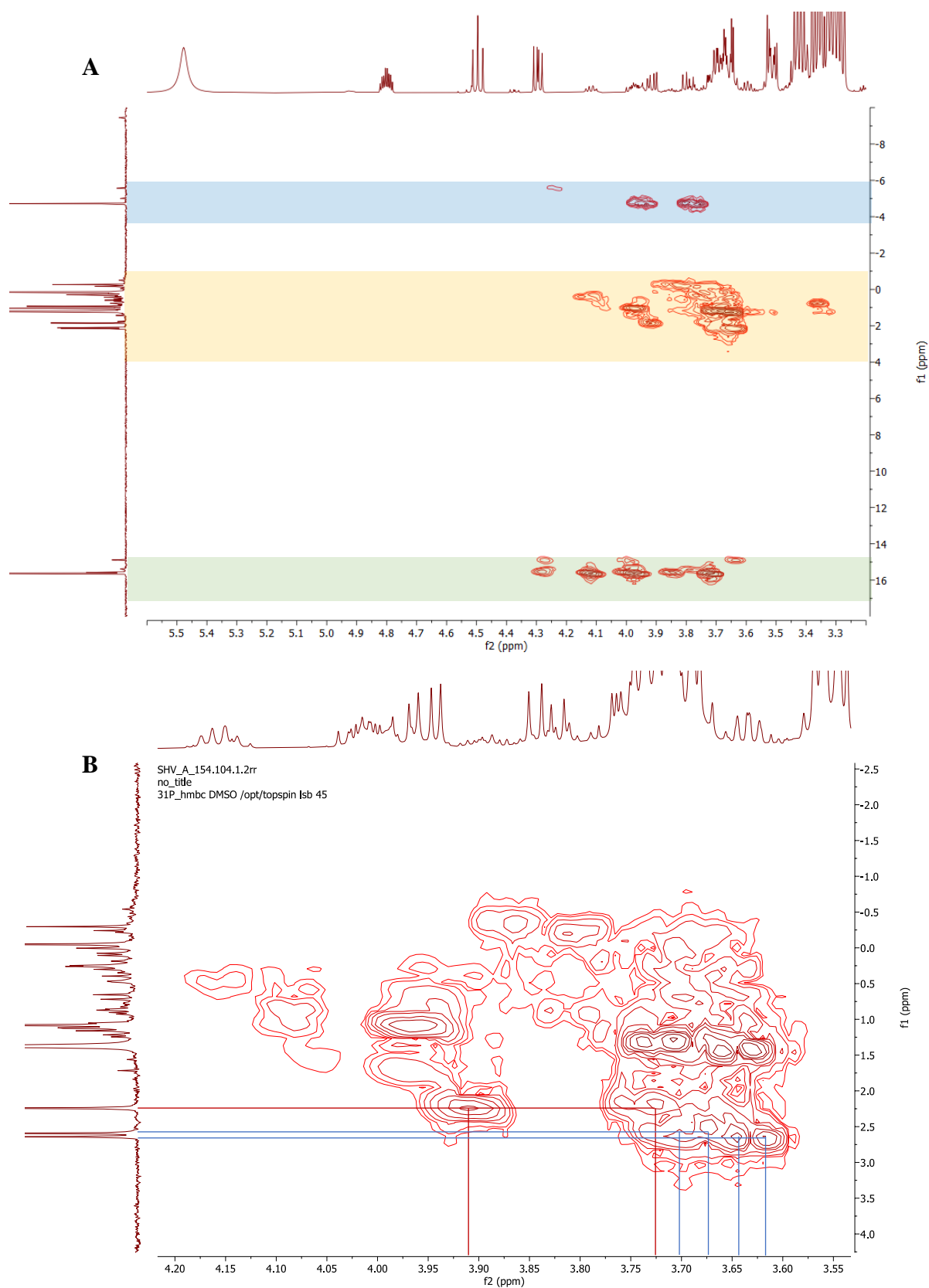


Figure 52. ^1H - ^{31}P HMBC spectrum (500 MHz for ^1H : horizontal axis, baseline-flattened, 202.5 MHz for $^{31}\text{P}\{^1\text{H}\}$: vertical axis) of the DMSO- d_6 extract of a neat 0.5 mmol scale mixture of glycerol (**5**), natural isotope abundance-urea (**2a**) and NaH_2PO_4 (**Pi**) (1:1:1 molar ratios) after 120 h of heating at 115 $^\circ\text{C}$. Correlation of signals ^1H and ^{31}P seen as cross-spots representing organic products in the reaction mixture. **A** – All ^{31}P signals. **B** – Acyclic organic phosphate esters.

Following these ^1H -coupled ^{31}P multiplicities, the observed organic and inorganic products can be divided into several groups: the signal at $\delta_{\text{P}_i} = 0.00$ ppm is due to inorganic ortho-phosphate PO_4^{-3} (**P_i**) as a residual part of the initial phosphorus source that remained unreacted and $\delta_{\text{PP}_i} = -9.32$ ppm is inorganic pyrophosphate $\text{P}_2\text{O}_7^{-4}$ (**PP_i**) as a by-product of the reaction. Non-terminal polyphosphate (**P_{ni}**) signals appear as ^1H -decoupled $^{31}\text{P}\{^1\text{H}\}$ triplets at -18 to -30 ppm, the corresponding terminal signals as $^{31}\text{P}\{^1\text{H}\}$ doublets at -8 to -12 ppm, both are rarely observed, mostly in nucleoside phosphorylation in water. The exact chemical shifts δ_{P_i} , δ_{PP_i} and $\delta_{\text{P}_{ni}}$ depend on the proton concentration of the solution, the more basic the more deshielded: δ_{P_i} mono-basic (around -0.4 ppm) < di-basic < tri-basic (up to $+3.4$ ppm). Organic products such as cyclic organic 5-membered ring phosphates (**5cGIP**) $\delta_{5\text{-mr}} = 12\text{-}20$ ppm (pale green zone), 6-membered rings (**6cGIP**) $\delta_{6\text{-mr}} = -4$ to -7 ppm (pale blue zone) and acyclic mono- (**GI-1P** and **GI-2P**) usually resonate at $\delta_{\text{acyclic}} = -1$ to $+2$ ppm (ochre zone). Conferring to $^{31}\text{P}\{^1\text{H}\}$ signals of mixtures containing dinucleoside phosphodiester (**Figure 51**), those of diglycerol phosphodiester (**[GI]₂P**) could be tentatively expected to resonate at higher field of this range, however, neither ^1H -coupled ^{31}P signals (turquoise line spectrum in **Figure 52**) nor ^{31}P DOSY spectra (not shown) were conclusive at this stage.

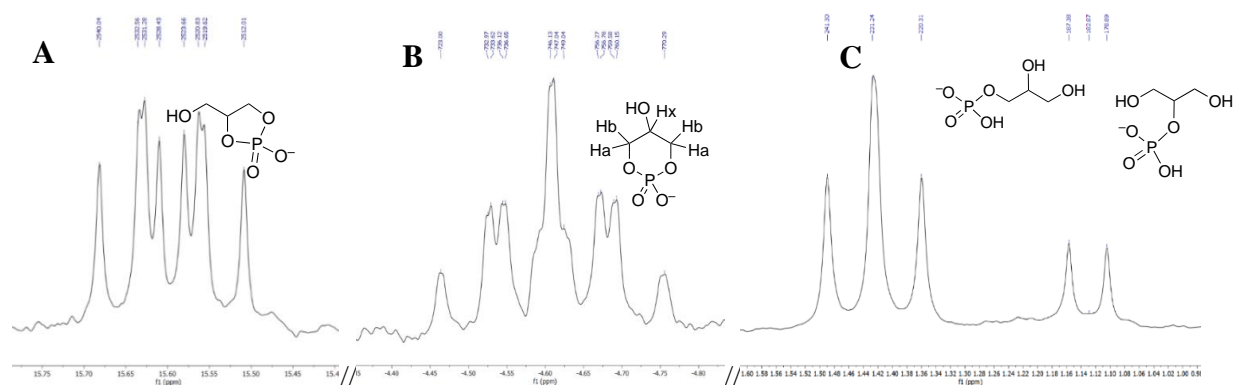


Figure 53. ^{31}P NMR spectra (^1H -coupled, 202.5 MHz, $\text{DMSO-}d_6$), selected signals from **Figure 51** of the extract of a 0.5 mmol scale mixture of glycerol (**5**), natural isotope abundance-urea (**2a**) and NaH_2PO_4 (**P_i**) (1:1:1) after 120 h of heating at 115°C .

A – zoom of the 5-membered ring cyclic phosphate; $\delta_{\text{P}} = 15.64$ ppm (*ddd*, $^3J_{\text{H,P}} = 11.6$ Hz, $^3J_{\text{H,P}} = 8.7$ Hz, $^3J_{\text{H,P}} = 7.6$ Hz).

B – zoom on 6-membered ring cyclic phosphate; $\delta_{\text{P}} = -4.56$ ppm (*ttd*, $^3J_{\text{Ha,P}} = 13.4$ Hz, $^3J_{\text{Hb,P}} = 10.2$ Hz, $^4J_{\text{Hx,P}} = 0.7$ Hz).

C – zoom on acyclic org. phosphates (1.60-0.9 ppm); δ_{P} (**GI1P**) = 1.43 (*t*, $^3J_{\text{H,P}} = 10.6$ Hz), δ_{P} (**G2P**) = 1.13 (*d*, $^3J_{\text{H,P}} = 8.5$ Hz).

1.1.2. Two persistent organic phosphorylated and carbonylated minor reaction products

Aside from the well-known and expected phosphorylated products, described in the previous section, we found two new persistent signals in all $\text{DMSO-}d_6$ solutions containing urea-assisted phosphorylation mixtures of glycerol. We have unfailingly observed other ^{31}P resonances, never observed as such in D_2O nor in $\text{DMSO-}d_6$ extracts of phosphorylation of glycerol in the absence of urea.

These resonances are shifted downfield with respect to all other acyclic product ^{31}P signals. They belong to two phosphorylated compounds, appear in changing concentrations and precise shapes as a function of reaction time and show complex multiplicities in their proton-coupled ^{31}P signals (**Figure 51**). One such glyceryl phosphate produces in proton-decoupled $^{31}\text{P}\{^1\text{H}\}$ NMR spectra two quite strongly deshielded peaks ($\delta_{\text{P}} = 2.35\text{-}2.45$ ppm) that seem to be a ^{31}P - ^{31}P doublet but are in fact two singlets.

We have discovered in different experiments (different batches, different reaction time periods) that not only their chemical shift varied with respect to that of P_i , which was expected from slight differences in pH (proton abundance), but also the difference in their relative chemical shifts $\Delta\delta_{\text{P}}$ varied as well (see **Figure 54A**). However, the ratio of their proton-decoupled $^{31}\text{P}\{^1\text{H}\}$ signal areas was exactly 1:1 in all cases (**Figure 54 A**). In proton-coupled ^{31}P NMR spectra they split into two quintets (2 *quint*) with the same coupling constant each or, when the $\Delta\delta_{\text{P}}$ happened to equal their coupling constant, they appear as an apparent sextet (**Figure 54 B and C**). The other deshielded phosphorylated glyceryl derivative resonates as an ordinary $^{31}\text{P}\{^1\text{H}\}$ singlet, always slightly more shielded than the double-resonance ($\delta_{\text{P}} = 2.0\text{-}2.2$ ppm), and is in all fully coupled ^{31}P NMR spectra a doublet of triplets (*dt*) or it coalesces into an apparent quartet (**Figure 54 B and D**).

Noteworthy is that the fully coupled ^{31}P resonance patterns for both compounds differ in their appearance depending on whether we used for the phosphorylation experiment natural isotope abundance-urea, ^{13}C urea or $^{15}\text{N}_2$ urea. The most marked differences were observed when ^{13}C urea was added, at lower field strength best visible in the more upfield signal (being a ^1H -decoupled singlet, lines **1-2** in **Figure 54 B**) and at slightly higher field strength best visible in the more downfield signal (resonating at two frequencies in the ^1H -decoupled spectrum, lines **1** and **3**, **Figure 54 B**). Minute barely significant differences are also observable in both signals when $^{15}\text{N}_2$ urea was used (lines **1, 4, 5** **Figure 54 B**). We ascribed those to the ^{15}N isotope effect either of carbamoyl groups (if present) or ammonium ions, i.e., the volatile counter cations of the organic phosphates, the other one being Na^+ .

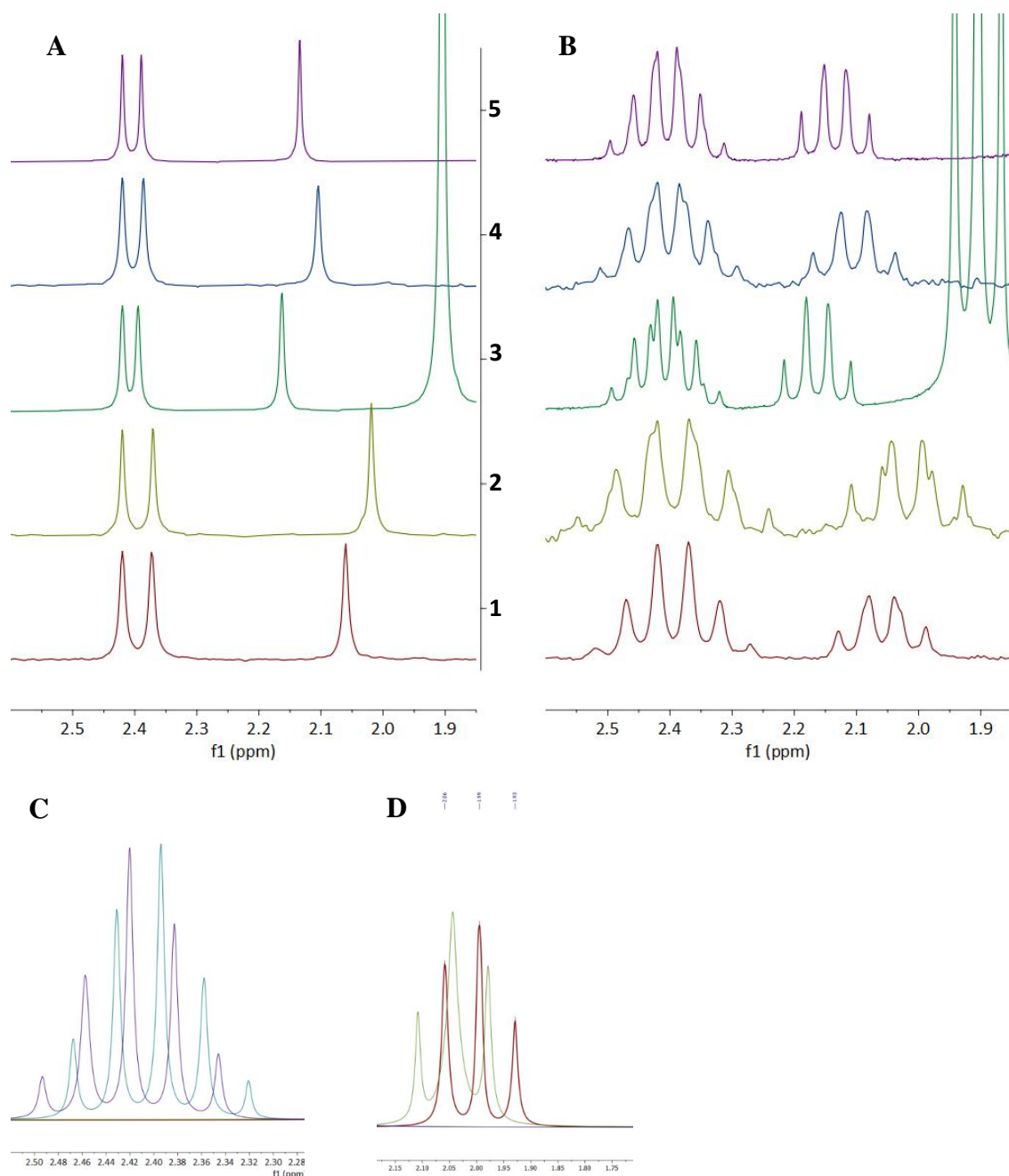


Figure 54. ^{31}P NMR spectra in $\text{DMSO-}d_6$, selected signals ($\delta_{\text{P}} = 2.7\text{-}1.7$, cf. **Figure 51**) at 202.5 MHz and 242.9 MHz. The stacked spectra are aligned on the peak maximum of the most downfield quintet ($\delta_{\text{P}} = 2.42$).

A – $^{31}\text{P}\{^1\text{H}\}$ NMR (^1H -decoupled); **B** – ^{31}P NMR (fully coupled);

C – Deconvoluted 2 *quint* from **B** line 3; **D** – Deconvoluted *dt* from **B** line 2.

Line 1 – unlabelled (202.5 MHz, $\text{DMSO-}d_6$): **5:2a:P_i** (1:1:1, 30 mmol each): $\delta_{\text{P}} = 2.42, 2.37$ (2 *quint*, $^3J_{\text{H,P}} = 9.5$ Hz each), 2.06 (*dt*, $^3J_{\text{H,P}} = 8.7, 9.7$ Hz). **Line 2** – ^{13}C -labelled: (202.5 MHz, $\text{DMSO-}d_6$): **5:2c:P_i** (1:1:1, 3 mmol each): $\delta_{\text{P}} = 2.42, 2.37$ (2 *quint*, $^3J_{\text{H,P}} = 10.3$ Hz each), 2.02 (*dt*, $^3J_{\text{H,P}} = 10.2, 8.1$ Hz). **Line 3** – ^{13}C -labelled: (242.9 MHz, $\text{DMSO-}d_6$): **5:2c:P_i** (1:1:1, 1 mmol each): $\delta_{\text{P}} = 2.42, 2.39$ (2 *quint*, $^3J_{\text{H,P}} = 8.9$ Hz each), 2.16 (*dt*, $^3J_{\text{H,P}} = 8.8, 8.5$ Hz). **Line 4** – ^{15}N -half labelled, half unlabelled: (202.5 MHz, $\text{DMSO-}d_6$) **5:2a:2b:P_i** (1:0.5:0.5:1, 1 mmol each): $\delta_{\text{P}} = 2.42, 2.39$ (2 *quint*, $^3J_{\text{H,P}} = 9.3$ Hz each), 2.10 (*dt*, $^3J_{\text{H,P}} = 9.0, 8.5$ Hz). **Line 5** – ^{15}N -labelled: (242.9 MHz, $\text{DMSO-}d_6$) **5:2b:P_i** (1:1:1, 1 mmol each), $\delta_{\text{P}} = 2.42, 2.39$ (2 *quint*, $^3J_{\text{H,P}} = 9.2$ Hz each), 2.13 (*dt*, $^3J_{\text{H,P}} = 9.0, 8.5$ Hz).

This meant that these minor compounds contained a carbonyl function in both molecules, apart from a phosphate group. A chemical explanation could be the presence of carbamates or cyclic carbonates in the acyclic glyceryl phosphate molecules. For confirmation, we conducted an experiment on commercial glyceryl phosphate (**5a**) with urea (**2a**) in the absence and presence of inorganic phosphate (**Figure 55**).

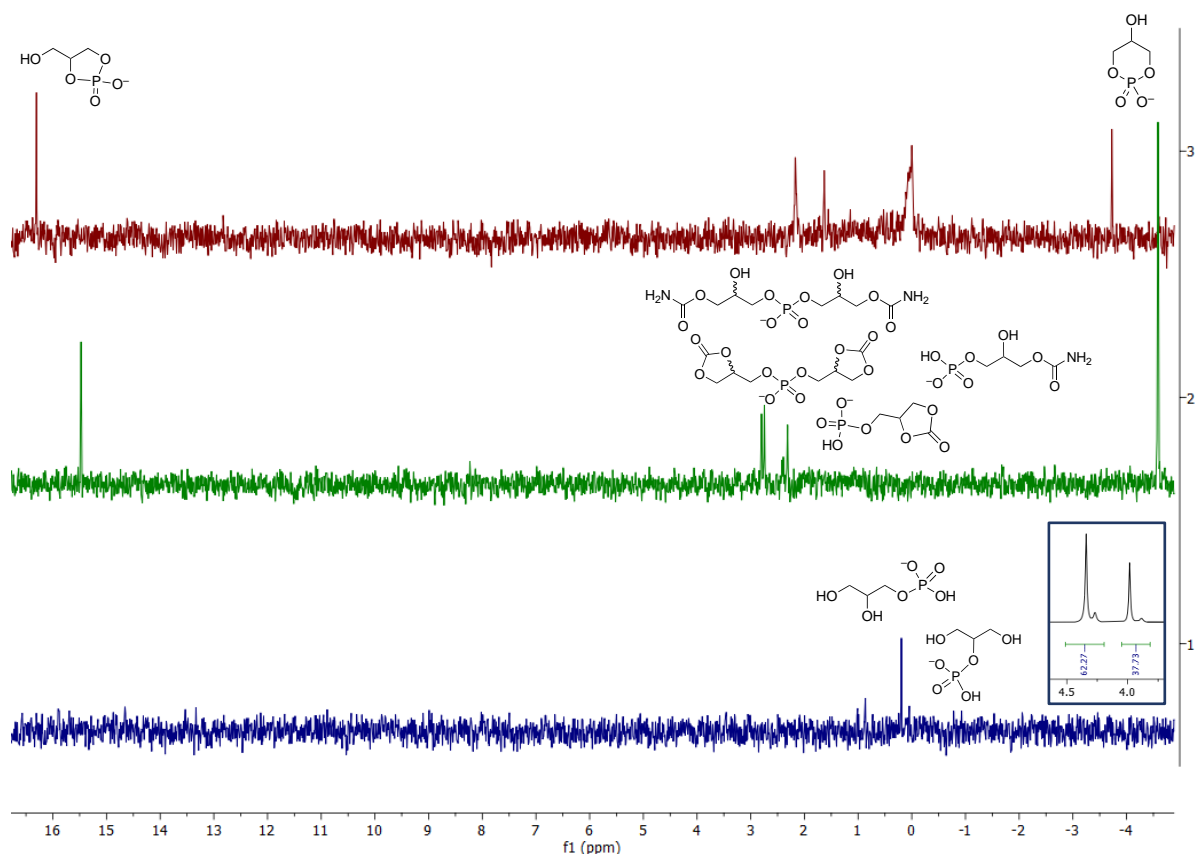


Figure 55. $^{31}\text{P}\{^1\text{H}\}$ NMR (202.5 MHz, $\text{DMSO-}d_6$) of the extract of 0.5 mmol scale mixture of:
1 – reference spectrum in $\text{DMSO-}d_6$ of commercial glyceryl phosphate (**5a**) without heating (insert: same in D_2O);
2 – glyceryl phosphate (**5a**) : natural isotope abundance-urea (**2a**) (1:1) after 96 hours of heating neat at $115\text{ }^\circ\text{C}$;
3 – glyceryl phosphate (**5a**): natural isotope abundance-urea (**2a**): NaH_2PO_4 (1:1:1) after 96 hours of heating at $115\text{ }^\circ\text{C}$.

Line 1 in **Figure 55** shows the $^{31}\text{P}\{^1\text{H}\}$ NMR reference spectrum of the starting molecules **5a** in $\text{DMSO-}d_6$. A better spectrum was obtained in D_2O , revealing a 63:37 ratio for glyceryl-1- and glyceryl-2-phosphates by peak area integration (see insert).

After heating a neat equimolar mixture of **5a** and urea for 4 days at $115\text{ }^\circ\text{C}$, the $\text{DMSO-}d_6$ extract showed in the $^{31}\text{P}\{^1\text{H}\}$ NMR spectrum that the starting molecules were absent. Instead, 15.9 % 5-membered ring cyclophosphate ($\delta_{\text{P}} = 15.5\text{ ppm}$) was observed, which could have cyclized from both **5a** isomers, and 53.5 % 6-membered ring cyclophosphate ($\delta_{\text{P}} = -4.6\text{ ppm}$), which could cyclize only from glyceryl-1-phosphate (lane 2 of **Figure 55**). In addition, more than three resonances appeared in between those of the cyclic phosphates, quite strongly downfield between 2.2 and 3.0 ppm. These are likely due to the carbamylation and/or

carbonylation of the glyceryl phosphates **5a**. We assign (see later for the justification) the double-resonances at the downfield-end of the acyclic phosphate region ($\delta_P = 2.9$ - 2.4 ppm) to diastereoisomeric dicarbonyl and/or dicarbamoyl diglyceryl phosphate diesters (17.6 %, double-resonance at $\delta_P \approx 2.9$) and the single resonance to 1,2-cyclic carbonyl or 1-carbamoylglycerol-3-phosphate or other acyclic phosphates (14.0 % at $\delta_P \approx 2.45$).

In line 3 of **Figure 55**, the broad peak at 0 ppm (53.1%) is due to unreacted inorganic phosphate **P_i** encompassing the signal of unreacted **5a**. The main organic products are 9.6 % 5-membered ring cyclophosphate ($\delta_P = 16.3$ ppm), 8.7 % 6-membered ring cyclophosphate ($\delta_P = -3.5$ ppm) and two signals in the normal acyclic glyceryl phosphate region (28.4 % at $\delta_P \approx 2.2$ - 1.5 ppm). In the presence of **P_i** added to **5a** and urea, the above mentioned double-resonances were not detected.

Subsequently, the solution from spectrum 2 of **Figure 55** was heated to 40 and 60°C, in order to observe the temperature effect on the ^{31}P NMR signals, and then D_2O was added (**Figure 56**). The spectra 1-3 of **Figure 56** show that, upon heating, the signal width and the difference in the chemical shift $\Delta\delta_P$ of the double-resonances became smaller (★major at 3.15-3.00 ppm, minor: see arrows). In the presence of 10 % v/v D_2O in $\text{DMSO-}d_6$ the double-resonance coalesced. In a similar experiment as shown in spectrum **A** of **Figure 51**, obtained after heating a neat equimolar mixture of glycerol (**5**), natural isotope abundance-urea (**2a**) and NaH_2PO_4 (1:1:1) for 120 hours at 115 °C, we diluted a 0.5 ml- $\text{DMSO-}d_6$ extract with 0.5 ml D_2O and the same coalescence of the corresponding signals, that is, of the double-resonance at $\delta_P = 2.64$ and 2.69 ppm in **Figure 51**, was observed (not shown).

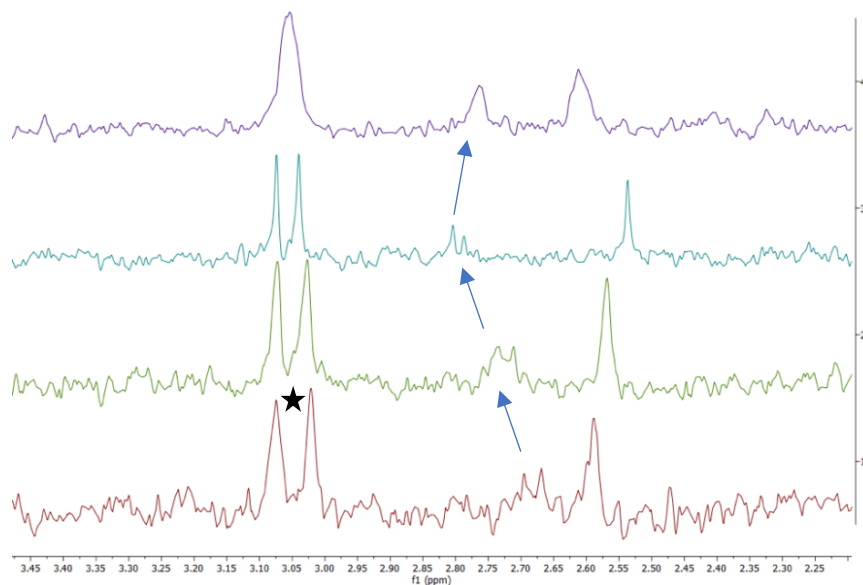
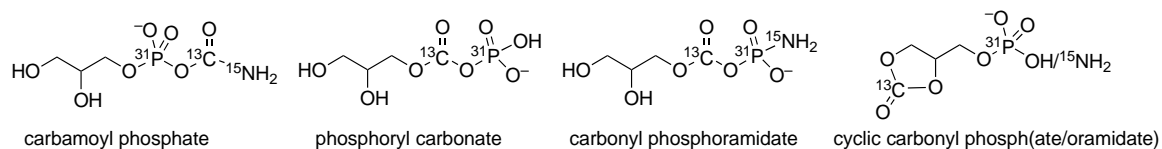


Figure 56. Stacked $^{31}\text{P}\{^1\text{H}\}$ NMR spectra at 202.5 MHz of selected signals at 2.2-3.5 ppm from spectrum 2 of **Figure 55** ($\text{DMSO-}d_6$) of the experiment crude mixture starting from commercial glyceryl phosphate (**5a**) and natural isotope abundance-urea (**2a**) (1:1) after 96 h of heating at 115 °C. The spectra are aligned on the most downfield peak at $\delta_P = 3.07$ of the larger double-resonance (star). Lane 1: spectrum made at room temperature. Lane 2: spectrum made at 40°C. Lane 3: spectrum made at 60°C. Lane 4: spectrum made at room temperature after adding 0.1 ml of D_2O to the stock solution ($\text{DMSO-}d_6 : \text{D}_2\text{O} \approx 9:1$ v/v). The arrows indicate the minor double-resonance.

1.1.3. Proton-decoupled heteronuclear multiple-bond correlation and J-modulation ^{13}C nuclear magnetic resonance spectroscopies

For a better understanding of the molecular structure of these minor phosphoglycerol carbonyl compounds, as they were recurrently produced in all urea-assisted glycerol phosphorylations under ‘dry’ conditions, we analysed the DMSO-*d*₆ extracts by NMR spectroscopy equipped with a quadruple resonance inverse cryoprobe (*QCI*).

In principle, the carbonyl group could either be attached to an oxygen atom of the glycerol backbone or directly bound to the phosphate group, which would imply the formation of carbamoyl phosphates or phosphoryl carbonates. Yet another possibility would be the formation of carbonyl phosphoramidates bearing a cyclic carbonate elsewhere in the molecule. These possibilities can be distinguished by using labelled urea and measuring any ^{1-3}J couplings in the reaction mixture and any correlation between ^{31}P , ^{15}N and ^{13}C by means of proton-decoupled $\{^1\text{H}\}$ HMBC spectroscopy.



DMSO-*d*₆ extracts of neat equimolar reaction mixtures containing glycerol (**5**), ^{13}C urea (**2b**) or $^{15}\text{N}_2$ urea (**2c**) and inorganic phosphate (**Pi**), that have been heated for 96 hours at 115 °C, have failed to give evidence for the presence of carbamoyl phosphates, phosphoryl carbonates or phosphoramidates: neither ^{13}C - ^{31}P couplings nor 2D correlations of resonances in the carbonyl ^{13}C frequency range were found whatsoever, and no ^{15}N - ^{31}P correlations either (not shown). All ^{13}C - ^{31}P couplings found through $^{13}\text{C}\{^{31}\text{P}\}$ decouplings and all heteronuclear cross correlations that have been observed between these nuclei by $\{^1\text{H}\}$ HMBC spectroscopy were those between non-carbonyl (glycerol) ^{13}C and ^{31}P nuclei (**Figure 57**).

A JMOD ^{13}C NMR spectrum allows us to confirm the structure and position of phosphorus in the molecule. At a ^{13}C field strength of 150.9 MHz (600 MHz for ^1H), ^{13}C signals that couple with a ^{31}P nucleus (> 1.5 Hz) appear as ^{13}C -doublets. In the ^1H -decoupled HMBC spectrum, we see short range ($^2\text{J}_{\text{C,P}}$) and longer range ($^3\text{J}_{\text{C,P}}$) correlations of carbon atoms of the glycerol part with phosphate groups. Thus, the display of JMOD ^{13}C NMR spectra of the glycerol carbon atoms allowed for the elucidation of the structures of both carbonylated phosphoglycerol products (**Figure 57 B**).

The $^{31}\text{P}\{^1\text{H}\}$ - $^{13}\text{C}\{^1\text{H}\}$ HMBC spectra taken at $\text{J}_{\text{C,P}} = 5$ Hz showed clearly the expected correlations for the 5-membered-ring glycerol cyclic phosphate: $\delta_{\text{P}} = 15.9$ with $\delta_{\text{C}} = 63.00$ ppm (*d*, $^2\text{J}_{\text{C,P}} = 4.8$ Hz, CH_2), $\delta_{\text{C}} = 65.46$ ppm (br *s*, $^3\text{J}_{\text{C,P}} < 1.5$ Hz, CH_2) and $\delta_{\text{C}} = 75.22$ ppm (br *s*, $^3\text{J}_{\text{C,P}} < 1.5$ Hz, CH), and the 6-membered-ring glycerol cyclic phosphate (**5cGIP** and **6cGIP**, cf. **Figure 57 A**): $\delta_{\text{P}} = -4.7$ with $\delta_{\text{C}} = 64.04$ ppm (*d*, $^2\text{J}_{\text{C,P}} = 4.8$ Hz, CH) and $\delta_{\text{C}} = 70.09$ ppm (*d*, $^3\text{J}_{\text{C,P}} = 5.7$ Hz, CH_2). The known acyclic glycerol phosphates could be more readily identified at $\text{J}_{\text{C,P}} = 10$ Hz. The $^{31}\text{P}\{^1\text{H}\}$ resonance at $\delta_{\text{P}} = 1.12$ ppm (triplet in proton-coupled ^{31}P) correlates with $\delta_{\text{C}} = 66.40$ ppm (*d*, $^2\text{J}_{\text{C,P}} = 5.4$ Hz, CH_2) and $\delta_{\text{C}} = 71.87$ ppm (*d*, $^3\text{J}_{\text{C,P}} = 5.3$ Hz, CH) which

is correct for glyceryl-1-phosphate. The smaller $^{31}\text{P}\{^1\text{H}\}$ resonance at $\delta_{\text{P}} = 1.03$ ppm (doublet in proton-coupled ^{31}P) correlates with $\delta_{\text{C}} = 63.03$ ppm (d , $^2\text{J}_{\text{C,P}} = 4.8$ Hz, CH_2) and $\delta_{\text{C}} = 76.87$ ppm (d , $^3\text{J}_{\text{C,P}} = 4.9$ Hz, CH) as expected from glyceryl-2-phosphate (both abbreviated **GIP**, cf. **Figure 57 B**).

In the same HMBC spectrum, the $^{31}\text{P}\{^1\text{H}\}$ single-resonance at $\delta_{\text{P}} = 1.38$ ppm (2.29 ppm in **Figure 51**, between 2.0 and 2.2 ppm in **Figure 54 A**) correlates with two different glyceryl moieties, so we should expect an asymmetric acyclic phosphodiester. This is consistent with the multiplicity of the ^1H -coupled ^{31}P resonance: a doublet of triplets at 202.5 MHz or a quartet at 242.9 MHz (dt or q , cf. **Figure 54 B**), and the ^1H - ^{31}P HMBC spectrum (red-brown correlation lines in **Figure 52**) indicating the connection of the phosphate with a secondary ($\delta_{\text{H}} \approx 3.91$ ppm) and a primary ($\delta_{\text{H}} \approx 3.72$ ppm) alcohol oxygen atom. The ^{13}C chemical shifts of one glyceryl residue: $\delta_{\text{C}} = 66.82$ ppm (d , $^2\text{J}_{\text{C,P}} = 5.7$ Hz, CH_2) and $\delta_{\text{C}} = 71.84$ ppm (d , $^3\text{J}_{\text{C,P}} = 5.2$ Hz, CH), are similar to those of 1-glyceryl phosphate and those of the other glyceryl residue: $\delta_{\text{C}} = 63.06$ ppm (d , $^3\text{J}_{\text{C,P}} = 4.2$ Hz, CH_2) and $\delta_{\text{C}} = 77.48$ ppm (d , $^2\text{J}_{\text{C,P}} = 5.1$ Hz, CH), resemble 2-glyceryl phosphate, although both carbon atoms that are closer to the phosphate ($^2\text{J}_{\text{C,P}}$ doublets) are much downfield-shifted when compared to the main glyceryl phosphates, by $\Delta\delta_{\text{CH}_2} = 0.42$.

Taken together and keeping in mind that the ^1H -coupled ^{31}P dt and q multiplicities are not visibly influenced by the presence of ^{15}N isotopes (**Figure 54 B** lines 1, 4 and 5) but strongly by the presence of ^{13}C carbonyls (**Figure 54 B** lines 1, 2 and 3), this molecule most likely is 1,3-dihydroxypropan-2-yl ((2-oxo-1,3-dioxolan-4-yl)methyl) phosphate or, in more descriptive words, a 5-membered ring 1,2-cyclic carbonate of a diglyceryl phosphodiester, one glyceryl of which is linked through the secondary and the other through the primary position (**diGICOP**, cf. **Figure 57 B**). The mono-anionic mass peak $m/z = 271.0224$ Dalton is indeed present in the negative ion mode mass spectrum of the methanolic extract of the unlabelled sample (**Figure 59**) and the signature of 1,2-cyclic carbonates is visible in the ^1H NMR spectrum of the mixture (**Figure 48**, **Figure 49**). The other 6-membered ring isomer (1,3-cyclic carbonate) or the variant containing two cyclic 1,2- and 1,3-carbonates cannot be categorically excluded; however, any acyclic carbonate (containing one to three carbonic acid monoester groups) seems too prone to decarboxylate after many days at 115 °C, and no MS evidence supports any of these alternatives.

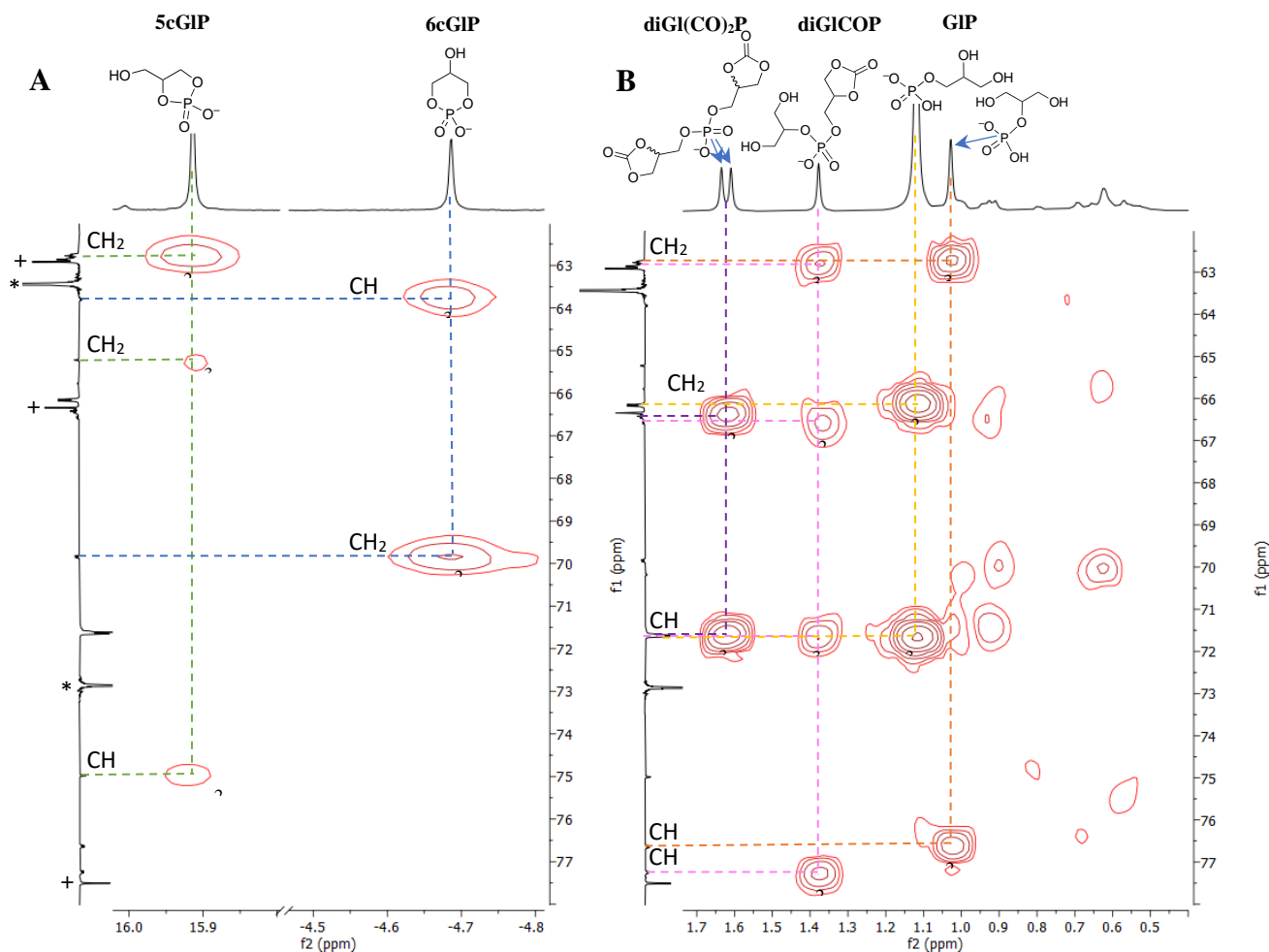


Figure 57. $^{31}\text{P}\{^1\text{H}\}\text{-}^{13}\text{C}\{^1\text{H}\}$ HMBC spectra (242.9 MHz for $^{31}\text{P}\{^1\text{H}\}$ [horizontal axis], 150.9 MHz for ^{13}C [vertical axis, JMOD], DMSO-*d*₆) of the extract from a neat mixture of glycerol (**5**), [^{13}C]urea (**2c**) and NaH_2PO_4 (**P_i**) (1:1:1, 0.5 mmol each) after heating for 96 hours at 115 °C. **A** – ^{13}C -middle field (62-78 ppm)/ ^{31}P -low-field (15.8-16.0 ppm) and high-field (–4.5 to –4.8 ppm) excerpts of HMBC taken at $J_{\text{C,P}} = 5$ Hz; * = glycerol; + = glyceryl-1,2-cyclic carbonate. **B** – ^{13}C -middle field (62-78 ppm)/ ^{31}P -middle-field (0.4-1.7 ppm) excerpt of HMBC taken at $J_{\text{C,P}} = 10$ Hz.

The correlation of ^{13}C and ^{31}P signals appears as cross-spots through 2-3 consecutive chemical bonds ($^{2-3}J_{\text{C,P}}$) in the molecules produced during the urea-assisted phosphorylation reaction. The C-P coupling ranges (2J or 3J) indicated on cross-spots are consistent with the multiplicity and coupling constants $J_{\text{H,P}}$ of the corresponding ^1H -coupled ^{31}P NMR resonances (**Figure 52** and **Figure 53C**).

Following the same pattern, we conclude that the $^{31}\text{P}\{^1\text{H}\}$ double-resonance at (here) $\delta_{\text{P}} = 1.63$ and 1.61 ppm (2.69 and 2.64 ppm in **Figure 51**, around 2.4 ppm in **Figure 54 A**) is due to an acyclic phosphate ester group linked to the primary position of glycerol, thus correlating with a $^{13}\text{C}\{^{31}\text{P}\}$ double-resonance at $\delta_{\text{C}} = 66.64$ and 66.68 ppm (2 *d*, $^2J_{\text{C,P}} = 5.7$ Hz each, 2 x CH_2) and with $\delta_{\text{C}} = 71.84$ (*d*, $^3J_{\text{C,P}} = 5.3$ Hz, CH). The ^1H - ^{31}P HMBC spectrum shows the connection of the phosphate with a primary alcohol only (^{31}P correlation with $\delta_{\text{H}} = 3.60$ -3.65 ppm, cf. **Figure 52B**). The fact that each $^{31}\text{P}\{^1\text{H}\}$ signal splits into a ^1H -coupled quintet (2 x *quint* around $\delta_{\text{P}} = 2.4$ ppm in **Figure 54 B**) means there are four magnetically equivalent protons in the vicinity of the ^{31}P nucleus, indicating the connection of the phosphate with two primary alcohol oxygen atoms. The shift in coupling pattern of the corresponding ^1H -coupled ^{31}P resonances in the absence or presence of ^{13}C -labelled atoms from [^{13}C]urea indicates the

presence of a carbonyl group in this molecule (lines 1 and 3 in **Figure 54 B**). However, the ^{31}P downfield shift of 0.2-0.4 ppm with respect to the aforementioned 1,2-cyclic carbonate **diGICOP** (**Figure 54 A**) suggests the presence of two carbonyl groups and the existence of only two ^{31}P - ^{13}C cross correlations for this molecule gives evidence for its symmetrical constitution, which means that it is *bis*-((2-oxo-1,3-dioxolan-4-yl)methyl) phosphate, that is, the symmetric phosphodiester of two primary 3-glyceryl-1,2-cyclic carbonates (**diGI(CO) $_2$ P**, cf. **Figure 57 B**).

The peculiarity of this molecule is that it shows a 1:1 double-resonance in anhydrous DMSO, both in $^{31}\text{P}\{^1\text{H}\}$ and $^{13}\text{C}\{^{31}\text{P}\}$ NMR spectra, that persists at elevated temperatures up to 60 °C and coalesces to a single somewhat broad resonance only in the presence of water, which is consistent with the existence of two equally probable diastereoisomers.

The remaining major (fully coupled) ^{13}C NMR resonances in this middle-field chemical shift range at 62-78 ppm do not couple or correlate by $\{^1\text{H}\}$ HMBC with the ^{31}P nucleus: three CH_2 singlets at $\delta_{\text{C}} = 63.16$ ppm (small *s*, CH_2), 63.68 ppm (large *s*, CH_2) and 66.58 ppm (small *s*, CH_2) besides two CH singlets at $\delta_{\text{C}} = 73.16$ ppm (medium *s*, CH) and 77.75 ppm (small *s*, CH), **Figure 57 A**. The large/medium signals are those of glycerol (marked with an asterisk *), the small signals are from glyceryl-1,2-cyclic carbonate (marked with a + sign). Both compounds are readily identified in the ^1H -spectrum (**Figure 48**, **Figure 49**), the cyclic carbonate is also in the $^{13}\text{C}\{^{31}\text{P}\}$ NMR spectrum of the ^{13}C -labelled sample (**Figure 58**). In this downfield chemical shift range, all carbonyls are seen best because they are fully enriched in this isotope. The corresponding mixture obtained after using $^{15}\text{N}_2$ urea is of course much less sensitive but still permits the identification of otherwise not observed residual urea (triplet), glyceryl carbamate (doublet) and cyclic carbonate (singlet), see **Figure 58 C**.

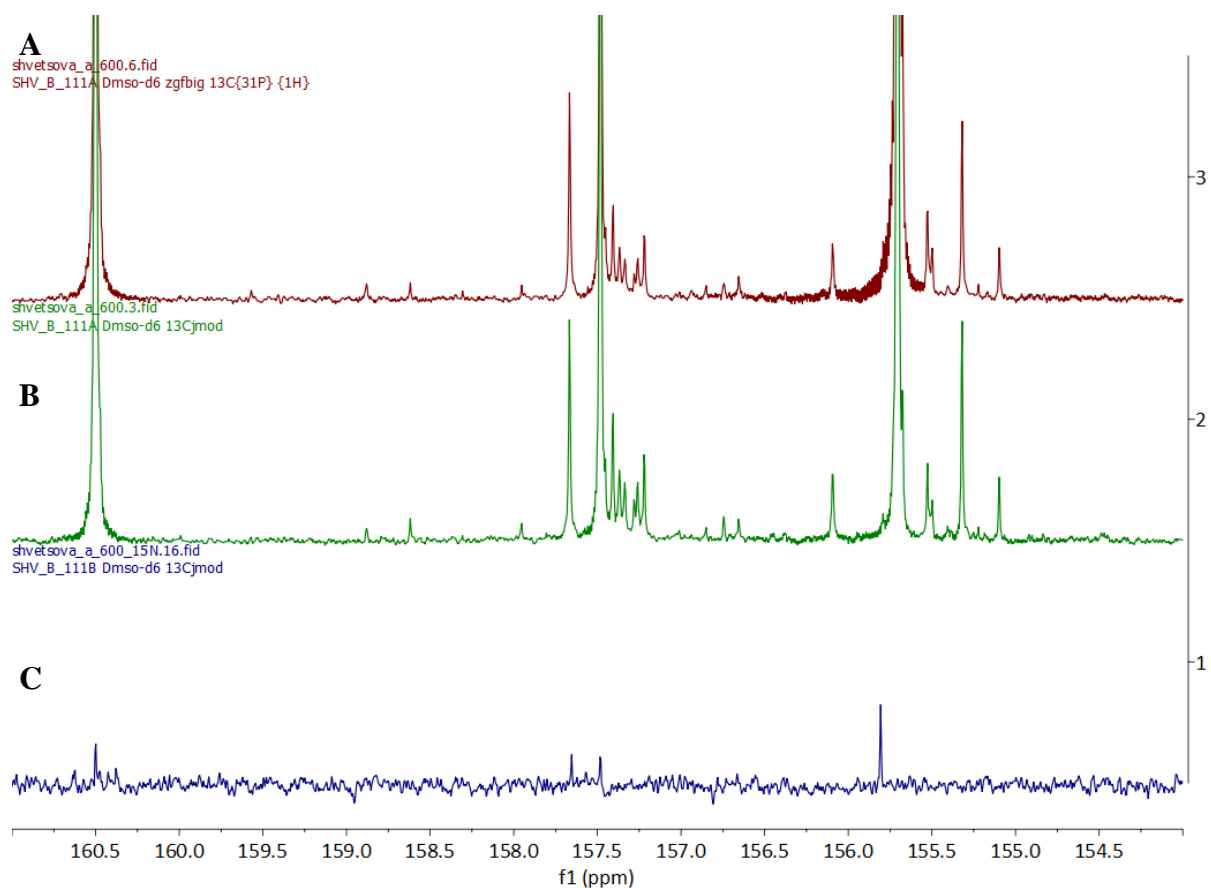


Figure 58. ^{13}C NMR (150.9 MHz) low-field excerpts of the DMSO-*d*₆ extracts from a neat mixture of **A** (red) $^{13}\text{C}\{^{31}\text{P}\}$ NMR, **B** (green) JMOD ^{13}C NMR both of glycerol (**5**), [^{13}C]urea (**2c**) and NaH_2PO_4 (**P**) (1:1:1, 0.5 mmol each); and **C** (blue) JMOD ^{13}C NMR of glycerol (**5**), [$^{15}\text{N}_2$]urea (**2b**) and NaH_2PO_4 (**P**) (1:1:1, 0.5 mmol each) all after heating neat mixtures for 96 hours at 115 °C. Leftmost: residual urea, central: carbamates, right-hand: cyclic carbonates.

1.1.4. High-resolution mass spectrometry and hydrophilic ion liquid chromatography

Another method that provided us with information about reaction products is mass spectrometry. Due to the small size and polarity of the glyceryl phosphates, the most optimal analysis was high-resolution (direct injection) MS in negative ion mode (**Figure 59**). Taking into consideration the exact masses of the compounds, we know the most probable atomic composition of the molecules but not their structure. For example, the 5- and 6-membered ring phosphates would have exactly the same mass, $m/z = 152.9958$ Dalton, similar to glyceryl-1-phosphate and glyceryl-2-phosphate, $m/z = 171.0064$ Dalton. Thus, in **Figure 59 D** the most probable isomers of the identified products are suggested.

HRMS also confirms the presence of diesters such as diglyceryl phosphate and diglyceryl diphosphates, along with the carbamoyl and cyclic carbonate derivatives of glyceryl phosphates suggested in the previous section. However, the mono-anionic mass peak $m/z = 297.0017$ Dalton is not present in the negative ion mode mass spectrum of the methanolic extract of the unlabelled sample (**Figure 59**).

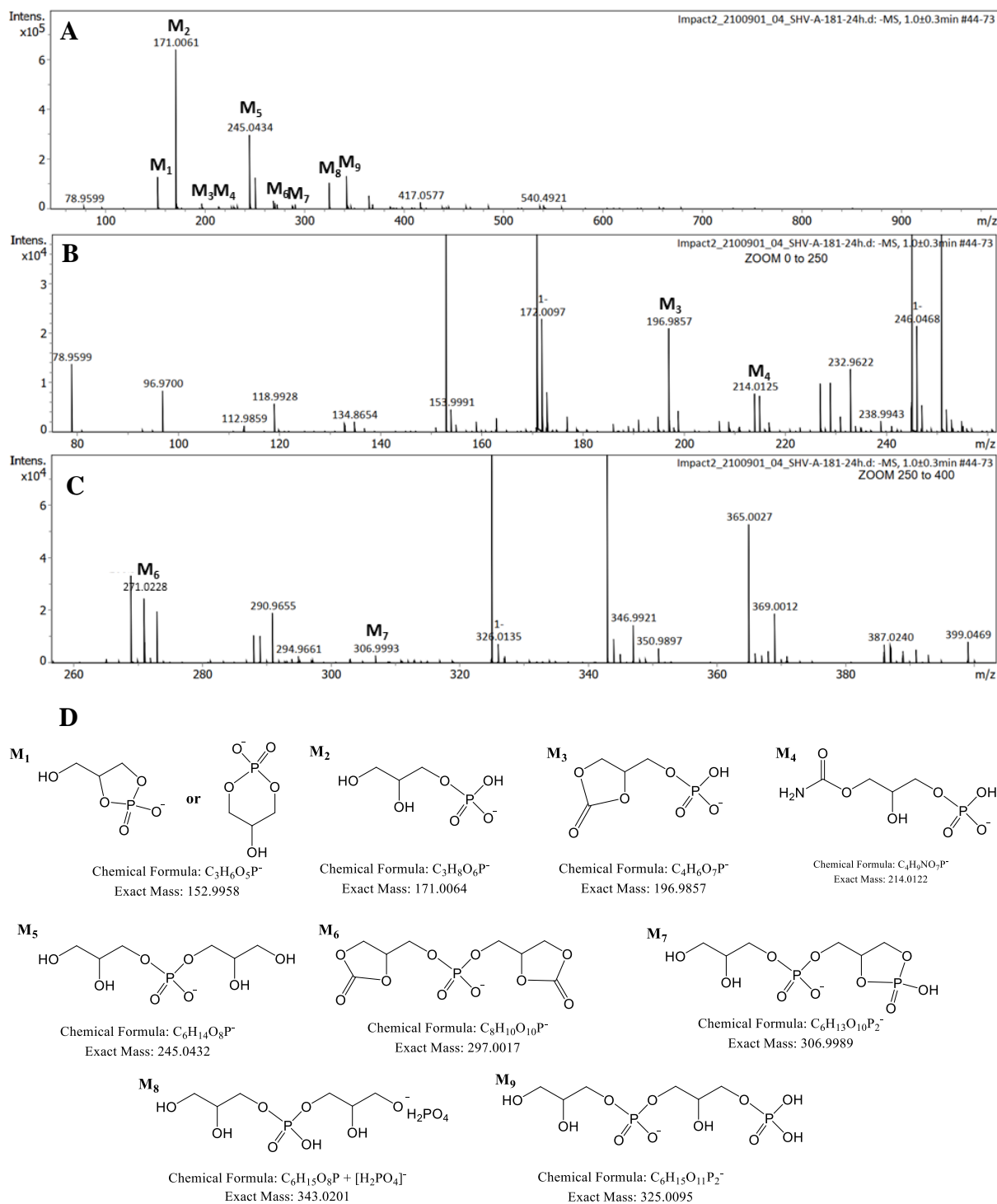


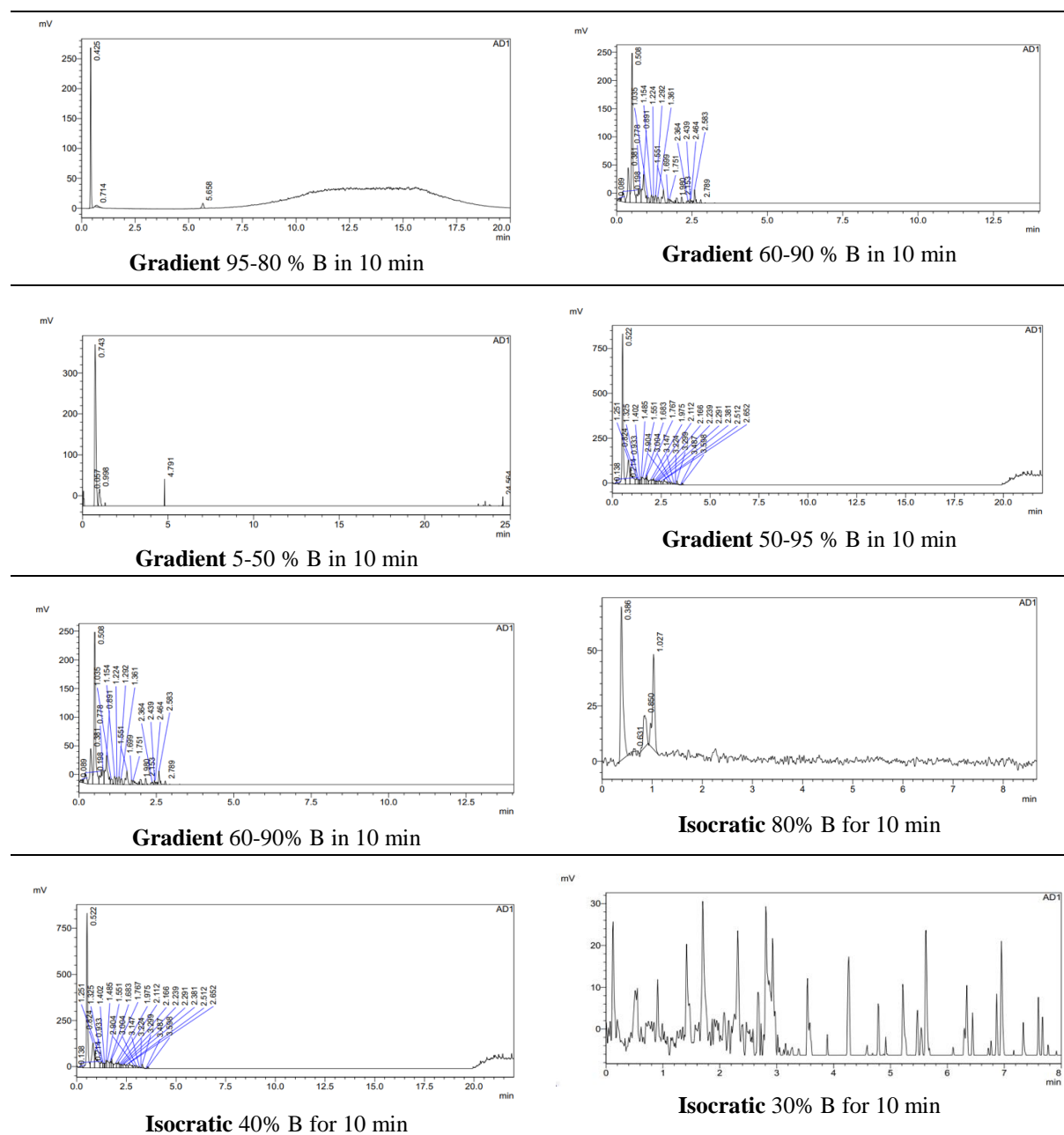
Figure 59. HRMS spectra (direct injection) in the negative ion mode of the methanolic extract of the crude mixture obtained from letting glycerol (**5**), urea (**2a**) and NaH_2PO_4 (**P_i**) (1:1:1, 0.5 mmol each) react for 24 h at 115 °C (neat). M/z $[H_2PO_4]^-$ 96.9696 = ESI^- common background ion; **A** – Total ion spectrum. **B**, **C** – Zoom on products. **D** – Assigned chemical structures (only 1-2 of several possible isomers shown) and monoisotopic masses of the charge-neutral molecules.

We attempted to find **diGICOP** and **diG(CO)₂P** in the crude mixture by LC-HRMS using the HILIC column (HILIC-HRMS). HILIC columns are very efficient tools that might be challenging to work with. It has a specific interaction mechanism that involves both hydrophilic

and hydrophobic interactions between the molecules and the stationary phase. This makes it very sensitive, even for isomers and other structurally similar small and polar compounds and provides high separation efficiency.

Before performing the HILIC-HRMS experiment, we optimised the separation protocol after trying several possible conditions and solvent systems by using HILIC-ELSD. The tested conditions and obtained chromatograms are shown in **Table 4**. The first tests at a very low pH of about 3 using ammonium formate buffer did not provide the expected separation. We then switched to the solvents A – 100 mM aqueous $\text{CH}_3\text{COONH}_4$ at pH 6.4, B – CH_3CN .

Table 4. HILIC-ELSD chromatograms of the methanolic extract of the crude mixture obtained by letting glycerol (**5**), urea (**2a**) and NaH_2PO_4 (**P_i**) (1:1:1, 0.5 mmol each) react for 96 h at 115 °C (neat).



Chromatograms demonstrated that the best condition was isocratic elution A/B = 55:45, as described in Materials and Methods section **2.3**. In **Figure 60**, the results of HILIC-HRMS

analysis in positive and negative ion modes are presented. There are similar products to the direct injection HRMS listed above, such as cyclic and acyclic mono- and diglyceryl phosphates (**Figure 60, C**). The methanolic extract of the unlabeled mixture does not show any identifiable carbamoyl or cyclic carbonate derivatives of glyceryl phosphates. However, the highest intensities of the extracted peaks in both positive and negative ion mode chromatograms match the mass of diglyceryl phosphate (peak no. 4 in **A** and, respectively, peak no. 5 in **C**, cf. **Figure 60**).

Further in the experimental part, a kinetic study of the time-dependent growth of the amounts of both carbonylated glyceryl phosphates as observed by ^1H , ^{13}C and $^{31}\text{P}\{^1\text{H}\}$ NMR spectroscopies is described in the section **2.4**.

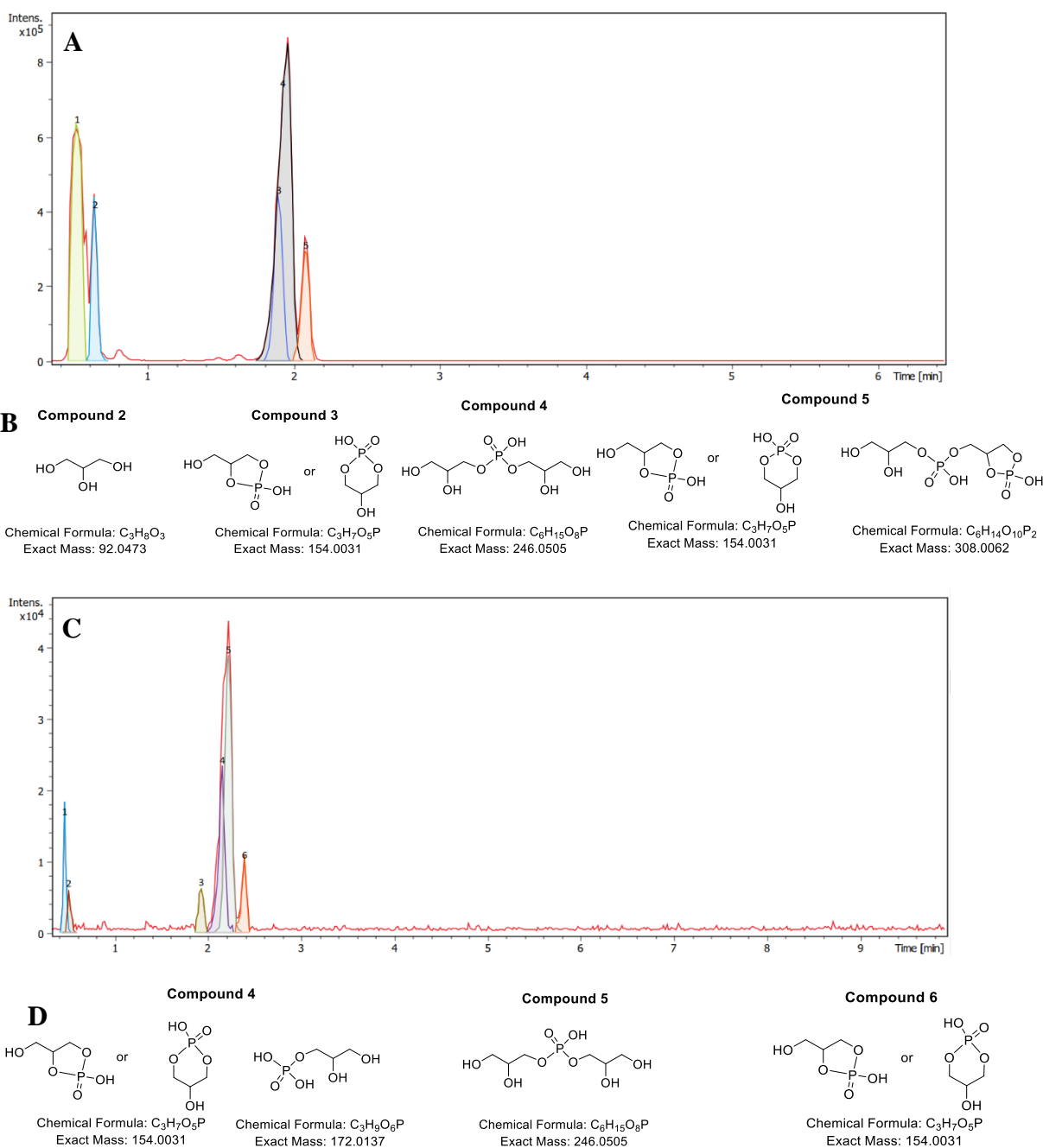


Figure 60. HILIC-HRMS spectra of the methanolic extract of the crude mixture obtained by letting glycerol (**5**), urea (**2a**) and NaH₂PO₄ (**P_i**) (1:1:1, 0.5 mmol each) react for 96 h at 115 °C (neat). **A** – positive ion mode chromatogram and numbered ion extracts. **B** – assigned chemical structures of the extracted ion peaks found in **A** (only the most probable acyclic isomers are shown) and monoisotopic masses of the charge-neutral molecules. Peak 1 of spectrum **A** contains only sodium acetate clusters (+82n). **C** – negative ion mode chromatogram and numbered ion extracts. **D** – assigned chemical structures of extracted ion peaks found in **C** (only the most probable acyclic isomers are shown) and monoisotopic masses of the charge-neutral molecules. Peaks 1 and 2 of spectrum **C** are acetate adducts of a fluorinated polymer (PTFE) (from the grease used on LC pump modules) and leftovers of MS calibrant. The mass of peak 3 of spectrum **C** is closest to glyceryl methyl phosphodiester that may occur from the reaction of glyceryl phosphate with the solvent (m/z 186.1139 found, m/z 186.0293 calculated for C₄H₁₁O₆P) but remains unidentified.

1.2. Urea-assisted phosphorylation of MPG

Having a good comprehension of the products obtained for glycerol phosphorylation, we moved on to the study of MPG. We could expect similar products due to the presence of glycerol in the molecule structure, except for 6-membered glyceryl cyclic phosphate. Similar analyses were performed on the **6:2a:P_i** crude mixture as described in section 1.1.

1.2.1. ¹H and ³¹P NMR and ¹H-³¹P HMBC spectroscopies

The ¹H NMR spectrum is more complicated than the ¹H NMR spectrum of pure MPG (**6**) (the characterization of pure MPG is described in methods and material section 3.1) due to the presence of phosphorylated and carbonylated products. Also, as a result of the thermal degradation of MPG (**6**), the presence of glycerol and considerable amounts of glyceryl phosphates are observed, as confirmed by ³¹P NMR (**Figure 63**) and LC-MS (**Figure 66**).

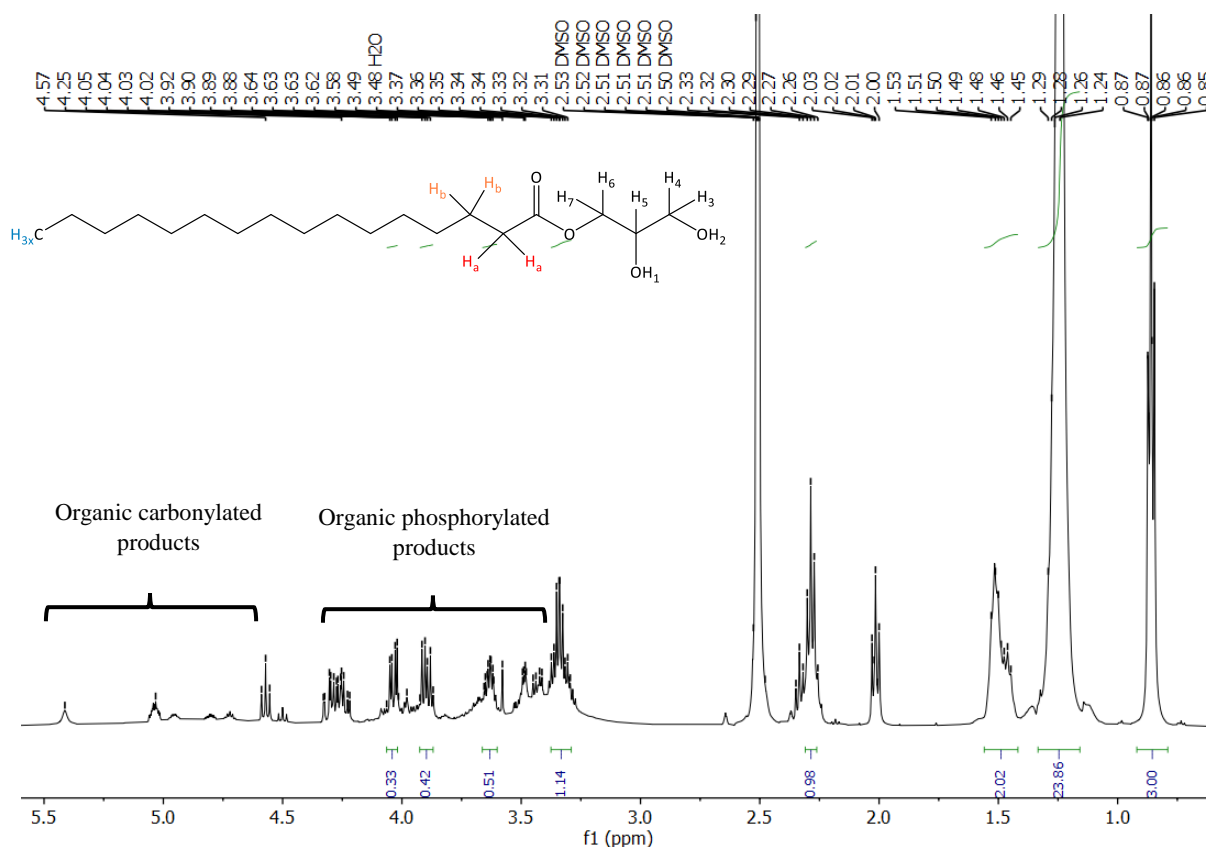


Figure 61. ¹H NMR spectrum (500 MHz, DMSO-*d*₆) of the extract of the crude reaction mixture from MPG (**6**), natural isotope-abundance urea (**2a**) and NaH₂PO₄ (**P_i**) (1:1:1, 3 mmol each) that was heated neat for 120 hours at 115 °C: δ_H (MPG signal appear with integrated peak areas, compare with **Figure 62**). Signals at 3.5-4.3 ppm are due to organic products of phosphorylation; signals at 4.3-5.5 ppm contain not reacted OH groups of MPG, also 1,2-cyclic carbonates.

The multiplicity pattern of organic phosphorylated products is more complicated to follow by ³¹P NMR due to the lower solubility of the MPG phosphorylation reaction mixture

when compared to that of glycerol phosphorylation. Consequently, lower signal intensities and a much higher signal-to-noise ratio are observed. However, it is possible to identify the main groups of products as in Figure 53 and the integration of the $^{31}\text{P}\{^1\text{H}\}$ peak areas for **5cGIP** — identified through the comparison of the ^1H - ^{31}P HMBC spectra of the reaction mixtures of glycerol and MPG (Figure 54 and Figure 65)—, the main acyclic 1-glyceryl phosphate and **6cGIP** allows for a rough estimation of the amount of MPG deacylation to palmitate, glyceryl phosphates, glyceryl cyclic carbonates and glycerol.

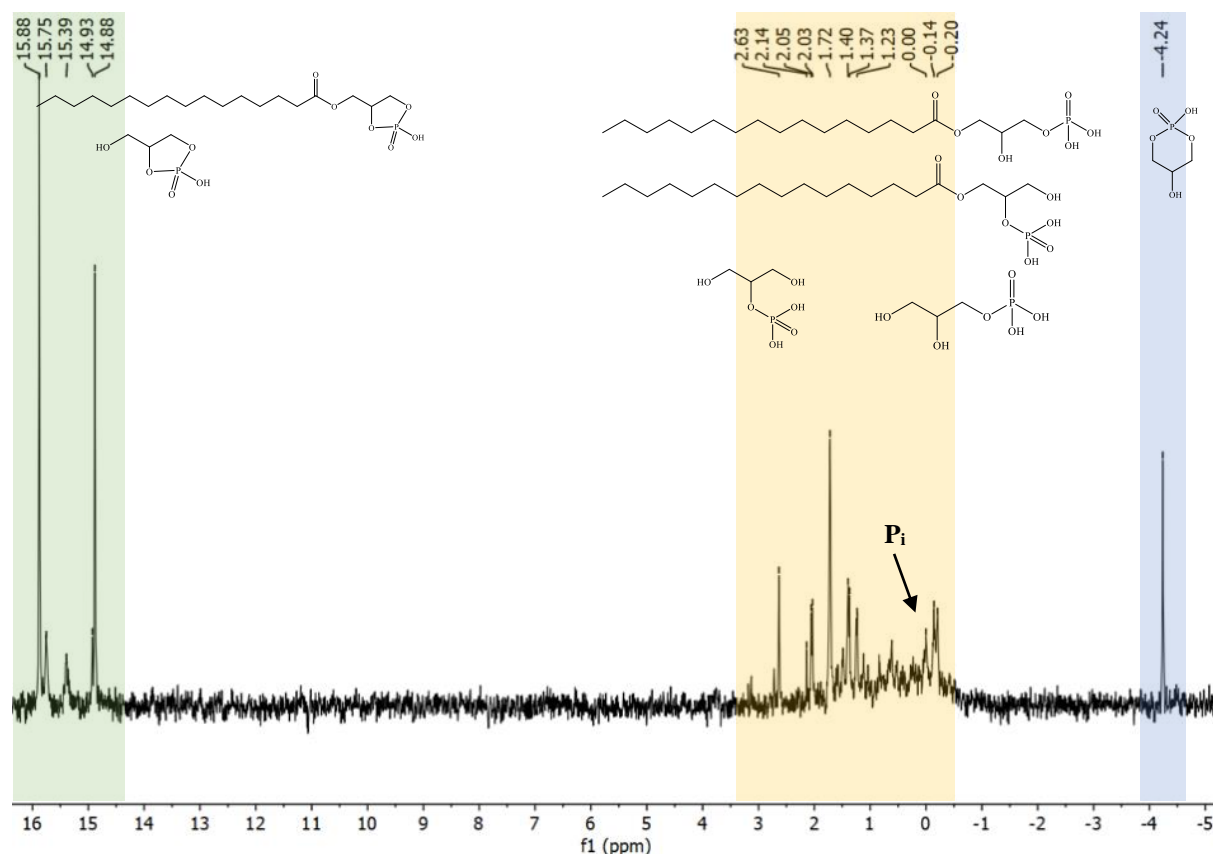


Figure 63. $^{31}\text{P}\{^1\text{H}\}$ NMR (202.5 MHz, $\text{DMSO-}d_6$) of the extract of the crude reaction mixture from MPG (**6**), natural isotope-abundance urea (**2a**) and NaH_2PO_4 (**Pi**) (1:1:1, 3 mmol each) that was heated neat for 120 hours at 115 °C. $\delta_{\text{P}} = 15.62\text{--}14.63$ (s, 5-membered ring cyclic phosphates containing **5cGIP** and **5cMPGP**, green), 2.38–0.46 (acyclic organo-phosphates containing **MPGP**, ochre), 0.00 (s, **Pi**), –4.49 (s, 6-membered ring glyceryl-1,3-cyclic phosphate **6cGIP**, blue).

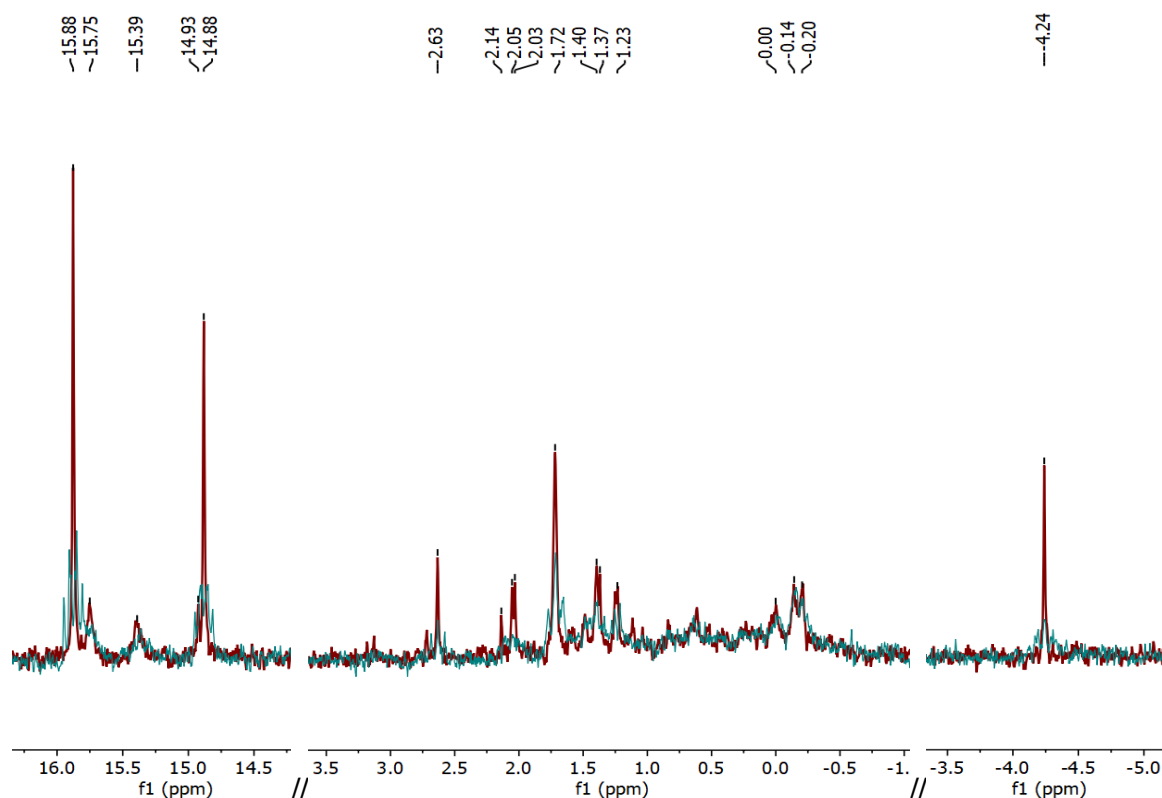


Figure 64. $^{31}\text{P}\{^1\text{H}\}$ NMR (red) and ^{31}P NMR spectra (blue) (202.5 MHz) in $\text{DMSO-}d_6$ of the extract of the crude reaction mixture from MPG (**6**), natural isotope-abundance urea (**2a**) and NaH_2PO_4 (**P_i**) (1:1:1, 3 mmol each) that was heated neat for 120 hours at 115 °C: $\delta_{\text{P}} = 15.88$ (*s/ddd*, 5-membered ring cyclic phosphate **5cGIP**), 14.88 (*s/ddd*, 5-membered ring cyclic phosphate **5cMPGP**), 2.38-0.46 (acyclic organo-phosphates containing **MPGP**) including 2.05 (*s/t*, acyclic primary monoester **MPG-1P**), 1.37 (*s/d*, acyclic secondary monoester **MPG-2P**); 1.75 (*s/t*, acyclic primary monoester **GI1P**), 0.00 (*s*, **P_i**); -4.24 (*s/tt(d)*, 6-membered ring cyclic phosphate **6cMPGP**).

If we calculate, by integrating the peak areas, the relative amount of ^{31}P signals that are surely depalmitoylated, namely, the larger most downfield signal from glyceryl-1,2-cyclic phosphate (marked **x** in **Figure 65**) and that from glyceryl-1,3-cyclic phosphate—the 6-membered ring cyclic phosphate is expected to form due to depalmitoylation followed by cyclisation much more likely than through acyl migration followed by cyclisation—then 53 % depalmitoylation constitutes a lower limit. This percentage could be higher if among the acyclic signals there were depalmitoylated phosphates as well.

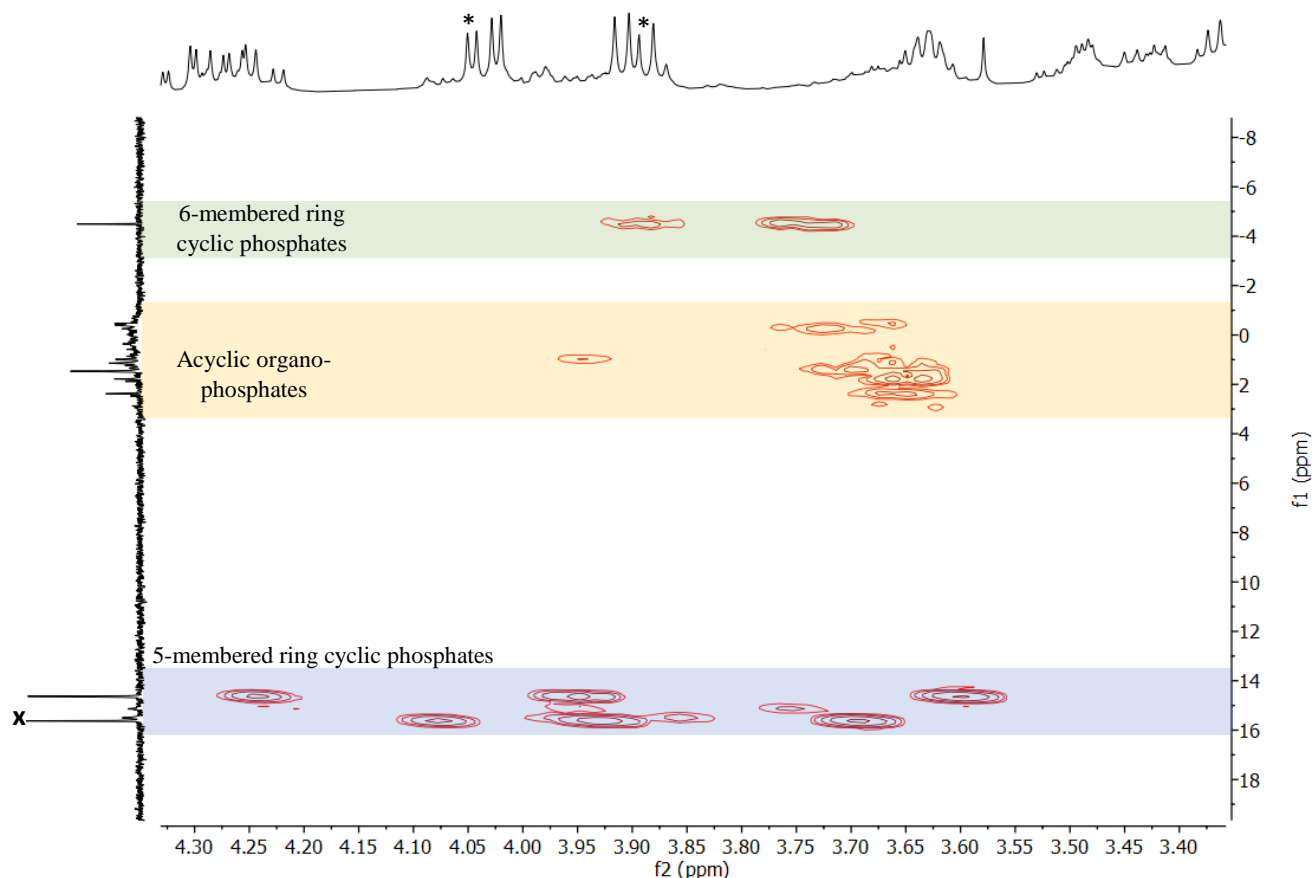


Figure 65. $^1\text{H}-^{31}\text{P}\{^1\text{H}\}$ HMBC spectrum (500 MHz, ^1H [horizontal axis], 202.5 MHz $^{31}\text{P}\{^1\text{H}\}$ [vertical axis]) in $\text{DMSO}-d_6$ of the extract of MPG (**6**), natural isotope abundance urea (**2a**) and NaH_2PO_4 (P_i) (1:1:1, 3 mmol each) heated neat for 120 hours at 115 °C. * = MPG (2 *dd*), x = 5cGIP.

1.2.2. Reversed-phase high-performance liquid chromatography coupled to high-resolution mass spectrometry (RPHPLC-HRMS)

MPG, compared to glycerol, has a long chain that helps to separate molecules well without using HILIC LC-MS. Thus, we performed reversed-phase LC-MS following the procedure described in Methods and Materials section 2.2. In **Figure 66**, we were able to identify all the products suggested by the above NMR analysis, such as 5- or 6-membered ring phosphates, acyclic glyceryl and MPG phosphates, along with carbamoyl and cyclic carbonate described in the previous section 1.1. Compounds **2**, **3** and **4** contain phosphorylated MPG with an additional glycerol molecule, each compound most likely belongs to different isomer of the same molecule (**Figure 66, B**). Other interesting products are compounds **12-14**, where we detected the presence of diMPG phosphate or two fatty acid chains on one phosphorylated glycerol molecule. This proves that in a dry-state experiment conducted at 115 °C for 120 hours, the membranogenic precursors may have indeed be synthesised on the early Earth.

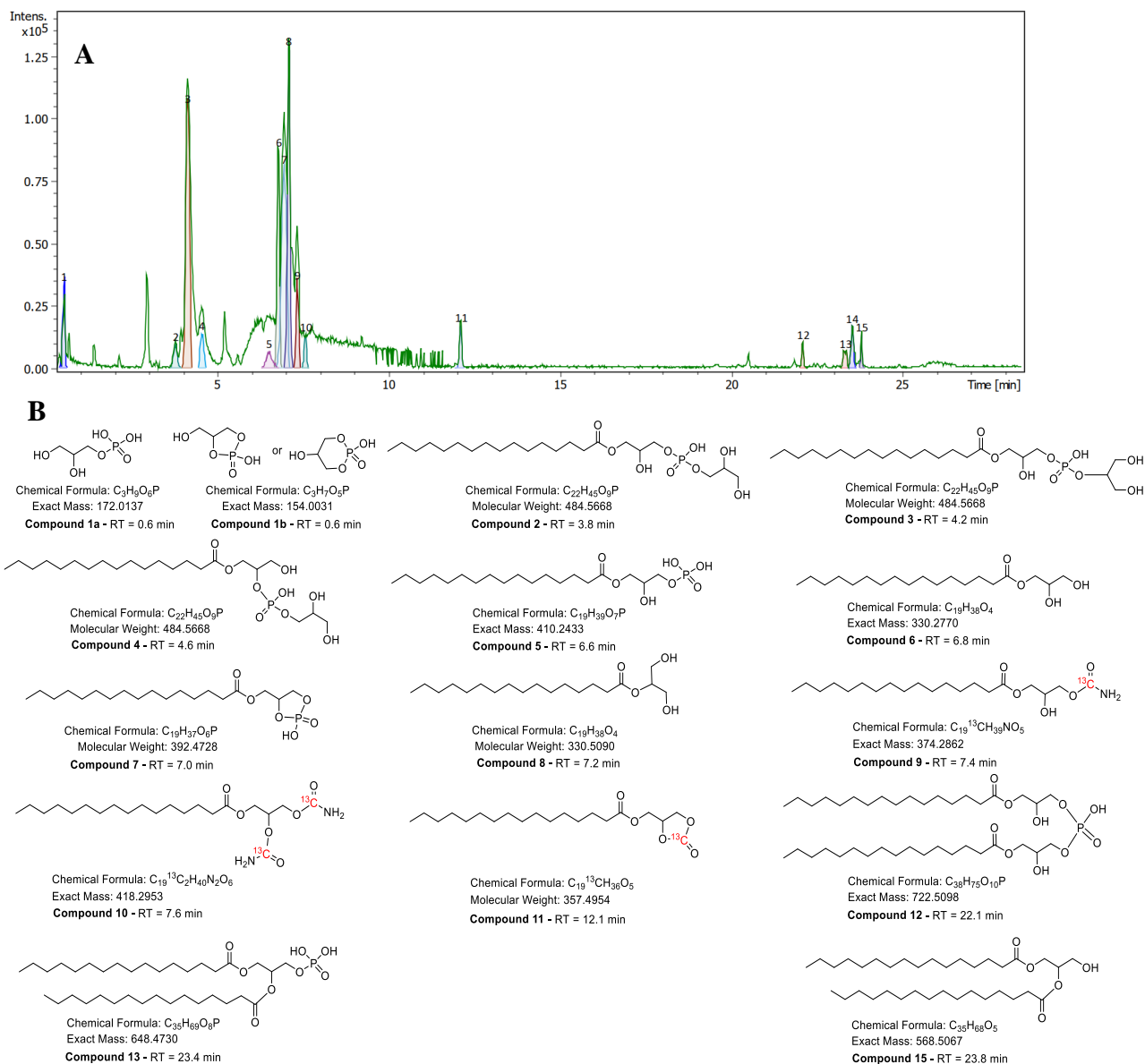


Figure 66. Exemplary chromatogram of a methanolic extract of the reaction mixture containing MPG (**6**), [¹³C]urea (**2c**) and NaH₂PO₄ (**P_i**) (1:1:1, 0.5 mmol each) that was heated neat for 48 hours at 115 °C. **A** – RP-UHPLC-HRMS chromatogram (green) with extracted negative ions (colored, numbered peaks). **B** – chemical structures and monoisotopic masses of the detected compounds in their charge-neutral forms. Suggested molecules corresponding to groups of peaks **2, 3, 4** (m/z 484.5668) and **6, 8** (m/z 330.5090) have different retention times R_T but the same m/z (see scheme), hence they are most likely isomers. Compound **5** shows up as a very broad peak ($R_T = 5.5\text{--}10$ min), it is the main phosphorylated product (area under the green line). Compound **14** ($R_T = 23.5$ min, m/z 540.4903) could not be identified.

Conclusions to the Section 1

Using available literature and experimental approach I identified the main products of the exemplary phosphorylation reaction of glycerol and its derivative MPG in the presence of monosodium dihydrogen phosphate and urea after 120 hours of heating at 115 °C analysed in DMSO-d₆.

¹H-coupled NMR provided information about two types of organic phosphorylated products: $\delta_{\text{H}} = 3.60\text{--}4.20$ ppm are glyceryl protons from phosphorylated organic products, $\delta_{\text{H}} = 4.30\text{--}4.95$ ppm are protons from organic carbonylated products (carbamate or cyclic carbonate) and $\delta_{\text{H}} = 3.51$ and 3.66 ppm are from carbonylated but not phosphorylated products.

Following these ¹H-coupled ³¹P multiplicities, the observed inorganic orthophosphate PO₄³⁻ (**P_i**, $\delta_{\text{P}_i} = 0.00$ ppm) is due to inorganic as a residual part of the initial phosphorus source that remained unreacted and inorganic pyrophosphate P₂O₇⁴⁻ (**PP_i**, $\delta_{\text{PP}_i} = -9.32$ ppm) is as a by-product of the reaction. Non-terminal polyphosphate (**P_{ni}**) signals appear as ¹H-decoupled ³¹P{¹H} triplets at -18 to -30 ppm. I detected presence of organic products such as cyclic organic 5-membered ring phosphates (**5cGIP**, $\delta_{5\text{-mr}} = 12\text{--}20$ ppm), 6-membered rings (**6cGIP**, $\delta_{6\text{-mr}} = -4$ to -7 ppm) and acyclic mono- (**GI-1P** and **GI-2P**, $\delta_{\text{acyclic}} = -1$ to $+2$ ppm).

Two new persistent signals on ³¹P NMR were discovered and described in all DMSO-d₆. They were observed only in the presence of urea and their resonances are shifted downfield with respect to all other acyclic product ³¹P signals. Two phosphorylated compounds appear in changing concentrations and precise shapes as a function of reaction time and show complex multiplicities in their proton-coupled ³¹P signals. The first displays two singlets with the ratio of their proton-decoupled ³¹P{¹H} signal areas exactly 1:1 in all cases, that in proton-coupled ³¹P NMR spectra split into two quintets (2 *quint*) with the same coupling constant. The second deshielded product resonates as an ordinary ³¹P{¹H} singlet ($\delta_{\text{P}} = 2.0\text{--}2.2$ ppm), and is in all fully coupled ³¹P NMR spectra a doublet of triplets (*dt*). Noteworthy is that the fully coupled ³¹P resonance patterns for both compounds differ in their appearance depending on whether we used for the phosphorylation experiment natural isotope abundance-urea, [¹³C]urea or [¹⁵N₂]urea. Studying in details their multiplicity over different labelled atom of urea, ³¹P{¹H}, ¹³C, ¹³C{³¹P} NMR, COSY, DOSY spectra and ³¹P-¹³C HSQC helped us identify those molecules as a 5-membered ring 1,2-cyclic carbonate of a diglyceryl phosphodiester, one glyceryl of which is linked through the secondary and the other through the primary position (**diGICOP**) and symmetric phosphodiester of two primary 3-glyceryl-1,2-cyclic carbonates (**diGI(CO)₂P**) respectively.

In reactions with MPG, similar products were described: **P_i**, **PP_i**, **5cMPGP**, **MPG-1P** and **MPG-2** along with the corresponding glyceryl phosphates including 6-membered rings (**6cGIP**) as the result of acylation reaction. Using LC-MS methods, I confirmed structures of the molecules described by NMR analyses. For MPG reactions were also discovered molecules with two fatty acid chain on one molecule of glycerol, that is prospective for further vesiculation of crude mixture.

III Results and discussion

2. Study of the mechanism and kinetic of urea-assisted alcohol phosphorylation

After identifying the main reaction products, we focused on the kinetic study of the phosphorylation reaction and the description of the reaction mechanism. Taking into consideration that urea works as a condensing agent, in other words, it is supposed to be hydrolysed during the reaction, thus helping to eject water. We first studied urea degradation and phosphorylation degree of reaction glycerol (or MPG) with P_i and labelled urea over a period of 0-120 hours at 115 °C.

2.1. Associative vs. dissociative mechanism

As discussed in the state-of-the-art section 4.1.1.4, there are two principal mechanisms of urea-assisted alcohol phosphorylation using orthophosphate. A condensing agent is needed to activate phosphate and is involved in the phosphorylation reaction. However, it is not clear whether this is going through “dissociative” or “associative” intermediate of urea and phosphate (**Figure 67**).

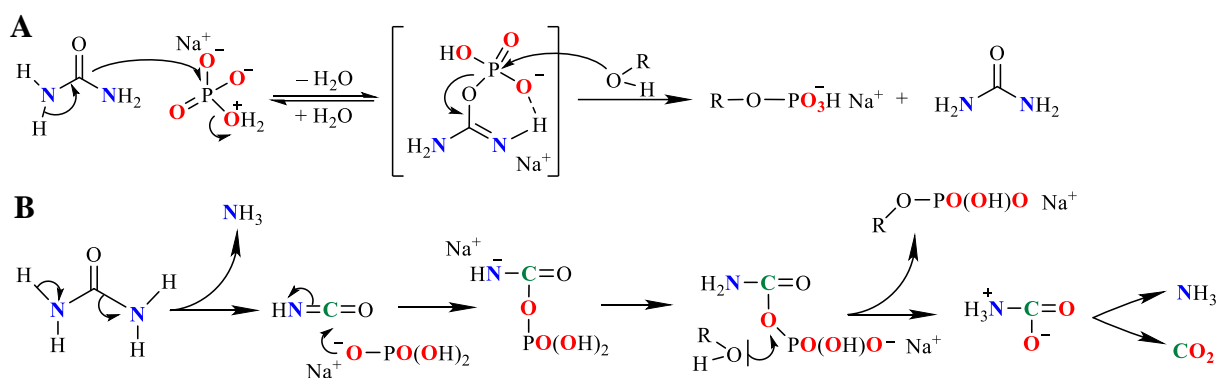


Figure 67. Principle mechanism schemes of urea-assisted alcohol phosphorylation. **A** – associative phosphate activation^{252,266,245} **B** – dissociative phosphate activation^{253,254,255} improved in this work†

The tentative associative pathway is based on the formation of a carbamimidic phosphoric anhydride intermediate from a rare dihydrogenphosphate tautomer in the first step of the reaction (**Figure 67, A**). In the next step, this intermediate reacts with a nucleophilic alcohol that leads to the formation of its phosphate and releases the molecule of urea back into the system.

The suggested dissociative mechanism goes through the thermal decomposition of urea at elevated temperatures into ammonia and isocyanic acid (**Figure 67, B**). It forms carbamoyl phosphate with dihydrogenphosphate, which later reacts with alcohol. Along with the phosphorylated product, carbamic acid is supposed to be formed and decomposed into ammonia and carbon dioxide. Both mechanisms could possibly produce diester phosphate or cyclic phosphate if phosphorylated alcohol plays the same role as inorganic dihydrogenphosphate.

Our collaborators, Professor Henry Chermette and Dr. Lynda Merzoud from the *Institut National de Physique des 2 Infinis (IP2I)* performed quantum theoretical method analyses of both mechanisms (not shown here)†. The results demonstrate that excess of urea (the minimum ratio is three molecules of urea per one molecule of dihydrogenphosphate) is necessary for the

formation of the proposed carbamimidic phosphoric anhydride. This step also has the highest energy barrier of the reaction 90.84 and 60.11 kcal/mol in the absence and presence of two molecules of water, respectively. At the same time, following the dissociative mechanism, they discovered the highest barrier was in the transition of starting molecules towards the formation of isocyanic acid, which was 51.36 and 30.39 kcal/mol in the absence and presence of two molecules of water, respectively.

This is a direct theoretical proof that the dissociative mechanism of reaction is more favorable; however, we cannot definitively decline some possible contributions to the reaction products from the associative mechanism because many more initial conditions (starting with more dihydrogen phosphate, urea and water molecules) could lead to lower barriers than 60 kcal/mol.

2.2. Tracing stable isotopes in volatiles evaporating from ‘dry’ phosphorylation reactions

Before the beginning of the thesis, my supervisors proposed a detailed dissociative mechanism (**Figure 68**) and designed an experimental set-up for its confirmation (methods and materials section **4.2**). My work was to confirm or discard it.

A major difference between the dissociative and associative mechanisms is the actual degradation of urea into ammonia and, on the later stages, its derivative carbamic acid decomposes into ammonia and carbon dioxide. Both volatiles would not be produced along the associative pathway. Urea, especially in the presence of inorganic phosphate and residual water, is known to thermally degrade (hydrolyse) to CO₂ and NH₃ even in the absence of any alcohol. Therefore, it was suggested to use stable isotopes of urea ([¹⁵N₂]urea, [¹³C]urea) and sodium dihydrogenphosphate (NaH₂P[¹⁸O₄]) for a better understanding of the reactants transformations. For this experiment, we used the system of round-bottom flask with a reaction mixture and two traps, one for nucleophilic (H₂O, NH₃) and a second one for electrophilic (CO₂) volatiles connected and kept under Ar atmosphere. The Ar flow carried gas produced from the crude mixture through the first trap filled with a solution of benzoyl chloride in toluene to trace ammonia and residual water (**Figure 68, B**), and then through the second one filled with phenyl magnesium bromide dissolved in tetrahydrofuran to trace carbon dioxide and isocyanic acid if present (**Figure 68, C**). The presence of labelled atoms in urea and phosphate allowed us to confirm the formation of those gasses from reagents and exclude air contamination. **Figure 68, A** suggests a complete reaction scheme with labelled urea and phosphate.

A series of experiments were performed to trace the isotopes in reactions with glycerol and MPG. Additional experiments were performed in the presence of [¹⁵N]formamide [¹⁵N]acetamide instead of urea (P_i consumption at 115 °C, 65 % and 3 % respectively). We studied in detail the content of each trap using LC-HRMS and direct injection HRMS. The list of experiments is presented in **Table 5**.

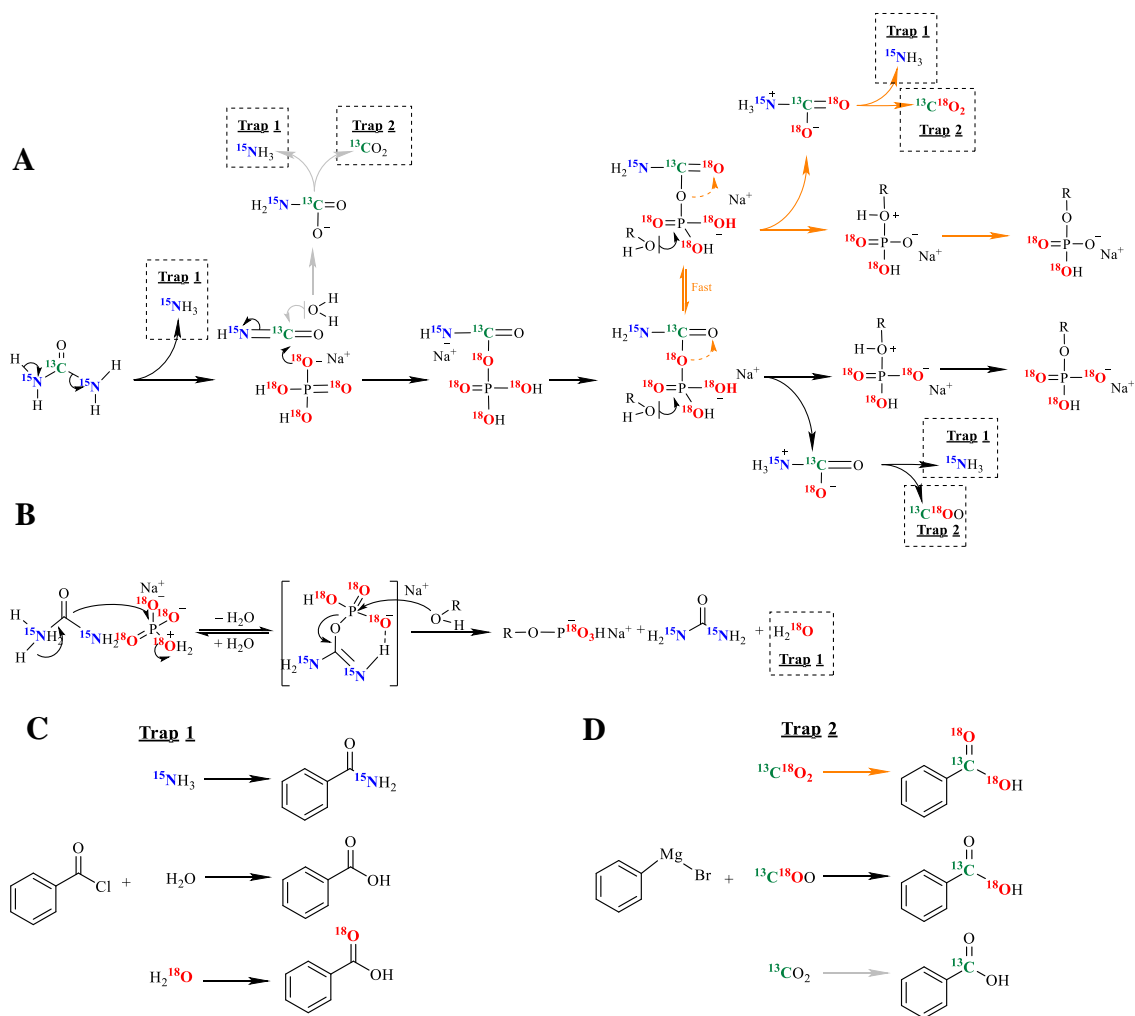


Figure 68. Detailed phosphorylation mechanism schemes of urea-assisted alcohol phosphorylation with labelled atoms of urea and phosphates marked. Two different urea isotopes were used ($^{15}\text{N}_2$ urea, ^{13}C urea), but in the scheme, they are shown as one. **Black** arrows describe the principal reaction pathway, **orange ones** suggest the intramolecular oxygen exchange in carbamoyl phosphate and **grey** represent reaction of water and isocyanic acid. **A** – dissociative mechanism; **B** – associative mechanism; **C** – principal reactions of trap 1; **D** – principal reactions of trap 2.

Table 5. List of experiments performed in the experimental setup shown in methods and materials section 4.2 for studying prebiotic reactions by tracing stable isotopes carried over in the gas phase.

Number of the experiment	Starting molecule	Cond. agent	P _i	Liquidiser	Reaction scale, mmol
1.1	MPG (6)	2b	[¹⁸ O ₄]P _i	-	3
1.2	6	2b	P _i	-	3
1.3	6	3b	[¹⁸ O ₄]P _i	-	3
1.4	6	4b	[¹⁸ O ₄]P _i	-	3
1.5	6	2c	[¹⁸ O ₄]P _i	-	3
1.6	6	2c	[¹⁸ O ₄]P _i	-	3
1.7	6	2c	[¹⁸ O ₄]P _i	-	10
1.8	6	2c	[¹⁸ O ₄]P _i	-	6
1.9	6	2c	[¹⁸ O ₄]P _i	-	6
1.10	6	2c	[¹⁸ O ₄]P _i	H ₂ O	6
1.11	6	2a	P _i	H ₂ O	10
1.12	Glycerol (5)	2a	P _i	H ₂ O	10

Table 6. Data used for estimation of average weight loss in reactions of starting molecule (5 or 6), urea (2a or 2b or 2c) and NaH₂PO₄ (P_i or [¹⁸O₄]P_i) (1:1:1):

m_{urea} (g) = initial mass of added urea;

Δw (g) = weight difference of crude mixture before and after heating;

Δm_{urea} (%) = percent of urea consumed during reaction*;

m_{water} (g) = Δw – m_{urea}: amount of residual water;

weight % water = m_{water} (g) · 100 % / w₁ (g) (crude mixture weight before heating);

m_{water} (mmol) = m_{water} (g) · 100 % / 18 g mol⁻¹: millimoles of residual water;

mol % water = m_{water} (mmol) / reaction scale.

Starting molecule	Urea	P _i	Reaction scale (mmol)	m _{urea} (g)	Δw (g)	Δm _{urea} (%)	m _{water} (g)	weight % water	m _{water} (mmol)	mol % water
Glycerol (5)	2a	P _i	30	1.81	2.66	100	0.86	10.44	4.75	0.16
	2c	P _i	3	0.18	0.31	100	0.13	16.67	0.71	0.24
	2a	P _i	3	0.18	0.06	35.40	-	-	-	-
MPG (6)	2c	[¹⁸ O ₄]P _i	10	0.61	1.18	100	0.57	10.93	3.14	0.31
	2c	[¹⁸ O ₄]P _i	5	0.31	0.63	100	0.33	12.31	1.82	0.36
	2b	P _i	3	0.18	0.29	100	0.10	6.88	0.58	0.19
	2c	[¹⁸ O ₄]P _i	5	0.31	0.40	100	0.09	3.57	0.51	0.10
	2a	P _i	3	0.18	0.21	100	0.03	1.56	0.14	0.05
	2c	[¹⁸ O ₄]P _i	3	0.18	0.21	100	0.02	1.44	0.12	0.04
	2a	P _i	3	0.18	0.20	100	0.02	1.14	0.10	0.03
	2a	P _i	3	0.18	0.19	100	0.01	0.74	0.06	0.02
	2b	[¹⁸ O ₄]P _i	3	0.19	0.14	77.54	-	-	-	-
	2c	[¹⁸ O ₄]P _i	3	0.19	0.14	75.72	-	-	-	-
	2a	P _i	3	0.18	0.14	76.31	-	-	-	-
	2a	P _i	3	0.18	0.09	47.83	-	-	-	-
	2c	P _i	3	0.18	0.18	96.02	-	-	-	-

* If m_{urea} (g) > Δw (g), Δm_{urea} (%) = Δm (g) · 100 % / m_{urea} (g)

If m_{urea} (g) < Δw (g), Δm_{urea} (%) = 100 %

2.2.1. Trap 1: Gaseous nucleophiles (ammonia, water) trapped as benzamide and benzoic acid

During the reaction, we observed the formation of a white precipitate that corresponded to benzamide in accordance with the **Figure 68, B**. For analyses, the content of trap 1 was separated into two aliquots, precipitated and analysed by LC-MS in positive-ion mode. In **Figure 69**, exemplary results were obtained in experiment **1.1**. The chromatograms and spectra of all other experiments performed are summarised in the **Appendix A1**.

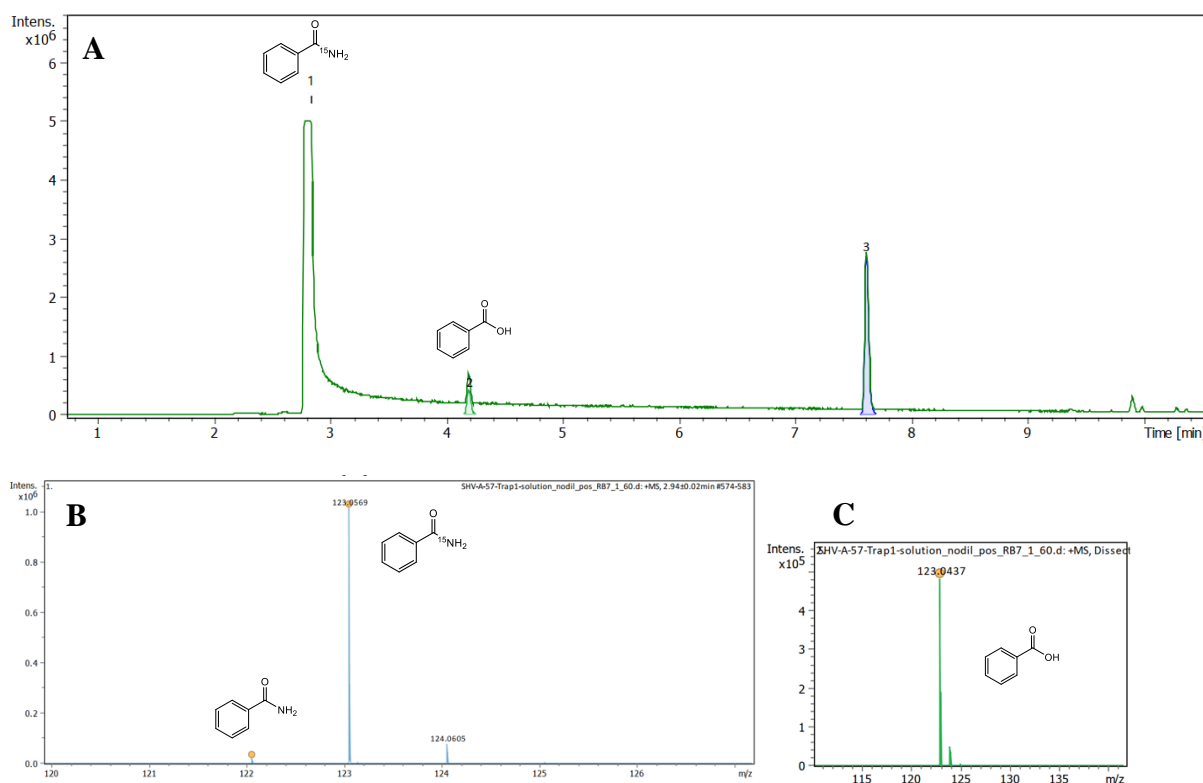


Figure 69. Exemplary results of HPLC-HRMS in positive-ion mode analysis of trap 1 solution of experiment **1.1**. **A** – total ion chromatogram with main signals. Peak 1 at $R_T = 3$ min: benzamide (C₇H₇NO and C₇H₇¹⁵NO); Peak 2 at $R_T = 4.2$ min: benzoic acid (C₇H₆O₂); Peak 3 at $R_T = 7.6$ min: contamination from vacuum filtration. **B** – high-resolution mass spectrum of peak 1 ($R_T = 3$ min). **C** – high-resolution mass spectrum of peak 2 ($R_T = 4.2$ min).

The main idea of this experiment was to measure the isotopolog ratios of the detected benzamide signals. All benzamide peaks trapped from [¹⁵N₂]urea-assisted (**2b**) and [¹⁵N]formamide-assisted (**3b**) phosphorylation of glycerol (**5**) and MPG (**6**) gave evidence for the elimination of ¹⁵NH₃ (**Table 7**). The presence of unlabelled benzoic acid in trap 1 can be explained by the presence of residual unlabelled water in some of the starting materials (up to 17 % water content by weight, **Table 6**) that could be carried by Ar flow. We made an attempt to quantify the amount of benzamide and benzoic acid in the trap 1 samples by using UHPLC (not shown here), but the data was not consistent from one experiment to another.

Table 7. Results of the study of isotope ratio of benzamide obtained in trap 1 after 5 days in experiments 1.1-1.4. The ratio was found by relation of absolute intensities of signals m/z 122.0600 ($[C_7H_7NO + H]^+$) and m/z 123.0571 ($[C_7H_7^{15}NO + H]^+$) on mass spectra of selected chromatogram peak. In all experiments there was no evidence of presence in trap 1 labeled benzoic acid (more details in **Appendix A1**).

Experiment	Part of trap 1 studied	Isotopolog ratio of benzamide, %	
		C_7H_7NO	$C_7H_7^{15}NO$
1.1	Solution	1.9	98.1
	Precipitate	2.8	97.2
1.2	Solution	3.2	96.8
	Precipitate	3.0	97.0
1.3	Solution	8.0	92.0
1.4	Solution	6.0	94.0

Another confirmation of the dissociative reaction pathway is the absence of ^{18}O -labelled benzoic acid. Following the first step of the associative mechanism of phosphate dehydration, we were supposed to obtain $H_2^{18}O$ that would be detected in the nucleophile trap 1. The presence of ^{18}O -labelled benzoic acid was never found in all the studied reactions (**Figure 70**). The control experiment with $[^{15}N]$ formamide and $[^{15}N]$ acetamide instead of urea also demonstrated the presence of labelled benzoic acid.

The deviations of the experimental values from the theoretical of isotopolog signal intensities for natural isotope-abundance benzoic acid are all within the experimental error margin for this analytical method (**Table 8**). More data of LC-MS, HRMS and LRMS analyses of the solutions and precipitates in trap 1 of this and other experiments can be found in **Appendix A1**.

Table 8. Comparison of the isotope ratio of MS signal intensities of benzoic acid found in trap 1 (peak 2, $R_T = 4.2$ min) in the experiments 1.1, 1.3 and 1.5 with the simulated isotopolog mass distribution of natural isotope-abundance benzoic acid.

m/z	Formula	Intensity of selected signals, %			Natural isotopolog pattern
		Experiment 1.5	Experiment 1.1	Experiment 1.3	
123.0438	$^{12}C_7^1H_7^{16}O_2$	92.07	92.05	91.89	92.25
124.0473	$^{12}C_6^{13}C^1H_7^{16}O_2$	7.36	7.36	7.53	7.13
125.0492	$^{12}C_5^{13}C_2^1H_7^{16}O_2$	0.57	0.59	0.58	0.62

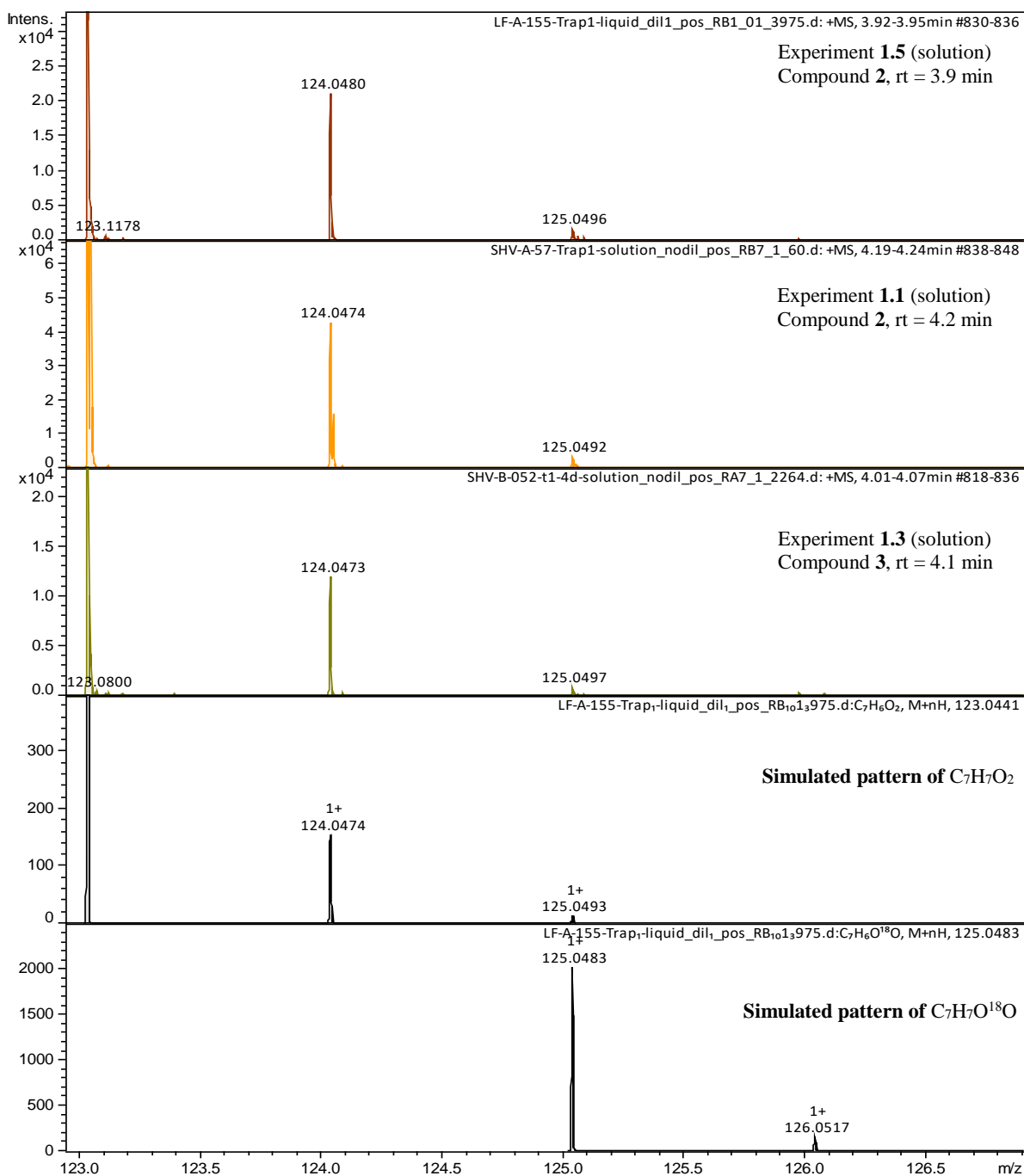


Figure 70. Comparison of the mass spectra of benzoic acid found in trap 1 (peak 2, $R_T = 4.2$ min) in the experiments **1.1**, **1.3** and **1.5** with the simulated isotopolog mass distribution of natural isotope-abundance benzoic acid and ^{18}O -labelled benzoic acid.

To be confident that the minor signal m/z 125.0492 in these isotopolog patterns indeed belonged to natural isotope-abundance benzoic acid $^{12}\text{C}_5^{13}\text{C}_2\text{H}_7^{16}\text{O}_2$ ($M+2$ for two ^{13}C) (**Table 9**) and was not m/z 125.0496 that would originate from ^{18}O -labelled benzoic acid, $M = ^{12}\text{C}_7\text{H}_7^{16}\text{O}^{18}\text{O}$, we used the “automatic signal assignment” (Bruker software) tool and forced the analytical program to fit formula $\text{C}_7\text{H}_7\text{O}^{18}\text{O}$ to signal 125.0492. The obtained data is summarised in **Table 9** (the assignment of benzoic acid to m/z 123.0444 is shown as an example of a good correspondence of the formula to the signal). The values of mSigma (isotopic pattern

fit factor) for the suggested ^{18}O -labelled benzoic acid and error margin are above the standard deviation or are indefinable.

Table 9. Results of using automagical tool for signal assignment of Bruker software.

Experiment	Measured m/z	Ion Formula	Sum Formula	error [ppm]	mSigma	Adduct
1.5	123.0444	$\text{C}_7\text{H}_7\text{O}_2$	$\text{C}_7\text{H}_6\text{O}_2$	-2.6	1.6	M+H
	125.0496	$\text{C}_7\text{H}_7\text{O}^{18}\text{O}$	$\text{C}_7\text{H}_6\text{O}^{18}\text{O}$	-10.5	n.a.	M+H
1.1	123.0438	$\text{C}_7\text{H}_7\text{O}_2$	$\text{C}_7\text{H}_6\text{O}_2$	2.2	1.4	M+H
	125.0492	$\text{C}_7\text{H}_7\text{O}^{18}\text{O}$	$\text{C}_7\text{H}_6\text{O}^{18}\text{O}$	-7.5	n.a.	M+H
1.3	123.044	$\text{C}_7\text{H}_7\text{O}_2$	$\text{C}_7\text{H}_6\text{O}_2$	0.1	2.7	M+H
	125.0497	$\text{C}_7\text{H}_7\text{O}^{18}\text{O}$	$\text{C}_7\text{H}_6\text{O}^{18}\text{O}$	-11.1	n.a.	M+H

Consequently, following the data in **Figure 70** and **Table 8-Table 9**, we can safely confirm the complete absence of measurable ^{18}O -isotopes in benzoic acid obtained in the experiments from trap 1.

2.2.2. Trap 2: CO_2 trapped as benzoic acid (benzamide from trapping HNCO not found by LC-MS)

Analyses of trap 2 were a big challenge in this work. In the first experiments, the content of trap 2 was kept at room temperature, and the produced chromatogram of the sample looked very complicated with over 60 different signals, where an expected benzoic acid was a very minor product, if it was present (**Figure 71**).

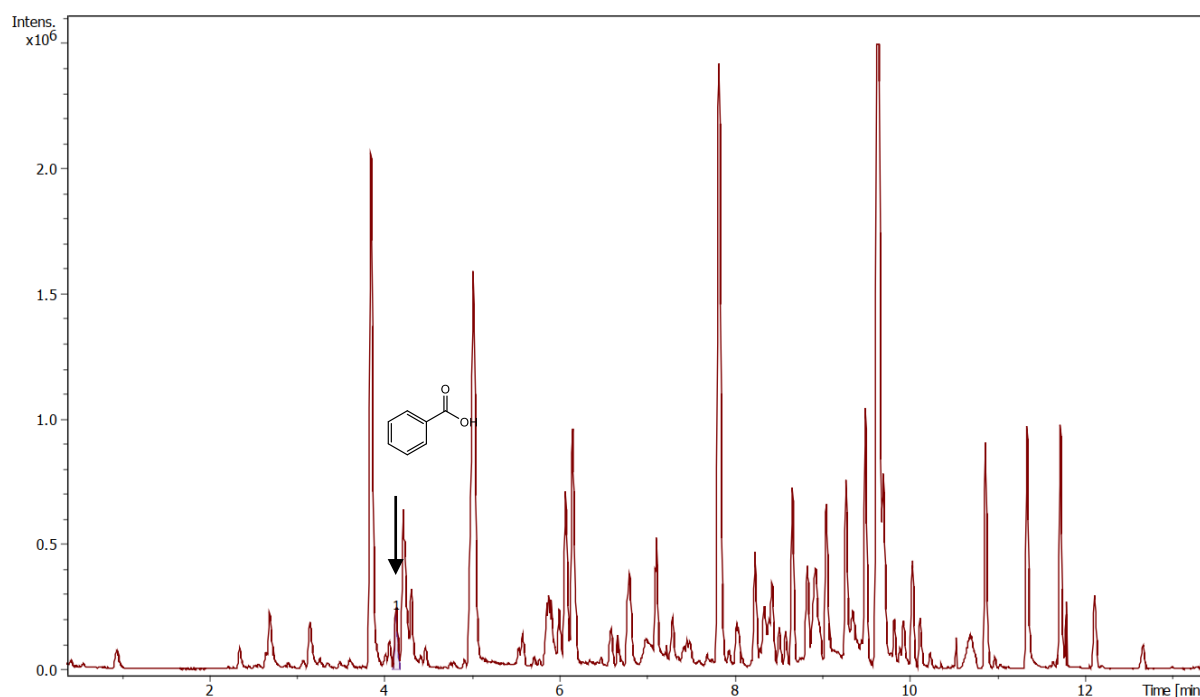


Figure 71. Chromatogram of the LC-MS analysis of trap 2 solution of experiment **1.2** after 120 h of heating. Peak 1 (rt = 4.1 min) benzoic acid ($\text{C}_7\text{H}_6\text{O}_2$). All other peaks are result of overphenylation of PhMgBr in THF under rt.

An attempt at analysing all the signals led us conclude that the majority of compounds are the results of overphenylation reactions due to the high activity of PhMgBr (**Table 10**, **Figure A268**).

Table 10. Full list of identified compounds of LC-MS analysis of trap 2 solution of experiment **1.1** after 120 h of heating. Chemical formulas were suggested by the “automagical signal assignment” tool (Bruker software).

Peak number	RT (min)	m/z of the main signal	Suggested chemical formula	Peak number	RT (min)	m/z of the main signal	Suggested chemical formula
1	1.7	73.0648	C ₄ H ₈ O	23	8.3	271.1481	C ₂₁ H ₁₈
2	2.7	117.0910	C ₆ H ₁₂ O ₂	24	8.6	354.2387	C ₁₈ H ₃₁ N ₃ O ₄
3	3.9	149.0961	C ₁₀ H ₁₂ O	25	8.7	287.1430	C ₂₁ H ₁₈ O
4	4.3	105.0699	C ₁₀ H ₁₀	26	8.9	228.2322	C ₁₄ H ₂₉ NO
5	4.3	167.0855	C ₁₃ H ₁₀	27	9.1	254.2478	C ₁₆ H ₃₁ NO
6	4.5	165.0900	C ₁₀ H ₁₂ O ₂	28	9.3	280.2635	C ₁₈ H ₃₃ NO
7	4.5	163.1117	C ₁₁ H ₁₄ O	29	9.6	256.2635	C ₁₆ H ₃₃ NO
8	4.8	101.0961	C ₆ H ₁₂ O	30	9.7	282.2791	C ₁₈ H ₃₅ NO
9	5.0	119.0855	C ₉ H ₁₀	31	10.1	284.2948	C ₁₈ H ₃₇ NO
10	5.1	177.0910	C ₁₁ H ₁₂ O ₂	32	10.2	310.3104	C ₂₀ H ₃₉ NO
11	5.3	149.0961	C ₁₀ H ₁₂ O	33	10.2	378.3155	C ₂₇ H ₃₉ N
12	5.9	135.0625	not found	34	10.7	419.3156	C ₂₆ H ₄₂ O ₄
13	6.1	145.1012	C ₁₁ H ₁₂	35	10.9	394.3468	C ₂₈ H ₄₃ N
14	6.2	167.0855	C ₁₃ H ₁₀	36	11.6	424.4513	C ₂₈ H ₅₇ NO
15	6.5	279.1356	C ₁₇ H ₂₀ O ₂	37	11.7	464.4826	C ₃₁ H ₆₁ NO
16	6.7	237.1274	C ₁₇ H ₁₆ O	38	11.8	452.4826	C ₃₀ H ₆₁ NO
17	6.9	221.1536	C ₁₄ H ₂₀ O ₂	39	11.9	478.4982	C ₃₂ H ₆₃ NO
18	6.9	183.0804	C ₁₃ H ₁₀ O	40	12.0	504.5139	C ₃₄ H ₆₅ NO
19	7.4	253.1223	C ₁₇ H ₁₆ O ₂	41	12.2	480.5139	C ₃₂ H ₆₅ NO
20	7.4	315.1743	C ₂₃ H ₂₂ O	42	12.3	506.5295	C ₃₄ H ₆₇ NO
21	7.8	331.1693	C ₂₃ H ₂₂ O ₂	43	12.7	508.5452	C ₃₄ H ₆₉ NO
22	7.9	243.1168	C ₁₉ H ₁₄	44	12.8	534.5608	C ₃₆ H ₇₁ NO

In the next steps of the experiment, we placed trap 2 in the chiller filled with acetone and dry ice. It slowed down the reactions of PhMgBr, and we successfully detected and measured the isotopolog ratio of benzoic acid (**Figure 72**).

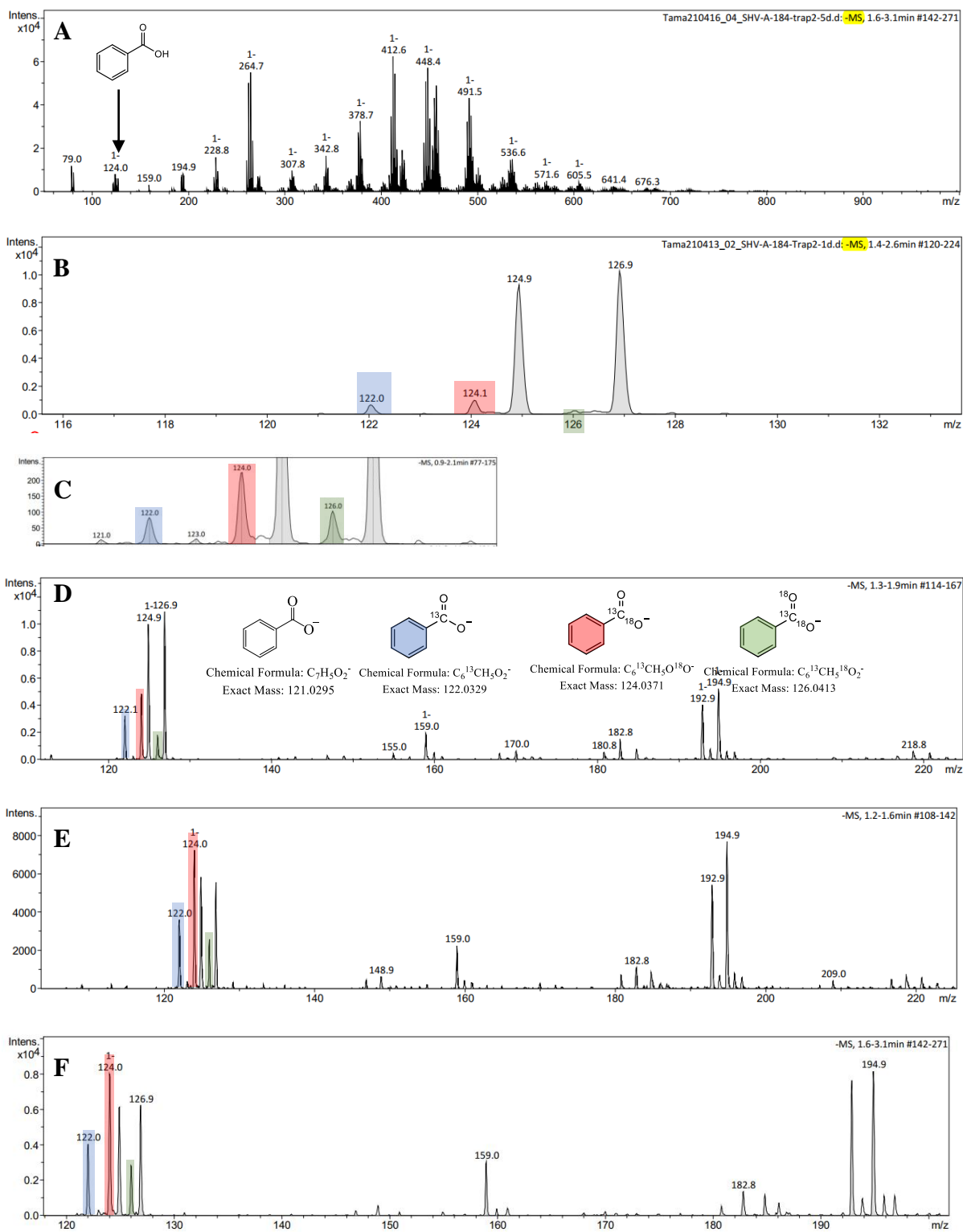


Figure 72. Results of low-resolution negative-ion mode mass analyses of trap 2 of experiment 1.7. **A** – total-ion chromatogram after 120 h of heating. **B-F** – sampling of trap 2 solution after 24, 48, 72, 96 and 120 hours after the start of the heating (sampling directly from the trap 2 during the reaction). $[^{13}C]$ benzoic acid (m/z 122.0330 $[M-H]^-$) marked blue, $[^{13}C^{18}O]$ benzoic acid (m/z 124.0371 $[M-H]^-$) red, $[^{13}C^{18}O_2]$ benzoic acid (m/z 126.0410 $[M-H]^-$) green.

In the fraction of benzoic acid, we identified four different isotopologs (**Figure 72, D**). Unlabeled isotope $C_7H_6O_2$ presents a very minor signal that is most likely originated from air pollution. Within the experiments, more than 85 % of the benzoic acid fraction was enriched with ^{13}C atom, originated from urea, 34-90 % enriched with $^{13}C^{18}O$ and only a very small part had max 24 % $^{13}C^{18}O_2$ (**Table 11**). Given the low concentration of benzoic acid in trap 2 solutions, the isotopolog enrichments measured over reaction time passing vary quite strongly but do not change the overall tendency of enrichment of a particular $C_7H_6O_2$ -isotopolog ($^{13}C^{16}O_2$, $^{13}C^{16}O^{18}O$ and $^{13}C^{18}O_2$) over time (**Table 11**). In the experiments where water was initially added to simulate wet-and-evaporating conditions, the same isotopologs except $^{13}C^{18}O_2$ were detected. More data of LC-MS, HRMS and LRMS analyses of trap 2 solution of other experiments can be found in **Appendix A1**.

Table 11. Results of the study of isotopolog ratios of benzoic acid obtained from trap 2 during 5 days of experiments **1.6**, **1.8** and **1.10**. The ratios were determined from the absolute intensities of signals m/z 121.0295 ($[C_7H_5O_2-H]^-$), 122.0329 ($[C_6H_5O_2^{13}C-H]^-$), 124.0371 ($[C_6H_5O^{13}C^{18}O-H]^-$) and 126.0413 ($[C_6H_5^{13}C^{18}O_2-H]^-$) in HRMS of the selected chromatogram peak (LRMS shown in **Figure 72**).

Heating time, h	Experiment 1.6				Experiment 1.8				Experiment 1.10			
	$C_7H_6O_2$	$C_6H_6O_2$ [^{13}C]	C_6H_6O [$^{13}C^{18}O$]	C_6H_6O [$^{13}C^{18}O_2$]	$C_7H_6O_2$	$C_6H_6O_2$ [^{13}C]	C_6H_6O [$^{13}C^{18}O$]	C_6H_6O [$^{13}C^{18}O_2$]	$C_7H_6O_2$	$C_6H_6O_2$ [^{13}C]	C_6H_6O [$^{13}C^{18}O$]	C_6H_6O [$^{13}C^{18}O_2$]
24	3.51	38.72	57.77	-	-	-	-	-	5.06	82.91	12.03	-
48	3.07	19.58	52.83	24.53	37.53	34.27	28.20	-	-	92.83	7.17	-
60	-	-	-	-	-	-	-	-	6.53	85.91	7.56	-
72	-	32.61	49.06	18.33	17.26	36.94	39.64	6.16	14.33	74.02	11.65	-
84	-	-	-	-	-	-	-	-	10.42	79.39	10.19	-
96	-	26.89	54.00	19.11	-	50.15	49.85	-	4.74	86.45	8.80	-
108	-	-	-	-	-	-	-	-	15.57	66.16	18.27	-
120	-	27.23	53.76	19.01	11.48	40.62	41.93	5.97	9.30	90.70	-	-

2.3. Inorganic cyanate (NCO^-) and carbamoyl phosphate (CP_i)

After demonstrating successful reasoning towards dissociative mechanisms, the missing piece was detecting the intermediates of the reaction – inorganic cyanate (NCO^-) and carbamoyl phosphate (CP_i).

The ^{13}C chemical shift of the cyanate anion (NCO^-) in D_2O has been reported to resonate at $\delta_C = 129.43$ or 129.54 ppm (s) at pH 8.5.²⁸⁵ The expected ^{13}C and ^{31}P chemical shifts and multiplicities of inorganic carbamoyl phosphate (CP_i) in water depend on the buffer, pH and internal or external references utilised at different magnetic field strengths B_0 : $\delta_P = -1.41$ ppm (s)²⁸⁵ and -1.75 to -2.5 ppm (s)²⁸⁶ both at $B_0 = 202.5$ MHz or $\delta_P = -4.35$ ppm (d, $J_{CP} = 4.7$ Hz) at $B_0 = 121.4$ MHz²⁸⁷ and $\delta_C = 157.39$ ppm (s) at $B_0 = 125.7$ MHz²⁸⁵ or 156.85 ppm (d, $J_{CP} = 4.7$ Hz) at $B_0 = 75.4$ MHz.²⁸⁷ We have never found any ^{13}C NMR peak resonating at around δ_C 130 ppm in any of our DMSO-*d*₆ or D_2O extracts, neither in early time points of the reaction with glycerol or MPG, nor in those urea-assisted phosphorylation experiments that have been carried out with [^{13}C]urea (**5c**). So, we focused our search for an NMR spectroscopic signature for CP_i .

As a reference compound, we tested the commercial dibasic hydrate of the lithium salt of **CP_i** as a 0.06 mM solution in DMSO-*d*₆:D₂O (5:1 v/v). Due to the low concentration of the solution and its poor solubility in DMSO-*d*₆, we did not detect any signals by ¹³C NMR spectroscopy. We did identify by ³¹P{¹H} NMR spectroscopy (red spectrum **Figure 73**) two signals corresponding to **CP_i** (−1.46 ppm) and **PP_i** (−7.78 ppm).

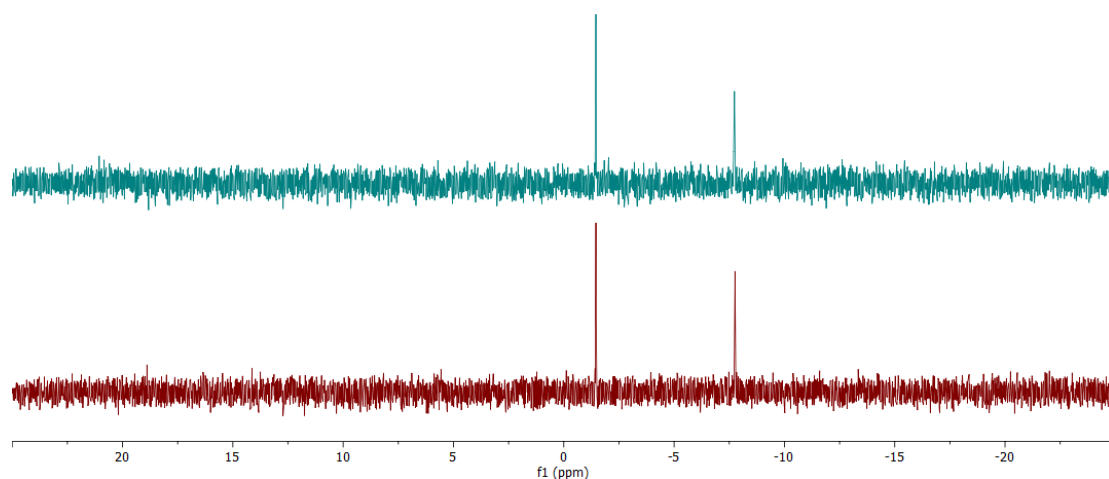


Figure 73. ³¹P{¹H} (red) and ³¹P (blue) NMR spectra (202.5 MHz, DMSO-*d*₆:D₂O 5:1 v/v) of 0.06 mM **CP_i** (5 mg dibasic lithium hydrate salt in 0.5-0.6 ml): $\delta_p = -1.46$ (s) **CP_i** and $\delta_p = -7.78$ (s) **PP_i**.

From the measured difference in decay rates of **P_i**, urea and MPG described later in section 2.4.2 (**Figure 88**) we could calculate the best range of reaction time when potentially a maximum amount of **CP_i** could be present, if it formed immediately after the (early) consumption of **P_i** and urea but before the (later) consumption of considerable amounts of MPG (measured by HPLC-ELSD), which in a neat reaction mixture was most probable after 2-3 hours of heating at 115 °C.

A crude mixture of glycerol (**5**), [¹³C]urea (**2c**) and **P_i** (1:1:1) was heated at 115°C for 2 hours. NMR acquisitions were made on "fresh" solutions of D₂O and DMSO-*d*₆ prepared just before the NMR experiment performed on a 600 MHz machine equipped with a QCI cryoprobe. Due to the presence of a ¹³C-labelled carbon atom in the urea molecule, **CP_i** was expected to present itself as a doublet by, possibly both, ³¹P NMR and, especially, by ¹³C NMR spectroscopy.²⁸⁷ After a series of experiments, we could positively confirm the absence of an NMR signal of **CP_i** in the crude mixture after 2 hours of heating at 115 °C (**Figure 74**, **Figure 75**).

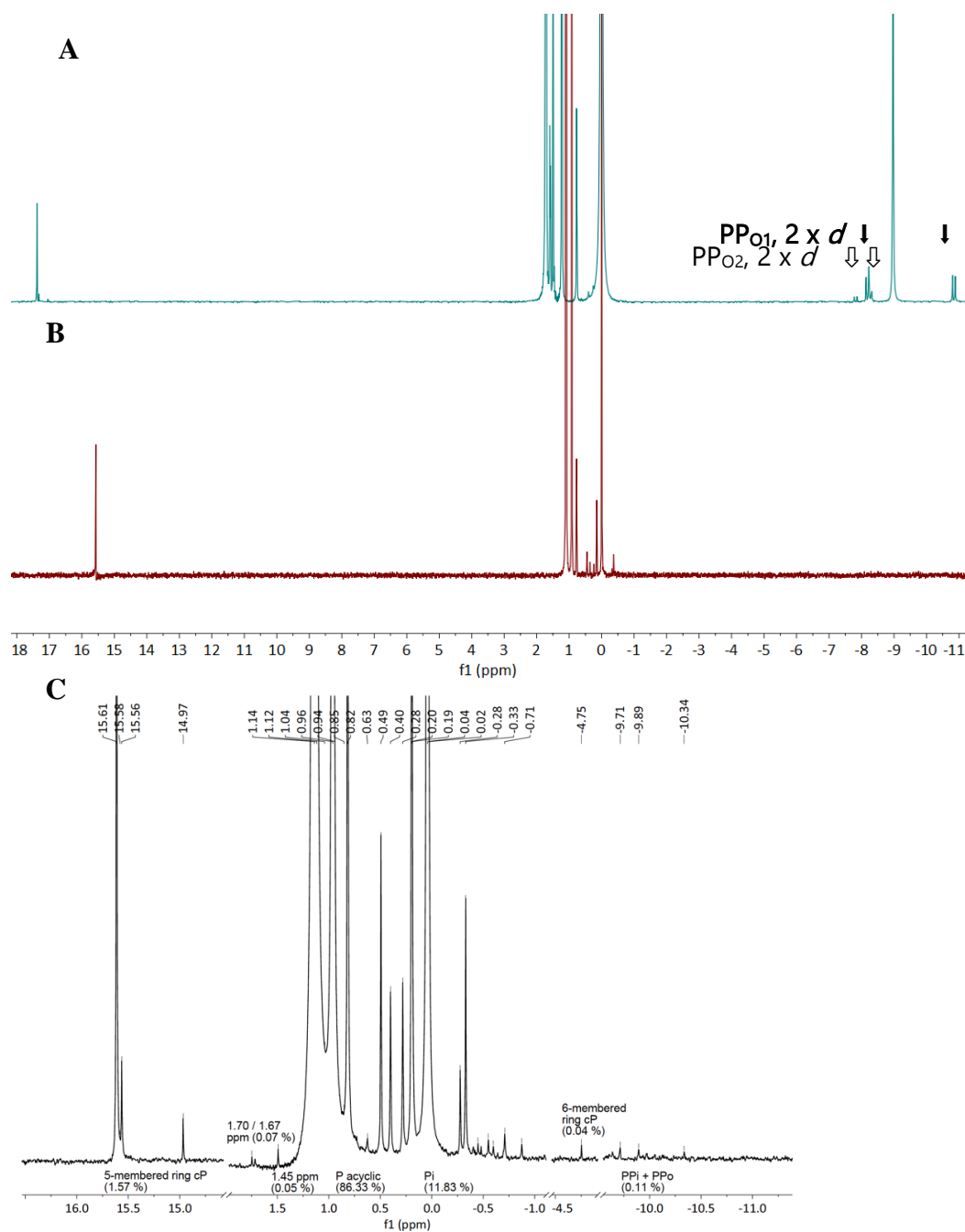


Figure 74. $^{31}\text{P}\{^1\text{H}\}$ NMR spectra (242.9 MHz) of freshly prepared extracts of a mixture of glycerol (**5**), ^{13}C urea (**2c**) and NaH_2PO_4 (**P_i**) (1:1:1, 0.5 mmol each) after 2 hours heating neat at 115 °C. **A** (blue) – in D_2O , **B** (red) and **C** (black)– in $\text{DMSO-}d_6$. **A** and **B**: 16 scans, **C**: 2059 scans. All spectra referenced to internal **P_i**: $\delta_{\text{P}_i} = 0.00$ ppm.

Apart from the large ^1H -coupled ^{13}C resonances of unreacted urea, that is, the huge singlet at 160.50 ppm in D_2O and $\text{DMSO-}d_6$, the large singlet at 157.0 ppm in D_2O and 157.57 ppm in $\text{DMSO-}d_6$, showing the early emergence of 1-glyceryl carbamate (see **Figure 58**, 2 hours spectrum) and the doublet CH and triplet CH_2 from unreacted glycerol, only tiny ^{31}P -coupled ^{13}C resonances appeared in the middle-field CH and CH_2 region from emerging 1-glyceryl phosphate and 2-glyceryl phosphate (**Figure 75**, see arrows and compare with JMOD ^{13}C NMR spectra, cf. **Figure 75**).

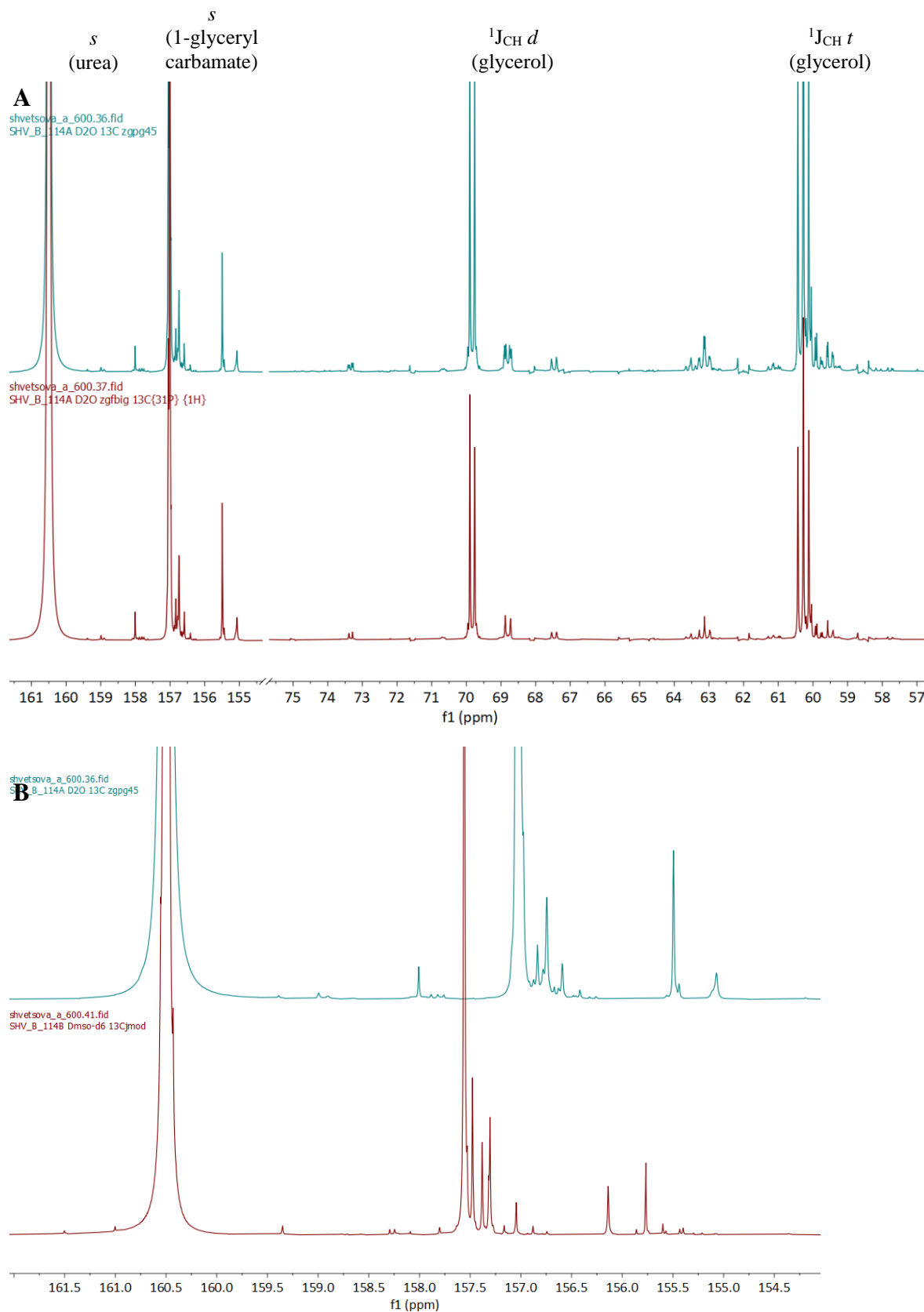


Figure 75. ^1H -coupled ^{13}C NMR spectra (150.9 MHz) of freshly prepared extracts of a mixture of glycerol (**5**), [^{13}C]urea (**2c**) and NaH_2PO_4 (**Pi**) (1:1:1, 0.5 mmol each) after 2 hours heating neat at 115 $^\circ\text{C}$. **A** – NMR solvent D_2O , **red**: $^{13}\text{C}\{^{31}\text{P}\}$ NMR ; **blue** ^{13}C NMR. **B** – 163-155 ppm zoom on ^{13}C NMR, **blue**: in D_2O ; **red** – in $\text{DMSO-}d_6$. Signals showing a J_{CP} coupling are marked with their $^1J_{\text{CH}}$ (*t* or *d*) and an empty arrow for 1-glyceryl phosphate and a filled arrow for 2-glyceryl phosphate.

There are no ^{31}P - ^{13}C couplings visible in the low-field (carbonyl) region of the fully coupled ^{13}C NMR spectrum. There are no ^{31}P resonances of whatever multiplicity visible between $\delta_{\text{p}} = -1.46$ and -4.5 ppm, not even between $\delta_{\text{p}} = -1.0$ and -8.0 ppm (**Figure 74**)²⁸⁵. Inorganic phosphate and pyrophosphate are better soluble in water than in DMSO; thus, on the **blue** spectrum, we can see that the P_i signal is more intense compared to that in the **red** spectrum. In water was detected a PP_i singlet ($\delta_{\text{PP}_i} = -8.08$ ppm) and two different PP_o resonances that could possibly belong to primary and secondary glyceryl pyrophosphates: $\delta_{\text{PP}_{o1}} = -7.29$ and -10.64 ($2 \times d$, $J = 20.9$ Hz) and $\delta_{\text{PP}_{o2}} = -6.93$ and -9.95 ($2 \times d$, $J = 20.7$ Hz). In the figure shown in **A** and **B**, 16 scans were made; however, when this scan number increased to 2059, PP_o , **diGI(CO) $_2$ P** and **diGICOP** (and others) were also visible in the DMSO-*d*₆ spectrum (**Figure 74 C**).

Even though we have never found the direct spectroscopic evidence of carbamoyl phosphate, the presence of carbamoylated products provides indirect evidence of its formation at certain stages of the reaction due to the presence of carbamoylated products. One possible explanation for the absence of the compound is its high reactivity, that results in the formation of new compounds faster than the time between cooling down the crude mixture and analysing it. Alternatively, if the compound is poorly soluble in the solvents used, it will not be extracted from the sample and will therefore not be detected.

2.4. Kinetic study of urea-assisted phosphorylation reactions

After identifying the main products and the most favourable reaction mechanism, we focused on the kinetic study of the phosphorylation to estimate the rate of phosphate consumption and compare it to the urea decay rate, together with the production of other detectable products. Hence, we first studied the urea degradation and phosphorylation degree of reaction glycerol (or MPG) with P_i and labelled urea over a period of 0-120 hours at 115 °C.

2.4.1. Phosphorylation of glycerol

We performed five independent series of experiments. Due to the small scale of reactions and the advantage of a carousel reactor to carry out many experiments at the same time, each reaction was performed in a separate open vessel and quenched at the defined reaction time. We kept using stable isotopes of urea ($[^{15}N_2]urea$, $[^{13}C]urea$) and dihydrogenphosphate ($NaH_2P[^{18}O_4]$) for tracking reaction products.

2.4.1.1. Degradation of urea

In the previous section, we discovered that urea degradation is an essential step of the phosphorylation reaction. 1H , ^{15}N and ^{13}C NMR of **2b** shown on figures **Figure 76**-**Figure 78**.

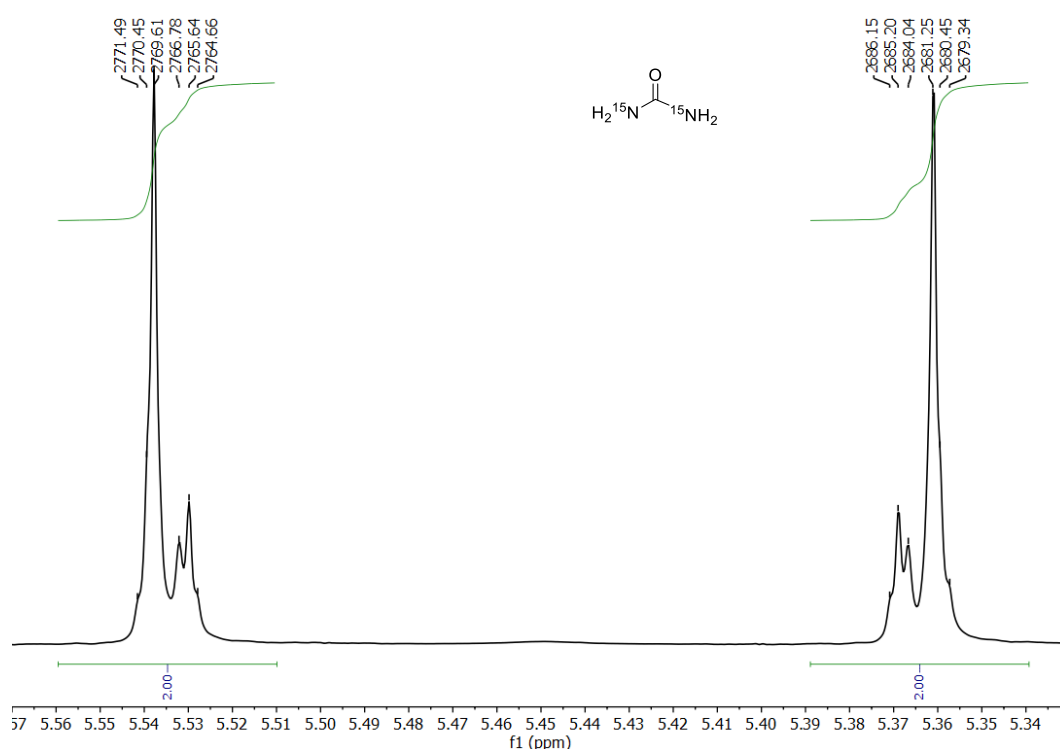


Figure 76. 1H NMR spectrum (500 MHz, $DMSO-d_6$) of 0.5 mM $[^{15}N_2]urea$ **2b** (500 MHz, $DMSO-d_6$), $\delta_H = 5.45$ (d, $^1J_{H,N} = 88.5$ Hz and long-range secondary-order $^3J_{H,N}$ couplings).

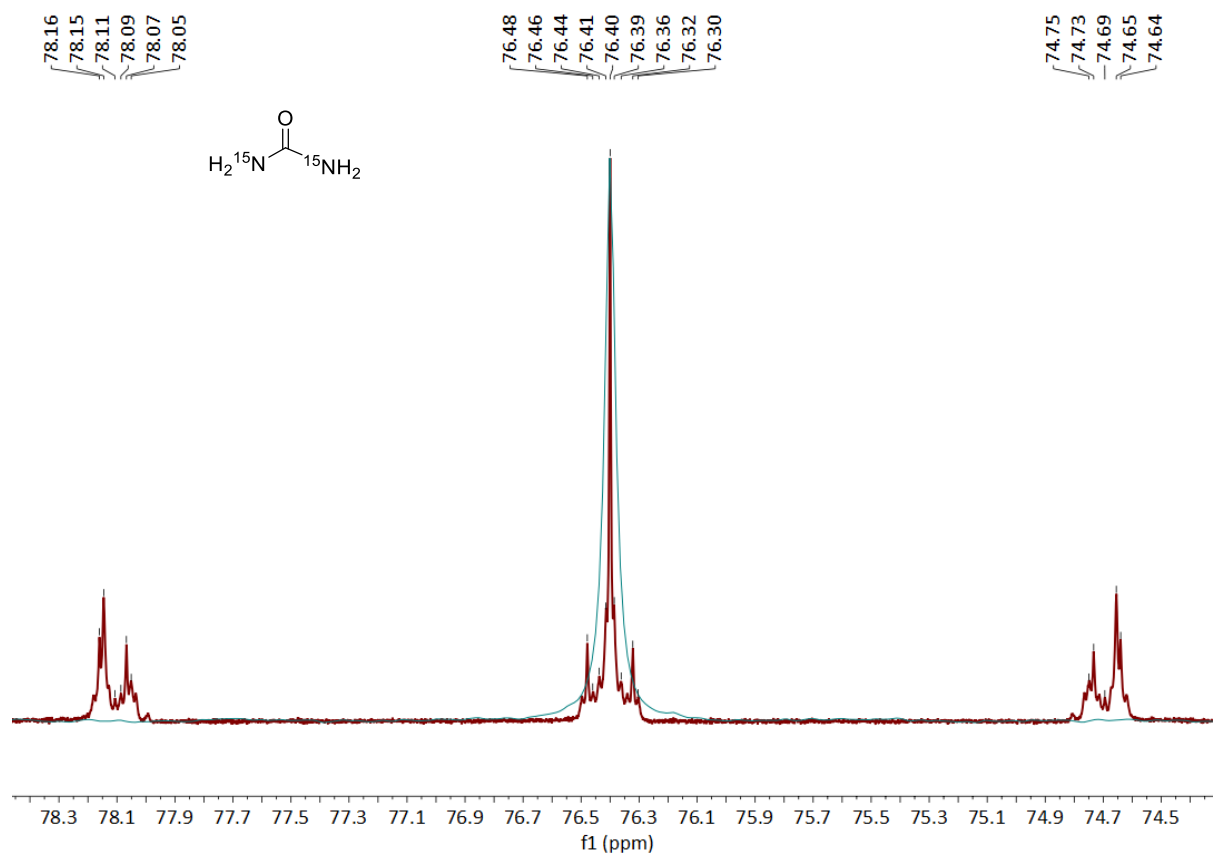


Figure 77 ^{15}N NMR spectrum (50.7 MHz, $\text{DMSO-}d_6$) of 0.5 mM **2b**. **Blue** – Proton decoupled $^{15}\text{N}\{^1\text{H}\}$ NMR spectrum at full spectral width: $\delta_{\text{N}} = 76.4$ ppm; **red** – Proton-coupled ^{15}N NMR spectrum: $\delta_{\text{N}} = 76.4$ ppm (*t*, $^1J_{\text{H,N}} = 88.5$ Hz and long-range secondary-order $^3J_{\text{H,N}}$ couplings).

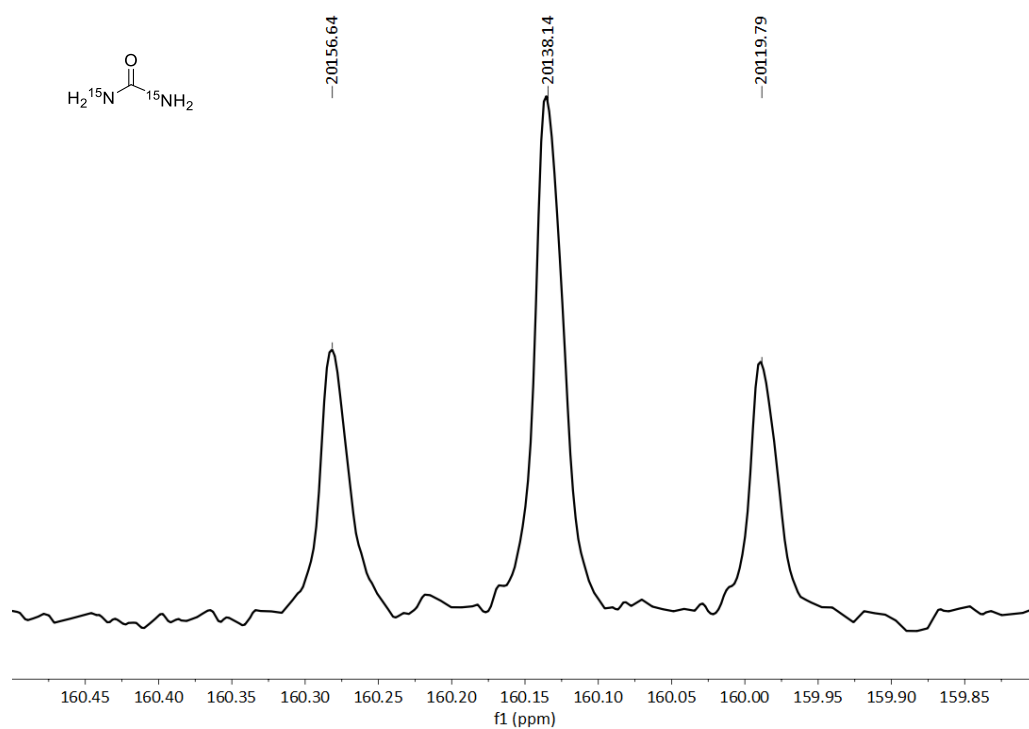


Figure 78. ^{13}C NMR spectrum (125.7 MHz, $\text{DMSO-}d_6$) 0.5 mM $[^{15}\text{N}_2]$ urea (**2b**), $\delta_{\text{C}} = 160.13$ ppm (*t*, $^1J_{\text{C,N}} = 18.6$ Hz).

In order to explore it, we heated an equimolar mixture of [$^{15}\text{N}_2$]urea and natural urea. The idea of using a mix of isotopes is to detect the appearance of [$^{14}\text{N},^{15}\text{N}$]urea that would be formed as a result of the re-addition of ammonia to isocyanic acid (**Figure 79**).

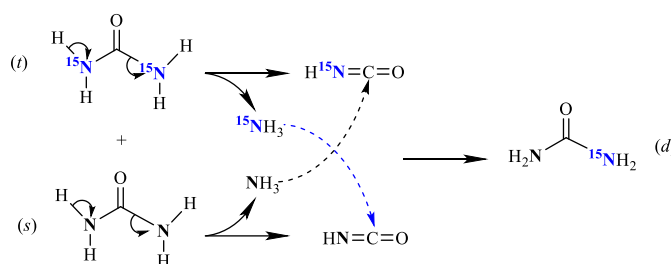


Figure 79. Scheme of urea degradation and N-exchange through isocyanic acid

This can be easily detected by ^{13}C NMR, where [^{14}N]urea is a singlet $\delta_{\text{C}} = 160.95$ ppm (s, **2a**) different from [$^{15}\text{N}_2$]urea triplet (**Figure 78**) due to the presence of labelled atoms $\delta_{\text{C}} = 160.94$ ppm (t, $^1J_{\text{C},\text{N}} = 18.6$ Hz, **2b**) (**Figure 81, A**). If the suggested exchange would appear we will detect the presence of a doublet that belongs to [$^{14}\text{N},^{15}\text{N}$]urea. At first, we heated a 1:1 **2a:2b** solution up to 100°C within 150 minutes directly in the spectrometer (**Figure 80**).

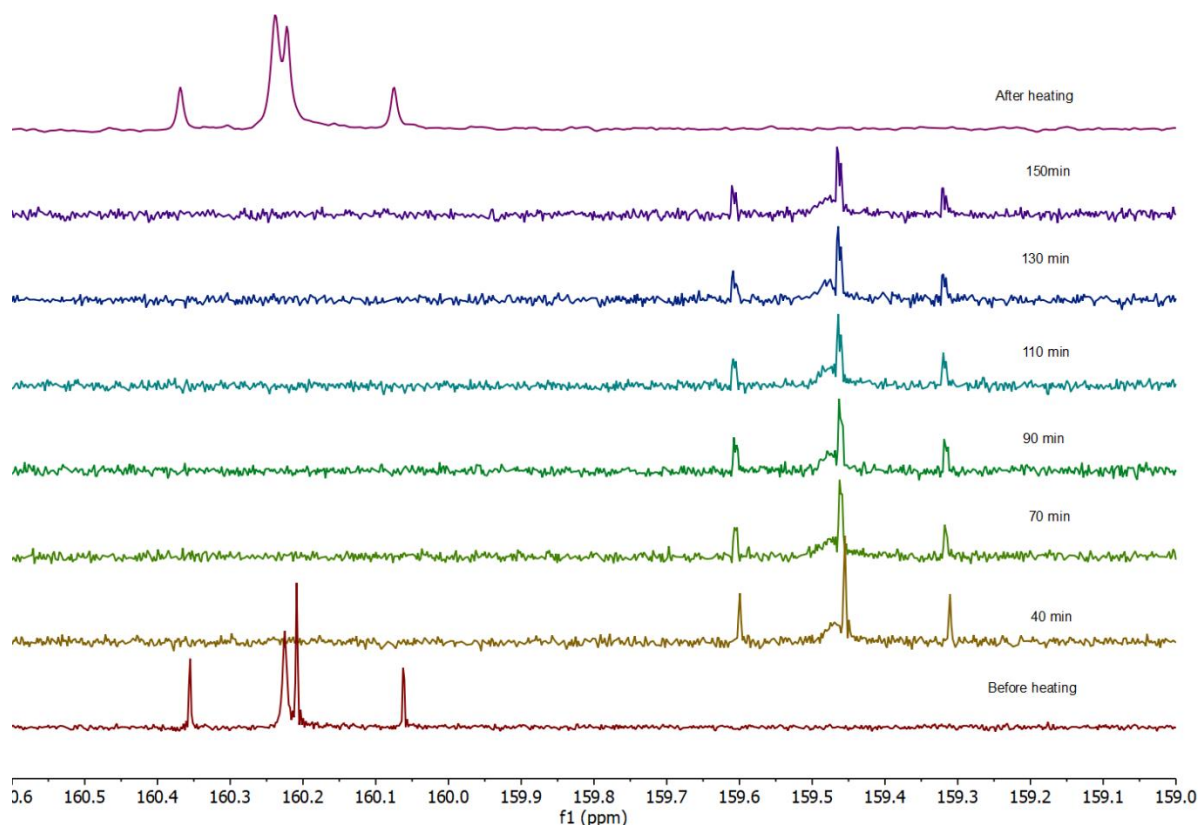


Figure 80. Stack of ^{13}C NMR spectra (500 MHz, $\text{DMSO}-d_6$) of the equimolar mixture of natural isotope-abundance urea (**2a**) and [$^{15}\text{N}_2$]urea (**2b**) (1:1, 0.5 mmol each). The sample was heated up to 100°C inside of NMR spectrometer and the NMR measurements were performed every 20-30 min. NMR spectra “before” and “after” (**Figure 81**) were made before heating and after cooling down respectively. After 150 min of experiment signals of doublet were not observed.

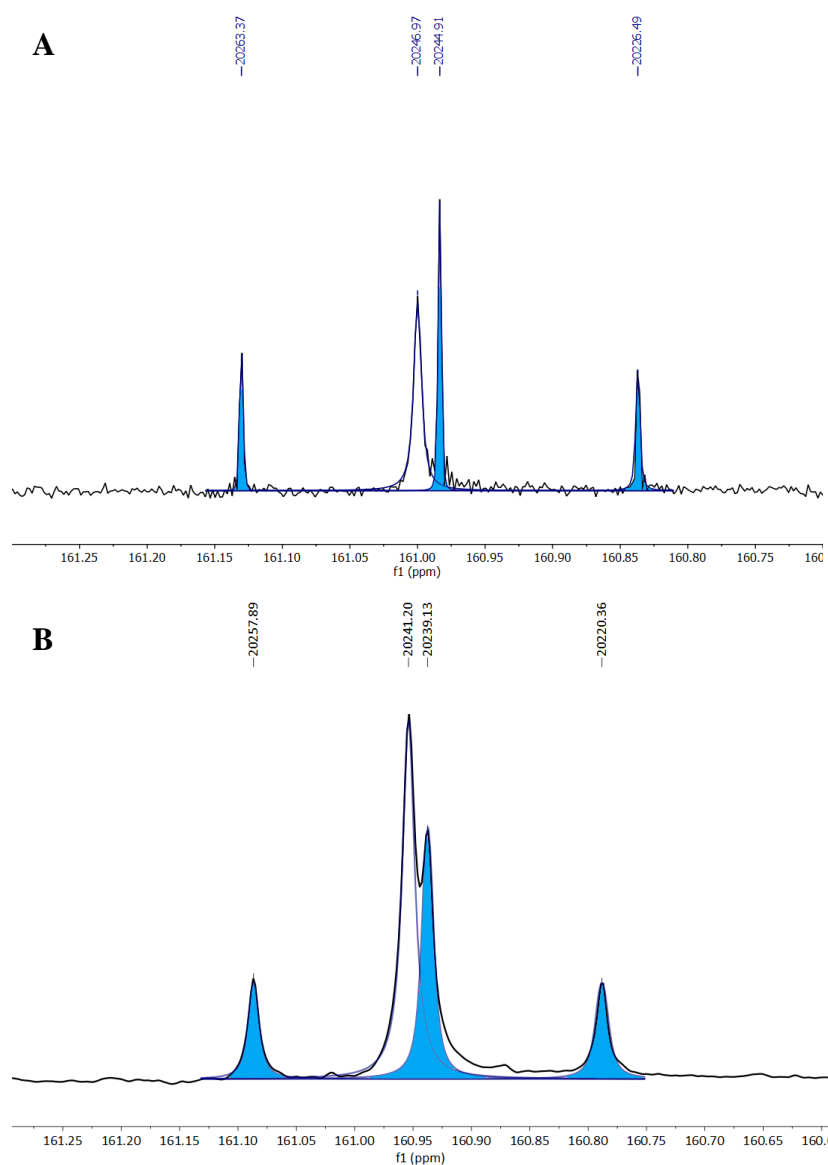


Figure 81. ^{13}C NMR spectra (125.7 MHz, $\text{DMSO-}d_6$) of the equimolar mixture of natural isotope-abundance urea (**2a**) and $^{15}\text{N}_2$ urea (**2b**) (1:1, 0.5 mmol each) taken both at rt: $\delta_{\text{C}} = 160.94$ ppm (*t*, $^1J_{\text{C,N}} = 18.6$ Hz, **2b**); $\delta_{\text{C}} = 160.95$ ppm (*s*, **2a**). Difference in frequencies (2.07 Hz) between **2a** and **2b** is due to the isotope effect for two ^{15}N nuclei versus two ^{14}N nuclei bonded to ^{13}C . **A** – before heating; **B** – after heating for 150 min up to 100 °C. Black line: spectrum, blue lines and cyan coloured peaks from deconvolution.

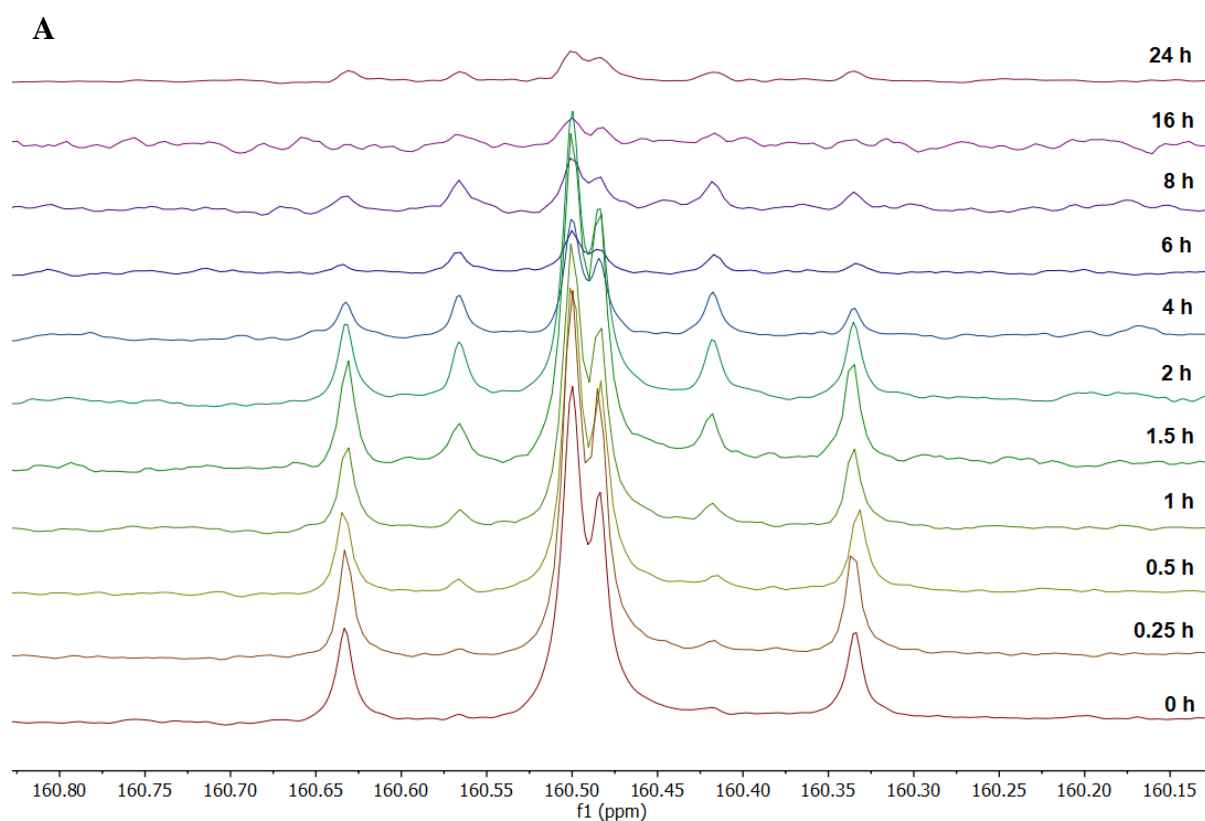
Table 12. Results from integration of ^{13}C NMR peaks of the deconvoluted urea signals of Figure 80 spectra (triplet versus singlet at [160.7-160.3 ppm]) before and after heating a $\text{DMSO-}d_6$ solution of the equimolar mixture of natural isotope-abundance urea (**2a**) and $^{15}\text{N}_2$ urea (**2b**) (1:1, 0.5 mmol each).

	Ratio of triplet versus singlet before heating, %	Ratio of triplet versus singlet after heating, %
Triplet	51.4	52.6
Singlet	48.6	47.4

Simply heating a DMSO-*d*₆ solution containing the 1:1 mixture of **2a** and **2b** to 100 °C for two hours (**Figure 80**) did not significantly change the amounts of unlabelled and labelled urea (**Table 12**), nor did any other signal appear in this timeframe. This meant that any change that would be observed in the presence of other compounds (**P_i**, glycerol) could be ascribed to their chemical potential.

2.4.1.2. Glycerol phosphorylation mixtures containing [¹⁵N₂]urea

The presence of equimolar amounts of urea (**2a:2b** 0.5:0.5 mol:mol), **P_i** and glycerol in a neat mixture that was heated at 115 °C. It gave clear evidence for the accelerated degradation of urea to ammonium cyanate within the same timeframe. The spectroscopic signature of [¹⁴N,¹⁵N]urea appeared very early in the reaction mixture, thus proving that eliminating ammonia before evaporating out of the neat mixture could re-attack isocyanate to form half-labelled urea molecules (**Figure 82**, **Figure 83**). The time-dependent degradation of urea could also be observed by ¹H NMR spectroscopy at 5.4-5.7 ppm (**Figure 84A**).



Continuation of the figure is on the next page

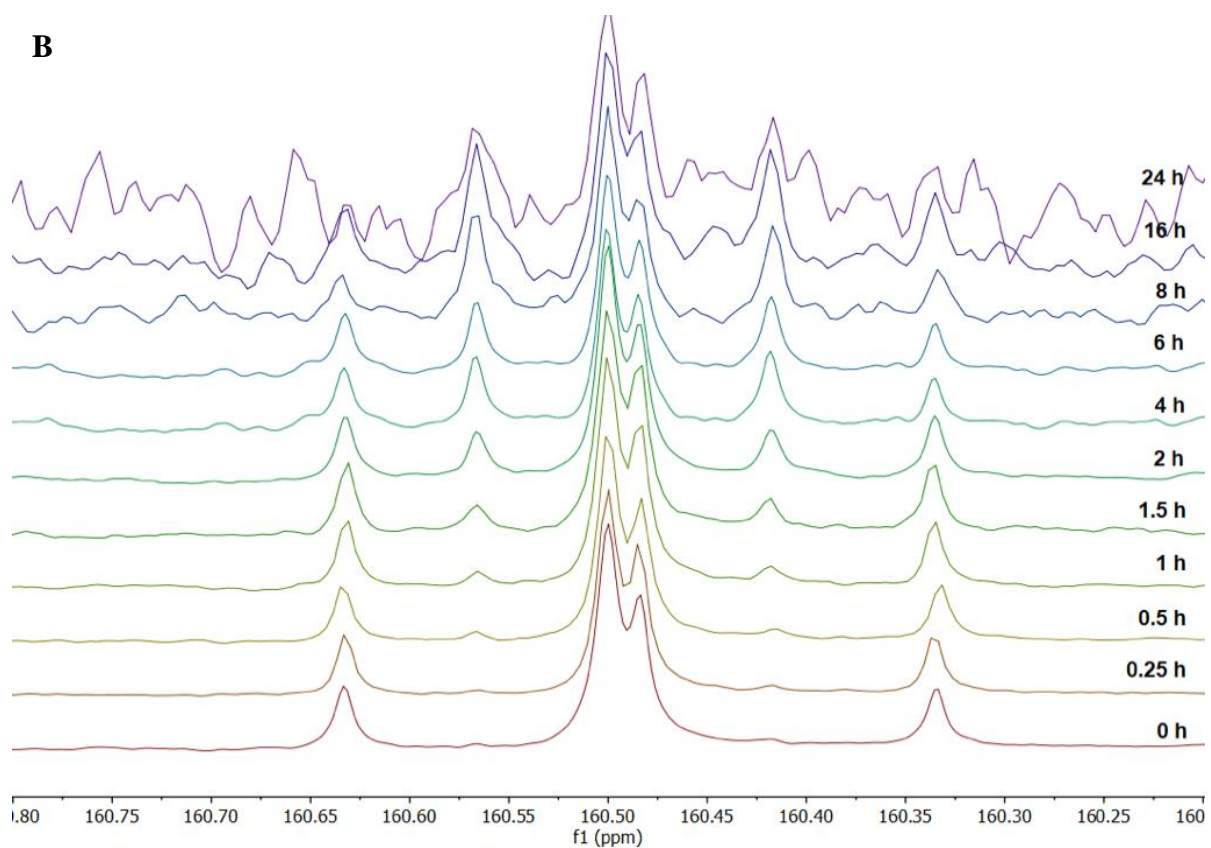


Figure 82. Stack of ^{13}C NMR spectra (125.8 MHz) zoomed on the urea signal of the DMSO- d_6 extract of a 0.5 mmol scale mixture of glycerol (**5**), natural isotope-abundance urea (**2a**), [$^{15}\text{N}_2$]urea (**2b**) and NaH_2PO_4 (**Pi**) (1:0.5:0.5:1 molar ratios) after heating neat for 0-24 hours at 115 °C. Spectra centered on the urea singlet at 160.5 ppm. $\delta_{\text{C}} = 160.50$ (s, **2a**), 160.48 (t, $^1J_{\text{C,N}} = 18.6$ Hz, **2b**), 160.49 (d, $^1J_{\text{C,N}} = 18.6$ Hz, [$^{14}\text{N},^{15}\text{N}$]urea). **A** – Stack of NMR spectra with experimental (absolute) intensities. **B** – Intensities of spectra adjusted to the intensity of the urea singlet at 0 h illustrating (in **B**) the gradually increasing signal-to-noise ratio with time passing owing to the degradation of urea (visible in **A**).

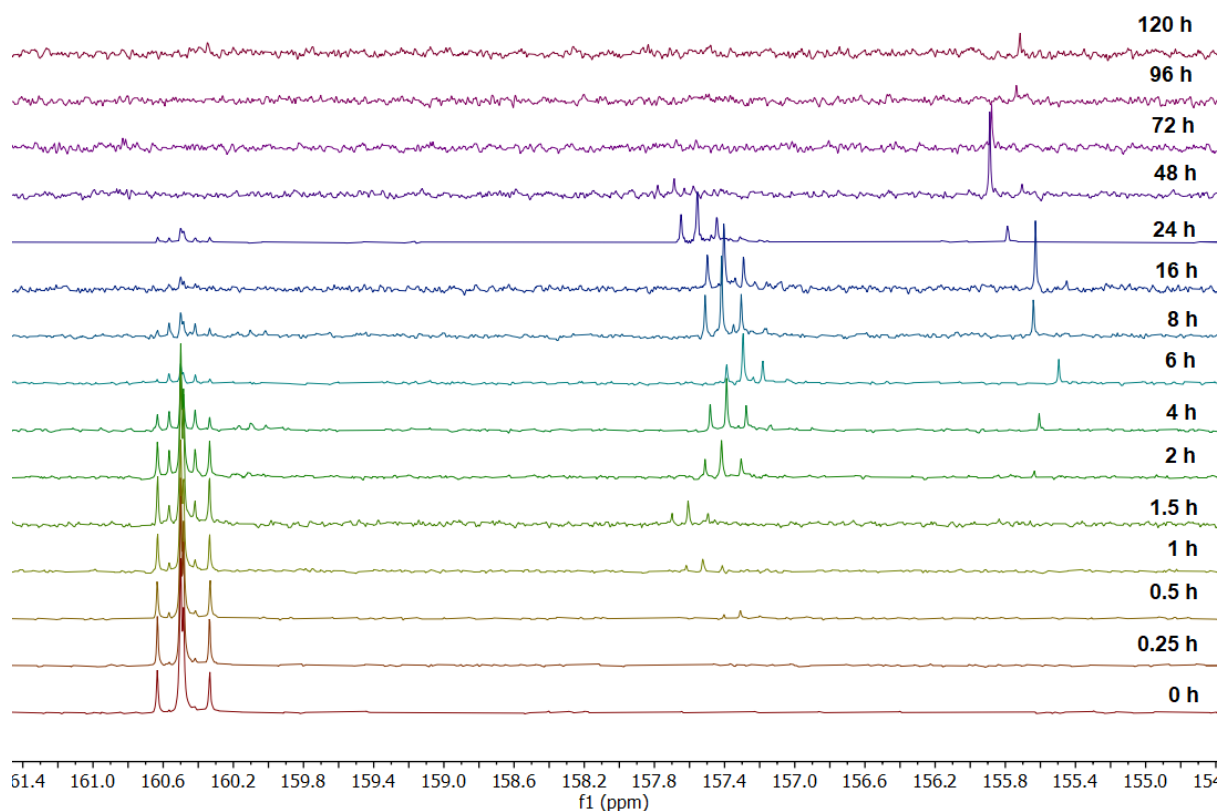


Figure 83. Stack of ^{13}C NMR spectra (125.8 MHz) at full spectral width of the DMSO- d_6 extracts of a 0.5 mmol scale mixture of glycerol (**5**), natural isotope-abundance urea (**2a**), [$^{15}\text{N}_2$]urea (**2b**) and NaH_2PO_4 (**Pi**) (1:0.5:0.5:1 molar ratios) after heating neat for 0-120 hours at 115 °C: $\delta_{\text{C}} = 160.50$ (*s*, **2a**), 160.48 (*t*, $^1J_{\text{C,N}} = 18.6$ Hz, **2b**), 165.49 (*d*, $^1J_{\text{C,N}} = 18.6$ Hz, [$^{14}\text{N},^{15}\text{N}$]urea), 157.8-157.4 (*s*, glyceryl- ^{14}N]carbamate; *d*, $^1J_{\text{C,N}} = 25.9$ Hz, glyceryl- ^{15}N]carbamate, isotope shift 1.1 Hz), 156.5-155.4 (*s*, glyceryl-1,2-cyclic carbonate). Stack centered on urea singlet at $\delta_{\text{C}} = 160.50$ ppm. Presence of carbamate and carbonate groups confirms interpretation of HRMS as shown in **Figure 59**.

The time-incremental ^{13}C , ^1H and ^{31}P NMR spectra of this reaction mixture (taken from extracts of independent reaction batches for each timepoint) show the evolution of the formation of different classes of organic compounds (**Figure 83**, **Figure 84**, **Figure 85**). The ^{13}C resonance at $\delta_{\text{C}} \approx 157.4$ ppm belongs to glyceryl carbamate, since it is a 1:1 mixture of singlet and doublet in this mixture containing $^{15}\text{N}_2$ -half-labelled urea, which is consistent with the ^{13}C NMR spectrum of the mixture that has been labelled with [^{13}C]urea. The singlet at > 155 ppm shows emerging glyceryl-1,2-cyclic carbonate.

From ^1H - ^1H COSY and ^1H - ^{31}P HMBC spectra (**Figure 50**, **Figure 52**) we cannot determine with certainty whether the carbamate and 1,2-cyclic carbonate are glycerol or glyceryl phosphate derivatives. However, the rapid appearance of the first ^{31}P signals from the 1-glyceryl and 3-glyceryl phosphates after 15 minutes at 115 °C (**Figure 85**), as well as the equally rapid emergence of a characteristic double ^1H - dd system at $\delta_{\text{H}} \approx 3.8$ and 3.9 ppm (**Figure 84A**) make us think that the major ^{13}C carbamate and cyclic carbonate signals are due to the corresponding primary glyceryl phosphate esters rather than glycerol without phosphate. Integrations of the ^{13}C and ^{31}P spectroscopic analyses are summarised in **Table 13-Table 16**. The obtained data was used for the kinetic fittings.

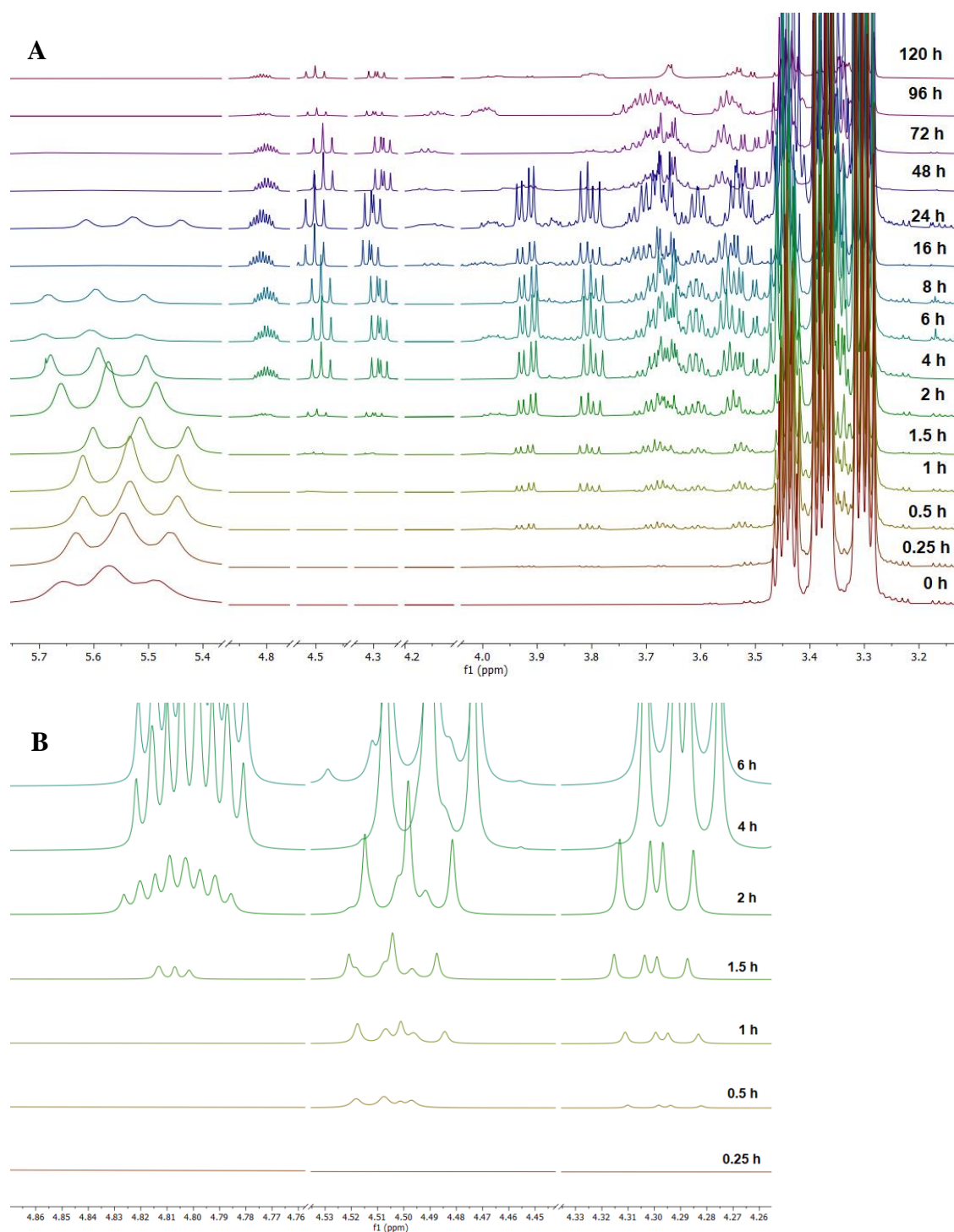


Figure 84. Stack of ¹H NMR spectra (500 MHz) of the DMSO-*d*₆ extract of a 0.5 mmol scale mixture of glycerol (**5**), natural isotope-abundance urea (**2a**), [¹⁵N₂]urea (**2b**) and NaH₂PO₄ (**P_i**) (1:0.5:0.5:1 molar ratios) after heating neat for 0-120 hours at 115 °C. Each time-point was an individual experiment. Spectra centered and the signal intensities adjusted to the residual *d*₅-quintet of DMSO-*d*₆ at δ_H = 2.52 ppm (not shown). δ_H (2 h) = 5.57 (br *s*, **2a** + carbamate), 5.58 (br *d*, ¹J_{H,N} = 84 Hz, **2b** + [¹⁵N]carbamate), 4.83-4.28 (*ddd*, *t*, *dd*, H_x, H_b and H_a of glyceryl-1,2-cyclic carbonate, **Figure 49**), 4.00-3.20 (mix of glyceryl phosphates, H_b' and H_a' of glyceryl-1,2-cyclic carbonate and glycerol). The decrease of the signal intensities in the late time points are due to lower solubility of the reaction mixtures. **A** – Spectrum width for all signals except solvent; **B** – Zoom into 4.90-4.25 ppm at 0.25-6 hours.

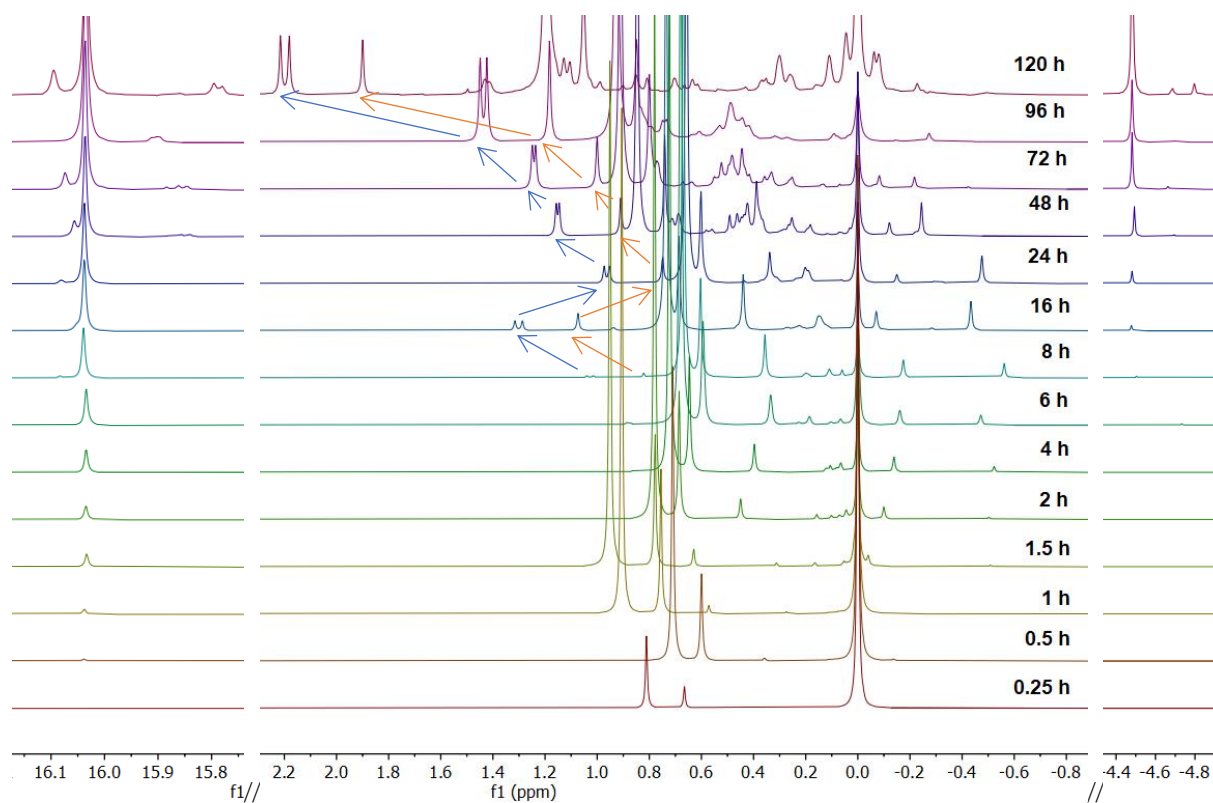


Figure 85. Stack of $^{31}\text{P}\{^1\text{H}\}$ NMR spectra (202.5 MHz) at full spectral width of the DMSO- d_6 extracts of a 0.5 mmol scale mixture of glycerol (**5**), natural isotope-abundance urea (**2a**), [$^{15}\text{N}_2$]urea (**2b**) and NaH_2PO_4 (**P_i**) (1:0.5:0.5:1 molar ratios) after heating neat for 0-120 hours at 115 °C. Stack centered on the **P_i** singlet at $\delta_{\text{P}_i} = 0.00$ ppm: $\delta_{\text{P}} = 15.8\text{-}16.2$ ppm (**5cGIP**), 2.2 to -0.5 ppm (**GI-1P**, **GI-2P**, **[GI]₂P**; cyclic carbonates, cf. blue and orange arrows), -4 to -7 (**6cGIP**).

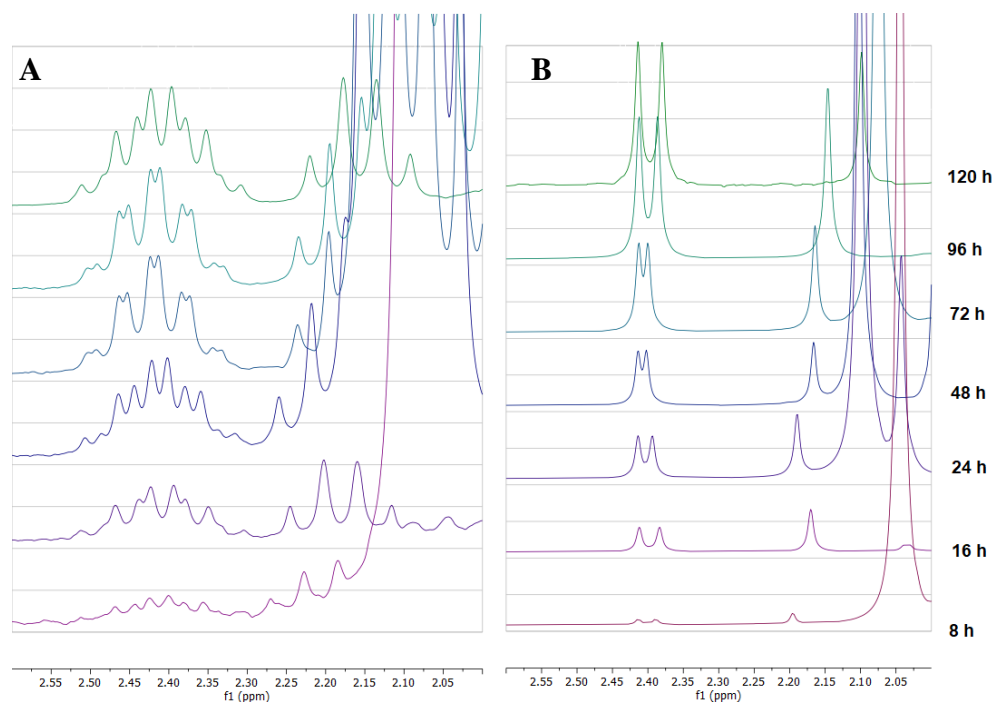


Figure 86. $^{31}\text{P}\{^1\text{H}\}$ NMR (202.5 MHz, DMSO- d_6) of selected zoom at 2.6-2.0 ppm of **Figure 85**; reaction times 8-120 h, at 115 °C. Stacks centered on the quintet's most downfield maxima at $\delta_{\text{P}} = 2.42$ ppm. **A** – ^{31}P NMR (^1H -coupled spectrum); **B** – $^{31}\text{P}\{^1\text{H}\}$ NMR (^1H -decoupled spectrum).

Table 13. Results from integrating ^{13}C NMR peaks of the deconvoluted urea signals (triplet versus doublet versus singlet at 160.7-160.3 ppm) depending on the heating time (**Figure 82**). DMSO-*d*₆ extracts of a 0.5 mmol scale mixture of glycerol (**5**), natural isotope-abundance urea (**2a**), [$^{15}\text{N}_2$]urea (**2b**) and NaH_2PO_4 (**P_i**) (1:0.5:0.5:1 molar ratios) after heating neat for 0-24 hours at 115 °C. Reactions were conducted in parallel in the carousel reactor (Materials and Methods section **4.1**), so each time point is an independent batch. We made a triplicate of each time point reaction. Error margins for all experiments were obtained following the signal-noise ratio as calculated by the MNova software, and by applying the Pythagorean theorem.²⁸⁸ For triplets and doublets the error margin was calculated from twice the signal-to-noise ratio of the highest peak.

Heating time, h	Triplet [$^{15}\text{N}_2$]urea, %	Error margin of triplet, %	Doublet [$^{14}\text{N}, ^{15}\text{N}$]urea, %	Error margin of doublet, %	Singlet [$^{14}\text{N}_2$]urea, %	Error margin of singlet, %
0	49.5	0.66	-	-	50.5	0.35
0.25	52.8	0.75	3.0	1.14	44.2	0.32
0.5	52.8	0.83	5.3	1.16	41.9	0.32
1	52.3	1.28	7.7	1.78	40.0	0.50
1.5	49.6	1.58	11.1	1.99	39.3	0.69
2	47.1	1.26	14.6	1.26	38.3	0.48
4	43.5	2.52	25.0	2.63	31.5	0.85
6	40.5	8.11	28.7	6.94	30.8	2.44
8	39.5	8.54	30.6	7.62	30.0	2.88
16	42.1	23.60	27.2	24.70	30.8	8.34
24	44.6	24.90	30.8	29.60	24.6	7.63

Table 14. Results from integrating ^1H NMR peaks of the deconvoluted 3-phosphoglyceryl-1,2-cyclic carbonate signals depending on the heating time. DMSO-*d*₆ extracts of a 0.5 mmol scale mixture of glycerol (**5**), natural isotope-abundance urea (**2a**), [$^{15}\text{N}_2$]urea (**2b**) and NaH_2PO_4 (**P_i**) (1:0.5:0.5:1 molar ratios) after heating neat for 0-120 hours at 115 °C. The integrated area of the *t* at $\delta_{\text{H}} \approx 4.5$ ppm was multiplied by five to respect five proton signals of the glyceryl-1,2-cyclic carbonate (H_x, H_a, H_b, H_a', H_b', cf. **Figure 49**) and compared to the total integral of all the signals of ^1H NMR. In all cases, the S-to-N ratio was negligible and was not considered in further calculations.

Heating time, h	0	0.25	0.5	1	1.5	2	4	6	8	16	24	48	72	96	120
Cyclic carbonate (sum of signals), %	-	-	0.15	0.38	1.17	1.95	6.07	6.93	8.32	14.42	8.40	15.48	11.05	4.73	16.62

Table 15. Results from integrating ^{13}C NMR peaks (**Figure 83**) of the carbonyl signals of urea [160.7-160.3 ppm], 3-phosphoglyceryl-1-carbamate* [157.8-157.4 ppm] and 3-phosphoglyceryl-1,2-cyclic

carbonate* [156.5-155.4 ppm] depending on the heating time at 115 °C obtained from DMSO-*d*6 extracts of mixture on a 0.5 mmol scale starting from glycerol (**5**), natural isotope-abundance urea (**2a**), [¹⁵N₂]urea (**2b**) and NaH₂PO₄ (**P_i**) (1:0.5:0.5:1 molar ratios). We calculated relative quantities of each compound by taking as 100 % the absolute integrated area of initial amount of urea before heating.

Heating time, h	Urea (multiplet), %	Error margin of urea, %	Carbamate (singlet and doublet), %	Error margin of carbamate, %	Cyclic carbonate (singlet), %	Error margin of cyclic carbonate, %
0	100	4.02	-	-	-	-
0.25	79.8	30.70	-	-	-	-
0.5	61.6	17.50	3.03	1.80	-	-
1	51.9	12.50	3.74	1.53	-	-
1.5	38.5	7.65	4.88	1.62	0.61	0.29
2	39.1	6.98	14.5	2.01	0.47	0.10
4	19.4	6.20	14.8	2.28	2.15	0.22
6	10.3	6.13	19.4	2.08	3.36	0.21
8	8.15	4.55	21.5	1.95	3.60	0.24
16	-	-	12.5	2.27	3.77	0.23
24	10.6	18.50	10.6	2.06	6.31	0.25
48	-	-	2.86	1.50	4.64	0.19
72	-	-	-	-	2.52	0.26
96	-	-	-	-	0.99	0.28
120	-	-	-	-	0.66	0.14

* the presence of the phosphate group is not proven but kinetically most probable.

In **Table 17**, results from urea-assisted phosphorylation reactions that were performed over time are summarised. These results give us an idea about the reproducibility of dry-state experiments over different repetitions at different scales.

Table 16. Results from integrating $^{31}\text{P}\{^1\text{H}\}$ NMR peaks depending on the heating time at 115 °C (**Figure 85**) of DMSO-*d*₆ extracts of a neat mixture of glycerol (**5**), natural isotope-abundance urea (**2a**), [$^{15}\text{N}_2$]urea (**2b**) and NaH_2PO_4 (**P_i**) (1:0.5:0.5:1 molar ratios) on a 0.5 mmol scale. The total conversion (conversion of initial amount of **P_i** to phosphorylated organic products) was determined by subtraction of inorganic compound quantities (**P_i** and **PP_i**) from the sum of all integrated peaks. The error margin was calculated from signal-to-noise ratio of the **P_i** peak. **GIP** comprise all acyclic organic phosphate peaks except those for **diGI(CO)₂P** and **diGICOP** (**Figure 57**).

Heating time, h	GIP, %	diGI(CO) ₂ P, %	diGICOP, %	5cGIP, %	6cGIP, %	P _i , %	PP _i , %	Total P _i conversion, %	Error margin of P _i , %
0	-	-	-	-	-	100.00	-	-	0.023
0.25	15.47	-	-	-	-	84.53	-	15.47	0.020
0.5	43.90	-	-	0.16	-	55.94	-	44.06	0.019
1	58.51	-	-	0.34	-	41.15	-	58.85	0.019
1.5	72.09	-	-	1.18	-	26.69	0.04	73.27	0.017
2	82.12	-	-	1.45	-	16.31	0.12	83.57	0.009
4	86.14	0.26	-	2.61	0.16	10.79	0.04	89.17	0.008
6	83.01	0.65	-	2.82	0.14	13.31	0.07	86.62	0.008
8	84.11	0.67	0.78	3.33	0.25	10.76	0.10	89.14	0.007
16	80.36	1.91	1.79	6.20	0.54	8.29	0.91	90.80	0.015
24	77.31	3.36	3.10	3.91	0.07	12.14	0.11	87.75	0.019
48	71.75	3.98	3.03	6.81	1.86	11.67	0.90	87.43	0.007
72	70.36	4.92	3.69	9.25	3.41	7.05	1.32	91.63	0.010
96	66.16	8.70	5.67	9.85	3.35	5.27	1.00	93.73	0.019
120	61.41	3.91	1.85	8.25	8.19	16.23	0.16	83.61	0.035

Table 17. Results from integrating $^{31}\text{P}\{^1\text{H}\}$ NMR spectra depending on a scale of the reaction. DMSO-*d*₆ extract of mixture 0.5-30 mmol scale glycerol (**5**), natural isotope-abundance urea (**2a**) and NaH_2PO_4 (**P_i**) (1:1:1). Calculation of the total conversion (conversion of initial amount of **P_i** to phosphorylated organic products) was made by subtraction of inorganic compounds quantities (**P_i** and **PP_i**) from the sum of all integrated peaks. Scales 3-30 mmoles were carried out in an open round-bottom flask (5-50 ml) with magnetic stirring and an oil heat bath; 0.5 mmol scale was performed using the carousel reactor (**Figure 46**) with small magnetic stirrers and electric heating.

Reaction scale, mmol	5cGIP, %	6cGIP, %	GIP [§] , %	P _i , %	PP _i , %	Total conversion, %
0.5	7.14	3.63	81.07	7.82	0.34	91.84
0.5	8.25	8.19	67.17	16.23	0.16	83.61
0.5	3.99	1.07	76.59	13.8	4.55	81.65
3*	12.08	10.05	72.58	4.88	0.41	94.71
3	10.40	4.57	77.76	6.86	0.41	92.73
10	5.42	3.32	89.17	2.09	-	97.91
30	4.56	6.79	83.53	5.12	-	94.88

*in this reaction [^{13}C]urea **2c** was used. § includes diGI(CO)₂P and diGICOP.

The software OriginPro was used to obtain fittings and calculate the decay or growth rate of fitted parameters from **Table 13-Table 16**. Depending on the tendency of the data certain models were chosen for the kinetic curves described in **Table 18**.

Table 18. List with the descriptions of the models of OriginPro software (version 9.9.0.225) used for kinetic studies of glycerol and MPG phosphorylation with urea assistance: x = heating time [seconds] ; y = relative $^{31}\text{P}\{^1\text{H}\}$, $^{13}\text{C}\{^1\text{H}\}$ or ^1H NMR peak area [%]. All y values are depicted on the fitted curves by using error margin weights implemented in the software.

Model	MnMolecular	ExpDec2	ExpGrowDec
Application	P _i consumption, production of [^{14}N , ^{15}N]urea	Total urea decay	3-phosphoglyceryl-1-carbamate and 3-phosphoglyceryl-1,2-cyclic carbonate growth and decay
Function	$y = A(1 - e^{-kx})$	$y = A_1 e^{-x/t_1} + A_2 e^{-x/t_2}$	$y = \begin{cases} A_d + A_g \left(e^{\frac{-x_c}{t_g}} - e^{\frac{-x_c}{t_d}} \right) & x \leq x_c \\ A_d e^{\frac{-(x-x_c)}{t_d}} & x > x_c \end{cases}$
Description	Exponential function for monomolecular growth model	Double-exponential decay function with time constant parameters	Exponential functions bearing one growth and one decay step
Optimized parameters found by error margin(y)-weighted fitting (Table 13)	A = amplitude of growth; k = apparent growth rate constant; $t_{1/2}$ = half-time growth rate	A_n = amplitude of decay; t_n = time constant; $t_{1/2n}$ = half-time of decay rate; k_n = decay rate constant.	x_c = center (“knee” in the curve); A_g (A_d) = amplitude of growth (decay); t_g (t_d) = growth (decay) time constant; k_g (k_d) = growth (decay) rate constant.
Derived parameters	$y_{max} = A$ $t_{1/2} = \frac{1}{k}$	$y_{max} = A_1 + A_2$ $t_{1/2n} = t_n * \ln(2)$ $k_n = \frac{1}{t_n}$	$y_{max} = A_g$; $k_g = \frac{1}{t_g}$; $k_d = \frac{1}{t_d}$

The kinetic curves obtained during the study of glycerol phosphorylation are summarised in **Figure 87** and **Figure 88**.

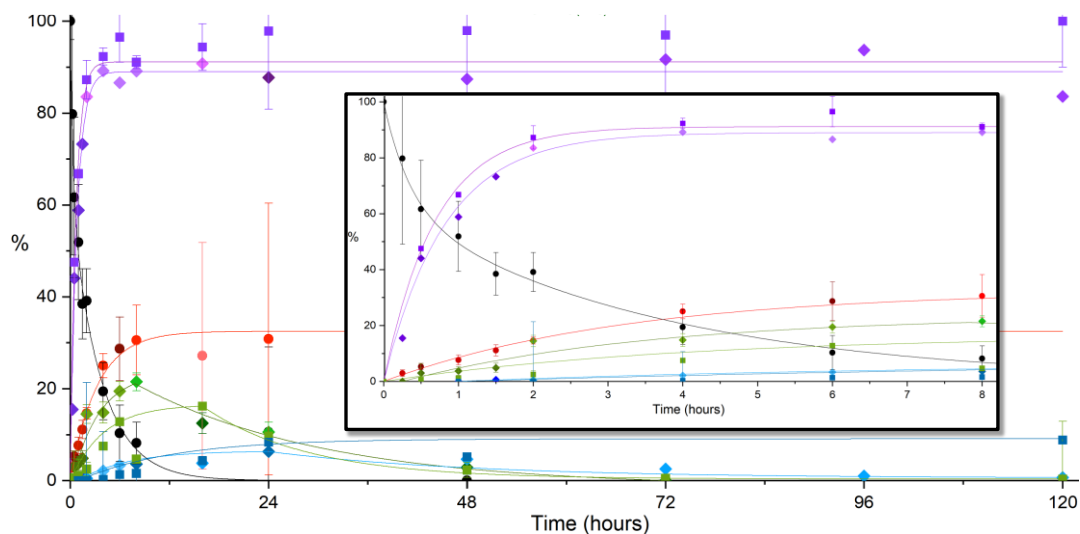


Figure 87. Kinetics of urea decay, nitrogen exchange on urea (circles), glycerol and MPG carbamoylation, their cyclisation to carbonate, and P_i consumption during phosphorylation of glycerol (diamonds) and MPG (squares) in the ‘dry state’, as observed by ¹³C and quantitative ³¹P NMR spectroscopies. Comparison of urea decay (**black** circles) with nitrogen exchange (**red** circles), amounts of glyceryl/MPG carbamate (**green** diamonds/squares), glyceryl/MPG cyclic carbonate (**blue** diamonds/squares) and P_i consumption during phosphorylation of glycerol/MPG (**violet-cyan** diamonds/squares) over 120 hours [insert: 0-8 hours]. Relative values [%] obtained from time-dependent NMR peak integration. Margins show signal-to-noise ratio of each corresponding ¹³C NMR peak and the ³¹P NMR peak for inorganic orthophosphate (estimation from the Pythagorean theorem, ³¹P NMR margins for glycerol experiments are very small). Exponential fittings all weighted by S-to-N margins. Different color shades of datapoints indicates independent experiments.

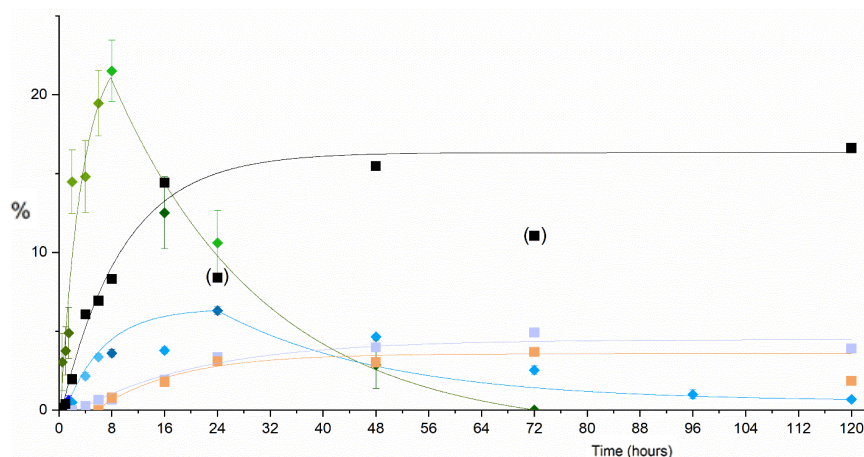


Figure 88. Results of kinetic study of the urea-assisted phosphorylation of glycerol (**5**). Curves show the kinetics of carbamoylation of glyceryl phosphate to: 3-phosphoglyceryl-1-carbamate (**green** ◊ from ¹³C NMR, followed by phosphodiester formation to diGI(CO)₂P and diGICOP (**pale violet** ■ and, respectively, **orange** ■ from ³¹P NMR, **Table 16**). Information used for fitting results taken from three series of independent experiments. Exponential fittings all weighted by error margins calculated from S-to-N ratios. In parentheses are outlier values that were not used for fitting.

Observing the reaction development over 120 hours, we noticed relatively fast Pi consumption growth and urea decay within the first hours of the reaction. Comparing N-exchange with urea decay, we noticed that urea is degrading faster than [¹⁵N₂]urea and [¹⁴N₂]urea reacting. The half-time growth rate of [¹⁴N, ¹⁵N]urea was about $t_{1/2} = 2.6$ hours (**Table 19**). After calculating the values of reaction constants, we discovered that Pi consumption is actually faster than urea decay. In general, we observed the system achieving equilibrium after 8-16 hours when urea was 90 % consumed.

Aside from urea and Pi, we also tracked the growth and decay of carbamate and cyclic carbonate within the reaction time. The carbamate detected by ¹³C NMR (**Figure 83**), similar to urea, had two isotopologs, glyceryl [¹⁴N]- and [¹⁵N]carbamate. It is formed within 8-16 hours (21.5 %) and then decays for the next 64 hours until it is completely absent. In the same way, cyclic carbonate follows a grow-decay pattern, reaching its maximum at 24 hours (6 %) and slowly decaying until the end of the study.

Table 19. Data obtained from kinetic studies of glycerol phosphorylation with urea assistance. Fittings performed by OriginPro software (version 9.9.0.225) using data from **Table 13-Table 16**.

Subject	Method of analysis	Model	k [h ⁻¹]	$t_{1/2}$ [h]	R ²	% max
Pi consumption	³¹ P{ ¹ H} NMR	Growth	1.20 ± 0.10	0.57 ± 0.04	0.98	89.1
[¹⁴ N, ¹⁵ N]urea	¹³ C{ ¹ H} NMR	Growth	0.27 ± 0.05	2.60 ± 0.40	0.99	35.8
Urea decay	¹³ C{ ¹ H} NMR	1 st step decay	2.90 ± 2.40	0.24 ± 0.14	0.99	100*
		2 nd step decay	0.28 ± 0.03	2.50 ± 0.03		
Carbamate	¹³ C{ ¹ H} NMR	Growth	0.30 ± 0.02	2.30 ± 1.60	0.97	21.5
		Decay	0.04 ± 0.02	16.00 ± 6.10		
	³¹ P{ ¹ H} NMR	Growth	0.05 ± 0.01	77.51 ± 16.10	0.96	4.92
Cyclic carbonate	¹³ C{ ¹ H} NMR	Growth	0.17 ± 0.23	4.10 ± 2.90	0.88	6.3
		Decay	0.04 ± 0.08	17.70 ± 13.80		
	³¹ P{ ¹ H} NMR	Growth	0.08 ± 0.02	52.6 ± 12.93	0.97	3.7
		¹ H NMR	Growth	0.11 ± 0.01		

* In the case of calculating urea's decay, we settle the integral of urea's signal to the first time point (0 hours) as the maximum amount in absolute values (100 %).

2.4.2. Phosphorylation of racemic monopalmitoylglycerol

The same experiments tracking changes of glycerol phosphorylation were studied in the MPG. For all NMR analyses, we extracted the products from the reaction mixture as described in Materials and Methods section 2.1. Nevertheless, we observed difficulties with the full dissolution in DMSO-*d*₆ of the crude mixtures after 24-48h of heating. After the centrifugation step of the sample preparation, the extracts of the late reaction mixtures were subdivided in three phases. The bottom phase was insoluble and remained as white as the initial crude mixture: the solvent was saturated with reaction products (and some part of unreacted P_i), so a part of the crude mixture remained insoluble. The middle fraction was a transparent solution that contained the extracted products and was used for NMR analysis. The top fraction was transparent but behaved like a gel and complicated the extraction process—the presence of

(deacylated) palmitate could be the cause of this effect. Because of the low volume of the fraction available for NMR analysis, signal intensities were low and the signal-to-noise ratio decreased in the 48-120 h spectra. To avoid these difficulties, in another series of experiments, we lowered the amount of the crude mixture, which solved the problem. We succeeded in obtaining parameters sufficient for building kinetic curves (**Figure 89-Figure 91**).

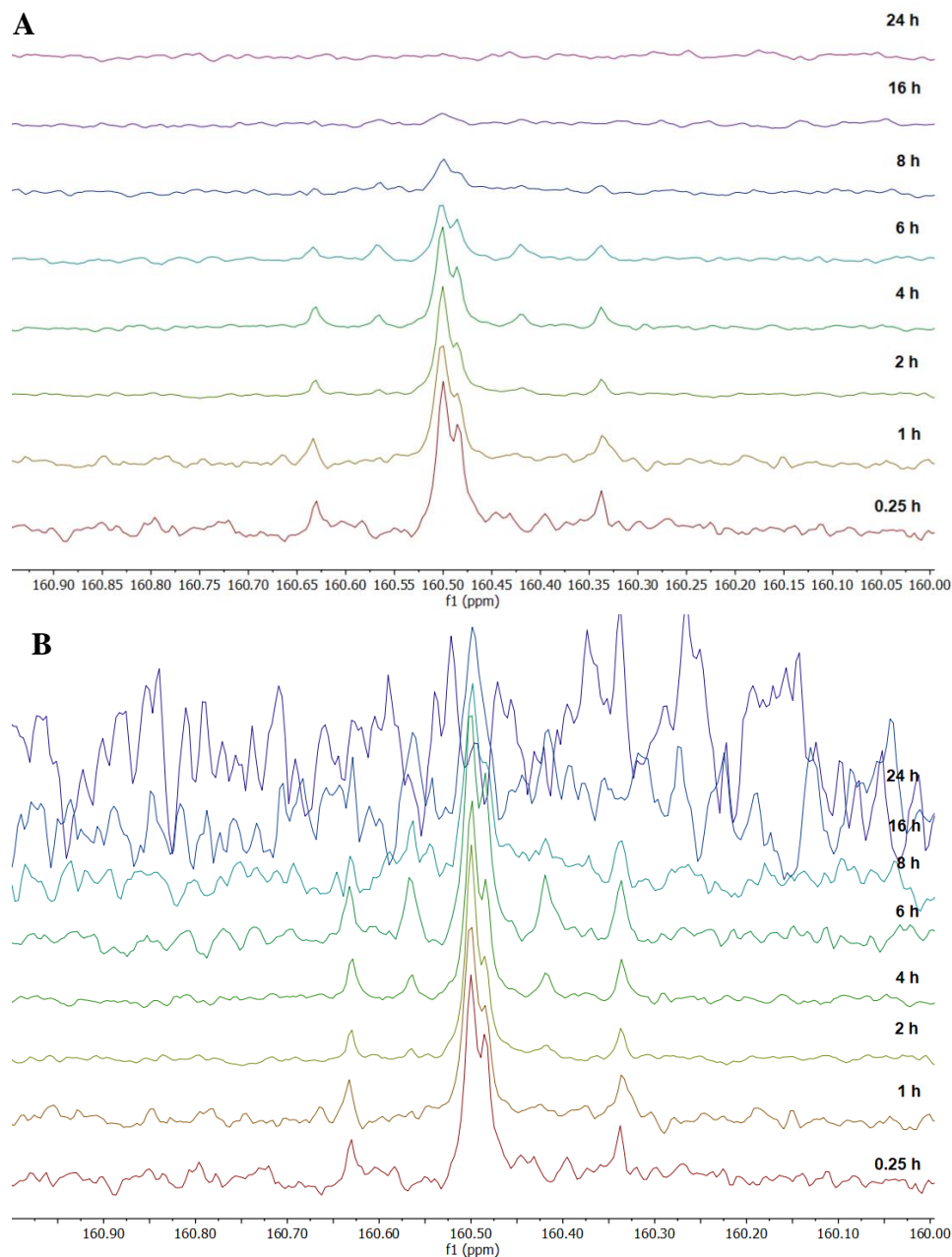


Figure 89. Stack of ^{13}C NMR spectra (125.8 MHz) zoomed on the urea signal of the DMSO- d_6 extract of a 0.5 mmol scale mixture of MPG (**6**), natural isotope-abundance urea (**2a**), [$^{15}\text{N}_2$]urea (**2b**) and NaH_2PO_4 (**Pi**) (1:0.5:0.5:1 molar ratios) after heating neat for 0-24 hours at 115 °C. Stack was referenced to urea singlet at 160.5 ppm: $\delta_{\text{C}} = 160.50$ ppm (*s*, **2a**), 160.48 (*t*, $^1J_{\text{C,N}} = 18.6$ Hz, **2b**), 160.49 (*d*, $^1J_{\text{C,N}} = 18.6$ Hz, [$^{14}\text{N},^{15}\text{N}$]urea). **A** – Stack of NMR spectra with experimental (absolute) intensities. **B** – Intensities of spectra adjusted to the intensity of the urea singlet at 0 h illustrating (in **B**) the gradually increasing signal-to-noise ratio with time passing owing to the degradation of urea (in **A**).

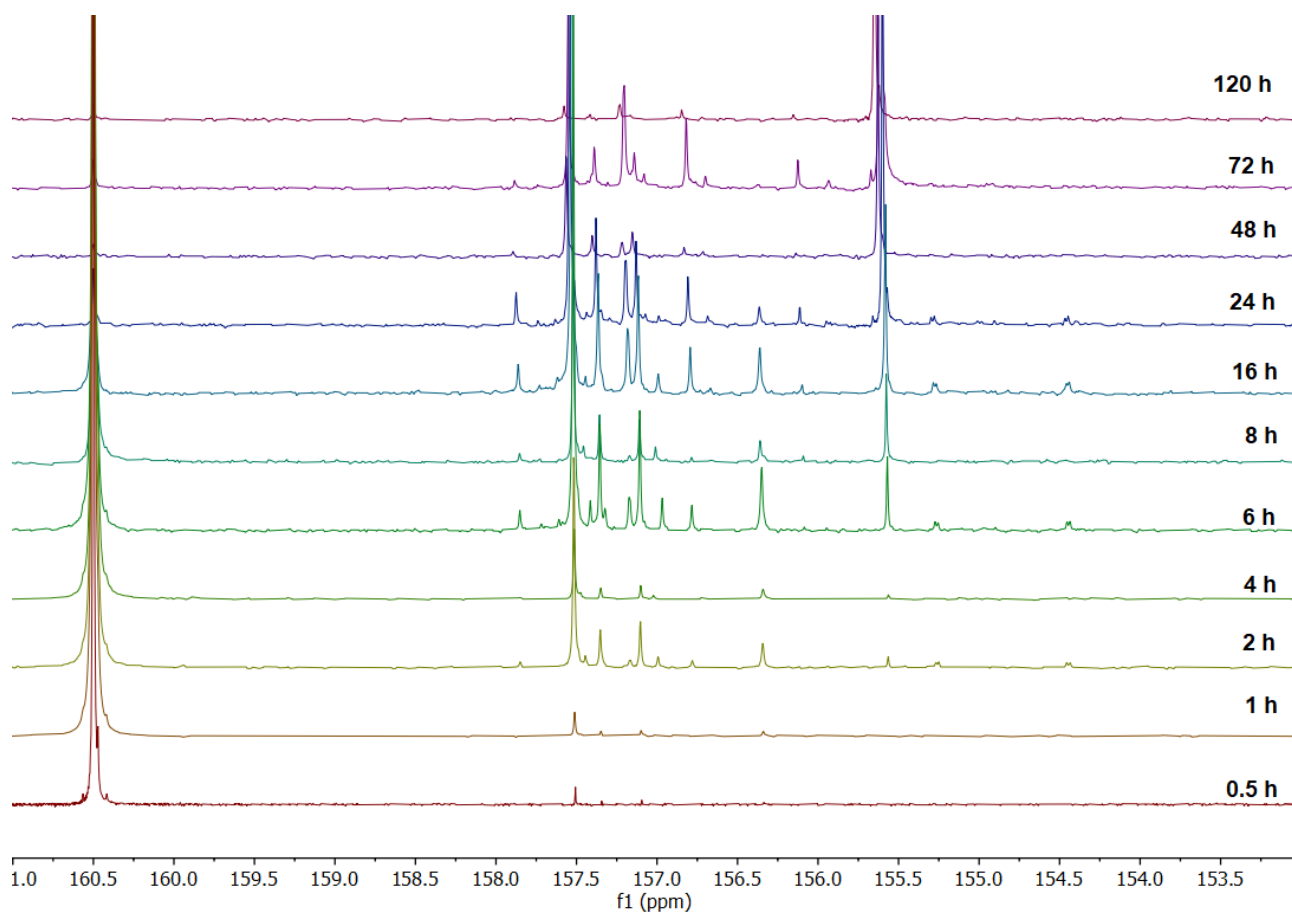


Figure 90. Stack of ^{13}C NMR spectra (125.8 MHz) at full spectral width of the DMSO- d_6 extracts of a 0.5 mmol scale mixture of MPG (**6**), [^{13}C]urea (**2c**) and NaH_2PO_4 (**P₁**) (1:0.5:0.5:1 molar ratios) after heating neat for 0-120 hours at 115 °C: δ_{C} = urea 160.50 (s, **2c**), 157.5 (s, MPG carbamate), 157.3, 157.1 (2 x s, MPG dicarbamate), 155.6 (s, MPG-2,3-cyclic carbonate). Stack centered on urea singlet at δ_{C} = 160.50 ppm. Presence of carbamate and carbonate groups confirms interpretation of HRMS as shown in **Figure 66**.

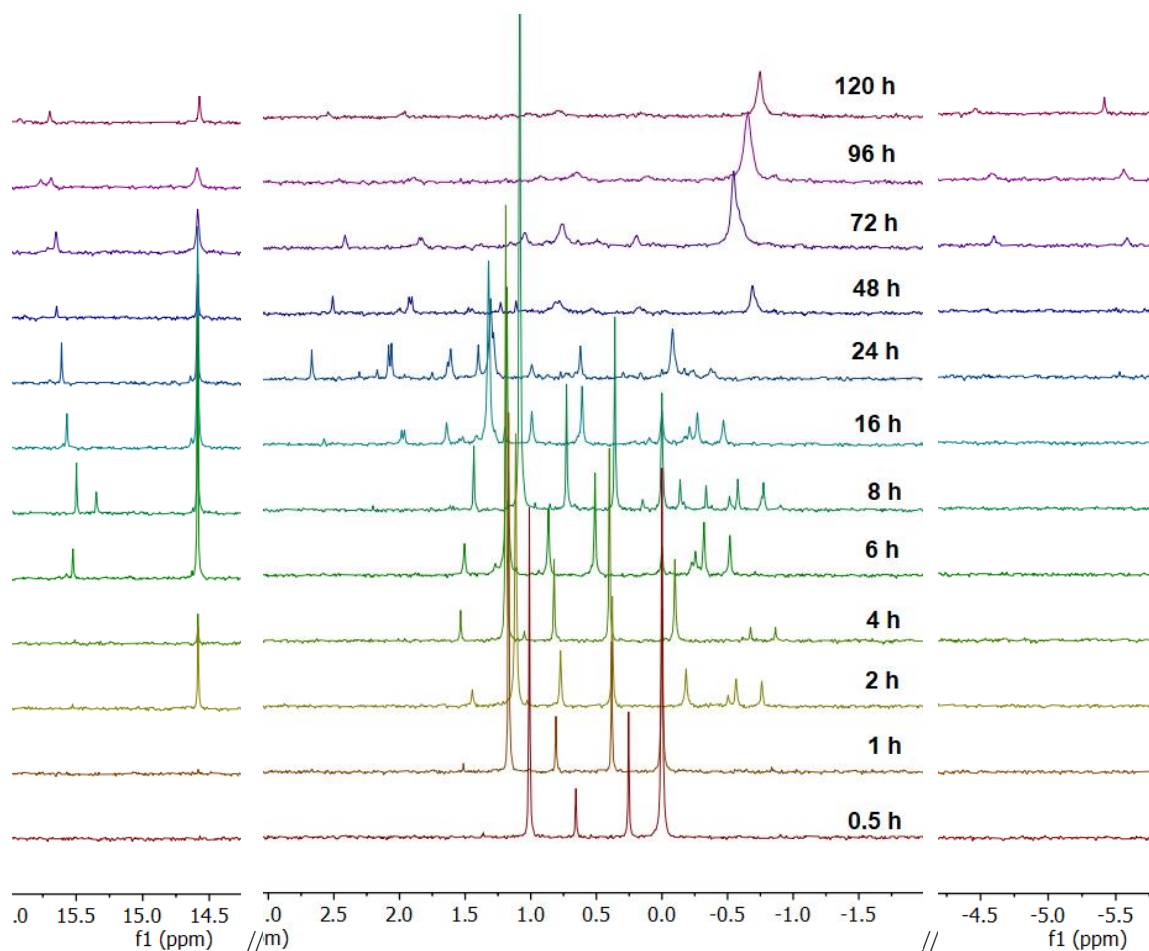


Figure 91. Stack of $^{31}\text{P}\{^1\text{H}\}$ NMR spectra (202.5 MHz) of the DMSO-*d*₆ extracts of a 0.5 mmol scale mixture of MPG (**6**), natural isotope-abundance urea (**2a**), [$^{15}\text{N}_2$]urea (**2b**) and NaH_2PO_4 (**P_i**) (1:0.5:0.5:1 molar ratios) after heating neat for 0-120 hours at 115 °C. Stack centered on **P_i** singlet at $\delta_{\text{P}_i} = 0.00$ ppm: $\delta_{\text{P}} = 15.5$ ppm (**5cGIP**), 14.5 ppm (**5cMPGP**), from 2.5 to -1.0 ppm (**MPG-1P**, **MPG -2P** and [**MPG**]₂**P**), 0.0 ppm (**P_i**), from -4.5 to -5.5 ppm (**6c MPGP**).

A kinetic study was also made for two 5-membered ring phosphorylated products of MPG and glycerol. After 16-48 h, urea was mostly consumed, and the production of 5-membered ring MPG phosphate slowed down. Over this period of time, the amount of **5cMPGP** decreased, which could be explained by the facilitation of further reactions because of the presence of **5cMPGP** as a new starting material. During the same time period, the amount of **5cGIP** remained relatively the same and its decay was slower than that of **5cMPGP**. The reason may be the facility of glycerol to be phosphorylated without the presence of urea. There are other signals in the 5-membered ring region; however, we do not have enough data to make a fitting and track their growth and decay. These products could be mono-cyclic glyceryl diphosphate **PGI5>P** and/or mono-cyclic diglyceryl diphosphate **GIPGI5>P**. In **Table 20**, the values were obtained from the integration of the $^{31}\text{P}\{^1\text{H}\}$ NMR peak areas (**Figure 91**) divided by the maximum phosphorylation of a single product being **5cMPGP** after 16 h and taken as 100%. All the data obtained after integrating ^{13}C and ^{31}P NMR data was summarised in **Table 21-Table 23**.

Table 20. Results from integrating $^{31}\text{P}\{^1\text{H}\}$ NMR peaks in the 5-membered cyclic phosphate region depending on the heating time. DMSO-*d*₆ extracts of MPG (**6**), [^{13}C]urea (**2c**) and NaH_2PO_4 (**Pi**) 1:1:1 (0.5 mmol each) heated neat at 115 °C. Values of conversions were calculated with respect to the maximum absolute intensity of **5cMPGP** at 16 h.

Heating time, h	5cGIP, %			5cMPGP, %
	15.6 ppm	15.5 ppm	14.55 ppm	14.5 ppm
0.5	-	-	-	-
1	-	-	-	1.3
2	-	1.3	-	30.7
4	-	1.6	-	8.9
6	-	10.2	-	96.3
8	-	15.2	-	65.8
16	-	16.8	6.0	100.0
24	2.6	13.9	3.7	50.2
48	-	4.8	-	21.3
72	7.1	17.5	5.3	39.7
96	12.0	11.7	-	35.5
120	4.0	6.3	2.4	17.4

Table 21. Results from integrating ^{13}C NMR peaks of the deconvoluted urea signals (triplet versus doublet versus singlet at 160.7-160.3 ppm) depending on the heating time (**Figure 90**). DMSO-*d*₆ extracts of a 0.5 mmol scale mixture of MPG (**6**), natural isotope-abundance urea (**2a**), [$^{15}\text{N}_2$]urea (**2b**) and NaH_2PO_4 (**Pi**) (1:0.5:0.5:1 molar ratios) after heating neat for 0-8 hours at 115 °C. After 8 hours of heating the signal/noise ratio of urea signal became too low to identify and deconvolute its multiplicity. Reactions were conducted in parallel in the carousel reactor (Materials and Methods section **4.1**), so each time point is an independent batch. Error margins for all experiments were obtained following the signal-noise ratio as calculated by the MNova software, and by applying the Pythagorean theorem.²⁸⁸ For triplets and doublets the error margin was calculated from twice the signal-to-noise ratio of the highest peak.

Heating time, h	Triplet [$^{15}\text{N}_2$]urea, %	Error margin of triplet, %	Doublet [$^{14}\text{N},^{15}\text{N}$]urea, %	Error margin of doublet, %	Singlet [$^{14}\text{N}_2$]urea, %	Error margin of singlet, %
0	49.5	0.66	-	-	50.5	0.35
0.25	53.10	5.10	-	-	46.90	3.19
0.75	44.90	25.81	10.73	17.44	44.37	11.93
1	39.03	5.90	10.46	12.13	50.51	3.16
2	32.90	2.02	9.37	3.98	57.73	1.21
4	38.48	2.70	11.74	3.74	49.78	1.48
6	47.03	5.47	20.57	6.15	32.40	1.95
8	39.25	10.65	17.17	9.23	43.58	5.03

Table 22. Results from integrating ^{13}C NMR peak areas of the carbonyl signals of urea [160.5 ppm], 3-phosphoglyceryl-1-carbamate [157.5 ppm], 3-phosphoglyceryl-1,2-cyclic carbonate [155.6 ppm] and glyceryl dicarbamate [157.3-157.1 ppm] depending on the heating time. Spectra from DMSO-*d*₆ extracts of MPG (**6**), [^{13}C]urea (**2c**) and NaH_2PO_4 (**P_i**) 1:1:1 (0.5 mmol each) after heating neat at 115 °C. We calculated relative quantities of each compound by taking as 100 % the absolute integrated area of initial amount of urea in the beginning of the experiment. Integrations obtained from spectra of **Figure 90**.

Heating time, h	Urea (s), %	Error margin of urea, %	Carbamate (s), %	Error margin of carbamate, %	Cyclic carbonate (s), %	Error margin of cyclic carbonate%	Dicarbamate (s), %	Error margin of dicarbamate %
0.5	100.0	0.06	0.62	5.77	-	-	0.14	20.62
1	99.73	0.05	1.13	3.54	-	-	0.30	14.71
4	86.28	0.06	2.49	1.46	0.13	21.19	0.43	7.24
2	73.96	0.07	7.51	0.53	0.26	10.40	1.47	2.46
6	46.15	0.11	12.82	0.28	1.34	2.25	2.61	1.39
8	22.02	0.23	4.68	0.80	1.55	1.98	0.98	3.95
16	11.95	0.47	16.20	0.29	4.33	0.91	3.17	1.50
24	1.51	2.84	9.68	0.31	8.38	0.32	2.00	1.92
48	0.37	13.23	2.34	1.66	5.17	0.68	0.59	6.92
72	0.79	6.00	0.43	0.95	23.67	0.15	1.30	4.81
120	0.40	11.15	0.33	12.59	8.85	0.37	0.23	40.32

Table 23. Results from integrating $^{31}\text{P}\{^1\text{H}\}$ NMR peak areas depending on the heating time. Spectra from DMSO-*d*₆ extracts of MPG (**6**), [^{13}C]urea (**2c**) and NaH_2PO_4 (**P_i**) 1:1:1 (0.5 mmol each) after heating neat at 115 °C. Calculation of total conversion (conversion of initial amount of **P_i** to phosphorylated organic products) was made by subtraction of inorganic compound quantities (**P_i** and **PP_i**) from the sum of all integrated peaks. Error margin was calculated from signal-to-noise ratio of **P_i** peak. Integrations obtained from spectra shown in **Figure 90-Figure 91**.

Heating time, h	MPGP, %	5cMPGP, %	6cMPGP, %	P_i , %	Total conversion, %	Error margin of P_i , %
0.5	47.54	-	-	52.46	47.54	0.44
1	66.37	0.42	-	33.21	66.79	0.95
2	83.97	8.33	-	7.70	92.30	4.20
4	84.45	2.82	-	12.73	87.27	1.85
6	78.06	18.46	-	3.48	96.52	5.43
8	78.94	12.14	-	8.92	91.08	1.39
16	71.57	22.80	-	5.63	94.37	5.07
24	82.64	14.79	-	2.14	97.86	17.04
48	83.45	13.86	0.65	2.04	97.96	52.36
72	80.42	13.5	3.05	3.03	96.97	16.58
120	78.61	16.68	4.71	-	100.00	-

Here in **Table 24**, phosphorylation yields over all the urea-assisted phosphorylation reactions of MPG are shown in order to demonstrate reproducibility.

Table 24. Reaction scale dependence of conversion from integrating $^{31}\text{P}\{^1\text{H}\}$ NMR peak areas. DMSO-*d6* extracts of mixture on a 0.5-30 mmol scale of MPG (**6**), urea (**2a** or **2b** or **2c**) and NaH_2PO_4 (**P_i** or $[\text{O}_4]\text{P}_i$) (1:1:1 molar ratios) after 120 h of heating neat at 115°C. Calculation of total conversion (conversion of initial amount of **P_i** to phosphorylated organic products) was made by subtraction of inorganic compound quantities (**P_i**) from the sum of all integrated peaks. Scales 3-30 mmol were carried out in a round-bottom flask (5-50 ml) with magnetic stirring and an oil heat bath. The 0.5 mmol scale reactions were performed using the Carousel reactor (**Figure 46**) with small magnetic stirrers and electric heating.

Reaction scale, mmol	5cMPGP, %	6cMPGP, %	MPGP, %	P _i , %	Total conversion, %
0.5	11.50	4.92	36.55	47.03	52.97
0.5*	2.38	25.21	1.93	70.48	29.52
0.5	12.85	29.44	9.95	47.76	52.24
0.5[§]	16.68	78.61	4.71	-	100.00
3	30.99	4.77	44.11	20.13	79.87
3	30.13	2.96	42.63	24.28	75.72
3	21.96	4.37	54.21	19.46	80.54
3	22.05	4.14	63.35	10.46	89.54
3	20.26	2.06	63.40	14.28	85.72
3	29.95	4.62	52.56	12.87	87.13
3[#]	35.87	8.71	46.03	9.39	90.61
3[§]	23.05	2.49	59.80	14.66	85.34
3^{*#}	49.04	9.76	32.84	8.36	91.64
3*	48.71	16.79	28.92	5.58	94.42
3^{§#}	37.10	6.00	51.94	4.96	95.04
6[#]	39.51	8.21	21.20	31.08	68.92
6^{§#}	42.65	8.19	42.57	6.59	93.41
10^{§#}	26.95	5.19	56.18	11.68	88.32

* – In the mentioned reaction was used $[\text{O}_4]\text{P}_i$ (2b)

§ – In the mentioned reaction was used $[\text{O}_4]\text{P}_i$ (2c)

– In the mentioned reaction was used $[\text{O}_4]\text{P}_i$

Unlike in the reaction of glycerol, we were able to compare time-dependent P_i consumption from ^{31}P NMR peak integration with the time-dependent decay of MPG obtained from ELSD-RP-HPLC analyses. After obtaining a calibration curve (**Figure 92**, **Table 25**), we could easily calculate MPG consumption (**Figure 93**, **Table 26**).

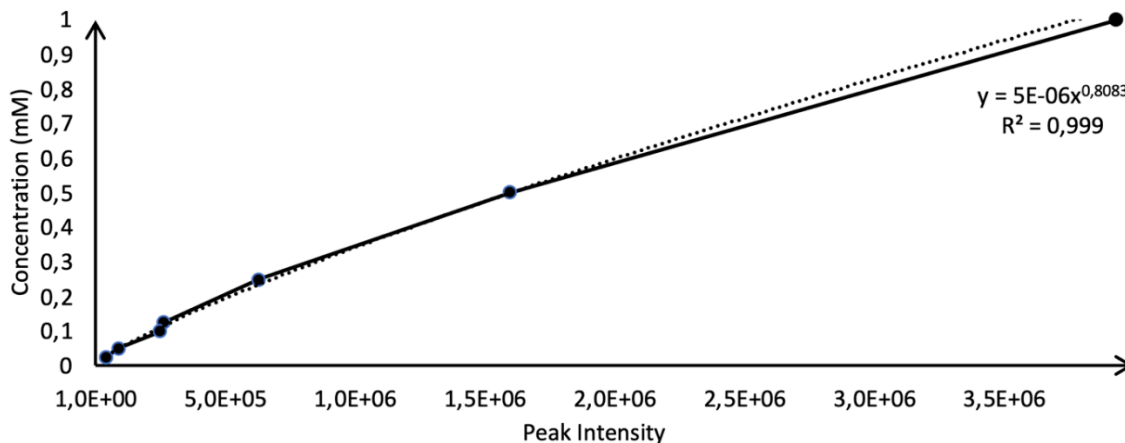


Figure 92. Calibration curve of pure MPG (**6**) for the determination of its concentration depending on the ELSD signal intensity in HPLC reference runs. 3.30 mg of synthesized pure MPG (**6**) was dissolved in 1 ml of MeOH. The solution was diluted in MeOH in order to obtain the appropriate concentrations (from 0.5 mM to 25 μM) and injected. An exponential trendline was used for the fitting and the obtained equation is shown in the figure.

Table 25. Intensities of the MPG (**6**) signal by ELSD from a HPLC chromatogram depending on its concentration in MeOH.

Signal intensity (arbitrary units)	Concentration (mM)
3934728	1.00
1596149	0.50
628127	0.25
261111	0.125
249353	0.10
90330	0.05
40632	0.025

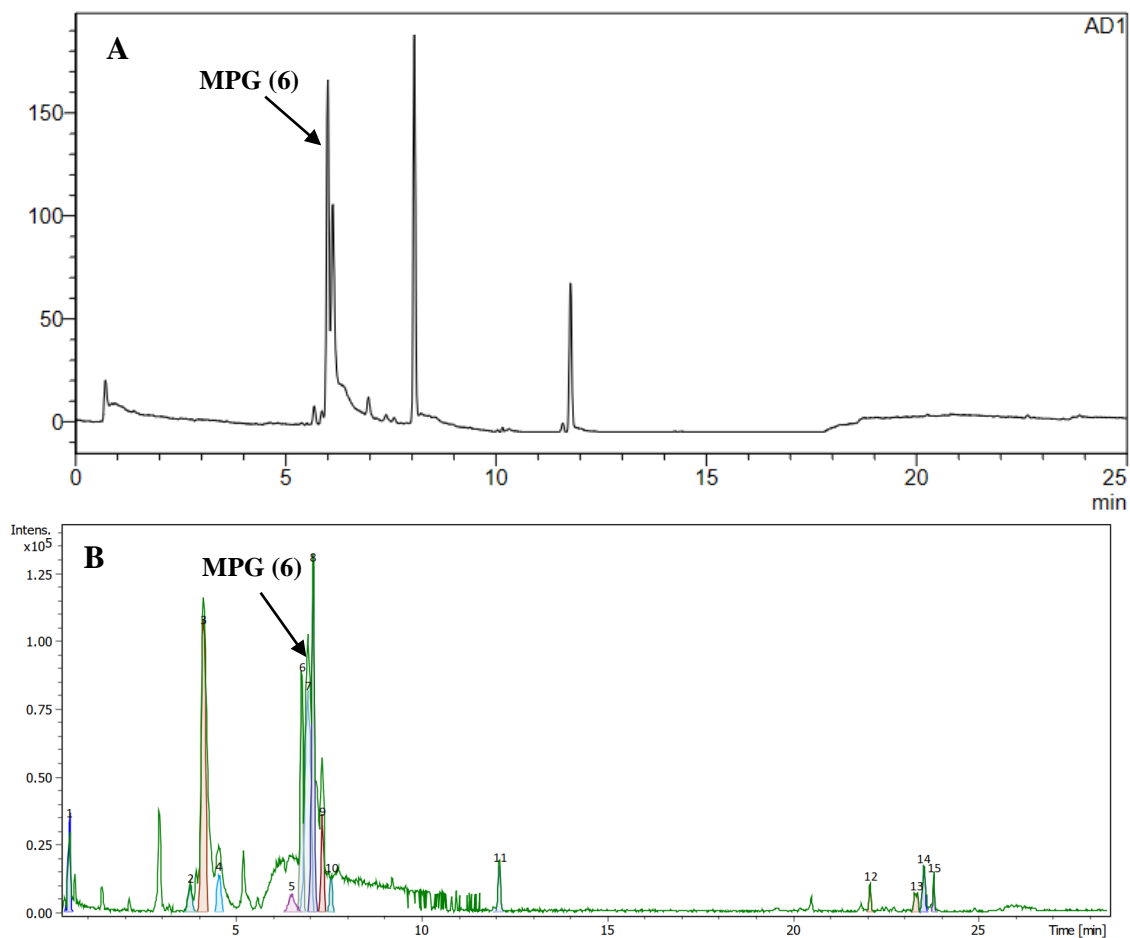


Figure 93. RP-UHPLC-HRMS chromatogram of a MeOH extract of a mixture of MPG (**6**), [^{13}C]urea (**2c**) and NaH_2PO_4 (**P_i**) (1:1:1 0;5 mmol each) after heating neat at 115 °C for 48 hours. **A** – ELSD chromatogram. **B** – Negative ion chromatogram (green, peaks slightly delayed with respect to ELSD) with extracted negative ions (colored, numbered peaks). The chemical structures and exact masses shown in **Figure 66**.

Table 26. Results from integrating HPLC-ELSD peak areas depending on the heating time of crude mixture. MeOH extracts of mixtures of MPG (**6**), [^{13}C]urea (**2c**) and NaH_2PO_4 (**P_i**) 1:1:1 (0.5 mmol each) after heating neat for 0-48 hours. Calculation of total conversion (conversion of initial amount of MPG to phosphorylated organic products) was made by subtraction of residual amount of MPG (MPG signal on chromatogram) from the sum of all integrated peaks. Error margin was calculated from the signal-to-noise ratio of the MPG peak.

Heating time, h	MPG consumption, %	Error margin of MPG consumption, %
0	-	-
0.5	22.61	0.002921841
1	12.06	0.002778086
2	21.12	0.004374836
4	37.05	0.006727664
6	43.51	0.004766217
16	86.36	0.048030740
24	76.42	0.024906600
48	78.91	0.081967213

Due to the solubility problem or possible fewer series of experiments described, the fitting for urea decay in reaction with MPG seems to be less accurate than in reaction with glycerol. However, there is no reason for urea decay to take a different direction, and even in reaction with another molecule, we assume that the trend should be the same.

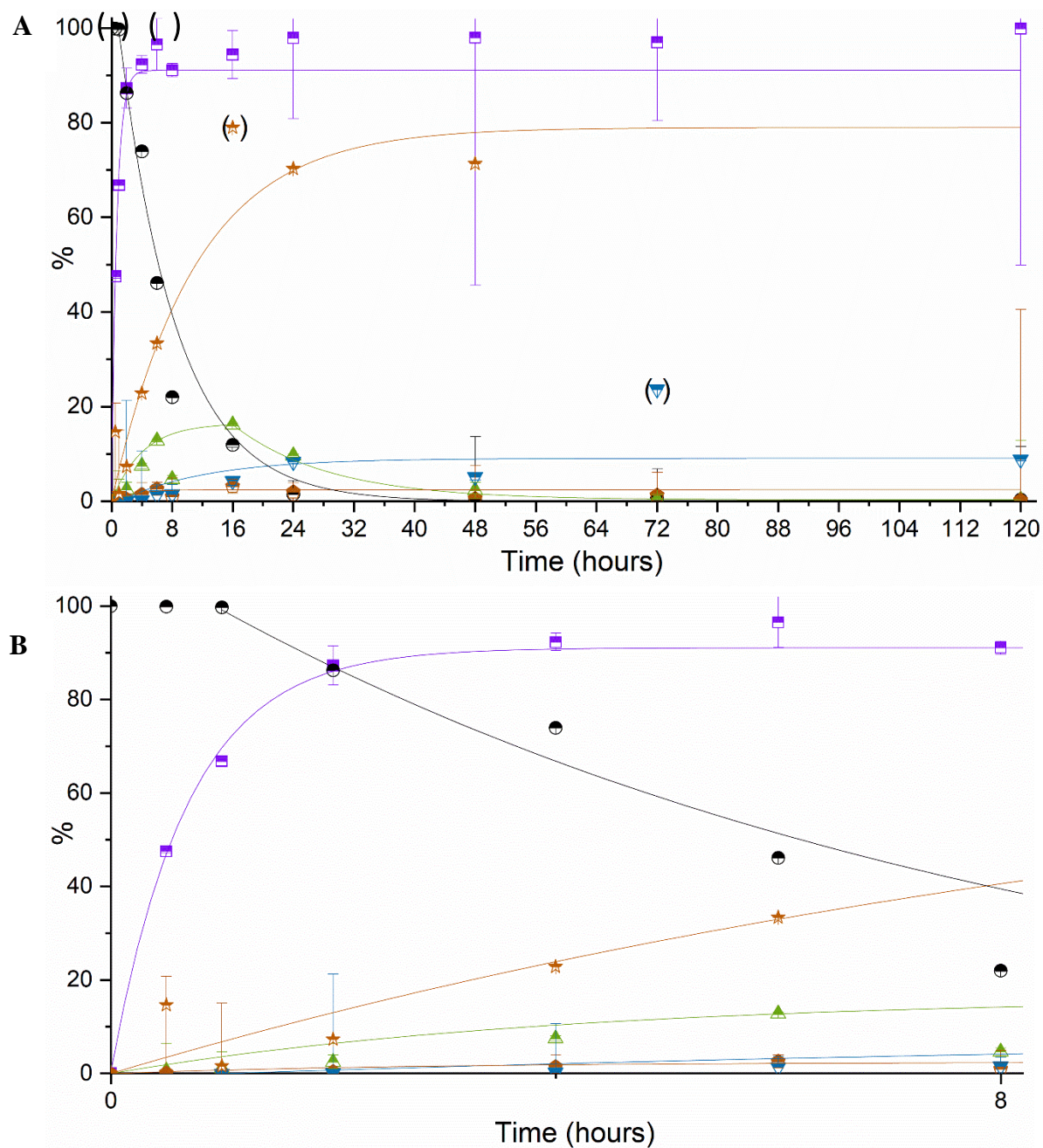


Figure 94. Results of kinetic study of MPG (6) phosphorylation through exponential fitting (cf. **Table 18**). Curves represent fitted urea decay (black half-filled circles), MPG carbamoylation (mono-carbamate green half-filled triangles and bi-carbamate brown ‘diamonds’), its cyclisation to carbonate (blue inverted half-filled triangles), P_i consumption (violet half-filled squares) and MPG consumption (brown half-filled stars ☆) during phosphorylation of MPG. Information used for fitting was obtained from **Table 21-Table 26** as the result of three series of independent experiments. Exponential fittings all weighted by S-to-N margins. In parentheses are outlier values that were not used for fittings. **A** – Full experimental length 0-120 hours. **B** – 0-8 hours (zoom).

As expected, the fitted parameters of the reaction with MPG are comparable with previously studied glycerol phosphorylation.

Table 27. Fitted parameters (rate constants etc.) from kinetic studies of urea-assisted MPG phosphorylation resulting from fittings shown in **Figure 94**

Subject	Method of analysis	Model	k [h^{-1}]	$t_{1/2}$ [h]	R^2	% max
P_i consumption	³¹ P{ ¹ H} NMR	Growth	1.45 ± 0.04	0.5 ± 0.01	0.99	100*
MPG consumption	HPLC	Growth	0.11 ± 0.01	6.4 ± 0.5	0.99	76.1
Urea	¹³ C{ ¹ H} NMR	1 st step decay	3.1 §	5.1 ± 0.14	0.94	100*
		2 nd step decay	3.6 §	5.5 ± 0.29		
Carbamate	¹³ C{ ¹ H} NMR	Growth	0.25 ± 0.24	2.8 ± 2.8	0.97	16.2
		Decay	0.08 ± 0.08	8.8 ± 5.8		
Carbonate	¹³ C{ ¹ H} NMR	Growth	0.09 ± 0.02	7.9 ± 2.1	0.99	8.8
Bicarbamate	¹³ C{ ¹ H} NMR	Growth	0.36 ± 0.25	1.9 ± 2.4	0.91	3.1

* Fixed (not fitted) parameter

Conclusions to the Section 2

I provided for the first time **experimental confirmation of the dissociative mechanism of urea-assisted phosphorylation of prebiotic alcohols** using the example of glycerol and mono-palmitoyl glycerol. Using stable isotope tracking, I confirmed the presence of labelled ammonia and carbon dioxide in traps as the result of the thermal degradation of labelled urea, which corresponds to the dissociative mechanism. The control experiment with [¹⁵N]formamide and [¹⁵N]acetamide instead of urea also demonstrated the presence of labelled CO₂.

Different variations of labelled atoms in CO₂ can be explained by different pathways of the main reaction, including the presence of residual water in the crude mixture and O-atom exchange in the PO₄³⁻ group. Another important proof of the dissociative mechanism is the lack of labelled oxygen in the nucleophilic trap that would correspond to labelled water obtained by the associative mechanism.

I studied in detail the kinetics of those reactions. I discovered that N-exchange and formation of isocyanic acid appear only in the presence of dihydrogenphosphate and alcohol. Observing the reaction development over 120 hours, we noticed relatively fast P_i consumption and urea decay within the first hours of the reaction. Comparing N-exchange with urea decay, we noticed that urea degrades faster than [¹⁵N₂]urea and [¹⁴N₂]urea reacts.

The values of reaction constants showed that P_i consumption is actually faster than urea decay. In general, we observed the system achieving equilibrium after 8-16 hours when urea was 90 % consumed. Aside from urea and P_i, we also tracked the growth and decay of carbamate and cyclic carbonate within the reaction time. Carbamate is formed within 8-16 hours (21.5 %) and then decays for the next 64 hours until it is completely absent. In the same way, cyclic carbonate follows a grow-decay pattern, reaching its maximum at 24 hours (6 %) and slowly decaying until the end of the study.

Same was done for MPG. Due to the solubility problem or possible fewer series of experiments described, the fitting of urea decay in reaction with MPG seems to be less accurate than in reaction with glycerol. However, the fitted parameters of the reaction with MPG are comparable with previously studied glycerol phosphorylation. In general, MPG consumption is lower than P_i, with a similar trend though. It can be due to the application of different analytical methods, as LC does not take into consideration glycerol phosphates and ³¹P identifies only phosphorylated products. A kinetic study for two 5-membered ring phosphorylated products of MPG and glycerol demonstrated that after 16–48 h, when urea was mostly consumed, the production of 5-membered ring MPG phosphate slowed down.

III Results and discussion

3. A scope of phosphorylation reactions of glycerol and its derivatives

After a thorough investigation of the urea-assisted phosphorylation reactions of urea (5) and MPG (6), it was interesting to explore possible variables of those reactions. In this section, we are going to discover the effect of:

- temperature effect on the phosphorylation reaction (115 vs. 75 °C);
- different condensing agents/catalyst/liquidifier to replace urea (cyanamide, formamide, N-methylformamide, acetamide and N-methylacetamide);
- dependence of phosphorylation on phosphate sources (orthophosphate with different protonation degrees, condensed phosphate, thiophosphates, natural minerals);
- phosphorylation of other prebiotic alcohols (nucleosides, BTG, DOG, pyruvic acid, geraniol and dodecanol).

Results can help us to expand our knowledge of phosphorylation reactions and obtain a better understanding of which prebiotic precursors could be formed in dry land conditions on the early Earth.

3.1. Dependence on condensing agent in phosphorylation of glycerol and MPG

Summarising state-of-the-art data, we selected potentially interesting reduced-nitrogen molecules that could be involved in phosphorylation reactions (**Figure 95**): cyanamide as a dehydrated precursor of urea; formamide known as a liquidiser could also have a condensing agent role; and its derivatives, carboxamides (N-methylformamide, acetamide and N-methylacetamide) that have a C(=O)NH₂ group, are small and reactive and remain non-volatile and liquid under prebiotically plausible conditions on the early Earth.

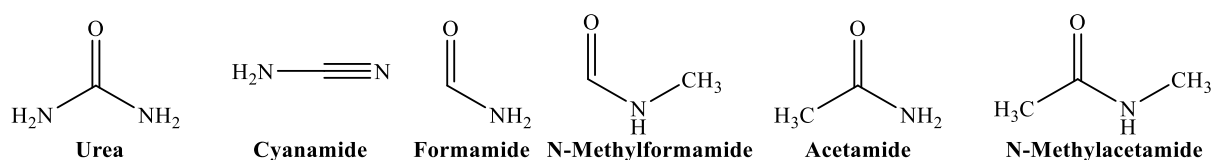


Figure 95. Prebiotic agents/catalyst/liquidiser that were studied in this section

The reaction products are similar to those described above in the identification of products section 1.1.1; thus, the spectra are not shown here. The reaction yields were identified using ¹H, ³¹P, ³¹P{¹H} NMR and ¹H-³¹P HMBC and quantified using the integration of product signal areas by ³¹P{¹H} NMR spectroscopy. The obtained results are summarised for glycerol in **Table 28** and **Figure 96** and for MPG in **Figure 97**.

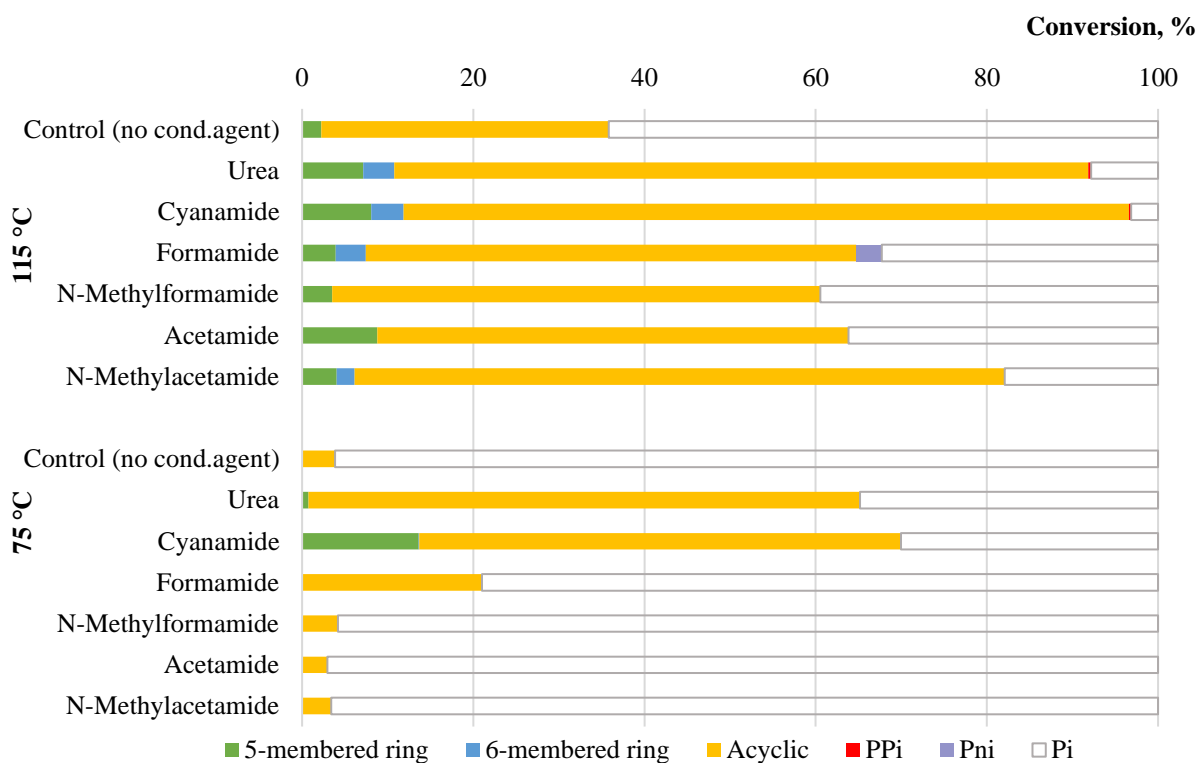


Figure 96. Summary of glycerol (**5**) phosphorylation after 120 h of heating at 75 and 115 °C in a 0.5 mmol scale reaction mixture containing **5**, **cond. agent** and **P_i** (1:1:1). Organic products: **5cGIP** (5-membered ring cyclic glyceryl phosphates), **GIP** (glyceryl mono-, diphosphates and di-glyceryl phosphates), **6cGIP** (6-membered ring cyclic glyceryl phosphates). Percent values from signal integration of quantitative ³¹P{¹H} NMR spectra taken in DMSO-*d*₆.

Table 28. Data to **Figure 96**. Total conversion of initial amount of **P_i** to phosphorylated organic products was calculated by subtracting inorganic compound area integrals (**P_i**, **PP_i**, **P_{ni}**) from the sum of all integrated ³¹P{¹H} NMR peak areas (in DMSO-*d*₆).

Temp., °C	Cond. agent	5cGIP, %	6cGIP, %	GIP, %	P _i , %	PP _i , %	P _{ni} , %	Total conversion, %
115	-	2.23	-	33.58	64.19	-	-	35.8135.
	2a	7.14	3.63	81.07	7.82	0.34	-	91.84
	1	8.09	3.76	84.74	3.15	0.26	-	96.59
	3a	3.93	3.50	57.30	32.29	-	2.98	64.73
	3c	3.53	-	57.03	39.44	-	-	60.56
	4a	8.79	-	55.05	36.16	-	-	63.84
	4c	4.03	2.10	75.96	17.91	-	-	82.09
75	-	-	-	3.84	96.16	-	-	3.84
	2a	0.74	-	64.46	34.80	-	-	65.20
	1	13.60	0.07	56.31	30.02	-	-	69.98
	3a	0.09	-	20.92	78.99	-	-	21.01
	3c	-	-	4.20	95.80	-	-	4.20
	4a	-	-	2.97	97.03	-	-	2.97
	4c	-	-	3.40	96.60	-	-	3.40

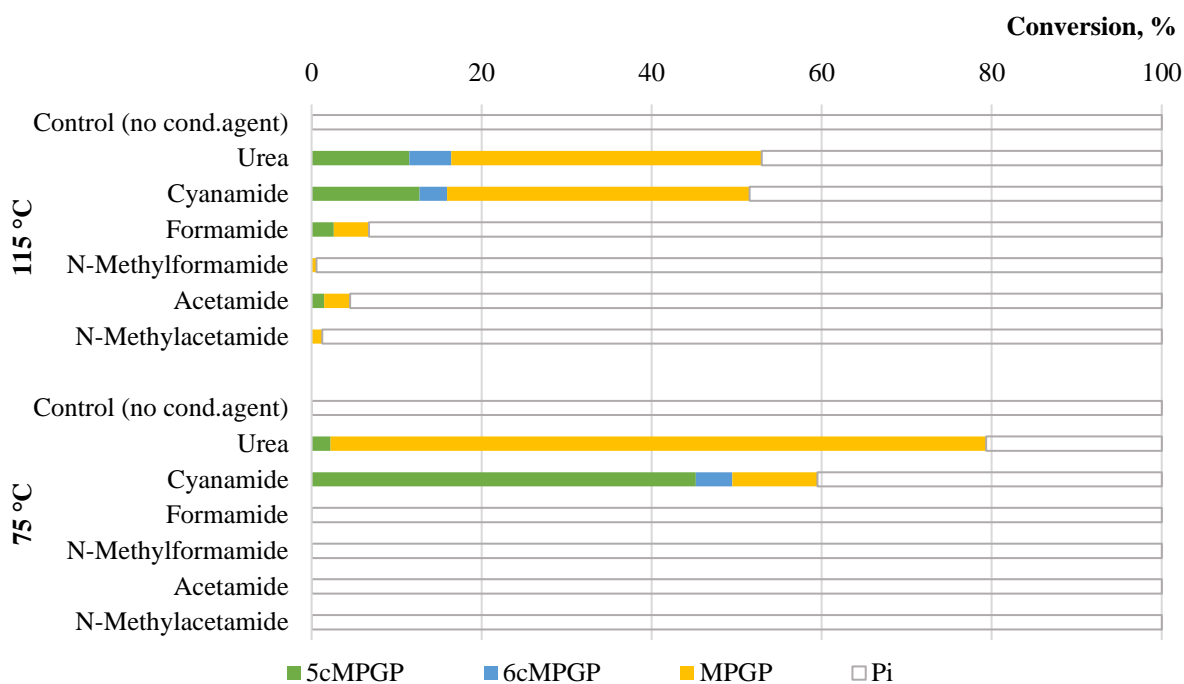


Figure 97. Summary of MPG (**6**) phosphorylation after 120 h of heating at 75 °C of **6**, **cond. agent** and **P_i** (1:1:1) on a 0.5 mmol scale depending on condensing agent. Organic products: **5cMPGP** (5-membered ring cyclic MPG phosphates), **MPGP** (MPG mono-, diphosphates and di-MPG phosphates), **6cMPGP** (6-membered ring cyclic MPG phosphates). Percent values from signal integration of quantitative ³¹P{¹H} NMR spectra taken in DMSO-*d*₆.

Table 29. Data to **Figure 97**. Total conversion of initial amount of **P_i** to phosphorylated organic products was calculated by subtracting inorganic compound integrals (**P_i**) from the sum of all integrated ³¹P{¹H} NMR peak areas (in DMSO-*d*₆). **PP_i**, **P_{ni}** were not detected in any of crude mixtures of those reactions.

Temp., °C	Cond. agent	5cMPGP, %	6cMPGP, %	MPGP, %	P _i , %	Total conversion, %
-	-	-	-	-	100.00	-
115	2a	11.50	4.92	36.55	47.03	52.97
	1	12.70	3.25	35.58	48.47	51.53
	3a	2.61	-	4.14	93.25	6.75
	3c	-	-	0.56	99.44	0.56
	4a	1.48	-	3.06	95.46	4.54
	4c	-	-	1.26	98.74	1.26
	-	-	-	-	-	100
75	2a	2.24	-	77.12	20.64	79.36
	1	45.20	4.28	10.03	40.49	59.51
	3a	-	-	-	100.0	-
	3c	-	-	-	100.0	-
	4a	-	-	-	100.0	-
	4c	-	-	-	100.0	-
	-	-	-	-	-	100.0

First of all, we performed a “negative” control reaction in the absence of any condensing agent, where a starting alcohol was heated with phosphate. After 120 hours, we see that at 115

°C, only glycerol was successfully phosphorylated into acyclic products (35.8 %). And even this yield is at least twice lower than in the presence of any condensing agent (60.5-96.6 %).

In the case of glycerol, we obtained organophosphates with any of the condensing agents tested at 115 °C; however, cooling down to 75 °C dramatically decreased the yield, and only reactions in the presence of urea (**2a**) and cyanamide (**1**) were sufficient, with slightly lower yields of 65.2 and 70.0 %, respectively. A possible explanation is that high temperatures favour some thermal degradation of carboxamides that favours phosphorylation. In reactions with MPG, the presence of a condensing agent is required, and similar to glycerol, the most efficient agents were urea and cyanamide at both 75 and 115 °C (51.5-79.4 %).

3.1.1. Effect of the molar excess of the condensing agent (catalyst, liquidiser) of phosphorylation of MPG (**6**)

After we investigated the ratio alcohol:cond.agent:Pi 1:1:1, it was interesting to explore the molar excess of the suggested above condensing agents, whether it would affect the phosphorylation degree. Thus, we performed experiments with 1, 2, 4 and 10 equivalents of the molar excess in the reaction with MPG at 115 °C. In **Figure 98** and **Figure 99** we demonstrated differences in $^{31}\text{P}\{^1\text{H}\}$ NMR depending on urea excess. All the obtained results are summarized in **Table 30** and **Figure 100**.

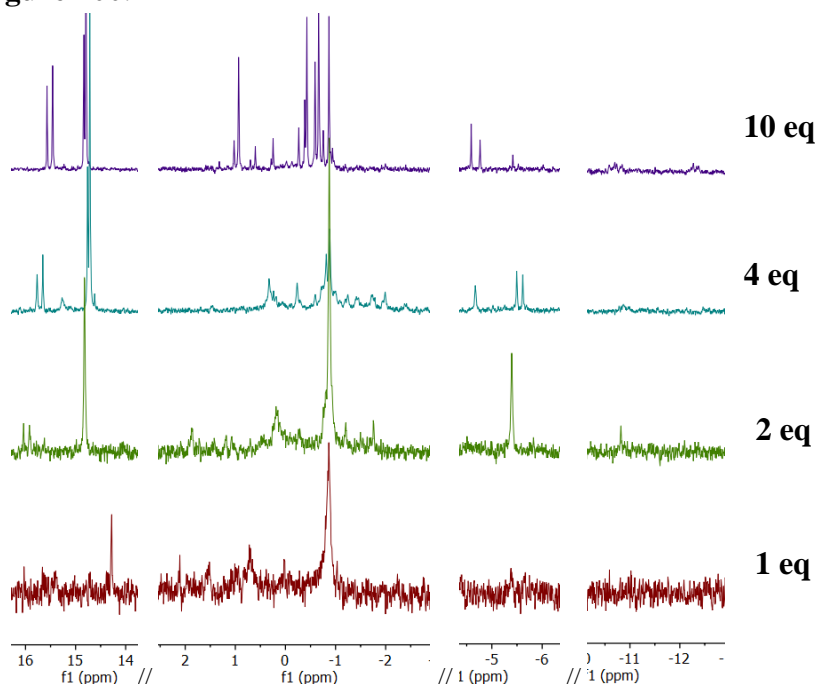


Figure 98. $^{31}\text{P}\{^1\text{H}\}$ NMR (202.5 MHz) of the DMSO-*d*₆ extracts of 0.5 mmol scale mixtures containing **6** (1 eq), **2a** (1, 2, 4 and 10 eq) and **P_i** (1 eq) after heating neat at 115 °C for 120 h: $\delta_{\text{P}} = 16\text{-}14$ ppm (**5cMPGP**), from 2 to -2 ppm (**MPG-1P**, **MPG-2P** and **[MPG]₂P**), 0.00 ppm (**P_i**), from -4.5 to -5.5 ppm (**6cMPGP**) and from -10 to -13 ppm (**PP_i**). Stack centered on **P_i** singlet at $\delta_{\text{P}} = 0.00$ ppm.

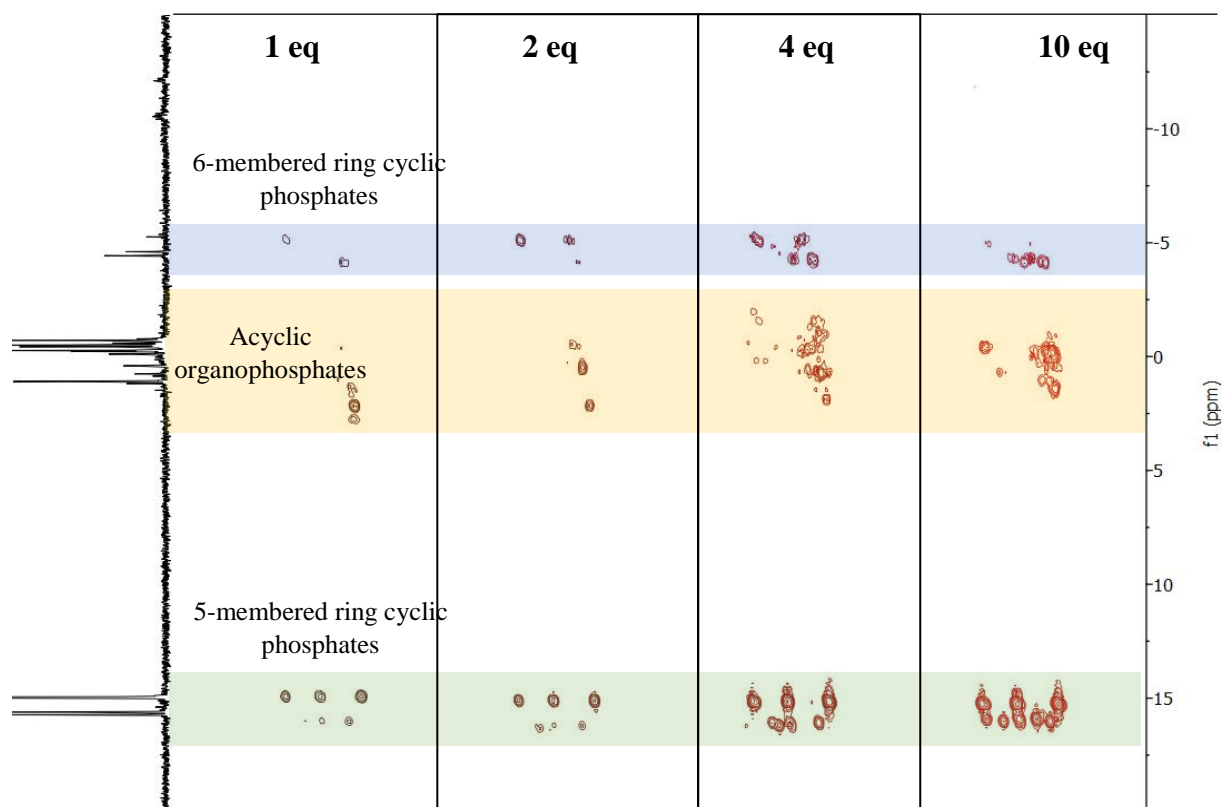


Figure 99. $^1\text{H}\text{-}^{31}\text{P}\{^1\text{H}\}$ HMBC spectra (500 MHz ^1H [horizontal axis], $\delta_{\text{H}} = 5\text{-}3$ ppm; 202.5 MHz $^{31}\text{P}\{^1\text{H}\}$ [vertical axis], DMSO-*d*₆) of the extract of mixture 0.5 mmol scale **6** (1 eq) : **2a** : P_i (1 eq) depending on molar excess of urea, reaction time 120 h at 115 °C. δ_{H} (ppm) = 16.6-14.3 (5-membered ring phosphates, green), 3.0 to -2.2 (acyclic phosphates, yellow) and -3.8 to -5.4 (6-membered ring phosphates, blue). Stacks were centered by P_i value 0 ppm.

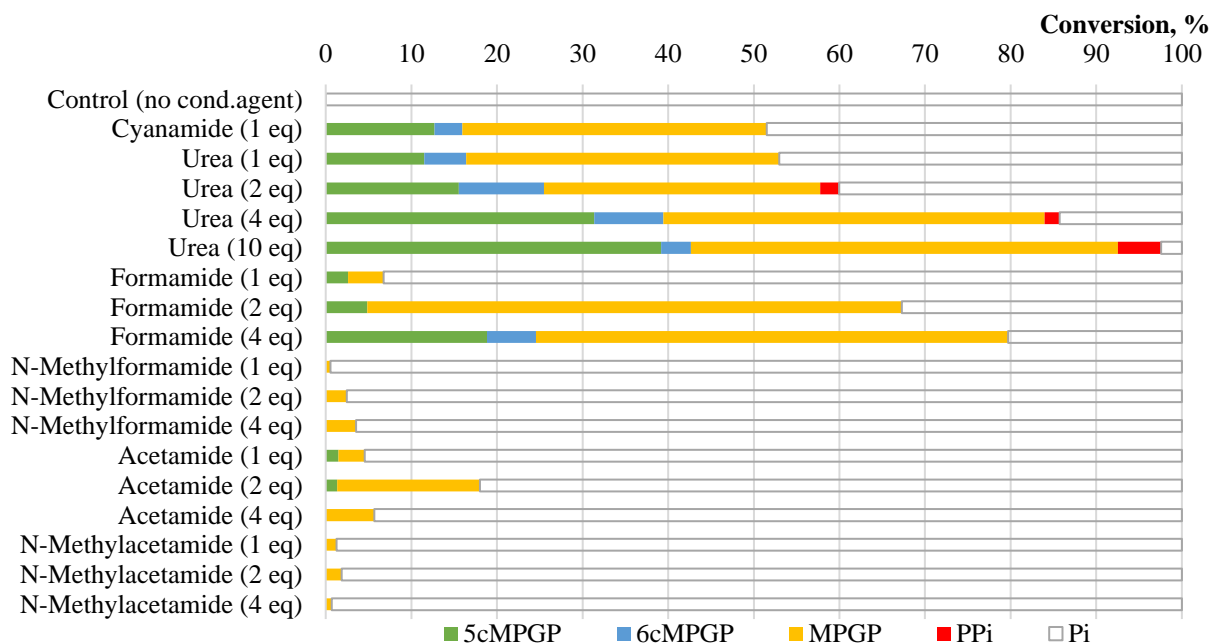


Figure 100. Summary of MPG (**6**) phosphorylation after 120 h of heating at 115 °C depending on molar excesses of condensing agent (0-10 eq) on a 0.5 mmol scale. Molar equivalents are indicated in the diagram with respect to **6** : P_i (1:1 eq). Percent values from peak area integration of quantitative $^{31}\text{P}\{^1\text{H}\}$ NMR spectra (Figure 98).

Table 30. Data to **Figure 100.** Total conversion of initial amount of **P_i** to phosphorylated organic products was calculated by subtracting inorganic compound integrals (**P_i**, **PP_i**) from the sum of all integrated ³¹P{¹H} NMR peaks (in DMSO-*d*₆).

Condensing agent	Molar eq. of cond. agent	5cMPGP, %	6cMPGP, %	MPGP, %	P _i , %	PP _i , %	Total conversion, %
-	-	-	-	-	100.00	-	-
1	1	12.70	3.25	35.58	48.47	-	51.53
2a	1	11.50	4.92	36.55	47.03	-	52.97
2a	2	15.56	9.92	32.26	40.05	2.21	57.74
2a	4	31.35	8.08	44.54	14.27	1.76	83.97
2a	10	39.17	3.47	49.89	2.42	5.05	92.53
3a	1	2.61	-	4.14	93.25	-	6.75
3a	2	4.85	-	62.43	32.72	-	67.28
3a	4	18.85	5.72	55.13	20.30	-	79.70
3c	1	-	-	0.56	99.44	-	0.56
3c	2	-	-	2.45	97.55	-	2.45
3c	4	-	-	3.53	96.47	-	3.53
4a	1	1.48	-	3.06	95.46	-	4.54
4a	2	1.35	-	16.65	82.00	-	18.00
4a	4	-	-	5.68	94.32	-	5.68
4c	1	-	-	1.26	98.74	-	1.26
4c	2	-	-	1.87	98.13	-	1.87
4c	4	-	-	0.69	99.31	-	0.69

From the obtained results, we can conclude that urea or formamide excess increases organophosphates production from 51.5 to 92.5 % and from 6.8 to 79.7 %, respectively. Even higher concentrations of other carboxamides did not make the phosphorylation degree sufficiently higher with the maximum yield in reaction with 2 eq of acetamide.

3.2. Dependence of phosphorylation of glycerol and MPG on phosphorous source

The next step was to examine the influence of different types of phosphate sources on the phosphorylation of glycerol and MPG. We explored

- effect of the protonation degree on the phosphorylation degree (Na_3PO_4 vs. Na_2HPO_4 vs. NaH_2PO_4);
- condensed phosphate (cTMP) as a potential phosphorus source;
- phosphorylation in the presence of thiophosphate (SP_i) and a competition between P_i and SP_i in urea-assisted phosphorylation;
- involvement of prebiotically plausible minerals or their analogues in phosphorylation reactions: vivianite, struvite and calcium pyrophosphate ($\text{Ca}_2\text{P}_2\text{O}_7$) as a model for canaphite.

These phosphate sources were selected based on the results of state-of-the-art research and could potentially be present on the early Earth.

3.2.1. Effect of protonation degree of sodium orthophosphate on phosphorylation of glycerol (5)

Orthophosphates, and in particular sodium dihydrogenphosphate, are known to be a common and abundant phosphate source on the early Earth. Thus, it was important to explore whether the protonation degree of sodium phosphate would have an influence on the phosphorylation reaction. pH values of Na_3PO_4 , Na_2HPO_4 , and NaH_2PO_4 were 12.8, 8.9 and 3.4, respectively, in a 0.5 mmol equimolar mixture with glycerol and urea.

In the **Figure 101**, $^{31}\text{P}\{^1\text{H}\}$ NMR spectra of negative control experiments in the absence of condensing agent are presented. As was demonstrated in **Figure 96**, glycerol can be phosphorylated directly by NaH_2PO_4 with yields 35.8 %; however, Na_2HPO_4 and Na_3PO_4 did not produce any organophosphates (**Table 31**). The same was observed in the urea-assisted reaction. Significant amounts of organic phosphates were obtained only in experiments using NaH_2PO_4 (91.84 %).

One of the possible explanations is that the more acidic a phosphate is, the more readily it can donate a phosphate group to another molecule. Monobasic sodium dihydrogenphosphate contains more H^+ ions than the dibasic and tribasic salts. These are available to protonate the phosphate group and make it more reactive (electrophilic), for example, to produce more reactive condensed phosphates such as inorganic pyrophosphate (PP_i). In the urea-assisted phosphorylation reactions, according to the dissociative phosphate activation mechanism, protons are needed to help eliminate ammonia from urea and carbamoyl phosphate.

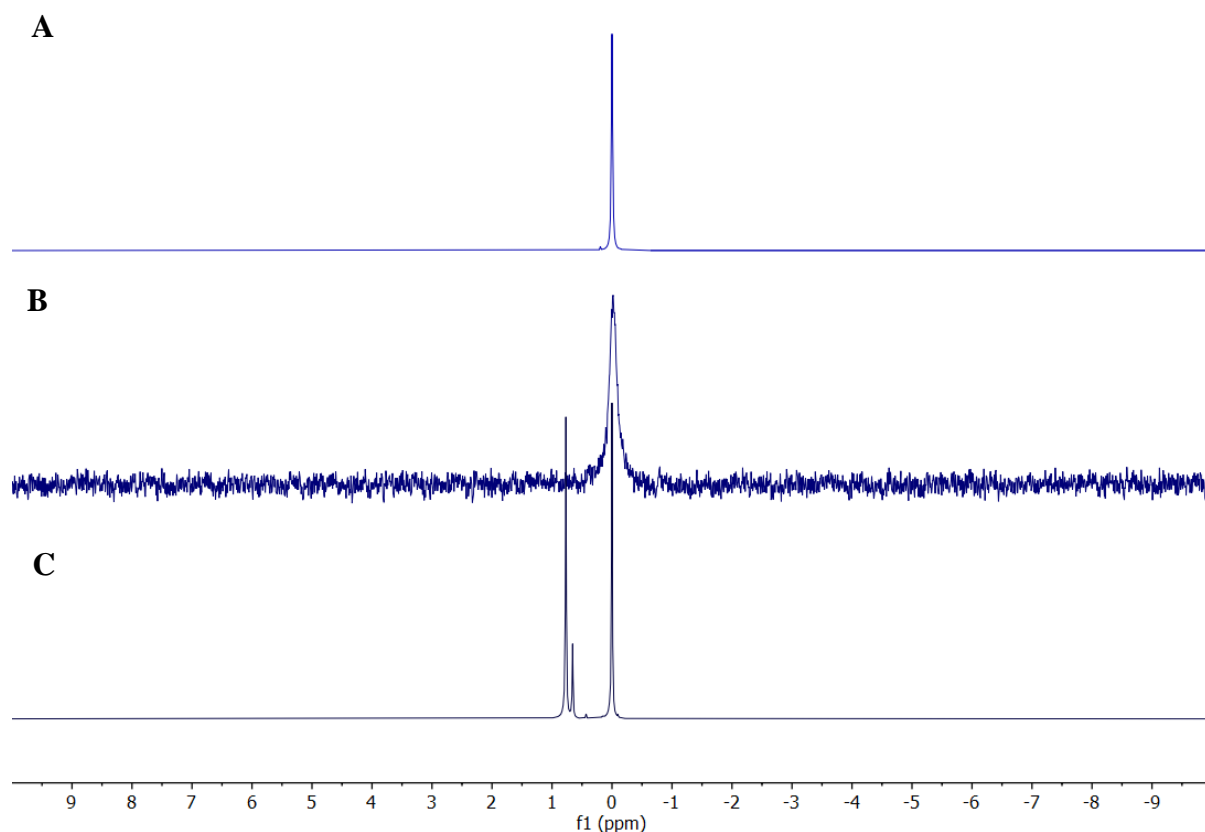


Figure 101. $^{31}\text{P}\{^1\text{H}\}$ NMR (202 MHz, $\text{DMSO-}d_6$) of reaction mixture 0.5 mmol scale after 120 h of heating neat at 115°C . Spectra were centred on P_i signal (0 ppm). **A** – **5** : Na_3PO_4 (1:1); **B** – **5** : Na_2HPO_4 = (1:1); **C** – **5** : NaH_2PO_4 = (1:1).

Table 31. Results from integrating $^{31}\text{P}\{^1\text{H}\}$ NMR peaks of $\text{DMSO-}d_6$ extract of 0.5 mmol scale mixture of **5**, **cond. agent** and P_i (1:1:1) after 120 h of heating neat at 115°C depending on protonation degree of inorganic phosphate. Calculation of total conversion (conversion of initial amount of P_i to phosphorylated organic products) was made by subtraction of inorganic compound quantities (P_i and PP_i) from the sum of all integrated peak areas.

Cond. agent	P_i	5cGIP, %	6cGIP, %	GIP, %	P_i , %	PP_i , %	Total conversion, %
-	Na_3PO_4	-	-	-	100.00	-	-
2a	Na_3PO_4	-	-	2.04	97.96	-	2.04
-	Na_2HPO_4	-	-	-	100.00	-	-
2a	Na_2HPO_4	-	-	-	100.00	-	-
-	NaH_2PO_4	2.23	-	33.58	64.19	-	35.81
2a	NaH_2PO_4	7.14	3.63	81.07	7.82	0.34	91.84

3.2.2. Experiments with cyclic trimetaphosphate (cTMP)

Another potentially interesting phosphate source is cyclic trimetaphosphate. Although it is still debated if the prebiotic conditions were favorable for its formation, cTMP was demonstrated as an excellent mediator in phosphorylation and condensation reactions. The spectrum of pure cTMP in water is shown in **Figure 102**.

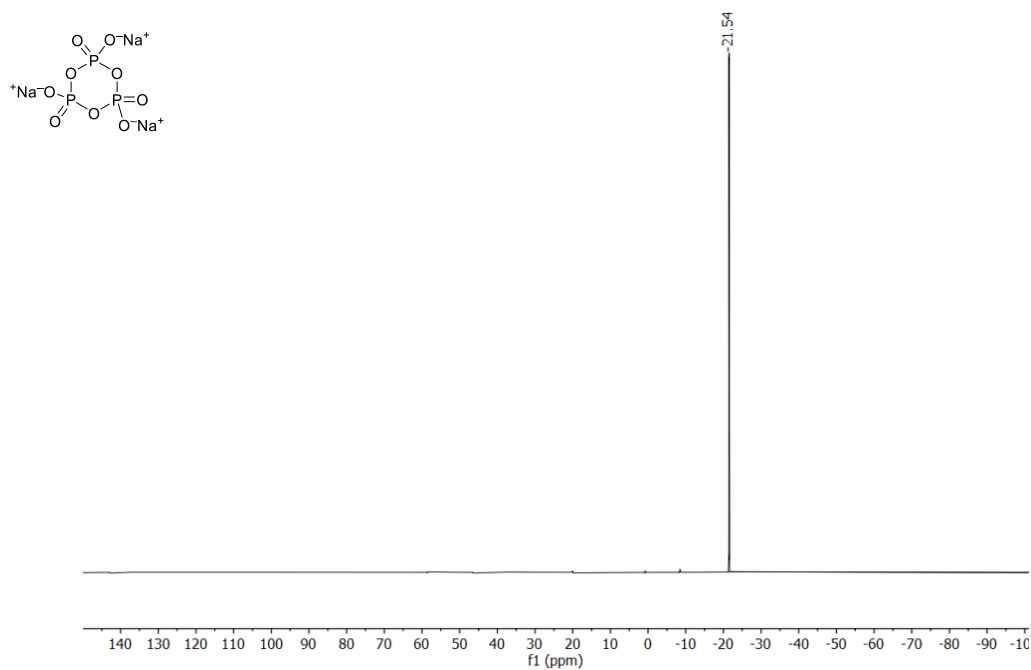


Figure 102. $^{31}\text{P}\{^1\text{H}\}$ NMR (202.5 MHz, D_2O) 0.5 mM cTMP. $\delta_{\text{P}}(\text{s}) = -21.5$.

Here, we studied the possibility of cTMP involvement in the phosphorylation of glycerol and MPG at 75 and 115 °C in dry conditions. The reaction mechanism for cTMP reactions is expected to be different from urea-assisted phosphorylation with P_i . It is most likely connected to the ring opening, thus helping cTMP to react. However, we decided to try it with condensing agents to see if the conversion into organic phosphates would be different.

In **Figure 103**, an exemplary $^{31}\text{P}\{^1\text{H}\}$ NMR spectrum of a mixture of 0.5 mmol scale **5:2a:cTMP** (1:1:1), reaction time 120 h at 115 °C is demonstrated. We can conclude that reaction conditions are favorable for ring-opening of cTMP due to the fact that we register the presence of P_i (0 ppm) and PP_i (-9.29) but not cTMP itself. The studied phosphate demonstrated an excellent conversion towards organic phosphate 71.6-98.2 % at both studied temperatures (**Figure 104, Table 32**). The presence of a condensing agent did not significantly increase yields (+3-8%), but more cyclic phosphates were detected in reactions with urea and cyanamide.

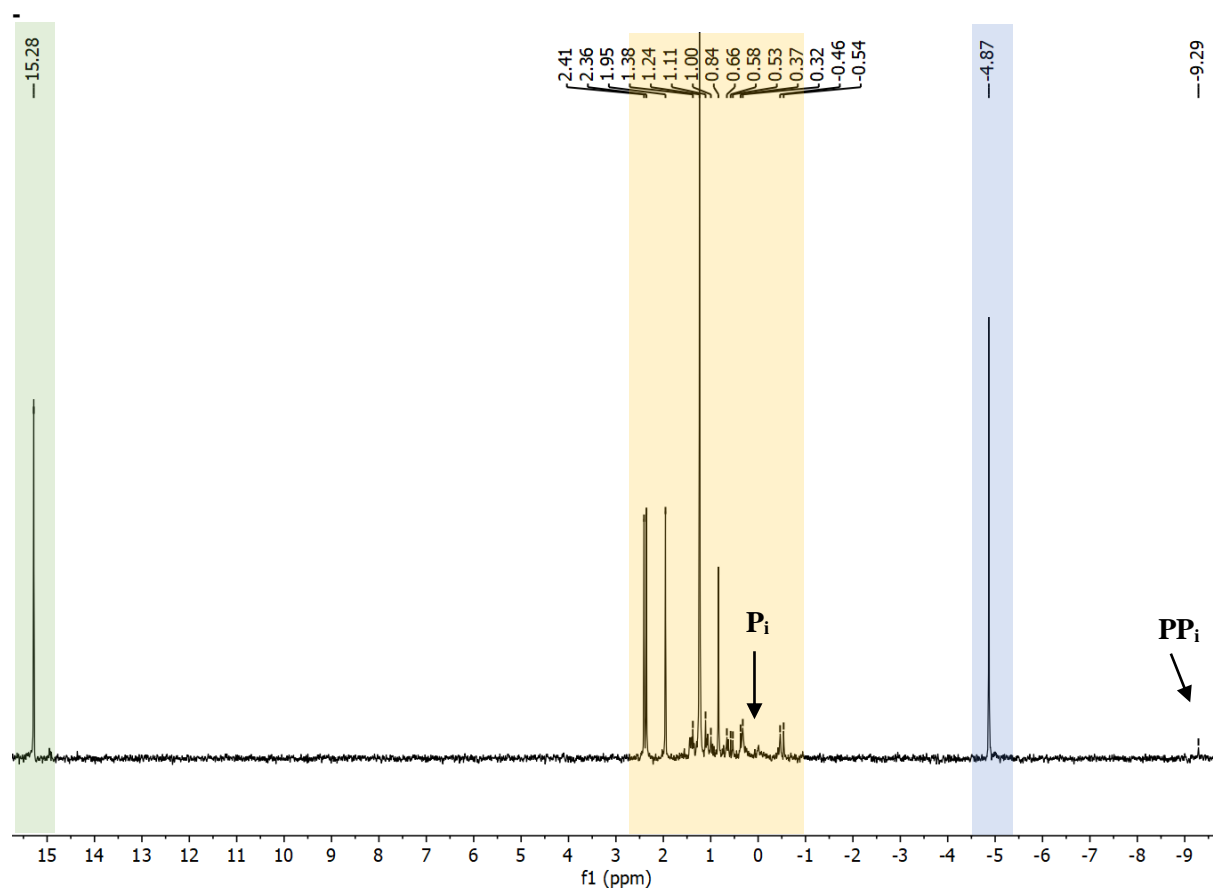


Figure 103. $^{31}\text{P}\{^1\text{H}\}$ NMR (202 MHz, $\text{DMSO-}d_6$) of the extract of mixture 0.5 mmol scale **5:2a:cTMP** (1:1:1), reaction time 120 h at 115 °C. $\delta_{\text{P}} = 15.28$ (**5cGIP**, green), from 2.41 to -0.54 (glyceryl-1-phosphates, glyceryl-2-phosphates, di-glyceryl phosphates, orange), 0 (**P_i**), -4.48 (**6cGIP**, blue), -9.29 (s, **PP_i**).

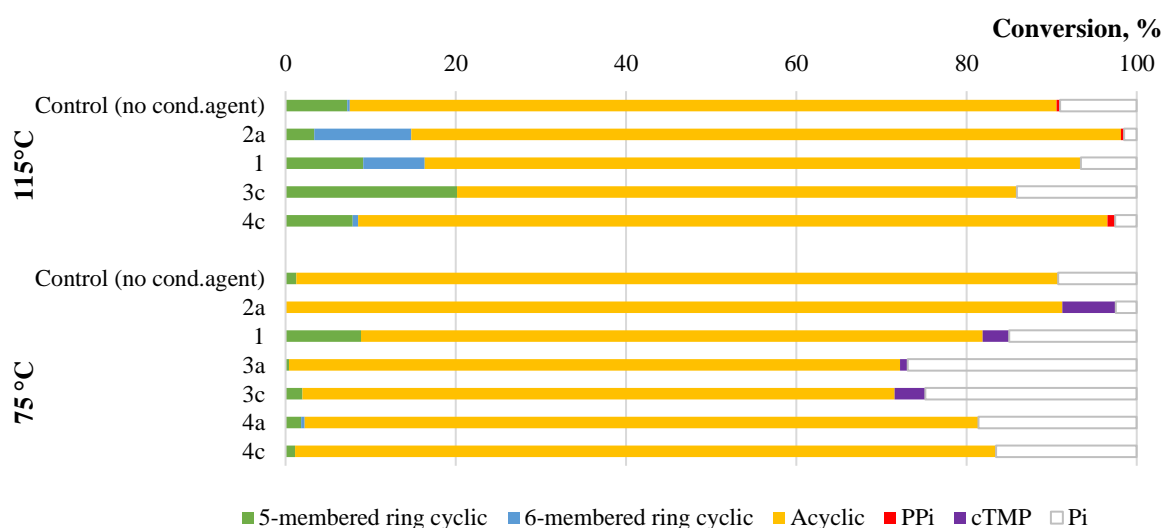


Figure 104. Summary of glycerol (**5**) phosphorylation after 120 h of heating at 75 and 115 °C in 0.5 mmol scale reaction mixture **5:cond.agent:cTMP** (1:1:1). In the case of experiments with **cTMP** signal of inorganic polyphosphates (-20 to -25 ppm) corresponds to **cTMP**.

Table 32. Data to **Figure 104**. Calculation of total conversion (conversion of initial amount of **cTMP** to phosphorylated organic products) was made by subtraction of inorganic compound quantities (**P_i**, **PP_i** and **cTMP**) from the sum of all integrated ³¹P{¹H} NMR peaks (in DMSO-*d*₆).

Temp., °C	Cond. agent	5cGIP, %	6cGIP, %	GIP, %	P _i , %	PP _i , %	cTMP, %	Total conversion, %
115	-	7.25	0.30	83.03	9.01	0.41	-	90.58
	2a	3.38	11.40	83.37	1.49	0.36	-	98.15
	1	9.14	7.20	77.10	6.56	-	-	93.44
	3c	20.15	-	65.77	14.08	-	-	85.92
	4c	7.87	0.66	88.03	2.55	0.89	-	96.56
	-	1.27	-	89.51	9.22	-	-	90.78
75	2a	-	-	91.26	2.46	-	6.28	91.26
	1	8.85	-	73.04	14.98	-	3.13	81.89
	3a	0.41	-	71.79	26.91	-	0.89	72.20
	3c	1.97	-	69.6	24.83	-	3.60	71.57
	4a	1.81	0.45	79.16	18.58	-	-	81.42
	4c	1.10	-	82.39	16.51	-	-	83.49

Equally great results were obtained in the phosphorylation of MPG (**6**) by **cTMP** at 115 °C 70.5-96.3 % (**Table 33**, **Figure 106**), as shown in the spectra of the reaction with glycerol in **Figure 105**. The presence of a condensing agent increased the fraction of 5- and 6-membered ring phosphates. Thus, **cTMP** appears to be a prospective and resultative phosphorylation agent for glycerol and its derivatives. However, it is important to note that there is still some debate about whether or not **cTMP** was actually present on the early Earth in sufficient quantities to support prebiotic phosphorylation reactions.

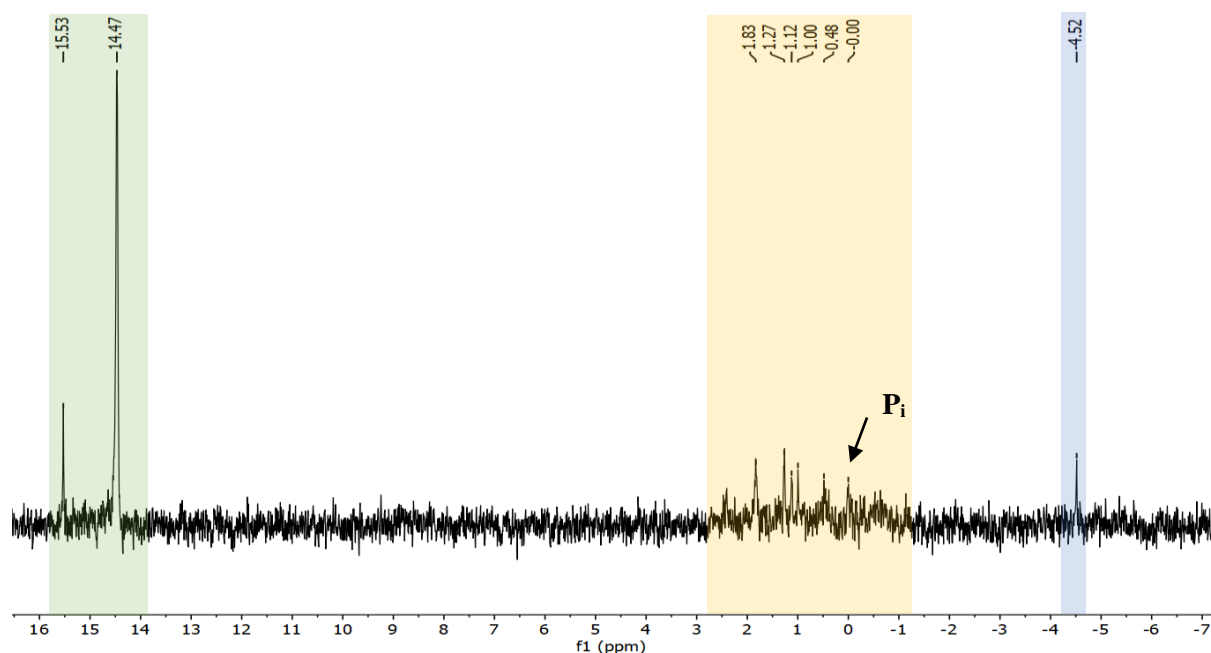


Figure 105. ³¹P{¹H} NMR (202 MHz, DMSO-*d*₆) of the extract of mixture 0.5 mmol scale **6** : **2a** : **cTMP** (1:1:1), reaction time 120 h at 115 °C. $\delta_P = 15.53, 14.47$ (**5cMPGP**, **5cGIP**, green), 1.83-0.48 (MPG-1-phosphates, MPG-2-phosphates, di-MPG phosphates, orange), 0 (**P_i**), -4.52 (**6cMPGP**, blue).

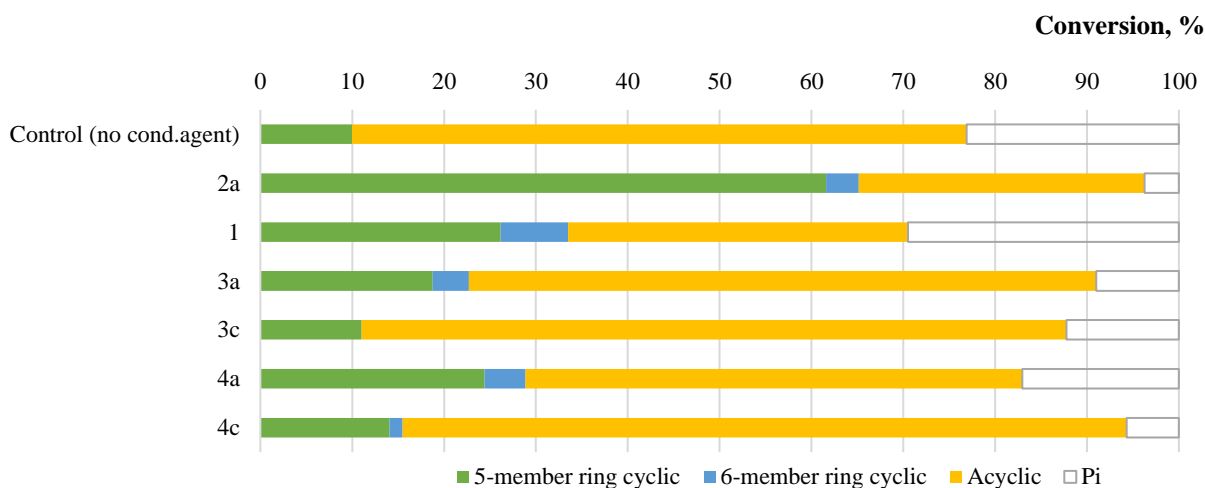


Figure 106. Summary of MPG (6) phosphorylation after 120 h of heating at 115 °C in 0.5 mmol scale reaction mixture **6:cond.agent:cTMP** (1:1:1).

Table 33. Data to **Figure 106**. Calculation of total conversion (conversion of initial amount of **cTMP** to phosphorylated organic products) was made by subtraction of inorganic compound quantities (**P_i**) from the sum of all integrated ³¹P{¹H} NMR peaks (in DMSO-*d*₆).

Cond. agent	5cMPPG, %	6cMPPG, %	MPGP, %	P _i , %	Total conversion, %
-	9.99	-	66.89	23.12	76.88
2a	61.59	3.55	31.13	3.73	96.27
1	26.16	7.36	37.01	29.47	70.53
3a	18.75	3.96	68.28	9.01	90.99
3c	11.02	-	76.73	12.25	87.75
4a	24.41	4.46	54.07	17.06	82.94
4c	14.06	1.43	78.81	5.70	94.30

In a similar series of experiments at 75 °C, the highest total conversion was obtained in reaction with **2a** (88% out of which 5-membered ring cyclic phosphates 6% and acyclic organophosphates 82%) and **1** (80 %). For all other tested carboxamides, we detected the presence of acyclic organophosphate signals; however, the conversion of products was not calculated.

3.2.3. Experiments with sodium thiophosphate (SP_i)

Another prebiotically plausible phosphate source is thiophosphates (SP_i). The spectra of pure commercial trisodium thiophosphate (**Figure 107, A**) with detected impurities P_i , PP_i and SPP_i that compose < 8% as indicated by the producer (**Figure 107, B**). Because the intensities of SPP_i signals do not change significantly during the reaction, they are not integrated and are not considered in further calculations.

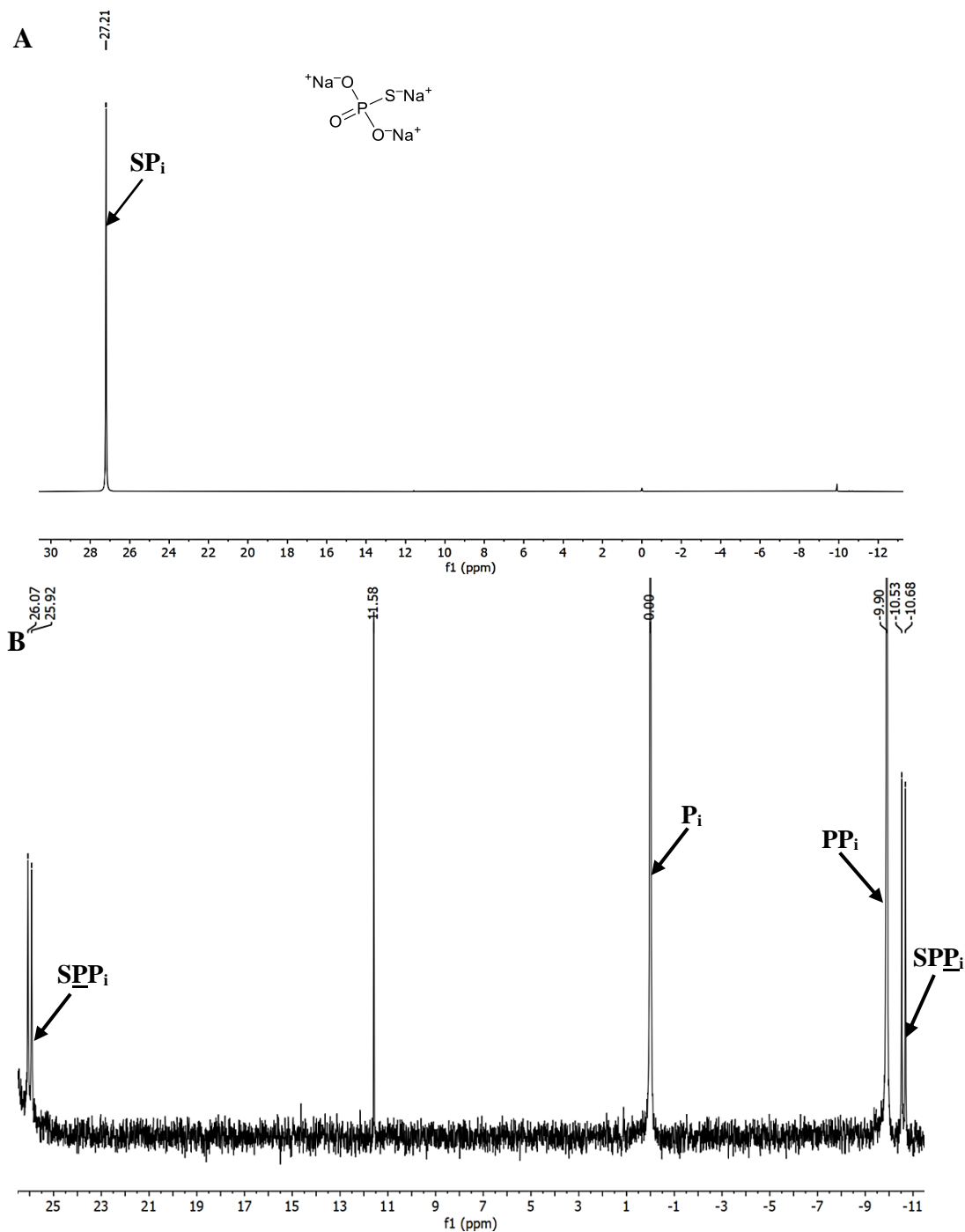


Figure 107. $^{31}\text{P}\{^1\text{H}\}$ NMR spectra (202 MHz) of commercial Na_3SPO_3 (SP_i) 0.5 mM in $\text{H}_2\text{O}/\text{D}_2\text{O} = 9:1$. δ_P (ppm) = 27.21 (s, SP_i), 26.00 (d, $J = 30.7$ Hz, SPP_i^*), 11.58 (s), 0.00 (s, P_i), -9.90 (s, PP_i), -10.60 (d, $J = 30.6$ Hz, SPP_i). The signal at 11.58 ppm is a singlet in the proton-coupled $^{31}\text{P}\{^1\text{H}\}$ NMR spectrum as well (not shown), its attribution unknown. **A** – full spectrum; **B** – zoom into minor signals of **A**.

The ^{31}P $\{^1\text{H}\}$ NMR spectrum of the **5:SP_i** reaction after 120 hours at 115 °C is shown in **Figure 108**. The obtained signals were identified by comparing $^{31}\text{P}\{^1\text{H}\}$ with ^{31}P and presented in **Figure 109**. Two main organic products are acyclic glyceryl-1 and 2-phosphates (21.70 %), along with a very small amount of glyceryl-1 and 2-thiophosphates (0.05 %).

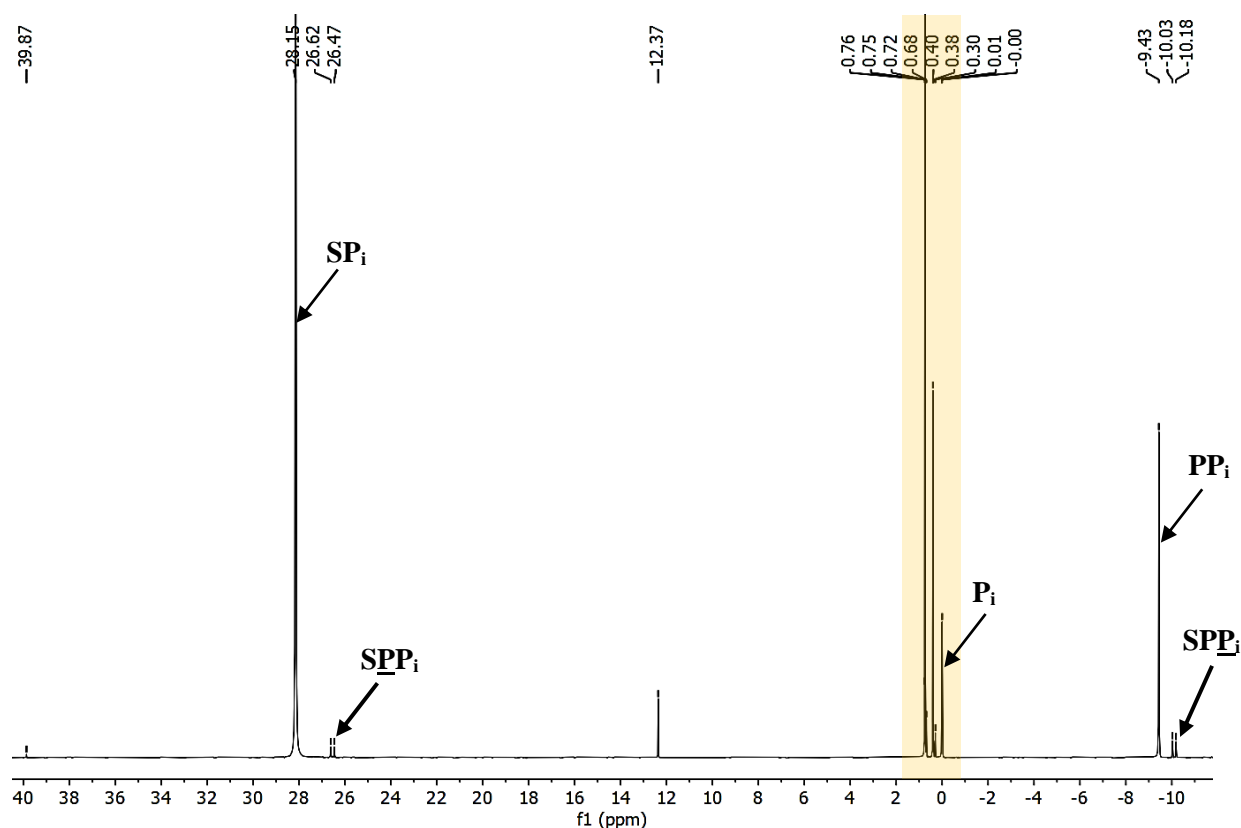


Figure 108. ^{31}P $\{^1\text{H}\}$ NMR spectrum (202 MHz) of crude mixture **5:SP_i** (1:1), 0.5 mmol scale reaction after 120 h of heating at 115 °C, then dissolved in $\text{H}_2\text{O}/\text{D}_2\text{O} = 9:1$. δ_{P} (ppm) = 39.87, 39.64 (2 x *s*, glyceryl thiophosphates, **GISP**, yellow), 28.15 (*s*, **SP_i**), 26.55 (*d*, $J = 31.0$ Hz, **SPP_i**), 12.37 (*s*), 0.75-0.63 (glyceryl-1-phosphates), 0.40-0.30 (glyceryl-2-phosphates), 0 (*s*, **P_i**), -9.43 (*s*, **PP_i**), -10.10 (*d*, $J = 31.0$ Hz, **SPP_i**). Orange zone: acyclic glyceryl phosphates, see zooms in **Figure 109**.

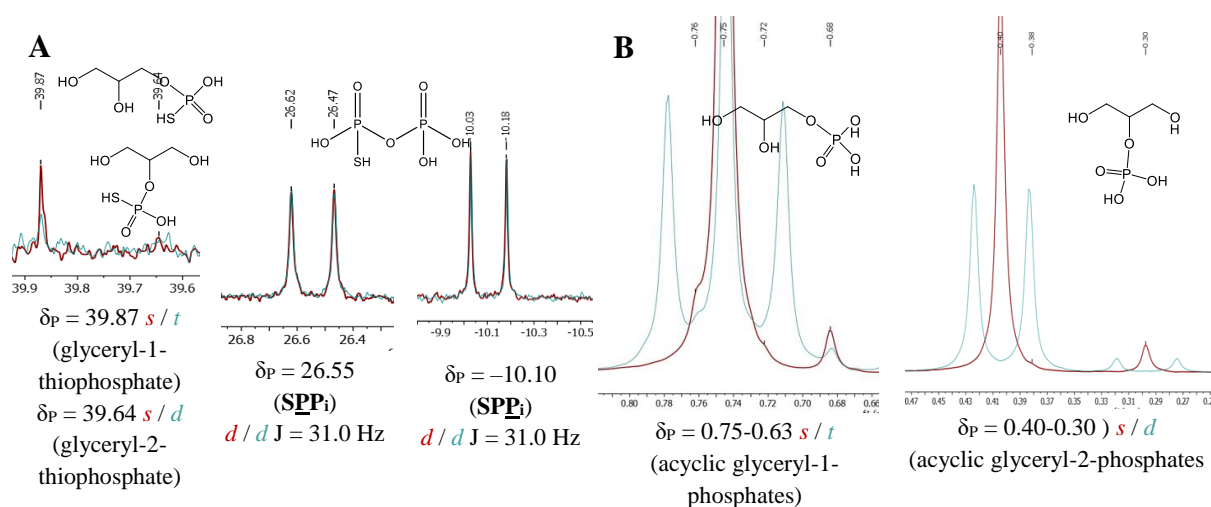


Figure 109. Zoomed zones of **Figure 108** (red-brown) superimposed on ^{31}P NMR spectrum (blue). **A** – thiophosphates; **B** – glyceryl phosphates (structure of only main compounds shown). Singlet at 12.37 ppm remains as a singlet in ^{31}P NMR (not shown).

We performed several series of experiments involving reactions with condensing agents **1** (**2a**) and reactions in the mixture of orthophosphates (1:1) with a different protonation degree. One of the most eventful $^{31}\text{P}\{^1\text{H}\}$ NMR spectrum of mixture **5:2a:SP_i:P_i** (1:1:0.5:0.5), 0.5 mmol scale reaction after 120 h of heating at 115 °C is demonstrated on **Figure 110** with detailed signal assignment on **Figure 111**. The results for glycerol phosphorylation are summarised in **Figure 112**, **Table 34** for 115 °C and **Figure 113**, **Table 35** for 75 °C.

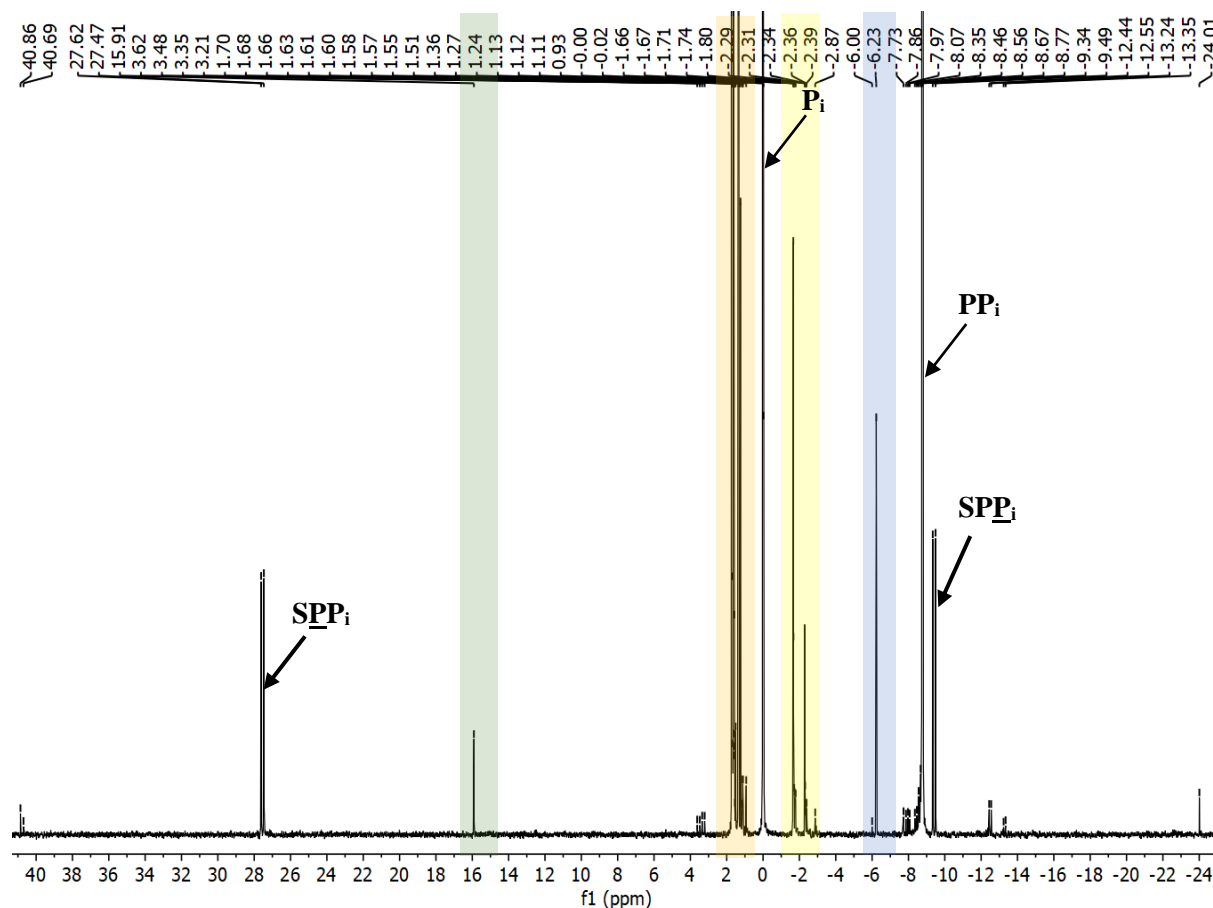


Figure 110. $^{31}\text{P}\{^1\text{H}\}$ NMR spectrum (202 MHz) of crude mixture **5:2a:SP_i:P_i** (1:1:0.5:0.5), 0.5 mmol scale reaction after 120 h of heating at 115 °C, then dissolved in $\text{H}_2\text{O}/\text{D}_2\text{O} = 9:1$. δ_{P} (ppm) = 40.86, 40.69 (2 x s, glyceryl thiophosphates, **GISP**), 27.52 (d, J = 31.0 Hz, **SPP_i**), 15.91 (s, 5-membered ring cyclic phosphate **5cGIP**, green), 3.51, 3.28 (2 x d, J = 29.0 Hz, J = 28.0 Hz), 1.70-1.51 (acyclic glyceryl-1-phosphates, **GI1P**, orange), 1.36-0.92 (acyclic glyceryl-2-phosphates, **GI2P**, orange), 0 (s, **P_i**), 1.36-0.9, -1.66 to -2.87 (acyclic diglycerol phosphates, (**GI**)₂**P**, yellow), -6.0, -6.23 (2 x s, 6-membered ring cyclic phosphates **6cGIP**, blue), -7.80 (d, J = 27.4 Hz), -8.02 (d, J = 19.4 Hz), -8.41 (d, J = 21.9 Hz, glyceryl-2-diphosphate **GIPP**), -8.61 (d, J = 22.1 Hz glyceryl-1-diphosphate **GIPP**), -8.77 (s, **PP_i**), -9.41 (d, J = 31.0 Hz, **SPP_i**), -12.50 (d, J = 22.1 Hz, glyceryl-1-diphosphate **GIPP**), -13.29 (d, J = 22.1 Hz, glyceryl-2-diphosphate **GIPP**), -24.01 (s, **P_{mi}**).

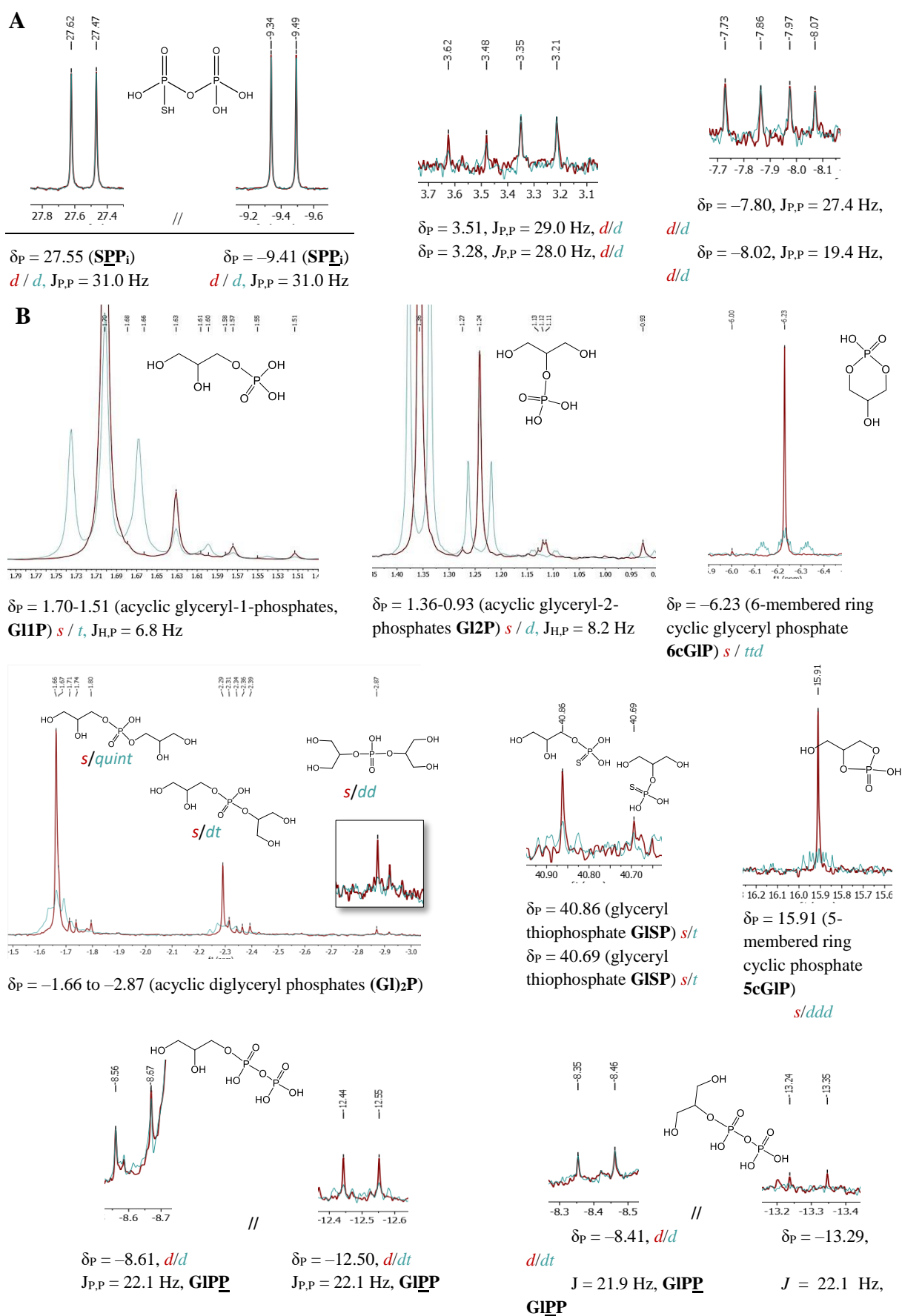


Figure 111. Zoomed zones of Figure 110 (red-brown) superimposed on ^{31}P NMR spectrum (blue). **A** – inorganic compounds; **B** – glyceryl phosphates (compound structures of attributed signals shown).

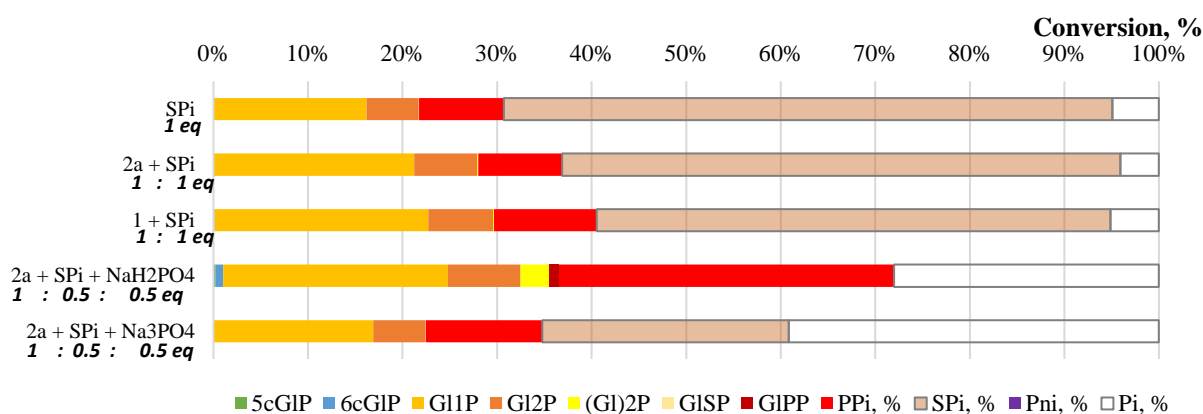


Figure 112. Summary of SP_i -driven phosphorylations of glycerol (**5**) after 120 h of heating at $115\text{ }^\circ\text{C}$, with and without urea (**2a**) or cyanamide (**1**), on a 0.5 mmol scale (no water added, ‘dry’ conditions). Molar equivalents are indicated in the diagram with respect to starting molecule **5** (1 eq). Organic products: **cGIP** (cyclic glyceryl phosphates), **G1IP** (glyceryl-1-phosphates), **G12P** (glyceryl-2-phosphates), **(G1)₂P** (diglyceryl phosphates), **GISP** (glyceryl thiophosphates); **GIPP** (glyceryl diphosphates). Percent values from signal integration of quantitative $^{31}\text{P}\{^1\text{H}\}$ NMR spectra taken in $\text{H}_2\text{O}/\text{D}_2\text{O}$ 9:1.

Table 34. Data to **Figure 112**. Total conversion of initial amount of SP_i and P_i to phosphorylated organic products was calculated by subtracting inorganic compound integrals (P_i , SP_i , PP_i , P_{ni}) from the sum of all integrated $^{31}\text{P}\{^1\text{H}\}$ NMR peak areas.

Cond. agent [‡]	Phosphate source	5cGIP %	6cGIP, %	Acyclic organo-phosphates, %					PP _i , %	SP _i , %	P _i , %	P _{ni} , %	Total conversion, %	
				G1P	G12P	(G1) ₂ P	GISP	GIPP						
-	SP _i	-	-	16.19	5.51	-	0.05	-	8.96	64.38	4.91	-	21.75	
2a	SP _i	-	0.02	21.21	6.67	0.09	0.02	-	8.86	59.04	4.07	0.02	28.01	
1	SP _i	-	0.03	22.63	6.83	0.09	-	-	10.88	54.33	5.13	-	29.66	
2a	SP _i §	NaH ₂ PO ₄	0.21	0.82	23.65	7.67	3.00	0.07	0.96	35.25	-	27.89	0.07	36.38
2a	SP _i ‡	Na ₃ PO ₄	-	-	16.90	5.52	-	0.02	-	12.32	26.05	39.15	-	22.44

[‡] Equimolar condensing agent with respect to phosphate source and starting compound **5** (1:1:1).

[§] Equimolar ratio between two phosphate sources with respect to 1 eq of starting compound **5** (0.5:0.5:1).

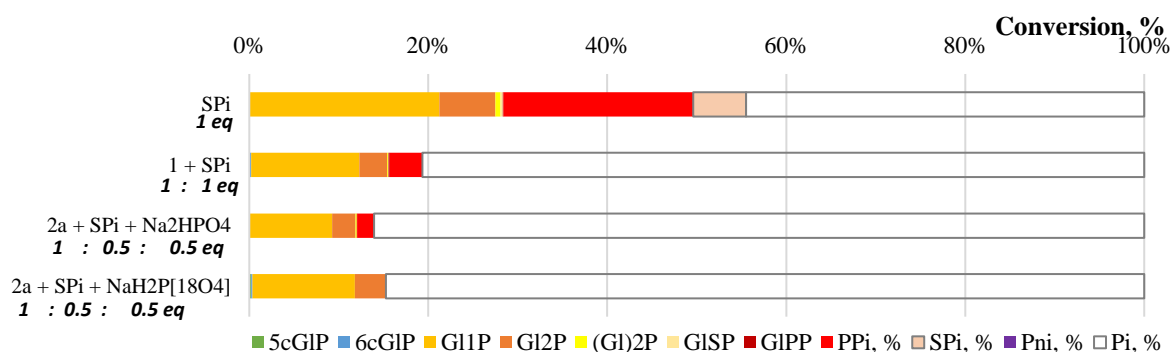


Figure 113. Summary of SP_i -driven phosphorylations of glycerol (**5**) after 120 h of heating at 75°C , with and without urea (**2a**) or cyanamide (**1**), on a 0.5 mmol scale in 1 ml D_2O ('wet and evaporating' conditions). Molar equivalents are indicated in the diagram with respect to starting molecule **5** (1 eq). Organic products: **cGIP** (cyclic glyceryl phosphates), **GI1P** (glyceryl-1-phosphates), **GI2P** (glyceryl-2-phosphates), **(GI)₂P** (diglyceryl phosphates), **GISP** (glyceryl thiophosphates); **GIPP** (glyceryl diphosphates). Percent values from signal integration of quantitative $^{31}\text{P}\{^1\text{H}\}$ NMR spectra taken in $\text{H}_2\text{O}/\text{D}_2\text{O}$ 9:1

Table 35. Data to **Figure 113**. Total conversion of initial amount of SP_i and P_i to phosphorylated organic products was calculated by subtracting inorganic compound integrals (P_i , SP_i , PP_i , P_{ni}) from the sum of all integrated $^{31}\text{P}\{^1\text{H}\}$ NMR peaks.

Condensing agent	Phosphorus source	Acyclic glyceryl phosphates, %											Total conversion, %	
		5cGIP, %	6cGIP, %	GI1P	GI2P	GIPGI	GISP	GIPP	PPi, %	SPi, %	Pni, %	Pi, %		
-	SP_i	-	0.03	0.01	21.19	6.26	0.58	0.25	0.07	21.2	5.91	0.02	44.48	28.39
1	SP_i	-	-	0.22	11.96	3.09	0.11	0.03	0.15	3.64	-	-	79.98	15.56
2a	SP_i	Na_2HPO_4	-	0.05	9.22	2.58	0.15	0.02	0.03	1.90	-	-	86.04	12.05
2a	SP_i^2	$\text{NaH}_2\text{P}[^{18}\text{O}_4]$	0.22	0.13	11.44	3.48	-	-	-	-	-	-	84.72	15.27

As in the negative control experiment, the involvement of urea increased yield up to 28-29 %, which is still lower compared to the P_i phosphorylation 91-95 % (**Figure 96**). The presence of orthophosphate does not help with producing organic phosphates but favours consuming SP_i . In all experiments, the presence of cyclic glyceryl phosphate was detected only in the reaction with $\text{SP}_i:\text{P}_i$ (1:1). We noticed that in the sequence $5:\text{SP}_i > 5:2a:\text{SP}_i > 5:2a:\text{SP}_i:\text{P}_i$ yields are increasing $21.75 > 28.01 > 36.38$ following adding condensing agent and dihydrogen phosphate. The mechanism of urea-assisted reaction was already explained before, but the presence of protons, provided by NaH_2PO_4 (P_i), apparently helps for the formation of H_2S as a good leaving group and intensifies the reaction. In a similar experiment, where tribasic phosphate was tested, we did not observe any yield increase. Lower temperatures do not help phosphorylation and the yields do not exceed 29 %.

Phosphorylation of MPG (**6**) was more challenging than previously described for glycerol due to the low solubility of the crude mixture in water and DMSO- d_6 . There are only two experiments which product yields were quantifiable: **6:2a:SP_i:P_i** (1:1:0.5:0.5), 0.5 mmol scale reaction after 120 h of heating at 75 °C, one in a dry mixture and another with an addition before heating a ml of water that would eventually evaporate during the experiments (**Figure 114**). The spectra and results suggest relatively high amounts of acyclic and cyclic products 61.5 and 93.9 % in dry and wet-to-dryness experiments, respectively (**Figure 115, Table 36**). These results should be compared carefully to the glycerol phosphorylation data, considering a different solvent. Most likely, **SP_i** as well as **SPP_i** and **PP_i** are less soluble in DMSO than water, which may have an influence on quantification results.

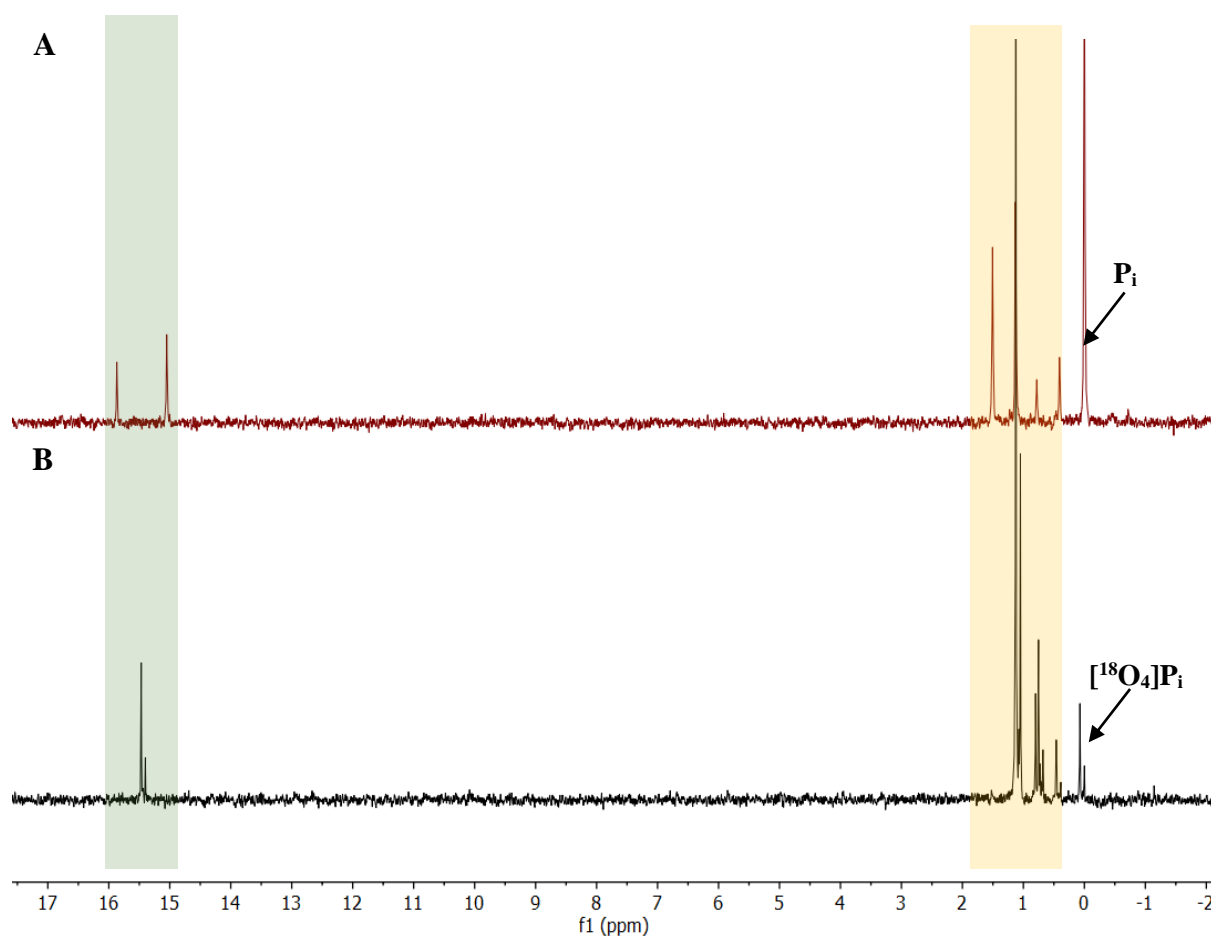


Figure 114. $^{31}\text{P}\{^1\text{H}\}$ NMR spectra (202 MHz) of crude mixture **6:2a:SP_i:P_i** (1:1:0.5:0.5), 0.5 mmol scale reaction after 120 h of heating at 75 °C, then dissolved in DMSO- d_6 . δ_{P} (ppm) = 16-15 (green zone: 2 x s, 5-membered ring cyclic MPG phosphates, **5-cMPGP**), 1.7-0.3 (orange zone: acyclic MPG phosphates = **MPG1P**, **MPG2P**, (**MPG**)₂**P**). **P_i** appears in B as two singlets $\delta_{\text{P}} = 0$ and -0.09 representing two isotopes of **P_i**, $^{16}\text{O}_4\text{P}_i$ from added and hydrolysed unlabelled **SP_i** and $^{18}\text{O}_4\text{P}_i$ from added of $\text{NaH}_2\text{P}^{18}\text{O}_4$ as **P_i** (the part that did not exchange its oxygen atoms with added D_2^{16}O); isotopic shift $\Delta\delta_{\text{P}}(^{16}\text{O}_4\text{P}_i - ^{18}\text{O}_4\text{P}_i) = 17.3$ Hz, i.e., 4.3 Hz per ^{18}O . **A** – without D_2O as a liquidiser (dry conditions); **B** – in 1 ml D_2O (‘wet and evaporating’ conditions).

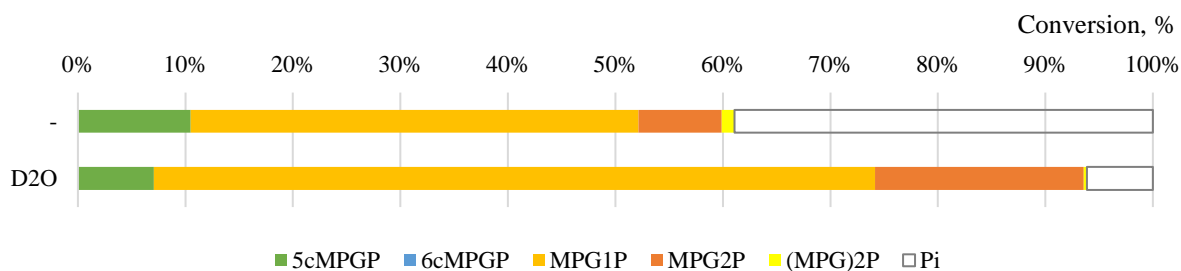


Figure 115. Summary of SP_i/P_i - and urea-driven phosphorylations of MPG (**6**) after 120 h of heating at 75 °C of **6:2a:P_i:SP_i** (1:1:0.5:0.5) on a 0.5 mmol scale, without and with 1 ml D₂O as liquidiser (water evaporated eventually). Organic products: **5cGIP** (5-membered ring cyclic MPG phosphates), **MPG1P** (MPG-1-phosphates), **MPG2P** (MPG-2-phosphates), **(MPG)₂P** (di-MPG phosphates). Percent values from signal integration of quantitative $^{31}\text{P}\{^1\text{H}\}$ NMR spectra taken in DMSO-*d*₆. NMR spectra for the dry reaction mixture were measured at 40°C to increase the solubility of the sample. Calculation of total conversion of the initial amount of SP_i and P_i to phosphorylated organic products was made by subtraction of inorganic compound quantities (P_i , SP_i , PP_i) from the sum of all integrated $^{31}\text{P}\{^1\text{H}\}$ NMR peaks.

Table 36. Data to Figure 115. Total conversion of initial amount of SP_i and P_i to phosphorylated organic products was calculated by subtracting inorganic compound integrals (P_i , SP_i , PP_i , Pn_i) from the sum of all integrated $^{31}\text{P}\{^1\text{H}\}$ NMR peaks.

Liqui- diser	5cMPGP, %	6cMPGP, %	Acyclic organo-phosphates, %			P_i , %	SP_i , %	PP_i , %	Total conver- sion, %
			MPG1P	MPG2P	(MPG) ₂ P				
-	10.57	-	41.91	7.8	1.21	39.17	-	-	61.49
D₂O	7.07	-	67.08	25.56	0.29	6.14	-	-	93.86

All other experiments with **6** and SP_i were complicated by the low solubility of the crude reaction mixtures in DMSO-*d*₆, despite being conducted at 40 °C in order to increase the solubility of the crude mixtures. We identified 5-membered ring cyclic phosphates and acyclic MPG phosphates as the main products of reactions in various ratios, but without quantification owing to too low signal-to-noise ratios. In the reactions of **6** and SP_i with and without cond. agent (**2a** or **1**) after heating for 120 h at 75 °C, the ratio of 5-membered ring cyclic MPG phosphates over acyclic MPG phosphates was 1:3. In experiments with a mix of phosphate sources, we measured this ratio as 1:4.5 and 1:1 from **6:2a:SP_i:Na₃PO₄** and, respectively, **6:2a:SP_i:NaH₂PO₄**.

3.2.3.1. Competition of SP_i and $[\text{}^{18}\text{O}_4]\text{P}_i$ in urea-assisted phosphorylation of glycerol and MPG

The increase in yields in reaction with mixed inorganic phosphates ($\text{P}_i:\text{SP}_i$) raised an interest in exploring the competition between them in product formation. To pursue this study, we used a labelled $[\text{}^{18}\text{O}]\text{P}_i$; thus, we were able to track phosphorylated molecules produced by orthophosphates against unlabelled thiophosphate by using HRMS.

In **Figure 116**, the total chromatogram of the crude mixture $5:2\text{a}:\text{SP}_i:[\text{}^{18}\text{O}]\text{P}_i$ (1:1:0.5:0.5); 0.5 mmol scale; reaction time 120 h at 115 °C in negative ion mode is shown. The main signals belong to glyceryl monophosphate and its isotopologs. Along with it, we identified glyceryl carbamate (phosphorylated and not phosphorylated), cyclic monoglyceryl phosphate and diglyceryl phosphate (**Table 37**). The ratio of unlabelled:labelled (to partly labelled) glyceryl phosphates was approximately 60:40. This demonstrated that SP_i is more efficient in phosphorylation reaction compared to P_i . Protonated SP_i because of the H_2S leaving group phosphorylate up to 69% of detected products.

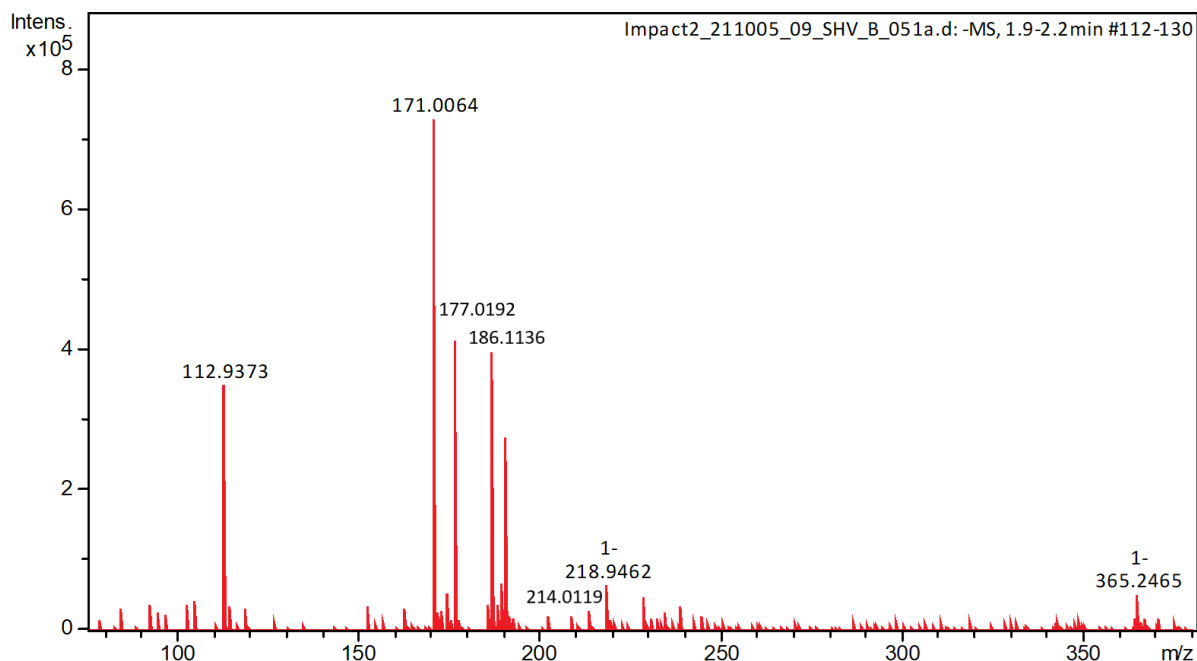
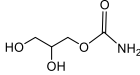
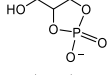
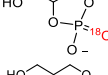
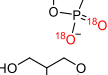
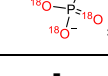
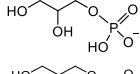
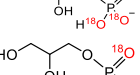
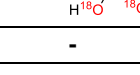
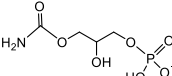
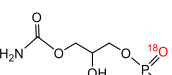
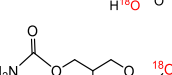
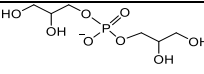
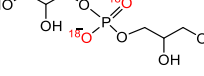
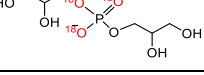


Figure 116. Negative ion mode HRMS of the methanolic extract of crude mixture $5:2\text{a}:\text{SP}_i:[\text{}^{18}\text{O}]\text{P}_i$ (1:1:0.5:0.5) ; 0.5 mmol scale ; reaction time 120 h at 115 °C.

Table 37. Interpretation of HRMS of **Figure 116** with suggested formulas, structures and measured relative isotopolog ratios per compound. Ion for all listed masses is $[M-H]^-$, if not specified otherwise.

Peak number	m/z of the main signal	Suggested chemical formula	Suggested chemical structure	Oxygen isotopolog ratio
1	134.0463	$C_4H_9NO_4$		-
	152.9959	$C_3H_7O_5P$		68.9
2	155.0002	$C_3H_7O_4P[^{18}O]$		3.3
	157.0045	$C_3H_7O_3P[^{18}O_2]$		23.1
	159.0085	$C_3H_7O_2P[^{18}O_3]$		4.7
3	170.9971	$C_3H_8O_6S$	-	-
4	171.0064	$C_3H_9O_6P$		61.0
	175.0150	$C_3H_9O_4P[^{18}O_2]$		4.4
	177.0192	$C_3H_9O_3P[^{18}O_3]$		34.6
5	186.1136	$C_9H_{17}NO_3$	-	-
6	186.9741	$C_3H_8O_5S_2$	-	-
7	214.0119	$C_4H_{10}NO_7P$		63.4
	218.0205	$C_4H_{10}NO_5P[^{18}O_2]$		4.3
	220.0250	$C_4H_{10}NO_4P[^{18}O_3]$		32.3
8	245.0433	$C_6H_{15}O_8P$		69.3
	249.0510	$C_6H_{15}O_6P[^{18}O_2]$		17.3
	251.0572	$C_6H_{15}O_5P[^{18}O_3]$		13.5
9	250.9633	$C_3H_9O_9PS$	-	65.4
	256.9761	$C_3H_9O_6PS[^{18}O_3]$	-	34.6
10	365.2465 $[M+Cl]^-$	$C_{19}H_{38}O_4$	-	-

* The position of one ^{18}O isotope is uncertain (resulting probably from reversible addition-elimination).

Similar to described above, the phosphorylation reaction of **6:2a:SP_i:[¹⁸O]P_i** (1:1:0.5:0.5), 0.5 mmol scale, reaction time 120 h at 115 °C was studied by HRMS (**Figure 117**). The results confirm that **SP_i** outperforms the competition with **P_i** by about 67-74 % and some products such as **5cMPPG**, **5cGIP**, **GIPGI**, and glyceryl carbamate were found only in unlabelled form (**Table 38**).

These results are consistent with the previous experiments and confirm that the presence of protons favours phosphorylation by thiophosphate and contributes up to 60–70 % to the total conversion of organic phosphates.

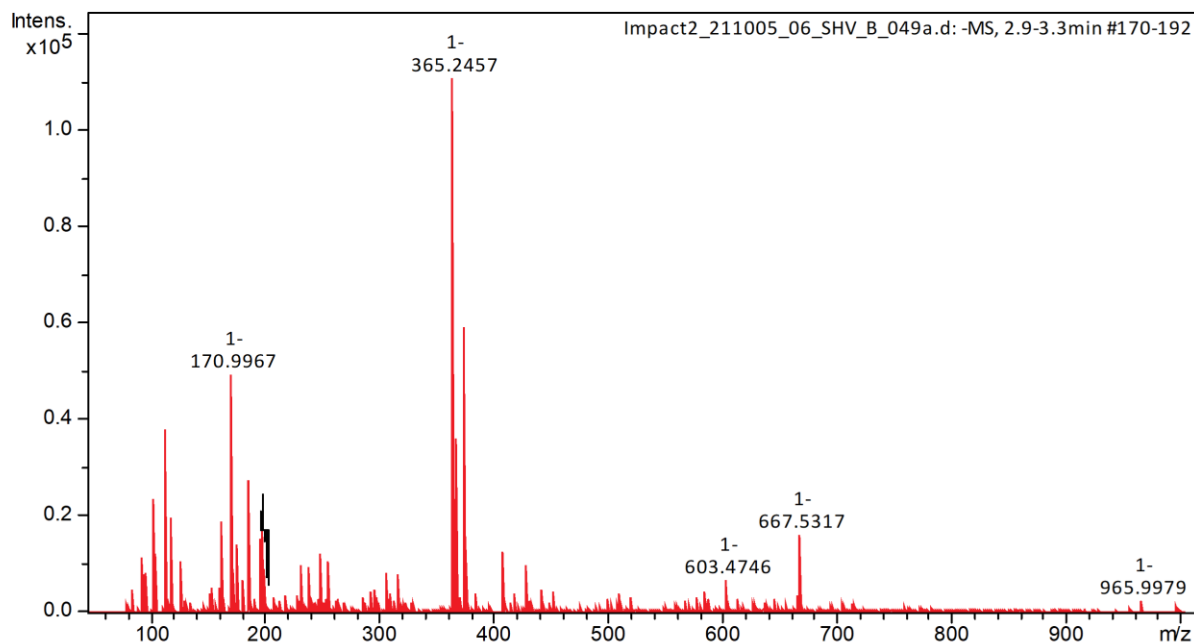


Figure 117. Negative ion mode HRMS of the methanolic extract of crude mixture **6:2a:SP_i:P_i** (1:1:0.5:0.5) ; 0.5 mmol scale ; reaction time 120 h at 115 °C.

Table 38. Interpretation of HRMS of **Figure 117** with suggested formulas, structures and measured relative isotopolog ratios per compound. Ion for all listed masses is $[M-H]^-$, if not specified otherwise.
* The position of one ^{18}O isotope is uncertain (resulting probably from reversible addition-elimination).

Peak number	m/z of the main signal ³	Suggested chemical formula	Suggested chemical structure	Isotopolog ratio
1	152.9956	$C_3H_7O_5P$		67.9
	157.0038	$C_3H_7O_4P[^{18}O]$		27.8
	159.0079	$C_3H_7O_3P[^{18}O_2]$		4.3
2	170.9967	$C_3H_8O_6S$	-	-
3	171.0058	$C_3H_9O_6P$		71.3
	173.0099	$C_3H_9O_5P[^{18}O]$		1.6
	175.0144	$C_3H_9O_4P[^{18}O_2]$		3.1
	177.0187	$C_3H_9O_3P[^{18}O_3]$		24.0
4	186.1132	$C_9H_{17}NO_3$	-	-
5	186.9735	$C_3H_8O_5S_2$	-	-
6	214.0113	$C_4H_{10}NO_7P$		74.4
	220.0244	$C_4H_{10}NO_4P[^{18}O_3]$		25.6
7	232.9616	$C_3H_8O_8P_2$		-
8	245.0424	$C_6H_{15}O_8P$		-
9	250.9633	$C_3H_9O_9PS$	-	-
10	375.2743 $[M- M+HCOOH-H]^-$	$C_{19}H_{38}O_4$		-
11	372.2749	$C_{20}H_{39}NO_5$		-
12	391.2252 $[M+Cl]^-$	$C_{20}H_{36}O_5$		-
13.1	409.2287	$C_{19}H_{38}O_7S$	-	-
13.2	411.2421	$C_{19}H_{39}O_6P[^{18}O]$		24.9
	413.2427	$C_{19}H_{39}O_5P[^{18}O_2]$		11.0
	415.2480	$C_{19}H_{39}O_4P[^{18}O_3]$		64.1
14	603.4746 $[M+Cl]^-$	$C_{35}H_{68}O_5$	-	-

3.2.4. Involving natural minerals and their analogues in phosphorylation of glycerol and MPG

Three commercially available and prebiotically plausible minerals were chosen to be tested in this work: natural vivianite, i.e., a blue rock grinded to powdered ($\text{Fe}_3(\text{PO}_4)_2 \cdot 8(\text{H}_2\text{O})$), synthetic struvite ($\text{NH}_4\text{MgPO}_4 \cdot 6\text{H}_2\text{O}$) and calcium pyrophosphate ($\text{Ca}_2\text{P}_2\text{O}_7$) as an analog of natural canaphite ($\text{CaNa}_2\text{P}_2\text{O}_7 \cdot 4\text{H}_2\text{O}$). The results are summarised in **Figure 118** and **Table 39**. We did not succeed phosphorylating MPG (**6**) with all three tested phosphate sources; however, glycerol phosphorylation seems to be prospective.

The work with vivianite was challenging due to the presence of ferrous iron in its composition. The initial treatment included using a saturated solution of EDTA (ethylenedinitrilotetraacetic acid disodium salt) to exchange Fe^{2+} ions with Na^+ . However, we did not succeed in obtaining a good-quality $^{31}\text{P}\{^1\text{H}\}$ NMR spectra of such solutions (and no ferrous EDTA precipitate after several weeks). Another successful approach was to use a saturated solution of Na_2S with a high pH (>10). Following this procedure, we obtained clear $^{31}\text{P}\{^1\text{H}\}$ NMR spectra that were used for the quantification. Although we overcame this challenge, the phosphorylation did not appear to be efficient, with the maximum yield of acyclic glyceryl phosphate in reaction **5:2a** 38 %.

Both struvite and canaphite analogues demonstrated equivalent phosphoester production in the presence and absence of condensing agent. A possible explanation for struvite is the presence of an ammonium cation that favours the phosphorylation reaction. Especially interesting seems to be the case of pyrophosphate-containing $\text{Ca}_2\text{P}_2\text{O}_7$. From $^{31}\text{P}\{^1\text{H}\}$ NMR no P_{Pi} signal was detected at the end of phosphorylation, which indicated that the initial material was completely consumed into phosphorylated products and P_i.

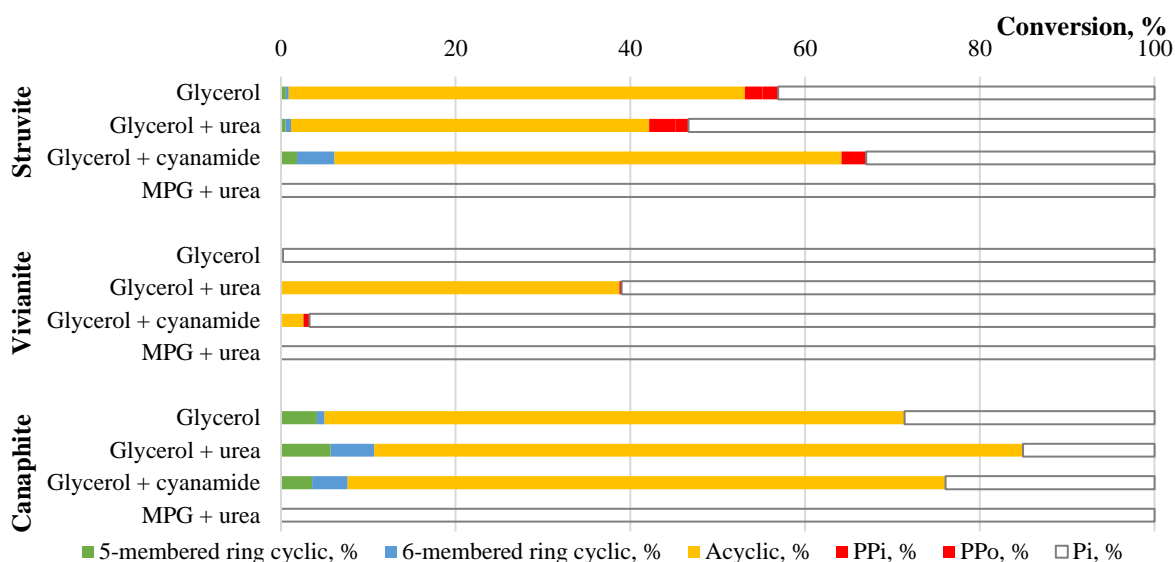


Figure 118. Summary of **minerals**-driven phosphorylations of glycerol (**5**) after 120 h of heating at 115 °C, with and without urea (**2a**) or cyanamide (**1**), on a 0.5 mmol scale. Organic products: **cGIP** (cyclic glyceryl phosphates), **G1IP** (glyceryl-1-phosphates), **G2IP** (glyceryl-2-phosphates), **(G1)₂P** (diglyceryl phosphates), **GISP** (glyceryl thiophosphates); **GIPP** (glyceryl diphosphates). Percent values from signal integration of quantitative $^{31}\text{P}\{^1\text{H}\}$ NMR spectra taken in D_2O for glycerol reactions and $\text{DMSO-}d_6$ for MPG.

Table 39. Data to **Figure 118**. Total conversion of initial amount of phosphates to phosphorylated organic products was calculated by subtracting inorganic compound integrals (**P_i**, **PP_i**) from the sum of all integrated $^{31}\text{P}\{^1\text{H}\}$ NMR peaks.

Phosphate source	Starting molecule	Cond. agent	5-membered ring cyclic, %	6-membered ring cyclic, %	Acyclic, %	PP _i , %	PP _o , %	P _i , %
Struvite	5	-	0.56	0.33	52.23	2.00	1.81	43.07
	5	2a	0.52	0.63	41.01	3.04	1.45	53.35
	5	1	1.84	4.28	58.07	1.40	1.39	33.02
	6	2a	-	-	-	-	-	100
Vivianite	5	-	-	-	-	0.24	-	99.76
	5	2a	-	-	38.75	0.26	-	60.99
	5	1	-	-	2.59	0.7	-	96.71
	6	2a	-	-	-	-	-	100
Canaphite analogue	5	-	4.11	0.90	66.39	-	-	28.60
	5	2a	5.69	4.97	74.30	-	-	15.04
	5	1	3.57	4.05	68.45	-	-	23.93
	6	2a	-	-	-	-	-	100

3.3. Phosphorylation of 2,3-bis-(tridecanoyl)glycerol: BTG (7)

After phosphorylation of glycerol and its monosubstituted derivatives with one fatty chain (MPG), it was important to study whether phosphorylation is possible in bi-substituted glycerol, such as BTG (7) and DOG (8). Reactions with BTG were carried at 115 and 75 °C (Figure 119, Figure 120) with only traces of phosphorylated products detected (Figure 123, Table 40).

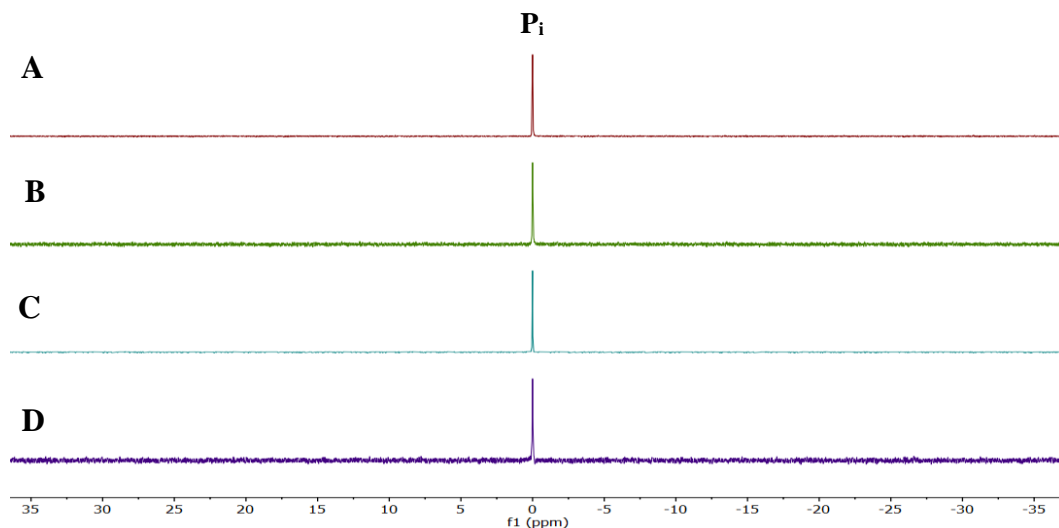


Figure 119. $^{31}\text{P}\{^1\text{H}\}$ NMR spectra (202.5 MHz) of crude mixtures of reactions with BTG (7) on a 0.5 mmol scale after 120 h of heating neat at 115 °C, then dissolved in DMSO-*d*6. On all shown spectra, we observe the presence of only one single resonance that belongs to P_i , $\delta_{\text{P}_i} = 0.00$ ppm: **A** – reaction 7: P_i (1:1); **B** – 7:2a: P_i (1:1:1); **C** – 7:1: P_i (1:1:1); **D** – 7:3a: P_i (1:1:1).

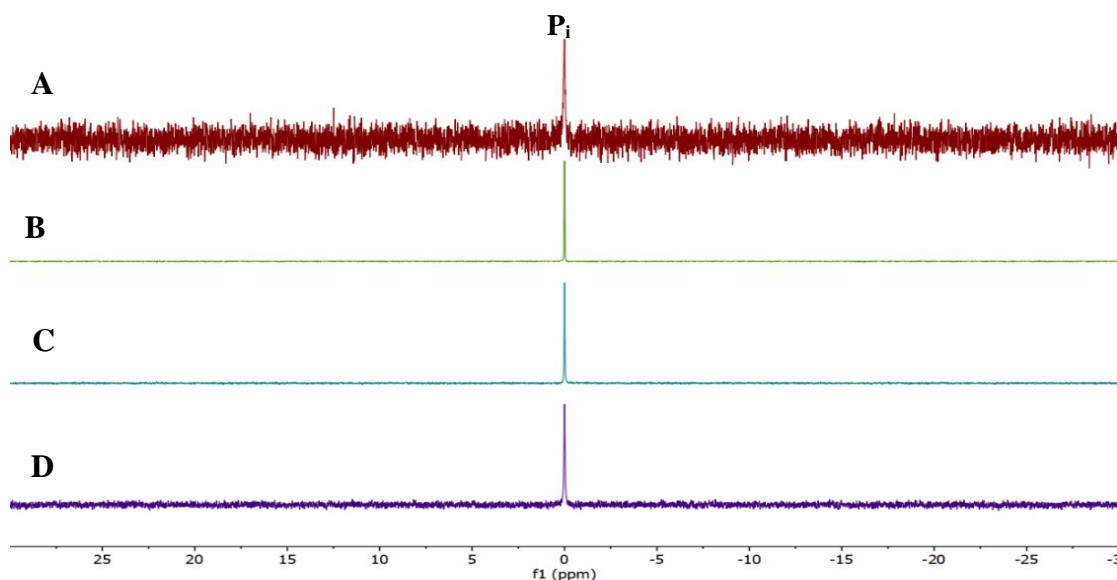


Figure 120. $^{31}\text{P}\{^1\text{H}\}$ NMR spectra (202.5 MHz) of crude mixtures of reactions with BTG (7) on a 0.5 mmol scale after 120 h of heating neat at 75 °C, then dissolved in DMSO-*d*6. On all shown spectra, we observe the presence of only one single resonance that belongs to P_i , $\delta_{\text{P}_i} = 0.00$ ppm: **A** – reaction 7: P_i (1:1); **B** – 7:2a: P_i (1:1:1); **C** – 7:1: P_i (1:1:1); **D** – 7:3a: P_i (1:1:1).

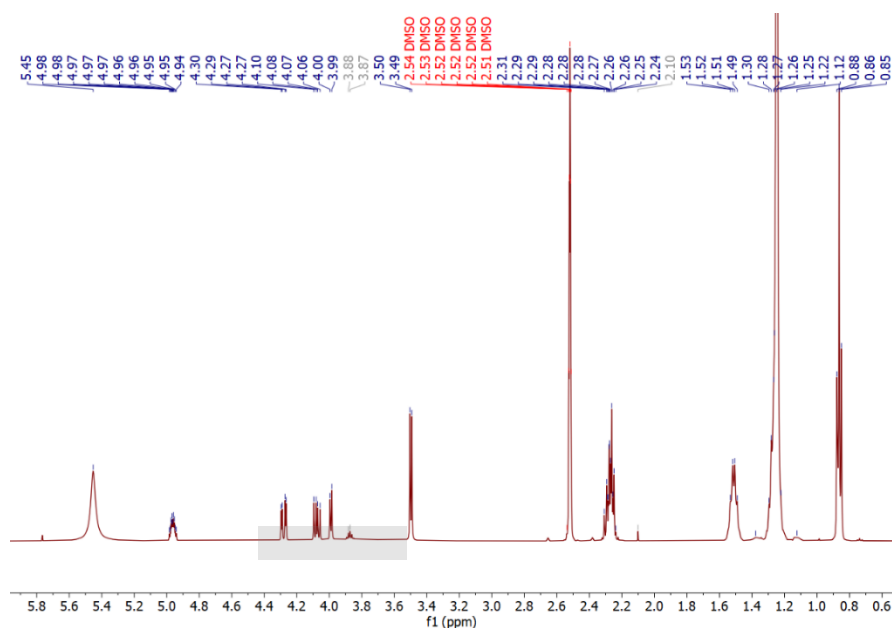


Figure 121. ^1H NMR spectrum (500 MHz) of crude reaction mixture with **BTG 7:1:cTMP** (1:1:1) on a 0.5 mmol scale after 120 h of heating neat at $115\text{ }^\circ\text{C}$, then dissolved in $\text{DMSO-}d_6$. δ_{H} (ppm) = 5.45 (*s*, 6H), 4.96 (*dtd*, $J = 10.7, 5.5, 3.0$ Hz, 1H), 4.28 (*dd*, $J = 12.0, 3.1$ Hz, 1H), 4.08 (*dd*, $J = 12.0, 7.2$ Hz, 1H), 3.99 (*d*, $J = 5.4$ Hz, 1H), 3.88 (*q*, $J = 5.3$ Hz, OH), 3.50 (*d*, $J = 5.6$ Hz, 2H), 2.31 (*s*, OH), 2.30 – 2.24 (*m*, 5H), 1.51 (*h*, $J = 6.9$ Hz, 6H), 1.25 (*s*, 42H), 0.86 (*t*, $J = 6.9$ Hz, 7H).

The structural assignment of ^1H NMR resonances of the starting molecule is shown in **Figure 41**. The grey zone is an area of organic products of phosphorylation. Out of the series of all reactions, only **BTG** with **cTMP** at $75\text{ }^\circ\text{C}$ were observed trace amounts of organic products of phosphorylation: acyclic **BTGP** and (most likely) 3-tridecanoylglycerol-1,2-cyclic phosphate (**5cTGP**) resulting from mono-deacylation of **BTG**.

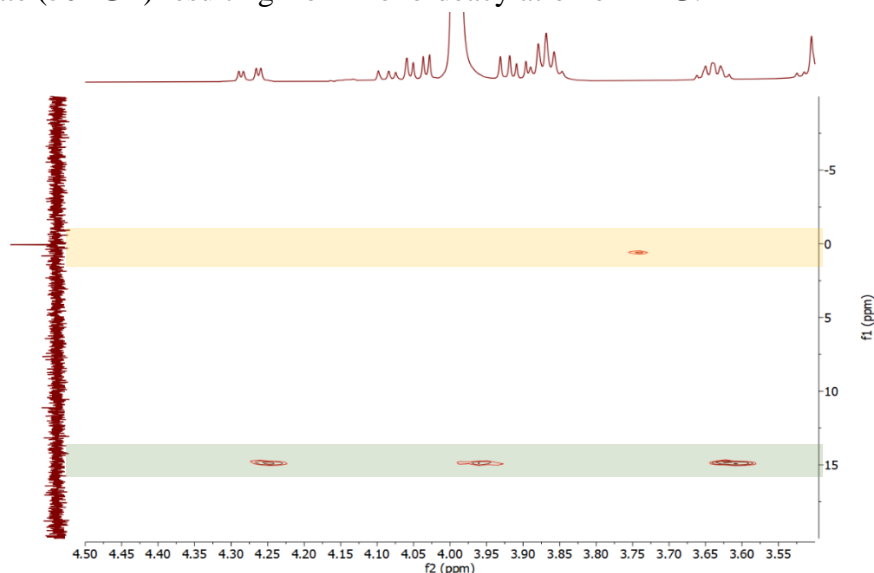


Figure 122. ^1H - ^{31}P HMBC spectrum (500 MHz for ^1H [horizontal axis], 202.5 MHz for $^{31}\text{P}\{^1\text{H}\}$ [vertical axis]) of crude mixture with **BTG 7:1:P_i** (1:1:1) on a 0.5 mmol scale after 120 h of heating neat at $75\text{ }^\circ\text{C}$, then dissolved in $\text{DMSO-}d_6$. Ochre (**BTGP**) and green (**5cTGP**) zones highlight organic products of phosphorylation. Quantities of products are very low, consequently it was impossible to identify these traces by $^{31}\text{P}\{^1\text{H}\}$ NMR spectroscopy.

Phosphorylated products are presented in reaction mixtures as traces, and the signals have intensities similar to noise. The only significant signal in all $^{31}\text{P}\{^1\text{H}\}$ NMR spectra of reactions with **7** was $\delta_{\text{P}} = 0$ ppm (**Pi**). However, we are able to see definitive traces of products in ^1H - ^{31}P HMBC. By cross-correlation, we identified product signals and integrated them (without signal broadening) into $^{31}\text{P}\{^1\text{H}\}$ NMR spectrum in accordance with the procedure described earlier (**Figure 123**, **Table 40**).

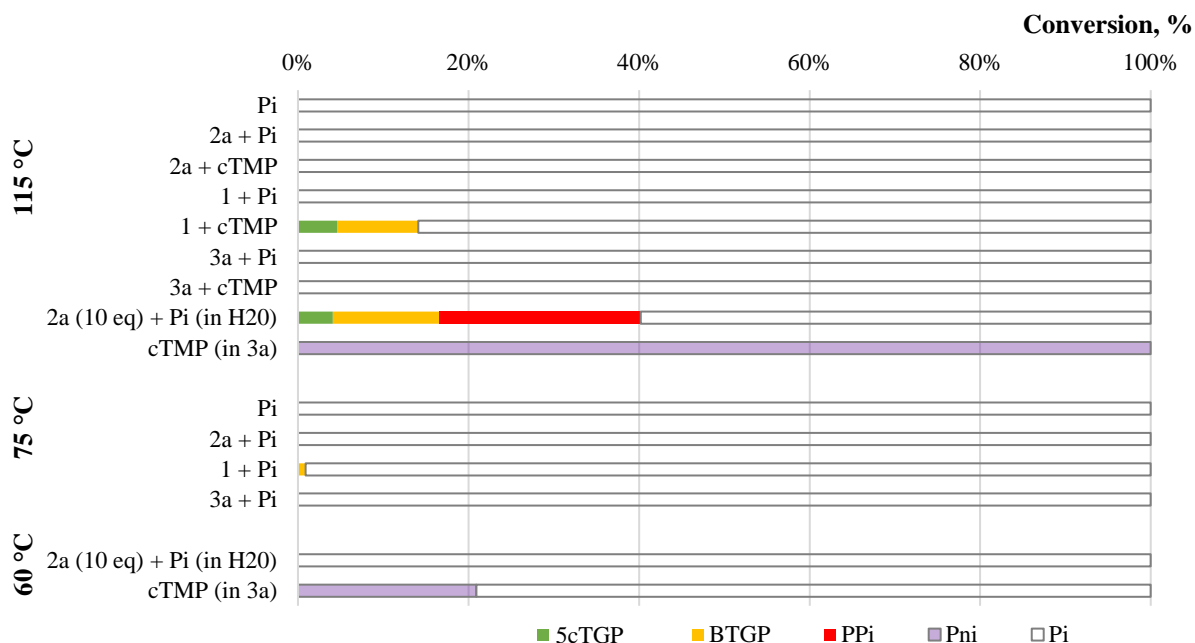


Figure 123. Summary of BTG (**7**) phosphorylations after 120 h of heating at 115°, 75° and 60 °C on a 0.5 mmol scale, without and with 1 ml H₂O (water evaporated eventually) or **3a** (0.5 eq with respect to starting molecule) as liquidisers. Organic products: **5cTGP** (3-tridecanoylglycerol-1,2-cyclic phosphate), **BTGP** (BTG monophosphate). Percent values from signal integration of quantitative $^{31}\text{P}\{^1\text{H}\}$ NMR spectra taken in DMSO-*d*₆ at 40 °C to increase the solubility of the sample. Molar ratios of reaction compounds are **7**:cond. agent:phosphorous source are 1:1:1, except when mentioned otherwise (10 eq excess in several reactions with **2a**).

Table 40. Data to **Figure 123**. Total conversion of initial amount of cTMP and P_i to phosphorylated organic products was calculated by subtracting inorganic compound integrals (P_i, PP_i, Pn_i) from the sum of all integrated ³¹P{¹H} NMR peak areas. Pn_i yield in reactions with cTMP is the signal of residual amount of cTMP. Molar ratios of reaction compounds are 7:cond. agent:phosphorous source are 1:1:1 respectively, except if mentioned otherwise (10 eq excess in several reactions with 2a).

Temp., °C	Cond. agent	Phosphorus source	Liquid -iser	5cBTGP, %	BTGP, %	Total con- version, %	PP _i , %	Pn _i , %	P _i , %
115	-	P _i	-	-	-	-	-	-	100.00
	2a	P _i	-	-	-	-	-	-	100.00
	2a (10 eq)	P _i	H ₂ O	4.09	12.46	16.55	23.6 6	-	59.79
	1	P _i	-	-	-	-	-	-	100.00
	3a	P _i	-	-	-	-	-	-	100.00
	2a	cTMP	-	-	-	-	-	-	100.00
	1	cTMP	-	4.57	9.55	14.12	-	-	85.88
	3a	cTMP	-	-	-	-	-	-	100.00
	-	cTMP	3a	-	-	-	-	100.00	-
75	-	P _i	-	-	-	-	-	-	100.00
	2a	P _i	-	-	-	-	-	-	100.00
	1	P _i	-	-	0.88	0.88	-	-	99.12
	3a	P _i	-	-	-	-	-	-	100.00
60	2a (10 eq)	P _i	H ₂ O	-	-	-	-	-	100.00
	-	cTMP	3a	-	-	-	-	20.91	79.09

3.4. Phosphorylation of 2,3-dioleoylglycerol: DOG (8)

As for the phosphorylation of BTG, we faced the same results in the case of DOG, the phosphorylation yields towards organic phosphates were <10 %, in reactions with different condensing agents **1** or **2a** and P_i (Figure 124).

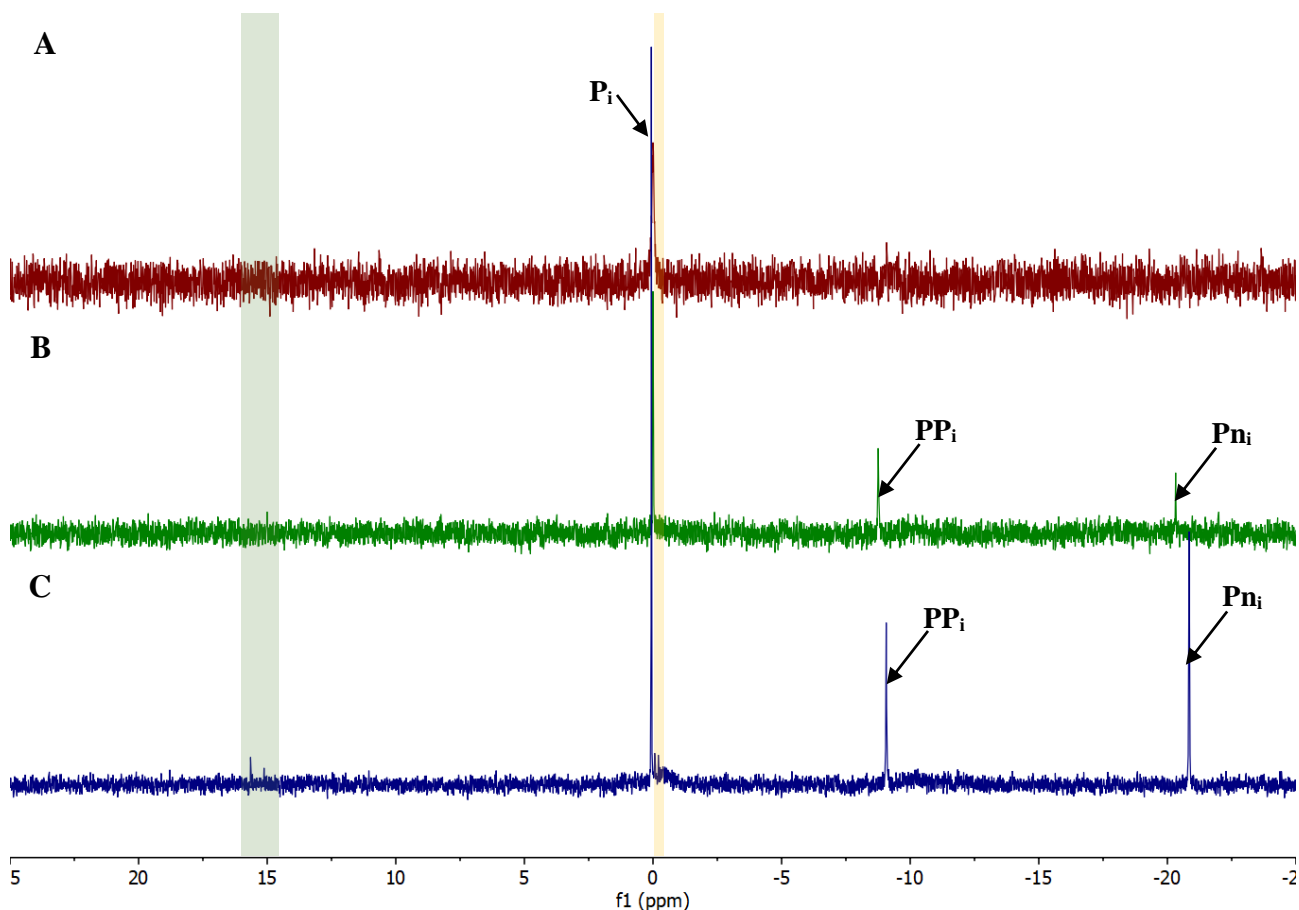


Figure 124. $^{31}P\{^1H\}$ NMR spectra (202.5 MHz) of reaction mixture with DOG **8:2a:P_i** (1:[1/5/10]:1), on a 0.5 mmol scale after 120 h of heating at 115 °C, then dissolved in DMSO-*d*₆. **A** – 1 eq of **2a**; δ_P (ppm) = 0.00 (*s*, P_i). **B** – 5 eq of **2a**; δ_P (ppm) = 15.01 (*s*, 5-membered ring cyclic MOG phosphate, **5cMOGP**, green zone); 0.00 (*s*, P_i); -8.78 (*s*, PP_i); -20.32 (*s*, P_{ni}). **C** – 10 eq of **2a**; δ_P (ppm) = 15.58, 15.06 (2 x *s*, 5-membered ring cyclic MOG phosphate, **5cMOGP**, green zone); 0.00 (*s*, P_i); -0.13, -0.27 (2 x *s*, acyclic phosphates, **DOGP**, ochre zone), -9.13 (*s*, PP_i); -20.91 (*s*, P_{ni}).

The presence of 5-membered and 6-membered ring cyclic phosphates can be explained in two ways, either as a result of the full deacylation to give glycerol that was phosphorylated to give **5cGIP** and **6cGIP**, or else (preferred option), the deacylation of the central oleoyl moiety to give after phosphorylation the 3-mono-oleoylglycerol-1,2-cyclic phosphate (**5cMOGP**) and, respectively, the deacylation of the terminal oleoyl moiety to give after phosphorylation 2-mono-oleoylglycerol-1,3-cyclic phosphate (**6cMOGP**).

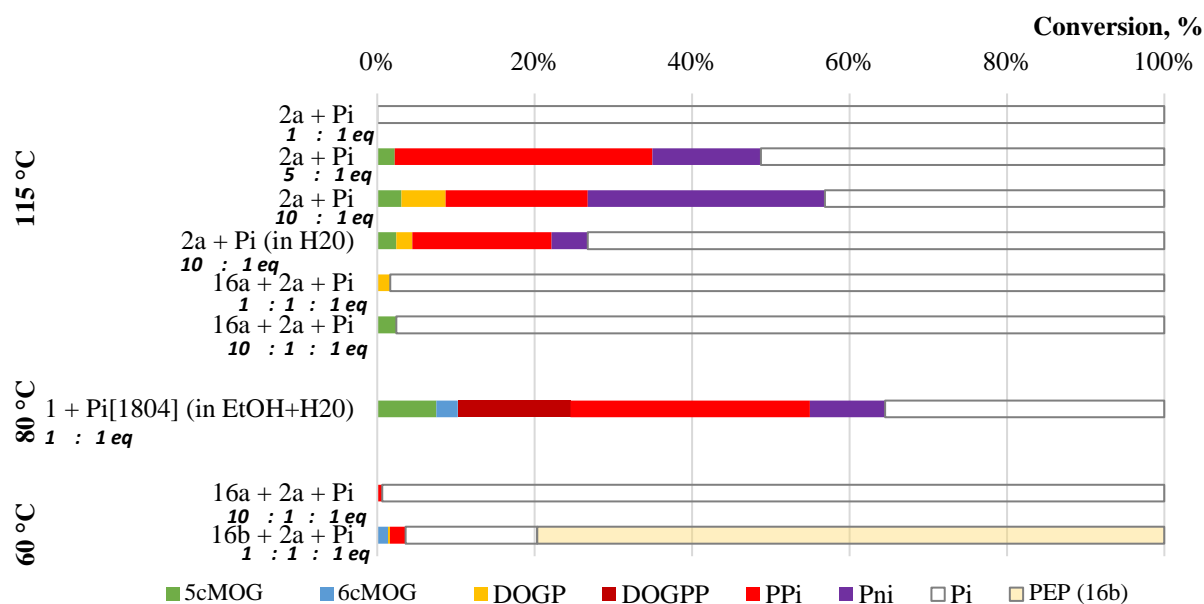


Figure 125. Summary of DOG (**8**) phosphorylation products after 120 h of heating at 115°, 80° and 60 °C on a 0.5 mmol scale, without and with 1 ml H₂O/EtOH (water and ethanol evaporated eventually) as a liquidiser. Added PEP (**16b**) that was transformed in the reaction. Organic products: **5cMOGP** (5-membered ring cyclic MOG phosphates), **6cMOGP** (6-membered ring cyclic MOG phosphates), **DOGP** (DOG monophosphate). Percent values from signal integration of quantitative ³¹P{¹H} NMR spectra taken in DMSO-*d*₆. Molar ratios of reaction compounds are indicated on the figure legend.

As for BTG (**Figure 123**), only a large molar excess of urea (10 equivalents 2a) or 1 equivalent cyanamide (1) allowed for significantly detectable (> 5 %) organic phosphorylation products of DOG (**Figure 125**, **Table 41**). Neither the addition of pyruvate (1 and 10 equivalents 16a) nor of phosphoenolpyruvate (1 equivalent 16b) at 60° or 115 °C would change this result.

Table 41. Data to **Figure 125**. Total conversion of initial amount of P_i to phosphorylated organic products was calculated by subtracting inorganic compound integrals (P_i, PP_i, Pn_i) from the sum of all integrated ³¹P{¹H} NMR peaks. In the last row, **16b** was used to intensify reaction where 16.7 and 79.7 % were not reacted P_i and **16b**, respectively.

Temp.	Cond. agent	Phosphorus source (1 eq)	Liquidiser or phosphate transfer reagent	5cMOGP, %	6cMOGP, %	DOGPP, %	DOG, %	PPI, %	Pni, %	Pi, %	Total conversion, %
115	2a (1eq)	P _i	-	-	-	-	-	-	-	100.00	-
115	2a (5 eq)	P _i	-	2.20	-	-	-	32.75	13.80	51.25	2.20
115	2a (10 eq)	P _i	-	3.09	-	5.60	-	18.07	30.11	43.13	8.69
115	2a (10 eq)	P _i	H ₂ O	2.41	-	2.03	-	17.70	4.62	73.24	4.44
115	2a (1 eq)	P _i	16a (1 eq)	-	-	1.64	-	-	-	98.36	1.64
115	2a (1 eq)	P _i	16a (10 eq)	2.42	-	-	-	-	-	97.58	2.42
80	1 (1 eq)	[¹⁸ O ₄]P _i	H ₂ O+EtOH	7.49	2.76	-	14.29	30.44	9.54	35.48	24.54
60	2a (1 eq)	P _i	16a (10 eq)	-	-	-	-	0.65	-	99.35	-
60	2a (1 eq)	P _i +16b	-	-	1.35	0.25	-	1.99	-	16.72 79.69	1.60

Conclusions to the Section 3

The “negative” control experiments (a starting alcohol was heated with phosphate) demonstrated that only glycerol and only at 115 °C was successfully phosphorylated into acyclic products (35.8 %) in the absence of condensing agent. Its presence increased the total yield of organic phosphorylated products up to 60.5-96.6 %. Cooling down to 75 °C dramatically decreased the yield, and only reactions in the presence of urea (**2a**) and cyanamide (**1**) were sufficient (65.2 and 70.0 %, respectively). A possible explanation is that high temperatures favour thermal degradation of carboxamides that in turn favours phosphorylation. In reactions with MPG, the presence of a condensing agent is mandatory, and as for glycerol, the most efficient were urea and cyanamide at both 75 and 115 °C (51.5-79.4 %). Excess of condensing agent leads to the formation of higher number of cyclic phosphorylated compounds and in general increase yields of organic products.

Out of tested oorthophosphates, I found that the protonation degree of sodium phosphate has an influence on the phosphorylation reaction. Glycerol can be phosphorylated directly by NaH_2PO_4 with yields 35.8 %; however, Na_2HPO_4 and Na_3PO_4 did not produce any organophosphates. One of the possible explanations is that the more acidic a phosphate is, the more readily it can donate a phosphate group to another molecule. In the urea-assisted phosphorylation reactions, according to the dissociative phosphate activation mechanism, protons are needed to help eliminate ammonia from urea and carbamoyl phosphate.

cTMP demonstrated an excellent conversion towards organic phosphate 71.6-98.2 % in reactions with glycerol and MPG at both studied temperatures. The presence of a condensing agent did not significantly increase yields (+3-8%), but more cyclic phosphates were detected in reactions with urea and cyanamide. Thus, I can conclude that reaction conditions are favorable for ring-opening of **cTMP** that helps the phosphorylation reaction of prebiotic precursors. However, whether or not **cTMP** was actually present on the early Earth in sufficient quantities to support prebiotic phosphorylation reactions is debated.

Another prebiotically plausible phosphate source is thiophosphates (**SP_i**). In “negative” control experiments two main organic products acyclic glyceryl-1 and 2-phosphates (21.70 %) were registered, along with a very small amount of glyceryl-1 and 2-thiophosphates (0.05 %). Urea increased yield up to 28-29 %, which is still low compared to the **P_i** phosphorylation 91-95 %.

The presence of dihydrogen phosphate helps with producing organic phosphates and favours consuming **SP_i**. In the sequence $5:\text{SP}_i > 5:2a:\text{SP}_i > 5:2a:\text{SP}_i:\text{P}_i$ yields are increasing 21.75 > 28.01 > 36.38 following adding condensing agent and dihydrogen phosphate. The protons, provided by NaH_2PO_4 (**P_i**), apparently helps for the formation of H_2S as a good leaving group and intensifies the reaction. In a similar experiment, tribasic phosphate did not increase the yield. Lower temperatures do not help phosphorylation and the yields do not exceed 29 %. Analysis of MPG (**6**) phosphorylation was challenging due to the low solubility of the crude mixture in water and $\text{DMSO-}d_6$. The spectra and results suggest relatively high amounts of acyclic and cyclic products 61.5 and 93.9 % in dry and wet-to-dryness experiments,

respectively. These results should be compared carefully to the glycerol phosphorylation data, given the different solvent.

In the competition between labelled [^{18}O] P_i ; and unlabelled SP_i) the ratio of unlabelled:labelled (to partly labelled) glyceryl phosphates was approximately 60:40. This demonstrated that SP_i is more efficient in phosphorylation reaction compared to P_i . Protonated SP_i because of the H_2S leaving group phosphorylate up to 69% of detected products. The results of the experiment with MPG confirm that SP_i outperforms the competition with P_i by about 67-74 % and some products such as **5cMPGP**, **5cGIP**, **GIPGI**, and glyceryl carbamate were found only in unlabelled form. Therefore, the presence of protons favours phosphorylation by thiophosphate and contributes up to 60–70 % to the total conversion of organic phosphates.

Out of tested natural minerals as a phosphorus source the least efficient for phosphorylation was vivianite, with the maximum yield of acyclic glyceryl phosphate in reaction **5:2a** 38 %. Both struvite and canaphite demonstrated equivalent phosphoester production in the presence and absence of condensing agent. A possible explanation for struvite is that an ammonium cation favours the phosphorylation reaction. In the case of canaphite the presence of pyrophosphate group might help the phosphorylation.

Phosphorylation of bi-substituted glycerol, such as **BTD (7)** and **DOG (8)** appear to be more complicated than expected. Reactions with **BTG** were carried at 115 and 75 °C with only traces of phosphorylated products. However, I was able to see definitive traces of products in ^1H - ^{31}P HMBC. The presence of mono-deacylated derivatives of **BTG** was detected in some of the reactions, resulted in 3-tridecanoylglycerol-1,2-cyclic phosphate (**5cTGP**). In the case of **DOG**, the phosphorylation yields towards organic phosphates were <10 %, in reactions with different condensing agents **1** or **2a** and P_i . Along with 5-membered ring cyclic phosphate, we detected presence of a 6-membered ring one as well, most likely belonging to glyceryl phosphates or deacylated **DOG** derivatives. A large molar excess of urea (10 equivalents **2a**) allowed the detectable (> 5 %) organic phosphorylation products of **DOG** and **BTG**. Neither the addition of pyruvate (1 and 10 equivalents **16a**) nor of phosphoenolpyruvate (1 equivalent **16b**) at 60° or 115 °C would change this result.

III Results and discussion

4. Phosphorylation other prebiotic alcohols

4.1. Phosphorylation of dodecan-1-ol

Another type of mono-alcohol that we studied is decanol-1 in reactions with **2a** and P_i (Figure 126, Figure 127) and in a system **2a:16:P_i** (Figure 128). It was not easy to phosphorylate by 1:1:1 ratio of the starting alcohol: cond. agent: P_i , as was done in previous experiments on glycerol or nucleosides. In Figure 126, we demonstrated the spectra obtained in a reaction mixture with 10 eq of **2a** and, even this way, we produced only inorganic phosphates.

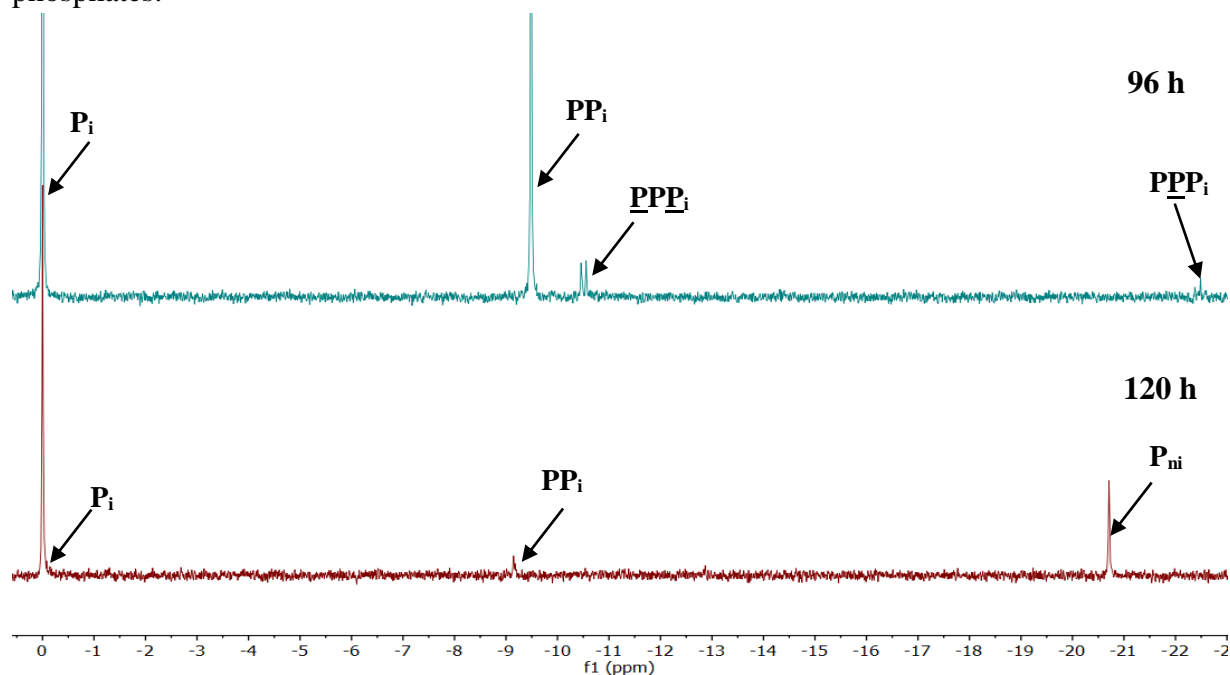


Figure 126. $^{31}P\{^1H\}$ NMR spectra (202.5 MHz, in $DMSO-d_6$) of reaction mixture **9a:2a:P_i** (1:10:1), 0.5 mmol scale at 115 °C in 1ml H_2O . Blue – after 96 h of heating; δ_P (ppm) = 0.00 (*s*, P_i), -9.49 (*s*, PP_i), -10.51 (*d*, $J = 19.7$ Hz PPP_i), -22.48 (*t*, $J = 19.7$ Hz PPP_i). Red – after 120 h of heating; δ_P (ppm) = 0.00 (*s*, P_i), -9.15 (*s*, PP_i), -20.71 (*s*, P_{ni}).

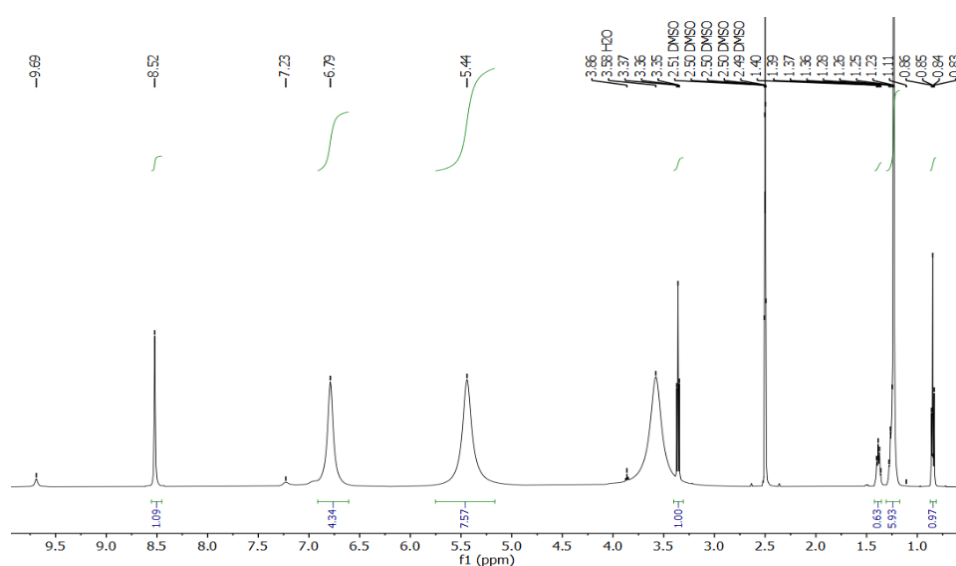


Figure 127. 1H NMR spectrum (500 MHz, $DMSO-d_6$) of crude mixtures of reaction **9a:2a:P_i** (1:10:1) 0.5 mmol scale in 1ml H_2O reaction after 120 h of heating at 115 °C. δ_H (ppm) = 8.52 (*s*, 1H), 6.79 (*s*, 4H), 5.44 (*s*, 7H), 3.36 (*t*, $J = 6.6$ Hz, 1H), 1.39 (*p*, $J = 6.9$ Hz, 1H), 1.23 (*s*, 6H), 0.88 – 0.81 (*m*, 1H).

For the experiments with a large molar excess of urea (**2a**), we performed ^1H - ^{31}P HMBC analyses that did not show any cross-correlation (not shown). We conclude that all signals in the $^{31}\text{P}\{^1\text{H}\}$ NMR spectra were inorganic phosphates. After 96 h we observed the presence of ^{31}P doublet and triplet signals, the area integration of which showed a 2:1 ratio, which is a signature for inorganic triphosphate **PPP_i**.

In another series of experiments, we studied the possibility of pyruvic acid (**16a**) involvement in the phosphorylation of dodecanol (**Figure 128**). ^{31}P signals of organic products in **Figure 128** (red) are very weak with a low signal/noise ratio. Nevertheless, we can tentatively observe phosphorylation of pyruvic acid (**5cPEP** and **PEP**), as well as 1-dodecyl phosphate **9b** (

Table 45, Figure 132).

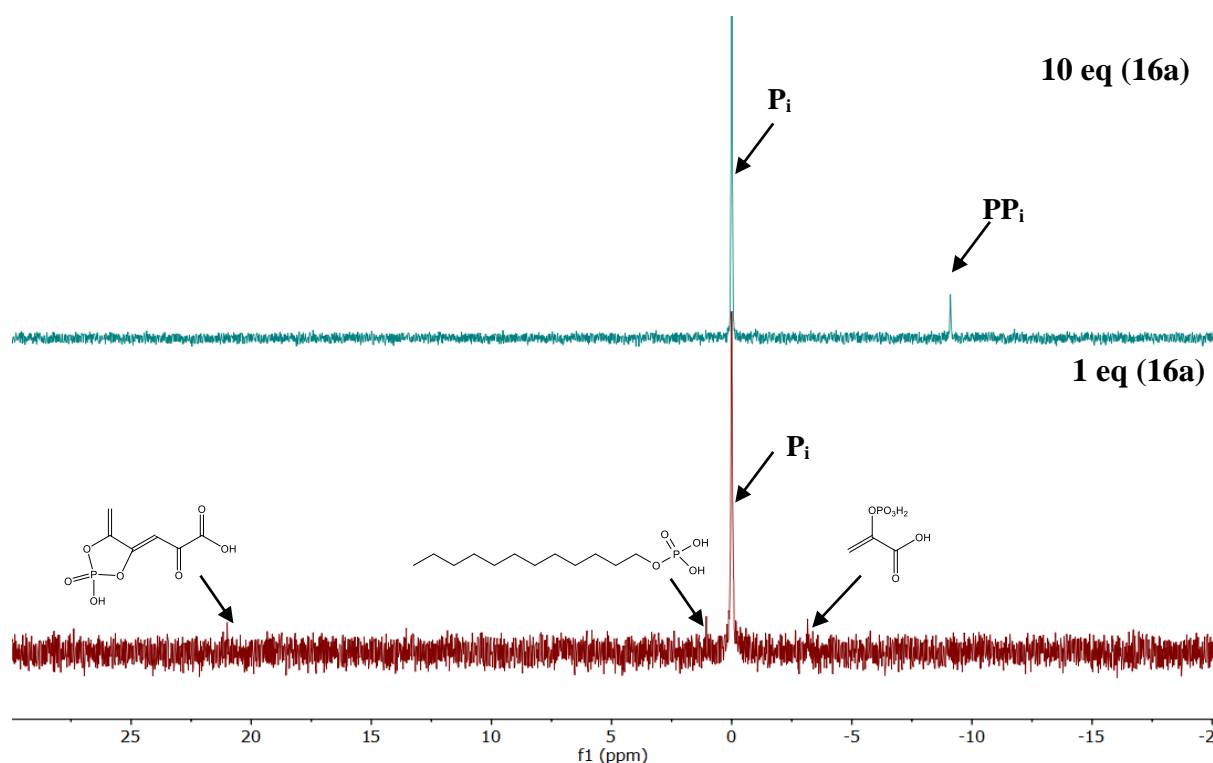


Figure 128. $^{31}\text{P}\{^1\text{H}\}$ NMR spectra (202 MHz, in $\text{DMSO-}d_6$) 0.5 mmol scale after 72 h of heating at 115 $^\circ\text{C}$ of reaction mixture: red **9:2a:16a:Pi** (1:1:1:1) δ_{P} (ppm) = 21.00 (s, 5-membered ring pyruvic phosphate **5cPEP**), 0.00 (s, **Pi**), -9.10 (s, **PPi**), 1.06 (s, dodecanoyl phosphate **DP**), -3.16 (s, phosphoenol pyruvate, **5cPEP**); blue **9:2a:16a:Pi** (1:1:10:1) δ_{P} (ppm) = 0.00 (s, **Pi**), -9.10 (s, **PPi**).

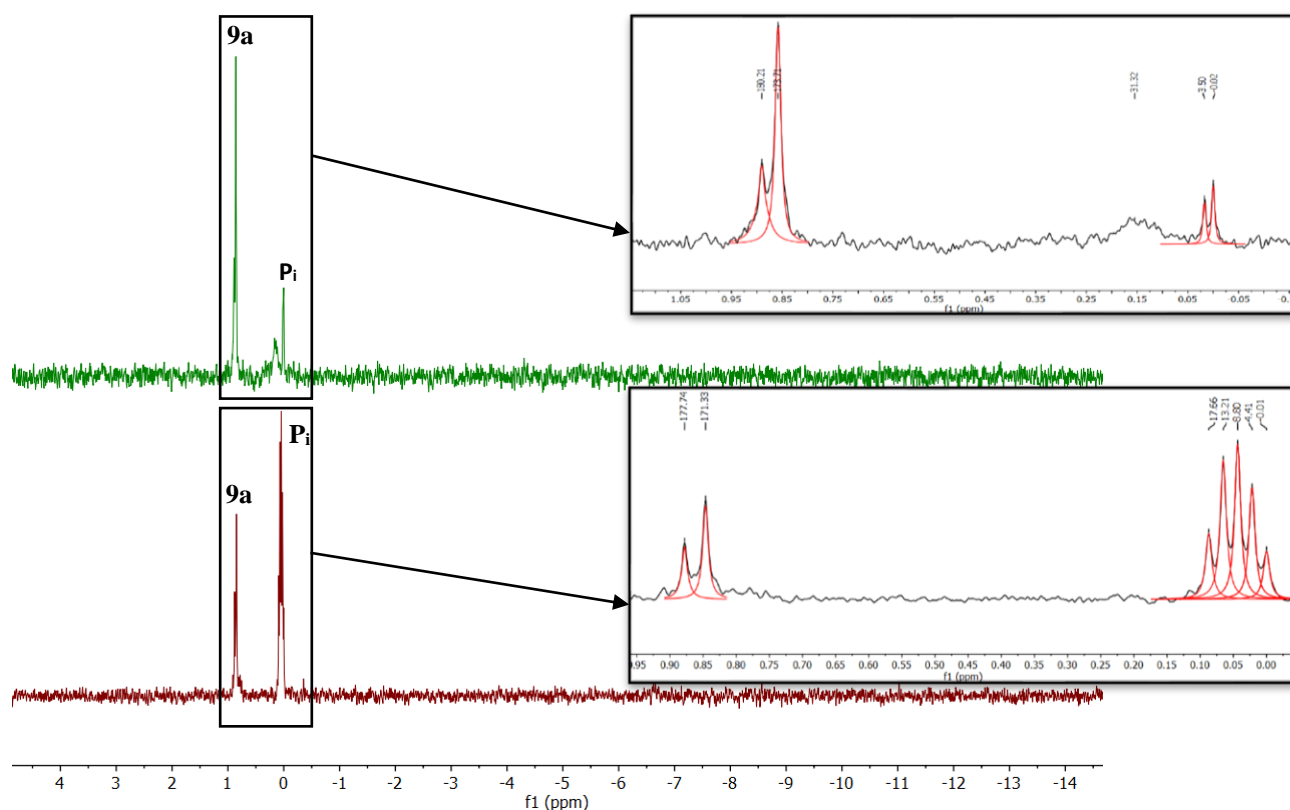


Figure 129. $^{31}\text{P}\{^1\text{H}\}$ NMR spectra (202.5 MHz, $\text{DMSO-}d_6$) 0.5 mmol scale after 72 h of heating at 115 °C of reaction mixture **9:1**: $[^{18}\text{O}_4]\text{P}_i$ (1:1:1). Upper (green) ‘dry’ without additional water: δ_{P} (ppm) = 0.88 and 0.85 (2 x *s*, $\Delta\nu = 6.5$ Hz two main ^{18}O isotopologs of **9a**); 0.17 (broad), 0.02 and 0.00 (2 x *s*, $\Delta\nu (^{18}\text{O}_1\text{--}^{16}\text{O}_1) = 3.5$ Hz, two main ^{18}O isotopologs of **P_i**). Lower (red) ‘to dryness’ reaction was started in 1 ml of H_2O that eventually evaporated: δ_{P} (ppm) = 0.88 and 0.85 (2 x *s*, $\Delta\nu (^{18}\text{O}_1\text{--}^{16}\text{O}_1) = 6.4$ Hz, two main ^{18}O isotopologs of **9a**); 0.09, 0.07, 0.04, 0.02 and 0 (5 x *s*, $\Delta\nu (^{18}\text{O}_1\text{--}^{16}\text{O}_1) = 4.4$ Hz, all five ^{18}O isotopologs of **P_i**). Peak frequencies in the inserts are given in Hertz.

In the reaction of dodecan-1-ol with cyanamide and labelled $[^{18}\text{O}_4]\text{P}_i$ giving 1-dodecyl phosphate (**9b**) we can observe through the isotopic shift effect the exchange of O atoms from unlabelled added water with the O atoms in inorganic phosphate but not 1-dodecyl phosphate.²⁸⁹ Following HRMS analysis of the starting phosphate salt $[^{18}\text{O}_4]\text{P}_i$ two most abundant isotopologs should be $\text{NaH}_2\text{P}[^{18}\text{O}_4]$ and $\text{NaH}_2\text{P}[^{16}\text{O},^{18}\text{O}_3]$. We can assume that two $^{31}\text{P}\{^1\text{H}\}$ singlets of **9b** are from $\text{C}_{12}\text{H}_{27}\text{OP}[^{18}\text{O}_3]$ ($\delta_{\text{P}} = 0.88$ ppm) and $\text{C}_{12}\text{H}_{27}\text{O}_2\text{P}[^{16}\text{O},^{18}\text{O}_2]$ ($\delta_{\text{P}} = 0.85$ ppm). In presence of natural isotope-abundances H_2O over 72 h of the reaction, we observe five $^{31}\text{P}\{^1\text{H}\}$ singlets of inorganic phosphate in an approximately statistical intensity distribution (row 2 in **Table 42**) that correspond to $\text{NaH}_2\text{P}[^{18}\text{O}_4]$ ($\delta_{\text{P}} = 0.09$ ppm), $\text{NaH}_2\text{P}[^{16}\text{O},^{18}\text{O}_3]$ ($\delta_{\text{P}} = 0.07$ ppm), $\text{NaH}_2\text{P}[^{16}\text{O}_2, ^{18}\text{O}_2]$ ($\delta_{\text{P}} = 0.04$ ppm), $\text{NaH}_2\text{P}[^{16}\text{O}_3, ^{18}\text{O}]$ ($\delta_{\text{P}} = 0.02$ ppm) and $\text{NaH}_2\text{P}[^{16}\text{O}_4]$ ($\delta_{\text{P}} = 0.00$ ppm). In the absence of added water, only two **P_i** isotopologs were detected (row 1 in **Table 42**). A similar effect was observed in **Figure 114B** in the reaction **6:2a:SP_i:P_i** (1:1:0.5:0.5).

Table 42. Isotopolog ratio of main signals obtained from $^{31}\text{P}\{^1\text{H}\}$ NMR spectra (**Figure 129**). Complex signals of singlets were deconvoluted and integrated separately after extraction with MNova software (zooms of **Figure 129**).

Liqui-diser	Isotopolog ratio				
	$\text{NaH}_2\text{P}[^{18}\text{O}_4]$, %	$\text{NaH}_2\text{P}[^{16}\text{O},^{18}\text{O}_3]$, %	$\text{NaH}_2\text{P}[^{16}\text{O}_2,^{18}\text{O}_2]$, %	$\text{NaH}_2\text{P}[^{16}\text{O}_3,^{18}\text{O}]$, %	$\text{NaH}_2\text{P}[^{16}\text{O}_4]$, %
-	41.7	58.3	-	-	-
H₂O	9.4	21.2	28.8	27.4	13.2

Liqui-diser	Isotopolog ratio				
	$\text{C}_{12}\text{H}_{27}^{16}\text{OP}[^{18}\text{O}_3]$, %	$\text{C}_{12}\text{H}_{27}^{16}\text{OP}[^{16}\text{O},^{18}\text{O}_2]$, %	-	-	-
-	62.6	37.4	-	-	-
H₂O	62.6	37.4	-	-	-

The presence of water seems to be essential for the dodecanol phosphorylation in the prebiotic conditions suggested in this work. Thus, we performed HRMS of **9a**, **1** and $[^{18}\text{O}_4]\text{P}_i$ (1:1:1) on a 0.5 mmol scale; reaction time 72 h at 115 °C to identify differences in reaction products in wet-to-evaporative (**Figure 130**) and dry (**Figure 131**) conditions. The results are summarised in **Table 43** and **Table 44**, respectively.

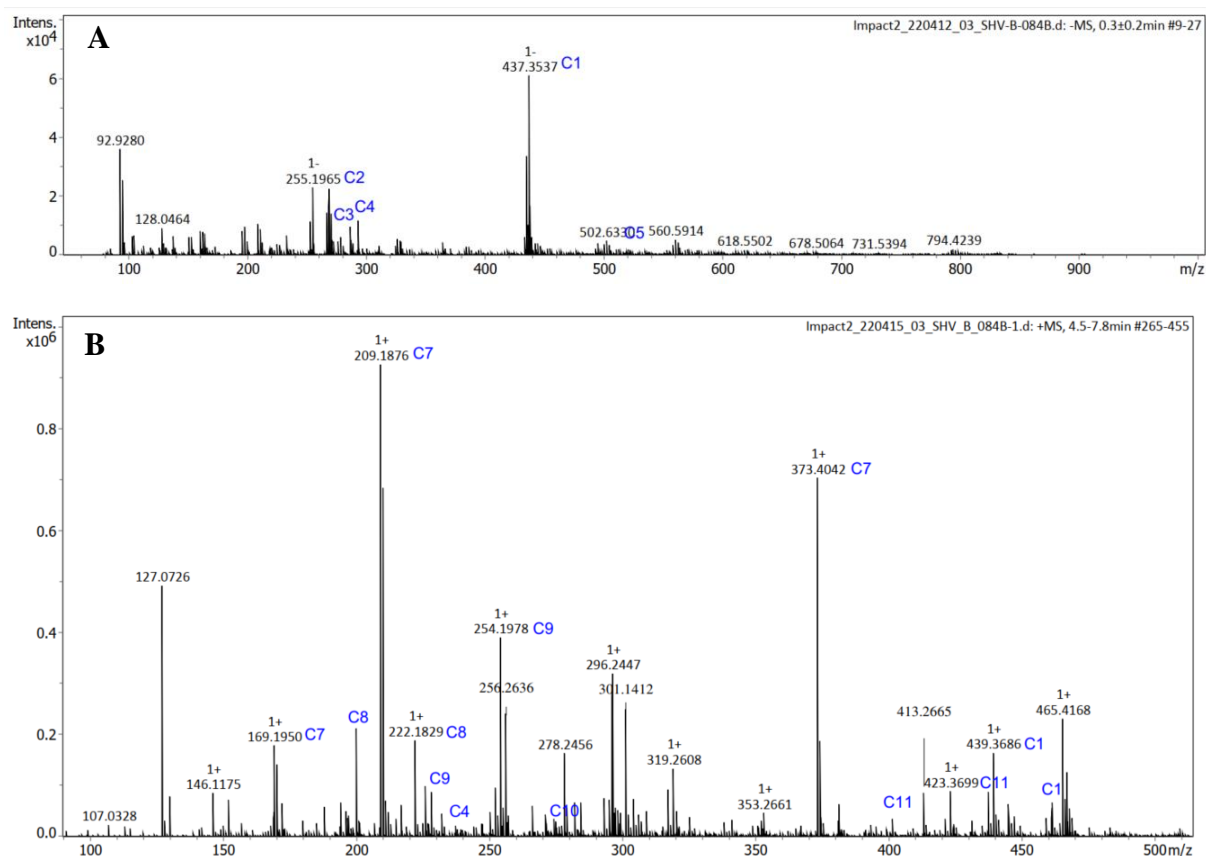
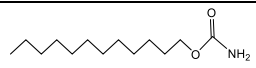
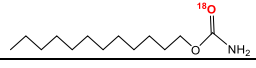
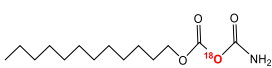
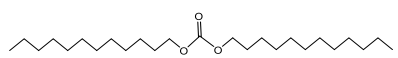
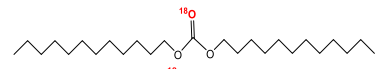
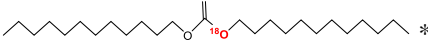


Figure 130. HRMS of the methanolic extract of crude mixture containing **9a**, **1** and $[^{18}\text{O}_4]\text{P}_i$ (1:1:1) on a 0.5 mmol scale ; reaction time 72 h at 115 °C starting in 1 ml H_2O . **A** – negative ion mode; **B** – positive ion mode. Numbers of compounds are the same as in **Table 43-Table 44** and **Figure 130-Figure 131**.

Table 43-1. Interpretation of HRMS of **Figure 130** with suggested formulas, structures and measured relative isotopolog ratios per compound. * The position of one ^{18}O isotope is uncertain (resulting probably from reversible addition-elimination). Numbers of compounds is the same for **Table 43-Table 44** and **Figure 130-Figure 131**.

Peak number	m/z of the main signal	Suggested chemical formula	Suggested chemical structure	Isotopolog ratio
1	433.3455 [M-H] ⁻	C ₂₄ H ₅₁ O ₄ P		5.8
	435.3497 [M-H] ⁻	C ₂₄ H ₅₁ O ₃ P[¹⁸ O]		31.4
	437.3539 [M-H] ⁻	C ₂₄ H ₅₁ O ₂ P[¹⁸ O ₂]		57.0
	439.3590 [M-H] ⁻	C ₂₄ H ₅₁ OP[¹⁸ O ₃]		5.8
2	253.1923 [M-H] ⁻	C ₁₄ H ₂₆ N ₂ O ₂		33.4
	255.1965 [M-H] ⁻	C ₁₄ H ₂₆ N ₂ O[¹⁸ O]		66.6
3	265.1539 [M-H] ⁻	C ₁₂ H ₂₇ O ₄ P		6.6
	267.1619 [M-H] ⁻	C ₁₂ H ₂₇ O ₃ P[¹⁸ O]		20.6
	269.1660 [M-H] ⁻	C ₁₂ H ₂₇ O ₂ P[¹⁸ O ₂]		40.9
	271.1704 [M-H] ⁻	C ₁₂ H ₂₇ OP[¹⁸ O ₃]		31.8
4	267.1619 [M+Cl] ⁻	C ₁₃ H ₂₆ O ₂ [¹⁸ O]		22.1
	269.1660 [M+Cl] ⁻	C ₁₃ H ₂₆ O[¹⁸ O ₂]		43.8
	271.1704 [M+Cl] ⁻	C ₁₃ H ₂₆ [¹⁸ O ₃]		34.1
5	513.3126 [M-H] ⁻	C ₂₄ H ₅₂ O ₇ P ₂		1.9
	515.3162 [M-H] ⁻	C ₂₄ H ₅₂ O ₆ P ₂ [¹⁸ O]		4.6
	517.3200 [M-H] ⁻	C ₂₄ H ₅₂ O ₅ P ₂ [¹⁸ O ₂]		13.8
	519.3242 [M-H] ⁻	C ₂₄ H ₅₂ O ₄ P ₂ [¹⁸ O ₃]		25.6
	521.3288 [M-H] ⁻	C ₂₄ H ₅₂ O ₃ P ₂ [¹⁸ O ₄]		34.1
	523.3326 [M-H] ⁻	C ₂₄ H ₅₂ O ₂ P ₂ [¹⁸ O ₅]		20.0
6	-	-	-	-
7	209.1876 [M+Na] ⁺	C ₁₂ H ₂₆ O		-

Table 43-2. Interpretation of HRMS of **Figure 130** with suggested formulas, structures and measured relative isotopolog ratios per compound. * The position of one ^{18}O isotope is uncertain (resulting probably from reversible addition-elimination). Numbers of compounds is the same for **Table 43-Table 44** and **Figure 130-Figure 131**.

Peak number	m/z of the main signal	Suggested chemical formula	Suggested chemical structure	Isotopolog ratio
8	222.1829 [M+Na] $^+$	$\text{C}_{12}\text{H}_{25}\text{NO}$	-	-
9	252.1939 [M+Na] $^+$	$\text{C}_{13}\text{H}_{27}\text{NO}_2$		19.7
	254.1977 [M+Na] $^+$	$\text{C}_{13}\text{H}_{27}\text{NO}[^{18}\text{O}]$		80.3
10	276.2049 [M+H] $^+$	$\text{C}_{14}\text{H}_{27}\text{NO}_3[^{18}\text{O}]$		-
11	399.3835 [M+H] $^+$	$\text{C}_{25}\text{H}_{50}\text{O}_3$		27.7
	421.3663 [M+Na] $^+$	$\text{C}_{25}\text{H}_{50}\text{O}_2[^{18}\text{O}]$		68.9
	423.3699 [M+Na] $^+$	$\text{C}_{25}\text{H}_{50}\text{O}[^{18}\text{O}_2]$		3.5

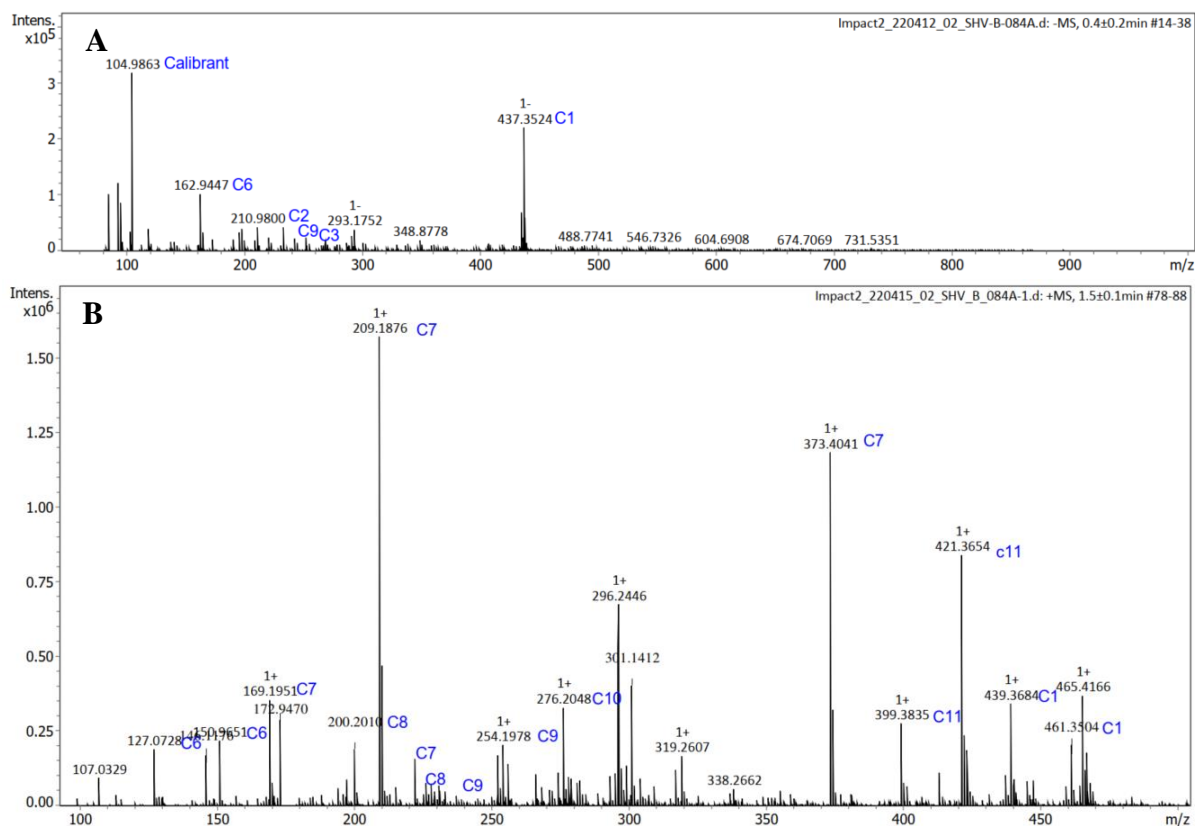


Figure 131. HRMS of the methanolic extract of crude mixture **9a:1:[$^{18}\text{O}_4$]**Pi (1:1:1); 0.5 mmol scale ; reaction time 72 h at 115 °C. **A** – negative ion mode; **B** – positive ion mode. Numbers of compounds is the same for **Table 43-Table 44** and **Figure 130-Figure 131**.

Table 44. Interpretation of HRMS of **Figure 131** with suggested formulas, structures and relative isotopolog ratios per compound. * The position of one ^{18}O isotope is uncertain (resulting probably from reversible addition-elimination). Numbers of compounds is the same for **Table 43-Table 44** and **Figure 130-Figure 131**.

Peak number	m/z of the main signal	Suggested chemical formula	Suggested chemical structure	Isotopolog ratio
1	433.3441 [M-H] ⁻	C ₂₄ H ₅₁ O ₄ P		2.6
	435.3482 [M-H] ⁻	C ₂₄ H ₅₁ O ₃ P[¹⁸ O]		22.1
	437.3524 [M-H] ⁻	C ₂₄ H ₅₁ O ₂ P[¹⁸ O ₂]		70.6
	439.3579 [M-H] ⁻	C ₂₄ H ₅₁ OP[¹⁸ O ₃]		4.7
2	253.1924 [M-H] ⁻	C ₁₄ H ₂₆ N ₂ O ₂		23.6
	255.1958 [M-H] ⁻	C ₁₄ H ₂₆ N ₂ O[¹⁸ O]		76.4
3	269.1649 [M-H] ⁻	C ₁₂ H ₂₇ O ₂ P[¹⁸ O ₂]		41.8
	271.1690 [M-H] ⁻	C ₁₂ H ₂₇ OP[¹⁸ O ₃]		58.2
4	-	-	-	-
5	-	-	-	-
6	148.9608 [M+Na] ⁺	CH ₃ O ₃ P		10.4
	150.9650 [M+Na] ⁺	CH ₃ O ₄ P[¹⁸ O]		89.6
7	209.1876 [M+Na] ⁺	C ₁₂ H ₂₆ O		-
8	222.1829 [M+Na] ⁺	C ₁₂ H ₂₅ NO	-	-
9	252.1938 [M+Na] ⁺	C ₁₃ H ₂₇ NO ₂		45.6
	254.1978 [M+Na] ⁺	C ₁₃ H ₂₇ NO[¹⁸ O]		54.4
10	274.2001 [M+H] ⁺	C ₁₄ H ₂₇ NO ₄		0.2
	276.2049 [M+H] ⁺	C ₁₄ H ₂₇ NO ₃ [¹⁸ O]		99.8
11	399.3835 [M+H] ⁺	C ₂₅ H ₅₀ O ₃		80.6
	401.3881 [M+H] ⁺	C ₂₅ H ₅₀ O ₂ [¹⁸ O]		18.6
	403.3934 [M+H] ⁺	C ₂₅ H ₅₀ O[¹⁸ O ₂]		0.7

The diversity and isotopolog ratio give us ideas about the phosphorylation reactions of dodecanol. We notice that in the presence of water, we have more phosphodiester. In general, phosphorylation of dodecanol appears to be the most efficient reaction with cyanamide rather than urea, or, alternatively, additional water needs to be present.

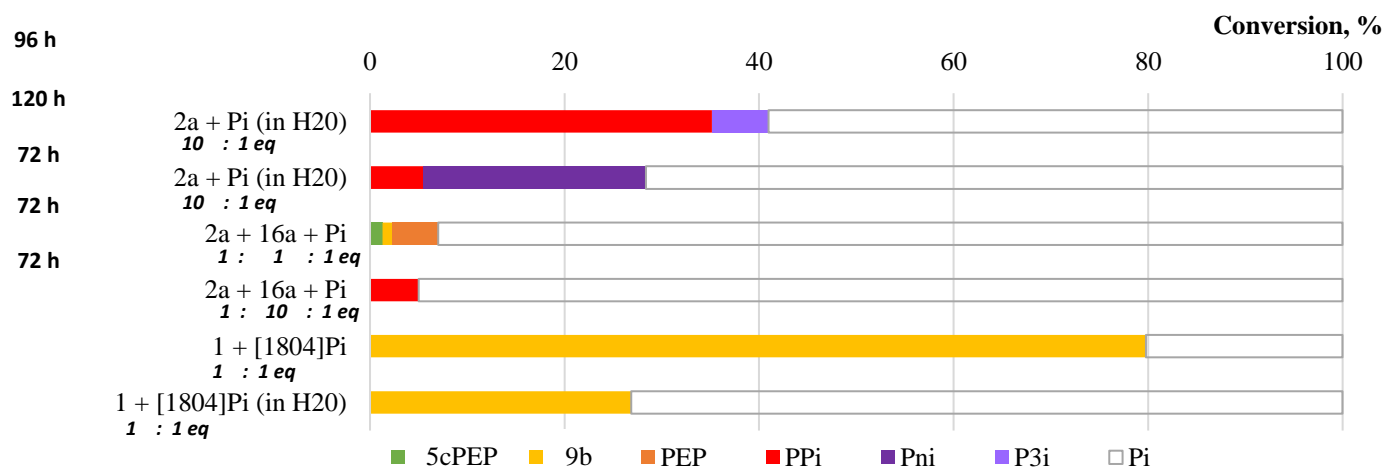


Figure 132. Summary of phosphorylations of dodecanol-1 (**9a**) after 72-120 h of heating at 115 °C on a 0.5 mmol scale. Percent values from signal integration of quantitative $^{31}\text{P}\{^1\text{H}\}$ NMR spectra taken in DMSO- d_6 .

Table 45. Data to **Figure 139**. Total conversion of initial amount of P_i to phosphorylated organic products was calculated by subtracting inorganic compound integrals (P_i , PP_i , Pn_i) from the sum of all integrated $^{31}\text{P}\{^1\text{H}\}$ NMR peak areas.

Cond. agent	Phosph. source (1 eq)	Liqui-diser	Reaction time, h	5cPE P, %	PEP, %	9b, %	P_i , %	PP_i , %	P_{3i} , %	P_{ni} , %	Total conv., %
2a (10 eq)	P_i	H_2O	120	-	-	-	59.01	35.16	5.83	-	-
2a (10 eq)	P_i	H_2O	96	-	-	-	71.64	5.53	-	22.83	-
2a:16a (1:1)	P_i	-	72	1.30	4.71	1.02	92.98	-	-	-	-
2a:16a (1:1)	P_i	-	72	-	-	-	95.01	4.99	-	-	-
1	$^{18}\text{O}_4\text{P}_i$	-	72	-	-	79.78	20.22	-	-	-	79.78
1	$^{18}\text{O}_4\text{P}_i$	H_2O	72	-	-	26.86	73.14	-	-	-	-

4.2. Phosphorylation of geraniol (10)

Here we describe our tentative and not yet completely explored research on geraniol phosphorylation. A few experiments that were performed revealed some new products that we did not figure out completely. It is possible, that the presence of unsaturated bonds affects the chemistry of phosphorylation, making it different from what was studied before. Here on the exemplar spectra we demonstrate the reaction products of geraniol with **2a** (or **1**) and **P_i** (**Figure 133-Figure 137**).

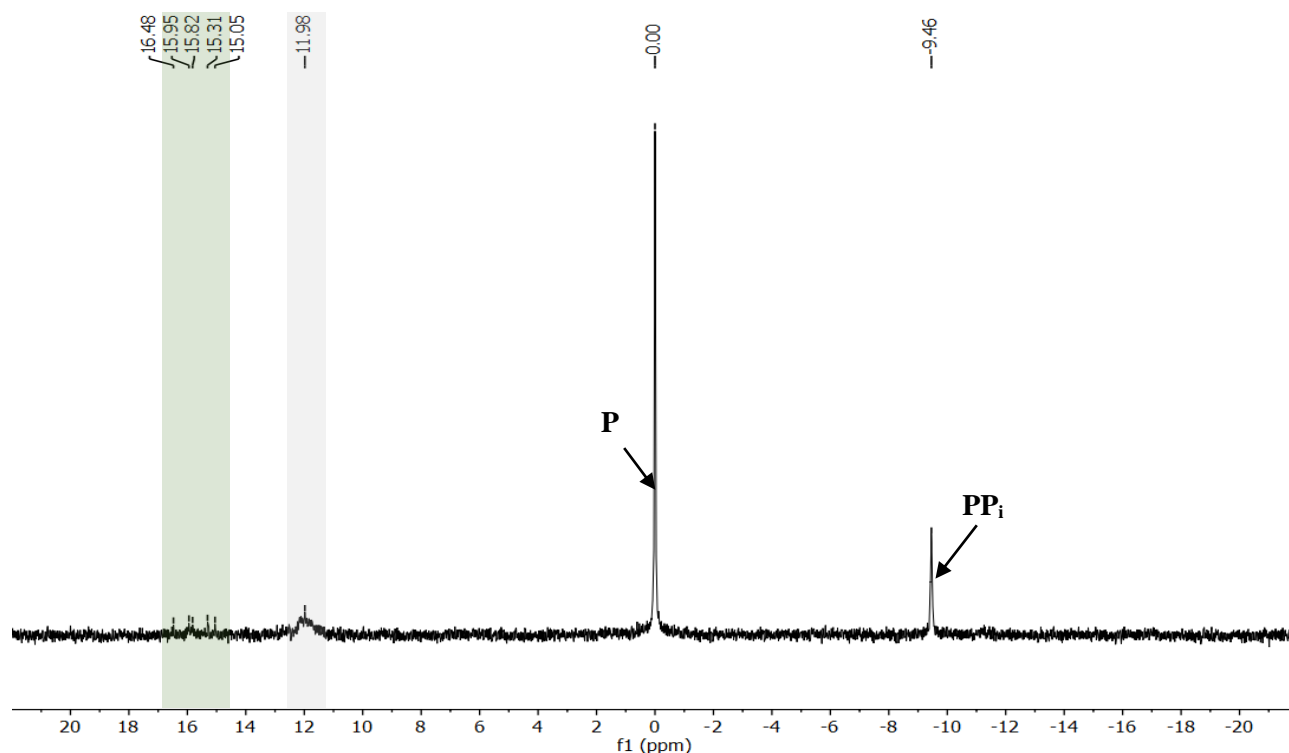


Figure 133. ³¹P{¹H} NMR spectrum (202.5 MHz, in DMSO-*d*₆) of reaction mixture **10:2a:P_i** (1:1:1), 0.5 mmol scale after 120 h of heating at 115 °C: δ_P (ppm) = 16.48-15.05 (*s*, 5-membered ring cyclic phosphates, **5cGeP**, green); 11.98 (broad *s*, **P_x**, gray); 0.00 (*s*, **P_i**); -9.46 (*s*, **PP_i**).

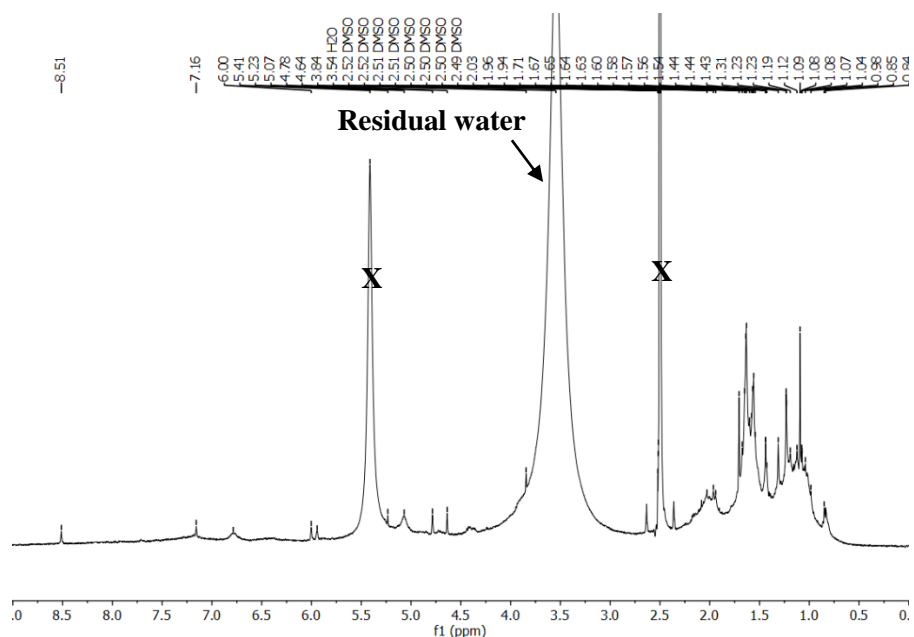


Figure 134. ^1H NMR spectrum (500 MHz, $\text{DMSO-}d_6$) of crude mixtures of reaction **10:2a:P_i** (1:1:1) 0.5 mmol scale reaction after 120 h of heating at 115 °C: δ_{H} (ppm) = 5.41 (br s, 53H), 2.63 (d, $J = 1.8$ Hz, 2H), 2.36 (d, $J = 1.9$ Hz, 2H), 1.71 (s, 1H), 1.66-1.60 (m, 14H), 1.59-1.52 (m, 9H), 1.47 – 1.41 (m, 2H), 1.31 (s, 1H), 1.23 (d, $J = 1.8$ Hz, 2H), 1.09 (s, 2H). **X** – residual water and $\text{DMSO-}d_6$.

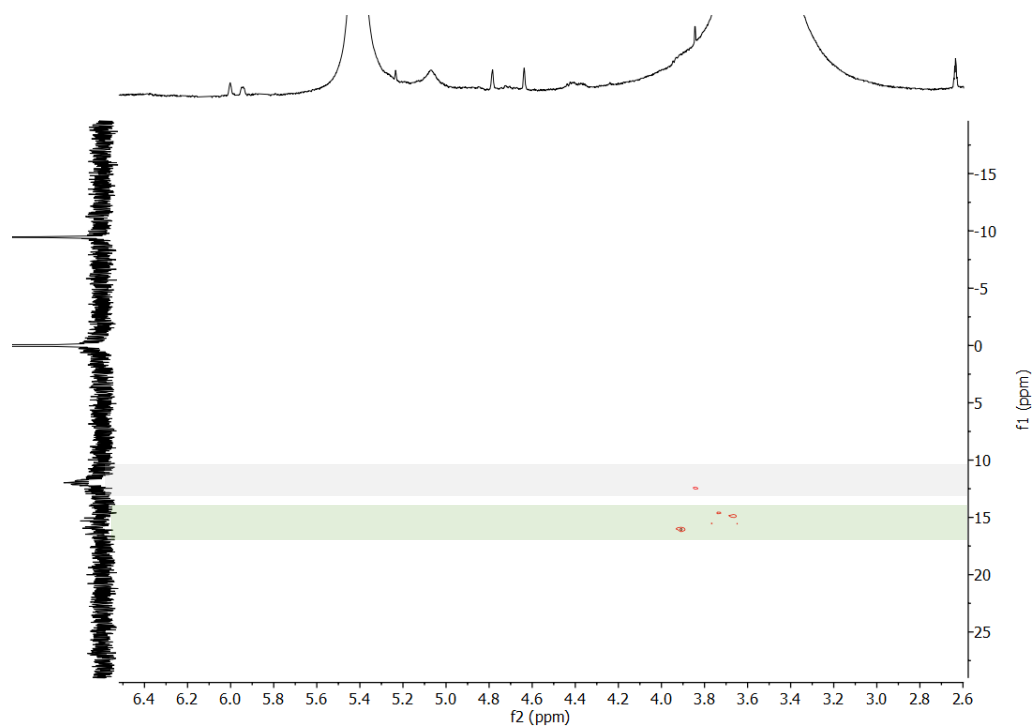


Figure 135. $^1\text{H-}^{31}\text{P}$ HMBC spectrum (500 MHz for ^1H [horizontal axis], 202.5 MHz for $^{31}\text{P}\{^1\text{H}\}$ [vertical axis], in $\text{DMSO-}d_6$) of crude mixtures of reaction **10:2a:P_i** (1:1:1) 0.5 mmol scale, after 120 h of heating at 115 °C. Green (**5cGeP**) and grey (**P_{xi}**) zones highlights organic products of phosphorylation.

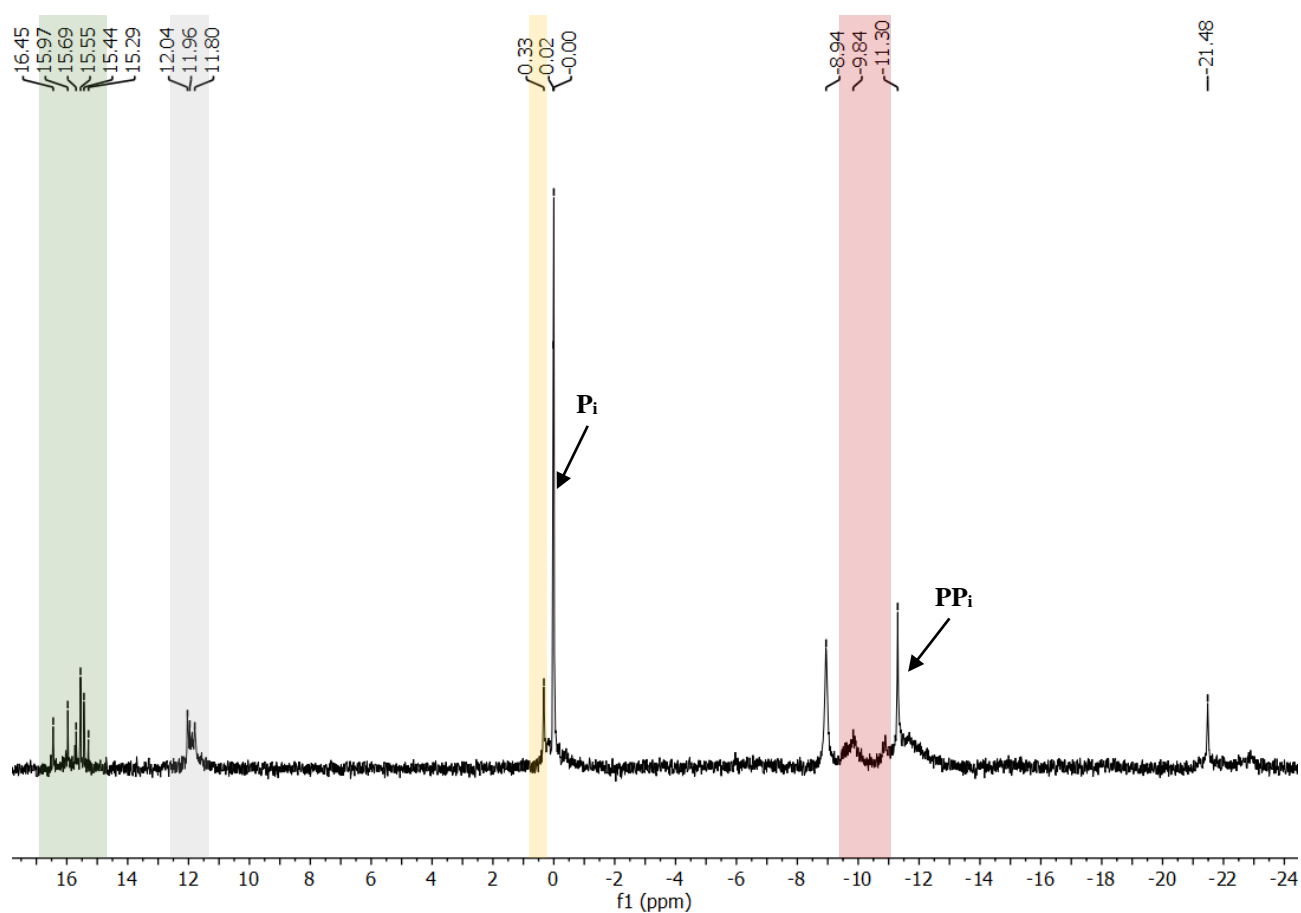


Figure 136. $^{31}\text{P}\{^1\text{H}\}$ NMR spectrum (202.5 MHz, in $\text{DMSO-}d_6$) of reaction mixture **10:1:P_i** (1:1:1), 0.5 mmol scale after 120 h of heating at 115 °C: δ_{P} (ppm) = 16.45-15.29 (*s*, 5-membered ring cyclic phosphate, **5cGeP**, green); 12.04-11.80 (broad *s*, **P_x**, gray); 0.33-0.2 (*s*, acyclic phosphate; **GeP**, ochre); 0.00 (*s*, **P_i**); -8.84 and -11.30 (2 x *s*, **PP_i**); -9.84 (organic diphosphate; **PP_o**, red); -21.48 (*s*, **P_{ni}**).

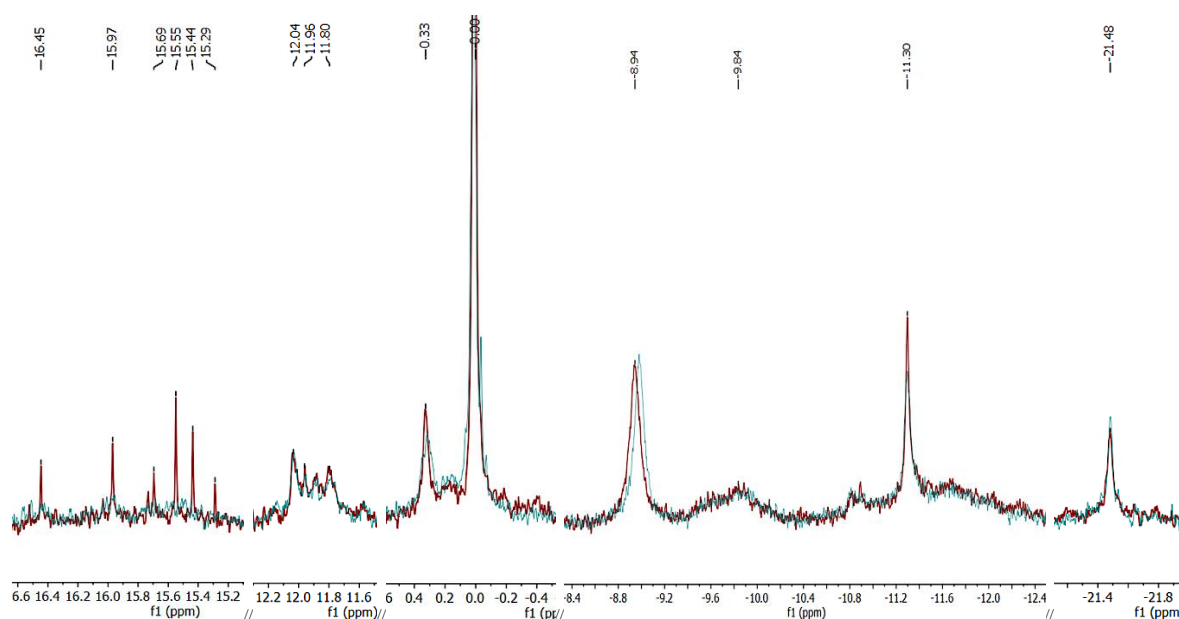


Figure 137. $^{31}\text{P}\{^1\text{H}\}$ NMR (red, **Figure 136**) and ^{31}P NMR spectra (blue) (202.5 MHz, in $\text{DMSO-}d_6$) of organic products **10:1:P₁** (1:1:1), 0.5 mmol scale after 120 h of heating at 115 °C.

Studying data from these figures, we confirm that signals at $\delta_{\text{P}} = 16.45\text{--}15.29$ ppm are organic phosphates, which may result from the phosphorylation of the C=C double-bonds of **10**. The signals at $\delta_{\text{P}} = 12.04\text{--}11.80$ (**P_x**) and at $-9.84\text{--}-10.8$ ppm (**PP_o**) are tentatively associated with cyclic monoterpene compounds that are phosphorylated, which could explain the absence of any clearly visible coupling between ^{31}P and ^1H nuclei.

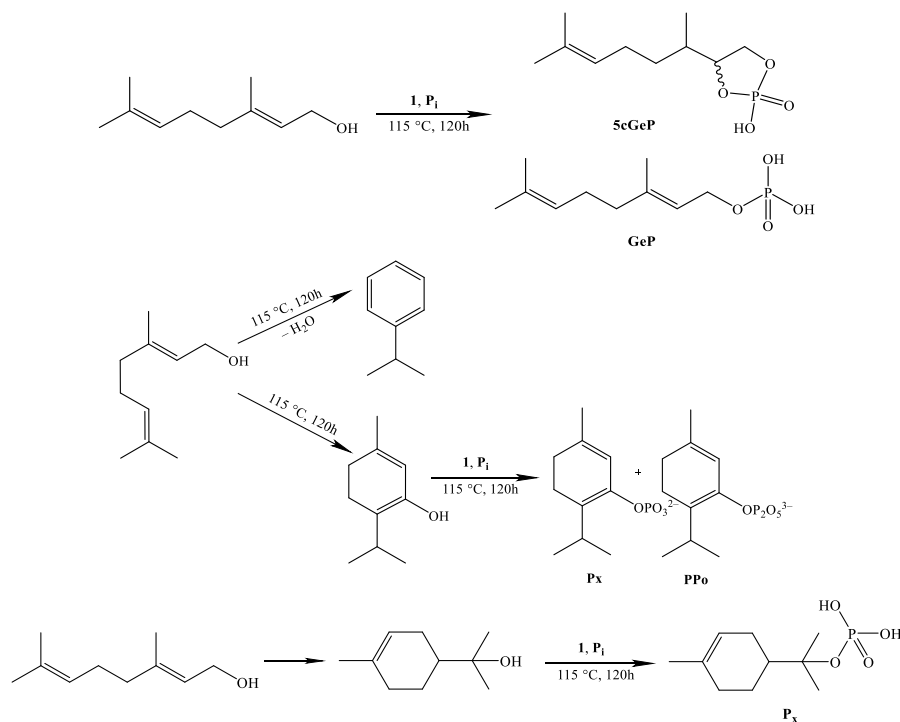


Figure 138. Tentative reaction of geraniol phosphorylation suggested C–C and C–O bonds represented as a wavy line, which shows the possibility of a *trans* and a *cis* isomer of this compound (giving two ^{31}P resonances).

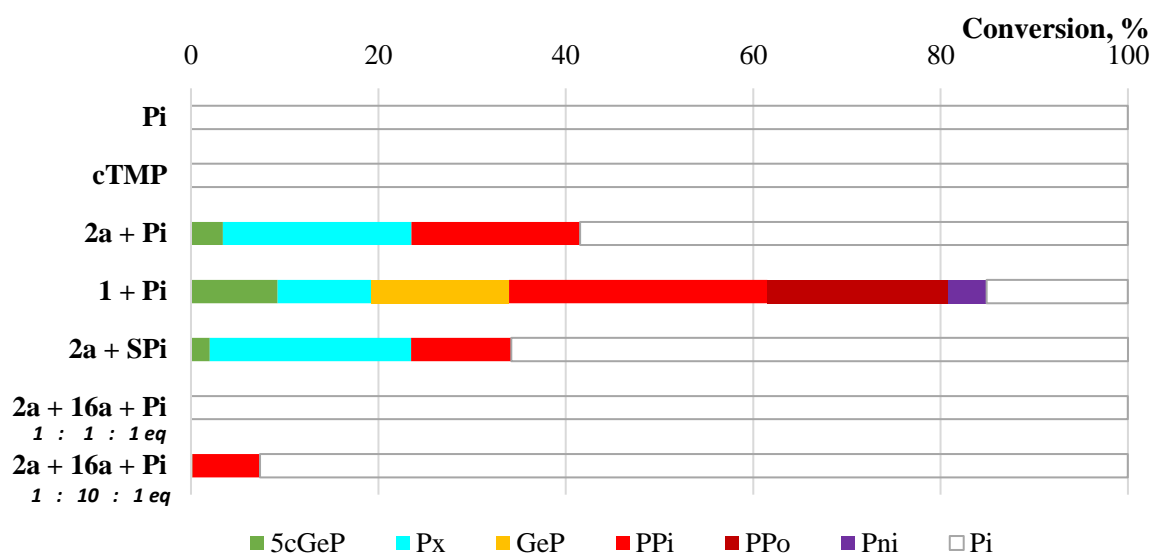


Figure 139. Summary of geraniol (**10**) phosphorylations after 120 h of heating at 115 °C on a 0.5 mmol scale. Percent values from signal integration of quantitative $^{31}\text{P}\{^1\text{H}\}$ NMR spectra taken in DMSO-*d*₆. Molar ratios of reaction compounds are 1 eq with respect to starting molecule **10** if not indicated otherwise.

In summary, heating neat equimolar mixtures of geraniol (**10**), urea (**2a**) and inorganic phosphate or thiophosphate (**P_i** or **SP_i**) for 5 days at 115 °C did not produce any organic phosphates above 5 %. The presence of pyruvic acid (**16a**) as an additive to **10** and **P_i** totally suppressed even the low amount of cyclic phosphates. The only high yields of organic phosphates denoted **5cGeP**, **GeP** and probably **P_x** and **PP_o** from **10** were obtained upon the action of cyanamide (**1**), which produced compounds of suggested but yet unconfirmed structures as shown above.

Table 46. Data to Figure 139. Total conversion of initial amount of **P_i** to phosphorylated organic products was calculated by subtracting inorganic compound integrals (**P_i**, **PP_i**, **P_{ni}**) from the sum of all integrated $^{31}\text{P}\{^1\text{H}\}$ NMR peak areas.

Cond. agent	Phosphorus source	5cGeP	P _x , %	GeP	PP _i , %	PP _o , %	P _{ni} , %	P _i , %
-	P_i	-	-	-	-	-	-	100
-	cTMP	-	-	-	-	-	-	100
2a	P_i	3.39	20.15	-	17.99	-	-	58.47
1	P_i	9.25	9.96	14.74	27.56	19.27	4.14	15.08
2a	SP_i	2.01	21.47	-	10.69	-	-	65.84
2a + 16a	P_i	-	-	-	-	-	-	100
2a + 16a (10 eq)	P_i	0.17	-	-	7.20	-	-	92.63

4.3. Phosphorylation of pyruvic acid (16a)

Another exciting and unexplored field is the phosphorylation reactions of pyruvic acid. Despite our efforts to involve it in reactions, including different temperatures, condensing agents, phosphates and other, we have obtained very few organic phosphorylated products. The dry prebiotic conditions favored polymerisation of pyruvic but not phosphorylation. On **Figure 140** and **Figure 141** you can notice a lack of P-signals and incidence of H-signals, respectively. Signals at $\delta_P = -4.36$ and -5.40 ppm are complicated to identify with certainty. Most likely, the first signal is from **PEP** and the second is another acyclic phosphorylated pyruvate derivative.

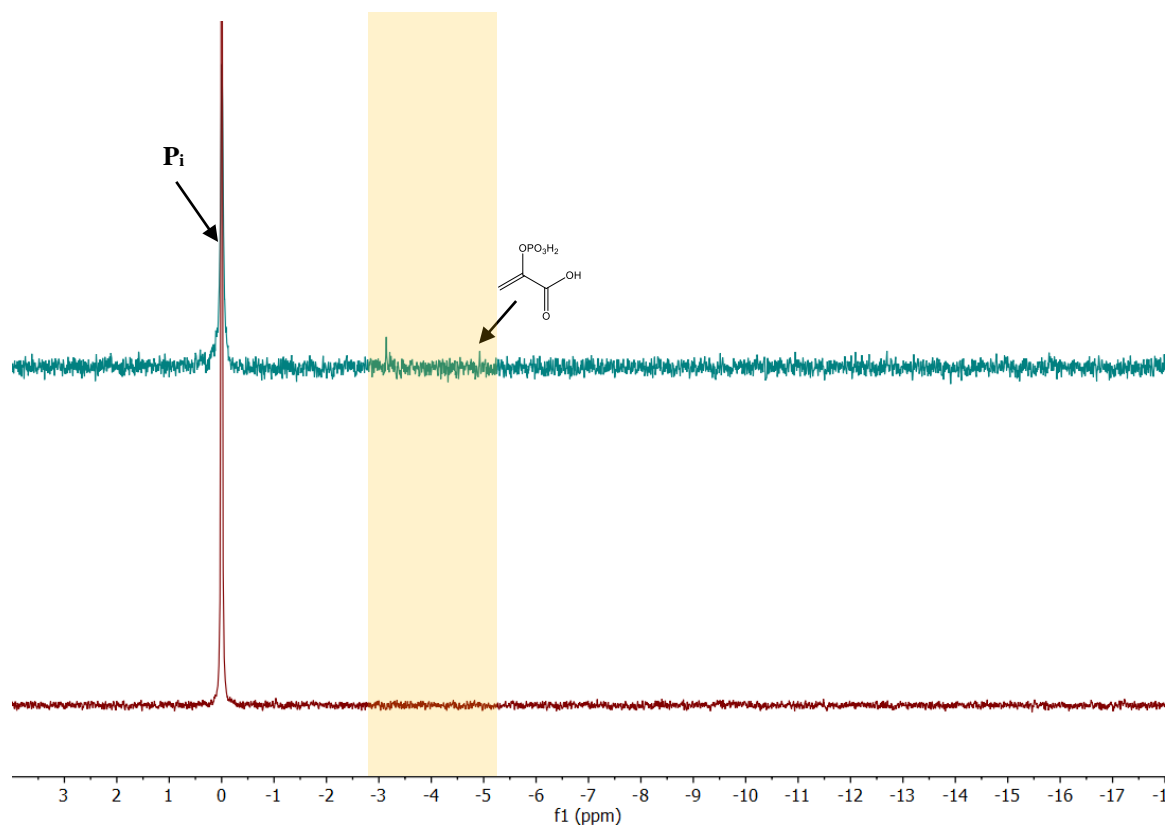


Figure 140. $^{31}\text{P}\{^1\text{H}\}$ NMR spectra (202.5 MHz, in $\text{DMSO-}d_6$) after 72 h of heating at 115 °C of reaction mixture on a 0.5 mmol scale, upper spectrum (blue) **16a:2a:P_i** (1:1:1): δ_P (ppm) = 0.00 (s, **P_i**), -3.13 and -4.92 (2 s, **PEP**, ochre zone), -9.50 (s, **PP_i**); lower spectrum (red) **16a:P_i** (1:1): δ_P (ppm) = 0.00 (s, **P_i**).

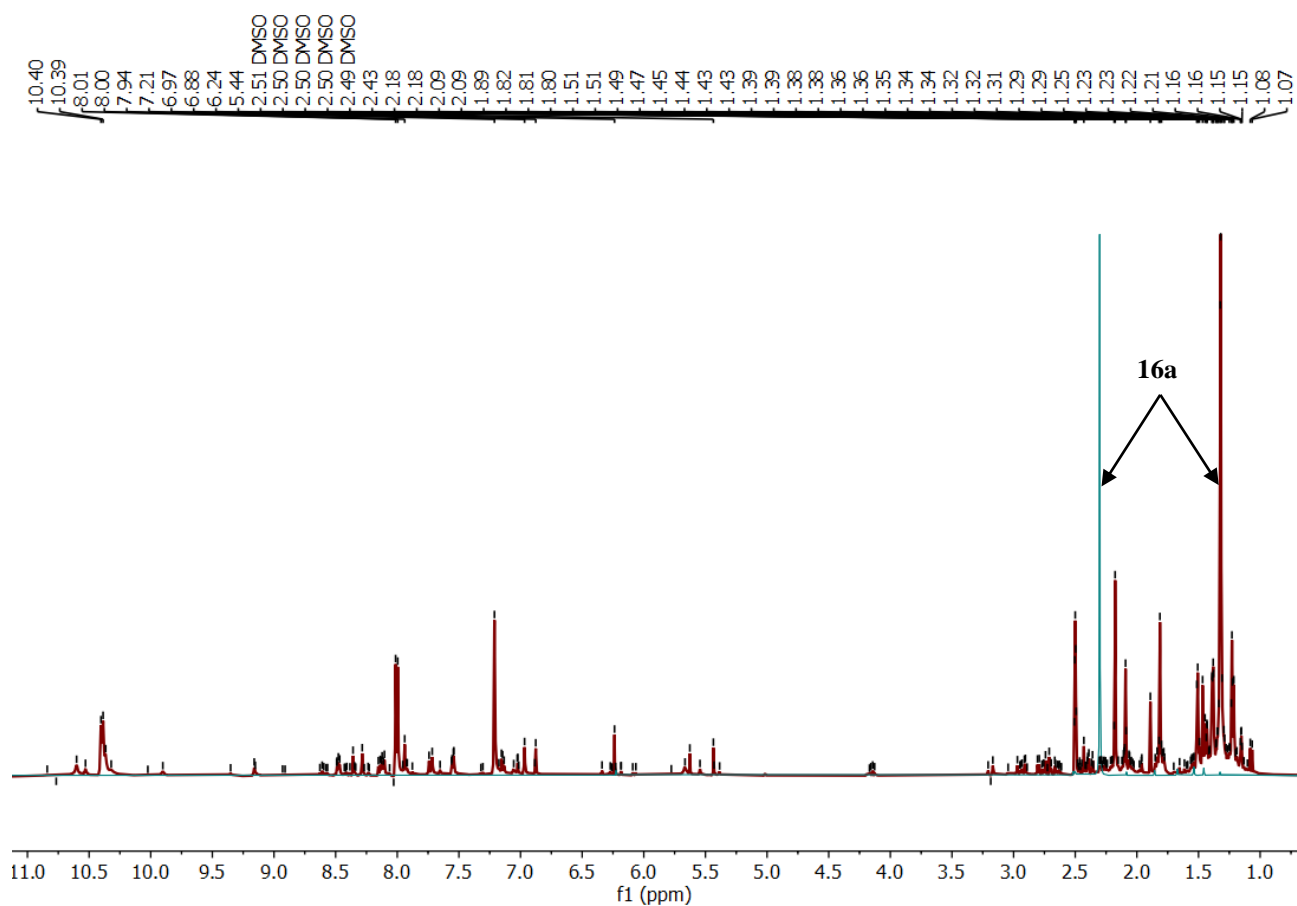
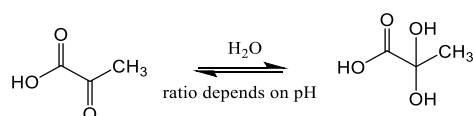


Figure 141. ^1H NMR spectra (500 MHz, $\text{DMSO-}d_6$): blue – 0.5 mM of **16a**: δ_{H} (ppm) = 2.3 (*s*, 3H); red – crude mixtures of reaction **16a**:**P_i** (1:1) 0.5 mmol scale after 48 h of heating at 75 °C, δ_{H} (ppm) = 10.39 (*t*, J = 9.5 Hz, 1H), 8.48 (*dd*, J = 8.8, 3.5 Hz), 8.16 – 8.09 (*m*), 8.00 (*d*, J = 8.6 Hz, 1H), 7.21 (*s*, 1H), 2.18 (*s*, 1H), 2.09 (*d*, J = 2.1 Hz), 1.89 (*s*), 1.81 (*s*), 1.51 (*d*, J = 3.7 Hz), 1.40 – 1.37 (*m*, 1H), 1.32 (*d*, J = 1.9 Hz, 3H), 1.23 (*d*, J = 2.2 Hz, 1H), 1.21 (*s*), 1.15 (*q*, J = 2.1 Hz).

Pyruvic acid (**16a**), depending on pH, can be present in two forms: as a ketoacid (oxo form) and as its hydrate:²⁹⁰



The ^1H NMR spectrum at δ_{H} = 2.2-2.4 ppm is the methyl group of the oxo form of **16a** and the one at δ_{H} = 1.4-1.6 ppm is the methyl group of pyruvic acid hydrate.²⁹⁰ After 120 h of heating **16a** with **P_i** in the absence of any condensing agent, we can observe the presence of the hydrated form. The occurrence of many smaller signals in the ^1H NMR spectrum and the absence of organic signals in the $^{31}\text{P}\{^1\text{H}\}$ NMR spectrum confirm the predominance of a polymerisation reaction over phosphorylation.

Thus, we can conclude that direct or condensing agent-assisted phosphorylation of pyruvic acid is hardly achievable in the prebiotic conditions suggested in this work (**Figure 142, Table 47**). The presence of **SP_i** and **cTMP** did not accelerate the reaction; therefore, another approach for pyruvic acid phosphorylation should be suggested.

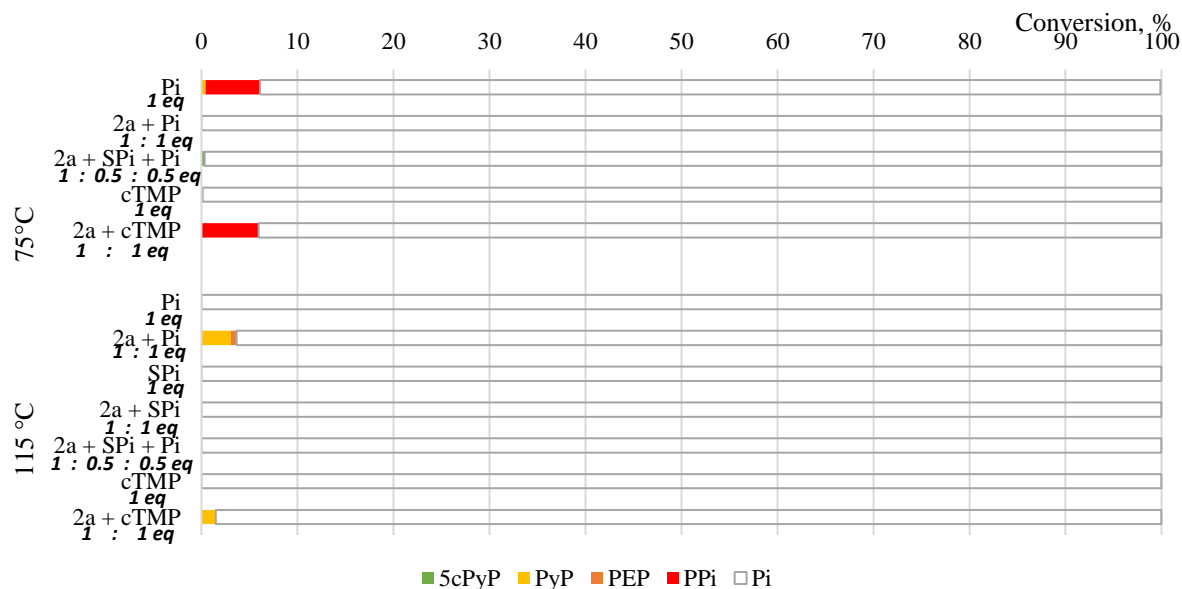


Figure 142. Summary of pyruvic acid (**16a**) phosphorylations after 48-72 h of heating at 75/115 °C, with and without urea (**2a**), on a 0.5 mmol scale. Molar equivalents are indicated in the diagram with respect to starting molecule **16a** (1 eq). Percent values from signal integration of quantitative ³¹P{¹H} NMR spectra taken in DMSO-*d*₆.

Table 47. Data to **Figure 142**. Total conversion of initial amount of **P_i** to phosphorylated organic products was calculated by subtracting inorganic compound integrals (**P_i** and **PP_i**) from the sum of all integrated ³¹P{¹H} NMR peak areas.

Reaction time and temp.	Cond. agent	Phosphate source	5cPyP, %	PyP, %	PEP, %	PPI, %	Pi, %
75 °C 48h	-	P_i	-	0.42	-	5.69	93.79
	2a	P_i	-	-	-	-	100
	2a	P_i:SP_i	0.34	-	-	-	99.66
	-	cTPM	-	-	0.14	-	99.86
	2a	cTPM	-	-	-	5.96	94.04
115 °C 72 h	-	P_i	-	-	-	-	100
	2a	P_i	-	3.06	0.61	-	96.33
	-	SP_i	-	-	-	-	100
	2a	SP_i	-	-	-	-	100
	2a	P_i:SP_i	-	-	-	-	100
115 °C	-	cTPM	-	-	-	-	100
	2a	cTPM	-	1.49	-	-	98.51

When we decided to analyse crude mixtures of pyruvic acid in water, and discovered a diversity of inorganic phosphates. In **Figure 143**, we observe the presence of doublet and triplet signals, which integration ratio is 2:1 respectively. Similar to **Figure 126**, it indicates the presence of inorganic triphosphate **PPP_i**. **Figure 144** is the corresponding to this reaction ¹H spectrum.

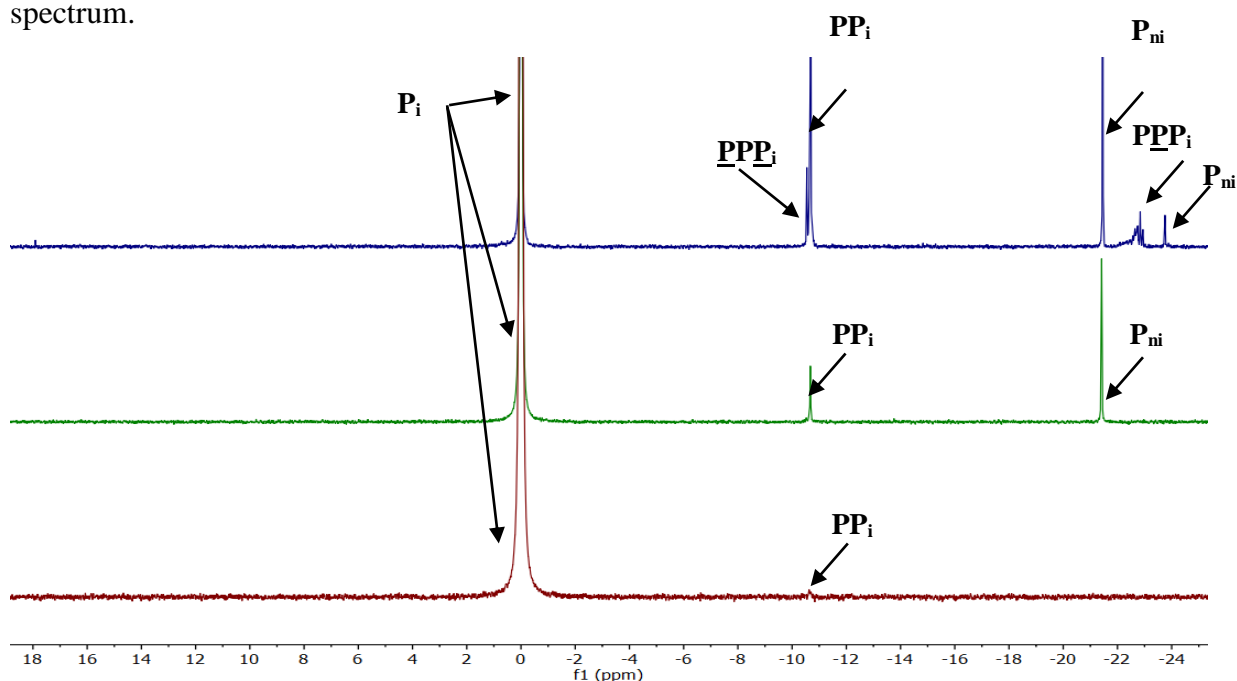


Figure 143. ³¹P{¹H} NMR spectra (202.5 MHz, in D₂O) after 120 h of heating at 115 °C of reaction mixture (on a 0.5 mmol scale); lower spectrum (**red**) **16a:P_i** (1:1): δ_P (ppm) = 0.00 (*s*, **P_i**), -10.63 (*s*, **PP_i**); middle spectrum (**green**) **16a:2a:P_i** (1:1:1): δ_P (ppm) = 0.00 (*s*, **P_i**), -10.67 (*s*, **PP_i**), -21.42 (*s*, **P_{ni}**); upper spectrum (**blue**) **16a:1:P_i** (1:1:1): δ_P (ppm) = 17.91 (*s*, **5cPyP**, blue), 0.00 (*s*, **P_i**), -10.59 (*d*, *J* = 19.4 Hz, **PPP_i**), -10.68 (*s*, **PP_i**), -21.46 and -23.75 (*s* and *s*, **P_{ni}**), -22.84 (*t*, *J* = 19.3 Hz, **PPP_i**).

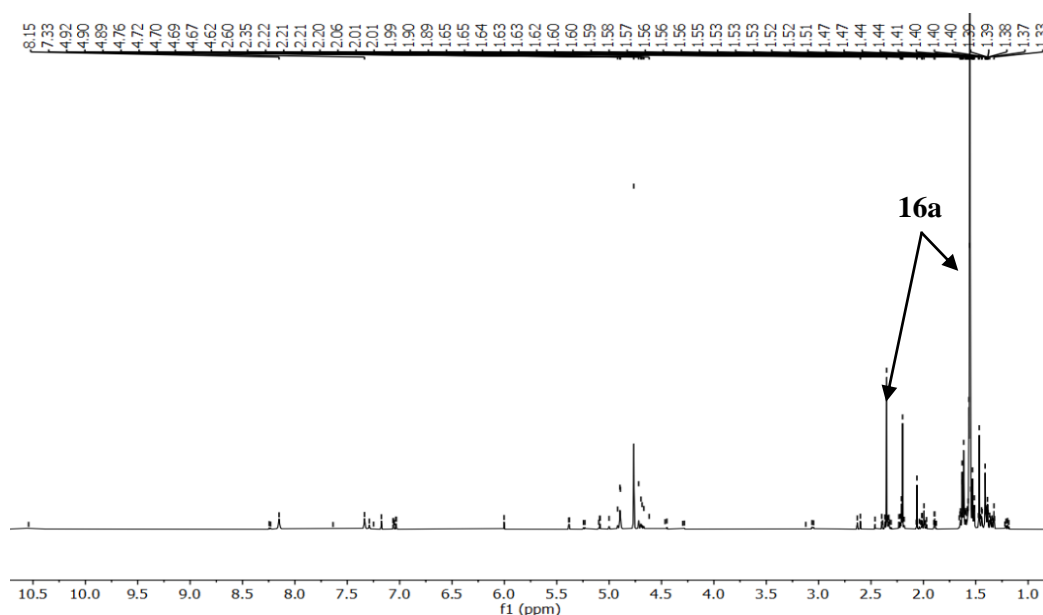


Figure 144. ¹H NMR spectrum (500 MHz, D₂O, water suppression) of crude mixtures of reaction **16a:1:P_i** (1:1:1) 0.5 mmol scale after 120 h of heating at 60 °C, δ_H (ppm) = 2.35 (*s*), 2.34 – 2.33 (*m*), 2.23 (*d*, *J* = 6.8 Hz), 2.20 (*s*), 1.62 (*d*, *J* = 7.2 Hz, 1H), 1.56 (*d*, *J* = 2.8 Hz, 1H), 1.56 (*s*, 3H), 1.47 (*s*).

A similar situation was observed in reaction with **cTMP** (Figure 145). **cTMP** is partly converted into inorganic mono-, di- and triphosphates. The presence of doublet and triplet integration ratio is 2:1, as in Figure 126 and Figure 143 confirms the structure of inorganic triphosphate **PPP_i**.

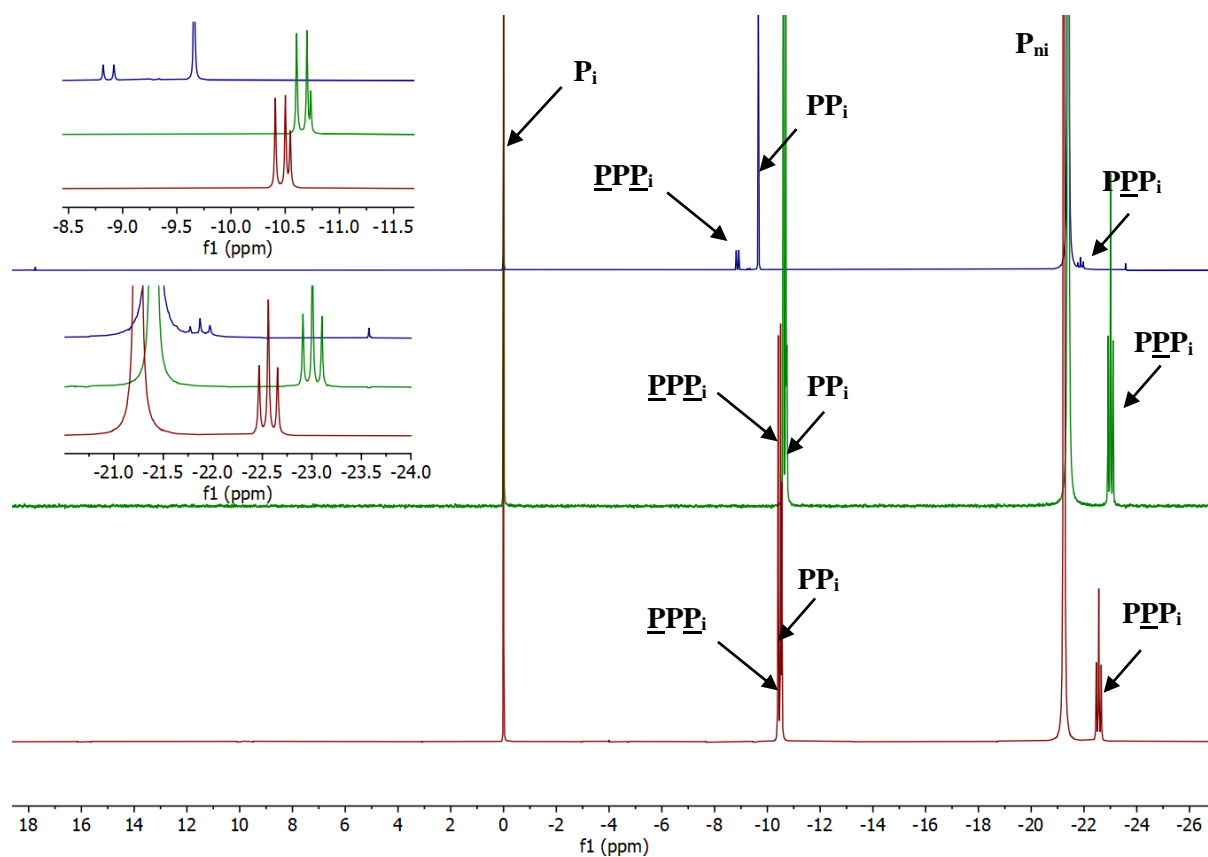


Figure 145. $^{31}\text{P}\{^1\text{H}\}$ NMR spectra (202.5 MHz, in D_2O) after 120 h of heating at 115 °C of reaction mixture (on a 0.5 mmol scale); lower spectrum (red) **16a:cTMP** (1:1) δ_{P} (ppm) = 0.00 (*s*, **P_i**), -10.46 (*d*, $J = 18.9$ Hz, **PPP_i**), -10.55 (*s*, **PP_i**); -21.24 (*s*, **P_{ni}**), -22.56 (*t*, $J = 19.0$ Hz, **PPP_i**); middle spectrum (green) **16a:2a:cTMP** (1:1:1) δ_{P} (ppm) = 0.00 (*s*, **P_i**), -10.65 (*d*, $J = 19.3$ Hz, **PP_i**), -10.74 (*s*, **PP_i**), -21.40 (*s*, **P_{ni}**), -23.01 (*t*, $J = 19.3$ Hz, **PPP_i**); upper spectrum (blue) **16a:1:cTMP** (1:1:1) δ_{P} (ppm) = 17.74 (*s*, **5cPyP**), 0.00 (*s*, **P_i**), -8.87 (*d*, $J = 20.1$ Hz, **PP_i**), -9.29 (*d*, $J = 19.8$ Hz), -9.66 (*s*, **PP_i**), -21.40 and -23.58 (*s* and *s*, **P_{ni}**), -21.87 (*t*, $J = 20.1$ Hz, **PPP_i**).

The last series of experiments were carried out with **SP_i** (**Figure 146**). We indeed produced phosphorylated products, such as cyclic and acyclic phosphoenol phosphates, but the yields were below 1 %. Unlike in the reaction of glycerol with pyruvic acid, the presence of Pi decreased the number of products. Most likely, inorganic di- and triphosphates were not detected in DMSO-*d*₆ because they are better soluble in water. These complex spectra were a great opportunity to work on the complex ³¹P{¹H} NMR data and improve my skills.

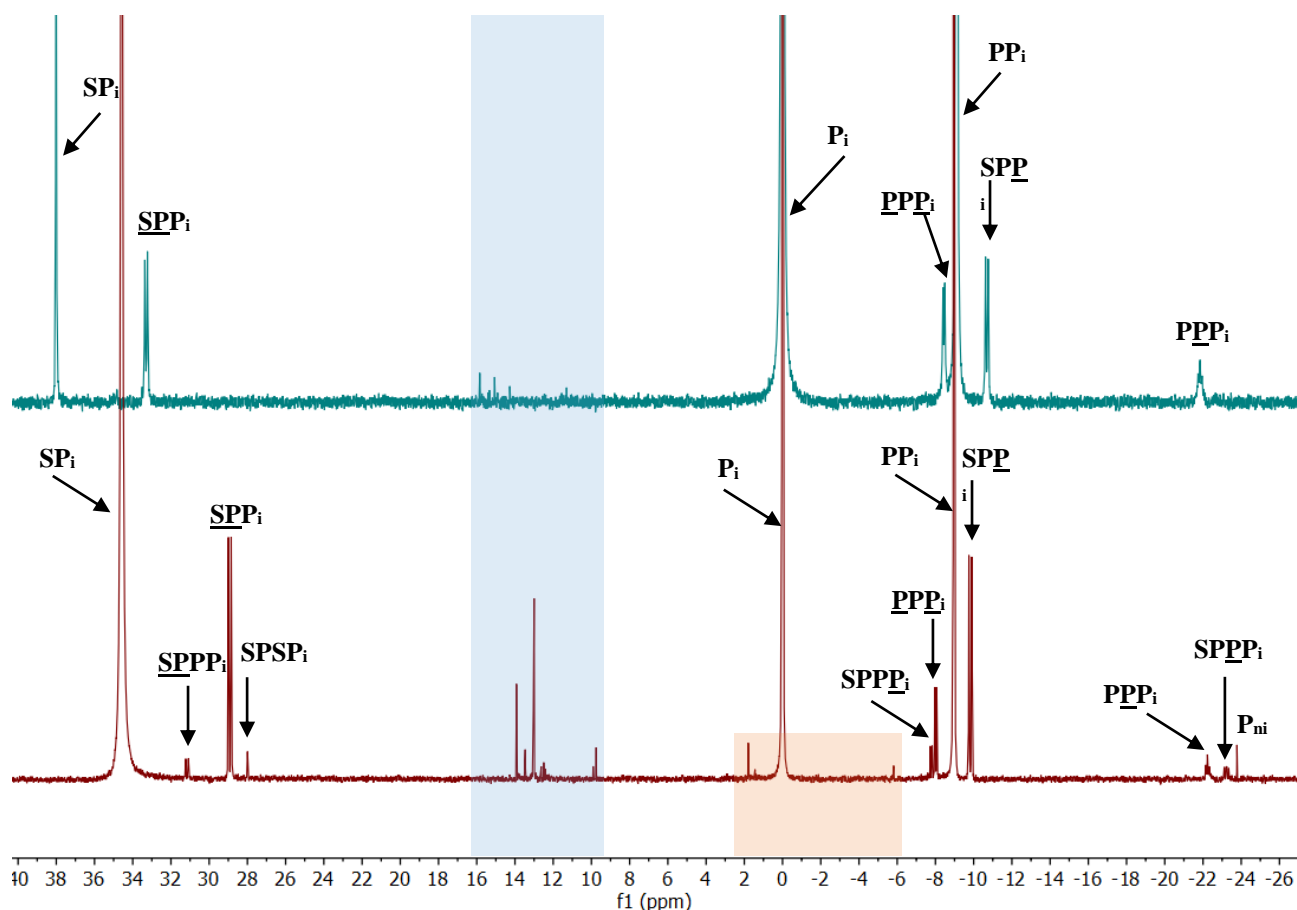
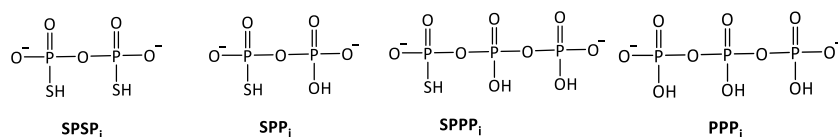


Figure 146. ³¹P{¹H} NMR spectra (202 MHz, in D₂O) after 120 h of heating at 115 °C of reaction mixture (0.5 mmol scale); upper spectrum (blue) **16a:2a:Pi:SP_i** (1:1:0.5:0.5) δ_P (ppm) = 38.01 (s, **SP_i**), 33.30 (*d*, *J* = 27.9 Hz, **SPP_i**), 15.84-14.27 (**5cPyP**, blue), 0.00(*s*, **P_i**), -8.44 (*d*, *J* = 20.0 Hz, **PPPi**), -9.11 (*s*, **PP_i**), -10.69 (*d*, *J* = 27.7 Hz, **SPP_i**), -21.85 (*t*, *J* = 20.4 Hz, **PPPi**); lower spectrum (red) **16a:2a:SP_i** (1:1:1) δ_P (ppm) = 34.58 (*s*, **SP_i**), 31.16 (*d*, *J* = 28.3 Hz, **SPPP_i**), 28.92 (*d*, *J* = 29.0 Hz, **SPP_i**), 28.00 (*s*, **SPSP_i**), 13.92-9.75 (**5cPyP**, blue), from 1.49 to -5.47 (**PyP**, orange) 0.00 (*s*, **P_i**), -7.78 (*d*, *J* = 19.3 Hz, **SPPP_i**), -8.02 (*d*, *J* = 19.3 Hz, **PPPi**), -8.97 (*s*, **PP_i**), -9.83 (*d*, *J* = 29.5 Hz, **SPP_i**), -22.23 (*t*, *J* = 18.8 Hz, **PPPi**); -23.23 (*dd*, *J* = 28.7, 18.9 Hz, **SPPP_i**), -23.78 (*s*, **P_{ni}**).



To finalise our work on pyruvic acid phosphorylation, we performed LRMS of the crude mixture **16a:2a:P_i** (1:1:1); 0.5 mmol scale; reaction time 120 h at 60 °C (**Figure 147**). As expected, we discovered many products of pyruvic acid polymerisation and we also detected phosphorylated products such as PEP and cyclic derivatives of pyruvate polymers (**Figure 148**).

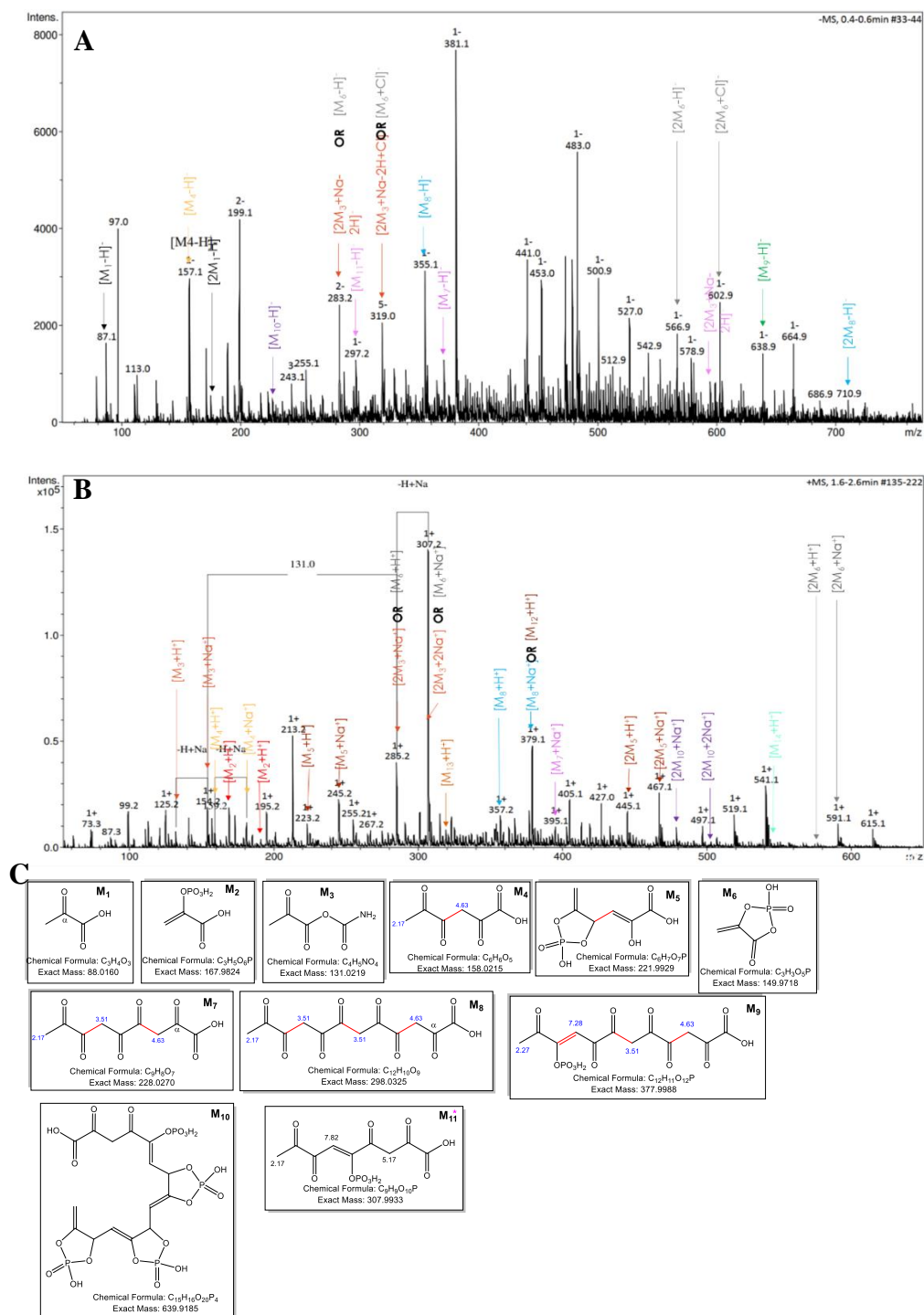


Figure 147. LRMS of the methanolic extract of crude mixture **16a:2a:P_i** (1:1:1); 0.5 mmol scale ; reaction time 120 h at 60 °C. **A** – negative ion mode; **B** – positive ion mode; **C** – Suggested molecular structures (only the most probable isomer shown) and monoisotopic exact masses of the compounds detected by LRMS. Values close to the main carbon chains are simulated chemical [ppm] shifts for ¹H NMR resonances (by ChemDraw™). Red C-C bonds = newly formed from **16a**.

As said before, dry and evaporative conditions suggested in the current work are more favourable for pyruvic acid polymerisation. The phosphorylation degree in all studied experiments never exceeded about 3 %.

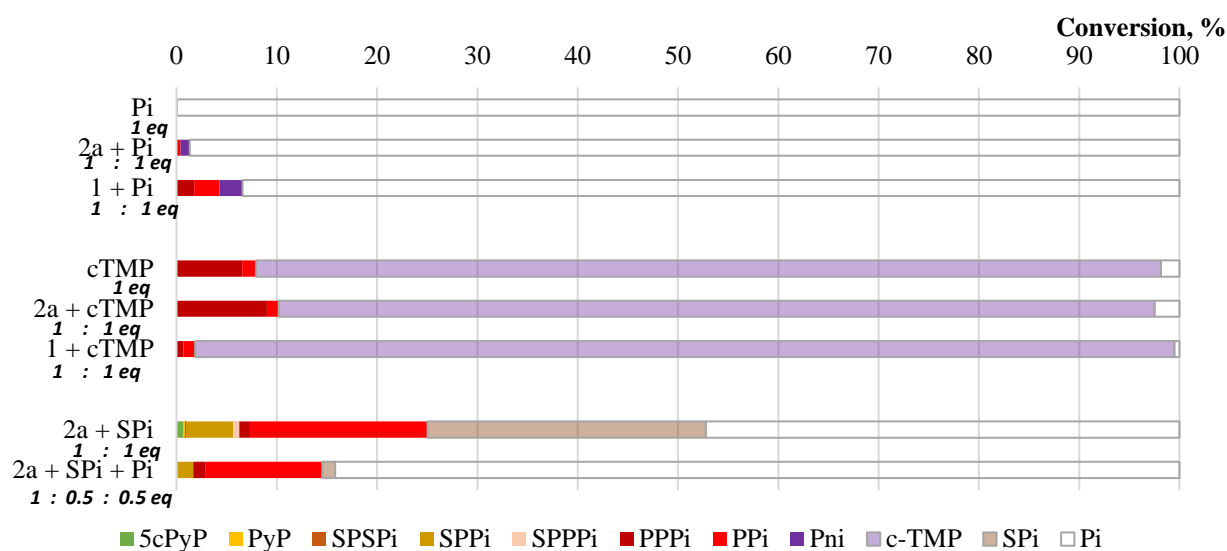


Figure 148. Summary of pyruvic acid (**16a**) phosphorylations after 120 h of heating at 60 °C, with and without cond. agent, on a 0.5 mmol scale. Molar equivalents are indicated in the diagram with respect to starting molecule **16a** (1 eq). Percent values from signal integration of quantitative $^{31}\text{P}\{^1\text{H}\}$ NMR spectra taken in D_2O .

Table 48. Data to **Figure 148**. Total conversion of initial amount of P_i to phosphorylated organic products was calculated by subtracting inorganic compound integrals from the sum of all integrated $^{31}\text{P}\{^1\text{H}\}$ NMR peak areas.

Cond agent	Phosphate source	5cPyP, %	PyP, %	SPSP _i , %	SPP _i , %	SPPP _i , %	PPP _i , %	PP _i , %	P _{ni} , %	cTMP, %	SP _i , %	P _i , %
-	P _i	-	-	-	-	-	-	0.05	-	-	-	99.95
2a	P _i	-	-	-	-	-	-	0.40	0.91	-	-	98.69
1	P _i	0.01	-	-	-	-	1.77	2.50	2.30	-	-	93.42
-	cTMP	-	-	-	-	-	6.56	1.38	-	90.22	-	1.84
2a	cTMP	-	-	-	-	-	9.03	1.17	-	87.33	-	2.47
1	cTMP	0.01	-	-	-	-	0.69	1.15	0.03	97.61	-	0.51
2a	SP _i	0.73	0.12	0.10	4.68	0.65	1.06	17.67	0.04	-	27.71	47.24
2a	P _i :SP _i	0.07	-	-	1.61	-	1.25	11.61	-	-	1.28	84.18

Conclusions to the Section 4

In the previous section, I showed that mono-alcohols are less reactive compared to glycerol (tri-ol) and MPG (di-ol). This holds true as well for dodecanol, geraniol, and pyruvic acid. I used two approaches for the phosphorylation of decanol in the presence of a condensing agent and reactions that involved pyruvic acid, or PEP. It was expected that it could intensify the production of phosphorylated organic products that did not appear. Nevertheless, we observed phosphorylation of pyruvic acid (**5cPEP** and **PEP**), as well as minor quantity of 1-dodecyl phosphate **9b**.

The highest yields were obtained with the addition of cyanamide; however, the presence of urea did not favour phosphorylation. For the experiments with a large molar excess of urea after 96 h, we observed only inorganic phosphates, including pyro- and triphosphate, **PP_i** and **PPP_i**. The most successful experiment with cyanamide was explored by HRMS, where the reaction was carried out in dry or wet-evaporative conditions. The presence of water seems to be essential for dodecanol phosphorylation. The diversity and isotopolog ratio give us ideas about the phosphorylation reactions of dodecanol; for example, more phosphodiester are detected in the wet-evaporative experiment.

As for dodecanol, geraniol as well did not appear to be easily phosphorylated. There are groups of the organic phosphorylated products that were not detected in other prebiotic experiments. It may be the result of the phosphorylation of the C=C double-bonds, we tentatively suggest them to be associated with cyclic monoterpene compounds that are phosphorylated and suggested possible mechanism of their formation. The only high yields of organic phosphates were obtained upon the action of cyanamide (25%). All the other experiments with urea and inorganic phosphate or thiophosphate did not produce any organic phosphates above 5 % and the presence of pyruvic acid as an additive totally suppressed even the low amount of cyclic phosphates. Those are the very first reaction results and NMR data described for the reaction of geraniol.

Another exciting and yet unexplored field is the phosphorylation of pyruvic acid. We have made a lot of efforts to involve it in reactions, including different temperatures, condensing agents, phosphates and other, but we have obtained very few organic phosphorylated products. The occurrence of many weak signals in the ¹H NMR spectrum and the absence of organic signals in the ³¹P{¹H} NMR spectrum confirm the predominance of a polymerisation reaction over phosphorylation. In LRMS analyses I described many products of pyruvic acid polymerisation and phosphorylated products such as PEP and cyclic derivatives of pyruvate polymers. Thus, I conclude that dry prebiotic conditions are favourable for polymerisation of pyruvic but not phosphorylation. The phosphorylation degree in all studied experiments never exceeded about 3 %.

Even though mono-ols are not easy to phosphorylate in the described condition, they could be part of membranogenic material and contribute to the formation of vesicles, or, in the case of pyruvic acid, produce some metabolites precursors through polymerisation reactions.

III Results and discussion

5. Phosphorylation of nucleosides

5.1. Phosphorylation of adenosine in the presence of water or formamide

Nucleosides were the next choice of plausible prebiotic alcohol to test in the phosphorylation reaction. Unlike glycerol and urea, they remain a solid powder under 75-115 °C, so their efficient phosphorylation and interaction with other dry solid reactants (Pi, urea) required a liquidifier. Thus, we performed phosphorylation reactions on adenosine (**11**) : urea (**2a**) : Pi (1:1:1) in the presence of water (**Figure 149**) or formamide.

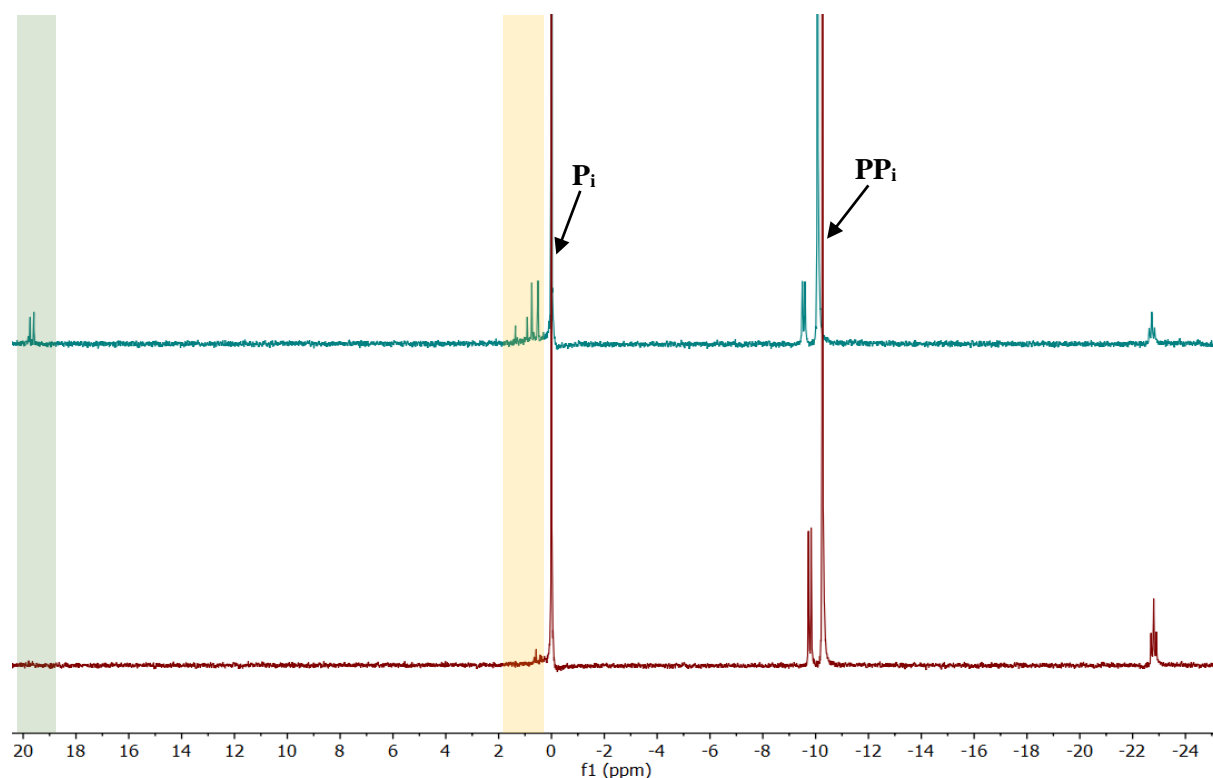


Figure 149. $^{31}\text{P}\{^1\text{H}\}$ NMR spectra (202.5 MHz, $\text{H}_2\text{O}/\text{D}_2\text{O} = 9:1$) 0.5 mmol scale reaction with 1 ml of H_2O added in the beginning of reaction after, 120 h of heating at 115 °C of crude mixtures: **Lower spectrum** – **11:1:Pi** (1:1:1); δ_{P} (ppm) = 0.58 (5'-, 3'- or 2'-acyclic adenosine phosphate, **Ap**, ochre), 0.00 (s, **Pi**), -9.78 (d, $J = 20.5$ Hz **PPPi**), -10.26 (s, **PPi**), -22.80 (t, $J = 20.3$ Hz **PPPi**); **upper spectrum** – **11:2a:Pi** (1:1:1); δ_{P} (ppm) = 19.73-19.59 (s, 2',3' 5-membered ring cyclic phosphates **A5>p**, green), 1.36-0.51 (5'-, 3'- and 2'-acyclic adenosine phosphates, **Ap**, ochre), 0.00 (s, **Pi**), -9.55 (d, $J = 20.5$ Hz **PPPi**), -10.07 (s, **PPi**), -22.73 (t, $J = 20.6$ Hz **PPPi**).

For these experiments in water, ^1H - ^{31}P HMBC spectra did not show any cross-correlations (not shown). We conclude that all signals in the above $^{31}\text{P}\{^1\text{H}\}$ NMR spectra are due to inorganic phosphates. In both experiments, the ratios of the $^{31}\text{P}\{^1\text{H}\}$ doublet and triplet resonances integrate in a 2:1 ratio, respectively; therefore, both signals belong to inorganic triphosphate. Summary: see next page.

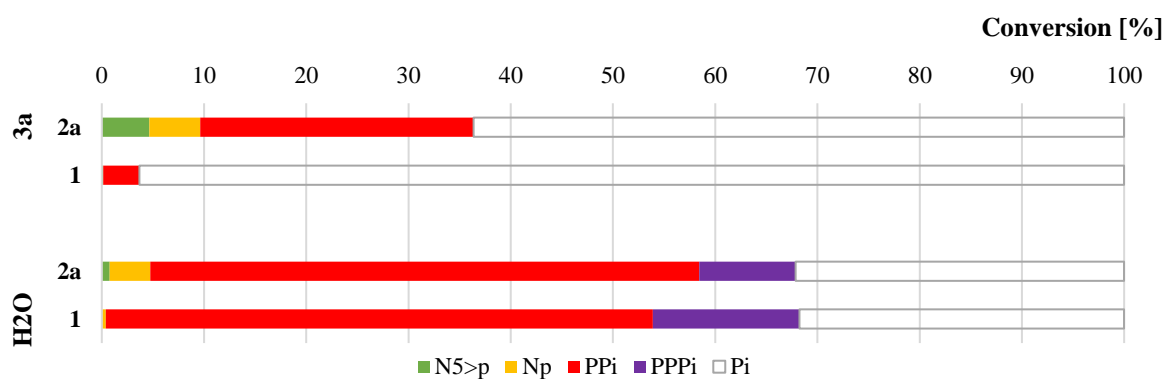


Figure 150. Summary of adenosine (**11**) phosphorylation in reaction **11:cond.agent:P_i** (1:1:1) with 1 ml of H₂O added in the beginning of the reaction or 0.5 eq **3a** as liquidiser, 0.5 mmol scale after 120 h of heating at 115 °C, then dissolved in H₂O/D₂O = 9:1. Percent values from signal integration of quantitative ³¹P{¹H} NMR spectrum.

Table 49. Data to **Figure 149**. Total conversion of initial amount of **P_i** to phosphorylated organic products was calculated by subtracting inorganic compound integrals (**P**, **PP_i** and **PPP_i**) from the sum of all integrated ³¹P{¹H} NMR peaks (in H₂O/D₂O = 9:1). Products **ApA** and **A6>p** were not detected.

Liquidiser	Condensing agent	A5>p, %	Ap, %	PP _i , %	PPP _i , %	P _i , %
3a	2a	4.64	4.99	26.74	-	63.63
	1	0.13	-	3.55	-	96.32
H₂O	2a	0.76	3.99	53.68	9.45	32.12
	1	-	0.40	53.51	14.34	31.75

Here, in fact, we experimentally proved that the presence of water prevents the phosphorylation adenosine or significantly slows it down. In the following sections, ‘**dry**’ nucleoside phosphorylations are carried out in the presence of 0.5 eq of formamide as a liquidiser for the starting molecule.

5.2. Experiments with different condensing agents (cyanamide **1** and urea **2a**)

We performed phosphorylation reactions of nucleosides A, C, G, U and T in the presence of urea (or cyanamide) and Pi. Here we demonstrated $^{31}\text{P}\{^1\text{H}\}$, ^1H and $^1\text{H}\text{-}^{31}\text{P}$ HMBC NMR spectra of each corresponding nucleosides: adenosine **Figure 151**-**Figure 153**, guanosine **Figure 154**-**Figure 156**, cytidine **Figure 157**-**Figure 159**, uridine **Figure 160**-**Figure 162** and thymidine **Figure 163**-**Figure 165**. The discussion starts after **Figure 165**.

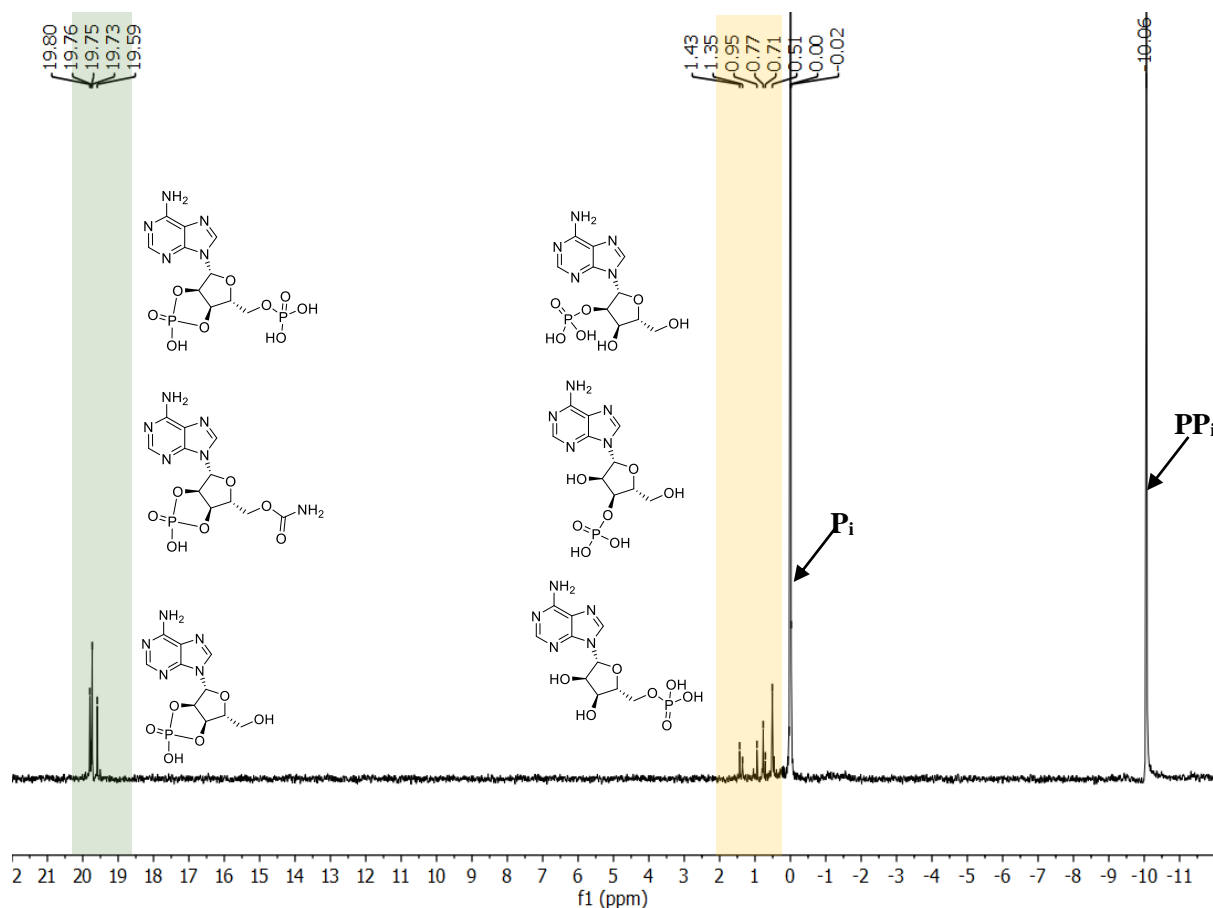


Figure 151. $^{31}\text{P}\{^1\text{H}\}$ NMR spectrum (202.5 MHz) of crude mixture containing **11**, **2a** and P_i (1:1:1) with 0.5 eq **3a** as liquidiser, 0.5 mmol scale reaction after 120 h of heating at 115 °C, then dissolved in $\text{H}_2\text{O}/\text{D}_2\text{O} = 9:1$. δ_{P} (ppm) = 19.80-19.59 (s, 2', 3' 5-membered ring cyclic phosphate **A5>p**, green), 1.43-0.51 (5', 3' or 2' acyclic adenosine-phosphates, **Ap**, ochre), 0 (s, P_i), -10.06 (s, PP_i). Acyclic phosphates can be due to di- or tri-phosphorylated or/and carbamoylated adenosine.

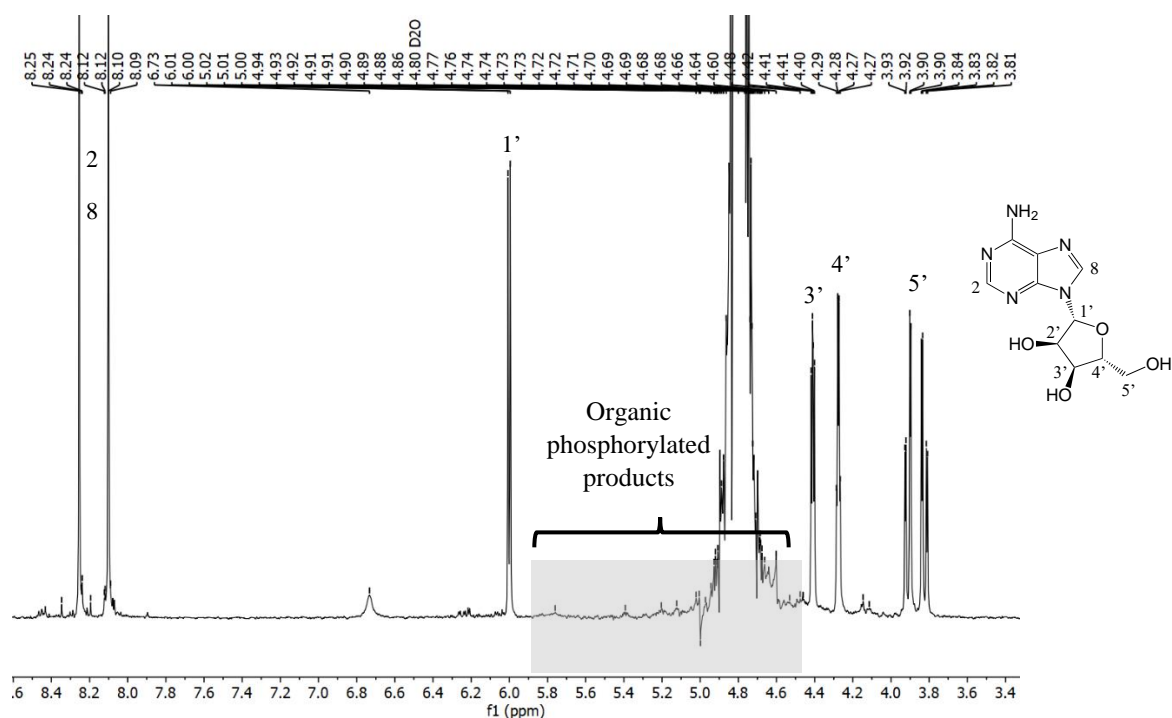


Figure 152. ^1H NMR spectrum (500 MHz) of crude mixture containing **11**, **2a** and **P_i** (1:1:1) with 0.5 eq **3a** as liquidiser, 0.5 mmol scale reaction after 120 h of heating at 115 °C, then dissolved in $\text{H}_2\text{O}/\text{D}_2\text{O} = 9:1$. δ_{H} (ppm) = 8.15 (s, 1H), 8.00 (s, 1H), 5.90 (d, $J = 6.1$ Hz, 1H), 4.31 (dd, $J = 5.2, 3.4$ Hz, 1H), 4.18 (q, $J = 3.3$ Hz, 1H), 3.81 (dd, $J = 12.9, 2.8$ Hz, 1H), 3.72 (dd, $J = 12.9, 3.6$ Hz, 1H). Spectrum labelled with proton resonances of unreacted nucleoside.

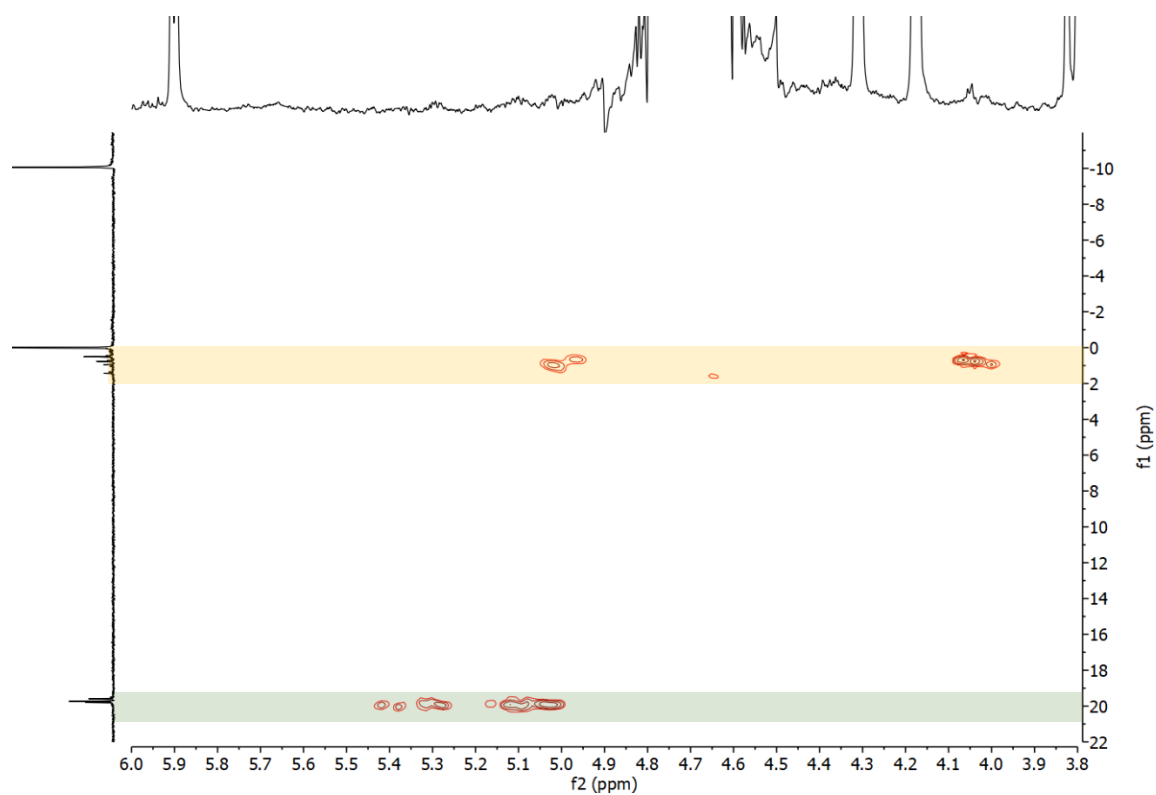


Figure 153. ^1H - ^{31}P HMBC spectrum (500 MHz for ^1H [horizontal axis], 202.5 MHz for $^{31}\text{P}\{^1\text{H}\}$ [vertical axis]) of crude mixture containing **11**, **2a** and **P_i** (1:1:1) with 0.5 eq **3a** as liquidiser, 0.5 mmol scale reaction after 120 h of heating at 115 °C, then dissolved in $\text{H}_2\text{O}/\text{D}_2\text{O} = 9:1$. Ochre (**Ap**) and green (**A5>p**) zones highlight organic products of phosphorylation.

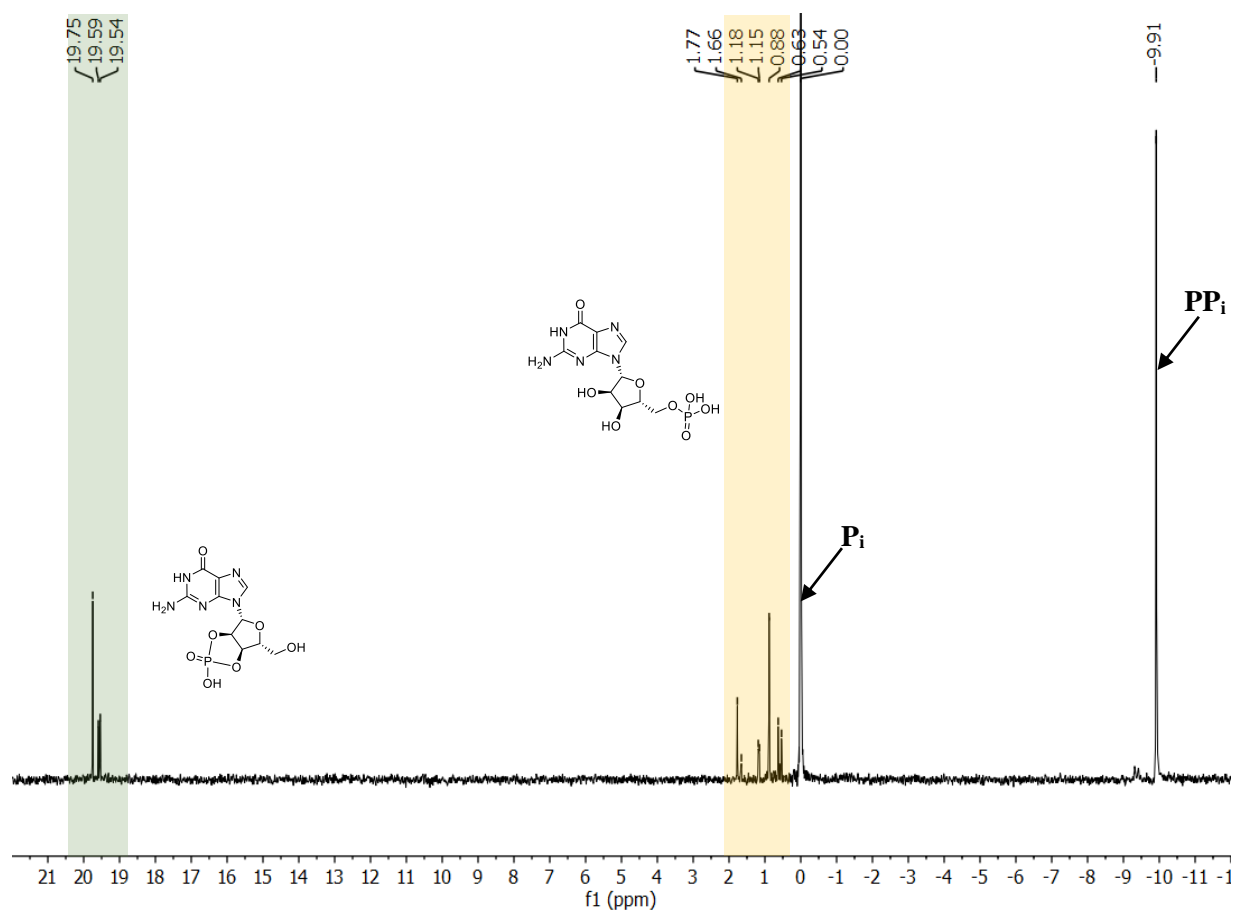


Figure 154. $^{31}\text{P}\{^1\text{H}\}$ NMR spectrum (202.5 MHz) of crude mixture containing **12**, **2a** and **P_i** (1:1:1) with 0.5 eq **3a** as liquidiser, 0.5 mmol scale reaction after 120 h of heating at 115 °C, then dissolved in $\text{H}_2\text{O}/\text{D}_2\text{O} = 9:1$. δ_{P} (ppm) = 19.75-19.54 (s, 2',3' 5-membered ring cyclic phosphate **G5>p**, green), 1.77-0.54 (5', 3' or 2' acyclic guanosine-phosphates, **Gp**, ochre), 0 (s, **P_i**), -9.91 (s, **PP_i**). Structures represent main groups of organic phosphorylated products.

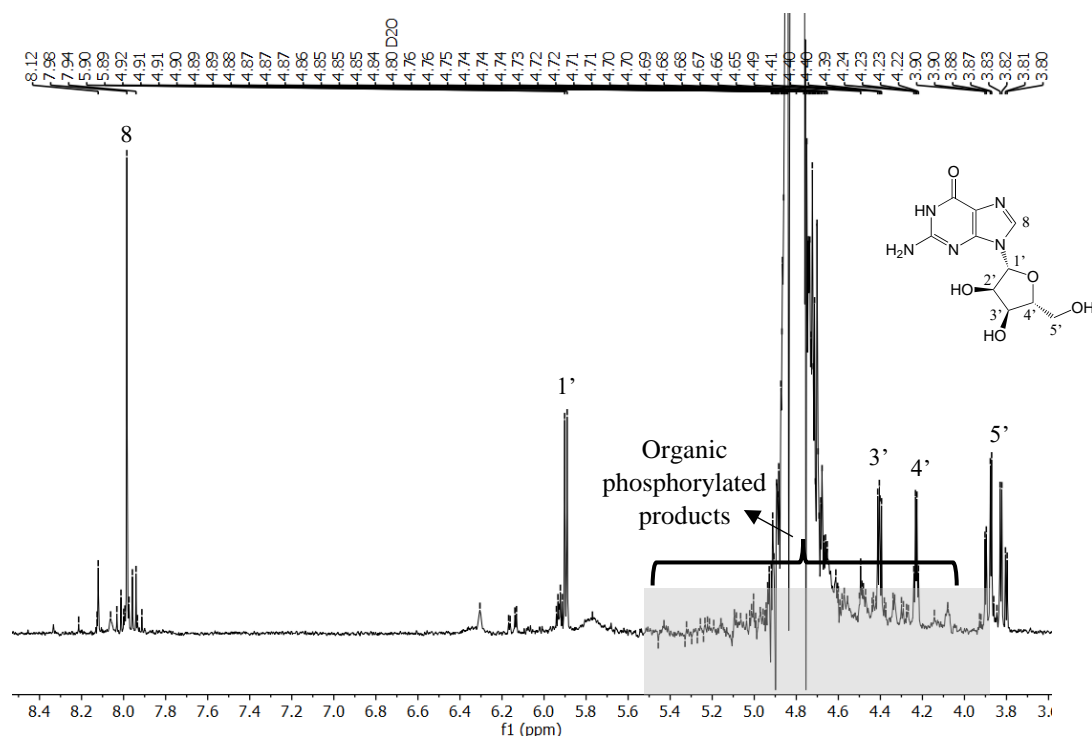


Figure 155. ^1H NMR spectrum (500 MHz) of crude mixture containing **12**, **2a** and **P_i** (1:1:1) with 0.5 eq **3a** as liquidiser, 0.5 mmol scale reaction after 120 h of heating at 115 °C, then dissolved in $\text{H}_2\text{O}/\text{D}_2\text{O} = 9:1$. δ_{H} (ppm) = 7.88 (*s*, 1H), 5.80 (*d*, $J = 5.9$ Hz, 1H), 4.30 (*dd*, $J = 5.3, 3.7$ Hz, 1H), 4.13 (*d*, $J = 3.5$ Hz, 1H), 3.79 (*dd*, $J = 12.7, 3.1$ Hz, 1H), 3.71 (*dd*, $J = 12.7, 4.1$ Hz, 1H). Spectrum labelled with proton resonances of unreacted nucleoside.

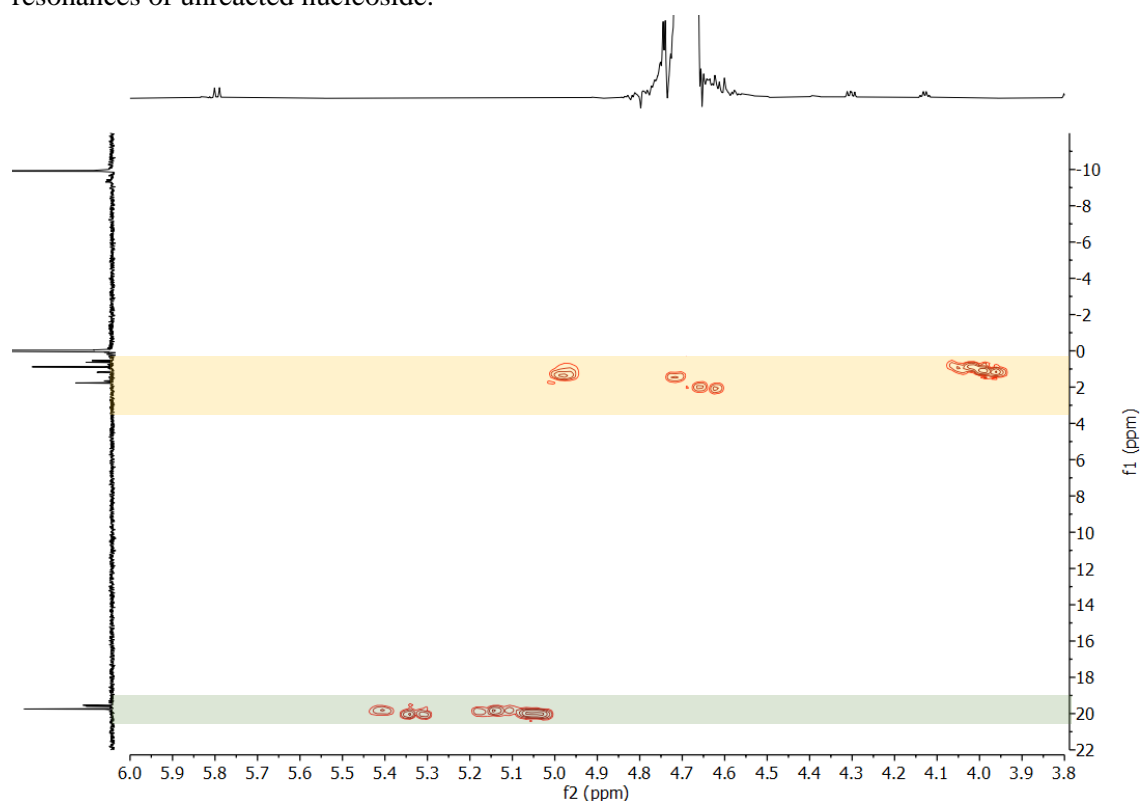


Figure 156. ^1H - ^{31}P HMBC spectrum (500 MHz for ^1H [horizontal axis], 202.5 MHz for $^{31}\text{P}\{^1\text{H}\}$ [vertical axis]) of crude mixture containing **12**, **2a** and **P_i** (1:1:1) with 0.5 eq **3a** as liquidiser, 0.5 mmol scale reaction after 120 h of heating at 115 °C, then dissolved in $\text{H}_2\text{O}/\text{D}_2\text{O} = 9:1$. Ochre (**G_p**) and green (**G₅>p**) zones highlight organic products of phosphorylation.

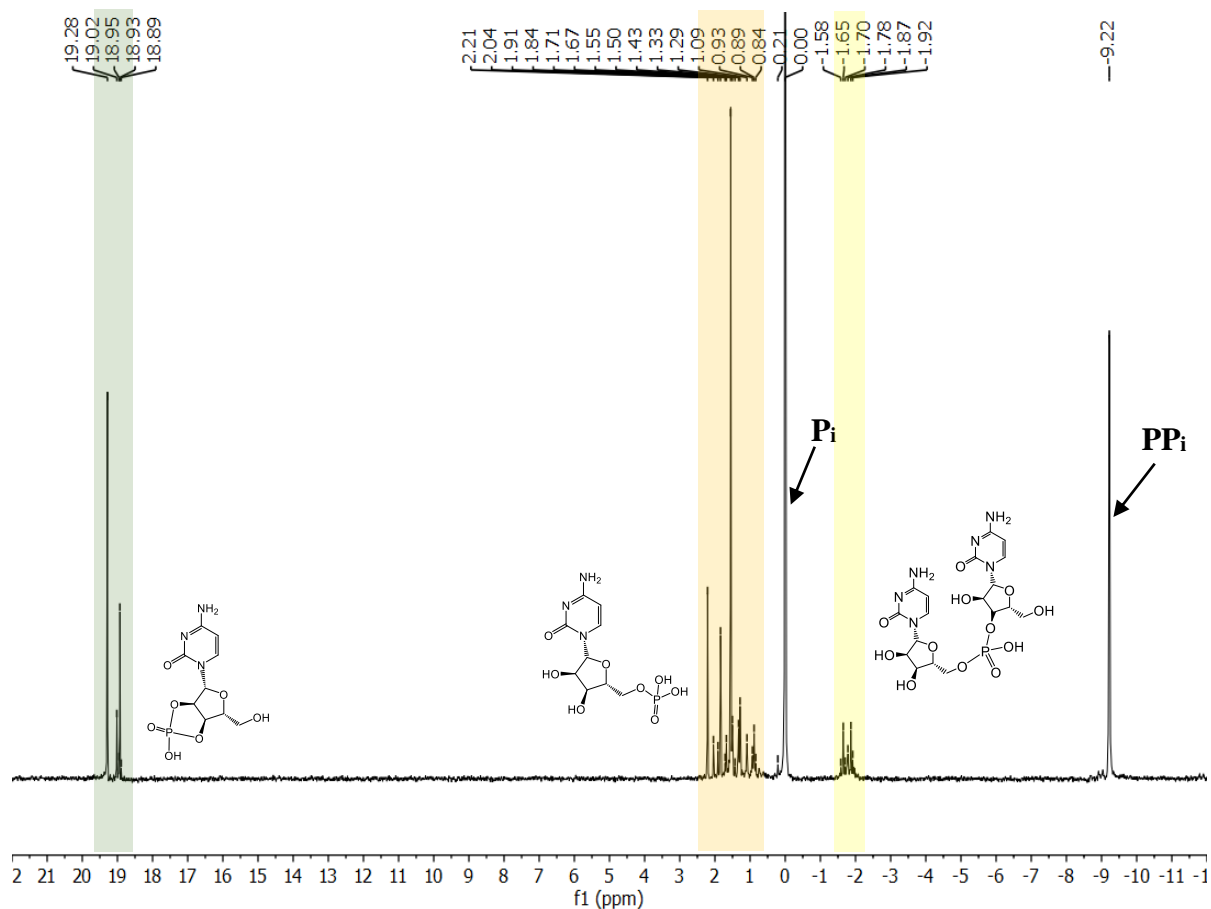


Figure 157. $^{31}\text{P}\{^1\text{H}\}$ NMR spectrum (202.5 MHz) of crude mixture containing **13**, **2a** and **P_i** (1:1:1) with 0.5 eq **3a** as liquidiser, 0.5 mmol scale reaction after 120 h of heating at 115 °C, then dissolved in $\text{H}_2\text{O}/\text{D}_2\text{O} = 9:1$. δ_{P} (ppm) = 19.28-18.89 (*s*, 2',3' 5-membered ring cyclic phosphate **C5>p**, green), 2.21-0.21 (5', 3' or 2' acyclic cytidine-phosphates, **Cp**, ochre), 0 (*s*, **P_i**), -1.58 to -1.92 (acyclic dicytidine phosphates, **CpC**, yellow), -9.22 (*s*, **PP_i**). Structures represent main groups of organic phosphorylated products.

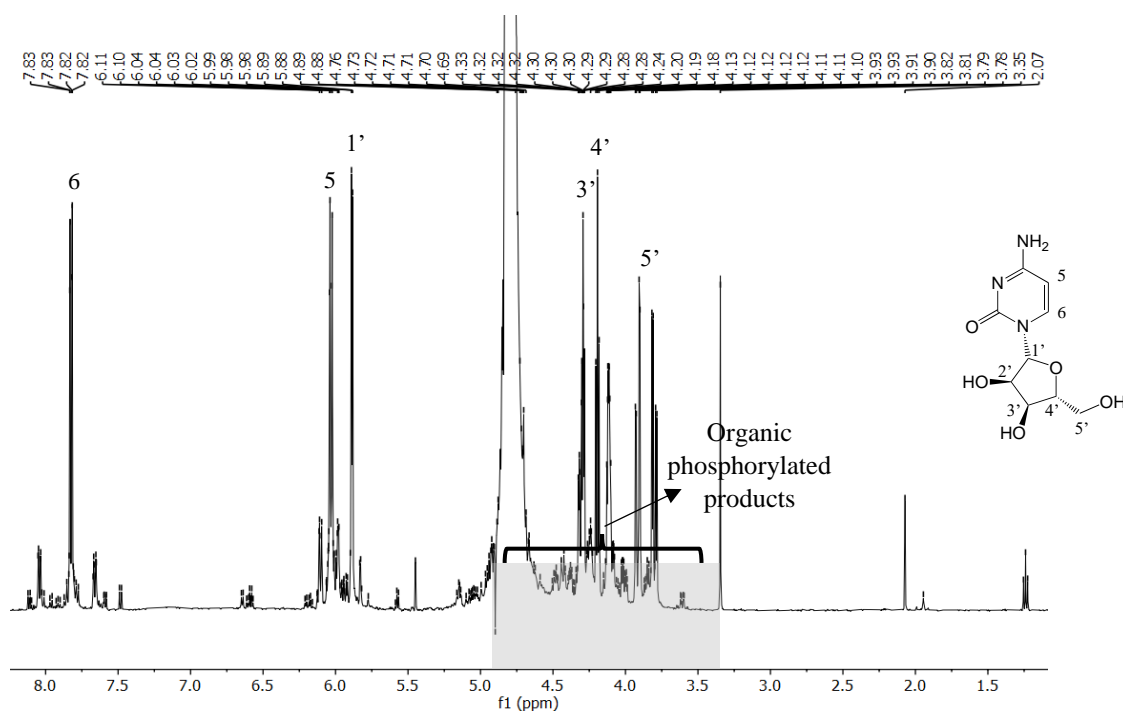


Figure 158. ^1H NMR spectrum (500 MHz) of crude mixture containing **13**, **2a** and **P_i** (1:1:1) with 0.5 eq **3a** as liquidiser, 0.5 mmol scale reaction after 120 h of heating at 115 °C, then dissolved in $\text{H}_2\text{O}/\text{D}_2\text{O} = 9:1$. δ_{H} (ppm) = 7.72 (*dd*, $J = 7.6, 1.1$ Hz, 1H), 5.93 (*dd*, $J = 7.5, 1.3$ Hz, 1H), 5.79 (*d*, $J = 4.0$ Hz, 1H), 4.19 (*ddd*, $J = 5.2, 4.0, 1.1$ Hz, 1H), 4.09 (*t*, $J = 5.7$ Hz, 1H), 3.82 (*dd*, $J = 12.8, 2.9$ Hz, 1H), 3.70 (*dd*, $J = 12.8, 4.5$ Hz, 1H). Spectrum labelled with proton resonances of unreacted nucleoside.

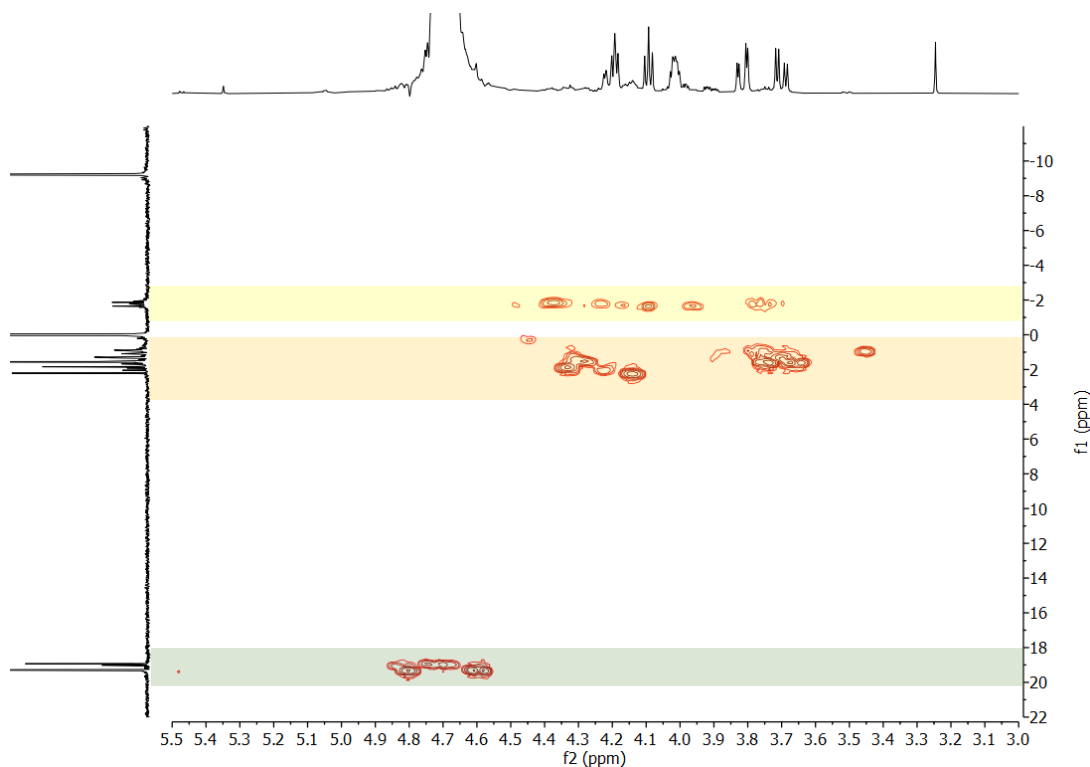


Figure 159. ^1H - ^{31}P HMBC spectrum (500 MHz for ^1H [horizontal axis], 202.5 MHz for $^{31}\text{P}\{^1\text{H}\}$ [vertical axis]) of crude mixture containing **13**, **2a** and **P_i** (1:1:1) with 0.5 eq **3a** as liquidiser, 0.5 mmol scale reaction after 120 h of heating at 115 °C, then dissolved in $\text{H}_2\text{O}/\text{D}_2\text{O} = 9:1$. Ochre (**C_p**), yellow (**C_{pC}**) and green (**C₅>p**) zones highlight organic products of phosphorylation.

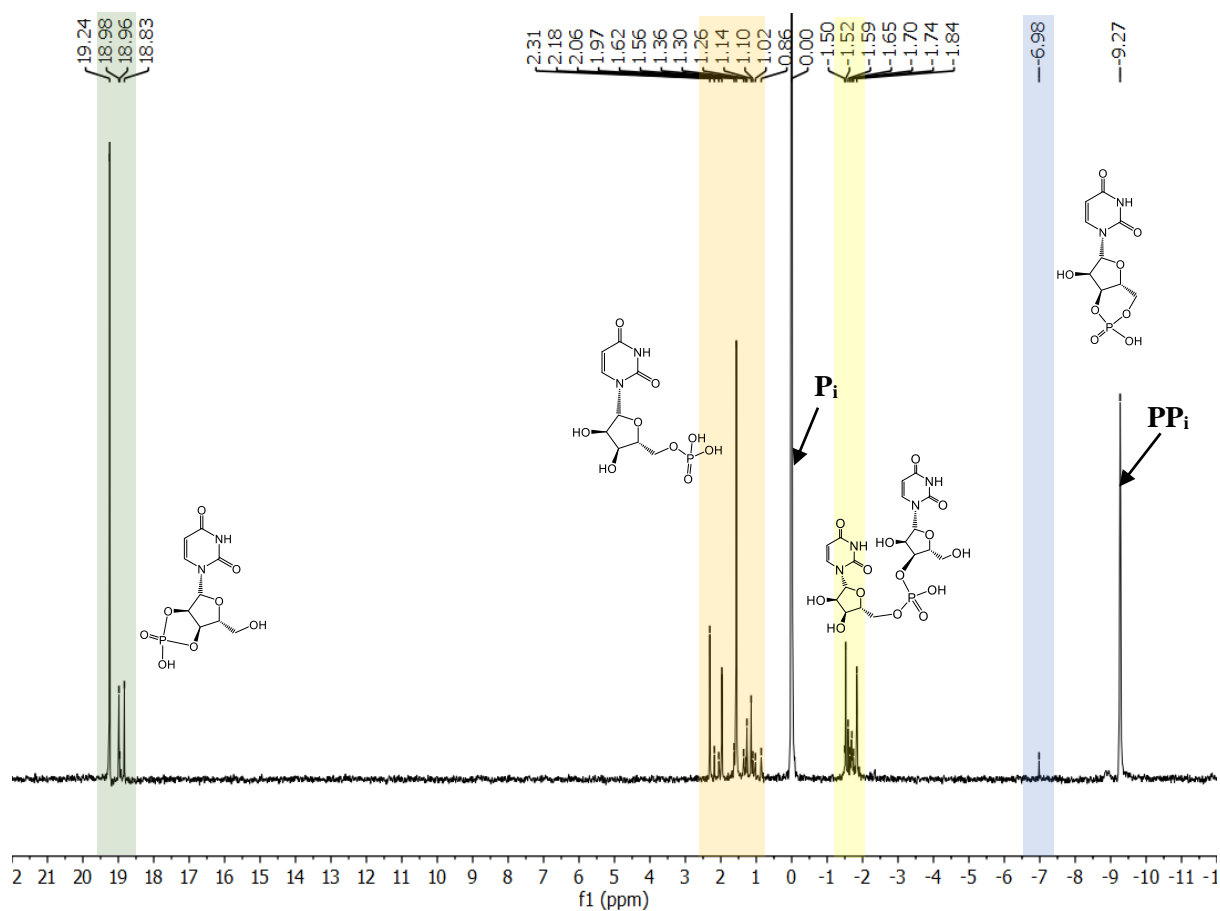


Figure 160. $^{31}\text{P}\{^1\text{H}\}$ NMR spectrum (202.5 MHz) of crude mixture containing **14**, **2a** and **P_i** (1:1:1) with 0.5 eq **3a** as liquidiser, 0.5 mmol scale reaction after 120 h of heating at 115 °C, then dissolved in $\text{H}_2\text{O}/\text{D}_2\text{O} = 9:1$. δ_{P} (ppm) = 19.24-18.83 (*s*, 2',3' 5-membered ring cyclic phosphate **U5>p**, green), 2.31-0.86 (5', 3' or 2' acyclic uridine-phosphates, **Up**, ochre), 0 (*s*, **P_i**), -1.50 to -1.84 (acyclic diuridine phosphates, **UpU**, yellow), -6.98 (*s*, 5',3' 6-membered ring cyclic phosphate **U6>p**, blue), -9.27 (*s*, **PP_i**). Structures represent main groups of organic phosphorylated products.

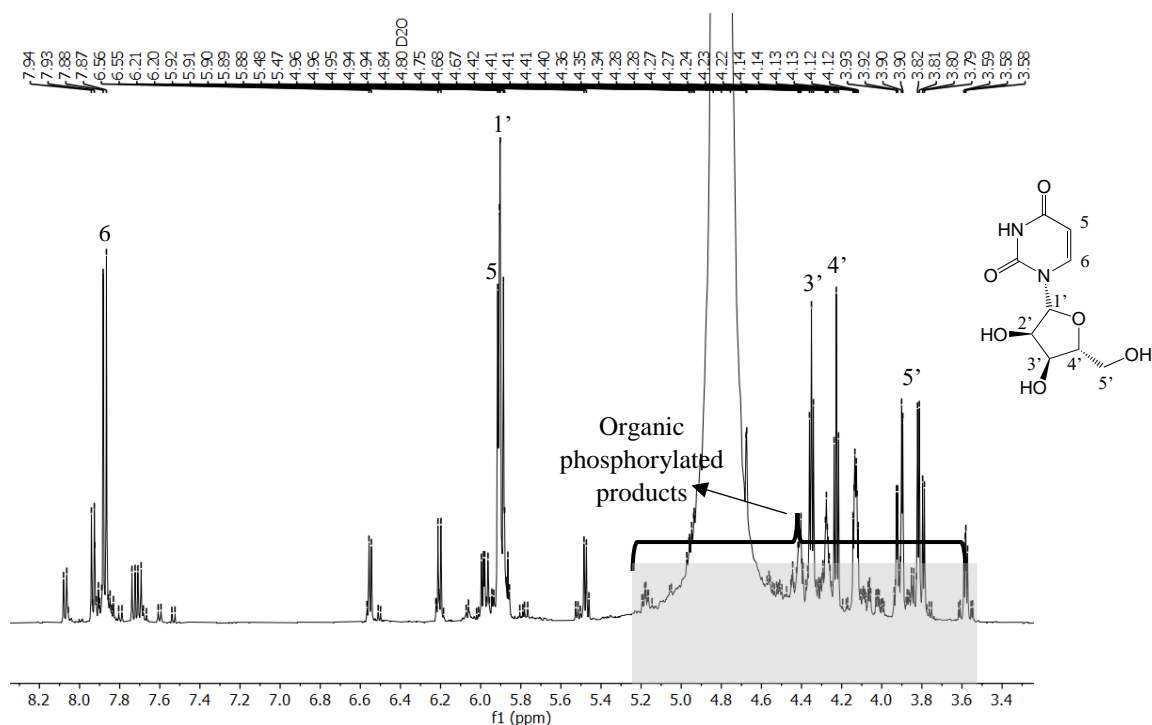


Figure 161. ^1H NMR spectrum (500 MHz) of crude mixture containing **14**, **2a** and **P_i** (1:1:1) with 0.5 eq **3a** as liquidiser, 0.5 mmol scale reaction after 120 h of heating at 115 °C, then dissolved in $\text{H}_2\text{O}/\text{D}_2\text{O} = 9:1$. δ_{H} (ppm) = ^1H NMR (500 MHz, D_2O) δ 7.87 (*d*, $J = 8.1$ Hz, 1H), 5.93 – 5.88 (*m*, 3H), 4.35 (*t*, $J = 4.9$ Hz, 1H), 4.23 (*t*, $J = 5.5$ Hz, 1H), 4.13 (*td*, $J = 4.8, 2.9$ Hz, 1H), 3.91 (*dd*, $J = 12.8, 3.0$ Hz, 1H), 3.80 (*dd*, $J = 12.8, 4.4$ Hz, 1H). Spectrum labelled with proton resonances of unreacted nucleoside.

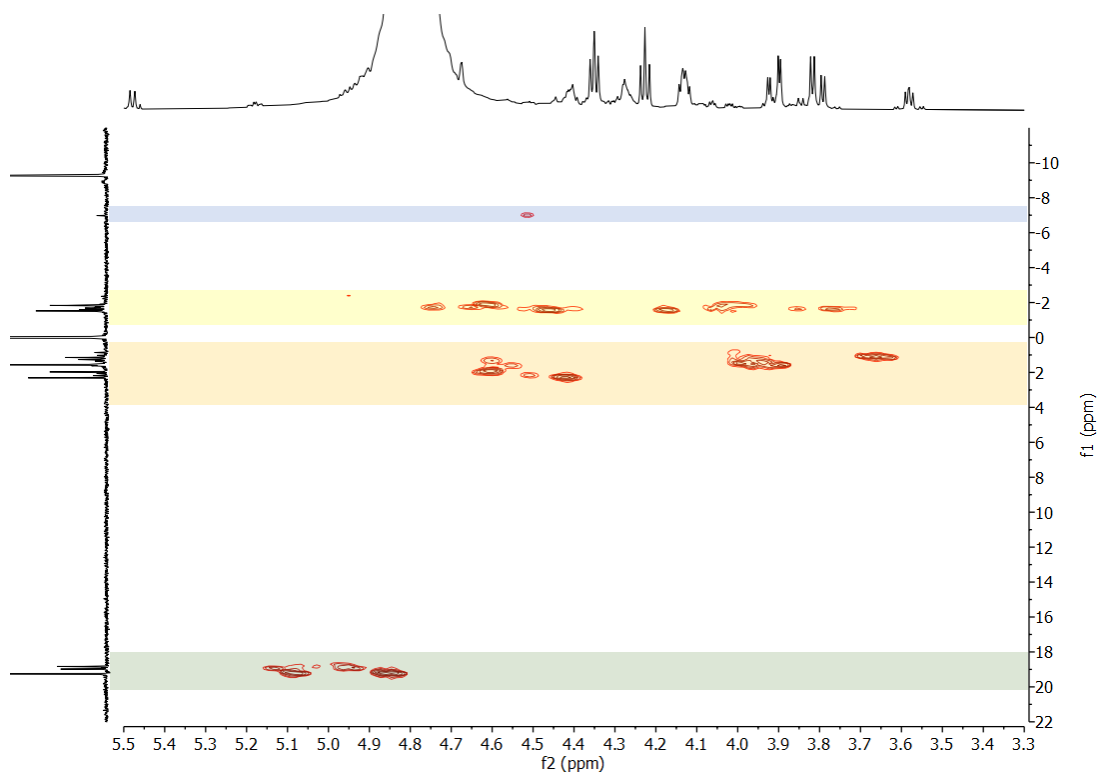


Figure 162. ^1H - ^{31}P HMBC spectrum (500 MHz for ^1H [horizontal axis], 202.5 MHz for $^{31}\text{P}\{^1\text{H}\}$ [vertical axis]) of crude mixture containing **14**, **2a** and **P_i** (1:1:1) with 0.5 eq **3a** as liquidiser, 0.5 mmol scale reaction after 120 h of heating at 115 °C, then dissolved in $\text{H}_2\text{O}/\text{D}_2\text{O} = 9:1$. Blue (**U5>p**), ochre (**Up**), yellow (**UpU**) and green (**U6>p**) zones highlight organic products of phosphorylation.

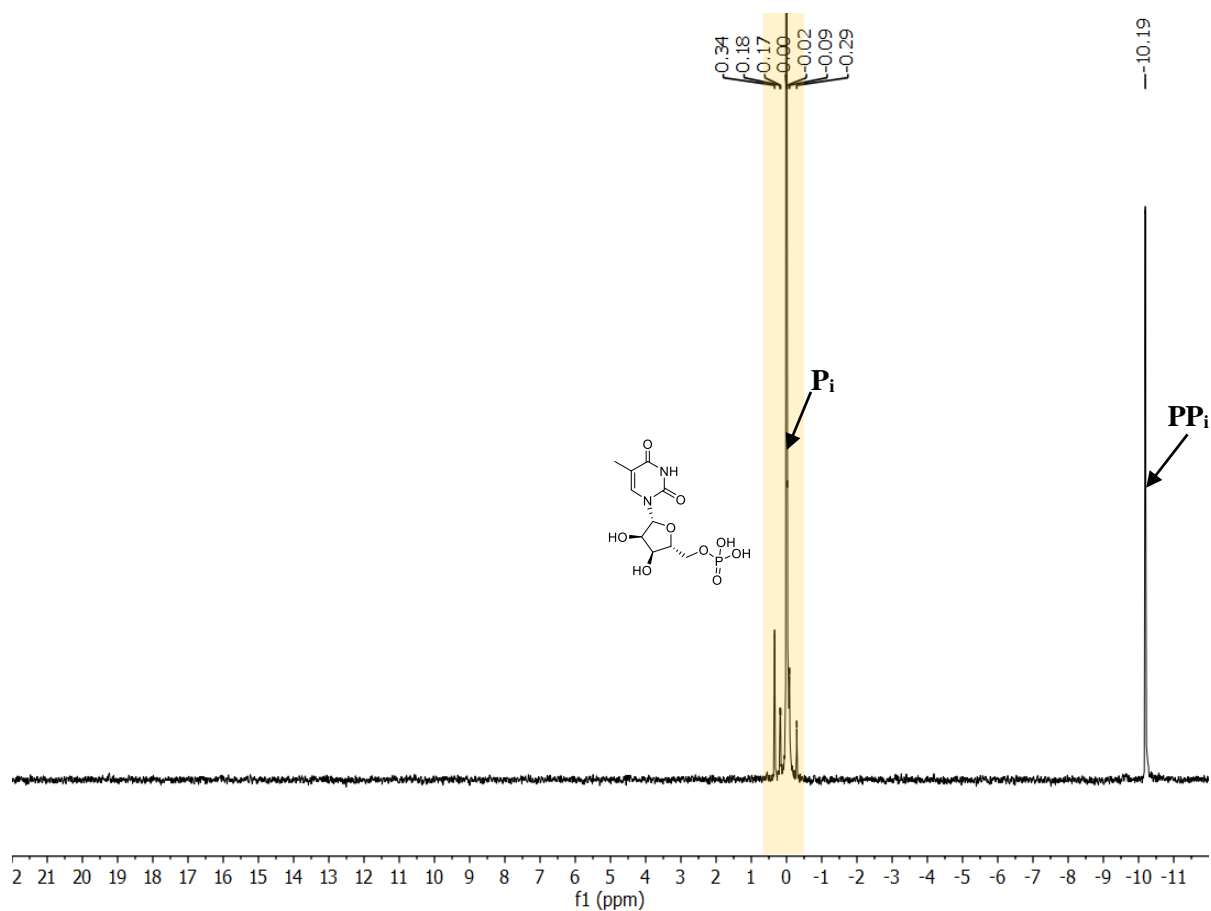


Figure 163. $^{31}\text{P}\{^1\text{H}\}$ NMR spectrum (202.5 MHz) of crude mixture containing **15**, **2a** and P_i (1:1:1) with 0.5 eq **3a** as liquidiser, 0.5 mmol scale reaction after 120 h of heating at 115 °C, then dissolved in $\text{H}_2\text{O}/\text{D}_2\text{O} = 9:1$. δ_{P} (ppm) = from 0.34 to -0.29 (5', 3' or 2' acyclic thymidine-phosphates, Tp , ochre), 0 (s, P_i), -10.19 (s, PP_i).

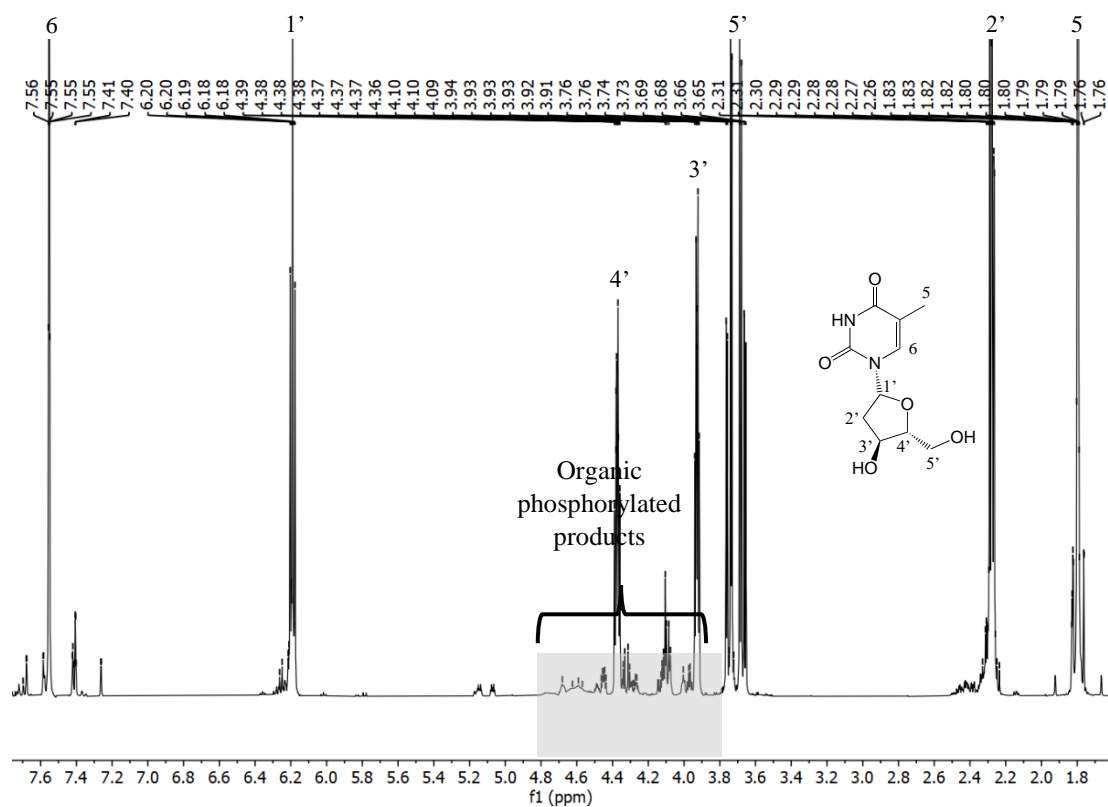


Figure 164. ^1H NMR spectrum (500 MHz, H_2O signal suppressed) of crude mixture containing **15**, **2a** and P_i (1:1:1) with 0.5 eq **3a** as liquidiser, 0.5 mmol scale reaction after 120 h of heating at 115 °C, then dissolved in $\text{H}_2\text{O}/\text{D}_2\text{O} = 9:1$. δ_{H} (ppm) = 7.55 (*q*, $J = 1.2$ Hz, 1H), 6.19 (*t*, $J = 6.8$ Hz, 1H), 4.37 (*ddd*, $J = 6.1, 4.8, 3.9$ Hz, 1H), 3.93 (*dt*, $J = 5.1, 3.7$ Hz, 1H), 3.75 (*dd*, $J = 12.5, 3.6$ Hz, 1H), 3.67 (*dd*, $J = 12.5, 5.0$ Hz, 1H), 2.30 – 2.26 (*m*, 2H), 1.80 (*d*, $J = 1.2$ Hz, 3H).

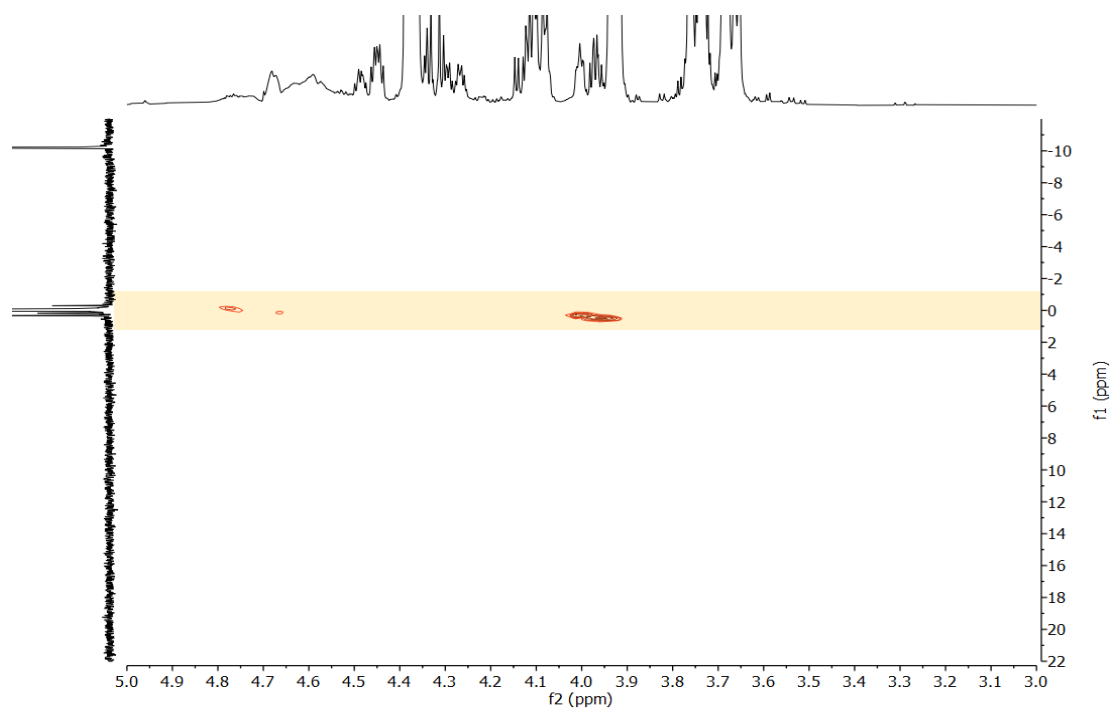


Figure 165. ^1H - ^{31}P HMBC spectrum (500 MHz for ^1H [horizontal axis], 202.5 MHz for $^{31}\text{P}\{^1\text{H}\}$ [vertical axis]) of crude mixture containing **15**, **2a** and P_i (1:1:1) with 0.5 eq **3a** as liquidiser, 0.5 mmol scale reaction after 120 h of heating at 115 °C, then dissolved in $\text{H}_2\text{O}/\text{D}_2\text{O} = 9:1$. Ochre (**TP**) zone highlights acyclic organic products of phosphorylation.

The identification of products was performed in the same manner as for glycerol and MPG. In summary, we conclude that phosphorylation was successfully achieved (**Table 50**). In the presence of urea, the total conversion of **P_i** is higher for pyrimidine rather than purines nucleosides 8-18 and 34-35 % respectively (**Figure 166**). Also, only in the case of cytidine and uridine, we obtained dinucleotides 4-7 %. There is the same tendency in reaction with cyanamide, although yields for all nucleosides are smaller than for urea (**Figure 167**). Phosphorylation experiments of adenosine (**11**) where urea (**2a**) was replaced with N-methylformamide (**3c**) or N-methylacetamide (**4c**) did not produce any organic products of phosphorylation at 115 °C.

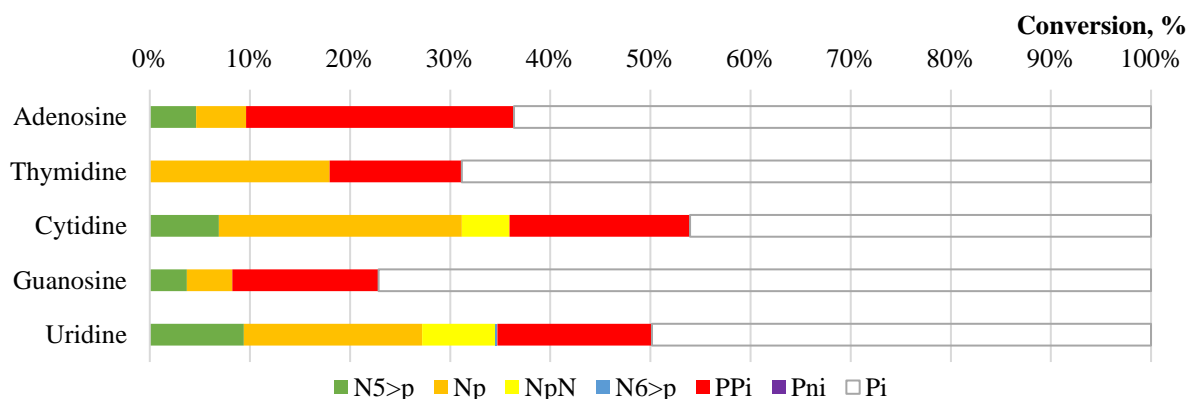


Figure 166. Summary of urea-assisted phosphorylation of nucleosides **N (11-15)** in **N:2a:P_i** (1:1:1) with 0.5 eq **3a** as liquidiser, 0.5 mmol scale reaction after 120 h of heating at 115 °C, then dissolved in H₂O/D₂O = 9:1. Percent values from signal integration of quantitative ³¹P{¹H} NMR spectra (**Figure 151-Figure 165**).

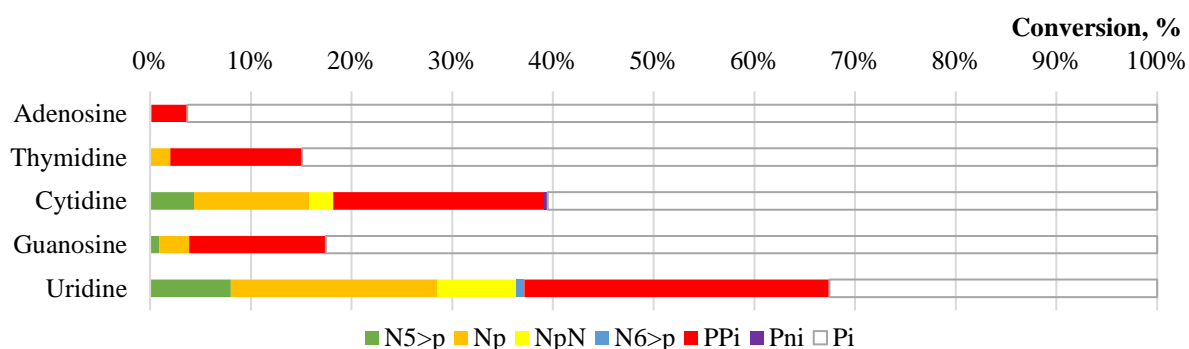


Figure 167. Summary of cyanamide-assisted phosphorylation of nucleosides **N (11-15)** phosphorylation in **N:1:P_i** (1:1:1) with 0.5 eq **3a** as liquidiser, 0.5 mmol scale reaction after 120 h of heating at 115 °C, then dissolved in H₂O/D₂O = 9:1. Percent values from signal integration of quantitative ³¹P{¹H} NMR spectra.

Table 50. Data to **Figure 166-Figure 167**. Total conversion of initial amount of **P_i** to phosphorylated organic products was calculated by subtracting inorganic compound integrals (**P_i**, **PP_i** and **P_{ni}**) from the sum of all integrated ³¹P NMR peak areas (in H₂O/D₂O = 9:1).

Condensing agent	Nucleoside	N5>p, %	Np, %	NpN, %	N6>p, %	PP _i , %	P _{ni} , %	P _i , %
2a	11	4.64	4.99	-	-	26.74	-	63.63
	12	3.70	4.54	-	-	14.62	-	77.14
	13	6.90	24.26	4.78	-	18.02	-	46.04
	14	9.41	17.78	7.32	0.19	15.46	-	49.84
	15	-	17.96	-	-	13.22	-	68.82
1	11	0.13	-	-	-	3.55	-	96.32
	12	0.91	2.98	-	-	13.57	-	82.54
	13	4.37	11.42	2.38	-	20.96	0.36	60.51
	14	8.02	20.54	7.84	0.75	30.31	-	32.54
	15	-	2.01	-	-	13.08	-	84.91

5.2.1. Temperature dependence of urea- and cyanamide-assisted adenosine phosphorylation

Comparing experimental results of adenosine phosphorylation in the presence of **2a** or **1** at 75 and 115 °C, we conclude that elevated temperatures are more favourable (**Figure 168**, **Table 51**).

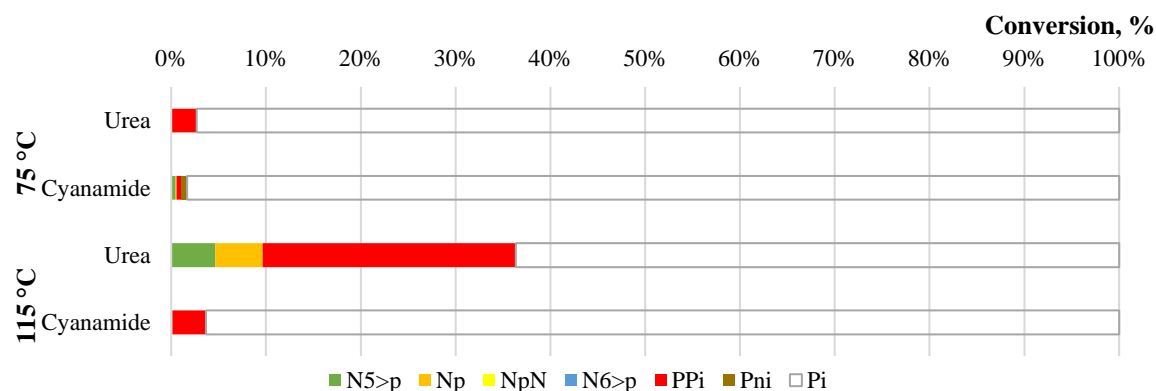


Figure 168. Summary of adenosine (**11**) phosphorylation in reaction **11:cond.agent:P_i** (1:1:1) with 0.5 eq **3a** as liquidiser, 0.5 mmol scale reaction after 120 h of heating at 75 or 115 °C, then dissolved in H₂O/D₂O = 9:1. Percent values from signal integration of quantitative ³¹P{¹H} NMR spectrum.

Table 51. Data to **Figure 168**. Total conversion of initial amount of **P_i** to phosphorylated organic products was calculated by subtracting inorganic compound integrals (**P**, and **PP_i**) from the sum of all integrated ³¹P{¹H} NMR peak areas (in H₂O/D₂O = 9:1). Products **ApA** and **A6>p** were not detected.

Temperature, °C	Condensing agent	N5>p, %	Np, %	PP _i , %	P _i , %
75	2a	-	-	2.68	97.32
	1	0.46	0.10	0.53	98.31
115	2a	4.64	4.99	26.74	63.63
	1	0.13	-	3.55	96.32

5.2.2. Effect of urea excess on phosphorylation of nucleosides

We explored the effect of excess of a condensing agent on the phosphorylation degree of nucleosides in the example of urea. In **Figure 169**, we show a stack of NMR spectra corresponding to each starting molecule (1 eq) and P_i (1 eq) in the presence of 4 eq of urea (**2a**). Each spectrum appears to be complex and more and more saturated with many different phosphorylated products.

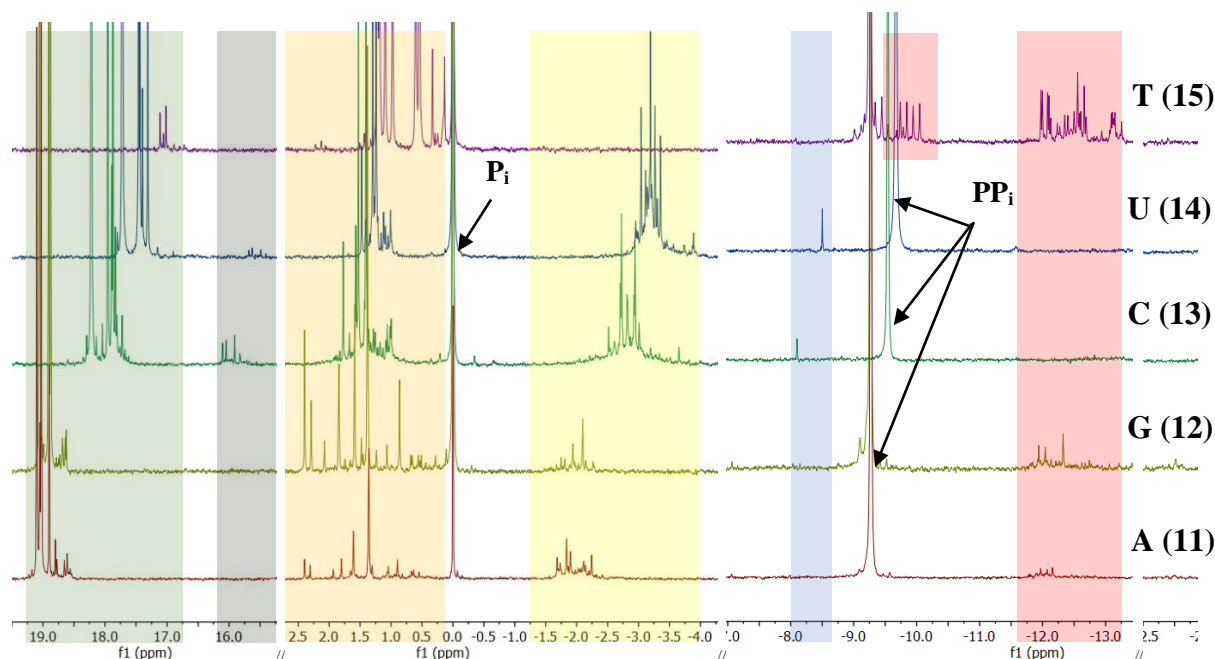


Figure 169. Stack of 1H NMR spectra (500 MHz, $H_2O/D_2O = 9:1$) of nucleoside (**N**) phosphorylations on a 0.5 mmol scale reactions of crude mixtures of **N:2a:P_i** (1:4:1) with 0.5 eq **3a** as liquidiser after 120 h of heating at 115 °C. δ_P (ppm) = 19.0-17.5 (*s*, 2',3' 5-membered ring cyclic phosphate **N5>p**, green), 16.5-15.0 (*s*, 2'3' 5-membered ring cyclic diphosphate **pN5>p**, grey, identified by analogy with intense acyclic dinucleotide signals), 2.5-0.5 (5', 3' or 2' acyclic phosphates, **Np**, ochre), 0 (*s*, **P_i**), from -1.50 to -4.0 (acyclic dinucleotide phosphates, **NpN**, yellow), from -7.0 to -8.5 (*s*, 5',3' 6-membered ring cyclic phosphate **N6>p**, blue), from -9.0 to -10.0 (*s*, **PP_i**); -9.5- -10.0 and -12- -13.5 (*n x d*, organic diphosphates **Npp**, pink); -25- -26 (*t*, organic triphosphates **Nppp**, very low quantity).

The detailed comparison for the reaction of adenosine with 4 eq of urea (**Figure 170**) demonstrates that in the excess of the condensing agent dinucleotides (yellow) and diphosphates (red) were formed, which were not detected in 1:1:1 **11:2a:P_i** ratio reactions. We also see the evolving 5-membered ring area, where more signals appear. Comparison of $^{31}P\{^1H\}$ and ^{31}P NMR provides us with a better idea about the structure of identified products (**Figure 171**). 1H and $^1H\text{-}^{31}P\{^1H\}$ are provided for more details in **Figure 172** and **Figure 173**.

The same experiments were performed for all other nucleosides, and the spectra are demonstrated for guanosine in **Figure 175-Figure 177** and thymidine **Figure 178-Figure 180**.

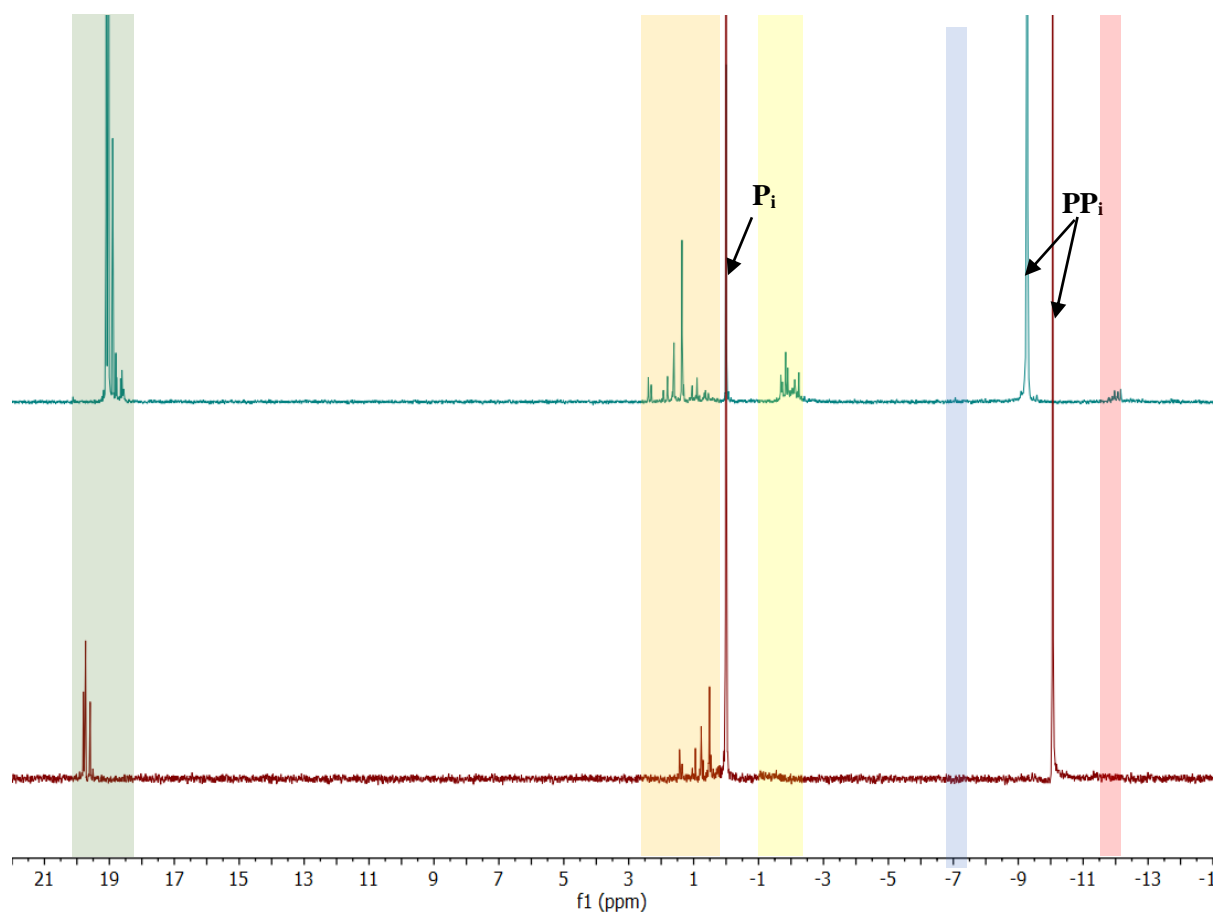


Figure 170. $^{31}\text{P}\{^1\text{H}\}$ NMR spectra (202.5 MHz, $\text{H}_2\text{O}/\text{D}_2\text{O} = 9:1$) 0.5 mmol scale reaction after 120 h of heating at 115 °C with 0.5 eq **3a** as liquidiser of crude mixtures: **Lower spectrum** – **11:2a:P_i** (1:1:1); **upper spectrum** – **11:2a:P_i** (1:4:1). δ_{P} (ppm) = 20.0-18.5 (*s*, 2',3' 5-membered ring cyclic phosphate **A5>p**, green), 2.5-0.5 (5', 3' or 2' acyclic adenosine-phosphates, **Ap**, ochre), 0 (*s*, **P_i**), from -1.50 to -2.5 (acyclic diadenosine phosphates, **ApA**, yellow), -7.0 (*s*, 5',3' 6-membered ring cyclic phosphate **A6>p**, blue), -9.0 and -10.0 (*s*, **PP_i**); -12.0 (2 x *d*, organic adenosine diphosphate **App**, pink).

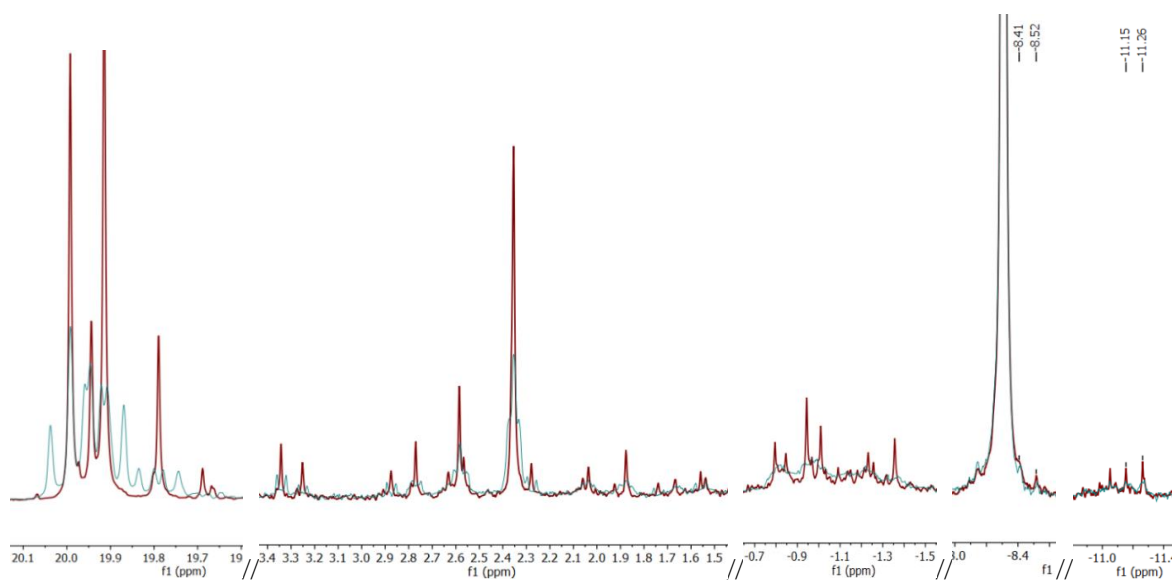


Figure 171. Selected $^{31}\text{P}\{^1\text{H}\}$ NMR signals (red, Figure 170) and ^{31}P NMR signals (blue) (202 MHz, $\text{H}_2\text{O}/\text{D}_2\text{O} = 9:1$) of organic products of 0.5 mmol scale reaction after 120 h of heating at 115 °C of crude mixture **11:2a:P_i** (1:4:1) with 0.5 eq **3a** as liquidiser.

^1H -coupled ^{31}P NMR multiplicity patterns (blue) of phosphorylated nucleosides correspond to those previous to **5** and **6** (Results and discussion section 1.1.1). However, due to the presence of higher number of similar products, the interpretation of each phosphorylated compounds is complicated. δ_{P} (ppm) = 20.1-19.7 (*s/m*, 2',3' 5-membered ring cyclic phosphates **A5>p**); 3.4-1.5 (acyclic organo-phosphates **Ap**, including *s/t* 5' and *s/d* 2' or 3' monoesters); from -0.7 to -1.5 (acyclic diester organo-phosphates **ApA**, due to many signals placed close to each other it is complicated to observe a certain multiplicity of each peak); -0.7 (not shown on the figure, 5',3' 6-membered ring cyclic phosphates **A6>p**, is too small to identify multiplicity); -8.46 and -11.21 (*d/d*, $J = 21.9$ Hz and *d/dd*, $J = 22.0$ Hz, adenosine diphosphate **App**); -8.1 and -11.05 (not identified).

LRMS of **11**, **2a** and **P_i** (1:4:1) with 0.5 eq **3a** as liquidiser, 0.5 mmol scale; reaction time 120 h under 115 ° gives us an idea about the main products (Figure 174, A). We identified cyclic and acyclic products of mono and dinucleotides; a full list suggested in Figure 174, B. The discussion starts before Figure 181.

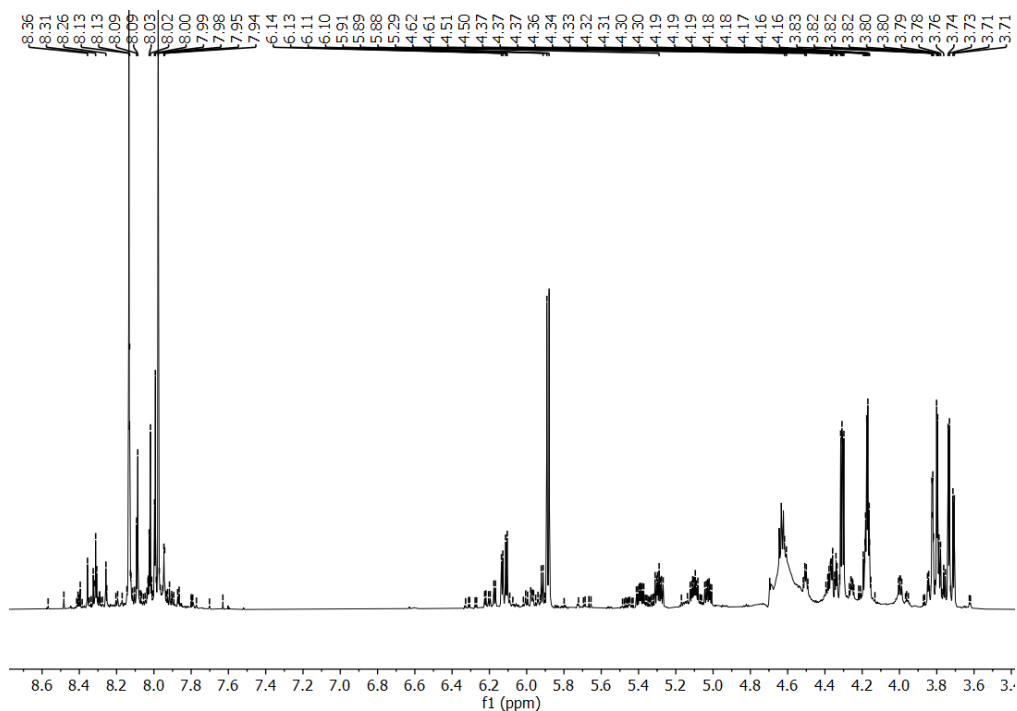


Figure 172. ^1H NMR spectrum (500 MHz, H_2O signal suppressed) of crude mixtures of reaction **11:2a:P₁** (1:4:1) with 0.5 eq **3a** as liquidiser, 0.5 mmol scale reaction after 120 h of heating at 115 °C, then dissolved in $\text{H}_2\text{O}/\text{D}_2\text{O} = 9:1$. δ_{H} (ppm) = 8.13 (*s*, 1H), 8.03 – 7.98 (*m*, 1H), 7.98 (*s*, 1H), 6.12 (*dd*, $J = 11.4, 4.0$ Hz, 1H), 5.89 (*d*, $J = 6.0$ Hz, 1H), 4.31 (*dd*, $J = 5.2, 3.4$ Hz, 1H), 4.17 (*q*, $J = 3.3$ Hz, 1H), 3.81 (*dd*, $J = 12.8, 2.7$ Hz, 1H), 3.72 (*dd*, $J = 12.9, 3.6$ Hz, 1H).

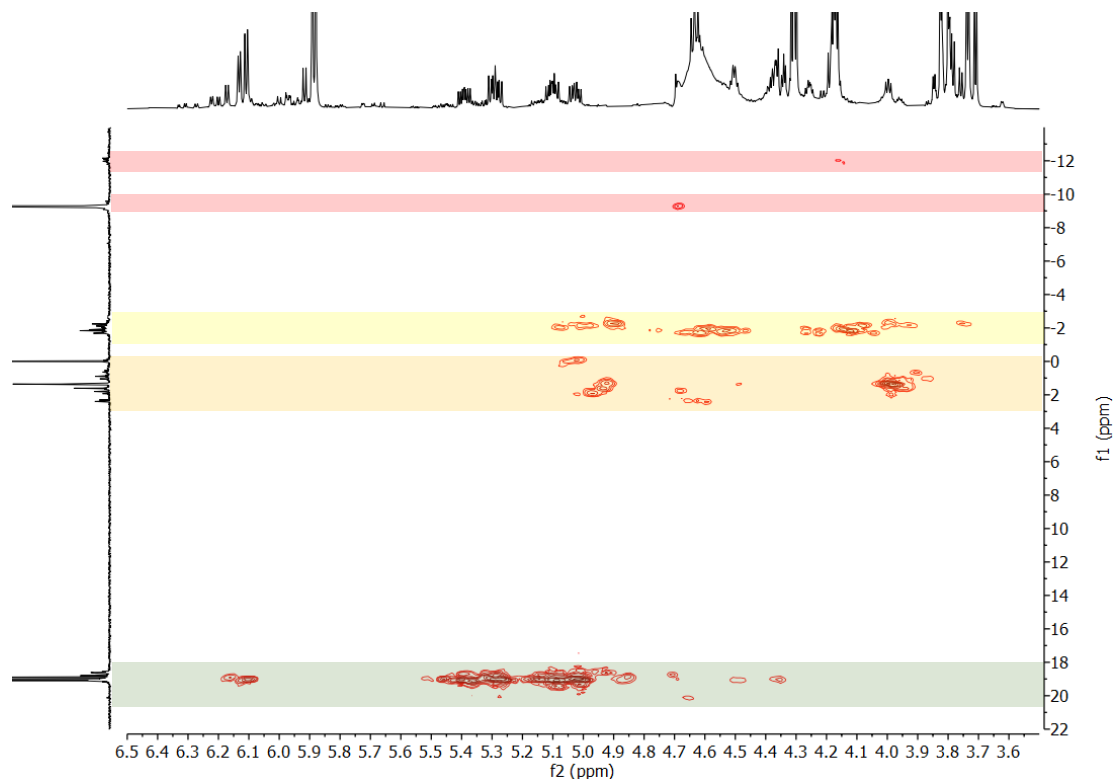


Figure 173. ^1H - ^{31}P HMBC spectrum (500 MHz for ^1H [horizontal axis], 202.5 MHz for $^{31}\text{P}\{^1\text{H}\}$ [vertical axis]) of crude mixtures of reactions **11:2a:P₁** (1:4:1) with 0.5 eq of **3a** as liquidiser, 0.5 mmol scale reaction after 120 h of heating at 115 °C, then dissolved in $\text{H}_2\text{O}/\text{D}_2\text{O} = 9:1$. Blue (**A5>p**), ochre (**Ap**), yellow (**ApA**) and pink (**App**) zones highlight organic products of phosphorylation.

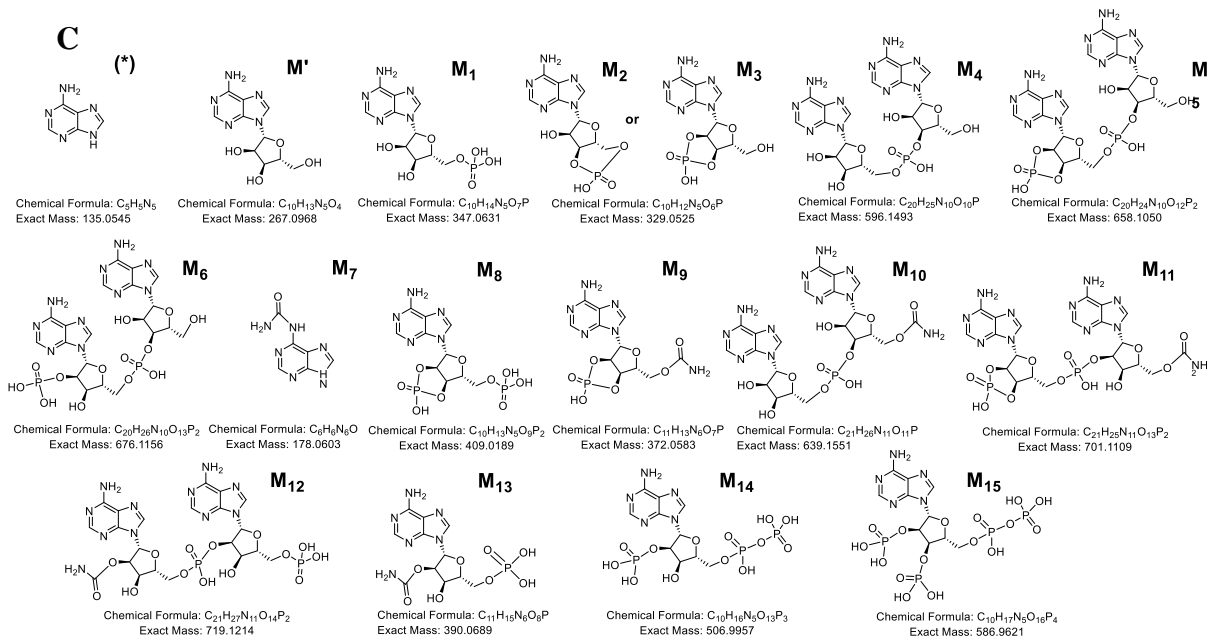
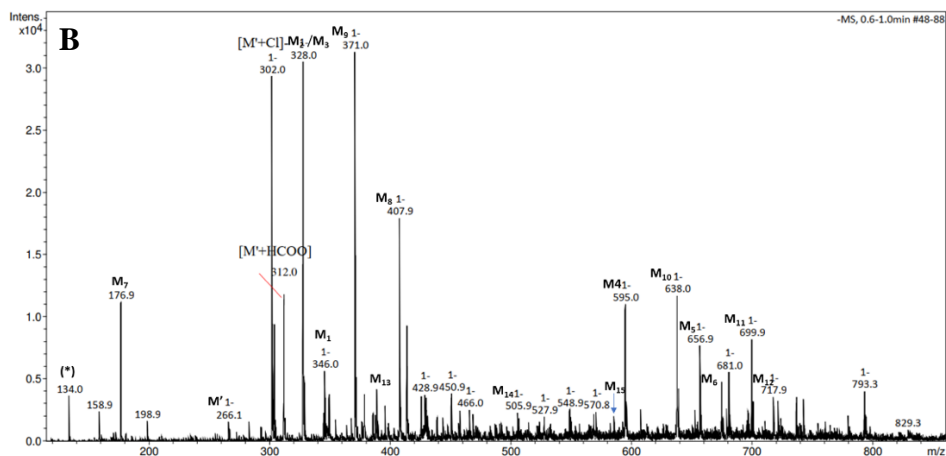
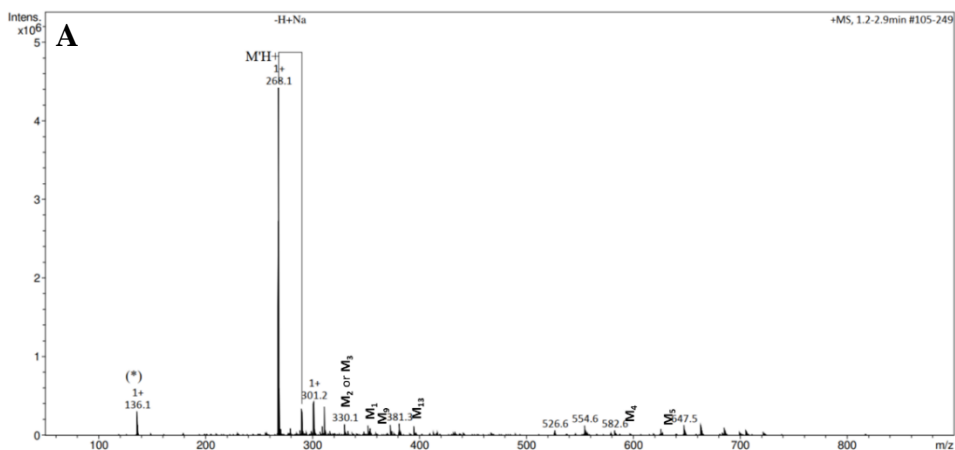


Figure 174. LRMS (direct injection) of the water extract of the crude mixture obtained by reacting **11**, **2a** and **P₁** (1:4:1) with 0.5 eq **3a** as liquidiser, 0.5 mmol scale; reaction time 120 h under 115 °C. **A** – Total ion spectrum in positive-ion mode; **B** – Total ion spectrum in negative-ion mode; **C** – Chemical structures (only the most probable isomer shown) and exact masses of the detected compounds.

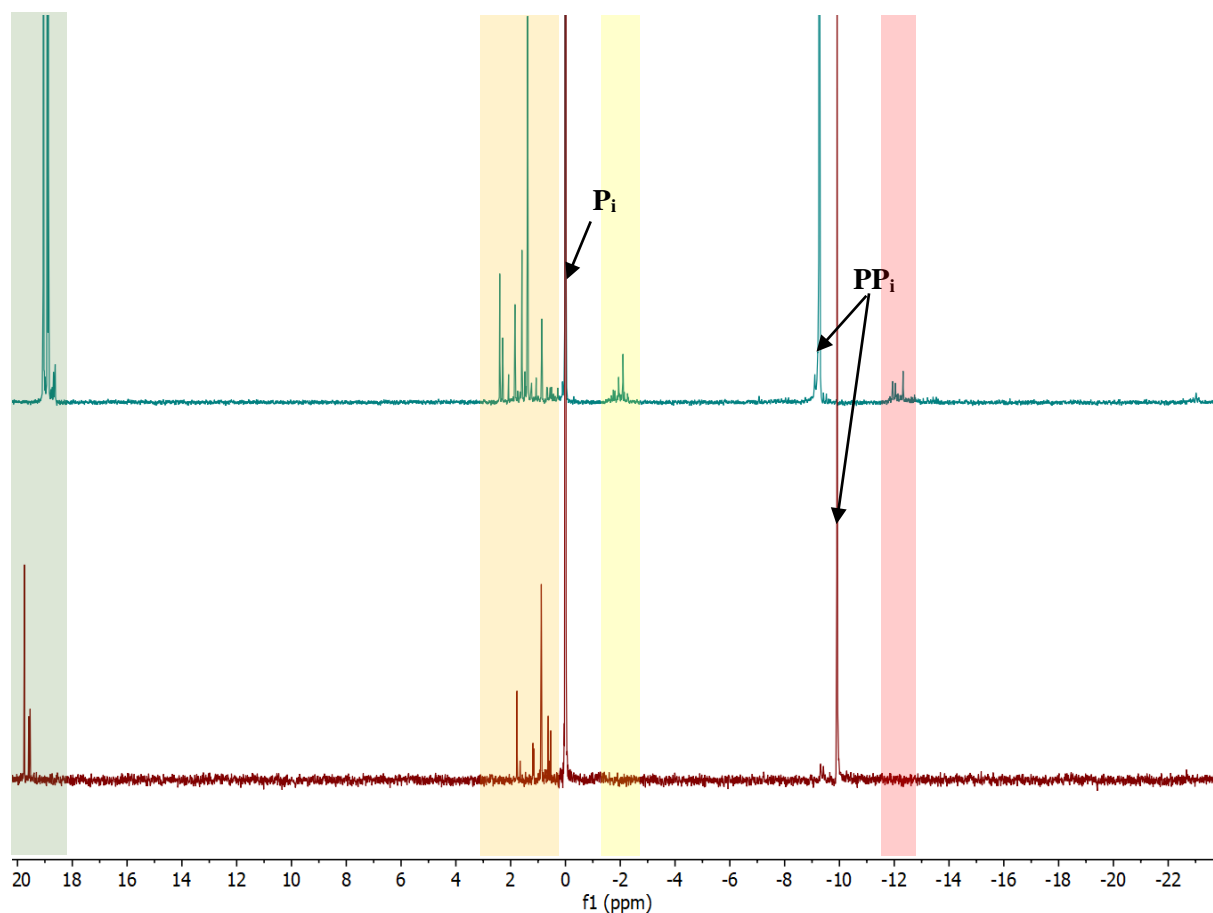


Figure 175. $^{31}\text{P}\{^1\text{H}\}$ NMR spectra (202.5 MHz, $\text{H}_2\text{O}/\text{D}_2\text{O} = 9:1$) 0.5 mmol scale reaction after 120 h of heating at 115 °C with 0.5 eq **3a** as liquidiser of crude mixtures: **Lower spectrum** – **12:2a:P_i** (1:1:1); **upper spectrum** – **12:2a:P_i** (1:4:1). δ_{P} (ppm) = 20.0-18.5 (*s*, 2',3' 5-membered ring cyclic phosphate **G5>p**, green), 2.5-0.5 (5', 3' or 2' acyclic phosphates, **Gp**, ochre), 0 (*s*, **P_i**), from -1.50 to -2.5 (acyclic diguanosine phosphates, **GpG**, yellow), -10.0 (*s*, **PP_i**). Signals that were identified only in experiment with 4 eq of **2a**: δ_{P} (ppm) = -9.47 and -11.99 (2 x *d*, *J* = 21.2 Hz, organic diphosphate **Gpp**, pink); -9.15, -12.68 and -23.02 (2 x *d* and *t*, *J* = 21.8 Hz, organic triphosphate **Gppp**).

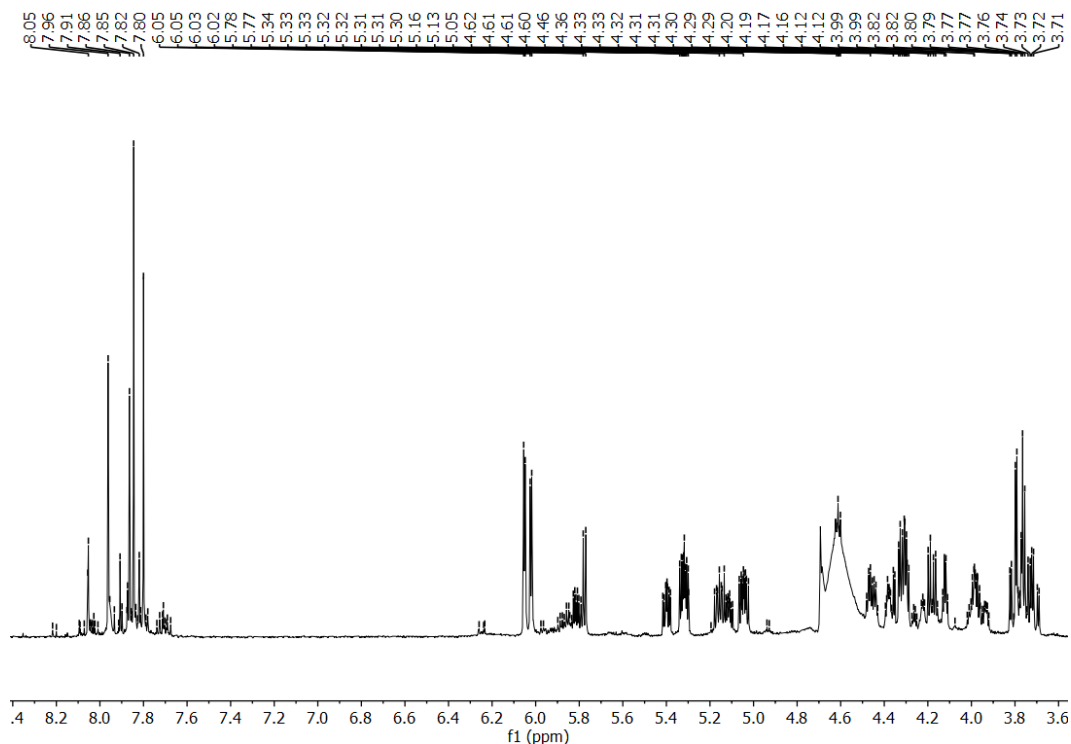


Figure 176. ^1H NMR spectrum (500 MHz, H_2O signal suppressed) of crude mixtures of reaction **12:2a:Pi** (1:4:1) with 0.5 eq **3a** as liquidiser, 0.5 mmol scale reaction after 120 h of heating at 115 °C, then dissolved in $\text{H}_2\text{O}/\text{D}_2\text{O} = 9:1$. δ_{H} (ppm) = 7.96 (s, 0H), 7.86 (s, 1H), 7.85 (s, 1H), 7.80 (s, 1H), 6.04 (dd, $J = 14.9, 3.5$ Hz, 2H), 5.83 – 5.79 (m, 1H), 5.78 (d, $J = 5.9$ Hz, 1H), 5.40 (ddd, $J = 7.8, 6.7, 3.0$ Hz, 1H), 5.35 – 5.29 (m, 2H), 5.18 – 5.12 (m, 1H), 5.04 (ddd, $J = 9.7, 6.8, 4.7$ Hz, 1H), 4.61 (t, $J = 4.5$ Hz, 0H), 4.46 (dq, $J = 12.2, 4.3$ Hz, 1H), 4.34 – 4.28 (m, 2H), 4.18 (dd, $J = 12.1, 5.1$ Hz, 1H), 4.12 (q, $J = 3.7$ Hz, 1H), 3.98 (ddd, $J = 8.2, 5.1, 4.1$ Hz, 1H), 3.81 – 3.75 (m, 2H), 3.73 (dd, $J = 8.0, 4.5$ Hz, 1H).

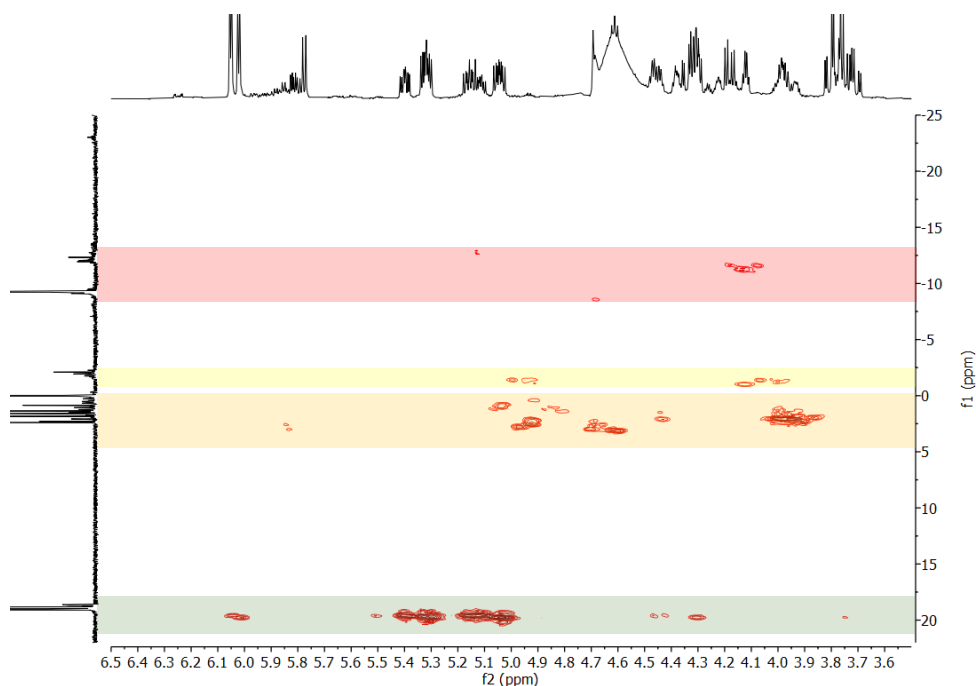


Figure 177. ^1H - ^{31}P HMBC spectrum (500 MHz for ^1H [horizontal axis], 202.5 MHz for $^{31}\text{P}\{^1\text{H}\}$ [vertical axis]) of crude mixtures of reaction **11:2a:Pi** (1:4:1) with 0.5 eq **3a** as liquidiser, 0.5 mmol scale reaction after 120 h of heating at 115 °C, then dissolved in $\text{H}_2\text{O}/\text{D}_2\text{O} = 9:1$. Blue (**G5>p**), ochre (**Gp**), yellow (**Gpp**) and pink (**Gpp**) zones highlight organic products of phosphorylation.

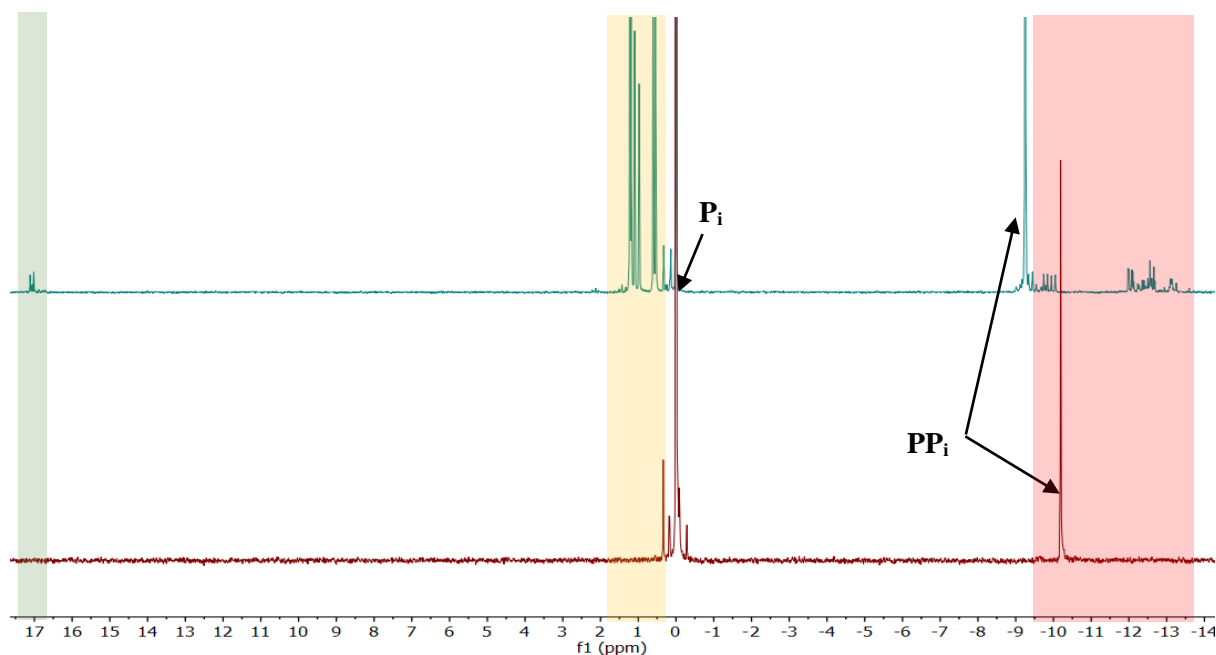


Figure 178. $^{31}\text{P}\{^1\text{H}\}$ NMR spectra (202.5 MHz, $\text{H}_2\text{O}/\text{D}_2\text{O} = 9:1$) 0.5 mmol scale reaction after 120 h of heating at 115 °C with 0.5 eq **3a** as liquidiser of crude mixtures: **Lower spectrum** – **15:2a:P_i** (1:1:1); **upper spectrum** – **15:2a:P_i** (1:4:1). δ_{P} (ppm) = 17.5-17.0 (*s*, 5-membered ring 3',4'- and 4',5'-cyclic phosphates of 2'-deoxyribose: **drib5>p**, green), 1.5-0.2 (5', 3' or 2' acyclic phosphates, **Tp**, ochre), 0 (*s*, **P_i**), -8 and -10.0 (*s*, **PP_i**). Signals that were identified only in experiment with 4 eq of **2a** organic diphosphates (**Gpp**, pink): δ_{P} (ppm) = -9.07 and -12.05 (2 x *d*, *J* = 21.1 Hz, **Tpp** and **Tpp**), -9.73 and -12.03 (2 x *d*, *J* = 21.3 Hz **Tpp** and **Tpp**), -10.00 and -12.61 (2 x *d*, *J* = 21.0 Hz **Tpp** and **Tpp**); other signals were not identified.

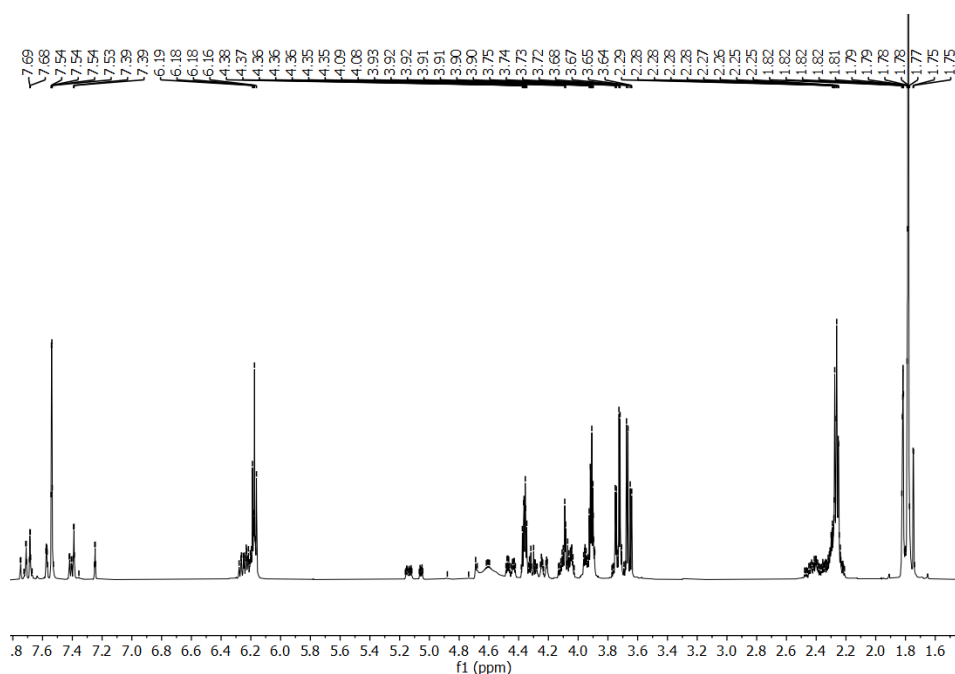


Figure 179. ^1H NMR spectrum (500 MHz, H_2O signal suppressed) of crude mixtures of reaction **15:2a:P_i** (1:4:1) with 0.5 eq **3a** as liquidiser, 0.5 mmol scale reaction after 120 h of heating at 115 °C, then dissolved in $\text{H}_2\text{O}/\text{D}_2\text{O} = 9:1$. δ_{H} (ppm) = 7.54 (*q*, *J* = 1.2 Hz, 1H), 6.18 (*t*, *J* = 6.7 Hz, 1H), 4.36 (*td*, *J* = 5.4, 4.0 Hz, 1H), 3.93 – 3.89 (*m*, 1H), 3.73 (*dd*, *J* = 12.5, 3.6 Hz, 1H), 3.66 (*dd*, *J* = 12.5, 5.0 Hz, 1H), 2.29 – 2.24 (*m*, 2H).

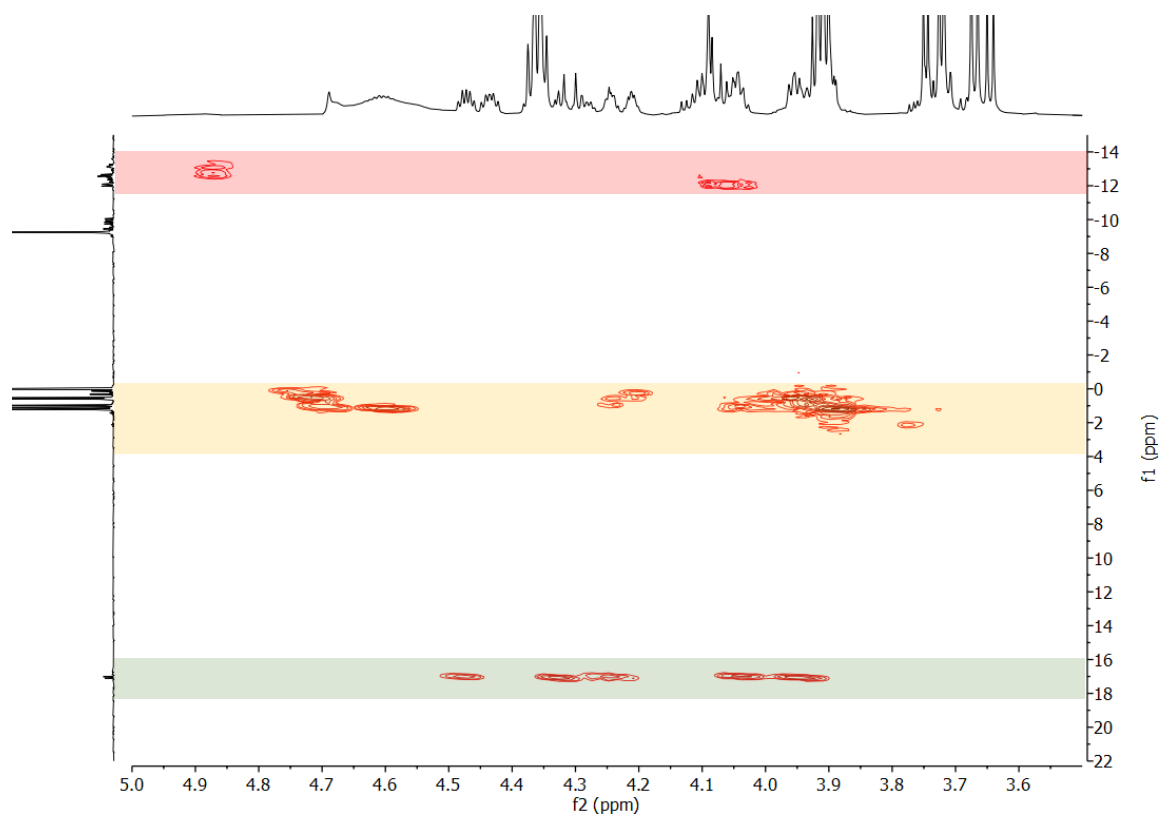


Figure 180. ^1H - ^{31}P HMBC spectrum (500 MHz for ^1H [horizontal axis], 202.5 MHz for $^{31}\text{P}\{^1\text{H}\}$ [vertical axis]) of crude mixtures of reactions **15:2a:P_i** (1:4:1) with 0.5 eq of **3a** as liquidiser, 0.5 mmol scale reaction after 120 h of heating at 115 °C, then dissolved in $\text{H}_2\text{O}/\text{D}_2\text{O} = 9:1$. Blue (**drib5>p** = 2'-deoxyribose-3',4'- and 4',5'-cyclic phosphates), ochre (**Tp**) and pink (**Tpp**) zones highlight organic products of phosphorylation.

In general, we can conclude that excess urea increases the phosphorylation yields of all types of organic products greatly. Particular interest is the formation of dinucleotides and a higher amount of cyclic phosphates, which could have potential for further polymerisation.

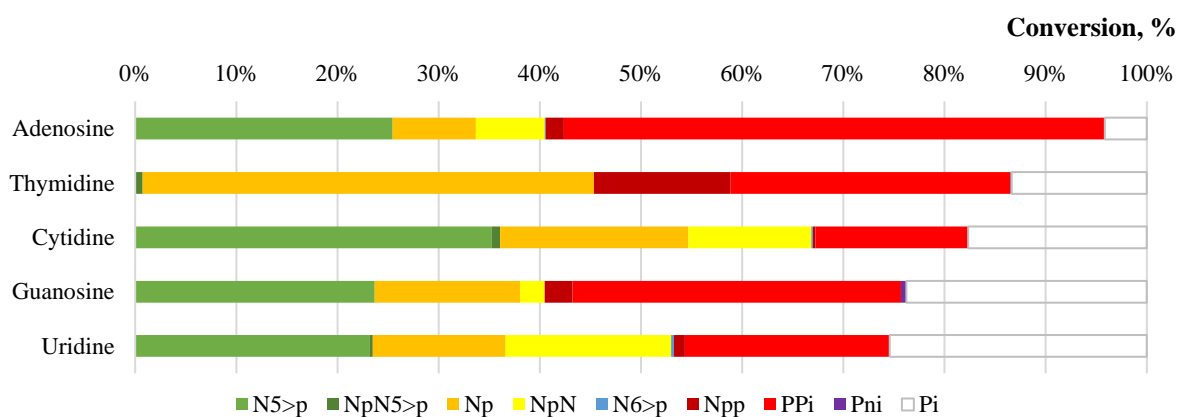


Figure 181. Summary of urea-assisted phosphorylation of nucleosides **N** (**11-15**) in **N:2a:P_i** (1:4:1) with 0.5 eq **3a** as liquidiser, 0.5 mmol scale reaction after 120 h of heating at 115 °C, then dissolved in $\text{H}_2\text{O}/\text{D}_2\text{O} = 9:1$. Percent values from signal integration of quantitative $^{31}\text{P}\{^1\text{H}\}$ NMR spectra (**Figure 169-Figure 180**). N5>p for thymidine is **drib5>p** = 2'-deoxyribose-3',4'- and 4',5'-cyclic phosphates.

Table 52. Data to **Figure 181**. Total conversion of initial amount of **P_i** to phosphorylated organic products was calculated by subtracting inorganic compound integrals (**P_i**, **PP_i** and **P_{ni}**) from the sum of all integrated ³¹P{¹H} NMR peak areas (in H₂O/D₂O = 9:1).

Nucleosid e	N5>p, %	NpN5>p, %	Np, %	NpN, %	N6>p, %	Npp, %	PP _i , %	P _{ni} , %	P _i , %
11	25.45	-	8.21	6.81	0.11	1.80	53.48	-	4.14
12	23.68	-	14.36	2.43	-	2.77	32.46	0.52	23.77
13	35.26	0.81	18.61	12.15	0.14	0.25	15.09	-	17.67
14	21.07	0.25	11.92	14.86	0.26	0.97	18.41	-	23.07
15	-	0.73	44.62	-	-	13.52	27.65	0.12	13.36

5.3. Experiments with cTMP and prebiotic minerals as a phosphorous source

Unlike in the experiment with glycerol, none of the nucleosides were sufficiently phosphorylated in the experiment with **cTMP**. The phosphate was partly converted to **P_i** and **PP_i**, but <1 % of phosphorylated organic products. An exemplary ³¹P{¹H} NMR spectrum of a crude mixture of reaction **11:2a:cTMP** (1:1:1) is demonstrated in **Figure 182**. The results of the integrations are summarised in **Figure 183** and **Table 53**.

In experiments with struvite, vivianite and the canaphite analogue, the same results were obtained, <1 % of phosphorylated organic products and a large **P_i** signal (not shown).

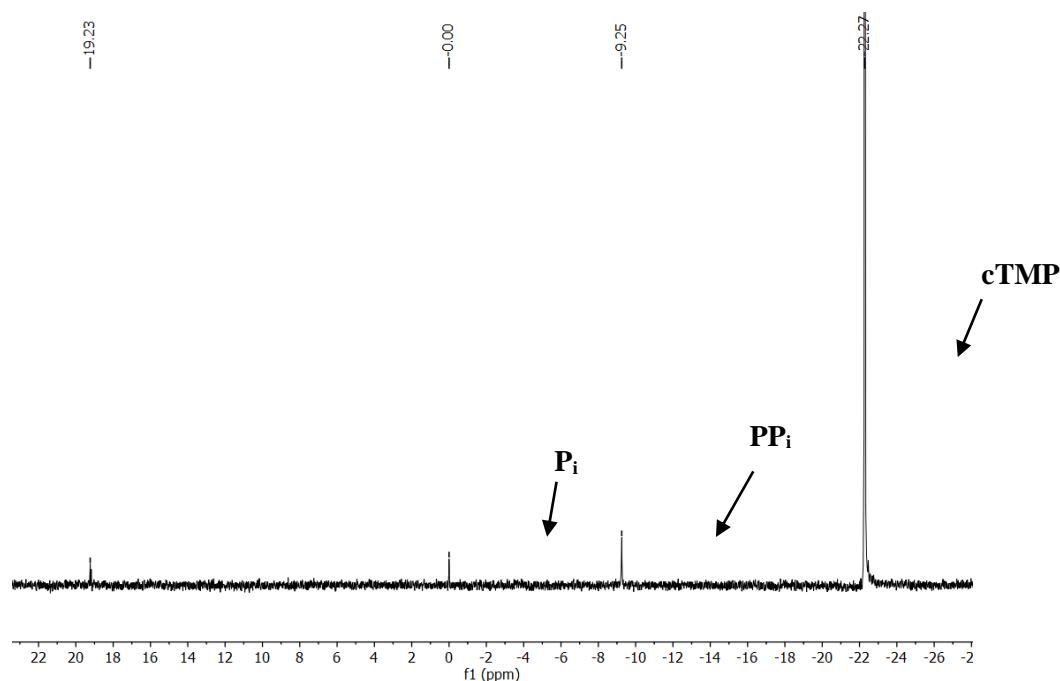


Figure 182. Exemplary ³¹P{¹H} NMR spectrum (202.5 MHz) of a crude mixture of reaction **11:2a:cTMP** (1:1:1) with 0.5 eq **3a** as liquidiser, 0.5 mmol scale reaction after 120 h of heating at 115 °C, then dissolved in H₂O/D₂O = 9:1. δ_P (ppm) = 19.23 (*s*, 2',3' 5-membered ring cyclic phosphate **A5>p**, green), 0 (*s*, **P_i**), -9.25 (*s*, **PP_i**), -22.27 (*s*, **cTMP**).

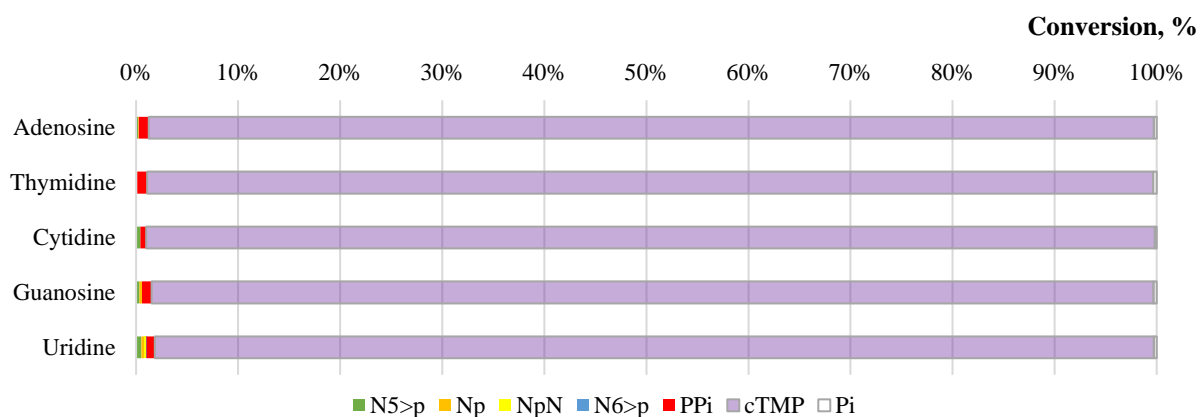


Figure 183. Summary of urea-assisted phosphorylation of nucleosides **N (11-15)** in **N:2a:cTMP (1:1:1)** with 0.5 eq **3a** as liquidiser, 0.5 mmol scale reaction after 120 h of heating at 115 °C, then dissolved in H₂O/D₂O = 9:1. Percent values from signal integration of quantitative ³¹P{¹H} NMR spectrum.

Table 53. Data to **Figure 183**. Total conversion of initial amount of **P_i** to phosphorylated organic products was calculated by subtracting inorganic compound integrals (**P_i**, **PP_i** and **cTMP**) from the sum of all integrated ³¹P{¹H} NMR peak areas (in H₂O/D₂O = 9:1).

Nucleoside	N5>p, %	Np, %	NpN, %	N6>p, %	PP _i , %	P _{ni} , %	P _i , %
11	0.19	0.07	-	-	0.99	98.47	0.28
12	0.34	0.23	-	-	0.94	98.17	0.32
13	0.42	-	-	-	0.58	98.80	0.20
14	0.51	0.28	0.19	0.04	0.80	97.91	0.27
15	-	0.11	-	-	0.97	98.58	0.34

Conclusions to the Section 5

Nucleosides were an obvious choice of plausible prebiotic alcohol to test in the phosphorylation reaction. As nucleosides remain as a solid powder under 75-115 °C, so efficient phosphorylation and interaction with other dry solid reactants (Pi, urea) required a liquidifier. I experimentally proved that the presence of water in the case of adenosine prevents phosphorylation or significantly slows it down, and that formamide is therefore the best choice as a liquidiser for those starting molecules.

In the presence of urea, the total conversion of **P_i** is higher for pyrimidine than for purines nucleosides, 8-18 and 34-35 % respectively. Also, only in the case of cytidine and uridine, we obtained dinucleotides 4-7 %. Elevated temperatures are more favourable for the phosphorylation of nucleosides. Dinucleotides and organic diphosphates were formed only with the excess of the condensing agent with respect to starting alcohol. It also increases yields of 5-membered ring organic phosphates. LRMS confirms the presence of the main products such as cyclic and acyclic mono and dinucleotides.

In experiments of phosphorylation of nucleosides with struvite, vivianite and the canaphite analogue, less than 1 % of phosphorylated organic products were produced. And unlike in the experiment with glycerol, none of the nucleosides were sufficiently phosphorylated in the experiment with **cTMP** (<1 % of organic phosphorylated products). It was partly converted into **P_i** and **PP_i**.

In general, we conclude that excess urea greatly increases the phosphorylation yields of all types of organic products, here with the formation of dinucleotides and a higher amount of cyclic phosphates, which could have potential for further polymerisation.

III Results and discussion

6. 'Messy' Chemistry

Nature is an open system (within our planet), and the chemistry on the early Earth most likely was ‘messy’ with several starting chemicals present at the same time, which makes tracking reactions more complicated. As said in the state-of-the-art chapter, there are no research papers reporting the production of phosphate and carboxylic esters in the same environment.³⁰⁸ However, this is a step that is required for the formation of membranogenic phospholipids from fatty acids, glycerol and a phosphate source. The same environment should also be favourable for nucleotide formation and their oligomerisation.

6.1. Urea-assisted phosphorylation of equimolar ‘dry’ mixtures of all ribonucleosides

After exploring the prebiotic conditions for nucleoside phosphorylation, we performed an experiment where A, C, G, and U were mixed with urea and P_i (0.25:0.25:0.25:0.25:1) with 1, 2 and 4 eq of urea (**Figure 184**). Expectedly higher amounts of 2a led to higher yields for cyclic 5-membered ring phosphates (**Figure 186, Table 54**). Other products with a relatively high excess of urea did not grow significantly. On the DOSY spectrum (**Figure 185**), we can see a molecular weight distribution with heavier molecules in the range of acyclic dinucleotides and 2',3'-cyclic nucleotides.

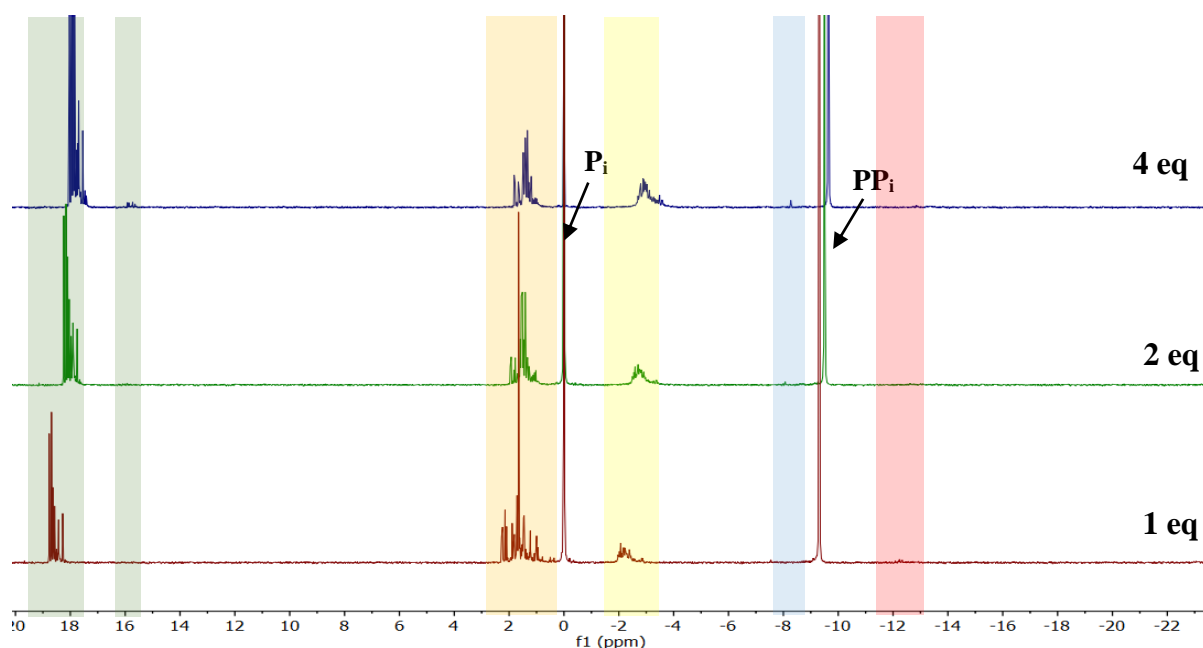


Figure 184. Stack of $^{31}P\{^1H\}$ NMR spectra (202.5 MHz, $H_2O/D_2O = 9:1$) 1 mmol scale reaction after 120 h of heating at 115 °C of crude mixtures of nucleosides **11:12:13:14:P_i** (0.25:0.25:0.25:0.25:1) with 1, 2 or 4 eq of **2a** with respect to **P_i** and 1 eq of **3a** as liquidiser. δ_P (ppm) = 19.0-17.0 (*s*, 2'3' 5-membered ring cyclic phosphate **N5>p**, green), 16.0-15.5 (*s*, 2'3' 5-membered ring cyclic diphosphate **pN5>p**, dark green), 2.5-0.5 (*s*, 5', 3' or 2' acyclic phosphates, **Np**, orange), 0 (*s*, **P_i**), from -2.0 to -3.5 (acyclic dinucleoside phosphates, **NpN**, yellow), from -7.0 to -8.5 (*s*, 5'3' 6-membered ring cyclic phosphate **N6>p**, blue), -9.5 (*s*, **PP_i**); -12.0 to -13.5 (*n x d*, organic diphosphates **Npp**, red).

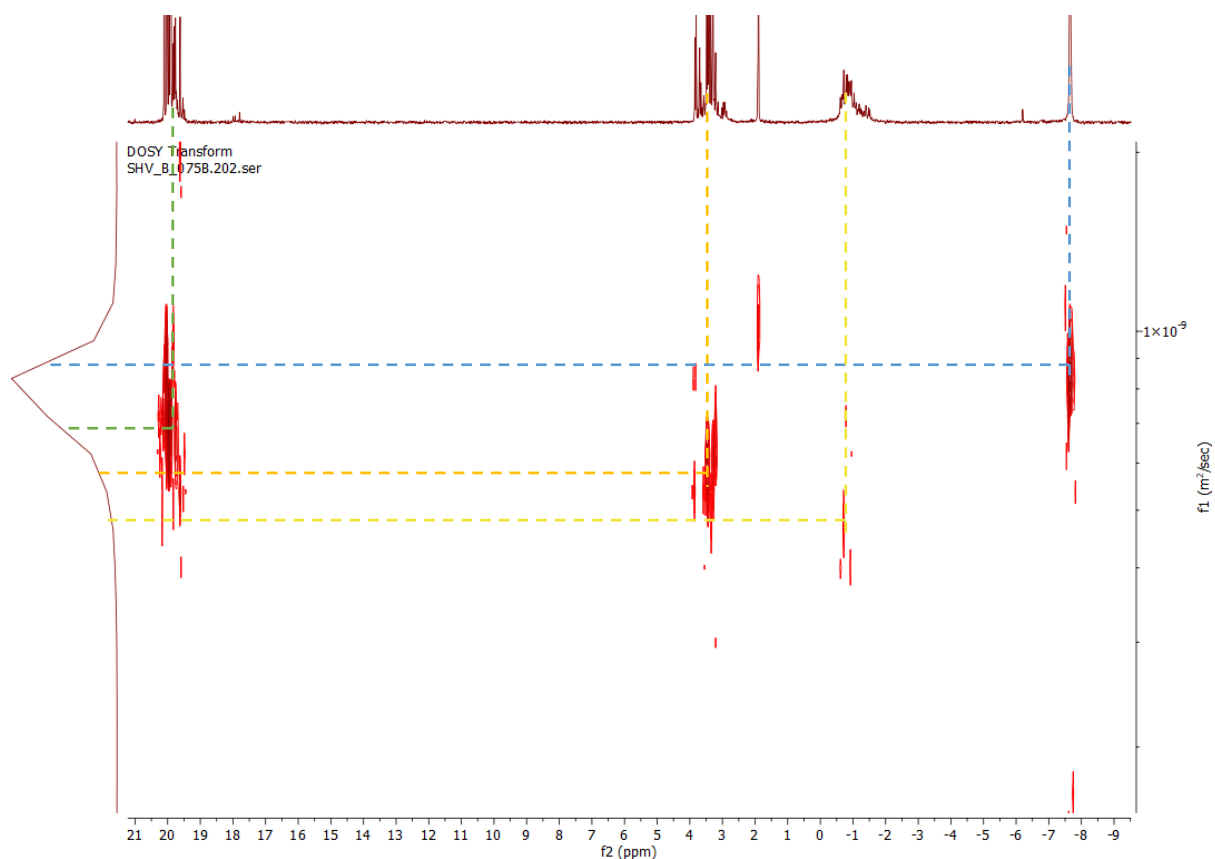


Figure 185. Stack $^{31}\text{P}\{^1\text{H}\}$ DOSY NMR (LED with decoupling during acquisition, acqu par : p30=2,5ms D20=150ms 16 increments, 128 scans, RD=5s expt=3h proc par : 2 zero fillings, ILT), (202.5 MHz, D_2O) of crude mixture containing 1 eq nucleosides (**11:12:13:14** 0.25:0.25:0.25:0.25), 4 eq **2a** and 1 eq **P_i**, 4 mmol scale reaction after 120 h of heating at 115 °C, then dissolved in D_2O .

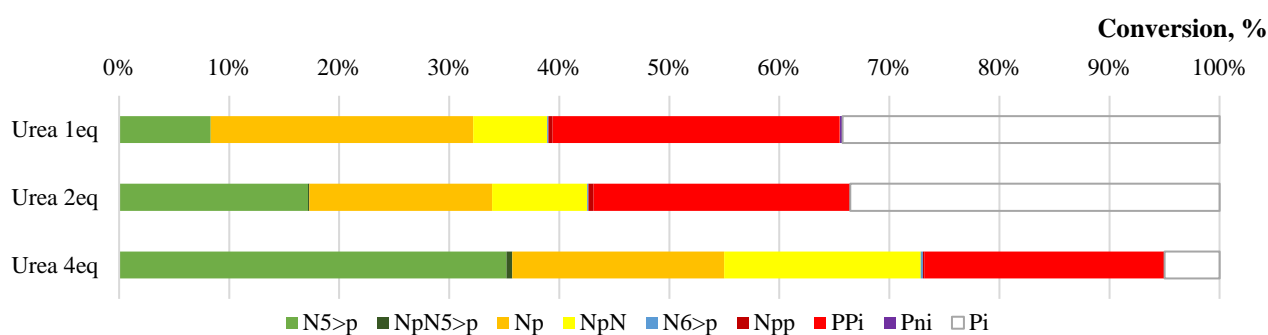


Figure 186. Summary of nucleosides mixture phosphorylation **11:12:13:14:P_i** (0.25:0.25:0.25:0.25:1) with 1, 2 or 4 eq **2a** with respect to **P_i** and 1 eq **3a** as liquidiser. 1 mmol scale reaction after 120 h of heating at 115 °C, then dissolved in $\text{H}_2\text{O}/\text{D}_2\text{O} = 9:1$. Percent values from signal integration of quantitative $^{31}\text{P}\{^1\text{H}\}$ NMR spectra (Figure 184).

Table 54. Data to **Figure 186**. Total conversion of initial amount of **P_i** to phosphorylated organic products was calculated by subtracting inorganic compound integrals (**P_i**, **PP_i** and **P_{ni}**) from the sum of all integrated ³¹P{¹H} NMR peak areas (in H₂O/D₂O = 9:1).

Amount of cond. agent 2a, eq	N5>p, %	NpN5>p, %	Np, %	NpN, %	N6>p, %	Npp, %	PP _i , %	P _{ni} , %	P _i , %
1	8.32	-	23.86	6.72	0.11	0.37	26.1	0.26	34.26
2	17.16	0.11	16.62	8.63	0.12	0.46	23.34	-	33.56
4	35.21	0.53	19.24	17.86	0.20	0.12	21.84	-	5.00

6.1.1. HPLC-HRMS analysis of urea-assisted phosphorylation of a dry equimolar mixture of all ribonucleosides

The promising experiment where **A**, **C**, **G** and **U** were mixed with urea and Pi (0.25:0.25:0.25:0.25:4:1) in the presence of 0.5 eq of formamide was studied by HPLC (**Figure 187, A**) and LC-MS (**Figure 187, B**) to obtain a better understanding of the types of products and their relative quantities with respect to the starting molecules, nucleosides. We were able to identify 55 signals and even more compounds contained in this crude mixture (**Table 55**). The main groups of products are displayed in **Figure 188**.

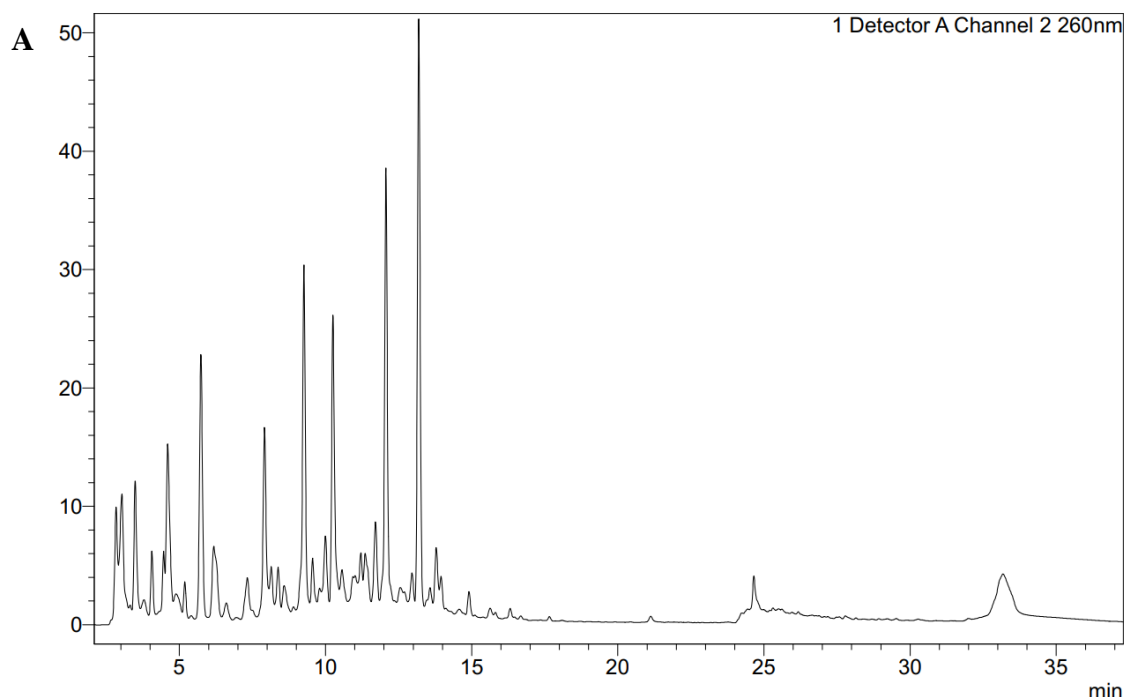


Figure continues on the next page

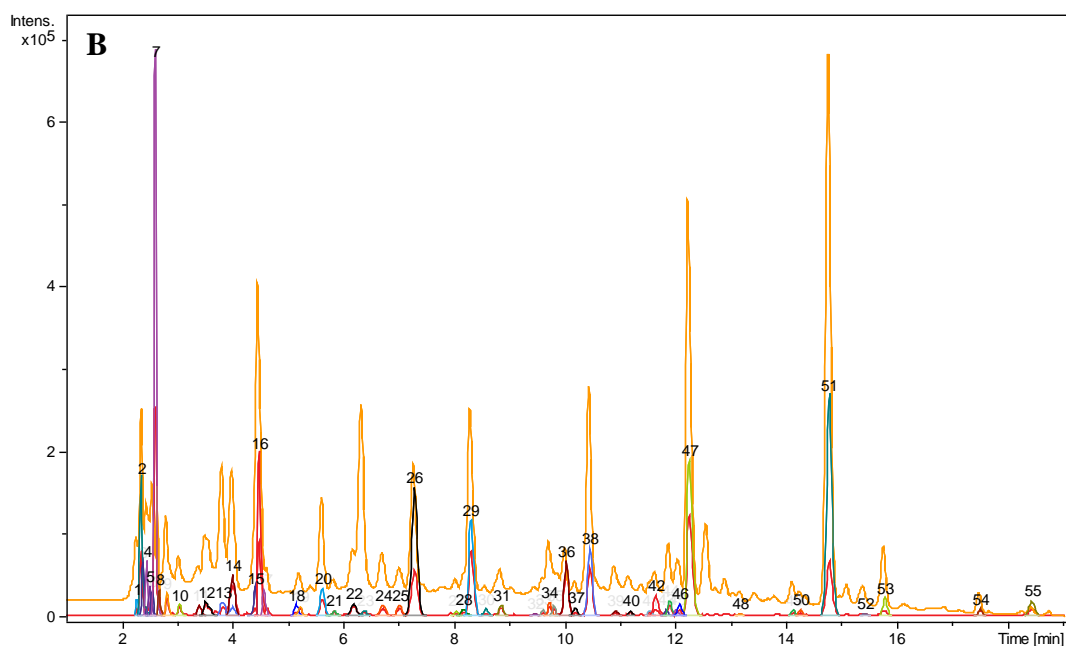


Figure 187. Chromatogram of H₂O extract of a 1 mmol scale mixture of **11:12:13:14:2a:P_i** (0.25:0.25:0.25:0.25:1:1 molar ratios) with 1 eq **3a** as liquidiser, heated neat at 115 °C for 120 h. **A** – UV(260 nm)-detected reversed-phase chromatogram, R_T = 0-37.5 min; **B** – RPHPLC-HRMS in negative ion mode of the same run: yellow – UV chromatogram (260 nm), R_T = 0-17.5 min, colored peaks – ion-extracted signals.

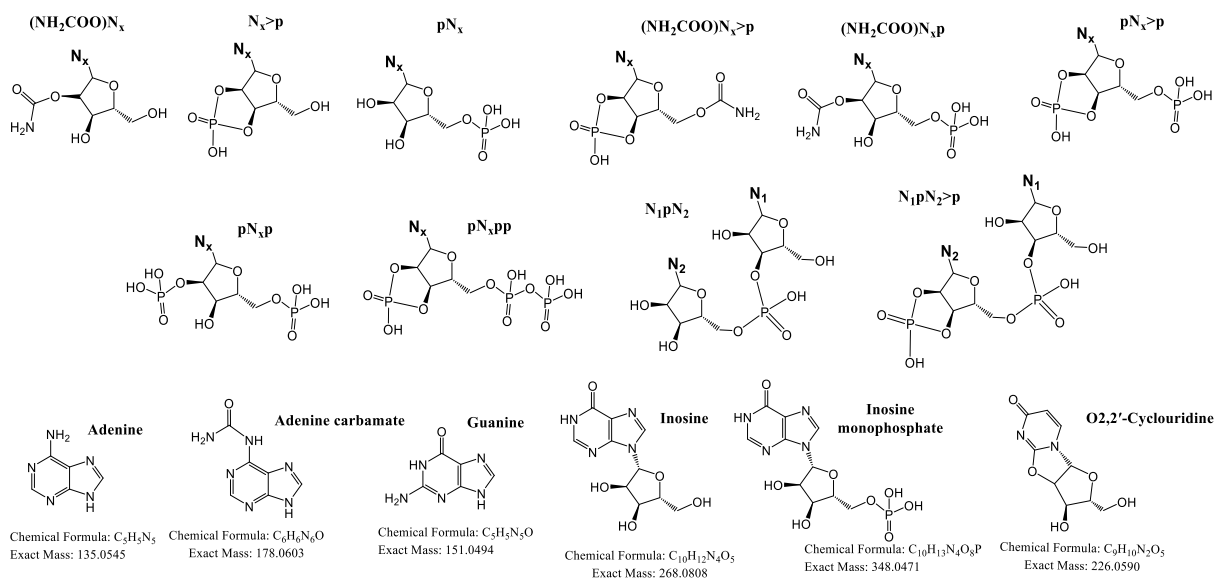


Figure 188. Chemical structures (only the most probable isomer shown) and exact masses of the main compounds each representing a group as detected by HPLC-HRMS (**Figure 187**, **Table 55**).

Table 55-1. Interpretation of HPLC-HRMS of **Figure 187** with suggested formulas, intensities and signal/noise ratio. Ion for all listed masses is $[M-H]^-$, if not specified otherwise. Calculations of yields were made with taking into a count extinction coefficient for purine and pyrimidine nucleobase^{291,292}. For the single peaks on chromatogram that correspond to two or more m/z peaks we counted as all molecules has equivalent amounts (for example Compound **1** showing area 1.14 and three molecules, so I assume that integral of each molecule is $1.14/3=0.38$).

Number of peaks	Compound	RT, min	Area (abs)	Area, %	Intensity (UV)	S/N
1	pGp, pCp, pUp	2.3	440.96	1.14	95	2038.5
2, 3	pC>p, pU>p, pAp,	2.4	1214.44	3.15	298	6364.8
4	pG>p, pGpp	2.5	804.12	2.08	179	3835.7
5, 6	pC, pU	2.6	815.47	2.11	178	3813.6
8	U>p, pA>p,	2.7	814.04	2.11	206	4401.6
9	pG	2.9	752.75	1.95	131	2809.9
10	pU	3.1	358.37	0.93	46	978.3
11	pU	3.4	369.23	0.96	52	1107
12	pA	3.6	852.38	2.21	81	1729.8
13	C>p	3.9	855.43	2.22	121	2593.2
14	C>p	4	1114.13	2.89	145	3120.5
15, 16	cU, U>p, UpU>p*	4.5	3127.07	8.10	586	12536.8
17	UpU>p	4.7	285.09	0.74	49	1056.4
18, 19	pI	5.3	237.37	0.62	29	620.2
20	C	5.7	746.52	1.93	110	2350.1
21	pG	5.9	287.68	0.75	30	638.3
22	pA	6.2	504.25	1.31	62	1320.7
23	guanine	6.4	680.86	1.76	76	1618.6
24	C>p	6.7	437.78	1.13	49	1037.6
25	(NH ₂ COO)U>p	7	498.13	1.29	49	1052.9
26	U	7.3	1713.94	4.44	240	5143.4
27	G	8.1	196.24	0.51	31	669.7
28	CpG>p, UpG>p,	8.2	207.25	0.54	42	909
29	G>p, GpG>p*	8.3	2668.66	6.92	402	8587.3
30	U	8.6	216.43	0.56	21	457.7
31	(NH ₂ COO)G>p	8.9	575.07	1.49	61	1302.6
32	-	9.5	165.79	0.43	21	457.4
33	UpG>p	9.6	234.9	0.61	39	827.6
34	I, pA, (NH ₂ COO)Ap, GpC	9.7	588.06	1.52	80	1697.8
35	U>p, G>p	9.5	296.41	0.77	104	2193.5
36	adenine, C	10	503.76	1.31	64	1366.8
37	(NH ₂ COO)G	10.2	225.83	0.59	26	563.6
38	G	10.5	2563.39	6.64	367	7839.2
39	ApC>p, ApU>p	10.9	539.99	1.40	51	1084.7
40	ApG>p	11.2	310.25	0.80	28	599.4
41	I, ApG>p	11.6	222.37	0.58	39	832.9
42	(NH ₂ COO)U	11.7	431.45	1.12	55	1184.8
43, 44	UpU, ApG, (NH ₂ COO)A>p	11.9	634.37	1.64	82	1756.6

Table 55-2. Interpretation of HPLC-HRMS of **Figure 187** with suggested formulas, intensities and signal/noise ratio.

Number of peaks	Compound	R _t , min	Area (abs)	Area, %	Intensity (UV)	S/N
45, 46	ApU>p, (NH ₂ COO)G, C>p	12.1	619.64	1.61	78	1650
47	A>p	12.3	3613.41	9.36	524	11199.5
48	GpU	13.2	217.35	0.56	28	592.5
49	A>p, ApA>p*	14.1	266.15	0.69	37	792.6
50	ApU	14.3	181.33	0.47	27	584
51	A	14.8	4870.2	12.62	715	15292.4
52	ApG	15.4	387.13	1.00	35	767.2
53	(NH ₂ COO)A, ApU	15.8	647.98	1.68	86	1848.6
54	ApA	17.5	191.68	0.50	29	612.4
55	(NH ₂ COO)Ade	18.4	104.35	0.27	11	242.7

* Dinucleotide corresponds to the same mass as adduct of cyclic monophosphate [2M-H]⁻

Such a detailed and differentiative analysis provided a lot of information. The conversion of starting molecules reaches 75.64 % and the majority of phosphorylated products are 2',3'-cyclic 37 % and acyclic 10 % mononucleotides (**Figure 189, Table 56**).

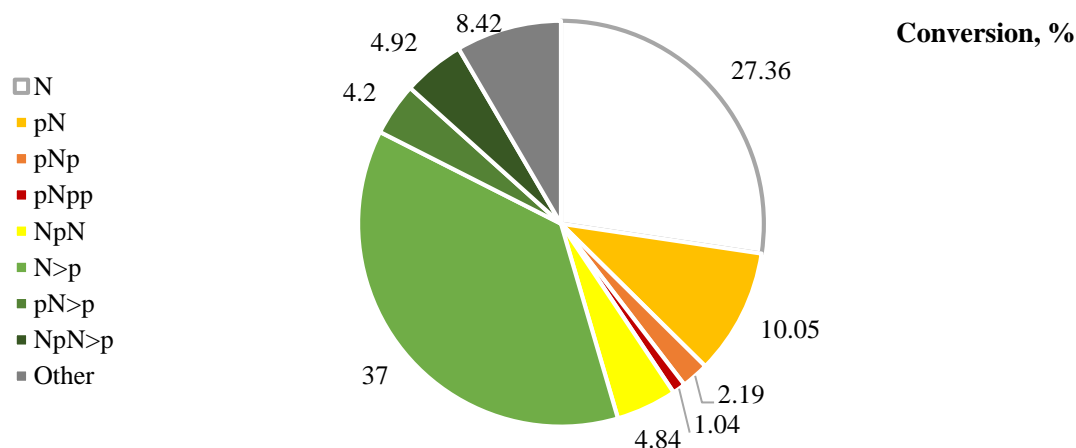


Figure 189. Summary of product distribution obtained from the urea-assisted phosphorylation of ribonucleoside mixture **11:12:13:14:2a:P₁** (0.25:0.25:0.25:0.25:1:4) and 1 eq **3a** as liquidiser. 1 mmol scale reaction after 120 h of heating at 115 °C, analysed by HPLC-HRMS. Percent values from signal integration of UV chromatogram (**Figure 187-B**).

Table 56. Data to **Figure 189** Calculations of yields were made by taking into account the difference in extinction coefficient for purine and pyrimidine nucleosides.^{291,292} Total conversion of initial number of nucleosides to phosphorylated and other organic products was calculated by subtracting not reacted nucleoside integrals (N) from the sum of all integrated peak areas (in H₂O).

Type of product	N	pN	N>p	pNp	pN>p	pNpp	NpN	NpN>p	Other
Conversion, %	27.36	10.05	37.00	2.19	4.20	1.04	4.84	4.92	8.42

Nucleosides were converted not only to organic phosphates but also to inosine hydrolysed from A. There is a slight unbalance at the end of the reaction between the equivalent amount of starting nucleotides and the predominance of uridine and adenosine against cytidine and guanosine (**Figure 190**, **Figure 191** and

Table 57).

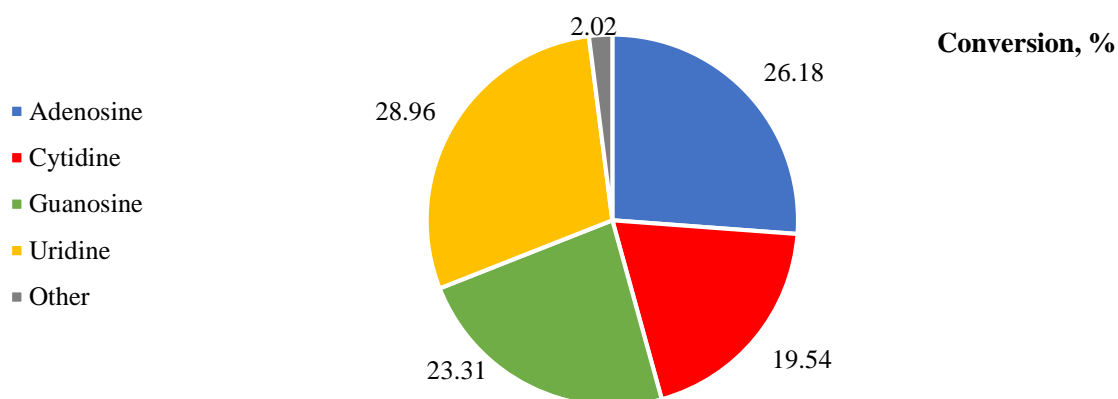


Figure 190. Summary of $^{31}\text{P}\{^1\text{H}\}$ signal intensity distribution depending on nucleobase obtained from crude mixture **11:12:13:14:2a:P_i** (0.25:0.25:0.25:0.25:1:4) with 1 eq **3a** as liquidiser. 1 mmol scale reaction after 120 h of heating at 115 °C, analysed by HPLC-HRMS. Percent values from signal integration of UV chromatogram (**Figure 187-B**).

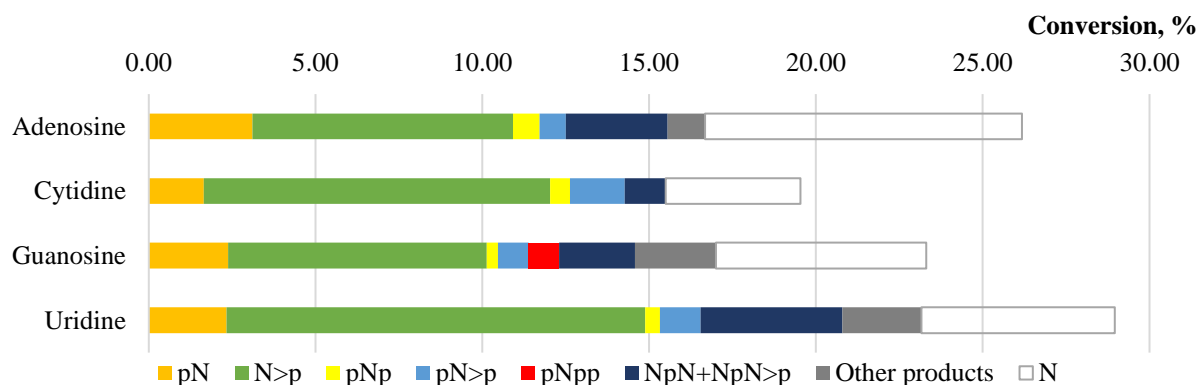


Figure 191. Summary of product distribution obtained from the urea-assisted phosphorylation of equimolar ribonucleoside mixture **11:12:13:14:2a:P_i** (0.25:0.25:0.25:0.25:1:4) with 1 eq **3a** as liquidiser. 1 mmol scale reaction after 120 h of heating at 115 °C, analysed by HPLC-HRMS. Percent values from signal integration of UV chromatogram (**Figure 187-B**).

Table 57. Data to **Figure 191**. Calculations of yields were made by taking into account the difference in extinction coefficient for purine and pyrimidine nucleosides.^{291,292} Total conversion of initial number of nucleosides to phosphorylated and other organic products was calculated by subtracting not reacted nucleoside integrals (N) from the sum of all integrated peaks (in H₂O).

Nucleoside	pN, %	N>p, %	pNp, %	pN>p, %	pNpp, %	NpN+NpN>p, %	Other products, %	N, %
11	4.28	10.60	1.05	1.06	-	3.45	1.49	12.62
12	2.70	8.80	0.38	1.04	1.04	2.58	2.75	7.15
13	1.06	6.78	0.38	1.05	-	0.65	-	2.59
14	2.02	10.83	0.38	1.05	-	3.66	2.05	5.00

The results of quantification of the same crude mixture by ³¹P{¹H} NMR and LC-MS appeared to be comparable with certain assumptions, such as shown in the same category PPI and other not phosphorylated products (**Figure 193, Table 58**). We could not obtain long oligonucleotide chains, but only dinucleotides. Although this attempt seems to be a first step towards “messy” chemistry.

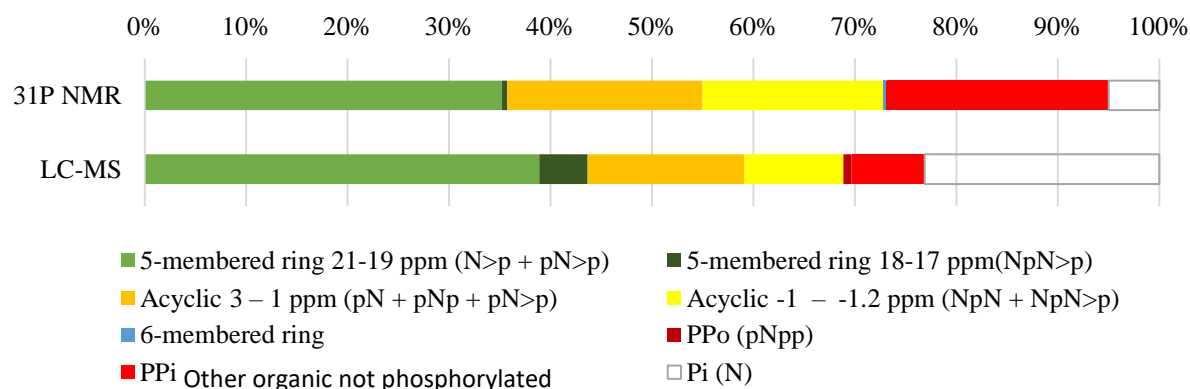


Figure 192. Comparison of product yields obtained by two different analytical methods, ³¹P{¹H} NMR (data from **Figure 184-Figure 186, Table 54**) and HPLC-MS (**Figure 187, Table 56**) of reaction **11:12:13:14:2a:P_i** (0.25:0.25:0.25:0.25:1:4) with 1 eq **3a** as liquidiser, 1 mmol scale reaction after 120 h of heating at 115 °C.

Table 58. Data to **Figure 192**. To be able to compare results obtained by two different analytical methods we used values from Table 54 and Table 56. For this case HPLC-MS total conversion of initial number of nucleosides to phosphorylated and other organic products was calculated by subtracting not reacted nucleoside integrals (**N**) from the sum of all integrated peaks (in H₂O) that was compared to total conversion of initial amount of **P_i** to phosphorylated organic products calculated by subtracting inorganic compound integrals (**P_i**, **PP_i** and **P_{mi}**) from the sum of all integrated ³¹P{¹H} NMR peak areas (in H₂O/D₂O = 9:1). In order to ‘match’ products we used the sum of products in HPLC-MS that contained phosphate groups in correspondence to ³¹P{¹H} NMR, after scaling the total number of products to 100 %.

	N5>p, %	NpN5>p, %	Np, %	NpN, %	N6>p, %	PP _i , %	-	PP _o , %	P _i , %
³¹ P{ ¹ H} NMR	35.21	0.53	19.24	17.86	0.20	21.84	-	0.12	5.00
LC-MS	38.87	4.79	15.45	9.75	-	-	7.17	0.83	23.14
	N>p + pN>p, %	NpN>p, %	pN + pNp + pN>p + pNpp, %	NpN + NpN>p, %	-	-	Other products, %	pNpp, %	N, %

6.1.2. Urea-assisted phosphorylation of a mixture of ribonucleosides in the presence of valine

We investigated whether the presence of amino acids in dry conditions would affect phosphorylation, and found that the presence of L- and D-valine slowed down the reaction and led to the formation of less phosphorylated products, and the inhibitory effect of L-valine was stronger than that of D-valine (**Figure 193**, **Figure 194**, **Table 59**).

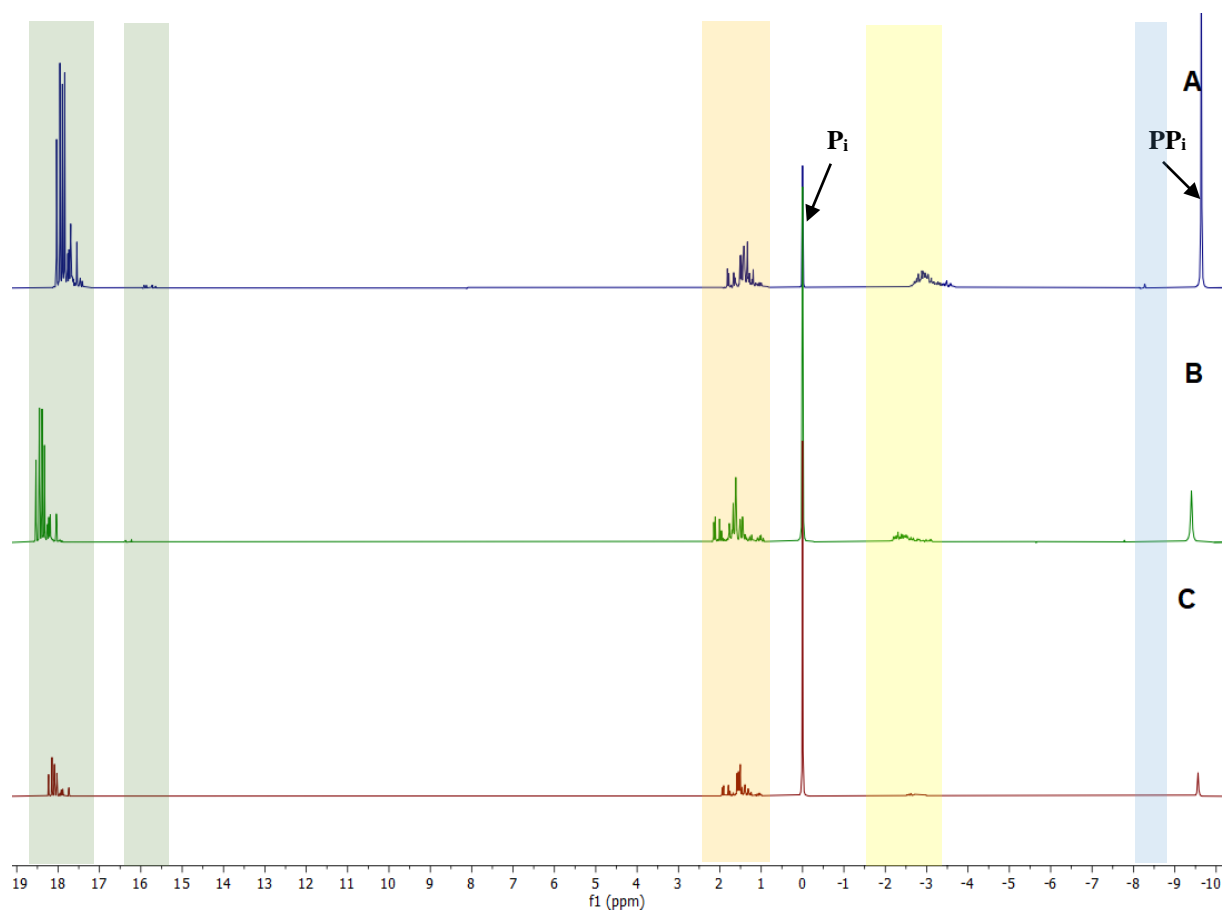


Figure 193. Stack of $^{31}\text{P}\{^1\text{H}\}$ NMR spectra (202.5 MHz, D_2O) of a 1 mmol scale reaction after 120 h of heating at 115 °C of crude mixtures of nucleosides **11:12:13:14:2a:P_i** (0.25:0.25:0.25:0.25:4:1) and 1 eq **3a** as liquidiser. **A** – spectrum from Figure 184; **B** – with 1 eq L-valine (**22a**) with respect to **P_i**; **C** – with 1 eq D-valine (**22b**) with respect to **P_i**. δ_{P} (ppm) = 19.0-17.0 (*s*, 2',3' 5-membered ring cyclic phosphates **N5>p**, green), 16.0-15.5 (*s*, 2',3' 5-membered ring cyclic diphosphate **pN5>p**, darker green, identified by analogy with signal intensities of acyclic dinucleotides), 2.5-0.5 (5', 3' or 2' acyclic phosphates, **Np**, ochre), 0.00 (*s*, **P_i**), from -2.0 to -3.5 (acyclic dinucleoside phosphates, **NpN**, yellow), from -7.0 to -8.5 (*s*, 5',3' 6-membered ring cyclic phosphate **N6>p**, blue), -9.5 (*s*, **PP_i**).

Table 59. Data to **Figure 193**. Total conversion of initial amount of **P_i** to phosphorylated organic products was calculated by subtracting inorganic compound integrals (**P_i** and **PP_i**) from the sum of all integrated ³¹P{¹H} NMR peak areas (in D₂O).

Type of product, 1eq	N5>p, %	NpN5>p, %	Np, %	NpN, %	N6>p, %	Npp, %	PP _i , %	P _i , %
L-Valine	24.07	0.25	28.83	11.25	0.09	-	11.64	23.87
D-Valine	14.14	0.22	27.36	6.38	0.10	-	7.99	43.81

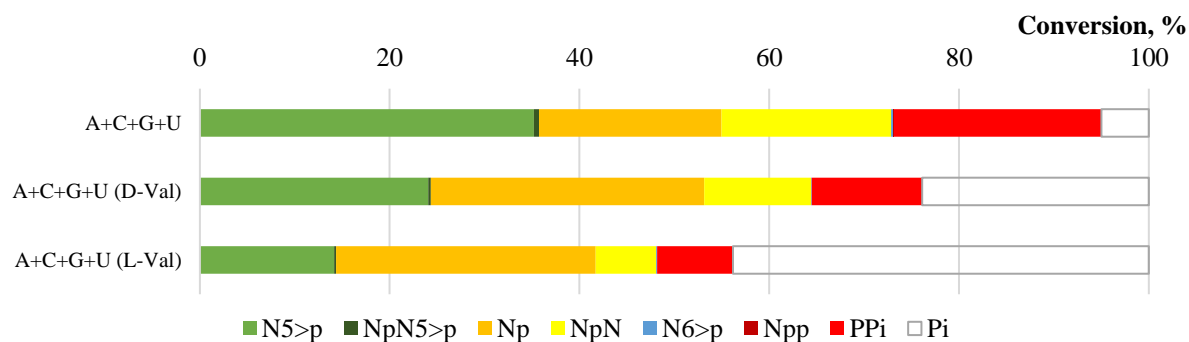


Figure 194. Summary of urea-assisted phosphorylation of ribonucleoside mixture **11:12:13:14:2a:P_i** (0.25:0.25:0.25:0.25:4:1) and 1 eq **3a** as liquidiser in absence and presence of amino acids **22a** and **22b**. 1 mmol scale reaction after 120 h of heating at 115 °C, then dissolved in D₂O on a 0.5 mmol scale. Percent values from signal integration of quantitative ³¹P{¹H} NMR spectrum (**Figure 193**).

6.2. One-pot experiment with urea as a condensing agent

We placed in the same pot four ribonucleosides (**A**, **C**, **G**, **U**), glycerol, four short saturated fatty acids ($\text{CH}_3(\text{CH}_2)_8\text{COOH}$, $\text{CH}_3(\text{CH}_2)_9\text{COOH}$, $\text{CH}_3(\text{CH}_2)_{10}\text{COOH}$, $\text{CH}_3(\text{CH}_2)_{11}\text{COOH}$) urea and NaH_2PO_4 . The neat mixture was heated at 115 °C for 2-5 days, and the products were analysed by HRMS and NMR.

We expected to see competition towards the formation of certain products or groups of products and to identify if those conditions could be favourable for spontaneous oligomerisation. According to our kinetic studies that showed that glycerol is phosphorylated fastest, and next best were nucleosides, we assumed that small amounts of phospholipids could be formed provided that glyceryl phosphates would indeed esterify fatty acids. Only small amounts of highly amphiphilic mono- and diacylated phospholipids are expected to suffice for the formation of bilayer membranes, ideally, vesicles. We did test such reaction mixtures to obtain some hints by NMR spectroscopy, mass spectrometry and fluorescence microscopy.

Due to the chemical diversity of expected reaction products, we used different solvents for the highest degree of extraction. As the best solvent for nucleic acid derivatives, water (D_2O and H_2O for NMR and MS, respectively) was selected. In the case of fatty acids and lipids, the most optimal solvents are $\text{DMSO-}d$ and MeOH for NMR and MS, respectively. $\text{DMSO-}d_6$ can be used for MS analyses in the negative-ion mode; however, overwhelming signals from the solvent will disturb identifying reaction products in positive-ion mode. Glycerol derivatives are expected to be soluble in all listed solvents. To achieve the best extraction, we used a fresh, separate sample for each solvent.

After success in urea-assisted phosphorylation of alcohols in dry conditions, the next logical step was to make the system more complex. The crude mixture contained 1 eq nucleosides (**A**:**C**:**G**:**U** 0.25:0.25:0.25:0.25), 1 eq glycerol (**5**), 1 eq fatty acids (C_{10} : C_{11} : C_{12} : C_{13} 0.25:0.25:0.25:0.25), 1 eq urea and 1 eq **P_i**. Reaction scale 4 mmol, heated for 48 hours at 115 °C. The reaction was carried out in the round bottom flask (250 ml) under middle-strength steering. In the beginning of the experiment, the crude mixture appeared in the form of a paste, that had partly solidified by the end of 48 hours.

6.2.1. NMR analyses of products

Starting with ^1H NMR, we detect the complexity of the reaction results. In **Figure 195**, a stack of D_2O extracts from the crude mixture is shown together with the reference spectra of the main expected products in water: **AMP**, **CMP**, **GMP** and **UMP** (**Figure 195**). We identify molecules similar to the suggested nucleotides in the mixture of many different products. Nucleoside-containing products resonate in the range $\delta_{\text{H}} = 7.75\text{-}8.25$ and 8.00 ppm (H6-pyrimidine and H2,H8-purine protons), 5.80-6.25 ppm (H5-pyrimidine and 1'-ribose protons) and 3.60-4.50 (2',3',4' and 5'-ribose protons). The products of phosphorylation are identified at 4.0-5.5 ppm. Glycerol is detected at $\delta_{\text{H}} = 3.40\text{-}3.60$ ppm and its phosphorylated products are found at 3.60-4.50 ppm. Mixed signals below 3.5 ppm are all from protons in fatty acids chains.

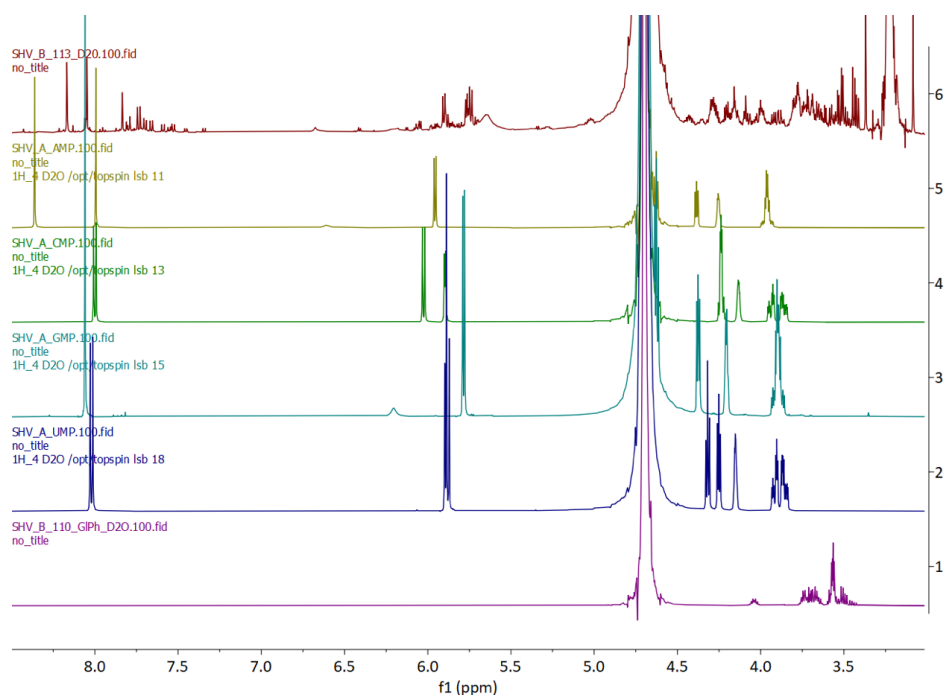


Figure 195. ^1H NMR spectrum (500 MHz) of **red** crude mixture containing 1 eq nucleosides (**11:12:13:14** 0.25:0.25:0.25:0.25), 1 eq glycerol (**5**), 1 eq fatty acids ($\text{C}_{10}:\text{C}_{11}:\text{C}_{12}:\text{C}_{13}$ 0.25:0.25:0.25:0.25), 1 eq **2a** and 1 eq **P_i**, 4 mmol scale reaction after 48 h of heating at 115 °C, then dissolved in D_2O . The stack was referenced to $\delta_{\text{H}} = 4.7$ ppm (*s*, D_2O). Reference spectra: **olive** – AMP, **green** – CMP, **light blue** – GMP, **dark blue** – UMP and **violet** – glyceryl phosphate.

Proton-decoupled $^{31}\text{P}\{^1\text{H}\}$ NMR spectra are more informative in terms of the identification of phosphorylated products. In **Figure 196A**, similar to previously studied nucleoside reactions: $\delta_{\text{P}} = 20\text{--}16$ ppm 5-membered ring cyclic phosphates; 2.5–0.5 ppm acyclic phosphate monoesters; 0.00 ppm referenced to **P_i**; -0.2 to -2.5 ppm acyclic phosphate diesters (dinucleotides and longer); -5.5 to -6.5 ppm 6-membered ring cyclic phosphates and -9.1 ppm for **PP_i**.

Looking carefully at the zoom of 5-membered ring products in **Figure 196B**, we could interpret most signals. The first four singlets, $\delta_{\text{P}} = 18.94, 18.86, 18.83$ and 18.80 ppm with relatively close intensities and integration values 2.36, 3.66, 2.54 and 2.24 %, respectively, are most likely due to 2'3'-cyclic nucleoside phosphates corresponding to **A**, **C**, **G** or **U**. Unfortunately, without synthetic reference compounds, it is impossible to distinguish one from the other. Other small signals at $\delta_{\text{P}} = 18.68\text{--}18.44$ ppm (2.89 %) can be from other nucleoside-containing cyclic phosphates, such as diphosphates or dinucleotides with another molecule connected to the phosphate ring.

The next singlet is the largest signal at 17.32 ppm and results in 13.52 % of 5-membered cyclic glyceryl phosphate. We interpret it knowing that glycerol is more reactive than nucleosides in general and that this singlet is shifted aside from the other signals. The same is true for signals $\delta_{\text{P}} = 16.95\text{--}17.09$ ppm (3.68 %) that are some minor derivatives of 5-membered cyclic glyceryl phosphate. The data obtained within $^{31}\text{P}\{^1\text{H}\}$ DOSY NMR (**Figure 197**) experiments is consistent.

The zoom into the acyclic products in **Figure 196C** is more challenging to interpret. Comparing this data with $^{31}\text{P}\{^1\text{H}\}$ DOSY (**Figure 197**), we see signals of phosphorylated monoesters at $\delta_{\text{P}} = 0.75\text{--}2.40$ ppm (29.39 %) of acyclic nucleotides and glyceryl phosphates together and the range -0.2 to -2.5 ppm represents heavier nucleotides, most likely dinucleotides. The large singlet at -4.81 ppm (5.50 %) is in the range of 6-membered rings. It is still possible to make 3',5'-cyclic phosphate from nucleosides, but most likely this signal is due to 6-membered ring glyceryl phosphate. In general, $^{31}\text{P}\{^1\text{H}\}$ DOSY NMR demonstrates the separation of four main product groups by molecular weight (more precisely, by their diffusion coefficient), as identified in **Figure 197**.

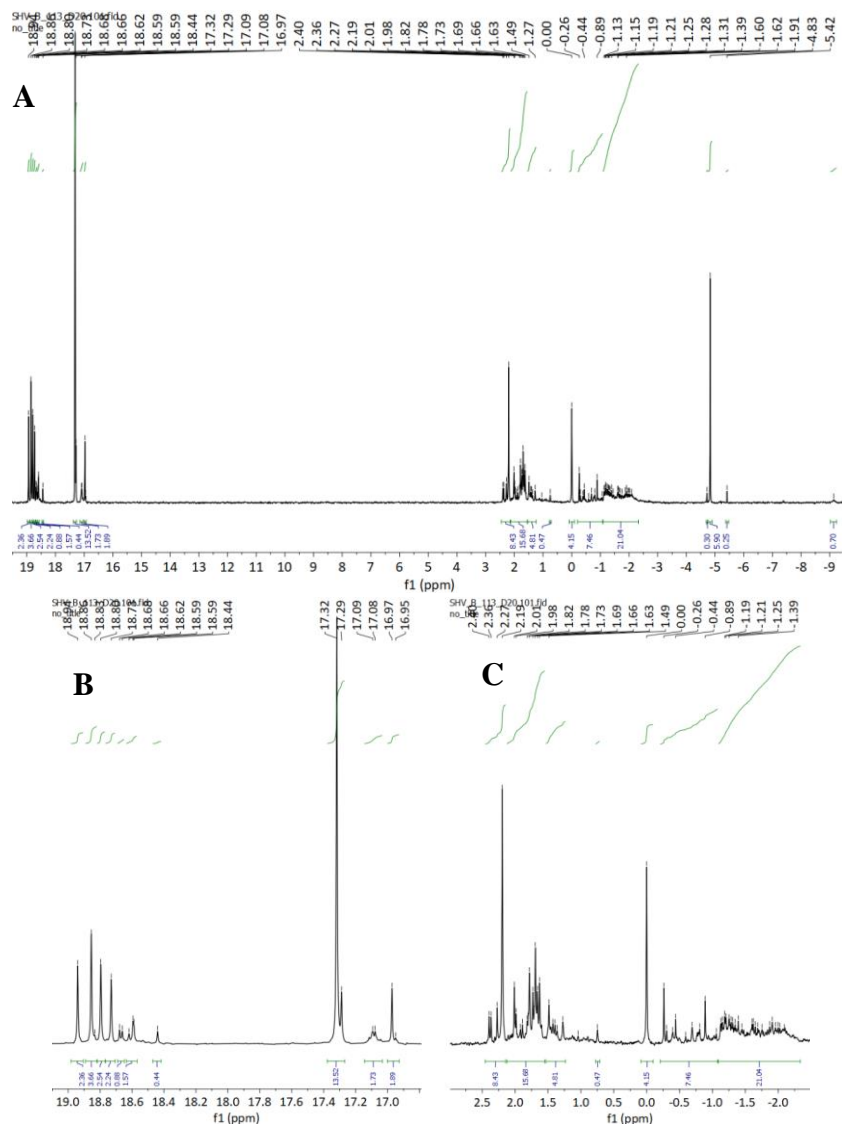


Figure 196. $^{31}\text{P}\{^1\text{H}\}$ NMR (202.5 MHz, D_2O) of crude mixture containing 1 eq nucleosides (**11:12:13:14** 0.25:0.25:0.25:0.25), 1 eq glycerol (**5**), 1 eq fatty acids ($\text{C}_{10}\text{:C}_{11}\text{:C}_{12}\text{:C}_{13}$ 0.25:0.25:0.25:0.25), 1 eq **2a** and 1 eq P_i , 4 mmol scale reaction after 48 h of heating at 115°C , then dissolved in D_2O . The spectrum was referenced to $\delta_{\text{P}} = 0.00$ ppm (*s*, P_i). **A** – full spectrum, **B** – zoom on 5-membered ring cyclic phosphates (19.2–16.8 ppm), **C** – zoom on acyclic phosphates (3.0 to -2.5 ppm).

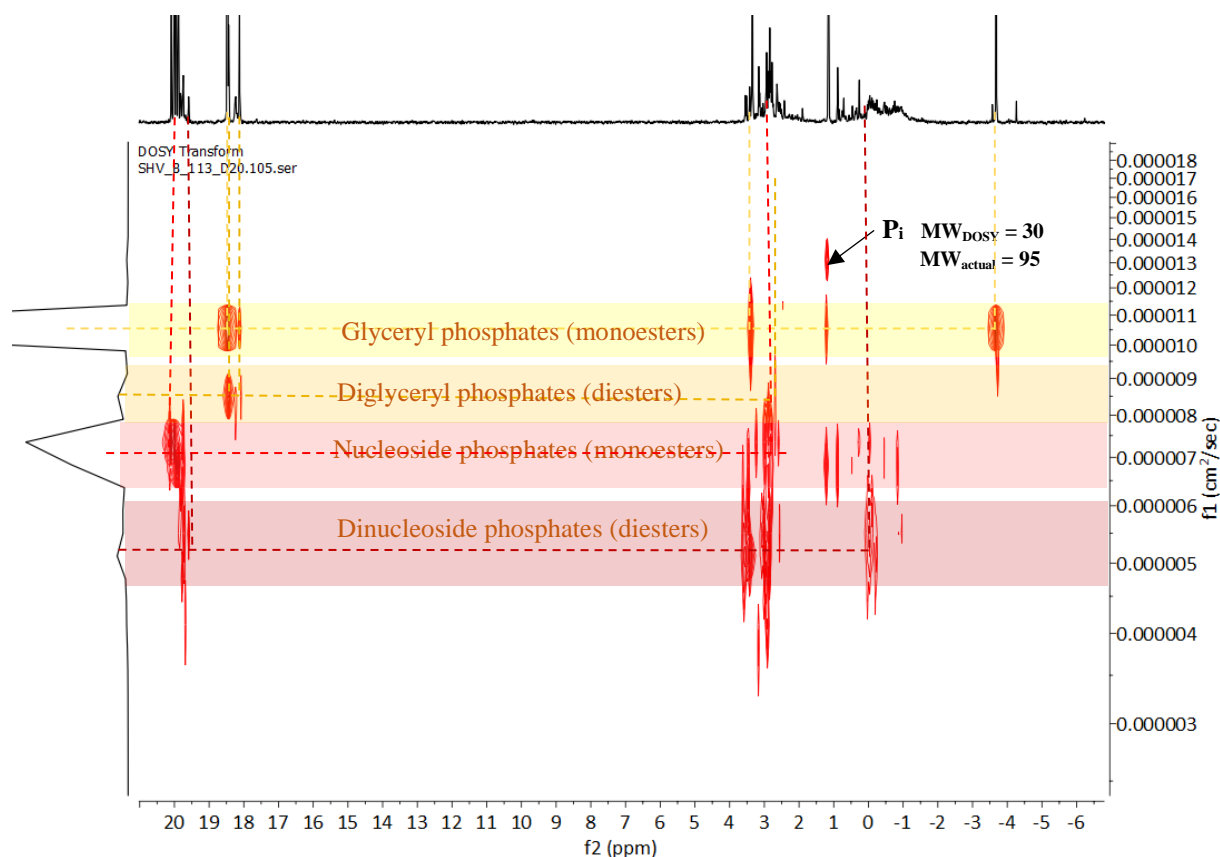


Figure 197. $^{31}\text{P}\{^1\text{H}\}$ DOSY NMR, peak fit DOSY transformation, (202.5 MHz, D_2O) of crude mixture containing 1 eq nucleosides (**11:12:13:14** 0.25:0.25:0.25:0.25), 1 eq glycerol (**5**), 1 eq fatty acids ($\text{C}_{10}:\text{C}_{11}:\text{C}_{12}:\text{C}_{13}$ 0.25:0.25:0.25:0.25), 1 eq **2a** and 1 eq P_i , 4 mmol scale reaction after 48 h of heating at 115 °C, then dissolved in D_2O . The spectrum was referenced to $\delta_{\text{P}} = 0.00$ ppm (*s*, P_i).

Another set of data was obtained by dissolving the same crude mixture in $\text{DMSO-}d_6$ to obtain more information about the products containing long-chain derivatives of fatty acids.

In the ^1H NMR spectrum of the crude mixture shown in **Figure 198**, the signals seem to be more crowded than in **Figure 195**. Signals at $\delta_{\text{H}} = 0.8\text{-}3.0$ ppm belong to the long-chain hydrogen atoms in fatty acids. The overcrowded area at 3.0-4.5 ppm shows numerous glyceryl derivatives and their phosphorylated products. All other signals most likely demonstrate that some of the nucleosides and possibly nucleotides are also partly soluble in $\text{DMSO-}d_6$.

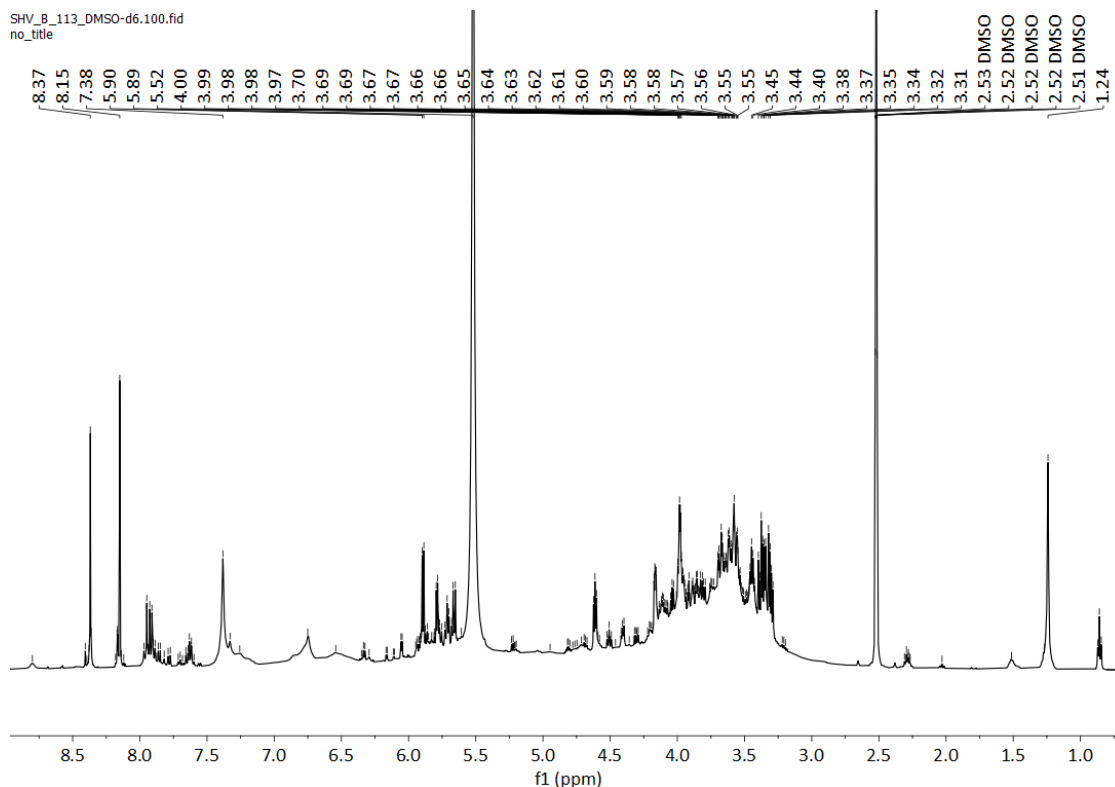


Figure 198. ^1H NMR spectrum (500 MHz) of crude mixture containing 1 eq nucleosides (**11:12:13:14** 0.25:0.25:0.25:0.25), 1 eq glycerol (**5**), 1 eq fatty acids ($\text{C}_{10}:\text{C}_{11}:\text{C}_{12}:\text{C}_{13}$ 0.25:0.25:0.25:0.25), 1 eq **2a** and 1 eq P_i , 4 mmol scale reaction after 48 h of heating at 115 °C, then dissolved in $\text{DMSO-}d_6$.

Although we identify on the ^{31}P NMR $\{^1\text{H}\}$ spectra the same groups of products, signals resonate too close to each other, which makes it almost impossible to differentiate (**Figure 199**). Looking into the details of the inserted zoom of 17.5–14.5 ppm range, we identify two sets of signals with comparable intensity at 17.02 and 16.97 with 16.83 and 16.73 ppm (total 17.62 %). Those signals look like doublets; however, there is no evidence of another set of doublets on the spectrum with the same coupling constant. Thus, we interpret them as **2'3'AMP** and **2'3'GMP** with **2'3'CMP** and **2'3'UMP**, or vice versa. In **Figure 196** δ_{P} (ppm) = 15.81 (17.65 %) is 5-membered ring cyclic glyceryl phosphate. The two last signals in the range of 15.56 and 15.11 ppm belong to more complex molecules such as phosphodiester (2.25 %).

In the mess of signals in the acyclic area, δ_{P} (ppm) = 2 to –1.5, it is impossible to identify the P_i signal or confirm its absence. Most likely, we have here a mixture of different kinds of acyclic phosphoesters that are hardly distinguishable (54.58 %). The singlet at –4.53 ppm can be attributed to 6-membered ring glyceryl phosphate (7.47 %) and another signal at –5.40 ppm, perhaps to one of its derivatives (0.44 %).

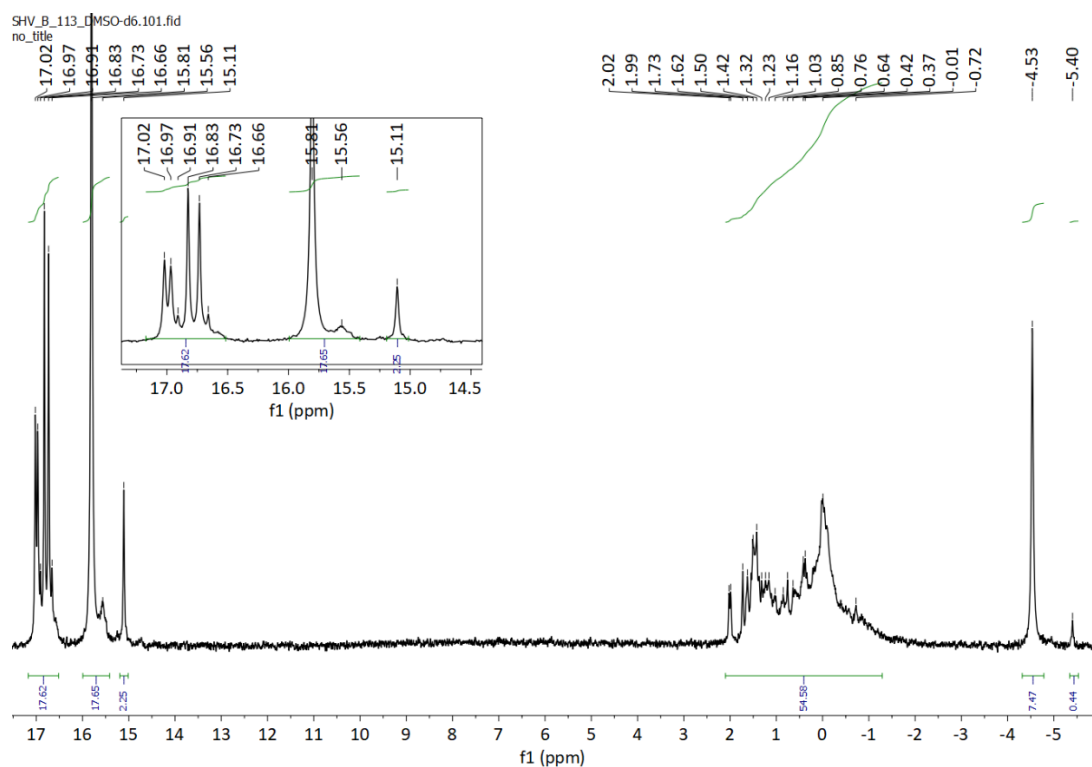


Figure 199. $^{31}\text{P}\{^1\text{H}\}$ NMR (202.5 MHz, $\text{DMSO-}d_6$) of the crude mixture containing 1 eq nucleosides (**11:12:13:14** 0.25:0.25:0.25:0.25), 1 eq glycerol (**5**), 1 eq fatty acids ($\text{C}_{10}:\text{C}_{11}:\text{C}_{12}:\text{C}_{13}$ 0.25:0.25:0.25:0.25), 1 eq **2a** and 1 eq **P_i**, 4 mmol scale reaction after 48 h of heating at 115 °C.

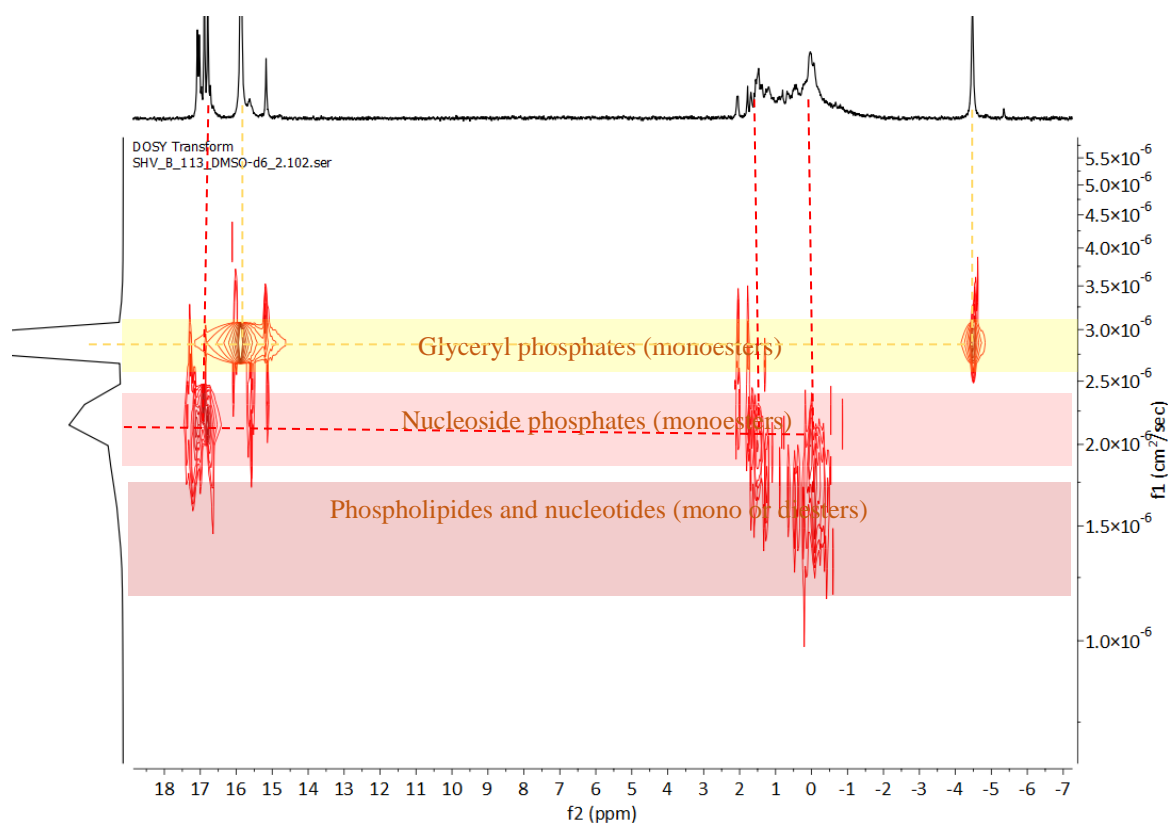


Figure 200. $^{31}\text{P}\{^1\text{H}\}$ DOSY NMR, peak fit DOSY transformation, (202.5 MHz, $\text{DMSO-}d_6$) of crude mixture containing 1 eq nucleosides (**11:12:13:14** 0.25:0.25:0.25:0.25), 1 eq glycerol (**5**), 1 eq fatty acids ($\text{C}_{10}:\text{C}_{11}:\text{C}_{12}:\text{C}_{13}$ 0.25:0.25:0.25:0.25), 1 eq **2a** and 1 eq **P_i**, 4 mmol scale reaction after 48 h of heating at 115 °C, then dissolved in $\text{DMSO-}d_6$.

$^{31}\text{P}\{^1\text{H}\}$ DOSY NMR spectrum (**Figure 200**) confirms our suggestions for glyceryl phosphates (highlighted in yellow). Part of the signals is in the same range as 2',3'-cyclic nucleotides proposed above (highlighted red), so we suggest that there are acyclic nucleotides present as well. In the acyclic area, we see a smooth diffusion from glyceryl monoesters towards some other heavier molecules in between the red and dark red zones that are heavier than mononucleotides, possibly phospholipids and dinucleotides.

6.2.2. MS analyses of products

Mass-spectrometry analyses of the crude mixture were performed in H_2O and MeOH , both in positive (LRMS) and negative (HRMS) ion modes.

In water, in positive-ion mode, we identified mostly starting molecules with the most intense signals m/z 244.1, 268.1 and 284.1 that correspond to C, A and G, respectively (**Figure 201**). Other compounds identified are nucleobases (**Ade** and **Ura**) carbamates (glyceryl, A and G carbamates) and **AMP (Ap)**.

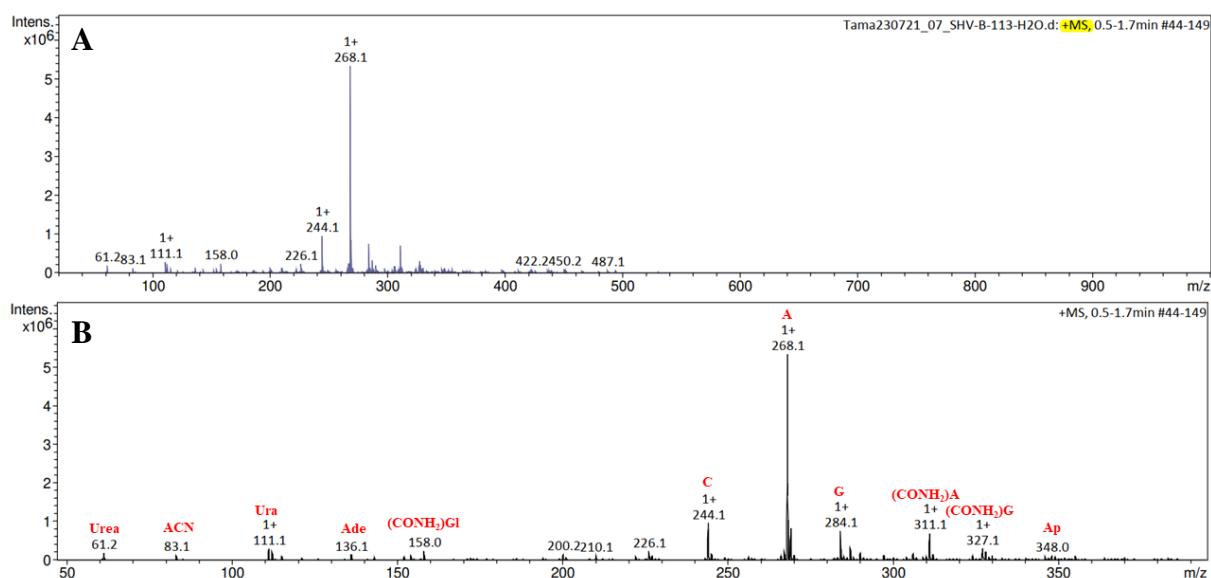
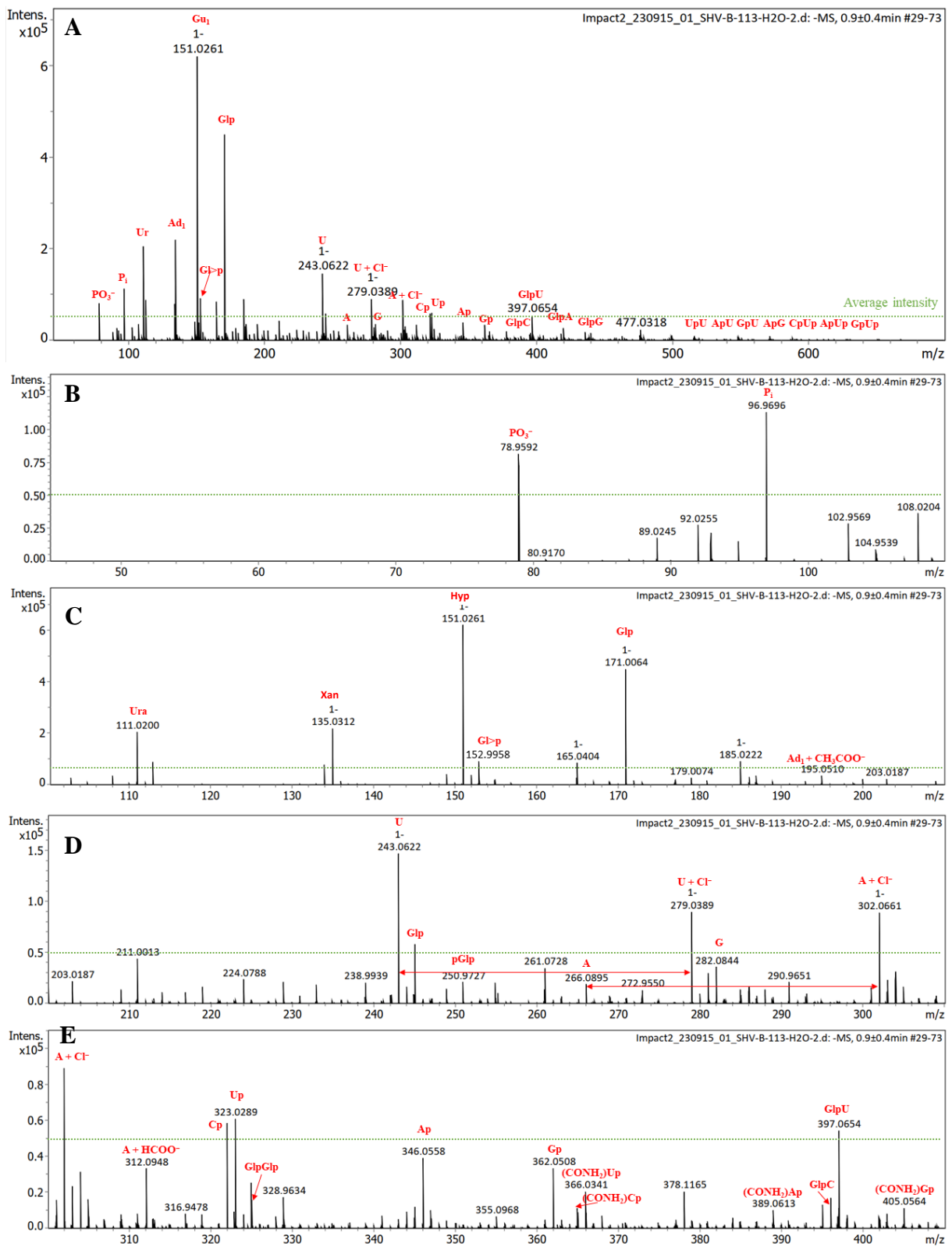


Figure 201. LRMS spectra (direct injection) in the positive-ion mode of the water extract of the crude mixture 1 eq nucleosides (**11:12:13:14** 0.25:0.25:0.25:0.25), 1 eq glycerol (**5**), 1 eq fatty acids ($\text{C}_{10}:\text{C}_{11}:\text{C}_{12}:\text{C}_{13}$ 0.25:0.25:0.25:0.25), 1 eq **2a** and 1 eq **Pi.**, 4 mmol scale reaction after 48 h of heating at 115 °C. **A** – full spectra, **B** – zoom m/z 50-400. **Red** abbreviations correspond to signal interpretations.

In negative-ion mode, we identified a large diversity of organic products. In **Figure 202**, we suggest a full spectrum and its zooms for each m/z 100 range.



Continuation of the figure is on the next page

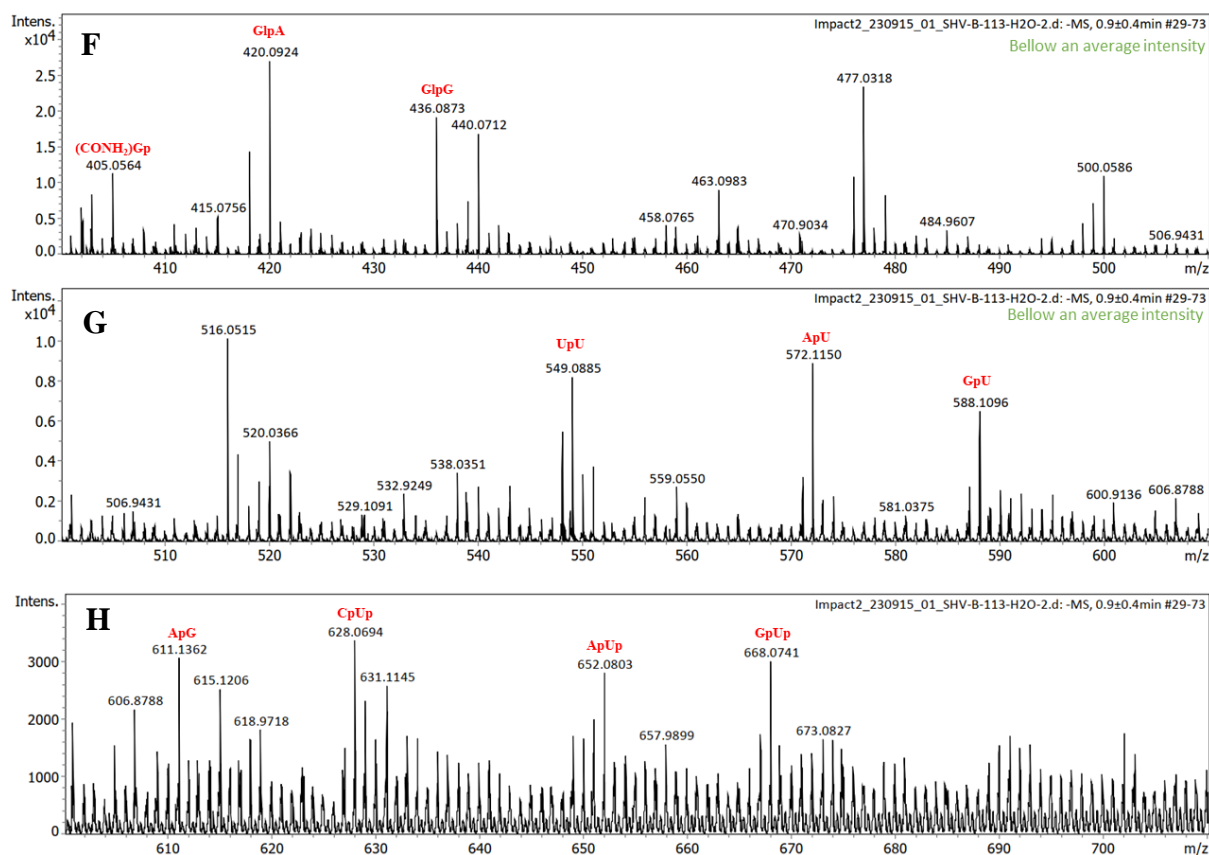


Figure 202. HRMS spectra (direct injection) in the negative-ion mode of the water extract of the crude mixture 1 eq nucleosides (11:12:13:14 0.25:0.25:0.25:0.25), 1 eq glycerol (**5**), 1 eq fatty acids (C₁₀:C₁₁:C₁₂:C₁₃ 0.25:0.25:0.25:0.25), 1 eq **2a** and 1 eq **P_i**, 4 mmol scale reaction after 48 h of heating at 115 °C. **A** – full spectra, **B-H** – zooms. Green line is an internal grade of the average intensity in that *m/z* range.

Surprisingly, we were unable to identify in either positive or negative ion mode the 5-membered ring phosphates of nucleosides that were detected by ³¹P{¹H} NMR (**Figure 196**). However, we confirmed the presence of diphosphorylated glycerol and nucleosides together with dinucleotides. There are still some minor signals that were not assigned. All the identified molecules (the structure of the most probable isomer) are presented in **Figure 203**.

In summary, the following main groups of products were identified:

- nucleobases uracil (Ura) and hydrolyzed derivatives of adenine and guanine, hypoxanthine (Hyp) and xanthine (Xan), respectively;
- nucleosides (**A**, **G**, **U**);
- acyclic (glycerol, **A**, **G**, **U**, **C**) and cyclic (glycerol) monophosphates;
- carbamoylated monophosphates (**A**, **G**, **U**, **C**);
- monoester diphosphate (glycerol);
- diesters (glycerol, **A**, **G**, **U**, **C** and their mixtures);
- diphosphates diesters (**A**, **G**, **U**, **C**).

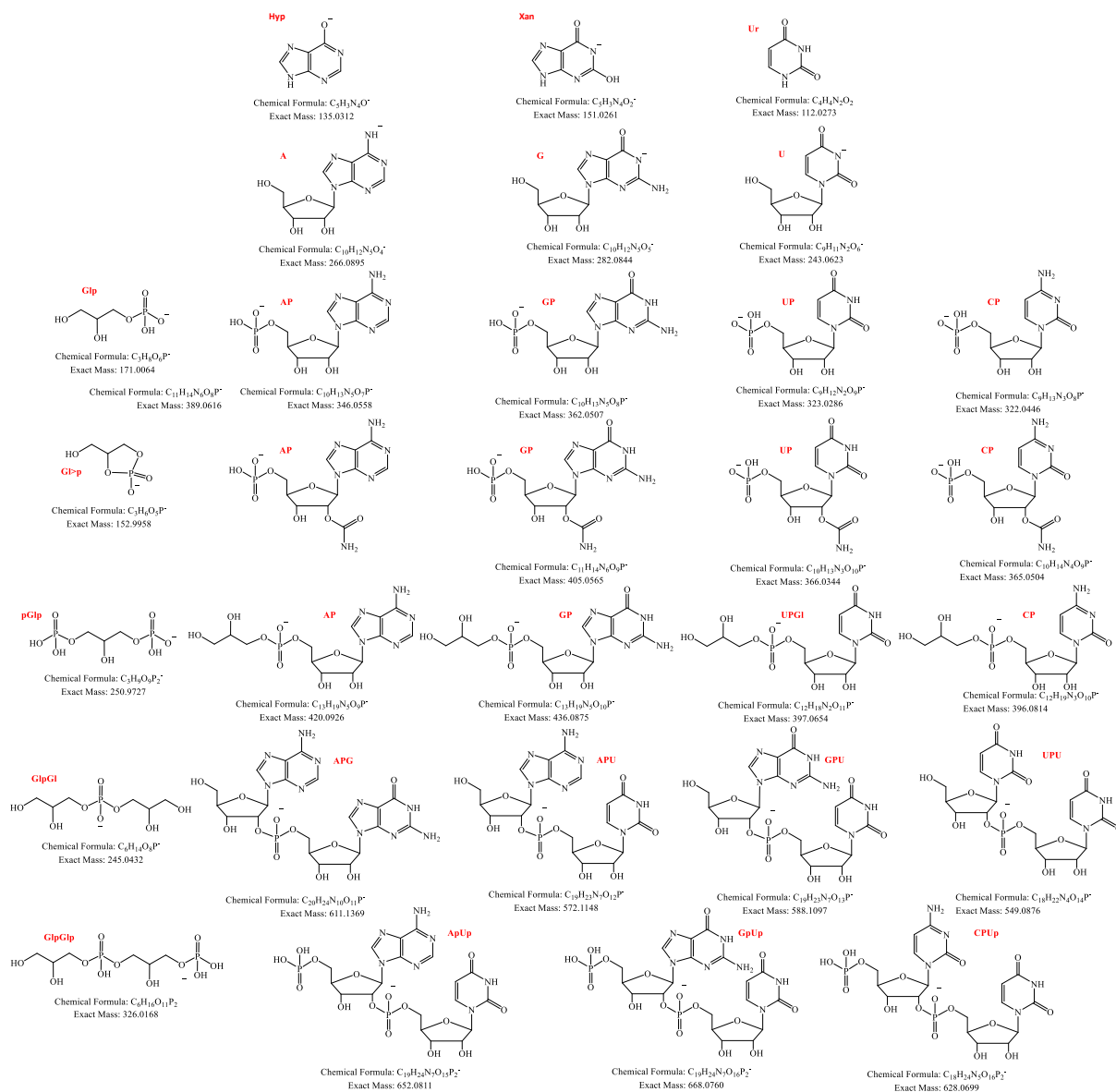


Figure 203. Chemical structures (only the most probable isomer shown) and exact masses of the detected compounds of **Figure 202** HRMS (direct injection) of the water extract of the crude mixture obtained by reacting 1 eq nucleosides (**11:12:13:14** 0.25:0.25:0.25:0.25), 1 eq glycerol (**5**), 1 eq fatty acids ($C_{10}:C_{11}:C_{12}:C_{13}$ 0.25:0.25:0.25:0.25), 1 eq **2a** and 1 eq **P_i**, 4 mmol scale reaction after 48 h of heating at 115 °C.

As expected, we did not find in water any long-chain containing compounds other than not esterified fatty acids. Thus, we performed similar MS experiments for the crude mixture dissolved in MeOH.

The positive-ion mass spectrum (**Figure 204**) was complicated by sodium formate clusters (pink). However, we identified signals from starting molecules **A**, **C** and **G**. The only signal of a long-chain compound found is **C₁₂** ($CH_3(CH_2)_{10}COOH$). It should be mentioned that this spectrum has low mass resolution, so it is possible that this signal in HRMS would not correspond to the exact mass of proposed formula.

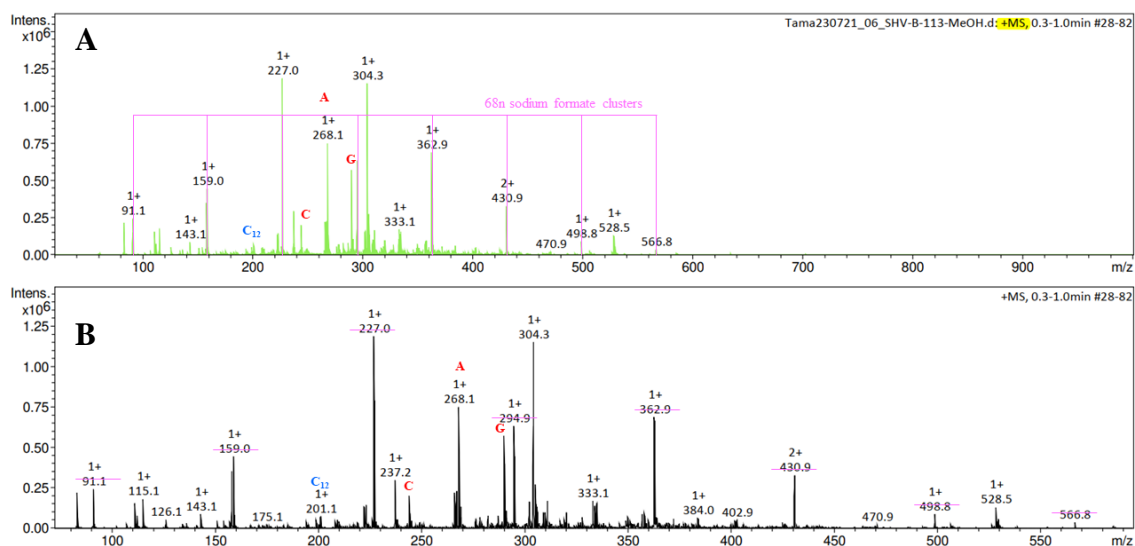


Figure 204. LRMS spectra (direct injection) in the positive-ion mode of the MeOH extract of the crude mixture containing 1 eq nucleosides (**11:12:13:14** 0.25:0.25:0.25:0.25), 1 eq glycerol (**5**), 1 eq fatty acids ($C_{10}:C_{11}:C_{12}:C_{13}$ 0.25:0.25:0.25:0.25), 1 eq **2a** and 1 eq **P_i**, 4 mmol scale reaction after 48 h of heating at 115 °C. **A** – full spectra, **B** – zoom m/z 50-600. **Red** abbreviations correspond to signal interpretations that were already identified in water and **blue** signals unique for MeOH extract.

In negative-ion mode HRMS (**Figure 206**), we discovered the presence of cyclic products. Apparently, they are more soluble in MeOH than in water. Although some new products were discovered (blue), long-chain derivatives were still not found. A possible solution was to use DMSO as a solvent. Similar to the solution in water, we did not obtain any oligomers longer than diester. The new compounds discovered in MeOH are suggested in **Figure 205** (the structure of the most probable isomer).

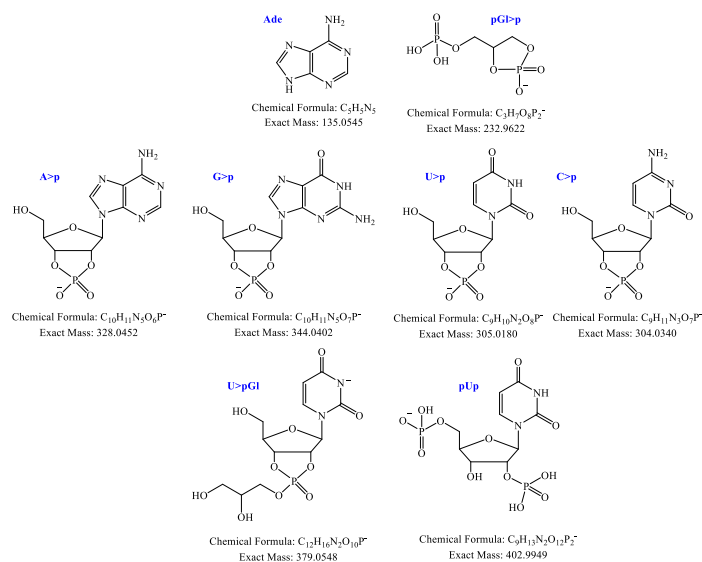
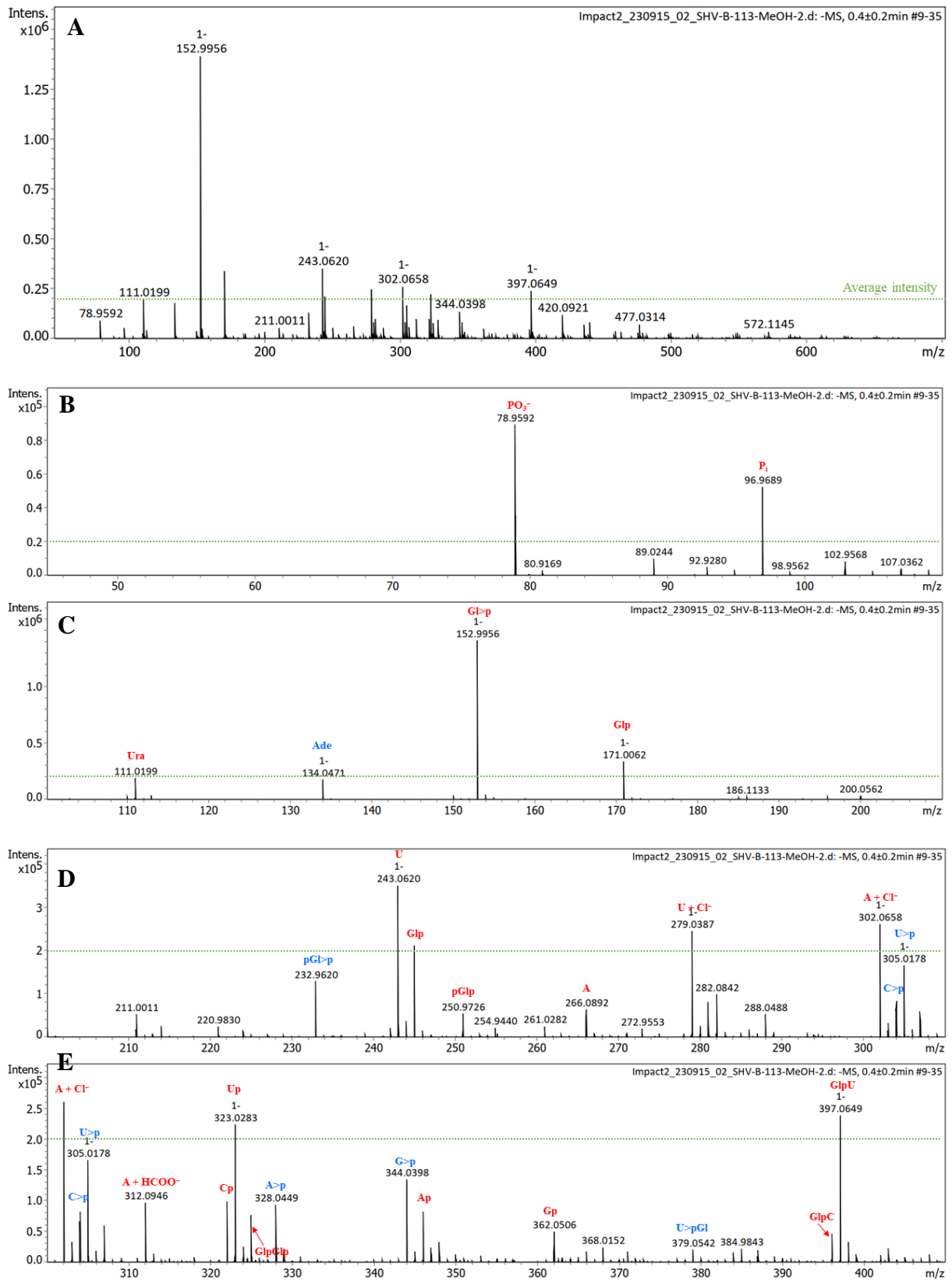


Figure 205. Chemical structures (only the most probable isomer shown) and monoisotopic exact masses of the detected compounds of **Figure 202** HRMS (direct injection) of the water extract of the crude mixture obtained by reacting 1 eq nucleosides (**11:12:13:14** 0.25:0.25:0.25:0.25), 1 eq glycerol (**5**), 1 eq fatty acids ($C_{10}:C_{11}:C_{12}:C_{13}$ 0.25:0.25:0.25:0.25), 1 eq **2a** and 1 eq **P_i**, 4 mmol scale reaction after 48 h of heating at 115 °C.



Continuation of the figure is on the next page

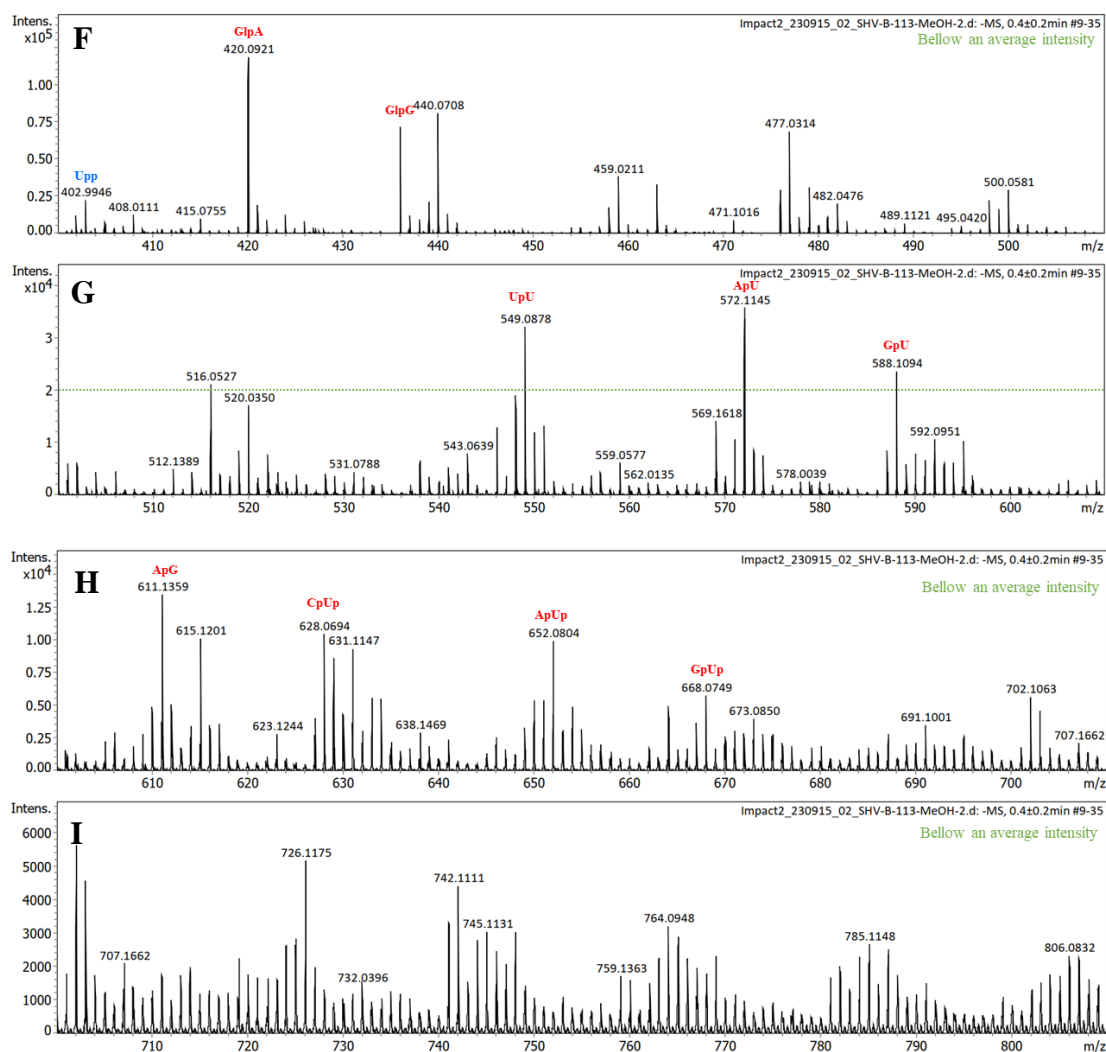


Figure 206. HRMS spectra (direct injection) in the negative-ion mode of the MeOH extract of the crude mixture containing 1 eq nucleosides (**11:12:13:14** 0.25:0.25:0.25:0.25), 1 eq glycerol (**5**), 1 eq fatty acids (C₁₀:C₁₁:C₁₂:C₁₃ 0.25:0.25:0.25:0.25), 1 eq **2a** and 1 eq **Pi.**, 4 mmol scale reaction after 48 h of heating at 115 °C. **A** – full spectra, **B-I** – zooms. Green line is an internal grade of the average intensity. **Red** abbreviations correspond to signals interpretation that were already identified in water and **blue** signals unique for MeOH extract.

Conclusions to the Section 6

The ‘messy chemistry’ experiments, where several prebiotic alcohols, such as nucleosides or nucleosides are mixed together with glycerol and fatty acids in the same environment aimed at heading toward the greater complexity characteristic of nature.

In experiments where A, C, G, and U were heated with urea and dihydrogen phosphate, the phosphorylated products were the same as for single nucleoside reactions, with increased yields with respect to higher amount of condensing agent. Comparing results obtained by NMR and LC-MS, I identified over 55 different products, including cyclic and acyclic mono-, di-, and triphosphates, along with mono- and dinucleotides. The conversion of starting molecules is 75.64 % and the majority of phosphorylated products are 2',3'-cyclic 37 % and acyclic 10 % mononucleotides. Nucleosides were converted to organic phosphates and inosine hydrolysed from A. There is a slight unbalance at the end of the reaction between the equivalent amount of starting nucleotides and the predominance of uridine and adenosine against cytidine and guanosine. The presence of aminoacids L- or D-valine slowed down the reaction and led to less phosphorylated products. The inhibitory effect of L-valine was stronger than that of D-valine.

We did not obtain long oligonucleotide chains, but only dinucleotides.

In another experiment performed with four ribonucleosides, glycerol, four short saturated fatty acids, urea and NaH_2PO_4 , I described 5- and 6-membered ring cyclic phosphates; acyclic phosphate mono- and diesters (dinucleotides and longer); along with P_i and PP_i . DOSY analysis suggests presence of several groups of products distributed by molecular weights. Although we identify on the ^{31}P NMR{ ^1H } spectra groups of products, signals resonate too close to each other, which makes it almost impossible to differentiate one product from another.

Mass-spectrometry analyses of the crude mixture performed in H_2O and MeOH demonstrated not only main groups but the masses of each individual product, most of them was assigned. In positive-ion mode, we identified mostly the starting molecules C, A and G, and other compounds such as nucleobases (**Ade** and **Ura**) carbamates (glyceryl, A and G carbamates) and **AMP**. In negative-ion mode, a large diversity of organic products belonging to phosphorylated and carbamoylated derivatives of nucleosides and glycerol were identified. I did not obtain any oligomers longer than diester.

I did not find in both solvents many long-chain containing compounds other than not esterified fatty acids. The only signal found is C_{12} ($\text{CH}_3(\text{CH}_2)_{10}\text{COOH}$). It should be mentioned that this spectrum has low mass resolution, so it is possible that this signal in HRMS would not correspond to the exact mass of proposed formula. A possible solution for absence of fatty acid derivatives is their low solubility in the solvent.

In summary, phosphorylation indeed happened. The conversion of phosphate (from the integration of $^{31}\text{P}\{^1\text{H}\}$ NMR) exceeds 95 %, and the resulting products are very diverse, including dinucleotides, glyceryl nucleoside phosphates and possibly phosphorylated derivatives of fatty acids. One of the many challenges for the analysis of complex prebiotic mixtures is the contrasted solubility of the products in different solvents.

Even though I did not achieve longer oligomers, the phosphorylated products accumulated in the suggested conditions could be polymerized after being transferred to other environments. A research avenue would be to confirm if this messy mixture is able to form vesicles that would be expected to encapsulate nucleotides, which would be a major organisational step in the direction of the prebiotic assembly of protocells.

III Results and discussion

7. High pressure induced experiments

7.1. High pressure induced phosphorylation of glycerol

Phosphorylation reactions under hydrothermal conditions are not a widely explored field in prebiotic chemistry yet. Only a few experiments have been described with very exciting results.²⁷⁷⁻²⁷⁹

Considering the results obtained with glycerol phosphorylation reaction at 115 °C and atmospheric pressure, we performed the same experiment under elevated pressure in a diamond anvil cell (DAC). The analyses of the results were conducted using in situ Raman spectroscopy (Methods and Materials section 4.3) as a function of pressure at 115 °C. We chose to perform the experiment at 115 °C for a better comparison with the results obtained in the previous section.

7.1.1. Assignment of the starting molecules Raman spectra

We first measured the reference Raman spectra of glycerol, urea and monosodium dihydrogen as reactants prior to carrying out the experiment (Figure 207).

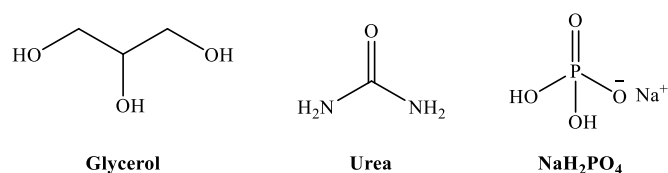


Figure 207. Molecular structure of starting materials

7.1.1.1. Glycerol

The Raman spectrum of pure commercial glycerol (5), measured in a glass vial, is shown in Figure 208. The interpretation of the spectrum was based on the interpretations of Mudalige & Pemberton,²⁹³ Gryniewicz-Ruzicka et al.²⁹⁴ and Mendelovici et al.²⁹⁵. Measured wavenumbers and their assignments are reported in Table 60.

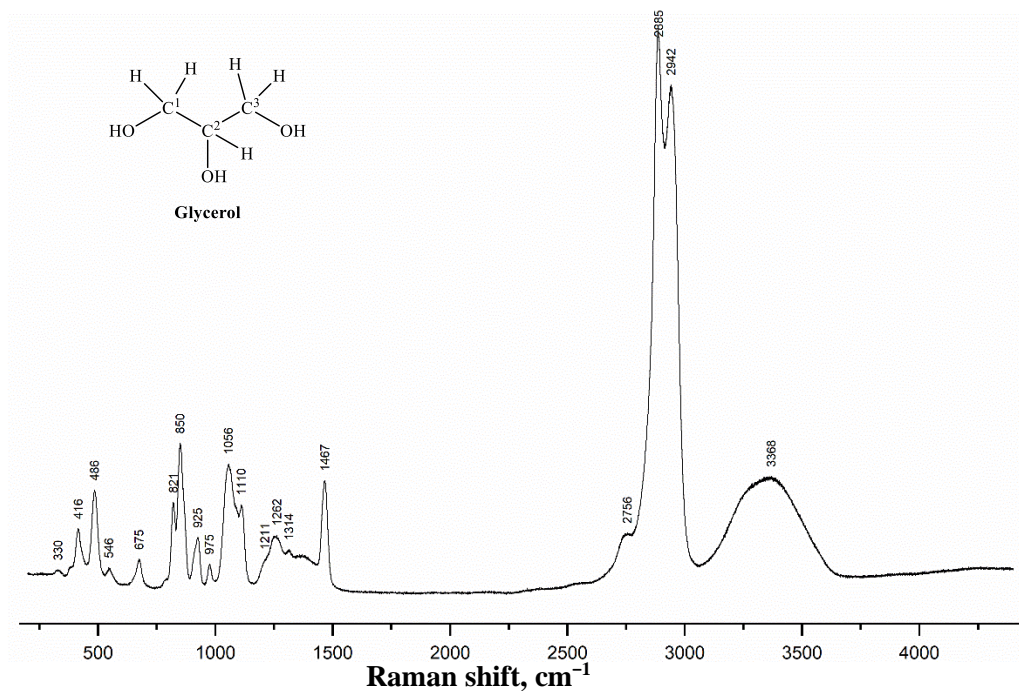


Figure 208. Raman spectrum of glycerol

Table 60. Raman vibrational data of glycerol (cm^{-1}) along with the proposed assignment

Wavenumber (cm^{-1}) measured	Wavenumber (cm^{-1}) form the literature ^{293,294,295}	Suggested assignments
330	326	Intermolecular H-bond
416	417	CCO rocking
486	488	CCO rocking
546	551	CCC bending
675	674, 676	C–C bending ²⁹⁴ OH bending ²⁹⁵
821	820	C–C stretching
850	848	C–C stretching
925	931	CH ₂ rocking
975	976	CH ₂ rocking
1056	1049, 1055	C – OH sym stretching C1, C3
1110	1109, 1113	C – OH stretching C2
1211	1207, 1204	CH ₂ twisting
1262	1254, 1256	CH ₂ twisting
1314	1311, 1316	CH ₂ twisting
1360	1357, 1364	COH bending
1467	1464, 1465	CH ₂ bending
2765	2752, 2770	CH stretching C2
2885	2887, 2902	CH sym. stretching C1, C3
2942	2949, 2956	CH asym. stretching C1, C3
3368	3240-3440, 3274-3400	CO–H assym.-sym. stretching

7.1.1.2. Urea

The experimental spectrum of pure commercial urea (2a) is displayed in the **Figure 209**. The interpretation of the spectrum was based on the assignments proposed by Lamelas et al.²⁹⁶ and Rousseau et al.²⁹⁷ and is summarised in **Table 61**.

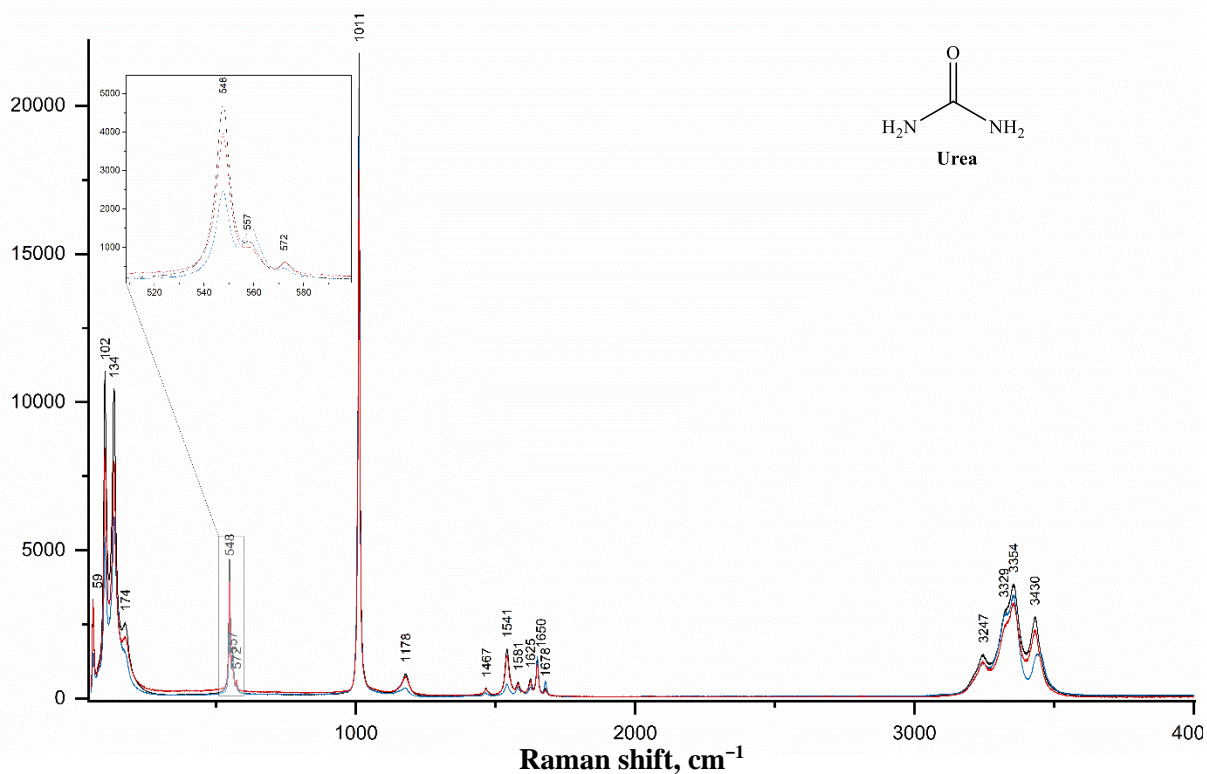


Figure 209. Raman spectra of dry crystals of urea. The three spectra were measured in different spots of the sample. Zoom on top left of the figure highlights the 500-600 cm^{-1} range of the spectrum

Table 61. Raman vibrational data of urea (cm^{-1}) along with an assignment

Wavenumber (cm^{-1}) measured	Wavenumber (cm^{-1}) from the literature ^{296,297}	Suggested assignments
548	547, 532	CN bending
572	576	CO bending
1011	1011, 1013	CN sym. stretching
1178	1178, 1149	NH ₂ rocking
1467	1470, 1471	CN asym. stretching
1541	1542	CO stretching
1581	1580, 1598	CO stretching
1625	1624, 1627	NH ₂ asym. bending
1650	1650	NH ₂ sym. bending
1678	1683	NH ₂ sym. bending
3329	3320, 3330	NH ₂ sym. stretching
3354	3356, 3345	NH ₂ sym. stretching
3430	3432, 3435	NH ₂ asym. stretching

7.1.1.3. Monosodium dihydrogen phosphate NaH₂PO₄ (P_i)

The Raman spectrum of pure commercial monosodium dihydrogen phosphate NaH₂PO₄ (P_i) is displayed in **Figure 210**. The interpretation relied on the assignments by Ghule et al.²⁹⁸ and Choi et al.²⁹⁹ and is summarised in **Table 62**.

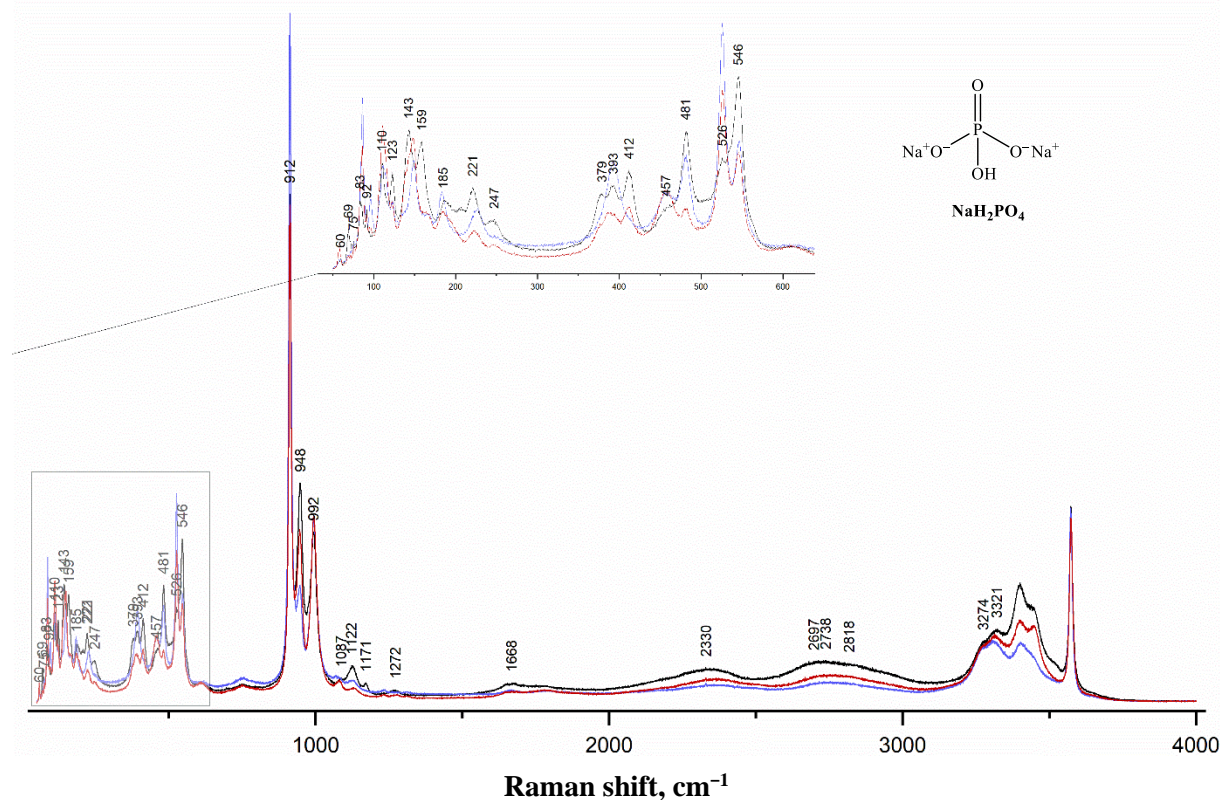


Figure 210. Raman spectra of dry powder of NaH₂PO₄. The three spectra were measured in different grains. Zoom on top of the figure highlights the 50-600 cm⁻¹ range of the spectrum

Table 62. Raman vibrational data of NaH₂PO₄ (cm⁻¹) along with an assignment

Wavenumber (cm ⁻¹) measured	Wavenumber (cm ⁻¹) in the literature ^{298,299}	Suggested assignments
60-247	-	Lattice vibrations
378-481	378-544, 350-570	PO ₄ ³⁻ bending
912-1272	800-1200	Skeletal stretching
2697-2818	2750-2920	OH stretching
3274-3442	3320-3450	H ₂ O
3573	3574	OH ⁻

7.1.1.4. Glyceryl phosphate

One of the main molecules that is expected to be produced as the result of the phosphorylation reaction is glyceryl phosphate. We describe it here before analysing the spectrum of the reaction products. The experimental spectrum of pure commercial glyceryl phosphate (**5a**) is displayed in **Figure 211** with the wavenumbers of the main Raman peaks.

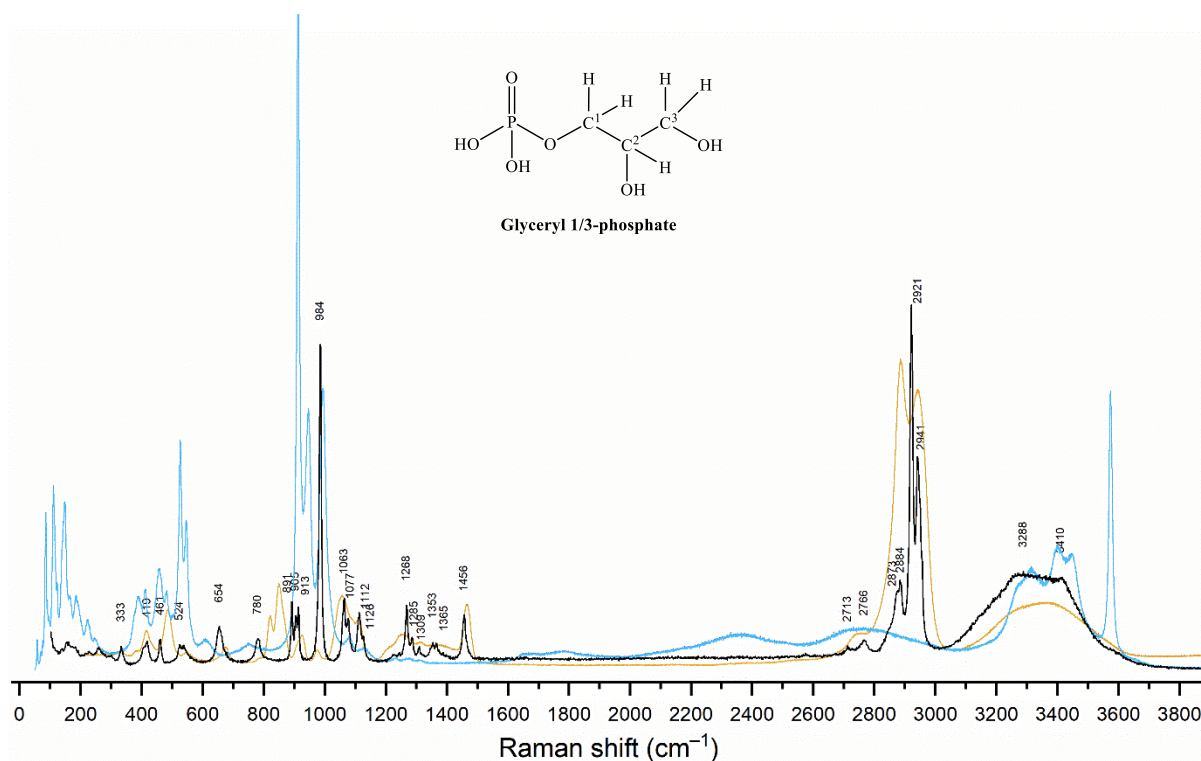


Figure 211. Raman spectra of dry powder glyceryl phosphate (**black**) compared to glycerol (**brown**) and **Pi** (**blue**).

By combining data obtained from the described before spectra of glycerol and **Pi**, we interpret each Raman peak including those like P–O–C stretching that are specific to organic phosphates. The Raman spectrum study of glyceryl phosphate was based on the interpretations of Zhu et al.³⁰⁰ and previously described starting molecules (**Table 60**, **Table 62**). In **Table 63**, Raman vibrational data for glyceryl phosphate is described.

Table 63. Raman vibrational data of glyceryl phosphate (cm^{-1}) along with an assignment, colours are identical to those used in **Figure 211**

Wavenumber measured	Wavenumber our references	Wavenumber from the literature	Suggested assignments
333	330	326	Intermolecular H-bond
419	416	417	CCO rocking
461	486	488	CCO rocking
524	481	378-544, 350-570	PO_4^{3-} bending
654	526	378-544, 350-570	PO_4^{3-} bending
780	-	674, 676	C–C bending ²⁹⁴ OH bending ²⁹⁵
891	-	832	Weak, sym. P–O–C stretching
905	912-1272	800-1200	Skeletal stretching
913	925	931	CH_2 rocking
984	-	1006, 963	asym. P–O–C stretching
1063	1056	1051	C – OH sym stretching C1, C3
1077	1087	-	Skeletal stretching
1112	1110	1109	C – OH stretching C2
1126	1122	1195	P=O stretch
1268	1262	1253	CH_2 twisting coupled with OH bending
1285	1272	800-1200	Skeletal stretching
1309	1314	-	CH_2 twisting
1353-1365	1360	1336	CH twisting coupled with OH bending
1456	1467	1459	CH_2 bending, scissoring
2713-2766	2765	-	CH stretching C2
2873-2884	2885	2841, 2896	CH sym. stretching C1, C3
2921-2941	2942	2948	CH asym. stretching C1, C3
3288-3410	3368	3487, 3334, 3150	CO–H asym.-sym. stretching
	3274-3442		H_2O

7.1.2. Experiments on glycerol phosphorylation under pressure

For studying glycerol under high pressure, ideally we would have chosen a ratio of 1:1:1 glycerol:urea: P_i . However, given the high viscosity of the mix, it was impossible to load it in the small pressure chamber of the DAC; therefore, we first loaded a dry mixture of 1:1 urea: P_i and filled the sample chamber with a microdroplet of glycerol.

The first experiment was performed with a large excess of glycerol, which led to its polymerisation. It was carried out in three steps: heating the crude mixture up to 115 °C, applying a moderate pressure of a few thousand bars at 115 °C, then cooling down and slowly releasing pressure.

Visually, through transmitted light, we could observe the dissolution of urea and P_i crystals in glycerol and then the slow formation of gas bubbles after 48 hours. They further

grew afterwards during the gradual pressure release (**Table 64**). Already after a couple hours of heating at 115 °C, we struggled with obtaining good-quality spectra due to overwhelming fluorescence (**Figure 212**). Most likely, during the experiment under pressure and temperature, the decomposition of glycerol was initiated due to its huge excess. Another evidence of it is the detection of CH₄ gas inside the large bubbles with a Raman shift 2917 cm⁻¹ (**Figure 212, red** spectra). It is known from the literature that condensation and polymerisation of glycerol molecules can be achieved at elevated temperatures^{301,302} as well as its decomposition into methane.³⁰³

Table 64. Images from microscope taken during the experiment, with excess of glycerol and corresponding to the spectra in **Figure 212**

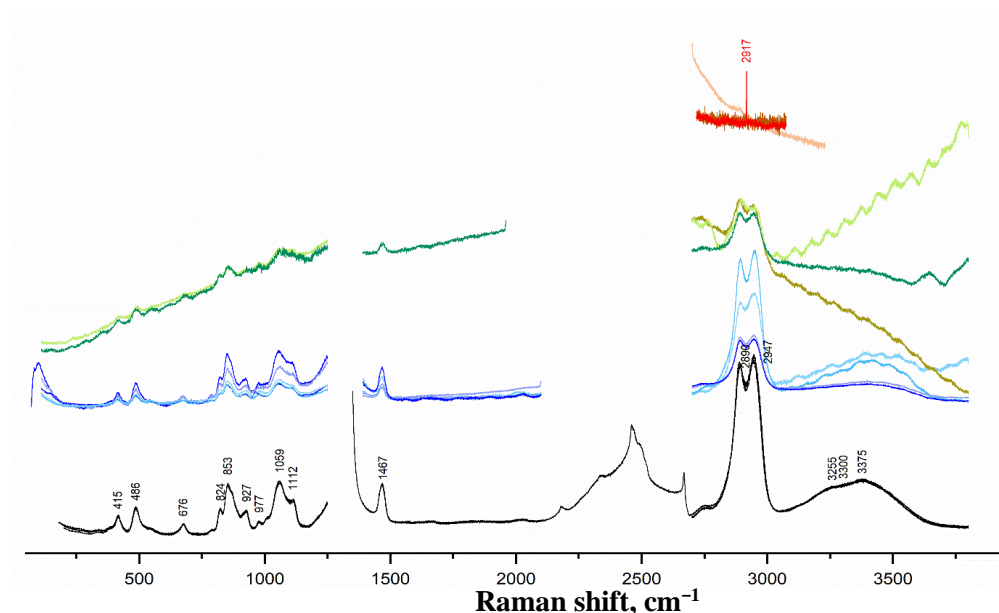
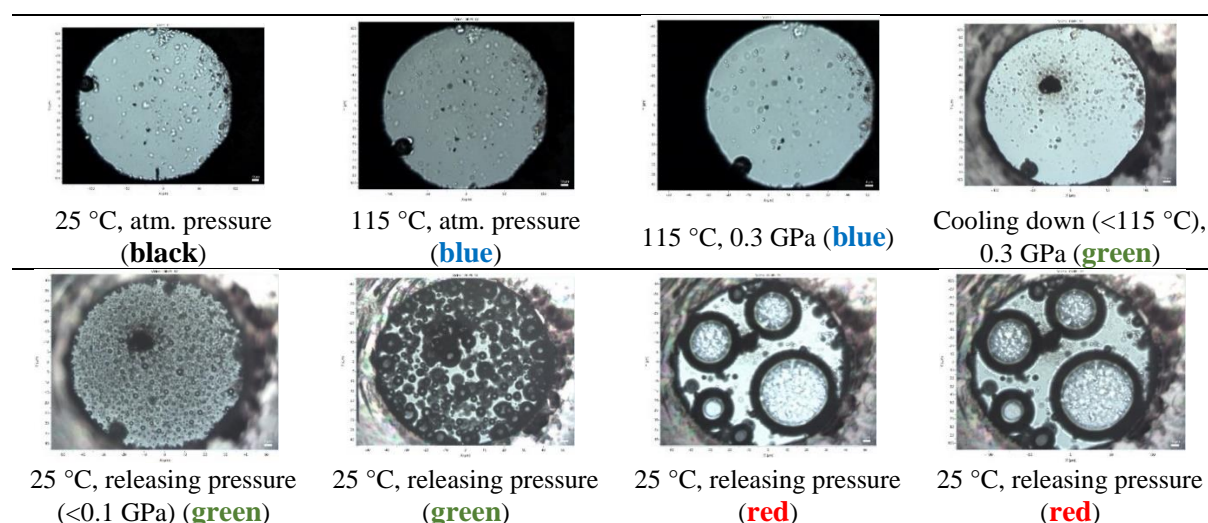


Figure 212. Raman spectra of crude mixture glycerol:urea:Pi as a function of temperature and pressure. For each point, acquisitions were made in several positions of the sample. Under pressure, the gaps between 1300-1350 cm⁻¹ and 2000-2400 cm⁻¹ are to avoid the very intense C–C vibration of the diamond anvil. **Black** – spectra before applying pressure and temperature, **blue** – spectra at 0.3 GPa and 115 °C, **green** – spectra after cooling down to rt, **red** – spectra inside of the produced bubbles (**Table 64**).

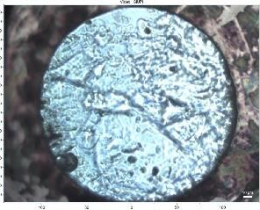
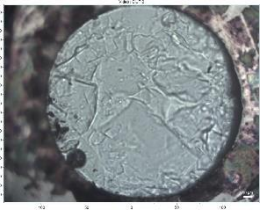
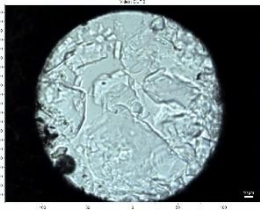
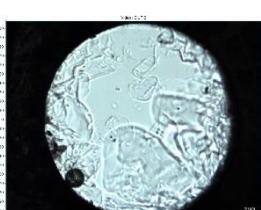
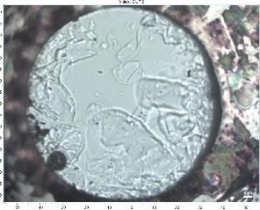
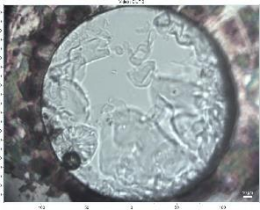
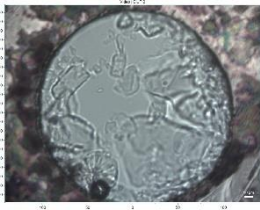
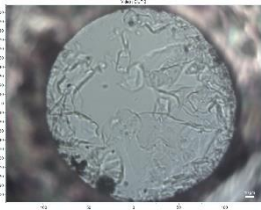
This result could be potentially interesting in terms of studying polymerisation and degradation of glycerol under hydrothermal conditions, which, however, was beyond the goal of this thesis. Thus, we changed the strategy for the second experiment. The DAC was densely filled with a dried and well-grinded mixture of urea: P_i (1:1) with the addition of a micro-droplet of glycerol, which was still in excess given the constraints to close the DAC.

The crude mixture was first sealed at 0.3 GPa and then heated up to 115°C. After reaching the desired temperature, the pressure was adjusted to 0.7 GPa and left overnight. The next day, we cooled it down and then the pressure was gradually released.

Each step of the experiment was controlled by Raman spectroscopy. At each stage of pressure and temperature, selected spectra were measured in different locations of the DAC and the results are summarised in **Figure 213**. Each spectrum has 1-3 duplicates not shown in the image to avoid overloading it.

Visually, we observed the melting of the solid crystals of urea and P_i and their migration inside the cell during heating and pressure release (**Table 65**). Compared to the previously described experiment, we did not observe the formation of bubbles or overwhelming fluorescence on the sample.

Table 65. Images from microscope registered during the experiment with excess of glycerol correspond to signals from spectra of **Figure 213**

			
25 °C, atm. pressure (red)	115 °C, 0.3 GPa (blue)	115 °C, 0.7 GPa, 6 hrs (green)	115 °C, 0.7 GPa, 21 hrs (brown)
			
115 °C, 0.7 GPa, 23 hrs (brown)	115 °C, 0.7 GPa, 26 hrs (brown)	25 °C, releasing pressure (brown)	25 °C, atm. pressure (purple)

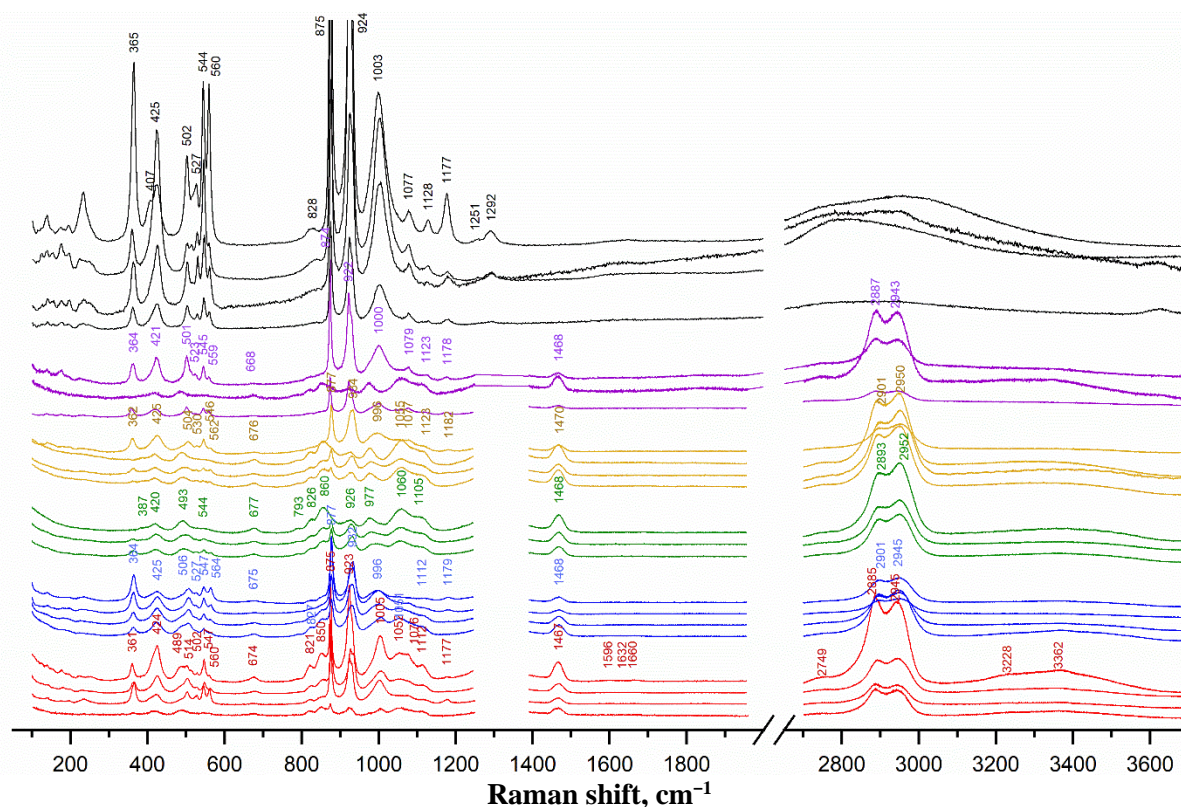


Figure 213. Raman spectra of crude mixture glycerol:urea: P_i as a function of temperature and pressure. For each point, acquisitions were made in several positions of the sample. The gaps between 1300-1350 cm^{-1} and 2000-2400 cm^{-1} are to avoid the very intense C–C vibration and the second order of the diamond anvil. **Red** – spectra before applying pressure and temperature, **blue** – spectra at 0.3 GPa and 115 °C, **green** – spectra at 0.7 GPa and 115 °C, **brown** – spectra below 0.7 GPa and cooling down, **purple** – spectra after cooling down to rt, atm. pressure, **black** – spectra after opening the cell. Spectra correspond to **Table 65**.

Even though the spectra in **Figure 213** seem to have different signal intensities depending on the spot where the Raman was registered, in general, signals seem to be consistent over the cell. Therefore, for easier products interpretation, we superimposed (**Figure 214, A**) and stacked (**Figure 214, B**) the spectra of the starting molecules, glyceryl phosphate and one of the final spectrum of the crude mixture glycerol:urea: P_i that was measured in the open DAC at the end of the experiment. In **Table 66**, we suggest an assignment of the final spectrum according to the literature.

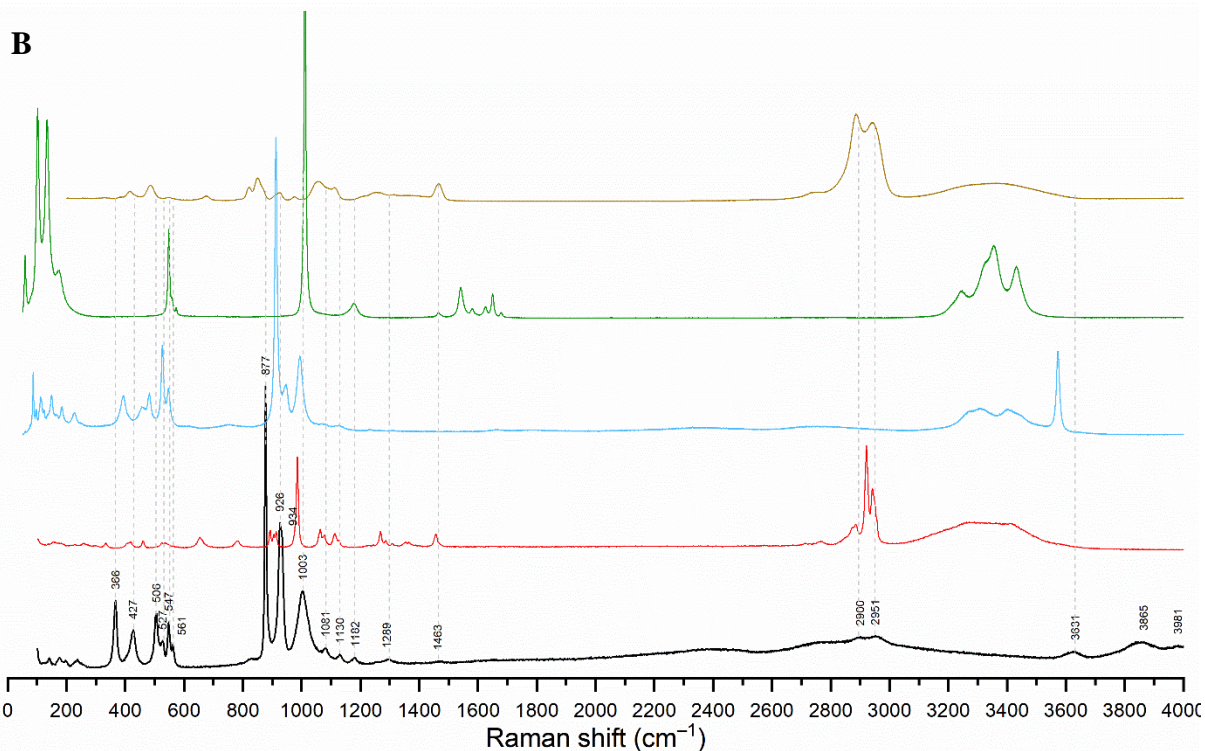
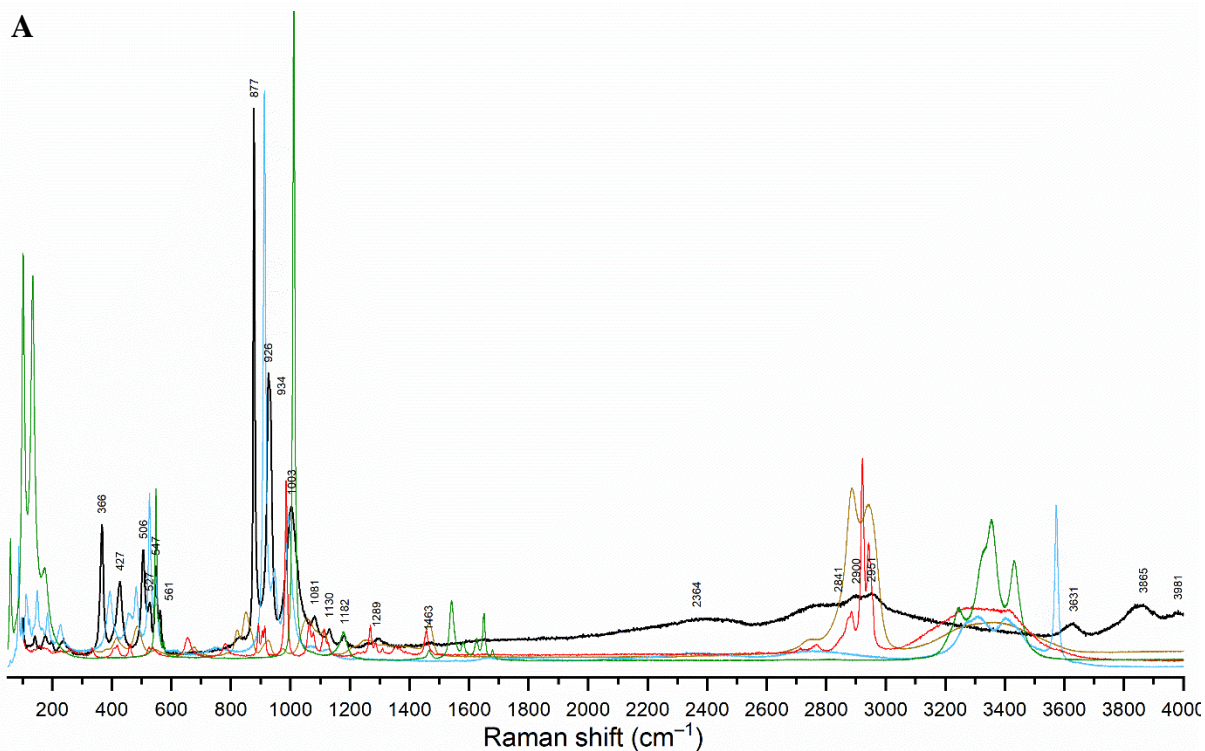


Figure 214. Selected Raman spectra of crude mixture of glycerol:urea:P_i (**black**) after 26 hours at 115°C and 0.7 GPa from **Figure 213** compared to the spectra of starting molecules glycerol (**red**), urea (**green**), P_i (**brown**) and glyceryl phosphate (**blue**) from **Figure 208-Figure 211**. **A** – superimposed spectra, **B** – stacked spectra.

Comparing the signals with the final spectrum (**black**), we notice a shift of the 912 cm⁻¹ P_i (**blue**) signal to the left to the lower wavenumber at 877 cm⁻¹ (**black**). This indicates that the PO₄ group is present in the mixture but in a different form, possibly phosphorylated

glycerol. This is also supported by the shift of CH and CH₂ groups 2885 and 2942 cm⁻¹ in glycerol (**brown**) to 2900 and 2951 cm⁻¹ in the crude mixture spectrum (**black**). Based on our experience with this reaction at 115°C and room pressure (see the previous section), it should be noted that we do not expect to get a single reaction product. The fact that most of the signals in the reaction mixture (**black**) are quite broad is consistent with the presence of several products with similar compositions in the mixture. Another important point is the presence of the symmetric and asymmetric P–O–C stretching at 780 and 984 cm⁻¹ for the reference spectrum (**red**) and 828 and 1003 cm⁻¹ for the obtained mixture (**black**), respectively. It is difficult to identify the exact type of phosphorylated product with absolute certainty; however, this provides evidence of the presence of phosphoester's bond.

An additional interesting point is the absence of the obvious urea triplet around 3200–3400 cm⁻¹ at the end of the experiment. In general, the pattern of the glyceryl phosphate spectrum (**red**) looks similar to the signals of the crude mixture (**black**) that are described in **Table 66**. Thus, in **Figure 213**, one may follow the advancement of the reaction by tracking the decrease of the signal in this region to its almost complete disappearance at the end of the reaction.

Table 66. Raman vibrational data of glyceryl phosphate (cm⁻¹) along with an assignment, colours correspond to signals from spectra of **Figure 214**

Wavenumber experiment	Wavenumber of glyceryl phosphate	Wavenumber of reference molecules	Wavenumber literature	Suggested assignments
366	333	330	326	Intermolecular H-bond
427	419	416	417	CCO rocking
		486	488	CCO rocking
506	461	481	378-544, 350-570	PO ₄ ³⁻ bending
527, 547, 561	524	526	378-544, 350-570	PO ₄ ³⁻ bending
-	654	675	674, 676	C–C bending ²⁹⁴ OH bending ²⁹⁵
828	780	-	832	Weak, sym. P–O–C stretching
877	891	912-1272	800-1200	Skeletal stretching
	905			
926-932	913	925	931	CH ₂ rocking
1003	984	-	1006, 963	asym. P–O–C stretching
-	1063	1056	1051	C – OH sym stretching C1, C3
1081	1077	1087	-	Skeletal stretching
-	1112	1110	1109	C – OH stretching C2
1130	1126	1122	1195	P=O stretch
1182	1268	1262	1253	CH ₂ twisting coupled with OH bending
1289	1285	1272	800-1200	Skeletal stretching
-	1309	1314	-	CH ₂ twisting
-	1353-1365	1360	1336	CH twisting coupled with OH bending
-	1456	1467	1459	CH ₂ bending, scissoring
2364	2713-2766	2765	-	CH stretching C2
2841	2873-2884	2885	2841, 2896	CH sym. stretching C1, C3
2900-2951	2921-2941	2942	2948	CH asym. stretching C1, C3
		3368	3487, 3334,	CO–H assym.-sym. stretching
3631	3288-3410	3274-3442	3150	H ₂ O

As the last step of this experiment, it was important to compare the obtained results with the similar reaction carried out in the previous section. For this purpose, we performed a vibrational study of one of the crude reaction mixtures of glycerol with urea and NaH_2PO_4 (1:1:1) after 120 hours of heating at 115 °C. A comparison of the spectra is given in **Figure 215**.

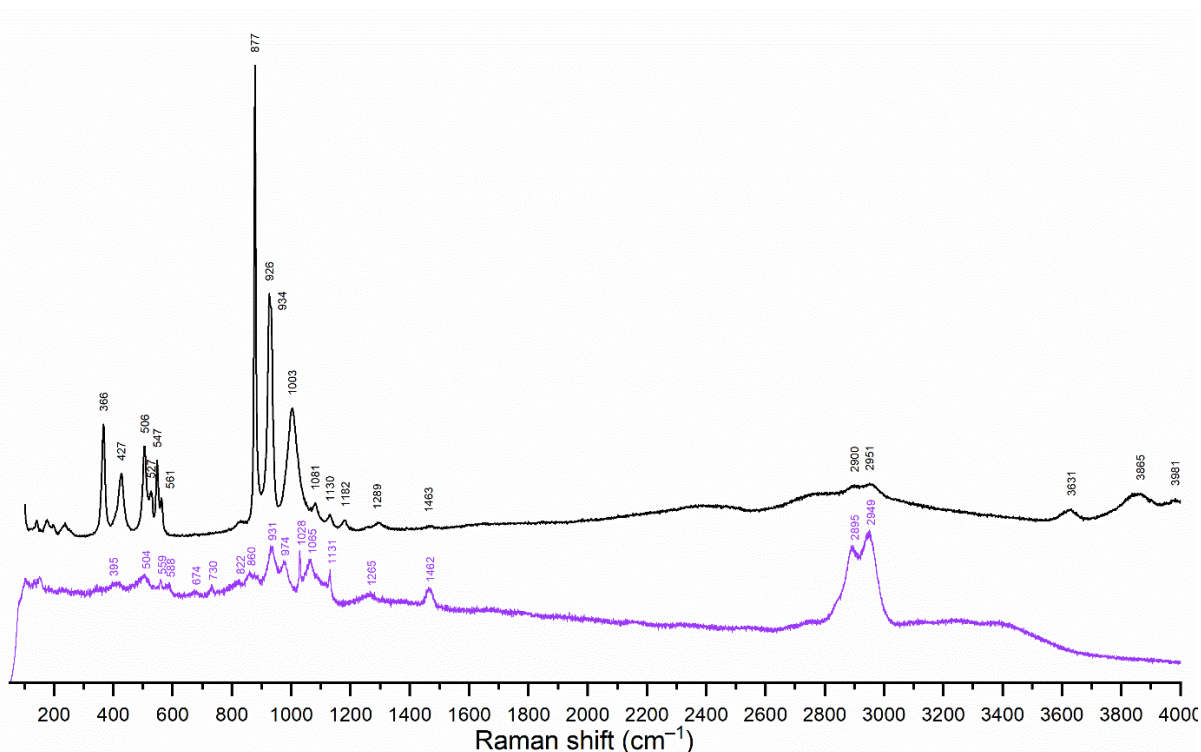


Figure 215. Selected Raman spectra of crude mixture glycerol:urea: P_i (**black**) from **Figure 213** (26 hrs at 115 °C and 0.7 GPa) compared to the spectra of crude mixture glycerol:urea: P_i (**purple**) obtained (Results and Discussion, section 1.1) after heating at 115 °C and room pressure for 120 hours.

Comparing the signals in **Figure 215**, we noticed that they do not correspond completely, which could be expected due to the different approaches to the phosphorylation process. As described before, the crude mixture may contain more than ten different organic products of phosphorylation. Unfortunately, the volume of the DAC sample is not large enough for performing MS or NMR analyses; however, potentially, in further research, it can be performed on another temperature-pressure vessel, such as a piston cylinder, to obtain larger samples suitable for NMR analysis. At this stage, we conclude from the vibrational analyses the presence of P–O–C sym. and asym. stretching at 822 and 974 cm^{-1} and complete consumption of urea.

7.2. Sodium N-formylcyanamide as a new potential condensing agent

Among organic molecules, cyanamide plays an important role in prebiotic chemistry. It could have been formed on the early Earth by UV irradiation from abundant small molecules such as water, methane, ammonia, etc³⁰⁴.

Cyanamide is a kinetically stable molecule with high activation barriers. Two tautomers are in equilibrium with the dominance of $\text{N}\equiv\text{C}-\text{NH}_2$ over $\text{HN}=\text{C}=\text{NH}$ (carbodiimide). In a slightly acidic environment, carbodiimide behaves as a dehydration agent and is capable of initiating condensation reactions^{305,306}. A possible source of protons could be NaH_2PO_4 , in the presence of which, with excess glycolaldehyde and cyanamide, it is possible to assemble pyrimidine ribonucleotides³⁰⁷.

Isocyanides (with the functional group $-\text{N}^+\equiv\text{C}^-$) have long been described as condensing agents in the synthesis of amino acids, peptides, and nucleotides³⁰⁸ as well as conductors of the acylation reaction of acyclic glyceryl phosphate by fatty acids ($\text{C}_8\text{-C}_{10}$) that leads to the production of stable vesicles³⁰⁹. In contrast to cyanamide or urea, methyl isonitrile (MeNC) is able to play a role in both phosphorylation and acylation reactions. However, its prebiotic plausibility is a debatable question. As a gas, MeNC could be hardly accumulated in the early Earth's environment, which hampers its role in prebiotic synthesis.

Along these lines, we suggest that N-cyanoformamide (systematic name, abbrev. NCF), more intuitively called N-formylcyanamide, could be an alternative prebiotic condensing agent. Due to the presence of an electron-withdrawing formyl group on cyanamide, it is expected to hydrolyse easier (faster) than cyanamide. NCF could be produced from cyanamide under alkaline conditions, for example, from calcium or sodium cyanamide salts and methyl formate, which could have been available on the early Earth through the disproportionation reaction of formaldehyde. As in a Tishchenko reaction,³¹⁰ where two aldehyde molecules disproportionate on a metal ion such as aluminium or a transition metal directly to an ester, prebiotic formaldehyde would disproportionate to formic acid methyl ester (methyl formate) without liberating methanol and formic acid. Methyl formate can act as a formylating agent of the cyanamide anion (**Figure 216**). The same reaction sequence applies to other, more complex electron-withdrawing groups on cyanamide, such as N-acetylcyanamide (systematic name: N-cyanoacetamide, NCA) and so on. NCA would result from the disproportionation of acetaldehyde on a metal ion, giving ethyl acetate that would acetylate cyanamide under alkaline conditions.

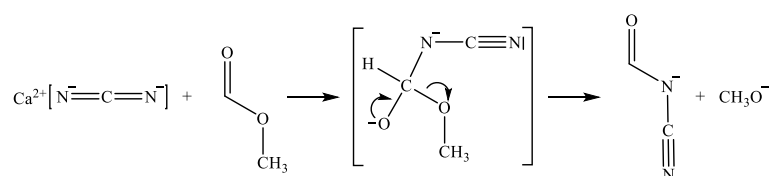


Figure 216. Tentative reaction scheme of sodium N-cyanoformamide prebiotic formation

These electron-poor cyanamide derivatives could equally serve as prebiotic condensing agents. Contrary to all known more complex derivatives, such as NCA, the simplest NCF is only stable as a salt, thus under unchanged alkaline conditions.³¹¹ Many acyl cyanamide

derivatives, such as NCF and NCA, are known as an industrial reactive intermediate for the synthesis of agrochemicals but have never been described or tested as a prebiotic molecule or salt. The sodium salt of NCF is stable under elevated temperatures (up to 301 °C), is soluble in water and slowly hydrolyses to formate, cyanamide then urea.³¹² We assume NCF to be as well as a condensing agent for fatty acids and alcohols for potential membranogenic processes.³¹³ The formation of prebiotic precursors with the assistance of NCF as a condensing agent could be a key to the formation of nucleotides and peptides.

Another interest for the N-cyanoforamamide molecule is applying hydrothermal conditions that may lead to the formation of the chemically very interesting molecule of carbamoylisonitrile (systematic name: N-isocyanocarbonylamide, ICA, **Figure 217**).

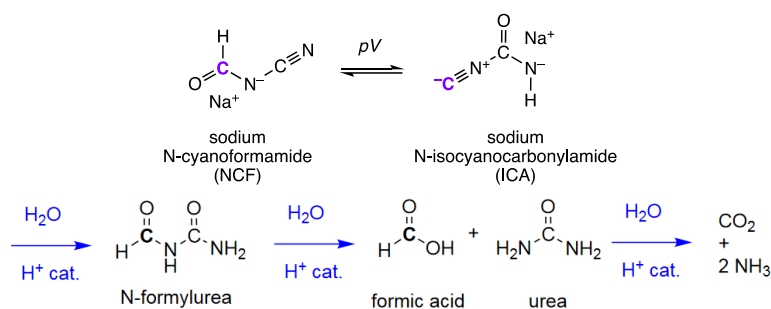


Figure 217. Tentative reaction scheme of sodium N-cyanoforamamide towards a hydrothermal intramolecular rearrangement to sodium N-isocyanocarbonylamide and further acid-catalysed hydrolysis of both as suggested in this work.

Should the transformation go along the described pathway, we expect to observe the appearance of a new N-H stretch vibration detectable by Raman spectroscopy. In addition to it, we anticipate the decay of C-H stretch vibration intensities as well as another C=O stretch and triple-bond CN vibrations appearance.

In later stages of the reaction, sodium N-cyanoforamamide could be hydrolysed (with the addition of water and protons) to N-formylurea, then formic acid and urea, and later carbon dioxide and ammonia.

In this chapter, the goal was to study the behaviour of sodium N-cyanoforamamide *in situ* under pressure in a diamond anvil cell using Raman spectroscopy, as well as to explore the possibility of the involvement of this molecule in phosphorylation reactions as a potential condensing agent.

7.2.1. Characterisation of starting molecule

The commercial sodium N-cyanoformamide that was synthesized on demand was analysed by LRMS and NMR spectroscopy.

As expected from literature³¹² we observe at $\delta_{\text{H}} = 8.49$ the proton of the carbonyl group (**Figure 218**). The additional signals are due to impurities that may have developed during long storage, as a result of its hygroscopicity and sensitivity to moisture. The estimated purity of the sodium N-cyanoformamide used in the experiments is calculated from the total integration of ^1H NMR signals and is about 44 % with respect to other minor proton signals.

In the ^{13}C NMR spectrum, we observe three main signals, two of which correspond to the starting molecule $\delta_{\text{C}} = 171.44$ and 123.07 ppm. The signal of the quaternary ^{13}C atom situated between two ^{14}N atoms is expected to be difficult to register (**Figure 219**).

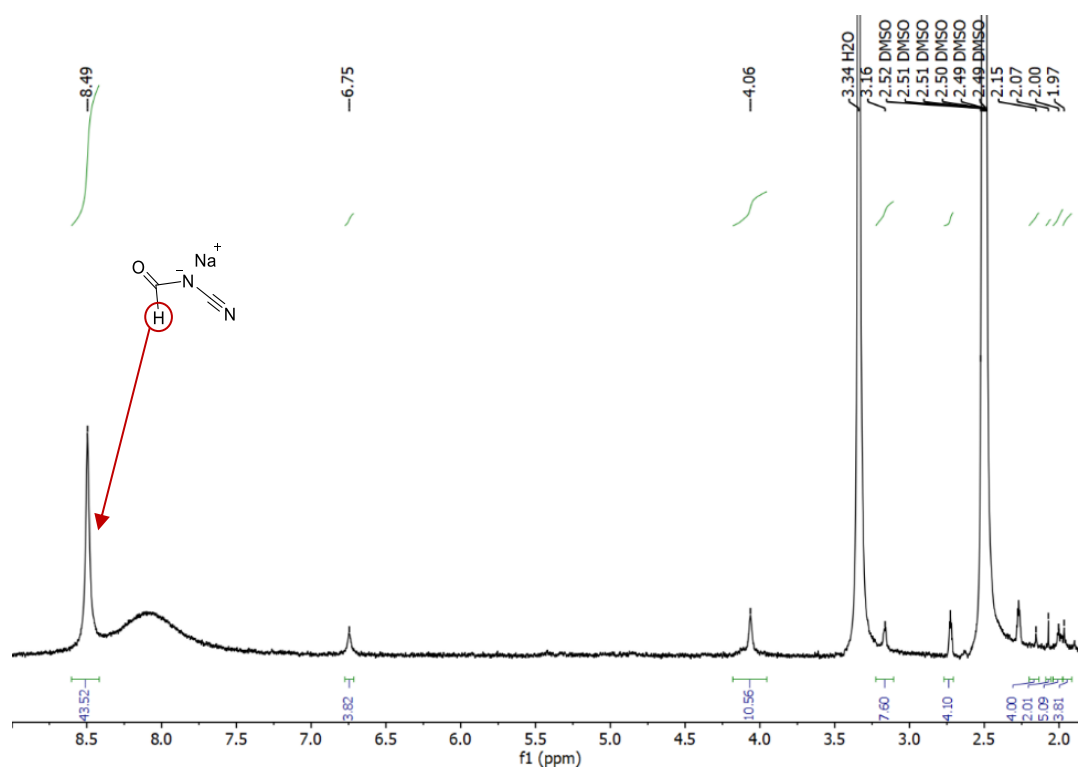


Figure 218. ^1H NMR (400 MHz, $\text{DMSO-}d_6$) 0.5 mM of sodium N-cyanoformamide: $\delta_{\text{H}} = 8.49$ (s, 1H).

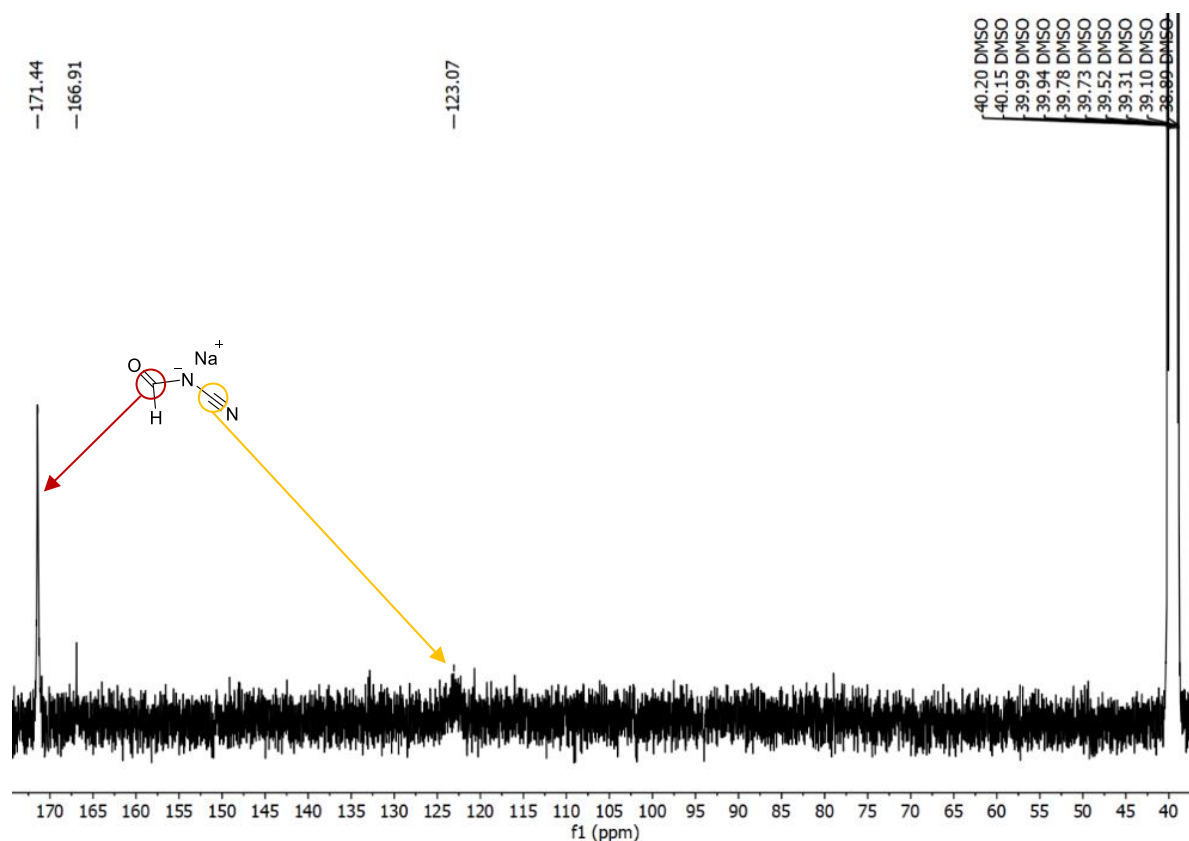


Figure 219. ^{13}C NMR (100 MHz, $\text{DMSO-}d_6$) 0.5 mM of sodium N-cyanoformamide: $\delta_{\text{C}} = 171.44$ ($\text{HC}(\underline{\text{C}}=\text{O})\text{NCN}$), 123.07 ($\text{HC}(\text{=O})\text{NC}\underline{\text{N}}$).

The analysis of NCF by LRMS using $\text{DMSO-}d_6$ as a solvent provides only the negative ion mode mass spectrum. Most signals can be explained by a variety of ion adducts of the NCF anion (**Figure 220**). The main signal, m/z 69.0, corresponds to the anion of NCF (M^-) [$\text{H}(\text{C}=\text{O})\text{N}^-\text{HC}\equiv\text{N}$] and all others correspond to MS-adducts of its multiplied mass and Na^+ , Cl^- . Minor signals are m/z 138.9 [$2\text{M}-\text{H}$] $^-$, 160.9 [$2\text{M}^- + 2 \text{Na}^+ - \text{H}$] $^-$, 218.8 [$2\text{M}^- + 2 \text{Na}^+ + \text{Cl}^-$] $^-$ etc.

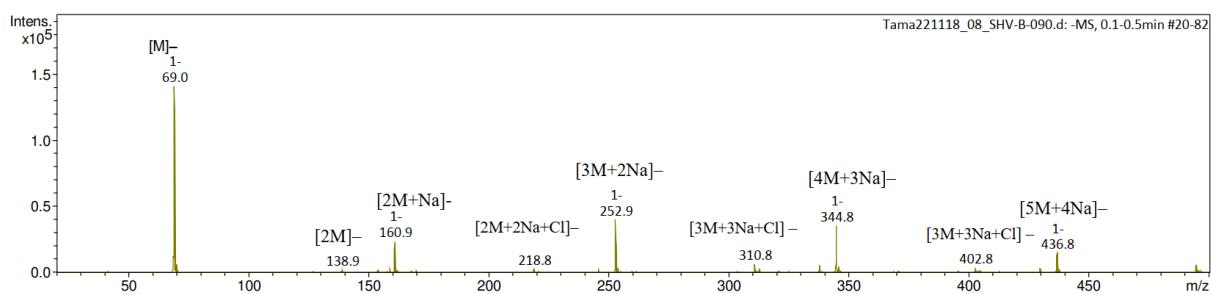


Figure 220. Low-resolution negative-ion mode mass spectrum of sodium N-cyanoformamide in $\text{DMSO-}d_6$.

When using MeOH as a solvent, in the negative ion mode of MS, the main signals of the spectrum correspond to clusters of m/z 68 [Na^+ , HCOO^-] (spectrum A, **Figure 221**). However, in positive ion mode, we did not detect the expected mass of NCF (spectrum B, **Figure 221**). The main signals, m/z 210, 304 and 528 are most likely the products of spontaneous polymerisation of NCF induced by electrospray ionisation in the MS source.^{234,235}

Due to the presence of CN, polymerisation and cyclisation follow the same pattern as in the case of cyanamide (**Figure 222**).^{314,315}

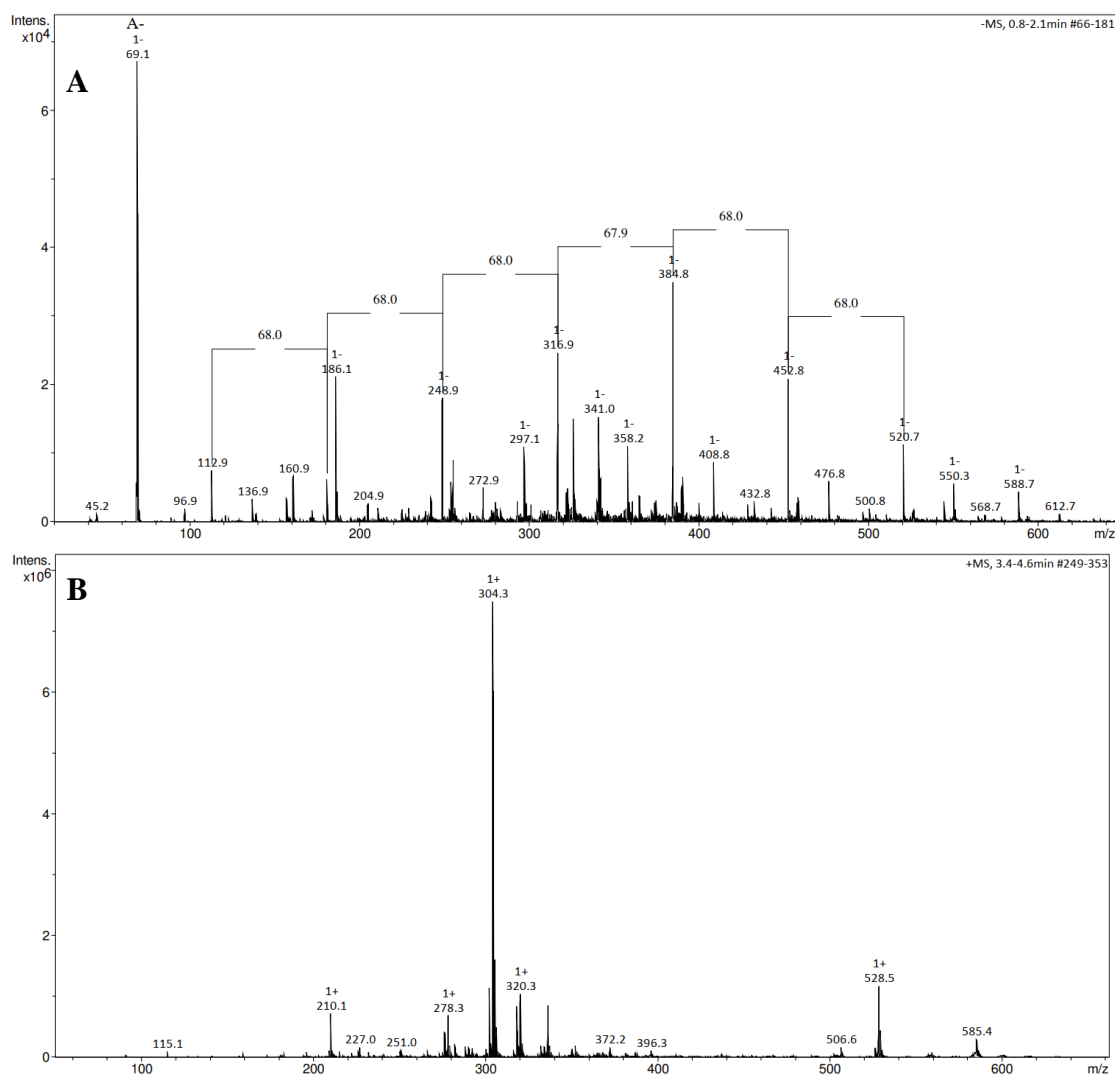


Figure 221. Low-resolution mass spectrum of sodium N-cyanofomamide in MeOH. **A** – negative-ion mode m/z 69.1 $[M-H]^-$; **B** – positive-ion mode.

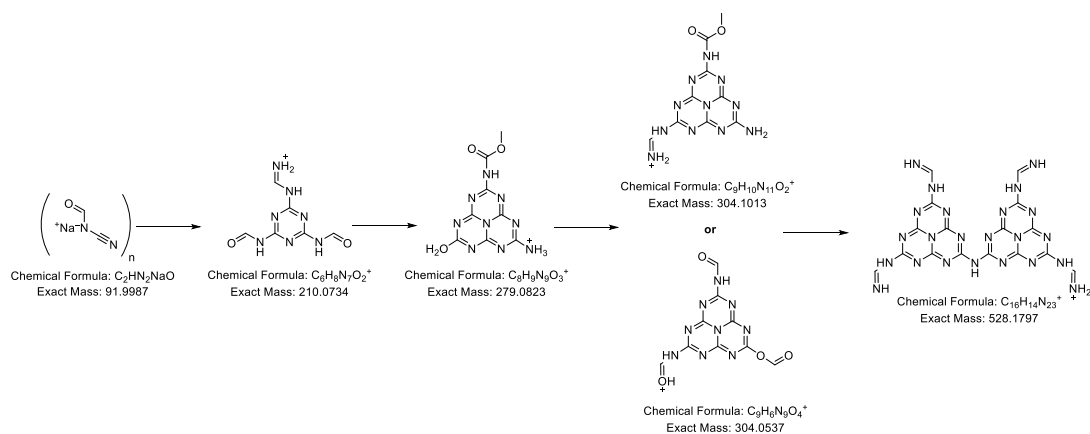


Figure 222. A tentative reaction scheme for sodium N-cyanofomamide polymerisation suggested in this work based on cyanamide polymerisation.

Prior to the *in-situ* study of dry sodium NCF under pressure, the vibrational Raman spectra of the NCF reactant were measured (**Figure 223**). Despite the small size of the molecule, the interpretation of the spectra was not straightforward, as there is no assignment available in the literature. The proposed assignment relies on the literature on isomeric cyanoformamide^{316,317} cyanamide³¹⁸ and formamide^{319,320}. Our interpretation of NCF Raman bands is summarised in **Table 67**. Note that we did not assign the lattice vibrational modes (below 400 cm⁻¹) since they are neither relevant to the present study nor described in the literature.

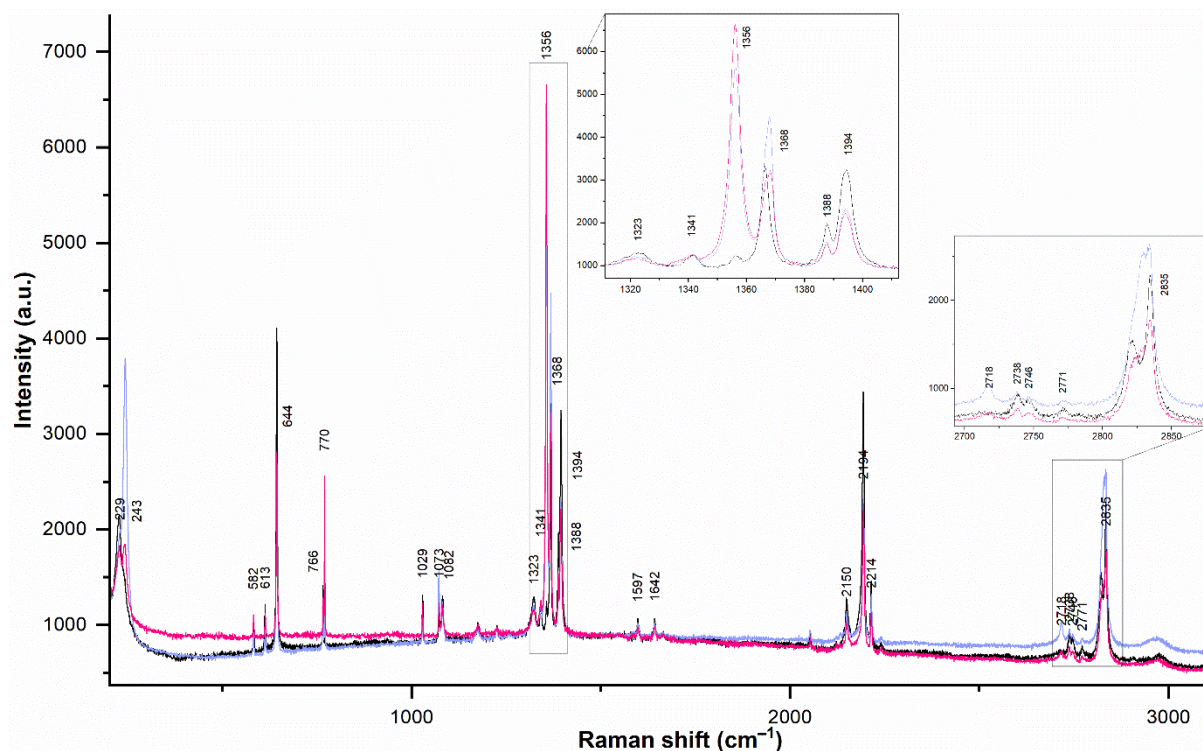


Figure 223. Raman spectra of dry powder of sodium N-cyanoformamide. The three spectra were measured in different spots of the sample

Given the high spectral resolution (<1 cm⁻¹) used in the present study, we think that we were able to identify the two *E* and *Z* conformers of NCF (**Figure 224**). In the spectra, most of the vibrations indeed appear in pairs, compared to singlets in the closely related molecules used for the assignment. We detected doublets that likely correspond to *E* and *Z* conformers for all major Raman vibrations: C1–H (2821–2835 cm⁻¹), N1–C1, N1–C2 (1323–1368 cm⁻¹), and C2≡N2 (2050–2214 cm⁻¹). In the solid state, such conformers may be stabilised through intermolecular salt bridges and therefore be in a slow exchange for Raman spectroscopy.

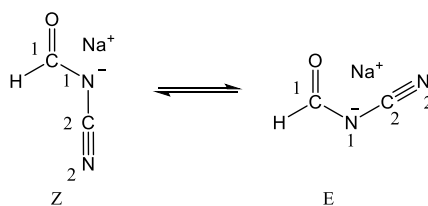


Figure 224. *E* and *Z* molecular conformations of sodium N-cyanoformamide

Table 67. Raman vibrational data of NCF (cm⁻¹) along with an assignment

Wavenumber experiment	Wavenumber literature ^{312,317-320}	Suggested assignments
582	570	N-C≡N in plane bending
613, 644	610	N-C=O bending
766, 770	753-755	C=O bending
1029	1018	C-H wagging
1073, 1082	1114	N-C≡N sym. stretching E, Z
1323, 1341	1309-1311	O-C ₁ -N ₁ asym. stretching E, Z
1356, 1368	1344-1356	C ₁ -N ₁ stretching, E, Z
1388, 1394	1390-1392	C-H bending
1597	1578	H-C-N sym. bending
1642	1621 (1680-1800)	C=O stretching
2150-2214	2250-2254	C≡N asym. stretching E, Z
2718-2771	-	C-H stretching, impurities
2821, 2835	2882-2887	C-H stretching E, Z

7.2.2. High pressure experiment with NCF at ambient temperature

Three high-pressure experiments were performed on NCF in a diamond anvil cell (DAC) up to 13 GPa. The spectra were collected at each pressure step, upon compression and decompression. A summary of one experiment is displayed in **Figure 225**. Raman spectra of the sample present data at the beginning (bottom line, red) and at the end of the experiment (top line, red), through the peak pressure at 10.2 GPa. We observe subtle reversible changes in the spectra from 8.0 GPa to the peak pressure and during decompression at 2.4 GPa (highlighted in grey).

We carefully tracked changes in the spectra from one pressure point to the next one and highlighted with colours all the changes that we could identify. A summary is displayed in **Figure 226 (A-D)**. Most of them are due to the expected compressibility of the NCF intramolecular bonds, some are characteristic of a reversible phase transition.

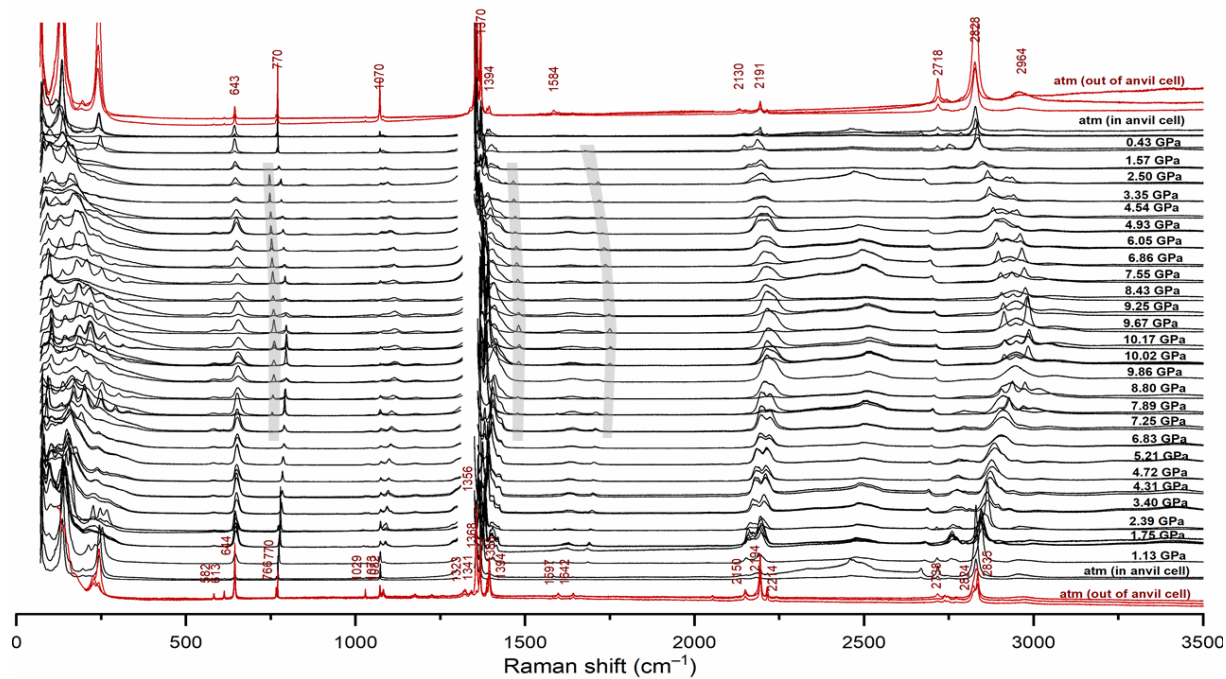
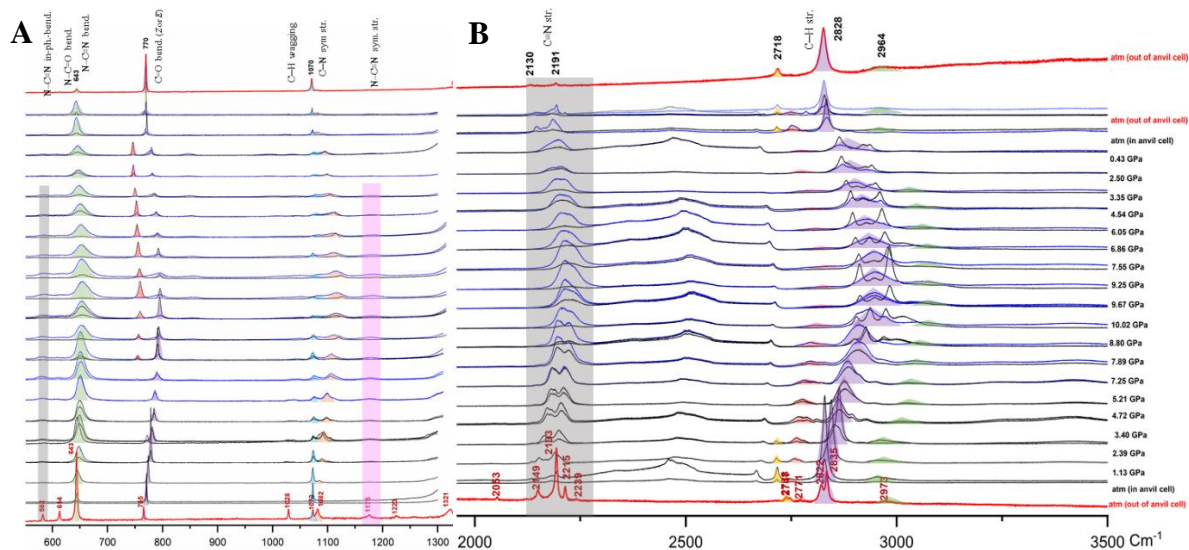


Figure 225. Raman spectra of dry sodium N-cyanofornamide as a function of pressure. For each pressure point, acquisitions were made in several positions of the sample. Under pressure, the gap between 1300 and 1350 cm^{-1} is to avoid the very intense C–C stretching vibration of the diamond anvil.



Continuation of the figure is on the next page

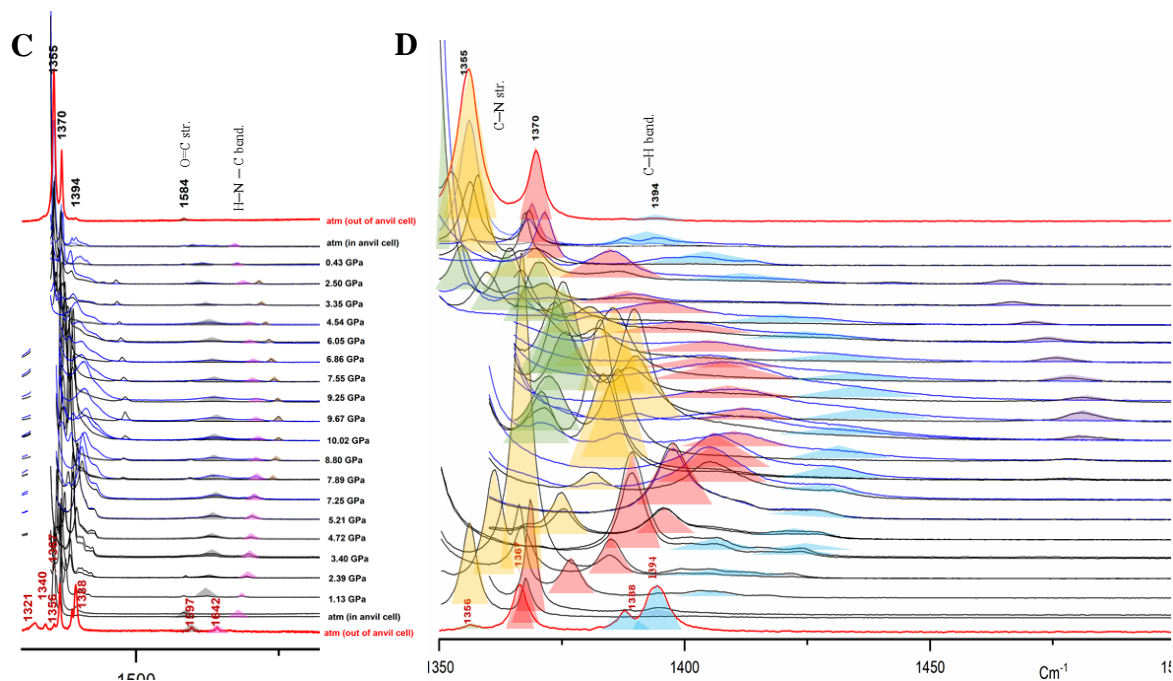


Figure 226. Selected regions of the Raman spectra of sodium N-cyanoforamide as a function of pressure, where reversible changes were observed. **A** – 550-1300 cm^{-1} ; **B** - 2000-3500 cm^{-1} ; **C** – 1350-2100 cm^{-1} ; **D** – 1350-1500 cm^{-1} .

Three new vibrations appeared upon compression at 8 GPa, at 750, 1480 and 1750 cm^{-1} , increased in intensity with pressure, reached their highest intensity at peak pressure. Upon decreasing pressure, these vibrations disappeared at 2.4 GPa, which represents a large hysteresis, characteristic of a first-order phase transition. This was beyond the scope of this work to go deeper into the crystallographic changes associated with this transition, as this simply shows subtle intramolecular rearrangements induced by lattice changes, which, however, do not influence the ultimate structure of the molecule. Most likely, we identified a rearrangement of the crystal structure, with NCF having a more symmetric structure at high pressure. This is supported by the disappearance of the pairwise vibrations of the *Z* and *E* conformers, as described in **Figure 224**.

The shifts of the Raman bands that could be followed during compression and decompression were measured and results are summarised in **Figure 227**.

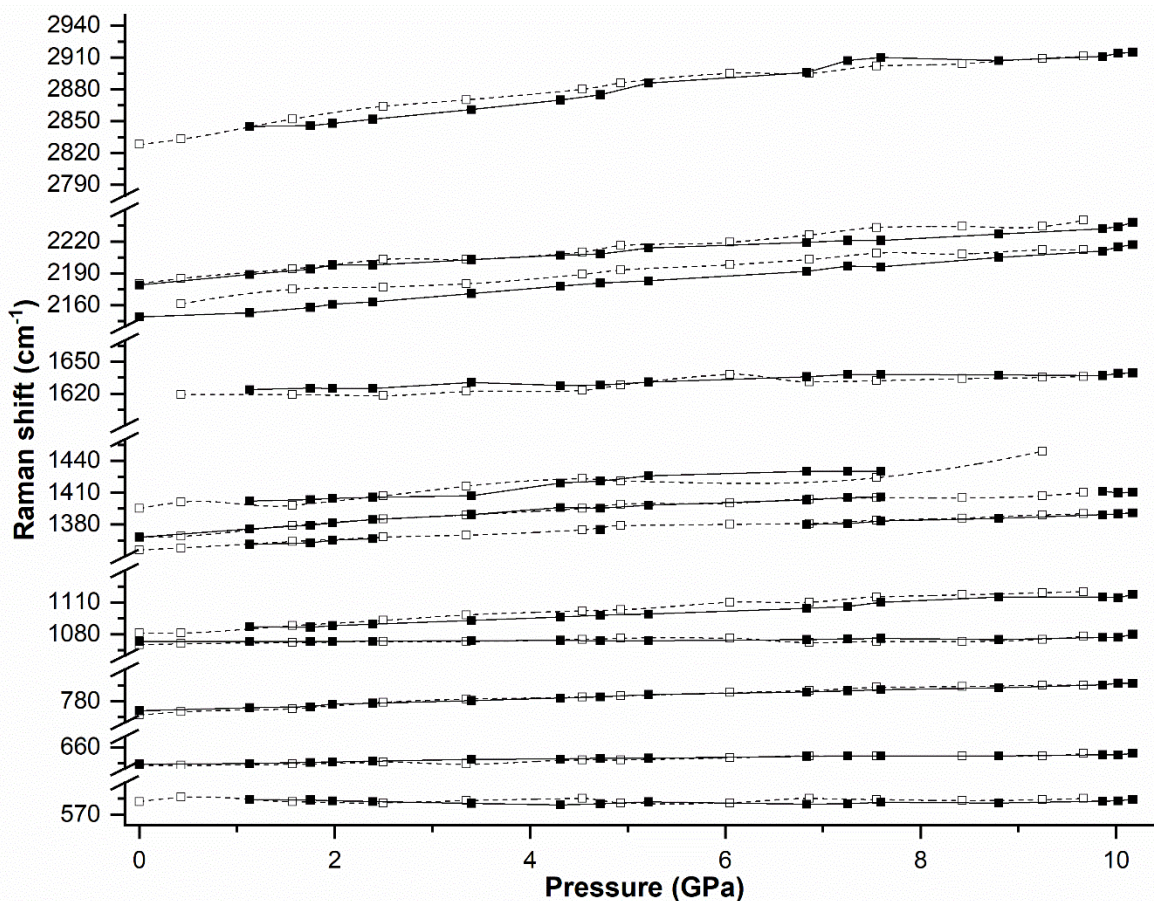


Figure 227. Pressure dependence of the Raman shifts. It demonstrates results from one of the independent sets of experiments. Black and white points represent changes with pressure increase and decrease, respectively. Straight and dashed lines connect pressure increase and decrease points, respectively.

Reviewing **Figure 217**, one sees that the expected changes in the sodium N-cyanoformamide (NCF) towards N-isocyanocarbonylamide (ICA) were not observed. In none of our experiments, did we find signal of expected NH vibrations at 1094 (NH rocking), 1595 (NH bending), or between 3190 and 3330 cm^{-1} (NH sym. and asym. stretching). Perhaps the application of pressure only is not sufficient to induce the changes, and the activation energy of the transition is too high. Additional heating of the sample would also be required.

To confirm the results obtained *in situ* in the DAC, we performed a larger-volume experiment in a Paris-Edinburgh cell. A few milligrams of NCF were kept under pressure at 7 GPa for one hour at room temperature. After recovery, the sample was measured by Raman spectroscopy and then dissolved in DMSO-*d*6 (0.5 mM scale) for NMR and MS analyses.

The Raman spectrum of the larger scale NCF sample does not demonstrate significant differences with the one obtained after pressure cycling in the DAC (**Figure 228**). We observe a similar tendency towards crystal structure reorganisation as was described in the smaller-scale DAC experiment.

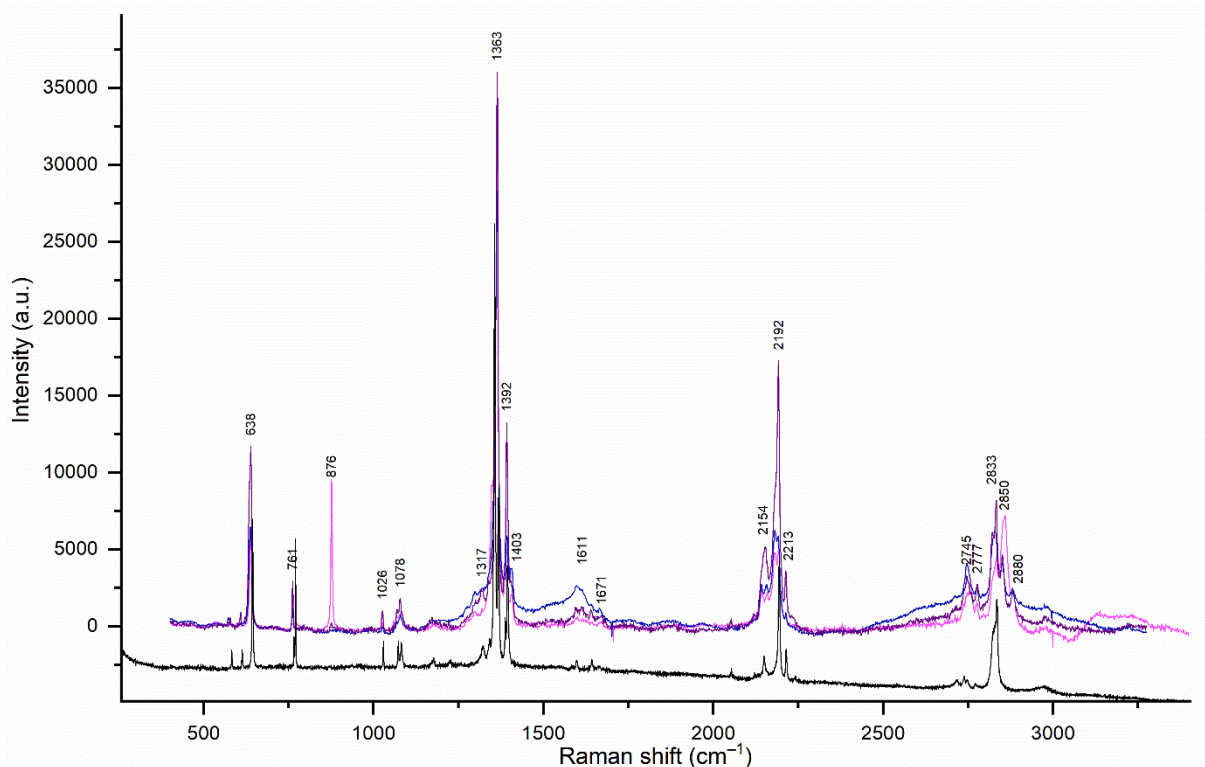


Figure 228. Raman spectra of sodium N-cyanoformamide, quenched, after 1 hour at 7 GPa. **Black** – spectrum of pure sodium NCF powder. Three **coloured** spectra were acquired at different locations on the recovered sample.

On such a small sample, ^1H NMR acquisition required more scans, which consequently enhanced the quality of the main signal at 8.5 ppm (**Figure 229**). Due to this fact, the signal seems to be more significant relative to the impurities (65%), compared to the spectra at the beginning of the experiment (44 %, **Figure 218**).

We do not observe major transformations or the appearance of new significant peaks. On the ^{13}C NMR spectrum (not shown here), we identified only one peak, $\delta_{\text{C}} = 166.3$, with an intensity close to the noise values.

The low-resolution mass spectrum in negative ion mode (**Figure 230**) is similar to the data from **Figure 220**. All the main signals have the same mass and the same relative intensities, indicating that no new molecules or products with higher weights were produced during the experiment.

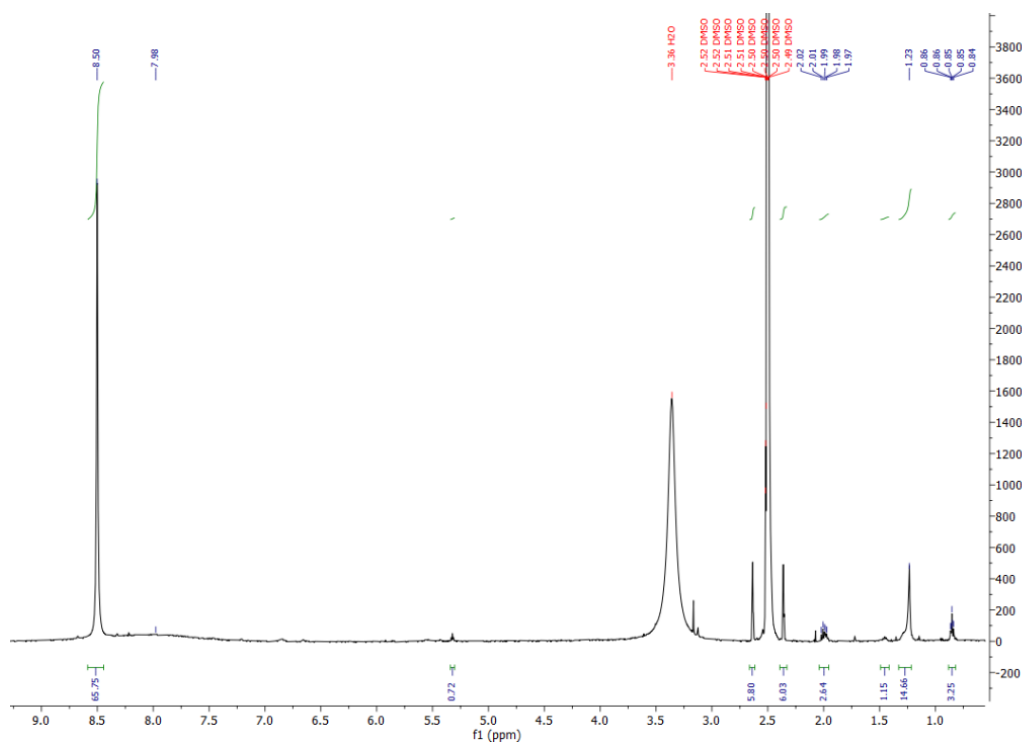


Figure 229. ^1H NMR (500 MHz, $\text{DMSO-}d_6$) 0.5 mM of sodium N-cyanofomamide after applying pressure: $\delta_{\text{H}} = 8.50$ (s, 1H).

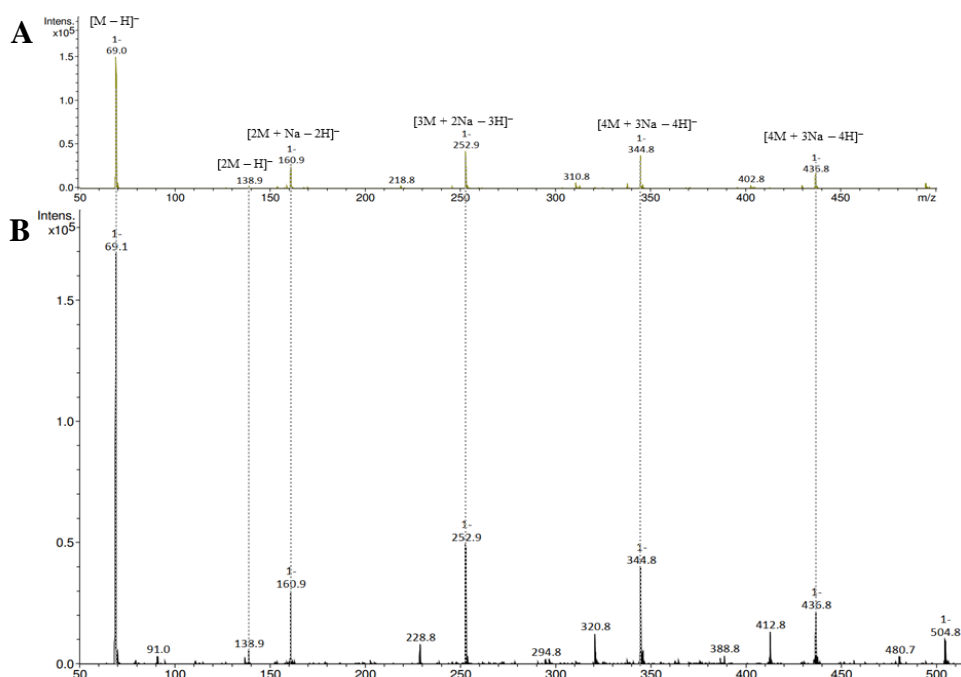


Figure 230. Low-resolution negative-ion mode mass spectra of sodium N-cyanofomamide in $\text{DMSO-}d_6$, m/z 69.0 $[\text{M}-\text{H}]^-$. **A** – pure sodium NCF before experiment (from **Figure 220**); **B** – sample after 1 hour under 7 GPa pressure.

In summary, the expected or other chemical transformation in the structure of the N-cyanofomamide molecule was not detected under pressure. The only difference detected between 2.5 and 10.17 GPa at 25 °C corresponds to crystalline re-orientation. The starting NCF

sample has transformed into a much more homogenous orientation (Raman peak pattern). The results of spectral analyses remain consistent on a larger and smaller scale.

7.2.3. High-pressure high-temperature experiment with NCF

The next step was obviously a study of NCF with simultaneous applications of pressure and temperature. The melting point of sodium NCF is 253 °C and the decomposition temperature is above 300 °C.³¹² The decomposition temperature of urea to transform it to, more precisely, to equilibrate it with ammonium cyanate, where a C-N bond has been cleaved, is about 130 °C. Thus, we chose this temperature and a pressure of about 10 GPa. The experiment was carried out in a gas-membrane driven DAC equipped with resistive heating.

A small amount of sodium NCF powder was loaded in the DAC with a ruby for pressure evaluation. It was first pressurised until 1.5 GPa to completely close the porosity of the powder and then heated. When the required temperature, as measured by a thermocouple touching one diamond anvil, was reached, pressure was gradually increased until 10.5 GPa. Then pressure was gradually released back to 1.5 GPa, and then the heating stopped. *In-situ* Raman spectra were measured in several locations of the sample at each pressure step (**Figure 231**).

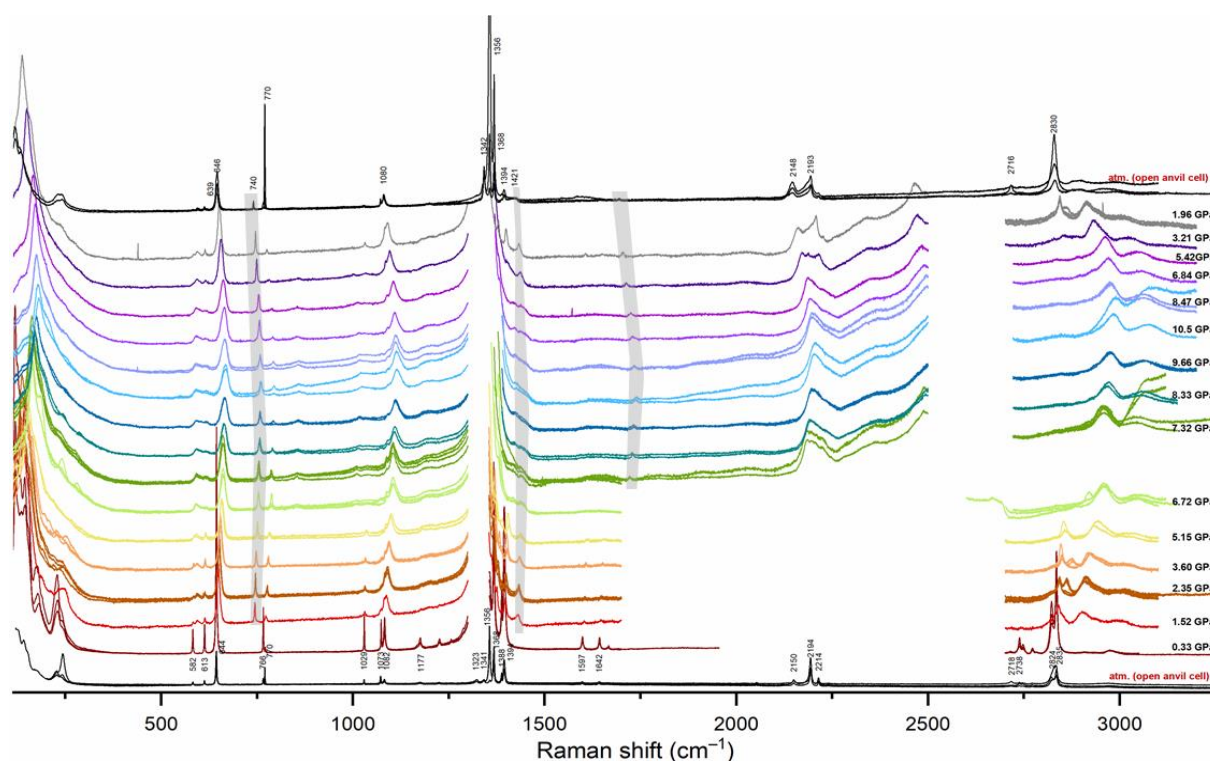


Figure 231. *In situ* Raman spectra of dry sodium N-cyanoformamide at 130°C as a function of pressure. For each pressure point spectra was made in several different places of sample. For the tests made through the DAC, the corresponding wavenumber of the diamond 1300–1350 and 2500–2700 cm^{-1} (C–C bond vibrations) was excluded.

In contrast to the experiments at ambient temperature, the changes that occurred under pressure and temperature started readily at 1.5 GPa when temperature was increased, and they

were quenchable. However, they clearly differ from those observed by Dai et al.³¹⁸ who described the oligomerization of solid-state cyanamide at 13 GPa at ambient temperature. If one may wonder why we did not extend our investigations to pressure in excess of 10 GPa, the answer lies in the environments that are represented by such pressures. They correspond to those of the mid-upper mantle, with temperature exceeding 1000°C and are no longer relevant to the subsurface where life could have emerged in the Hadean. Although the possibility of transfer upwards through convection into the livable depths of the Hadean Earth where they would produce from simpler compounds: lipids, nucleotides, oligonucleotides, peptides and so forth remains.

As a consequence, we performed a larger scale experiment in the Paris-Edinburgh press with a sample of 3 mg, at 7 GPa and 130°C for 1 hour (**Figure 232**).

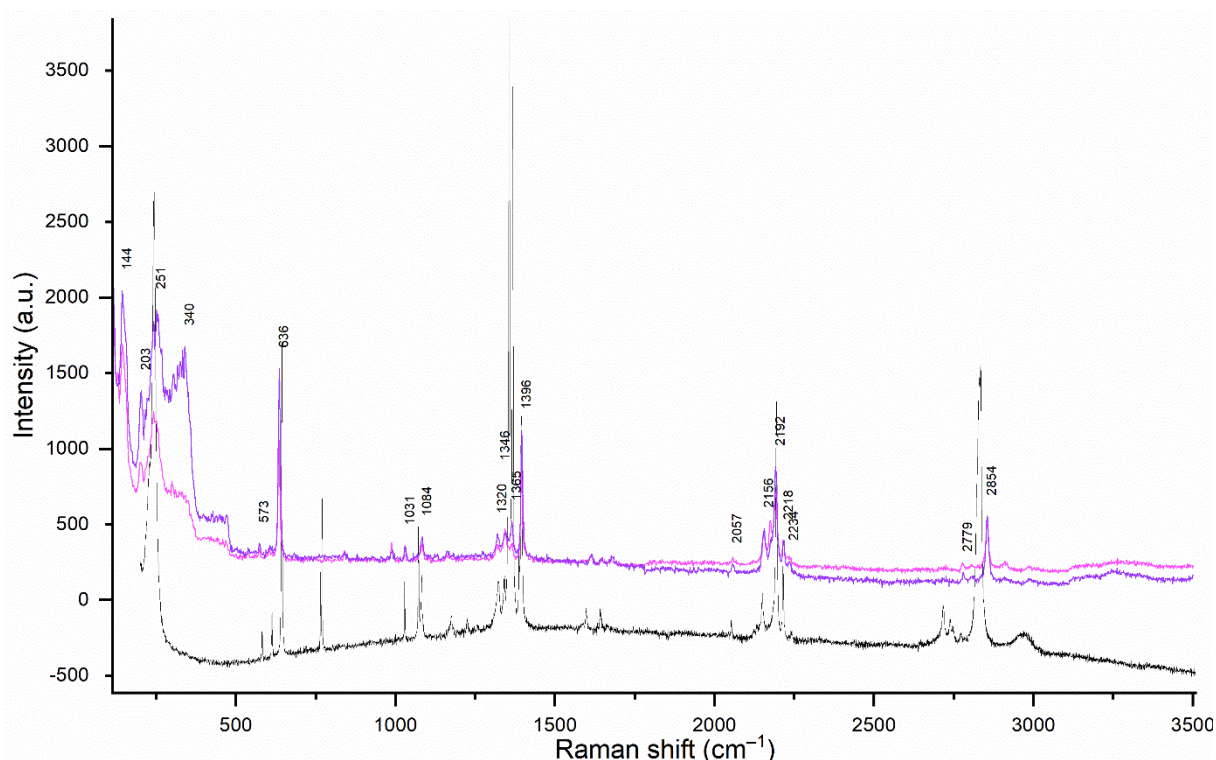


Figure 232. Raman spectra of dry sodium N-cyanofornamide after 1 hour under 7 GPa at 130 ° C. **Black** – spectrum of NCF before heating. Two **coloured** spectra represent different spots on the sample where an acquisition was made.

The experiment results were similar to the transformations that were described previously. The differences between the initial and obtained spectra consist of slightly different intensities but with the same Raman shift.

The sample obtained in the large-scale experiment was analysed and compared with previous NMR and MS data to understand and summarise the observed alterations (**Figure 233- Figure 235**).

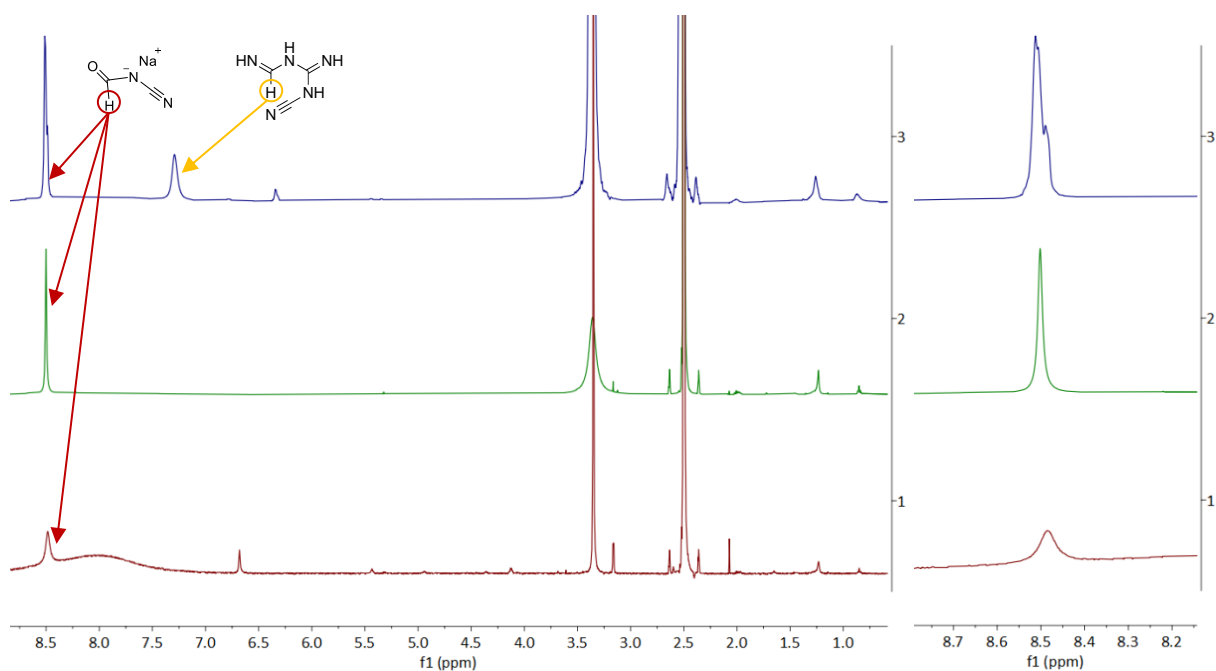


Figure 233. ^1H NMR (500 MHz, $\text{DMSO-}d_6$) spectra of 0.5 mM of dry sodium N-cyanoformamide: **red** – pure from **Figure 218** (4 scans), **green** – after applying pressure in the large-scale experiment from **Figure 229** (64 scans), **blue** – after applying pressure and temperature in the large-scale experiment (128 scans). The main signal is NCF $\delta_{\text{H}} = 8.50$ (1H). **A** – full spectra, **B** – zoom on the NCF signal 8.5 ppm.

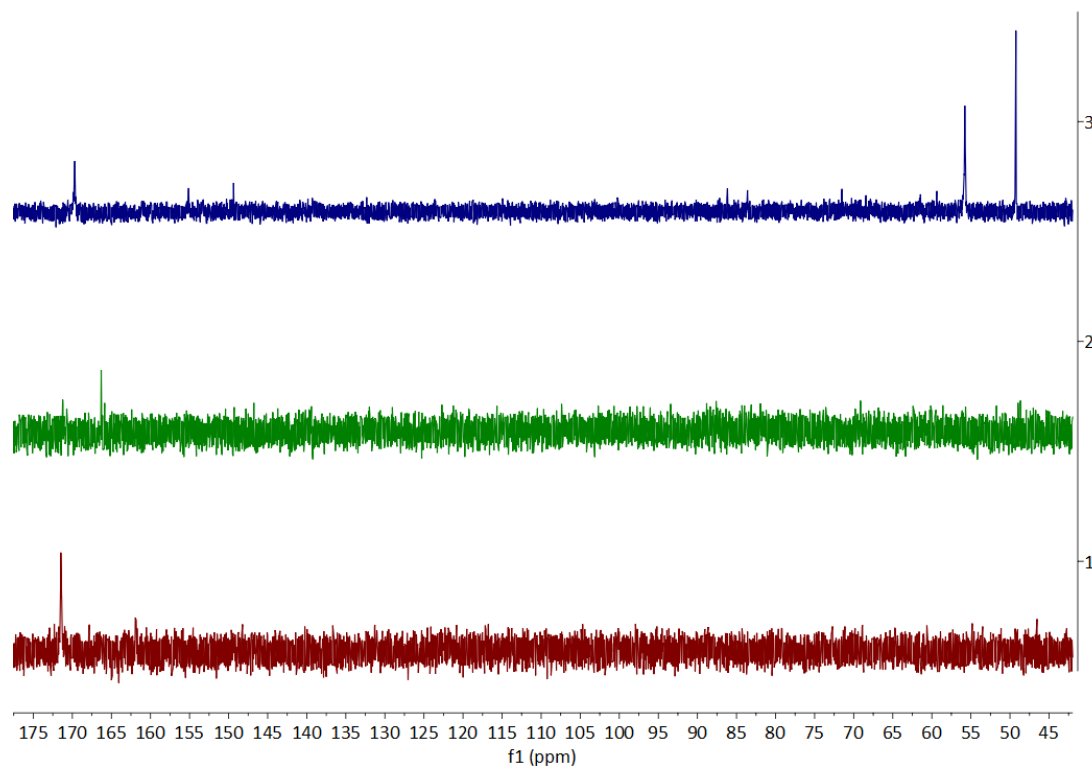


Figure 234. ^{13}C NMR (75.5 MHz, $\text{DMSO-}d_6$) spectra of 0.5 mM of dry sodium N-cyanoformamide: **red** – pure from **Figure 219**, **green** – after applying pressure, **blue** – after applying pressure and temperature (128 scans). The main signals belong to NCF: $\delta_{\text{C}} = 171.44$ ($\text{HC}(\text{=O})\text{NCN}$), 123.07 ($\text{HC}(\text{=O})\text{NCN}$).

On the spectrum obtained after applying pressure and temperature together (**Figure 233, A, blue**), the amount of NCF $\delta_H = 8.50$ is 25 %, compared to 65 % (**Figure 233, A, green**) and 44 % (**Figure 233, A, red**) of the starting molecule and pressure experiment, respectively. It means that the starting molecule was consumed into another product $\delta_H = 7.29$ ($s, 1H$) with a yield of 25 %. This signal could correspond to the amidine dimer of NCF that was identified in another experiment (**Figure 239**). The signal of 7.29 ppm could correspond to the CH bond of the formamidine group (marked yellow) that is expected in the range of 7.5-10.5 ppm, depending on the molecule.^{321,322} Another alteration of the spectrum of the last experiment is seen by looking at the zoom of the main signal (**Figure 233, B**). In the spectrum of pure sodium NCF and the one affected only by pressure, it appears as a singlet (**red and green**). However, in the experiment under pressure and temperature (**blue**), it consists of three signals. It could represent the presence of NCF isomers or oligomers in the reaction mixture.

Another proof of the presence of the suggested products is obtained by ^{13}C NMR spectroscopy (**Figure 234**). Compared to previous experiments (**Figure 234, red and green**), we clearly see the presence of several new signals in the 90-55 and 150-160 ppm ranges. They could correspond to different heteroatom-substituted and carboxylic acid carbon atoms, respectively, that were not present in other spectra.

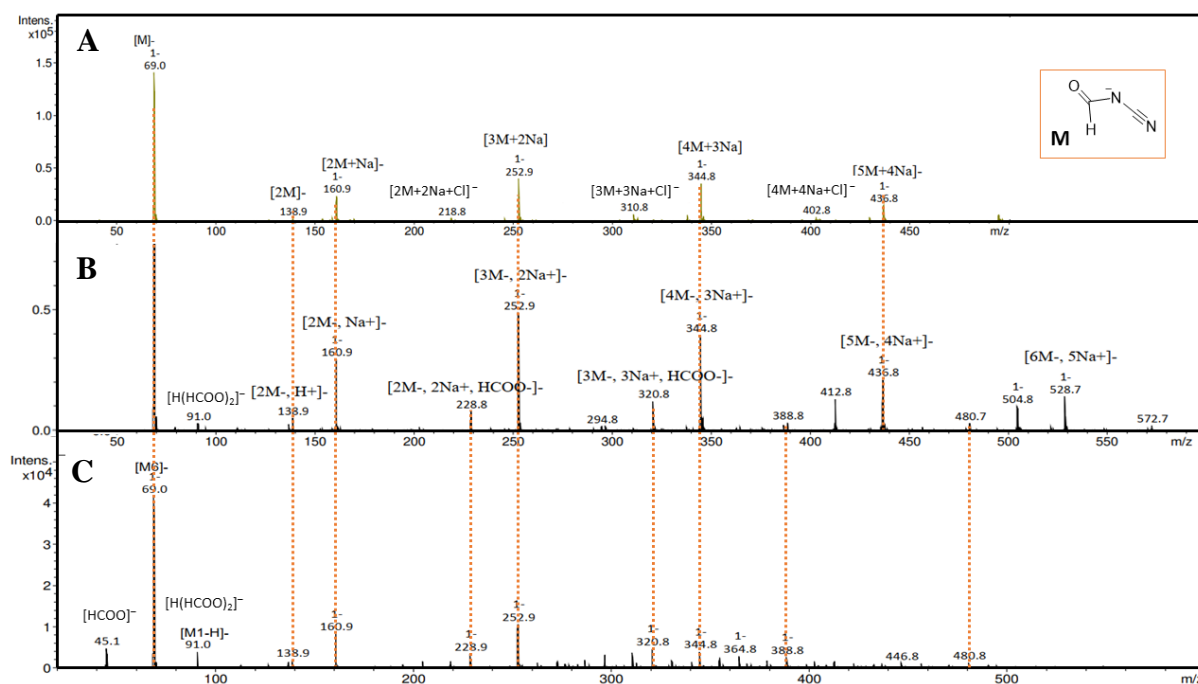


Figure 235. Low-resolution negative-ion mode mass spectra of sodium N-cyanoformamide in DMSO- d_6 : m/z 69.0 $[M-H]^-$. **A** – dry sodium NCF before experiment (from **Figure 220**); **B** – sample after 1 hour under 7 GPa pressure (from **Figure 230**); **C** – sample after 1 hour under 7 GPa and 130 °C.

There are no significant changes in the mass spectra (**Figure 235**) compared to the initial MS of sodium NCF and the experiment under pressure only. The main signal in all experiments remains m/z 69.0 $[M-H]^-$, which corresponds to the NCF anion. Along with it, we observed increased formation of hydrolysed formate $[HCOO]^-$ m/z 45. Although, we should mention here that the isonitrile isomer of NCF or its dimer and oligomer might have exactly the same mass

as the starting molecule and its adducts but be more reactive, which would make the change undetectable by MS.

In conclusion, the reactivity of sodium N-cyanofornamide can be induced only by applying elevated temperature and pressure. Otherwise, only insignificant intermolecular changes were observed, which reverted back to their original state almost completely when the pressure was released.

The need for temperature for the molecule activation is explored in the next section by experiments at elevated temperature (rt-115 °C) and atmospheric pressure, and its involvement in prebiotic reactions of phosphorylation.

7.2.4. NCF in prebiotic synthesis of phosphate esters

In the introduction, we mentioned that N-cyanofornamide could be a potentially important molecule for prebiotic chemistry, although only limited information is currently available about its possible contribution to phosphorylation. Along with urea and cyanamide, sodium N-cyanofornamide could be a potential reaction agent. Here, we performed reactions with NCF as a condensing agent in the phosphorylation of glycerol and MPG (2:1:1) and nucleosides – adenosine and cytidine (4:1:1), with NaH₂PO₄. Such molar proportions were chosen considering the presence of impurities in the NCF starting material—2 mol equivalents of NCF if sodium NCF were chemically pure. Experiments were carried out in a carousel reactor as described in the methods and materials chapter (Methods and Materials, section 4.1) and analysed by NMR and MS methods.

Here we show the NMR spectra of the experiment with glycerol:NCF:NaH₂PO₄ (**P_i**) (1:2:1); after 120 h of heating at 115 °C as an example of the products analyses. On ¹H NMR (**Figure 236**), one of the main signals, δ_H = 8.49 (s), belongs to unreacted NCF. Signals between 8.5 and 4.0 ppm most likely correspond to organic products that are the results of NCF polymerisation. We also observe the presence of unreacted glycerol and phosphorylated organic products δ_H = 3.5-3.1 and 4.3-3.5, respectively.

³¹P NMR is most informative for the identification of the phosphorylated products (**Figure 237**) where we observe five main signals. The first two correspond to 5- and 6-membered ring cyclic phosphates (15.83 and -4.32 ppm), with 7.8 and 15.8 % yield, respectively; this is confirmed by their multiplicities on proton-decoupled ³¹P NMR (**Figure 237, blue**). Other products are acyclic phosphates, represented by a broad peak at -1.88 ppm. We assume that there are several similar (glyceryl phosphates or acyclic phosphodiester) products with unreadable proton-decoupled ³¹P NMR due to their small amounts and crowding. Possibly it also contains a signal of not-reacted **P_i**.

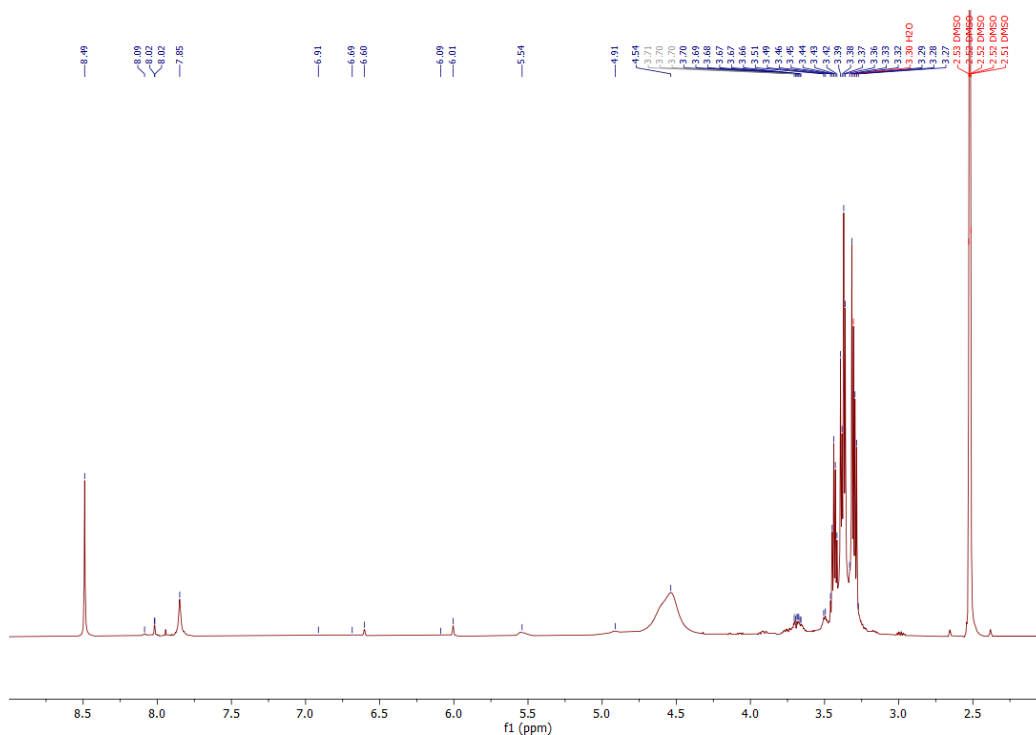


Figure 236. ^1H NMR (500 MHz, $\text{DMSO-}d_6$) of the extract of 0.5 mmol scale mixture glycerol:NCF: NaH_2PO_4 (P_i) (1:2:1); after 120 h of heating at 115 °C. $\delta_{\text{H}} = 8.49$ (s, NCF), 4.3-3.5 (phosphorylated organic products), 3.5-3.1 (glycerol).

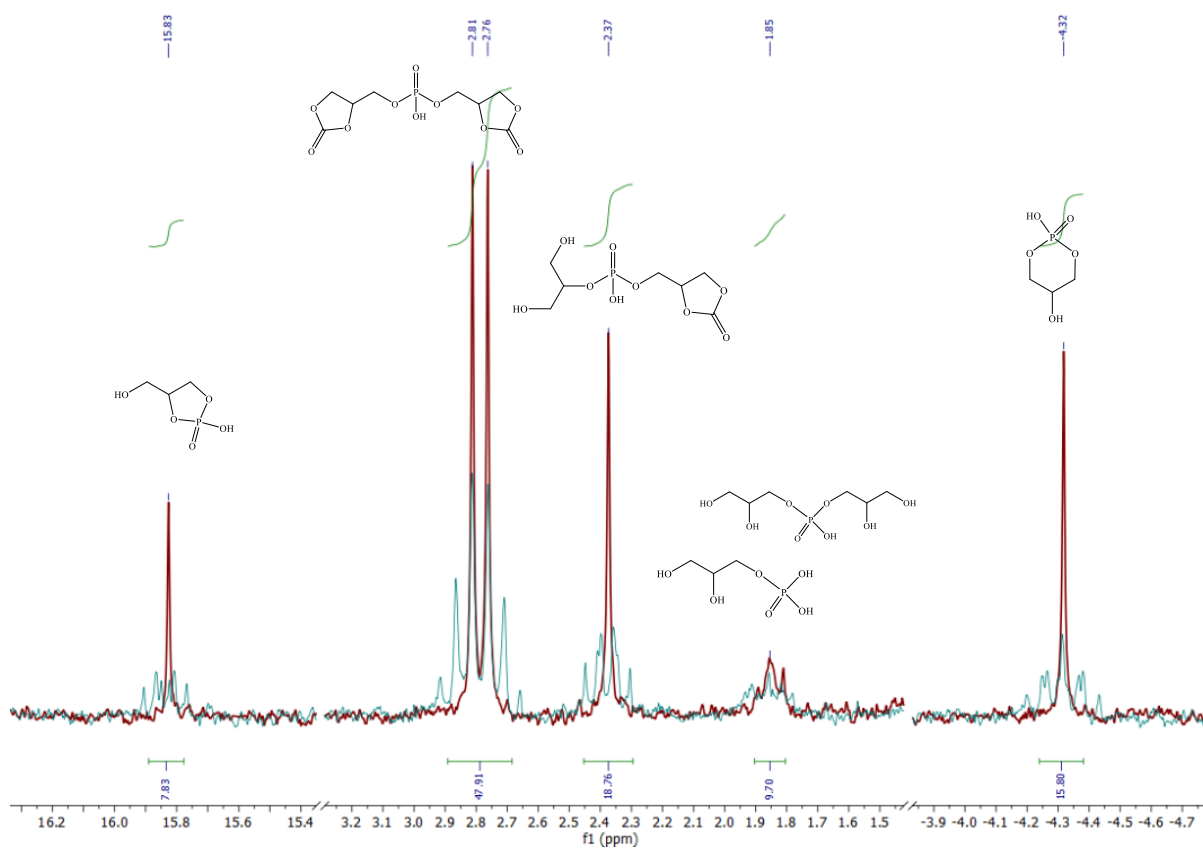


Figure 237. ^{31}P NMR (blue) and $^{31}\text{P}\{^1\text{H}\}$ NMR spectra (red) (202.5 MHz, $\text{DMSO-}d_6$) of the extract of glycerol, NCF and NaH_2PO_4 (P_i) (1:2:1, 0.5 mmol each) after heating neat at 115 °C for 120 h C.

The main products in the ^{31}P NMR spectra are $\delta_{\text{p}} = 2.37$ and 2.79 , which correspond to the aforementioned 1,2-cyclic carbonate **diGICOP** (18.8 %) and symmetric phosphodiester of two primary 3-glyceryl-1,2-cyclic carbonates **diGl(CO) $_2$ P** (47.9 %) (described in the section on identification of main products **1.1.2**). In general, glycerol phosphorylation in the presence of NCF appears to be more selective towards cyclic carbonates. The reactions studied had major products, primary and secondary glyceryl phosphates, in a complex mix with other phosphorylated products. For a better understanding of product size distribution, we performed a ^{31}P DOSY (diffusion-ordered) NMR experiment (**Figure 238**). The data provides information on the distribution of molecular weights, or the number of glycerol molecules attached to a phosphate. We conclude that the molecular weights of the products are not significantly different from each other to be distinguished by differences in diffusion rate constants.

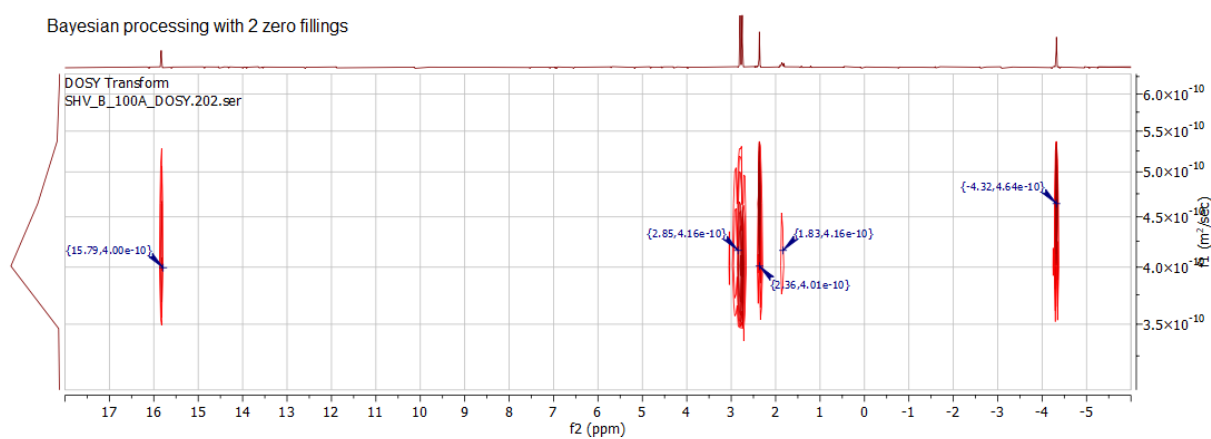


Figure 238. ^{31}P [^1H] DOSY NMR (202.5 MHz, Bayesian processing with 2 zero fillings, in $\text{DMSO-}d_6$) of the extract of glycerol, NCF and NaH_2PO_4 (**P_i**) (1:2:1, 0.5 mmol each) after heating neat at $115\text{ }^\circ\text{C}$ for 120 h.

Although selectivity towards certain phosphorylated products appears to be an exciting result, we need to take into consideration other products of the reaction. To pursue this search, we performed LS-MS analyses. Due to the relatively small size of the glyceryl derivative molecules and their high polarity, the crude mixture was analysed by the HILIC column (described in Methods and Materials **2.2**).

The analysis was performed in both positive (**Figure 239**) and negative (**Figure 240**) ion modes, demonstrating the presence of non-phosphorylated products of polymerisation reactions similar to those produced due to ionisation in the MS source (**Figure 222**). The main peaks from HILIC-HRMS in positive ion mode (**Figure 239**) consist of the amidine dimer of NCF, melamine and glyceryl melamine (Compound **2**, RT 0.6 min), and ammeline (Compound **3**, RT 0.7 min) as major peaks, along with minor amounts of ammelide (Compound **4**, RT 1.2 min) and diglyceryl phosphate (Compound **5**, RT 2.0 min).

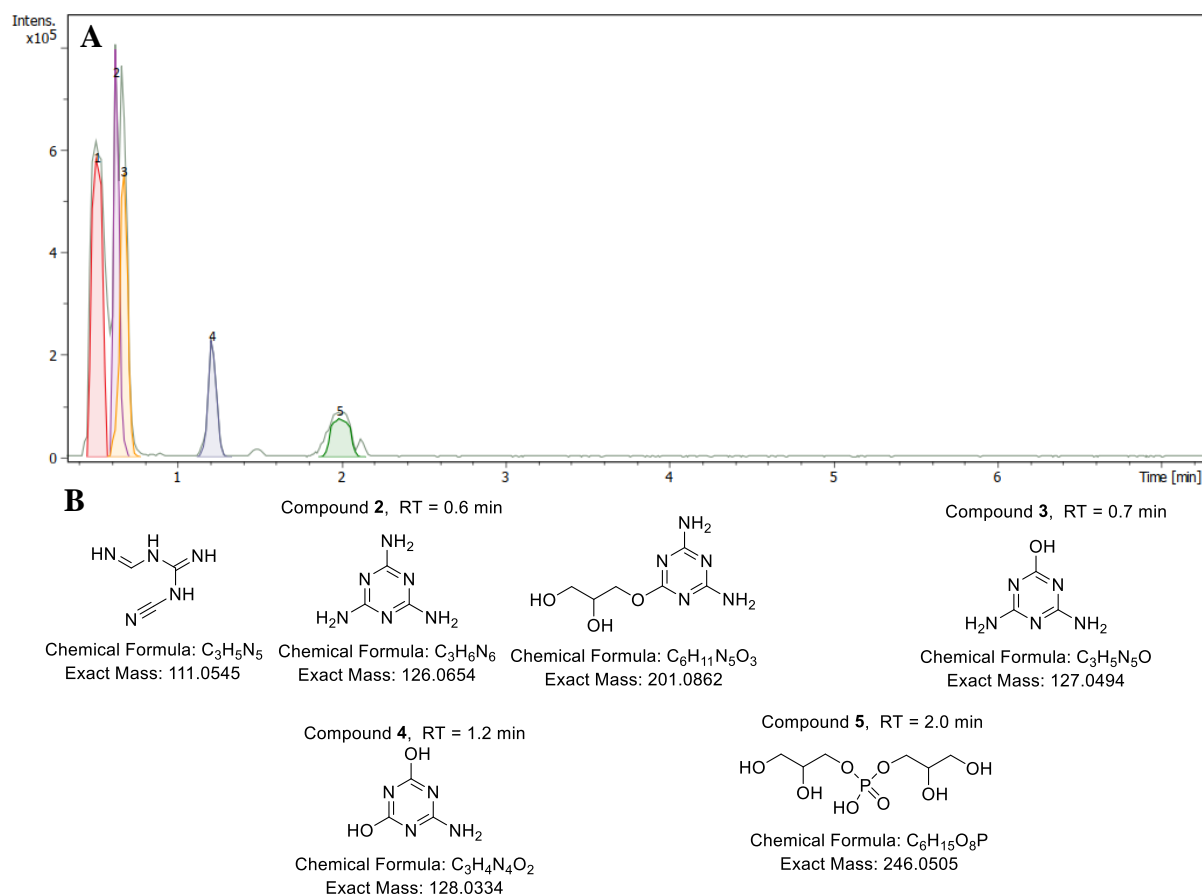


Figure 239. Results of HILIC-HRMS chromatography in the positive ion mode of the crude acetonitrile extract of crude mixture obtained by reacting glycerol, NCF and NaH_2PO_4 (**P1**) (1:2:1, 0.5 mmol each) after heating neat at 115 °C for 120 h. **A** – total HILIC with ion-extracted signals. **B** – the chemical structures and relative masses of the detected compounds. The compound **1** is produced due to the clusters of sodium acetate buffer and is not considered a reaction product.

The HILIC-HRMS in negative ion mode revealed more products (**Figure 240**). Unlike in positive ion mode, the main peak contains cyclic phosphate (5- or 6-membered rings are hardly distinguishable by MS analyses due to exactly the same molecular mass) and diglyceryl phosphate (Compound **5**, RT 2.1 min). Also significant is the presence of mono- and diglyceryl derivatives with cyanuric acid or ammelide (Compounds **2**, **2.1**, **3**, **3.1**).

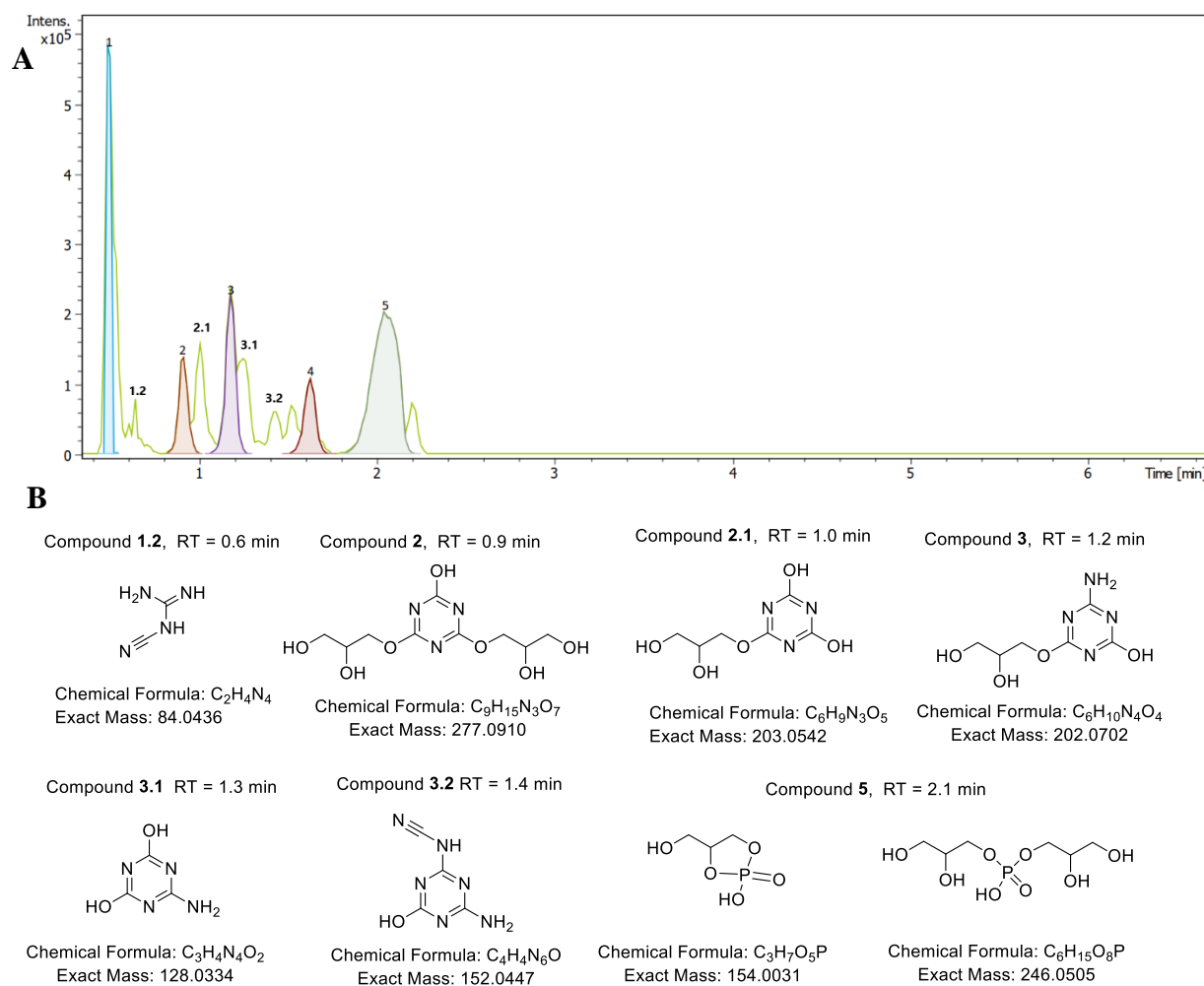


Figure 240. Results of LC-MS chromatography in the negative ion mode of the acetonitrile extract of crude mixture obtained by reacting glycerol, NCF and NaH₂PO₄ (**P₁**) (1:2:1, 0.5 mmol each) after heating neat at 115 °C for 120 h. **A** – total HILIC with ion-extracted signals. **B** – the chemical structures and relative masses of the detected compounds. Compound **1** is produced due to the clusters of sodium acetate buffer and is not considered a reaction product.

As in the experiments with glycerol, urea and **P₁** (**Figure 60**), we did not observe the main phosphorylated organic compounds detected by ³¹P NMR (**diGICOP** and **diGI(CO)₂P**) on the HILIC-HRMS chromatograms. However, it should be mentioned that the HILIC column is a very particular analytical tool that can be very sensitive and selective towards certain molecules but not efficient towards others. It is possible that the column that we used was not optimal for our experiment, and using another type of HILIC column may give a different result.

To compare this data to the experiments with pure sodium N-cyanoguanidine, we also performed low-resolution total-ion MS. In positive ion mode (**Figure 241, A**), we identified NCF polymerisation products similar to **Figure 221** along with a glyceryl diphosphate (shown on the spectra), but none of the products discovered by HILIC column analysis. However, in negative ion mode (**Figure 241, B**), we found organic products previously detected (numbering of compounds as in **Figure 240**) along with new products identified only in this spectrum, such as glyceryl phosphate and its derivatives (molecules corresponding to signals on **Figure 241, C**).

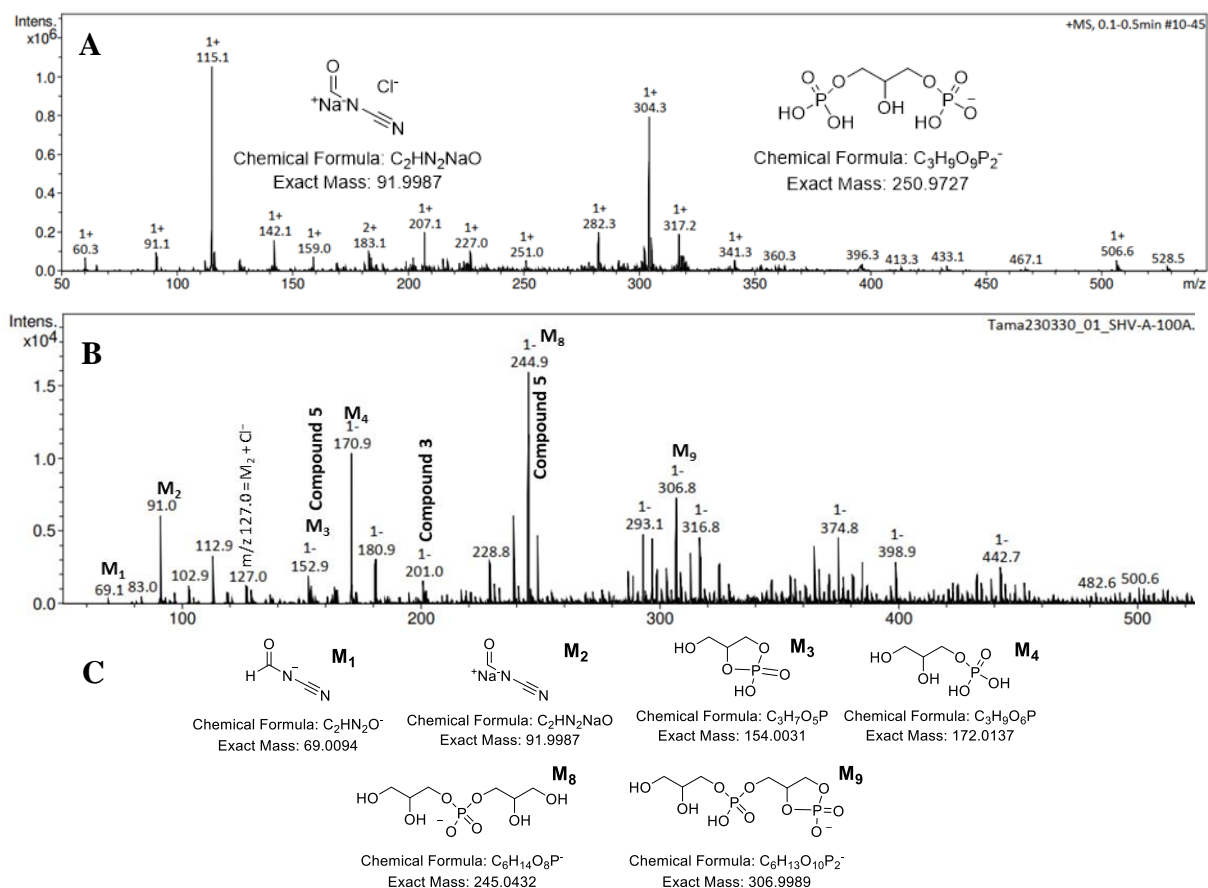


Figure 241. Low-resolution mass spectra of the MeOH extract of crude mixture obtained by reacting glycerol, NCF and NaH₂PO₄ (**P_i**) (1:2:1, 0.5 mmol each) after heating neat at 115 °C for 120 h. **A** – positive-ion mode; **B** – negative-ion mode; **C** – the chemical structures and relative masses of the detected compounds.

It is possible that new phosphorylated molecules were too polar for the LC-MS method and passed through the column without separation or were completely decarboxylated during ionisation. Another point is that low-resolution MS leaves some uncertainties about the exact molecular mass of the compounds that could potentially mislead their identification.

In both mass spectrometry methods, a variety of cyclic polymerised products derived from NCF were detected. As mentioned before, NCF has a tendency for spontaneous polymerisation induced by MS electrospray ionisation sources, and possibly some of the identified melamine cyclic derivatives were not present in the initial crude mixture of glycerol phosphorylation.^{234, 235} Nevertheless, the predisposition of NCF towards cyclisation reactions is clear due to the variety of phosphorylated and non-phosphorylated products in its presence.

Phosphorylation of glycerol with the assistance of N-cyanofomamide and NaH₂PO₄ was studied at different temperatures and later with different starting molecules (MPG and nucleosides). The summary of reaction results carried out at prebiotic conditions is presented in **Figure 243**.

The results show that temperatures lower than 115 °C are not sufficient for phosphorylating the tested alcohols except glycerol. From the diagram, we conclude that in the case of glycerol, to push the reaction, an elevated temperature was needed, and only at 115 °C

did we register the presence of phosphorylated cyclic glyceryl carbonates. For the reaction of MPG, organic products of phosphorylation were detected in a very low amount only at 75 °C of 5-membered ring organic phosphates and **PP_i** (the intensity of signals was close to the noise values, not shown). Phosphorylation of nucleosides did not produce nucleosides in significant quantities in all tested conditions, even with the involvement of formamide as a liquidiser (**Figure 242**).

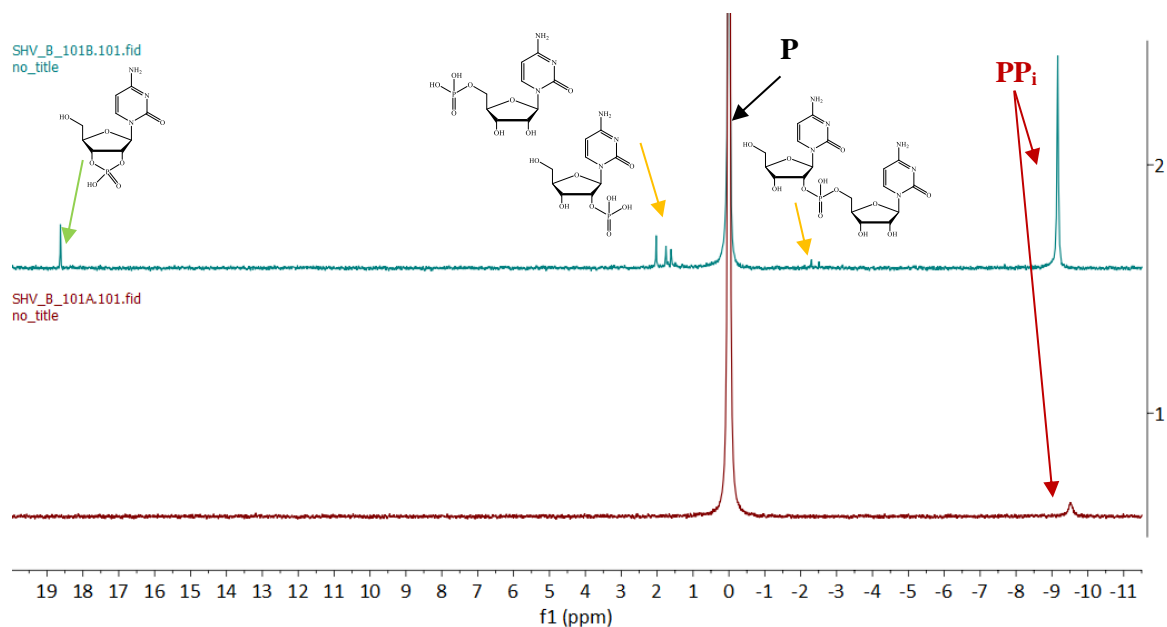


Figure 242. ³¹P and ³¹P{¹H} NMR spectra (202.5 MHz, D₂O) of the extract of a 0.5 mmol scale mixture (1:4:1) after 120 h heating neat at 115 °C: **blue** – cytidine:NCF:NaH₂PO₄, **red** – adenosine:NCF:NaH₂PO₄.

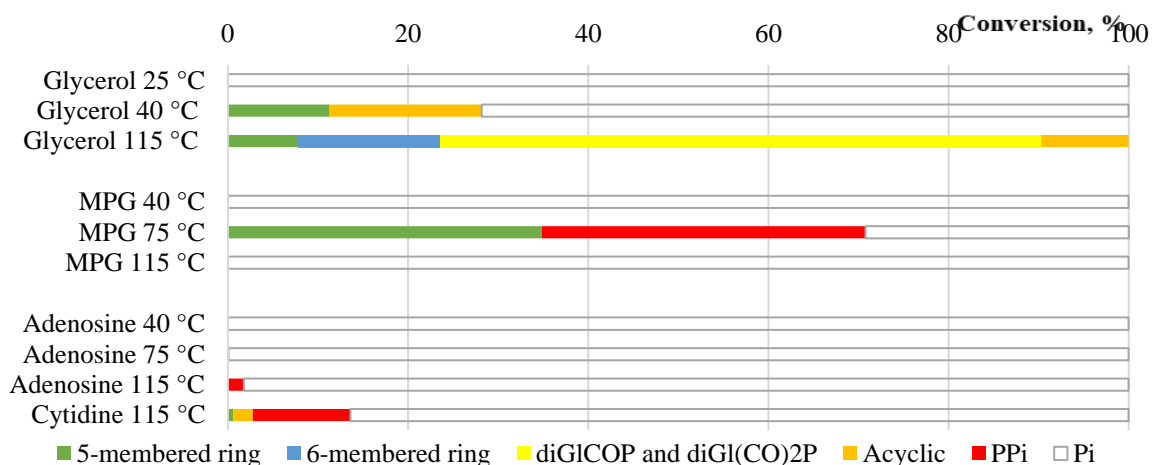


Figure 243. Summary of the phosphorylation of alcohols after 120 h of heating at 25, 40, 75 and 115 °C, with NCF and NaH₂PO₄ (P_i) on a 0.5 mmol scale (no water added, ‘dry’ conditions). Reaction products: organic cyclic (5- and 6-membered rings) and acyclic phosphates and inorganic pyrophosphate (PP_i). Percent values are from the integration of quantitative ³¹P{¹H} NMR spectra taken in DMSO-*d*₆ for glycerol and MPG and D₂O for nucleosides reactions.

As a summary, sodium N-cyanofornamide is an effective condensing agent in the phosphorylation reaction with glycerol. The phosphorylation degree towards organic phosphates at 75 and 115 °C is significantly higher compared to the negative control experiment (**Figure 101**). This molecule has particular interest due to its tendency to produce different types of cyclic products. Possibly, this reaction can be optimised by using another phosphate source or molar ratio of starting products in further research.

Conclusions to the section 7

Thereby, I conclude that phosphorylation of glycerol was demonstrated at high pressure and high temperatures for the first time; urea was consumed and phosphoester bounds were formed. A qualitative vibrational analysis of the obtained crude mixture is still awaiting confirmation from complementary analytical methods.

The organic salt sodium N-cyanoformamide was suggested for the first time as a potential prebiotic molecule for hydrothermal and prebiotic reactions on the early Earth. We demonstrated that it is a promising condensing agent for glycerol phosphorylation. For the first time, a detailed vibrational and spectral (NMR, MS) analysis of sodium N-cyanoformamide was described, and we revealed its ability for spontaneous polymerisation under MS-source ionisation.

The pressure-induced alterations in the NCF molecule demonstrated that an elevated temperature (above 75 °C) is required for its activation and involvement in the chemical reactions. Some reversible intramolecular changes occur under the application of pressure alone; however. The mechanism of intramolecular change of N-cyanoformamide into N-isocyanocarbonylamide, suggested in the beginning, was not confirmed. Raman analysis did not reveal changes towards the formation of N–H and the vanishing of C–H bonds. Assuming that NCF might be sensitive to the presence of water, we conclude that hydrothermal conditions are not optimal for its availability, accumulation and involvement in chemical reactions on the early Earth.

Sodium N-cyanoformamide may be more promising for phosphorylation and acylation reactions under dry conditions. It is very important to note its potential for cyclisation reactions. The highest degree of phosphorylation was achieved in reaction with glycerol. Perhaps other prebiotic molecules at elevated NCF concentrations could also be involved in the reaction in future studies. For glycerol, the selective formation of acyclic phosphodiester ($\geq 67\%$) is a remarkable difference to urea-assisted counterpart, which is interesting in the context of the ubiquity of PG (phosphoglyceryl) polar headgroups in modern phospholipids.

Final conclusions and future prospective

After summarising the experimental results and concluding the discussion, here are the following suggestions for the aims set in this project:

The First aim of the thesis was to understand the conditions that are most favourable for the phosphorylation of organic precursors on the early Earth.

- I experimentally confirmed the possibility of phosphorylation of alcohols (glycerol, *rac*-mono-palmitoylglycerol, nucleosides) in dry prebiotic conditions relevant to the early Earth. At elevated temperatures (75, 115 °C) in the presence of a condensing agent (urea, cyanamide) with inorganic phosphate, a conversion up to 95 % was achieved (according to ³¹P NMR) after 24-120 hours.
- Mono-alcohols (dodecanol, geraniol, *rac*-1,2-dioleoylglycerol and *rac*-1,2-bis-tridecanoyl glycerol) were complicated to involve in phosphorylation reactions. It resulted in <10 % yields (according to ³¹P NMR) in the presence of condensing agent excess (10 eq. of urea with respect to the starting alcohol) or wet-to-evaporative conditions. In the case of pyruvic acid, the tested prebiotic conditions favoured polymerisation instead of phosphorylation.
- The presence of phosphoester bonds was discovered (by Raman spectroscopy) in a hydrothermal experiment of urea-assisted glycerol phosphorylation: at elevated temperature (115 °C) and pressure <1 GPa after 48 hours.

Such harsh reaction conditions appeared to be effective for the phosphorylation of prebiotic alcohols. Even more, my colleagues succeeded in obtaining† stable vesicles from a crude mixture obtained by urea-assisted phosphorylation of MPG obtained in this work. This makes the suggested reactions prospective for future research on membranogenic compounds.

Further research could also include exploring other conditions and reactants in hydrothermal conditions and applying additional analytical methods for a better understanding of the phosphorylated products. It would be interesting to involve nucleotides in the suggested reactions. Hydrothermal conditions might be prospective for not only phosphorylation but also spontaneous polymerisation of prebiotic precursors of membranes and other biopolymers.

The Second aim of the thesis was to explore plausible prebiotic conditions, agents that could be involved, and factors that could possibly affect phosphorylation reactions.

- The presence of a condensing agent is essential for the phosphorylation of all the studied alcohols except glycerol. In dry reactions, the most efficient prebiotic condensing agents were urea and cyanamide. Carboxamides favour phosphorylation only in reaction with glycerol at high temperature 115 °C due to their thermal destruction. Excess urea with respect to the starting alcohol enhanced yields greatly and favoured the formation of cyclic phosphorylated products.
- cTMP appeared to be the most efficient source of phosphate in reactions with glycerol and its derivatives with/without condensing agent, probably due to the ring-opening reactions that favour phosphorylation. Comparable results were achieved in the urea-dihydrogen phosphate pair; this phosphorylation pathway was efficient for nucleoside

production as well. Also, the presence of protons from NaH_2PO_4 in the crude mixture helped phosphorylation, whereas mono- and disodium phosphates were not sufficient for producing phosphoesters. Thiophosphate by itself was involved in the phosphorylation, with yields lower than dihydrogen phosphate. However, in the reactions of the pair $\text{NaH}_2\text{PO}_4:\text{Na}_3\text{SPO}_3$, as a phosphorus source, the thiophosphate was completely consumed after five days of heating at $115\text{ }^\circ\text{C}$. In competition analyses of this experiment with labelled orthophosphate, we discovered that Na_3SPO_3 thermodynamically overcame NaH_2PO_4 and produced 60-70 % of phosphorylated products.

- Out of the tested prebiotically plausible minerals, vivianite was the least efficient. We had initially assumed that the presence of Fe^{2+} would facilitate the reaction; however, only glycerol phosphorylation occurred. Struvite does not require a condensing agent due to the presence of an ammonia group that also provides protons. Canaphite, which is a pyrophosphate source, led to high yields of monophosphorylated products only (>70%).

In general, elevated temperatures were more favourable for the phosphorylation of prebiotic alcohols. The explored frameworks of plausible phosphorylation reactions proved urea: NaH_2PO_4 as the most effective phosphorylation reactant. It was also the most universal. For most alcohols tested during this thesis, we obtained good yields using urea-dihydrogen phosphate tandem, unlike, for example, cTMP, which was efficient only for glycerol derivatives.

Further research would involve placing phosphorylation reactions in conditions in which natural phosphate-containing minerals could be formed (using schreibersite, for example, in evaporative conditions). Another direction could be to explore reaction networks or 'messy' chemistry, where the synthesis involved more of the 'raw' building blocks (precursors of nucleobases or sugars, for example) with inorganic phosphate sources.

The Third aim of the thesis was to confirm the mechanism of urea-assisted phosphorylation of prebiotic alcohols that could provide a key to understanding the role of the condensing agent and explaining its necessity.

- We proposed the most detailed identification and description of the main phosphorylated products by combining several NMR spectroscopy methods. We identified two new phosphorylated products, 5-membered ring 1,2-cyclic carbonate of a diglyceryl phosphodiester (one glyceryl of which is linked through the secondary and the other through the primary and secondary positions), that were never suggested before.

- For the first time, the kinetics of the phosphorylation reaction were studied, and the phosphorylation degree was compared to the decomposition rate of urea in the reactions of MPG and glycerol.

- In this work, we indeed experimentally proved the dissociative urea-assisted phosphorylation of prebiotic alcohols, by trapping the products of urea degradation, ammonia and carbon dioxide and proving their origin from urea by using its stable isotopes ^{15}N and ^{13}C . We also discarded any contribution of the associative urea-assisted pathway by using ^{18}O isotopes present in inorganic phosphate.

The Forth aim of the thesis was to place in a united, challenging environment all pieces of the explored reaction, such as precursors of membrane and RNA, to discover their competition and interaction in the reaction network. Two ‘messy’ experiments were performed:

- A mix of nucleosides (A, C, G and U) was phosphorylated in the presence of excess urea and dihydrogen phosphate at 115 °C for 120 hours. LC-MS analysis demonstrated the presence of dinucleotides and diphosphate nucleotides, although the majority were cyclic and acyclic mononucleotides. We detected a slight unbalance at the end of the reaction between the equivalent amounts of starting nucleotides and the predominance of uridine and adenosine against cytidine and guanosine.

- In another experiment, nucleosides (A, C, G and U) were mixed with glycerol, fatty acids ($\text{CH}_3(\text{CH}_2)_8\text{COOH}$, $\text{CH}_3(\text{CH}_2)_9\text{COOH}$, $\text{CH}_3(\text{CH}_2)_{10}\text{COOH}$, $\text{CH}_3(\text{CH}_2)_{11}\text{COOH}$) urea and NaH_2PO_4 and reacted at 115 °C for 120 hours. We obtained cyclic and acyclic monophosphates along with phosphodiester of nucleosides and glycerol. Unfortunately, we did not detect any derivatives of fatty acids by HRMS, though there is indirect evidence of their presence on NMR spectra.

We carried out all reactions in a constant dry condition and some of the experiments involved the addition of water only in the beginning before heating. The next step would be to try the same reactions in a dry-wet cycling mode, which could be favourable for obtaining products longer than monomers and dimers in higher amounts.

In both 'messy' experiments, we did not achieve the synthesis of molecules bigger than diesters. It is possible that the prebiotic conditions that were explored in this work are favourable for the phosphorylation step of prebiotic precursors assembly. Accumulated in one environment, those products could be transferred to others, where being exposed to new conditions led to polymerisation, as an example.

There are indeed vast prospects for 'messy' chemistry experiments. As was discussed in the states of the arts, more and more scientists are moving from ‘pure’ and perfected experiments to complex systems chemistry. There are many plausible set-ups that are awaiting exploration and a huge undiscovered field of possible experiments within the framework of prebiotic chemistry. Overall, this work represents a unique collaboration of astrobiology, geology, organic and analytic chemistry. We started with a simple prebiotic reaction of glycerol phosphorylation, studied it in detail and expanded it to different reactants and conditions and then placed it in a big picture of the origin of life study.

Appendix A1 Tracing stable isotopes in urea-assisted phosphorylation reactions

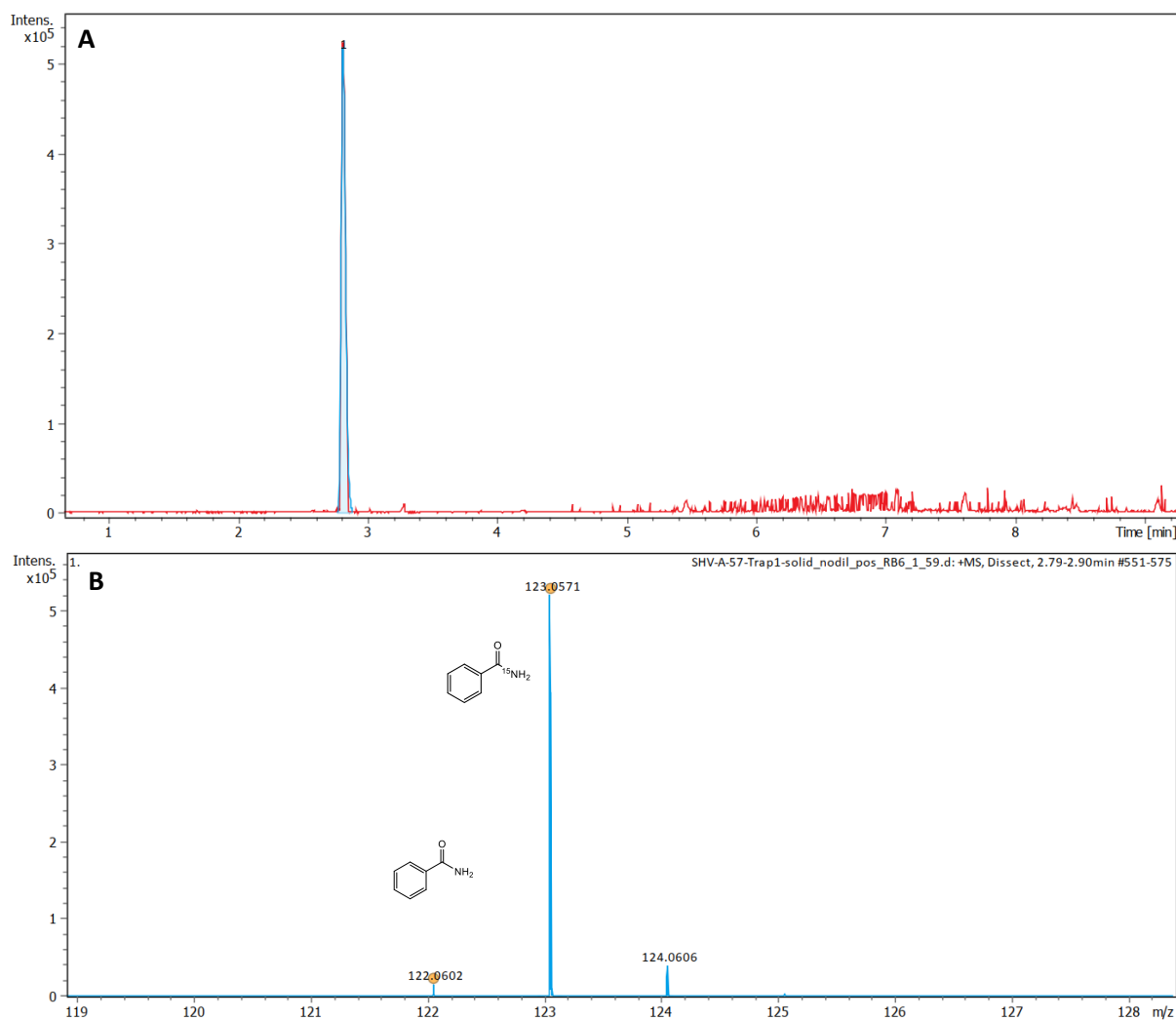


Figure A244. Results of LC-MS analysis of trap 1 precipitate of experiment **1.1** after 120 h of heating.

A – chromatogram of the experiment.

B – mass spectra of peak 1 ($rt = 2.9$ min) benzamide (C_7H_7NO and $C_7H_7^{15}NO$).

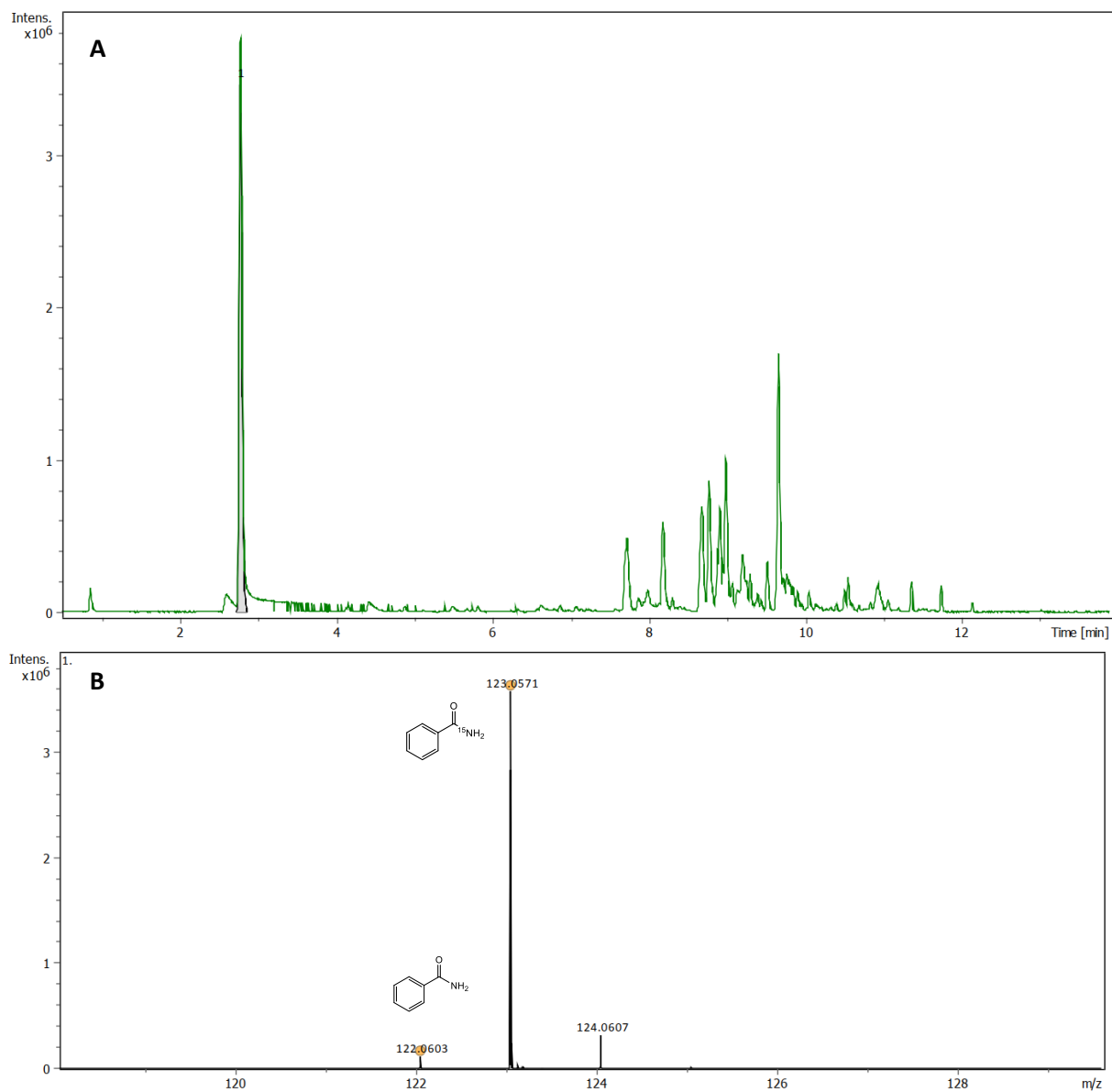


Figure A245. Results of LC-MS analysis of trap 1 solution of experiment **1.2** after 120 h of heating.

A – chromatogram with main signal: *t* $rt = 3$ min, benzamide (C_7H_7NO and $C_7H_7^{15}NO$); signals after 8 min are contamination from vacuum filtration.

B – mass spectra of main peak ($rt = 3$ min).

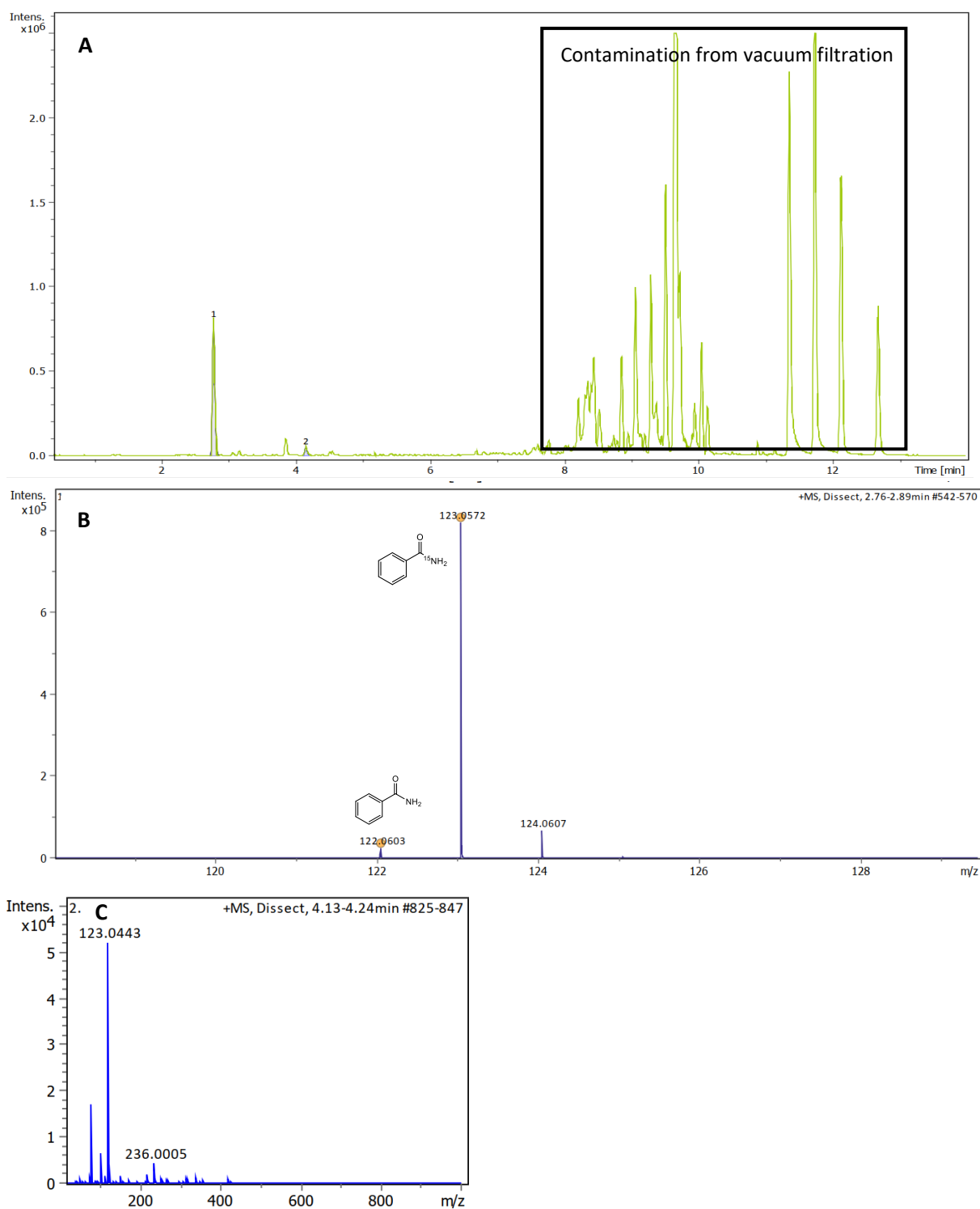


Figure A246. Results of LC-MS analysis of trap 1 precipitate of experiment **1.2** after 120 h of heating.

A - chromatogram with main signals: **1** $rt = 2.8$ min, benzamide (C_7H_7NO and $C_7H_7^{15}NO$); **2** $rt = 4.2$ min, benzoic acid ($C_7H_6O_2$).

B – mass spectra of peak 1 ($rt = 2.8$ min).

C – mass spectra of peak 2 ($rt = 4.2$ min).

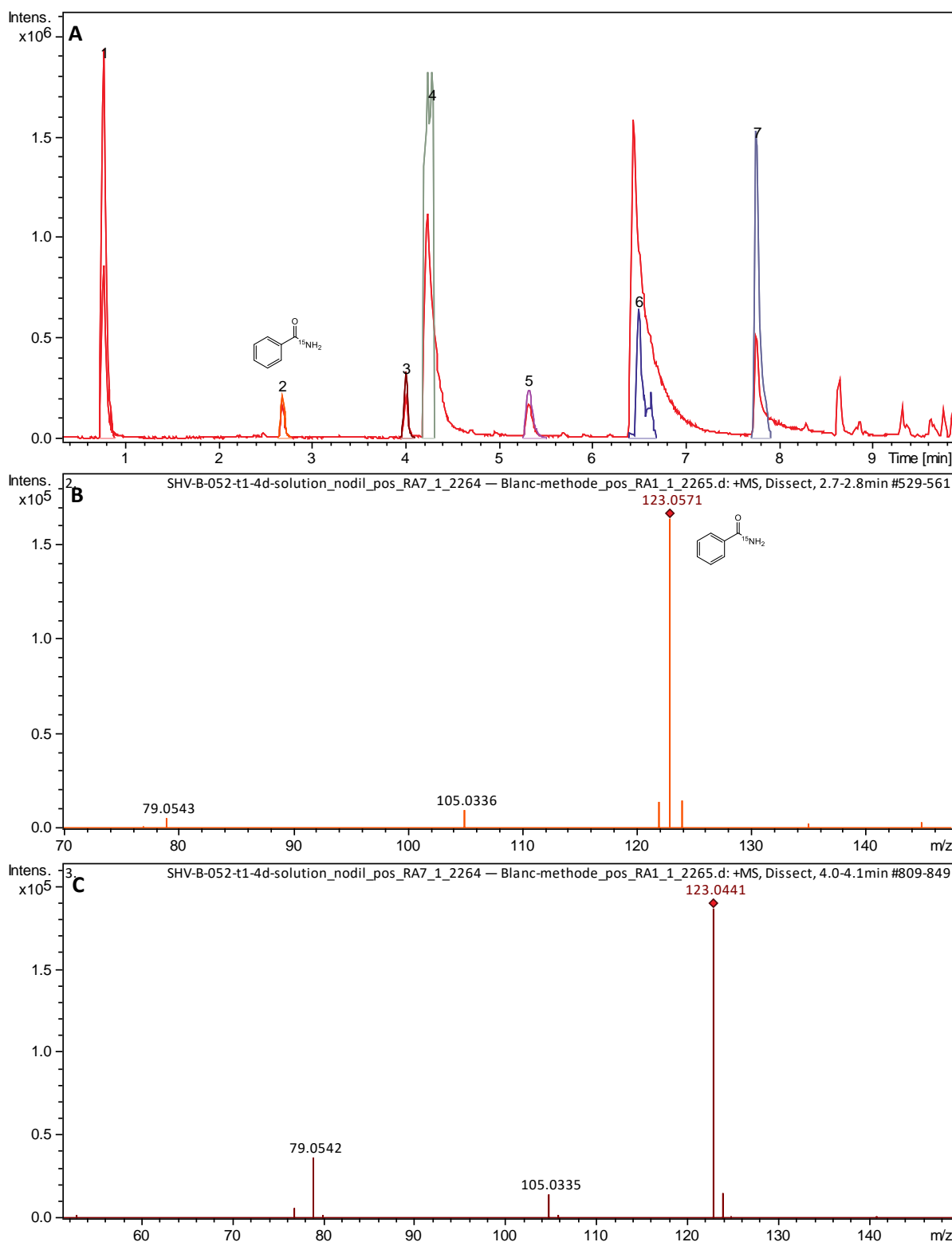


Figure A247. Results of LC-MS analysis of trap 1 solution of experiment **1.3** after 120 h of heating. **A** – chromatogram of the experiment: **2** $rt = 2.8$ min, benzamide (C_7H_7NO and $C_7H_7^{15}NO$); **3** $rt = 4.1$ min, benzoic acid ($C_7H_6O_2$). **B** – mass spectra of peak 2 ($rt = 2.8$ min). **C** – mass spectra of peak 3 ($rt = 4.1$ min).

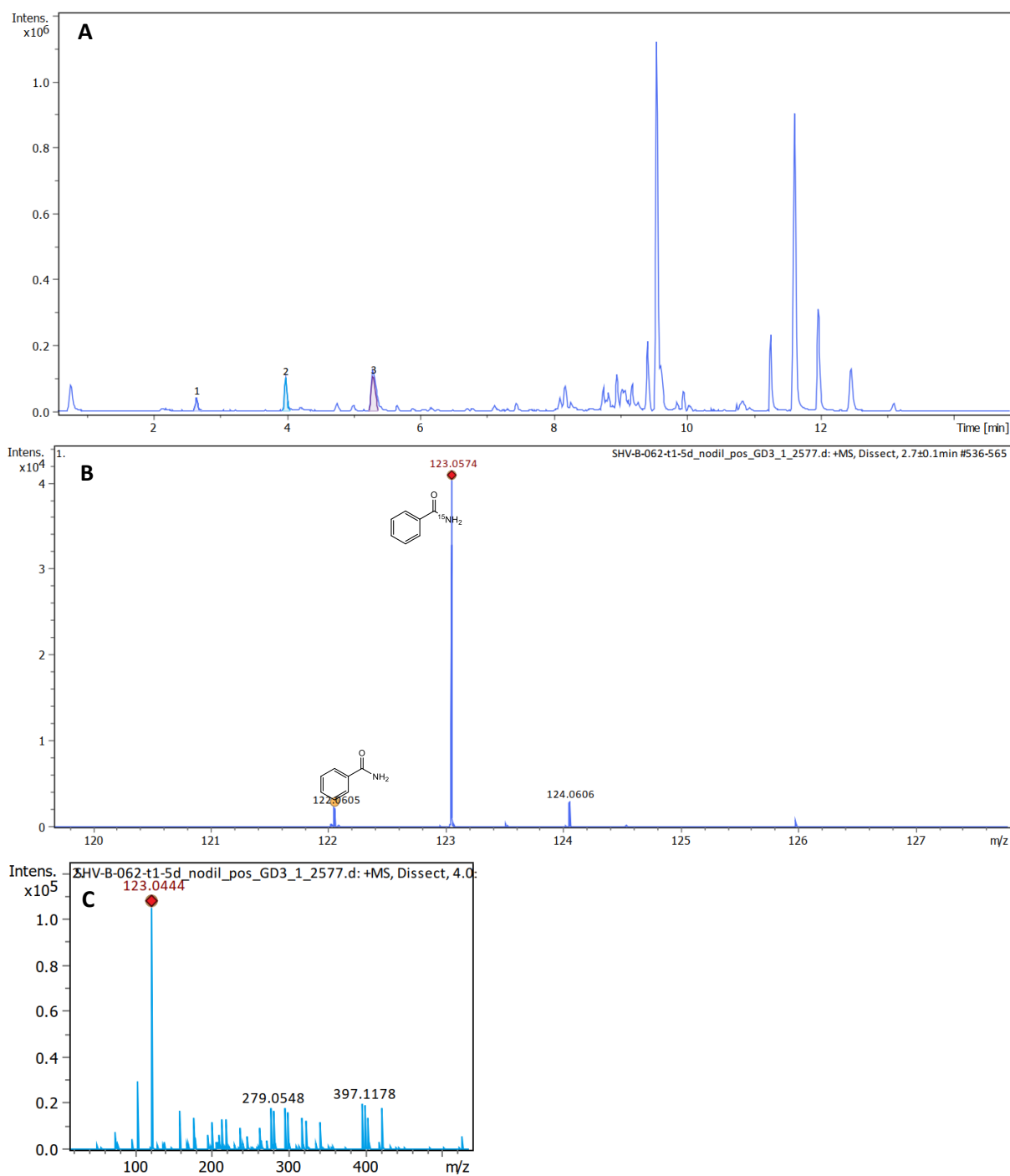


Figure A248. Results of LC-MS analysis of trap 1 solution of experiment **1.4** after 120 h of heating.

A – chromatogram of the experiment: **1** $rt = 2.7$ min, benzamide (C_7H_7NO and $C_7H_7^{15}NO$); **2** $rt = 4.0$ min, benzoic acid ($C_7H_6O_2$).

B – mass spectra of peak 1 ($rt = 2.7$ min).

C – mass spectra of peak 3 ($rt = 4.0$ min).

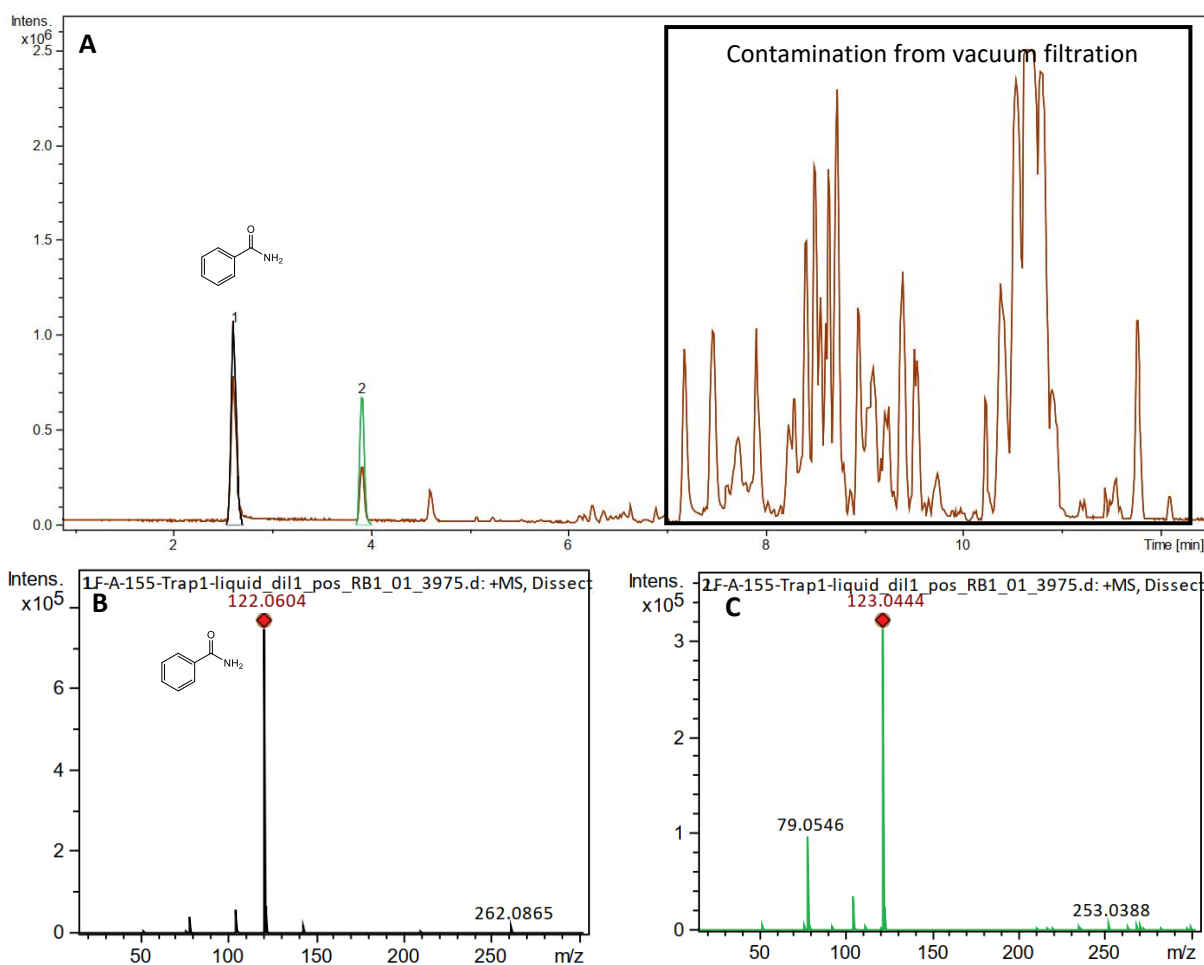


Figure A249. Results of LC-MS analysis of trap 1 solution of experiment 1.5 after 120 h of heating.

A – chromatogram with main signals: **1** rt = 2.7 min, benzamide (C₇H₇NO); **2** rt = 3.9 min, benzoic acid (C₇H₆O₂).

B – mass spectra of peak 1 (rt = 2.7 min).

C – mass spectra of peak 2 (rt = 4.2 min).

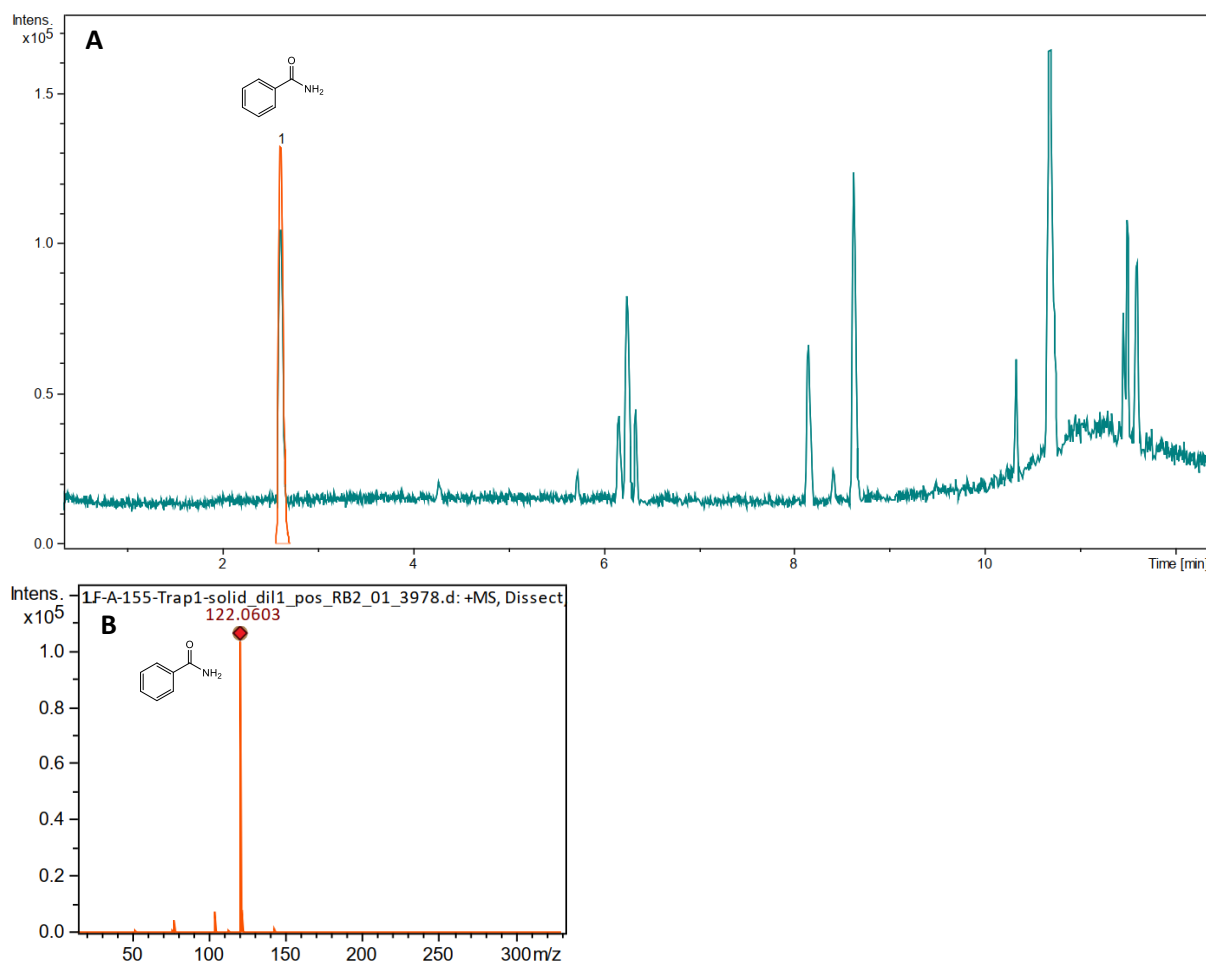


Figure A250. Results of LC-MS analysis of trap 1 precipitate of experiment **1.5** after 120 h of heating.

A – chromatogram of the experiment.

B – mass spectra of peak 1 (rt = 2.9 min) benzamide (C_7H_7NO).

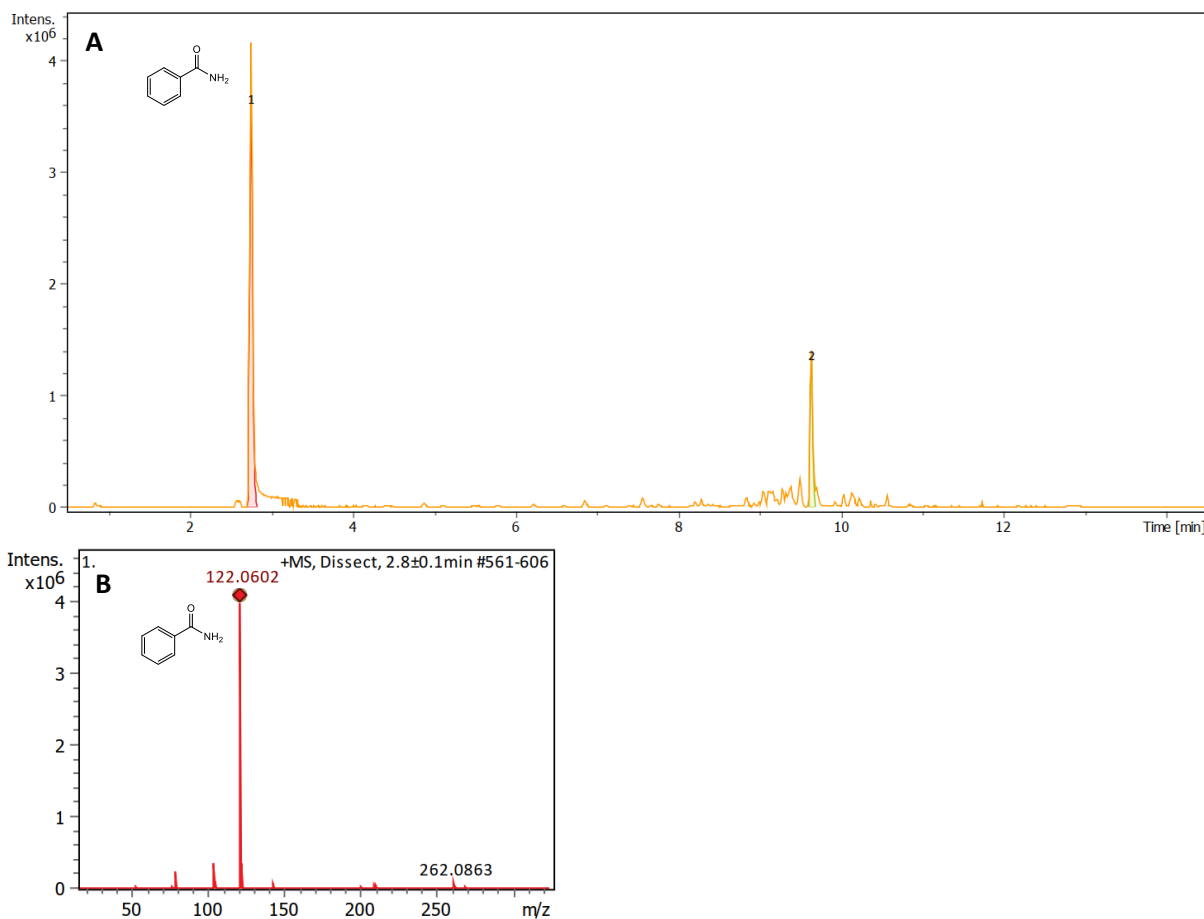


Figure A251. Results of LC-MS analysis of trap 1 solution of experiment **1.6** after 120 h of heating.

A – chromatogram of the experiment.

B – mass spectra of peak 1 (rt = 2.8 min) benzamide (C₇H₇NO).

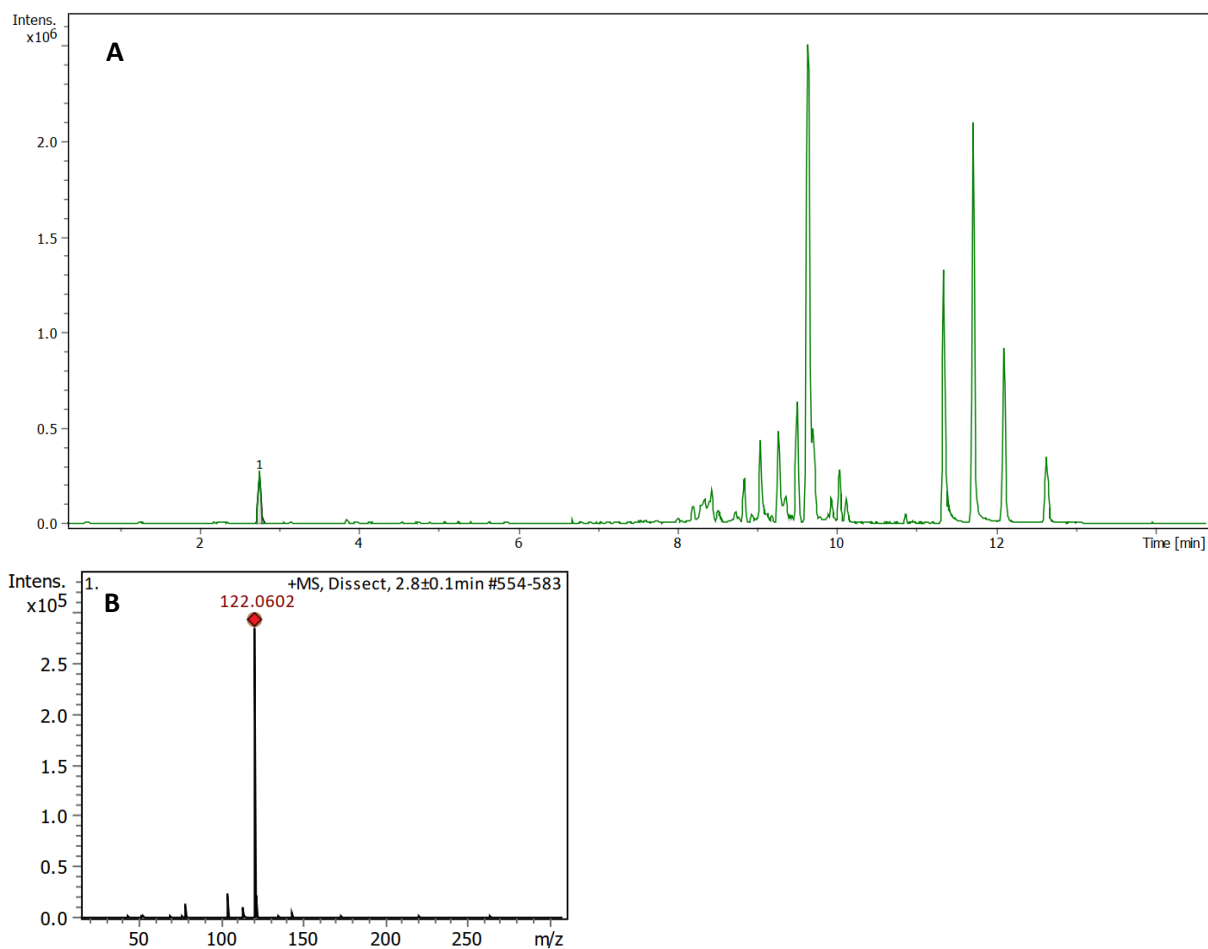


Figure A252. Results of LC-MS analysis of trap 1 precipitate of experiment **1.5** after 120 h of heating.

A – chromatogram of the experiment.

B – mass spectra of peak 1 (rt = 2.9 min) benzamide (C_7H_7NO).

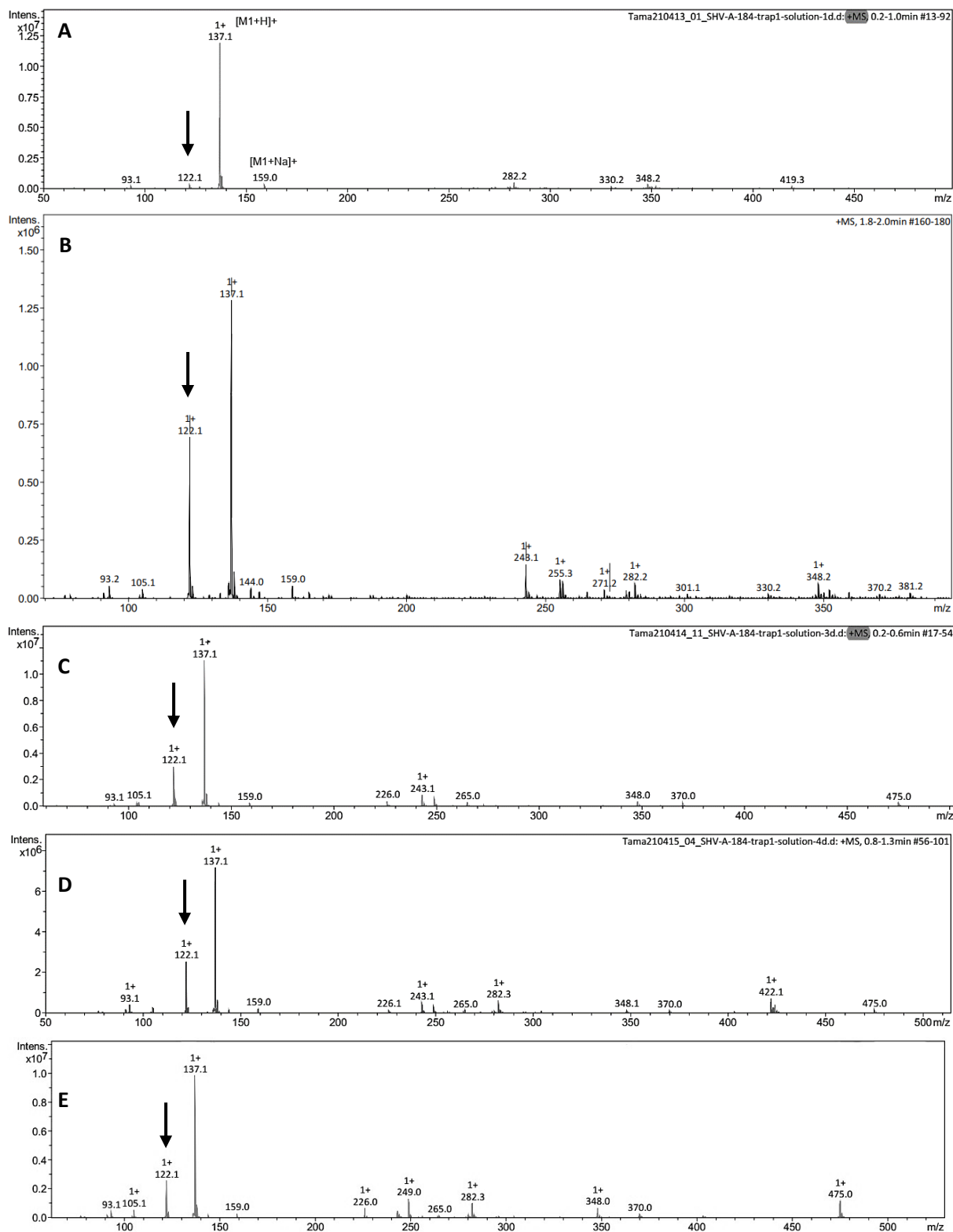


Figure A253. Results of low-resolution positive ion mode mass analyses of trap 1 of experiment 1.7.

A-E – sampling of solution was made after 24, 48, 72, 96 and 120 h of heating (sampling directly from the trap 2 during the reaction). Arrow shows presence of benzamide in the studied solution.

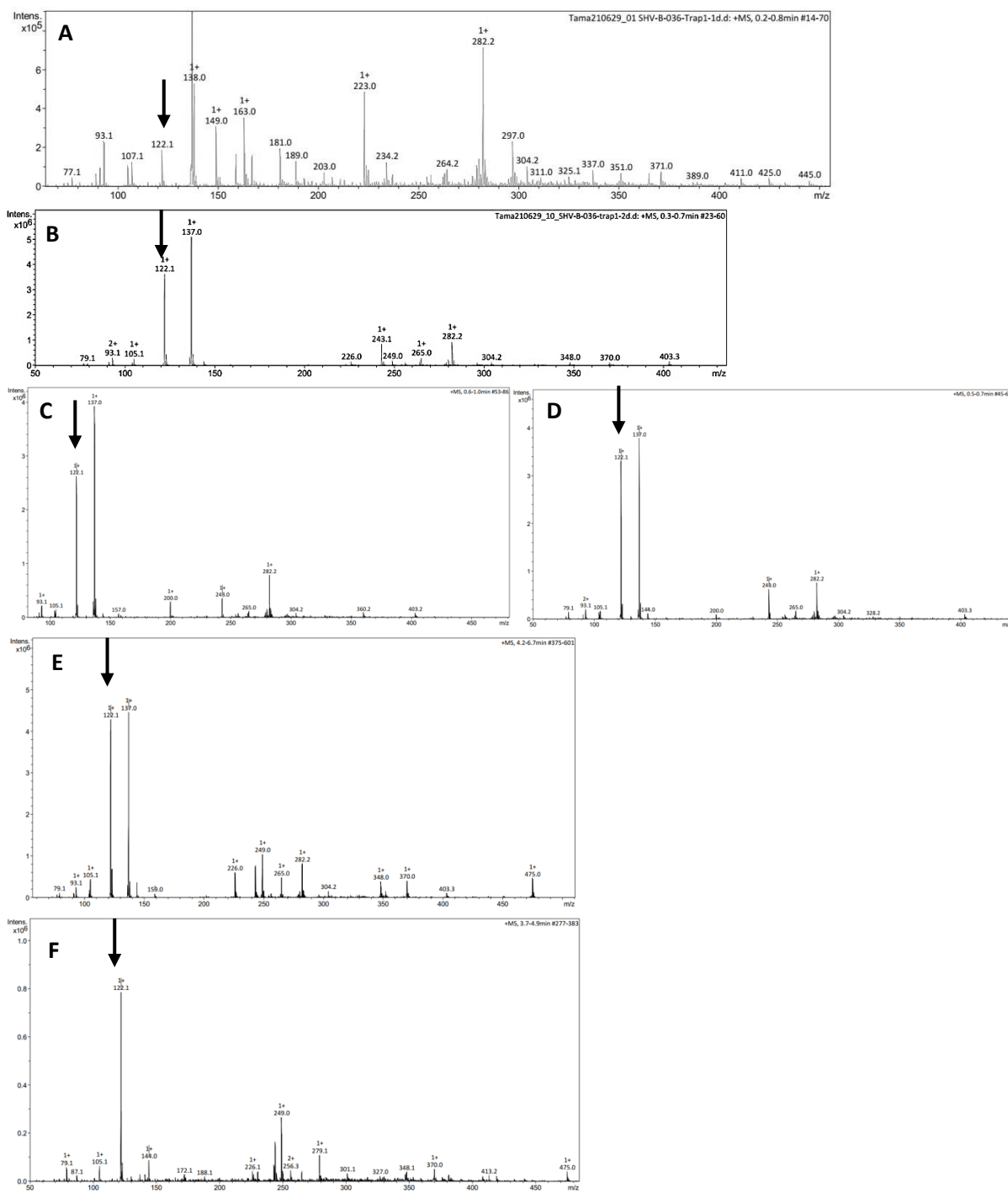


Figure A254. Results of low-resolution positive ion mode mass analyses of trap 1 of experiment 1.8.

A-D – sampling of solution was made after 24, 48, 72 and 96 h of heating (sampling directly from the trap 2 during the reaction).

E – sample of trap 1 solution

F – sample of trap 1 precipitate after the end of the reaction and filtration.

Arrow shows presence of benzamide in the studied solution.

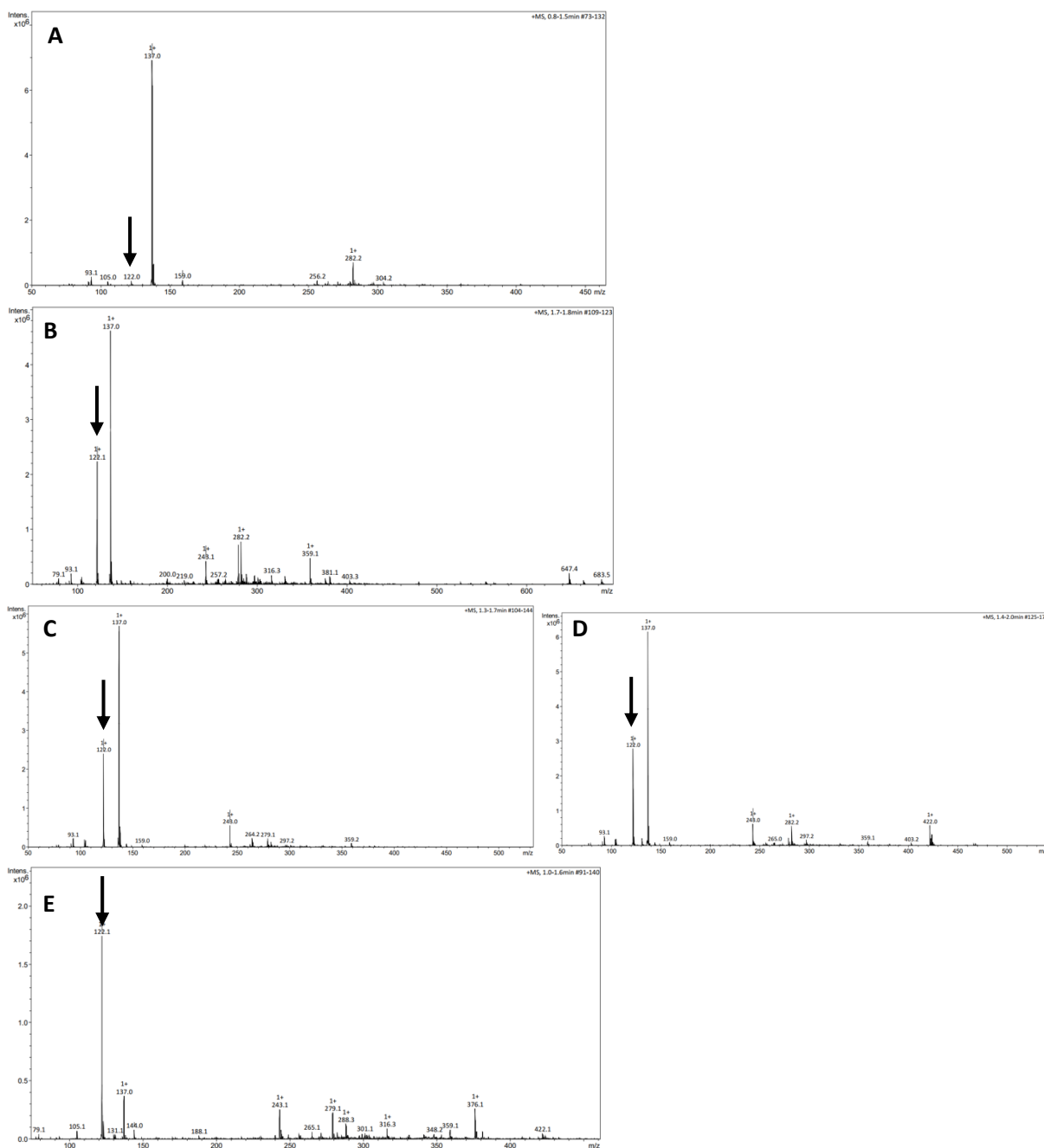


Figure A255. Results of low-resolution positive ion mode mass analyses of trap 1 of experiment **1.9**.

A-C – sampling of solution was made after 24, 48 and 96 h of heating (sampling directly from the trap 2 during the reaction).

D – sample of trap 1 solution

E – sample of trap 1 precipitate after the end of the reaction and filtration.

Arrow shows presence of benzamide in the studied solution.

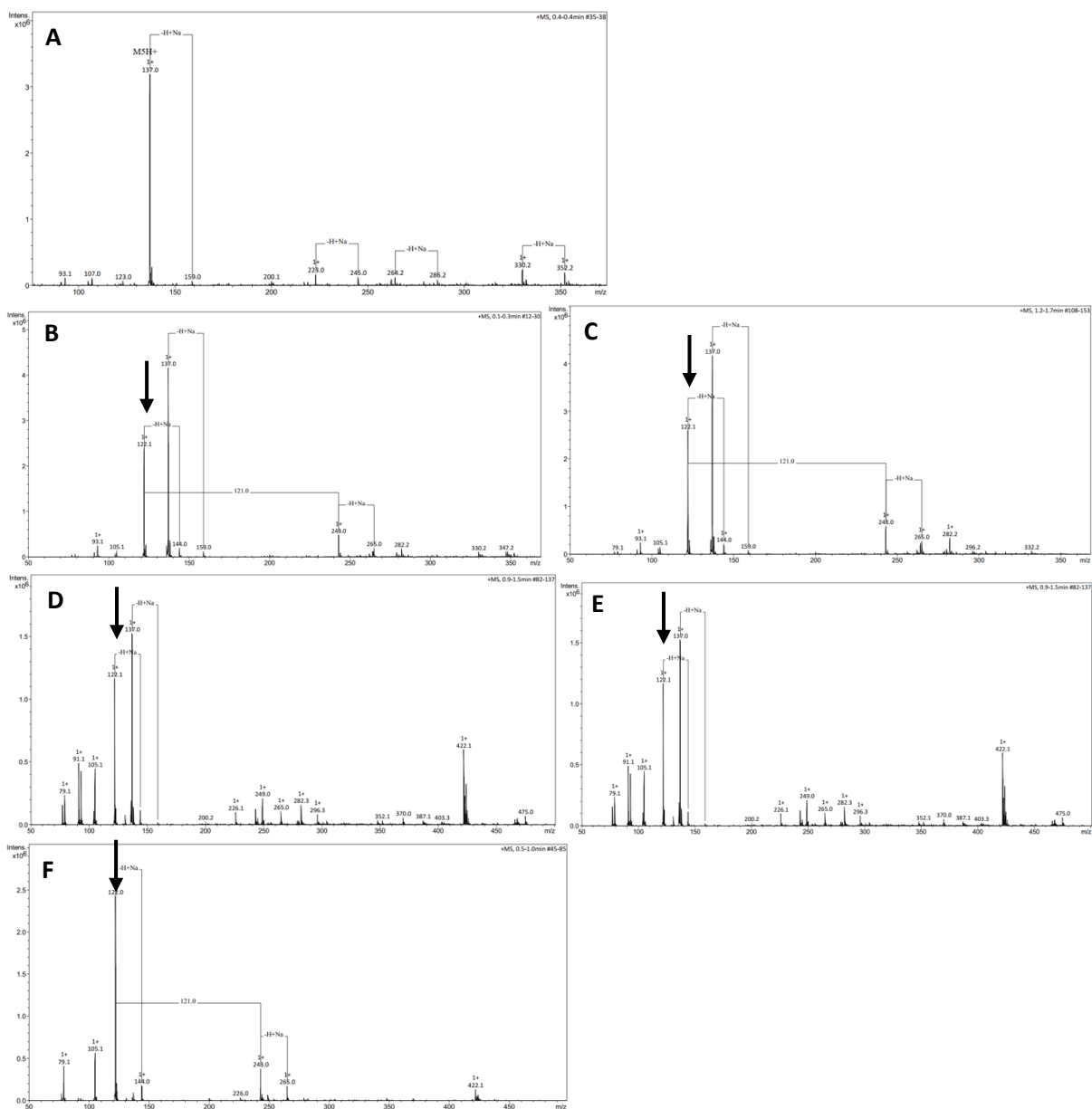


Figure A256. Results of low-resolution positive ion mode mass analyses of trap 1 of experiment **1.10**.

A-D – sampling of solution was made after 24, 48, 72 and 96 h of heating (sampling directly from the trap 2 during the reaction).

E – sample of trap 1 solution

F – sample of trap 1 precipitate after the end of the reaction and filtration.

Arrow shows presence of benzamide in the studied solution.

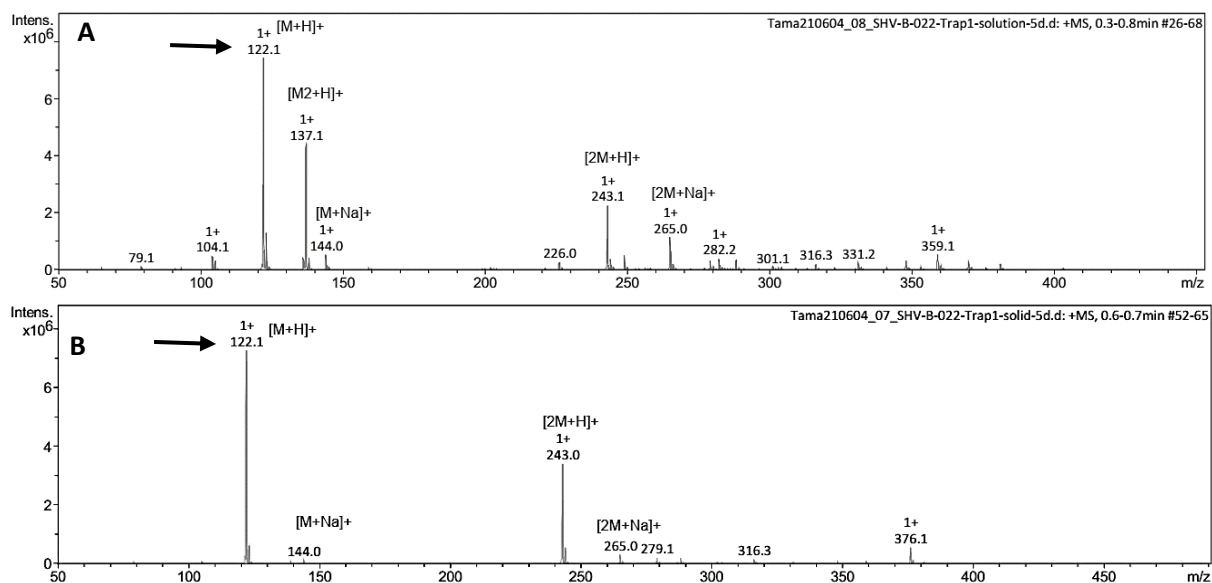


Figure A257. Results of low-resolution positive ion mode mass analyses of trap 1 of experiment **1.11** after 120 h of heating.

A – sample of trap 1 solution

B – sample of trap 1 precipitate after the end of the reaction and filtration.

Arrow shows presence of benzamide in the studied solution.

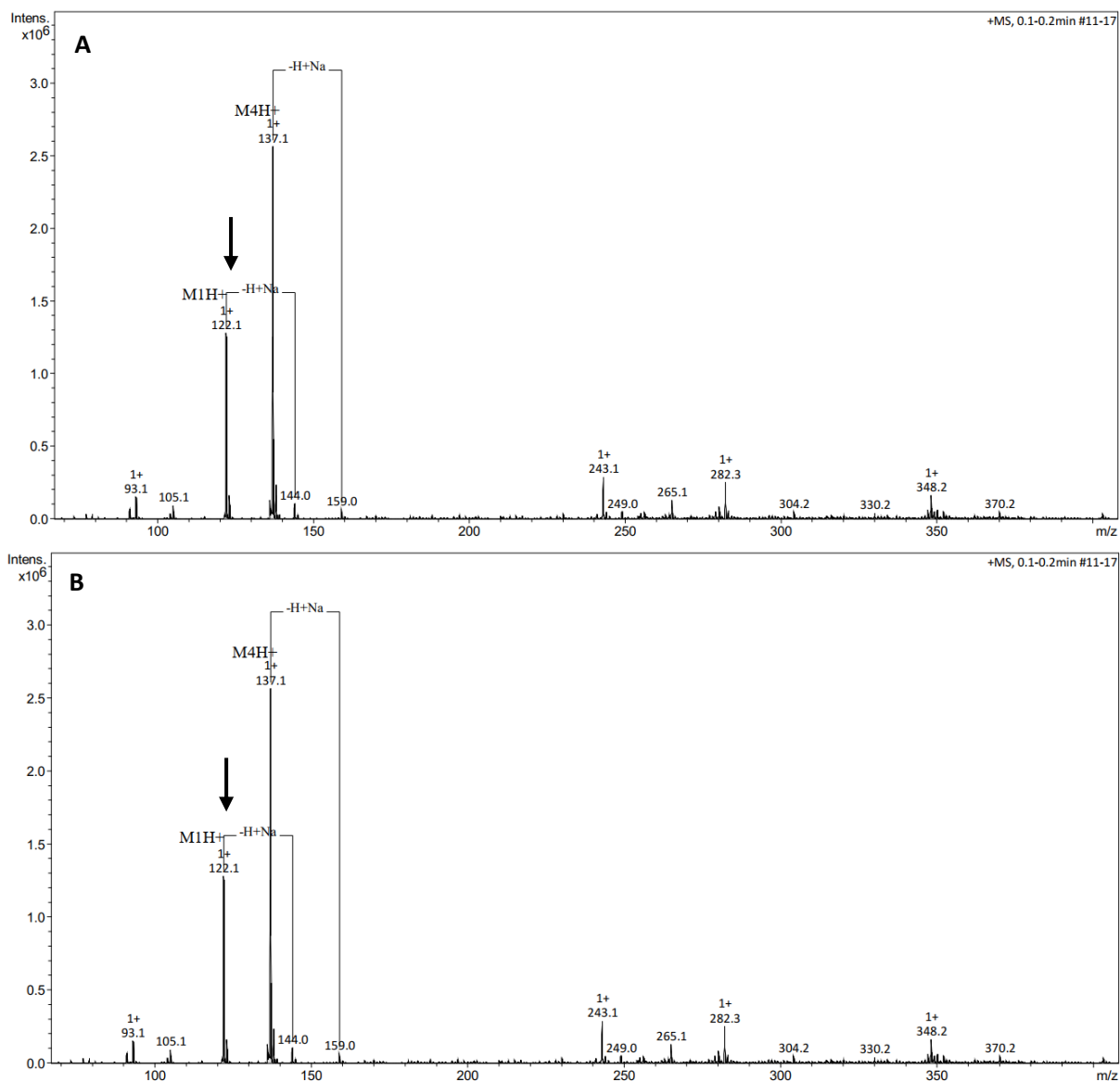


Figure A258. Results of low-resolution positive ion mode mass analyses of trap 1 of experiment **1.12** after 120 h of heating.

A – sample of trap 1 solution

B – sample of trap 1 precipitate after the end of the reaction and filtration.

Arrow shows presence of benzamide in the studied solution.

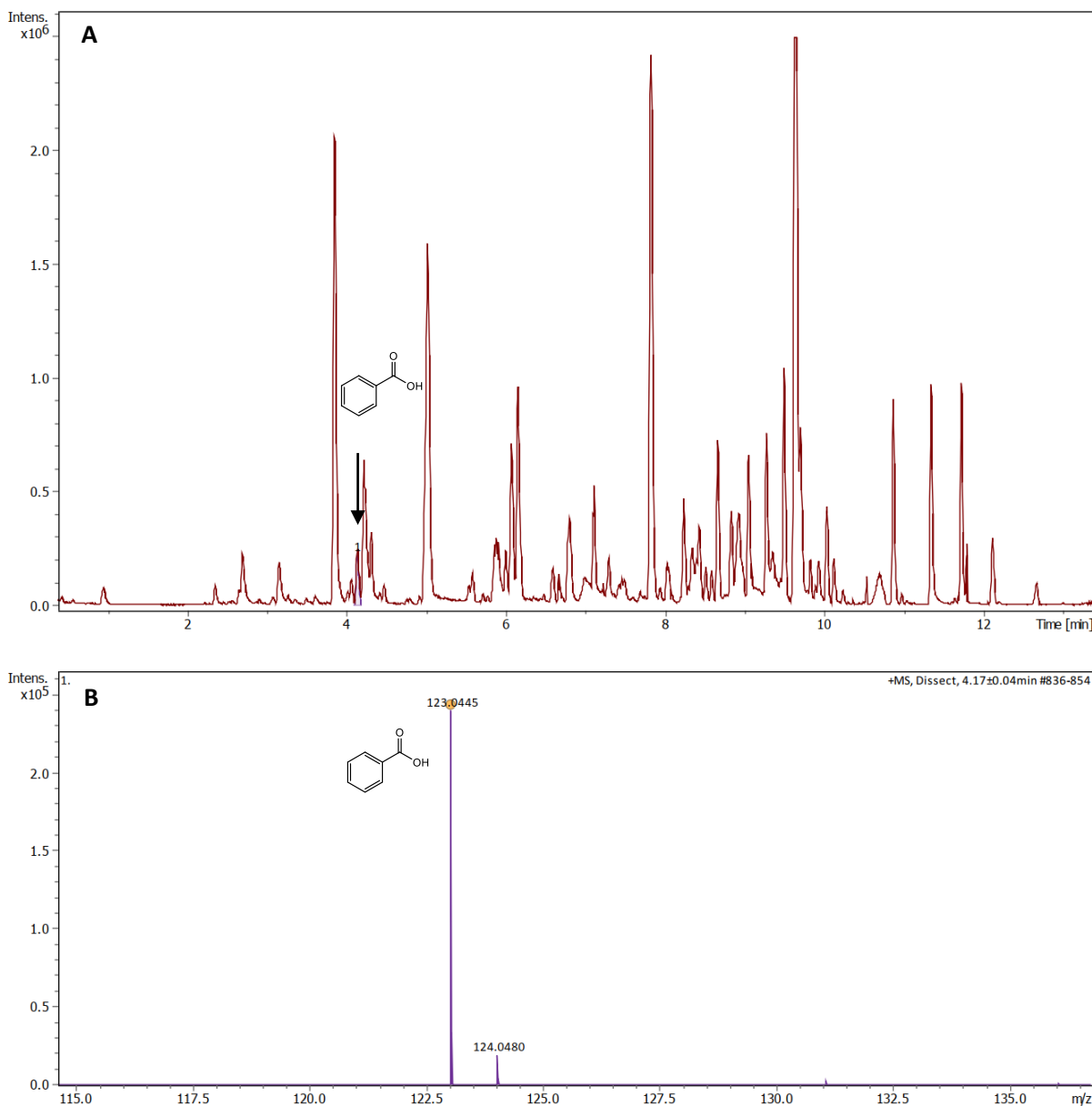


Figure A259. Results of LC-MS analysis of trap 2 solution of experiment **1.2** after 120 h of heating.

A – chromatogram of the experiment.

B – mass spectra of peak 1 (rt = 4.1 min) benzoic acid ($C_7H_6O_2$).

All other peaks are result of overphenylation of PhMgBr in THF under rt.

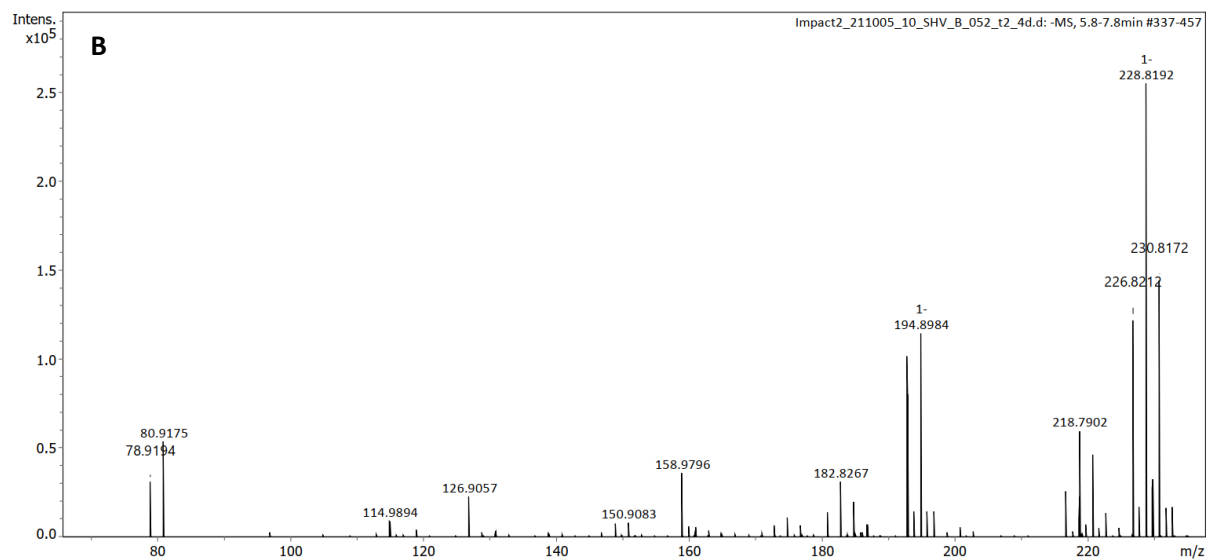
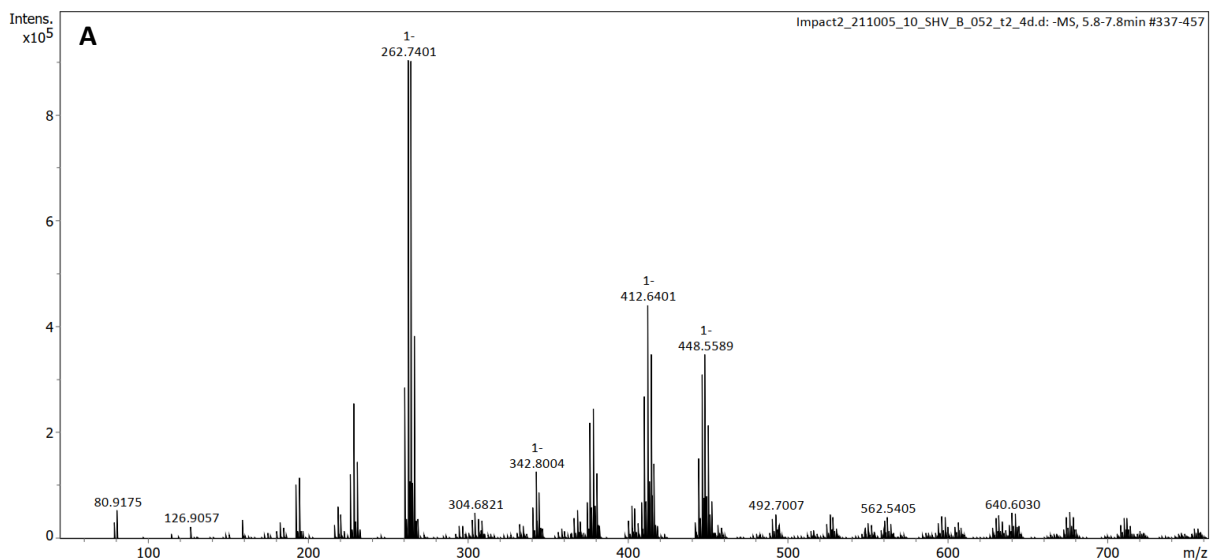


Figure A260. Results of high-resolution negative ion mode mass analyses of trap 2 of experiment **1.3** after 120 h of heating.

A – chromatogram of the experiment.

B – zoom in area 70-240 m/z.

Benzoic acid is absent due to different phosphorylation mechanism in reaction with formamide (**3b**).

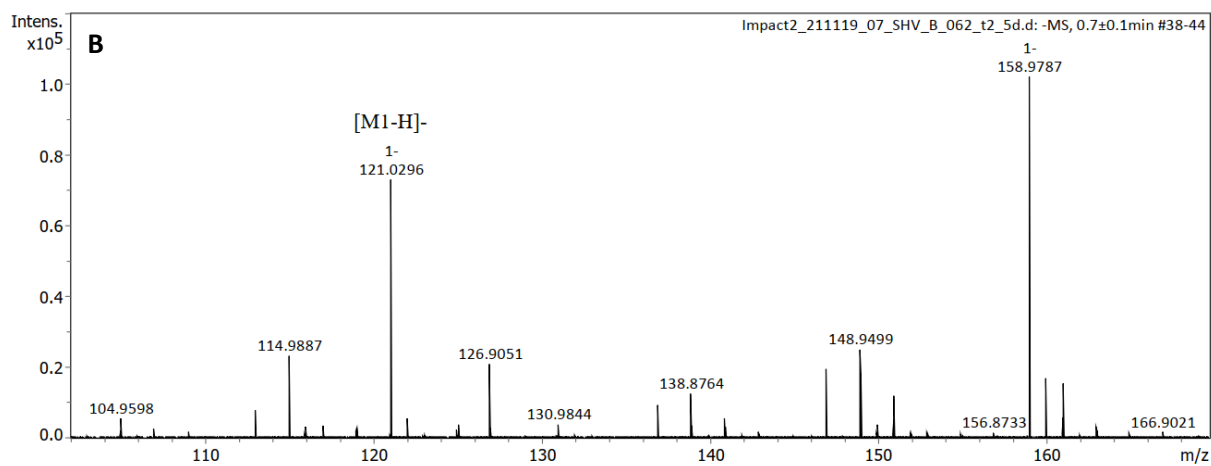
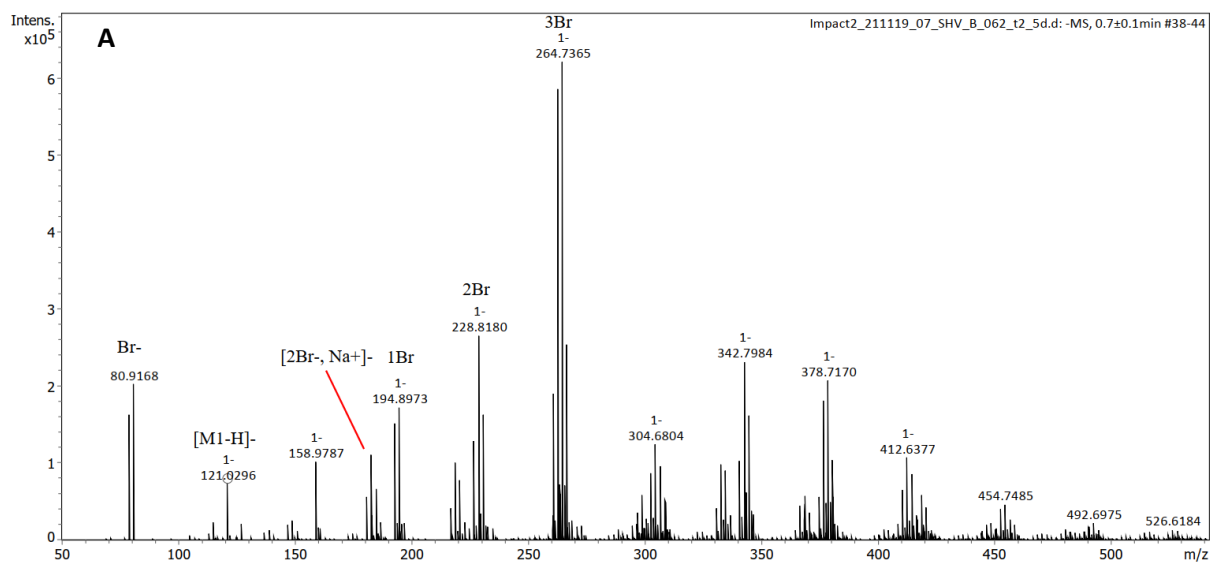


Figure A261. Results of high-resolution negative ion mode mass analyses of trap 2 of experiment **1.4** after 120 h of heating.

A – chromatogram of the experiment.

B – zoom in area 100-170 m/z.

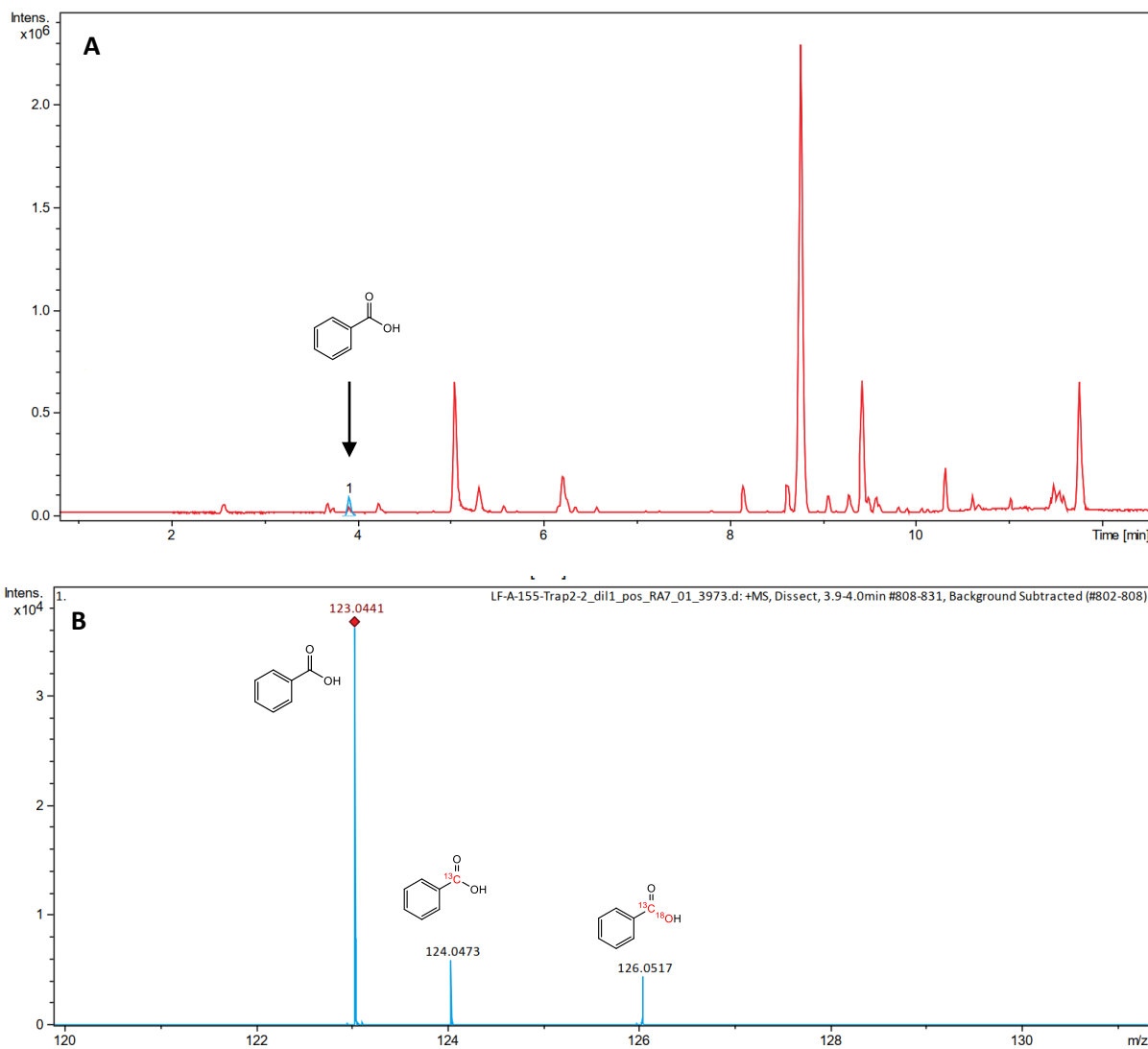


Figure A262. Results of LC-MS analysis of trap 2 solution of experiment **1.5** after 120 h of heating.

A – chromatogram of the experiment.

B – mass spectra of peak 1 ($rt = 4.1$ min) benzoic acid ($C_7H_6O_2$, $C_6H_6O_2^{13}C$, $C_6H_6O^{13}C^{18}O$).

All other peaks are result of overphenilation of PhMgBr in THF under r.t.

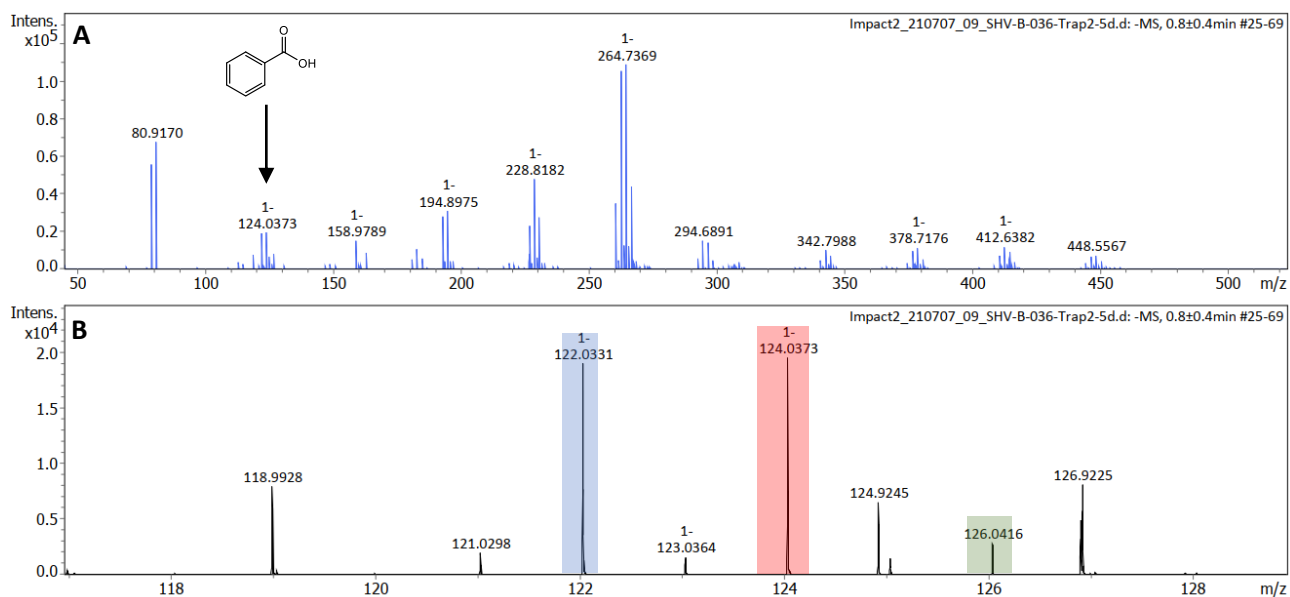


Figure A263. Results of high-resolution negative ion mode mass analyses of trap 2 of experiment **1.8**.

A – total ion chromatogram after 120 h of heating.

B – zoom for benzoic acid area.

^{13}C benzoic acid (mass $[\text{m/z}-\text{H}]^-$ 122.0331) is marked as blue line, $^{13}\text{C}^{18}\text{O}$ benzoic acid (mass $[\text{m/z}-\text{H}]^-$ 124.0373) red, $^{13}\text{C}^{18}\text{O}_2$ benzoic acid (mass $[\text{m/z}-\text{H}]^-$ 126.0416) green.

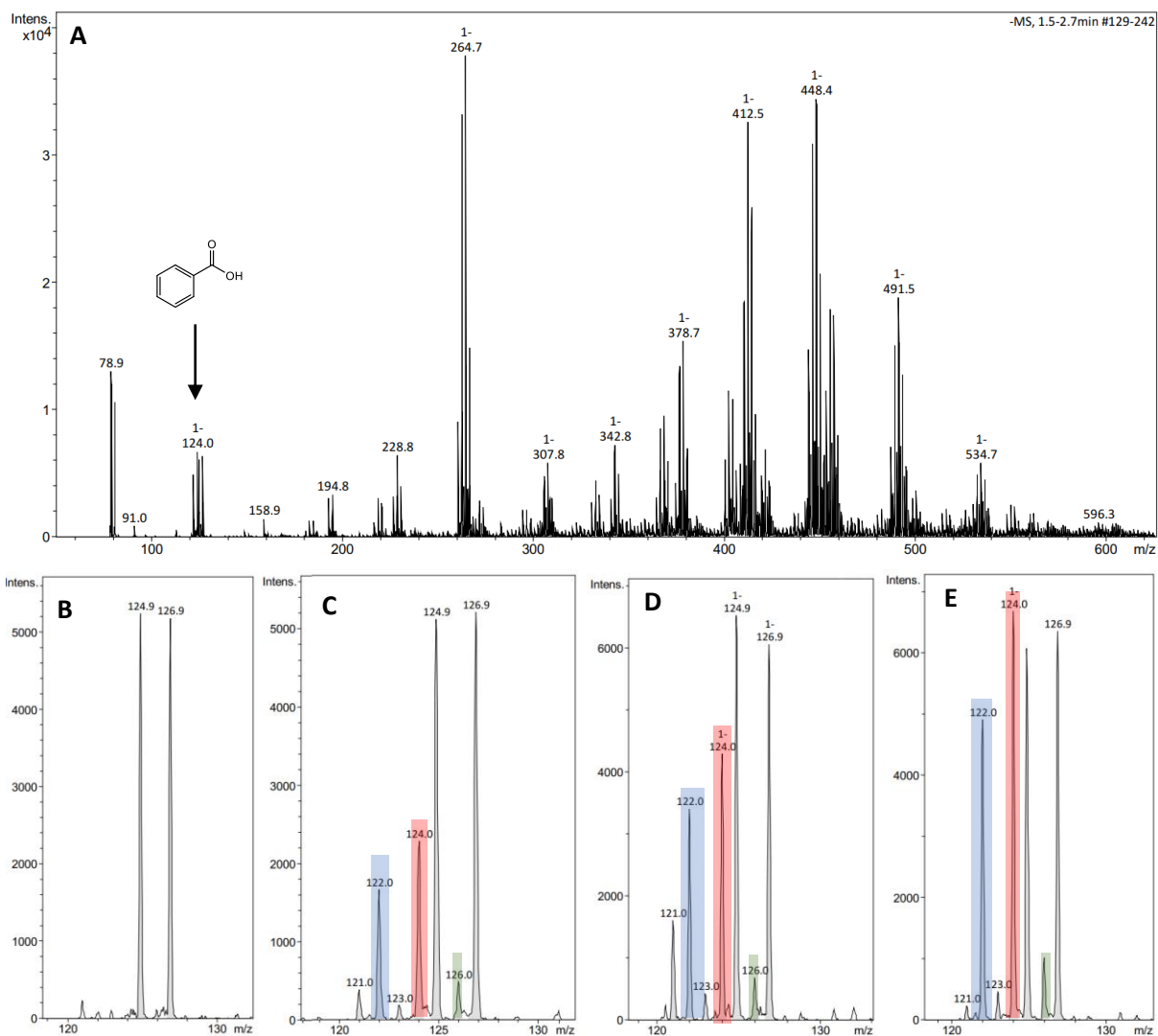


Figure A264. Results of low-resolution negative ion mode mass analyses of trap 2 of experiment **1.9**.

A – total ion chromatogram after 120 h of heating.

B-E – sampling of solution was made after 24, 48, 96 and 120 h after start of the heating (sampling directly from the trap 2 during the reaction).

Blue color [¹³C]benzoic acid (mass [m/z-H]⁻122.0330), red [¹³C¹⁸O]benzoic acid (mass [m/z-H]⁻124.0371), [¹³C¹⁸O₂]benzoic acid (mass [m/z-H]⁻126.0410) green.

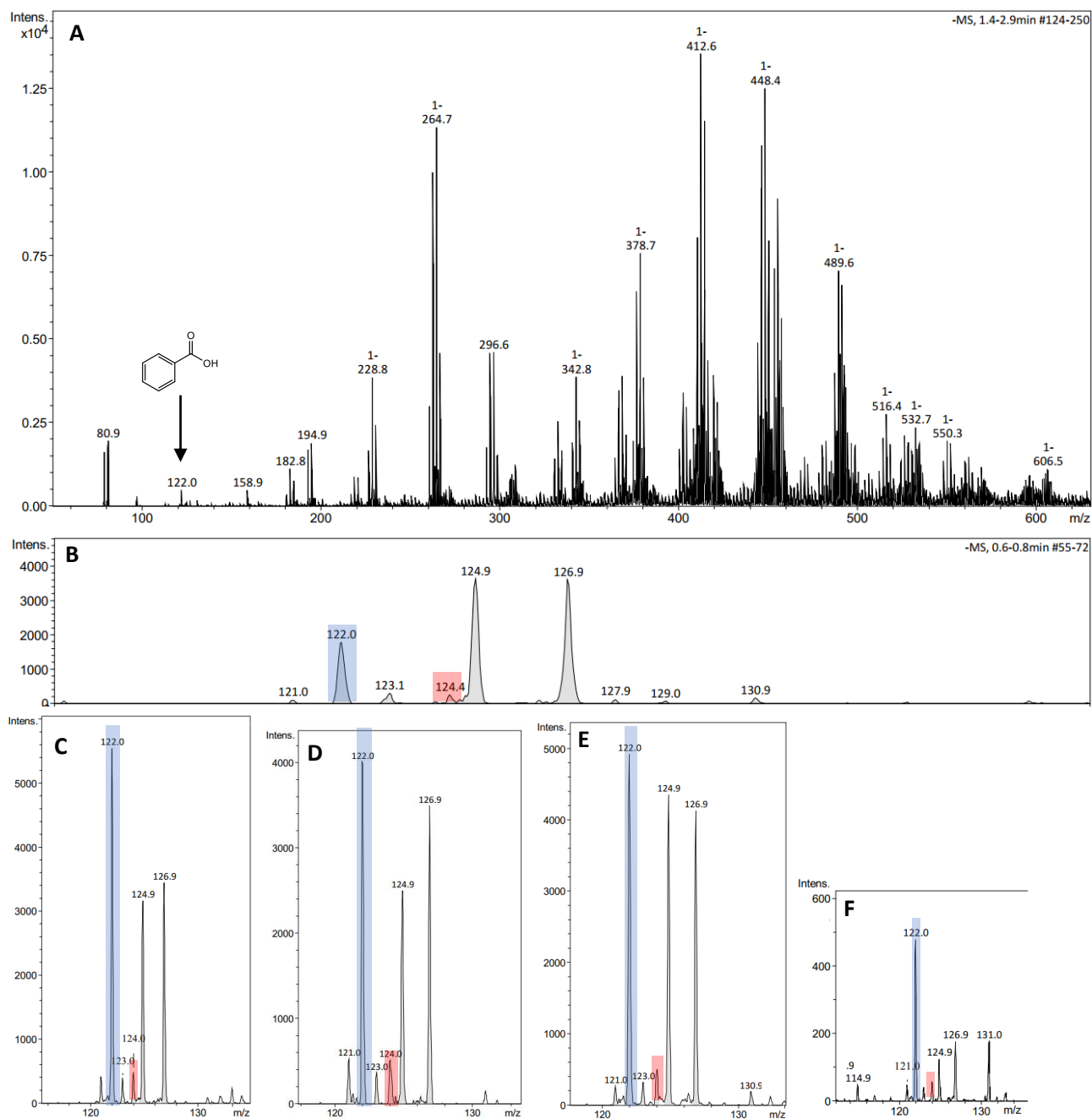


Figure A265. Results of low-resolution negative ion mode mass analyses of trap 2 of experiment **1.10**.

A – total ion chromatogram after 120 h of heating.

B-F – sampling of solution was made after 24, 48, 72, 96 and 120 h after start of the heating (sampling directly from the trap 2 during the reaction).

Blue color [^{13}C]benzoic acid (mass $[\text{m/z}-\text{H}]^{-}$ 122.0330), red [$^{13}\text{C}^{18}\text{O}$]benzoic acid (mass $[\text{m/z}-\text{H}]^{-}$ 124.0371).

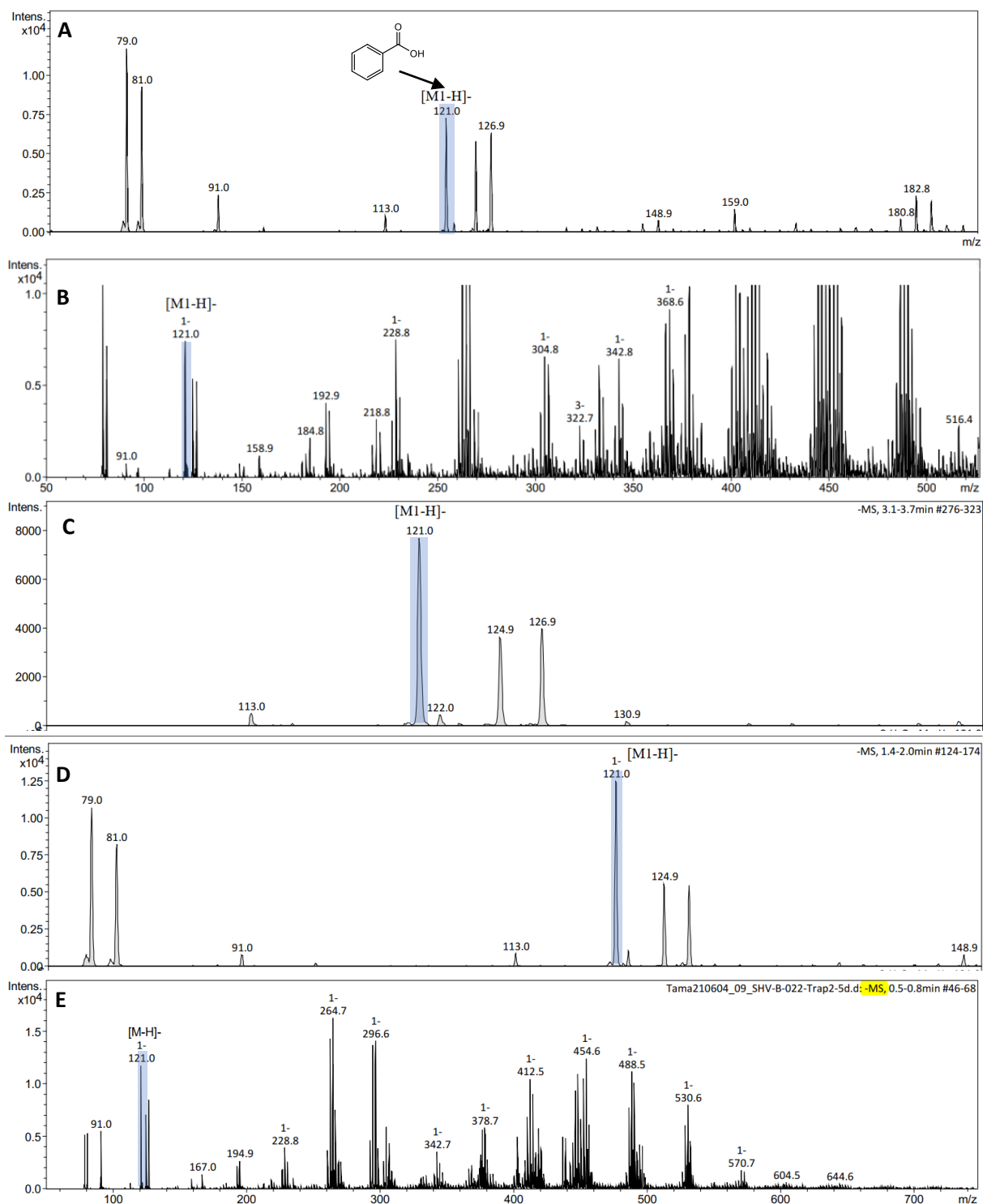


Figure A266. Results of low-resolution negative ion mode mass analyses of trap 2 of experiment **1.11**.

A-E – sampling of solution was made after 24, 48, 72, 96 and 120 h after start of the heating (sampling directly from the trap 2 during the reaction).

Blue color benzoic acid (mass [m/z-H]⁻122.0330).

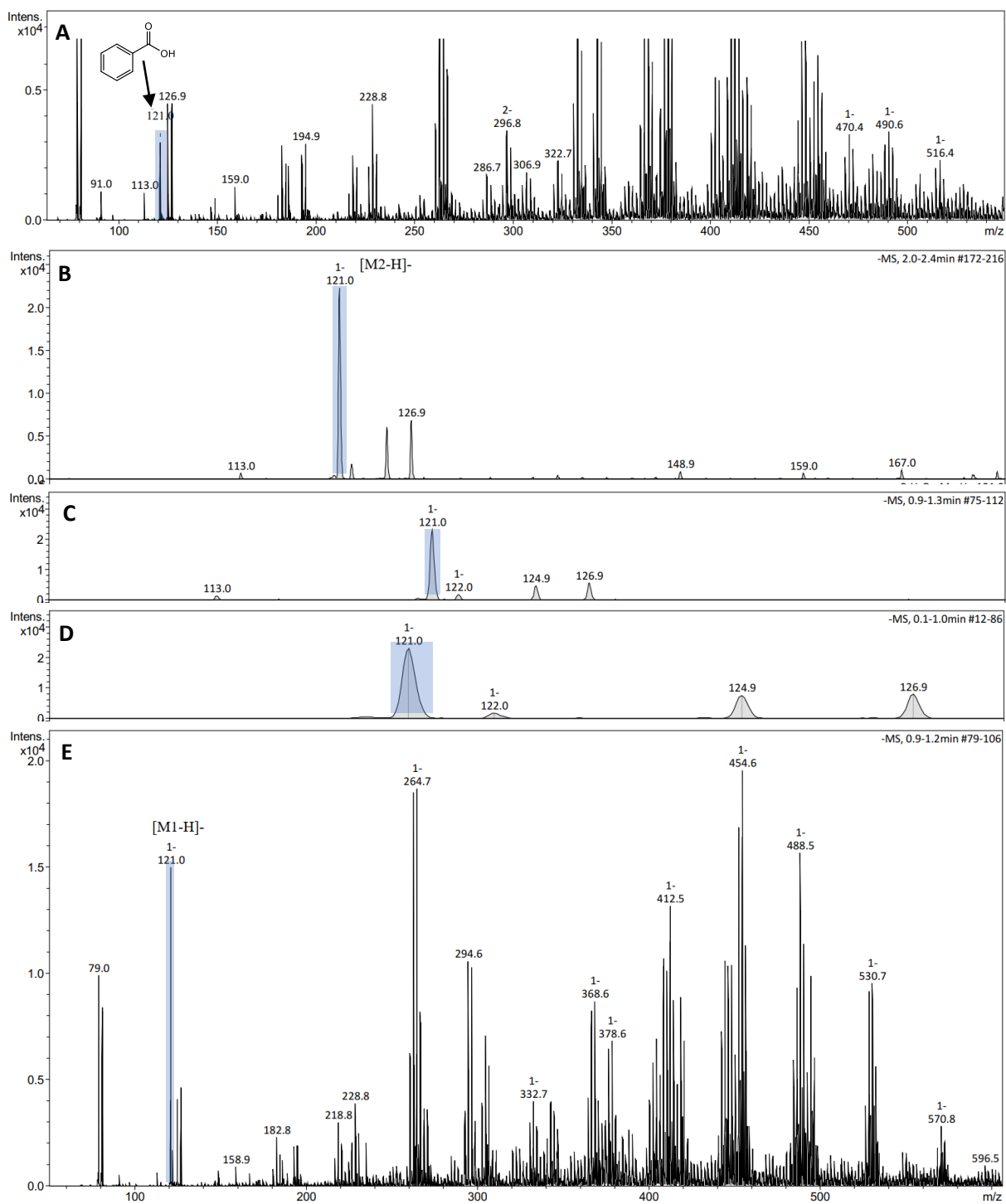


Figure A267. Results of low-resolution negative ion mode mass analyses of trap 2 of experiment **1.12**.

A-E – sampling of solution was made after 24, 48, 72, 96 and 120 h after start of the heating (sampling directly from the trap 2 during the reaction).

Blue color benzoic acid (mass $[m/z-H]^-122.0330$).

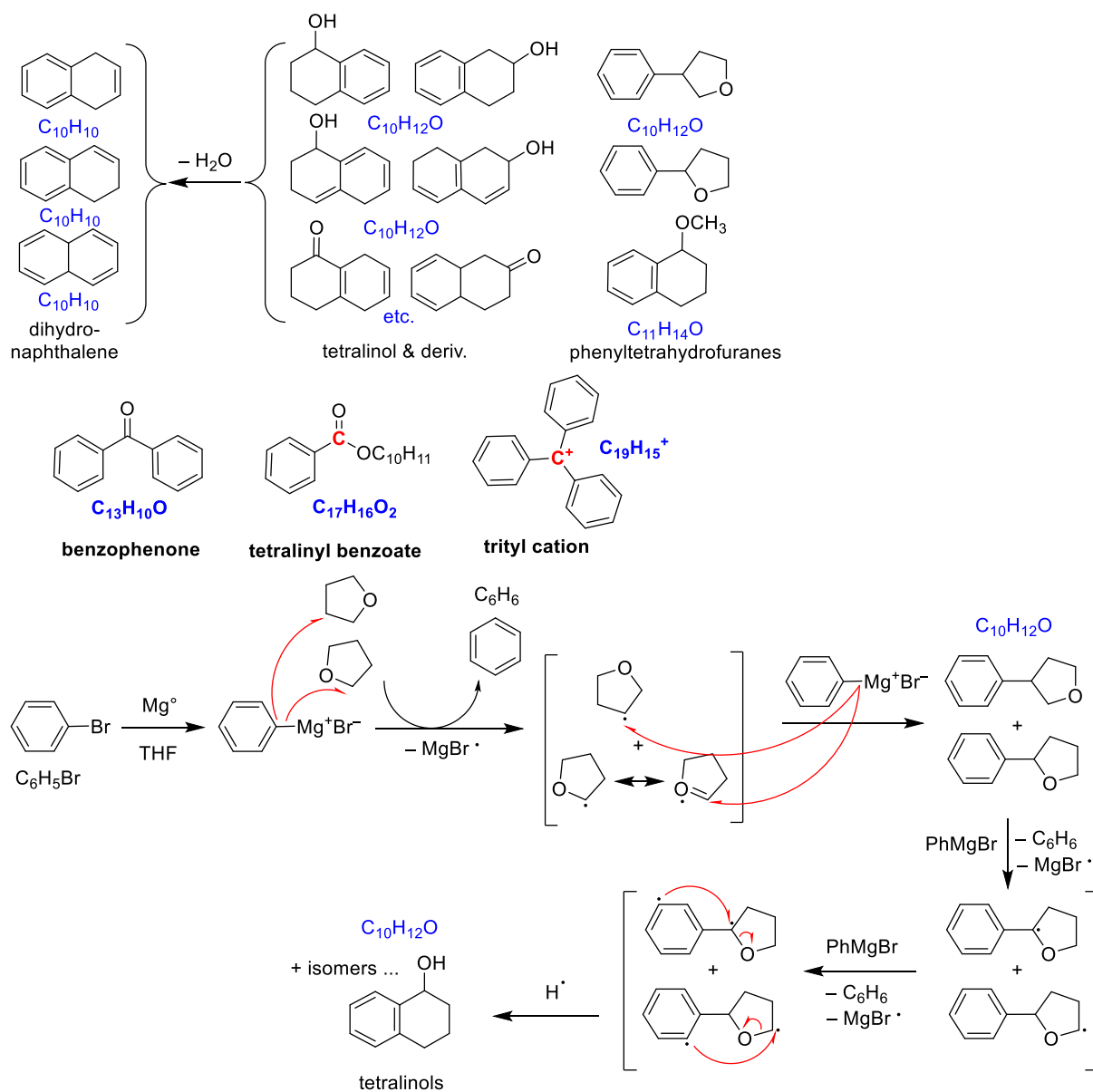


Figure A268. Suggested “families” of products and proposition for mechanism of reaction that could occur in trap 2 after 120 h of heating under rt.

List of citations

- ¹ Pasek, M. A., Dworkin, J. P., & Lauretta, D. S. (2007). A radical pathway for organic phosphorylation during schreibersite corrosion with implications for the origin of life. *Geochimica et Cosmochimica Acta*, 71(7), 1721–1736. <https://doi.org/10.1016/j.gca.2006.12.018>
- ² Nelson, D. L. & Cox, M. M. (2004) Principles of Biochemistry 4th edn, *Lehninger Ch. 13*, 493–497 (W. H. Freeman 2004)
- ³ Westheimer, F. H. (1987). Why Nature Chose Phosphates. *Science*, 235, 1173–1178. <https://doi.org/10.1126/science.2434996>
- ⁴ Fernández-García, C., Coggins, A. J., & Powner, M. W. (2017). A chemist's perspective on the role of phosphorus at the origins of life. *Life*, 7(3). <https://doi.org/10.3390/life7030031>
- ⁵ Keefe, A. D., & Miller, S. L. (1995). Are Polyphosphates or Phosphate Esters Prebiotic Reagents? *J Mol Evol*, 41, 693–702. <https://doi.org/10.1007/BF00173147>
- ⁶ Schwartz, A. W. (2006). Phosphorus in prebiotic chemistry. *Philosophical Transactions of the Royal Society B: Biological Sciences*, 361(1474), 1743–1749. <https://doi.org/10.1098/rstb.2006.1901>
- ⁷ Hao, J., Knoll, A. H., Huang, F., Schieber, J., Hazen, R. M., & Daniel, I. (2020). Cycling phosphorus on the Archean Earth: Part II. Phosphorus limitation on primary production in Archean ecosystems. *Geochimica et Cosmochimica Acta*, 280, 360–377. <https://doi.org/10.1016/j.gca.2020.04.005>
- ⁸ Walton, C. R., Shorttle, O., Jenner, F. E., Williams, H. M., Morrison, S. M., Downs, R. T., Zerkle, A., Hazen, R. M., & Pasek, M. (2021). Phosphorus mineral evolution and prebiotic chemistry: from minerals to microbes. *Earth-Science Reviews*, 221. <https://doi.org/10.1016/j.earscirev.2021.103806>
- ⁹ Pasek, M. A. (2017). Schreibersite on the early Earth: Scenarios for prebiotic phosphorylation. *Geoscience Frontiers*, 8(2), 329–335. <https://doi.org/10.1016/j.gsf.2016.06.008>
- ¹⁰ Pasek, M. A., & Lauretta, D. S. (2005). Aqueous Corrosion of Phosphide Minerals from Iron Meteorites: A Highly Reactive Source of Prebiotic Phosphorus on the Surface of the Early Earth. *Astrobiology*, 5(4), 515–535. <https://doi.org/10.1089/ast.2005.5.515>
- ¹¹ Lohrmann R, & Orgel L E. (1968). Prebiotic Synthesis: Phosphorylation in Aqueous Solution. *Science*, 161(3836), 64–66. <https://doi.org/10.1126/science.161.3836.64>
- ¹² Powner, M. W., Gerland, B., & Sutherland, J. D. (2009). Synthesis of activated pyrimidine ribonucleotides in prebiotically plausible conditions. *Nature*, 459(7244), 239–242. <https://doi.org/10.1038/nature08013>
- ¹³ Altamura, E., Comte, A., D'Onofrio, A., Roussillon, C., Fayolle, D., Buchet, R., Mavelli, F., Stano, P., Fiore, M., & Strazewski, P. (2020). Racemic phospholipids for origin of life studies. *Symmetry*, 12(7). <https://doi.org/10.3390/sym12071108>
- ¹⁴ Russell, M. J., Daniel, R. M., Hall, A. J., & Sherringham, J. A. (1994). A Hydrothermally Precipitated Catalytic Iron Sulphide Membrane as a First Step Toward Life. *Journal of Molecular Evolution*, 39, 231–243. <https://doi.org/10.1007/BF00160147>
- ¹⁵ Ozawa, K., Nemoto, A., Imai, E., Honda, H., Hatori, K., & Matsuno, K. (2004). Phosphorylation of nucleotide molecules in hydrothermal environments. *Orig Life Evol Biosph*, 34(5), 465–471. <https://doi.org/10.1023/b:orig.0000043121.65714.05>
- ¹⁶ Martin, W., & Russell, M. J. (2007). On the origin of biochemistry at an alkaline hydrothermal vent. *Philosophical Transactions of the Royal Society B: Biological Sciences*, 362(1486), 1887–1926. <https://doi.org/10.1098/rstb.2006.1881>

-
- ¹⁷ Canup, R. M. (2004). Simulations of a late lunar-forming impact. *Icarus*, 168(2), 433–456. <https://doi.org/10.1016/j.icarus.2003.09.028>
- ¹⁸ Benz, W., Cameron, A. G. W., & Melosh, H. J. (1989). The Origin of the Moon and the Single-Impact Hypothesis III. *ICARUS*, 81, 113–131. [https://doi.org/10.1016/0019-1035\(89\)90129-2](https://doi.org/10.1016/0019-1035(89)90129-2)
- ¹⁹ Wood, B. J., & Halliday, A. N. (2005). Cooling of the Earth and core formation after the giant impact. *Nature*, 437(7063), 1345–1348. <https://doi.org/10.1038/nature04129>
- ²⁰ Monteux, J., Andraut, D., & Samuel, H. (2016). On the cooling of a deep terrestrial magma ocean. *Earth and Planetary Science Letters*, 448, 140–149. <https://doi.org/10.1016/j.epsl.2016.05.010>
- ²¹ Blichert-Toft, J., & Albarède, F. (2008). Hafnium isotopes in Jack Hills zircons and the formation of the Hadean crust. *Earth and Planetary Science Letters*, 265(3–4), 686–702. <https://doi.org/10.1016/j.epsl.2007.10.054>
- ²² Valley, J. W., Cavosie, A. J., Ushikubo, T., Reinhard, D. A., Lawrence, D. F., Larson, D. J., Clifton, P. H., Kelly, T. F., Wilde, S. A., Moser, D. E., & Spicuzza, M. J. (2014). Hadean age for a post-magma-ocean zircon confirmed by atom-probe tomography. *Nature Geoscience*, 7(3), 219–223. <https://doi.org/10.1038/ngeo2075>
- ²³ Harrison T. M., Blichert-Toft J., Müller W., Albarede F., Holden P., and Mojzsis S. J. (2005) Heterogeneous Hadean Hafnium: Evidence of Continental Crust at 4.4 to 4.5 Ga. *Science*, 310, 1947-1950. <https://doi.org/10.1126/science.1117926>
- ²⁴ Guo, M., & Korenaga, J. (2020). Argon constraints on the early growth of felsic continental crust. *Science Advances*, 6(21). <https://doi.org/10.1126/sciadv.aaz6234>
- ²⁵ Rosas, J. C., & Korenaga, J. (2018). Rapid crustal growth and efficient crustal recycling in the early Earth: Implications for Hadean and Archean geodynamics. *Earth and Planetary Science Letters*, 494, 42–49. <https://doi.org/10.1016/j.epsl.2018.04.051>
- ²⁶ Hawkesworth, C. J., Dhuime, B., Pietranik, A. B., Cawood, P. A., Kemp, A. I. S., & Storey, C. D. (2010). The generation and evolution of the continental crust. *Journal of the Geological Society*, 167(2), 229–248. <https://doi.org/10.1144/0016-76492009-072>
- ²⁷ O'neil, J., Carlson, R. W., Paquette, J.-L., & Francis, D. (2012). Formation age and metamorphic history of the Nuvvuagittuq Greenstone Belt. *Precambrian Research, Elsevier*, 220–221, 23–44. <https://doi.org/10.1016/j.precamres.2012.07.009>
- ²⁸ Korenaga, J. (2018). Crustal evolution and mantle dynamics through Earth history. *Philosophical Transactions of the Royal Society A: Mathematical, Physical and Engineering Sciences*, 376(2132). <https://doi.org/10.1098/rsta.2017.0408>
- ²⁹ Goldreich, P. (1966). History of the lunar orbit. *Reviews of Geophysics*, 4(4), 411. <https://doi.org/10.1029/RG004i004p00411>
- ³⁰ Touma, J., & Wisdom, J. (1994). Evolution of the Earth-Moon system. *The Astronomical Journal*, 108, 1943. <https://doi.org/10.1086/117209>
- ³¹ Heller, R., Duda, J. P., Winkler, M., Reitner, J., & Gizon, L. (2021). Habitability of the early Earth: liquid water under a faint young Sun facilitated by strong tidal heating due to a closer Moon. *PalZ*, 95(4), 563–575. <https://doi.org/10.1007/s12542-021-00582-7>
- ³² Mojzsis S J, Harrison T M, & Pidgeon R T. (2001). Oxygen-isotope evidence from ancient zircons for liquid water at the Earth's surface 4,300 Myr ago. *Nature*, 409, 178–181. <https://doi.org/10.1038/35051557>
- ³³ Wilde, S. A., Valley, J. W., Peck, W. H., & Graham, C. M. (2001). Evidence from detrital zircons for the existence of continental crust and oceans on the Earth 4.4 Gyr ago. *Nature*, 409, 175–178. <https://doi.org/10.1038/35051550>
- ³⁴ Sagan, C., & Chyba, C. (1997). The Early Faint Sun Paradox: Organic Shielding of Ultraviolet-Labile Greenhouse Gases. *Science*, 276, 1217–1221. <https://doi.org/10.1126/science.276.5316.1217>

-
- ³⁵ Hsiao, C., Chou, I. C., Okafor, C. D., Bowman, J. C., O'neill, E. B., Athavale, S. S., Petrov, A. S., Hud, N. v., Wartell, R. M., Harvey, S. C., & Williams, L. D. (2013). RNA with iron(II) as a cofactor catalyses electron transfer. *Nature Chemistry*, 5(6), 525–528. <https://doi.org/10.1038/nchem.1649>
- ³⁶ Charnay, B., Wolf, E. T., Marty, B., & Forget, F. (2020). Is the Faint Young Sun Problem for Earth Solved? *Space Science Reviews*, 216(5). <https://doi.org/10.1007/s11214-020-00711-9>
- ³⁷ Spencer, J. (2019). The faint young sun problem revisited. *GSA Today*, 29(12), 4–10. <https://doi.org/10.1130/GSATG403A.1>
- ³⁸ Sleep, N. H. (2010). The Hadean-Archaeon environment. *Cold Spring Harbor Perspectives in Biology*, 2(6). <https://doi.org/10.1101/cshperspect.a002527>
- ³⁹ Owen, T., Cess, R., & Ramanathan, V. (1979). Enhanced CO₂ greenhouse to compensate for reduced solar luminosity on early Earth. *Nature*, 277, 640–642. <https://doi.org/10.1038/277640a0>
- ⁴⁰ Sleep, N. H., & Zahnle, K. (2001). Carbon dioxide cycling and implications for climate on ancient Earth. *Journal of Geophysical Research*, 106. <https://doi.org/10.1029/2000JE001247>
- ⁴¹ Pavlov, A. A., Kasting, J. F., Brown, L. L., Rages, K. A., & Freedman, R. (2000). Greenhouse warming by CH₄ in the atmosphere of early Earth. *Journal of Geophysical Research: Planets*, 105(E5), 11981–11990. <https://doi.org/10.1029/1999JE001134>
- ⁴² Zahnle, K., Arndt, N., Cockell, C., Halliday, A., Nisbet, E., Selsis, F., & Sleep, N. H. (2007). Emergence of a habitable planet. *Space Science Reviews*, 129(1–3), 35–78. <https://doi.org/10.1007/s11214-007-9225-z>
- ⁴³ Trainer, M. G., Pavlov, A. A., Langley Dewitt, H., Jimenez, J. L., McKay, C. P., Toon, O. B., & Tolbert, M. A. (2006). Organic haze on Titan and the early Earth. *Proceedings of the National Academy of Sciences of the United States of America*, 103(48), 18033–18042. <https://doi.org/10.1073/pnas.0608561103>
- ⁴⁴ Hartmann, J., Moosdorf, N., Lauerwald, R., Hinderer, M., & West, A. J. (2014). Global chemical weathering and associated p-release - the role of lithology, temperature and soil properties. *Chemical Geology*, 363, 145–163. <https://doi.org/10.1016/j.chemgeo.2013.10.025>
- ⁴⁵ Goldblatt, C., Claire, M. W., Lenton, T. M., Matthews, A. J., Watson, A. J., & Zahnle, K. J. (2009). Nitrogen-enhanced greenhouse warming on early Earth. *Nature Geoscience*, 2(12), 891–896. <https://doi.org/10.1038/ngeo692>
- ⁴⁶ Truche, L., McCollom, T. M., & Martinez, I. (2020). Hydrogen and abiotic hydrocarbons: Molecules that change the world. *Elements*, 16(1), 13–18. <https://doi.org/10.2138/GSELEMENTS.16.1.13>
- ⁴⁷ Nisbet, E. G., & Sleep, N. H. (2001). The habitat and nature of early life. *Nature*, 409(6823), 1083–1091. <https://doi.org/10.1038/35059210>
- ⁴⁸ Marty, B., Avicé, G., Bekaert, D. v., & Broadley, M. W. (2018). Salinity of the Archaeon oceans from analysis of fluid inclusions in quartz. *Comptes Rendus - Geoscience*, 350(4), 154–163. <https://doi.org/10.1016/j.crte.2017.12.002>
- ⁴⁹ Catling, D. C., & Zahnle, K. J. (2020). The Archean atmosphere. *Science Advances*, 6(9). <https://doi.org/10.1126/sciadv.aax1420>
- ⁵⁰ Johnson, B., & Goldblatt, C. (2015). The nitrogen budget of Earth. *Earth-Science Reviews*, 148, 150–173. <https://doi.org/10.1016/j.earscirev.2015.05.006>
- ⁵¹ Lyons, T. W., Reinhard, C. T., & Planavsky, N. J. (2014). The rise of oxygen in Earth's early ocean and atmosphere. *Nature*, 506(7488), 307–315. <https://doi.org/10.1038/nature13068>
- ⁵² Kasting, J. F. (2013). What caused the rise of atmospheric O₂? *Chemical Geology*, 362, 13–25. <https://doi.org/10.1016/j.chemgeo.2013.05.039>
- ⁵³ Trail, D., Watson, E. B., & Tailby, N. D. (2011). The oxidation state of Hadean magmas and implications for early Earth's atmosphere. *Nature*, 480(7375), 79–82. <https://doi.org/10.1038/nature10655>

-
- ⁵⁴ Zahnle, K. J., Lupu, R., Catling, D. C., & Wogan, N. (2020). Creation and evolution of impact-generated reduced atmospheres of early earth. *Planetary Science Journal*, *1*(1). <https://doi.org/10.3847/PSJ/ab7e2c>
- ⁵⁵ Macleod, G., Mckeown, C., Hall, A. J., & Russell, M. J. (1994). Hydrothermal and oceanic pH conditions of possible relevance to the origin of life. *Origins Life Evol Biosphere.*, *24*, 19–41. <https://doi.org/10.1126/science.aal4151>.
- ⁵⁶ Halevy, I., & Bachan, A. (2017). The geologic history of seawater pH. *Science*, *355*(6329), 1069–1071. <https://doi.org/10.1126/science.aal4151>
- ⁵⁷ Hsiao, C., Chou, I. C., Okafor, C. D., Bowman, J. C., O’neill, E. B., Athavale, S. S., Petrov, A. S., Hud, N. v., Wartell, R. M., Harvey, S. C., & Williams, L. D. (2013). RNA with iron(II) as a cofactor catalyses electron transfer. *Nature Chemistry*, *5*(6), 525–528. <https://doi.org/10.1038/nchem.1649>
- ⁵⁸ Pasek, M. A., Gull, M., & Herschy, B. (2017). Phosphorylation on the early earth. In *Chemical Geology* (Vol. 475, pp. 149–170). Elsevier B.V. <https://doi.org/10.1016/j.chemgeo.2017.11.008>
- ⁵⁹ Toner, J. D., & Catling, D. C. (2020). A carbonate-rich lake solution to the phosphate problem of the origin of life. *PNAS*, *117*(2), 883–888. <https://doi.org/10.1073/pnas.1916109117>
- ⁶⁰ Spitzer, J., & Poolman, B. (2009). The Role of Biomacromolecular Crowding, Ionic Strength, and Physicochemical Gradients in the Complexities of Life’s Emergence. *Microbiology and Molecular Biology Reviews*, *73*(2), 371–388. <https://doi.org/10.1128/mmbr.00010-09>
- ⁶¹ Borquez, E., Cleaves, H. J., Lazcano, A., & Miller, S. L. (2005). An Investigation of Prebiotic Purine Synthesis from the Hydrolysis of HCN Polymers. *Orig Life Evol Biosph.*, *35*, 79–90.
- ⁶² Chyba, C. F., & Sagan, C. E. (1992). Endogenous production, exogenous delivery and impact-shock synthesis of organic molecules, an inventory for the origins of life. *Nature*, *355*, 125–132. <https://doi.org/10.1038/355125a0>
- ⁶³ Sephton, M. A. (2004). Organic matter in ancient meteorites. *Astronomy and Geophysics*, *45*(2), 2.08-2.14. <https://doi.org/10.1046/j.1468-4004.2003.45208.x>
- ⁶⁴ Modica, P., Martins, Z., Meinert, C., & Zanda, B. (2018). The Amino Acid Distribution in Laboratory Analogs of Extraterrestrial Organic Matter: A Comparison to CM Chondrites. *The Astro-Physical Journal*, *865*(1), 41. <https://doi.org/10.3847/1538-4357/aada8a.insu-01897632>
- ⁶⁵ Kvenvolden, K., & Lawless, J. (1970). Extraterrestrial Amino-acids and Hydrocarbons in the Murchison Meteorite. *Nature*, *228*, 923–926. <https://doi.org/10.1038/228923a0>
- ⁶⁶ Elsila, J. E., Aponte, J. C., Blackmond, D. G., Burton, A. S., Dworkin, J. P., & Glavin, D. P. (2016). Meteoritic amino acids: Diversity in compositions reflects parent body histories. *ACS Central Science*, *2*(6), 370–379. <https://doi.org/10.1021/acscentsci.6b00074>
- ⁶⁷ Martins, Z., Botta, O., Fogel, M. L., Sephton, M. A., Glavin, D. P., Watson, J. S., Dworkin, J. P., Schwartz, A. W., & Ehrenfreund, P. (2008). Extraterrestrial nucleobases in the Murchison meteorite. *Earth and Planetary Science Letters*, *270*, 130–136. <https://doi.org/10.1016/j.epsl.2008.03.026>
- ⁶⁸ Callahan, M. P., Smith, K. E., James, H., Ii, C., Ruzicka, J., Stern, J. C., Glavin, D. P., House, C. H., & Dworkin, J. P. (2011). Carbonaceous meteorites contain a wide range of extraterrestrial nucleobases. *Academy of Sciences of the United States of America*, *108*(34), 13995–13998. <https://doi.org/10.1073/pnas.1106493108>
- ⁶⁹ Stoks, P. G., & Schwartz, A. W. (1981). Nitrogen-heterocyclic compounds in meteorites: significance and mechanisms of formation. *Geochimica et Cosmochimica Acta*, *45*(4), 563–569. [https://doi.org/10.1016/0016-7037\(81\)90189-7](https://doi.org/10.1016/0016-7037(81)90189-7)
- ⁷⁰ Cooper, G., Kimmich, N., & Belisle, W. (2001). Carbonaceous meteorites as a source of sugar-related organic compounds for the early Earth. *Nature*, *414*, 879–883. <https://doi.org/10.1038/414879a>
- ⁷¹ Yuen G., Blair N., & des Marais D. (1984). Carbon isotope composition of low molecular weight hydrocarbons and monocarboxylic acids from Murchison meteorite. *Nature*, *307*, 252–254. <https://doi.org/10.1038/307252a0>

-
- ⁷² Pendleton, Y. J., & Allamandola, L. J. (2002). The Organic Refractory Material in the Diffuse Interstellar Medium: Mid-Infrared Spectroscopic Constraints. *The Astrophysical Journal Supplement Series*, 138, 75–98. <https://doi.org/10.1086/322999>
- ⁷³ Brinton K.L.F., & Bada J.L. (1996). A reexamination of amino acids in lunar soils- exogenous organic material during impact delivery. *Geochimica et Cosmochimica Acta*, 60(2), 349–354. [https://doi.org/10.1016/0016-7037\(95\)00404-1](https://doi.org/10.1016/0016-7037(95)00404-1)
- ⁷⁴ Remusat, L., Robert, F., & Derenne, S. (2007). The insoluble organic matter in carbonaceous chondrites: Chemical structure, isotopic composition and origin. *Comptes Rendus - Geoscience*, 339(14–15), 895–906. <https://doi.org/10.1016/j.crte.2007.10.001>
- ⁷⁵ Pizzarello, S., Williams, L. B., Lehman, J., Holland, G. P., & Yarger, J. L. (2011). Abundant ammonia in primitive asteroids and the case for a possible exobiology. *Proceedings of the National Academy of Science*, 108(11), 4303–4306. <https://doi.org/10.1073/pnas.1014961108>
- ⁷⁶ Martins, Z., Price, M. C., Goldman, N., Sephton, M. A., & Burchell, M. J. (2013). Shock synthesis of amino acids from impacting cometary and icy planet surface analogues. *Nature Geoscience*, 6(12), 1045–1049. <https://doi.org/10.1038/ngeo1930>
- ⁷⁷ Pasek, M., & Lauretta, D. (2008). Extraterrestrial flux of potentially prebiotic C, N, and P to the early earth. *Origins of Life and Evolution of Biospheres*, 38(1), 5–21. <https://doi.org/10.1007/s11084-007-9110-5>
- ⁷⁸ Macia E. (2019) The Chemical Evolution of Phosphorus-Chapter 1., ISBN: 9781771888042
- ⁷⁹ Westall, F., Hickman-Lewis, K., Hinman, N., Gautret, P., Campbell, K. A., Bréhéret, J. G., Foucher, F., Hubert, A., Sorieul, S., Dass, A. v., Kee, T. P., Georgelin, T., & Brack, A. (2018). A Hydrothermal-Sedimentary Context for the Origin of Life. *Astrobiology*, 18(3), 259–293. <https://doi.org/10.1089/ast.2017.1680>
- ⁸⁰ Martin, W., Baross, J., Kelley, D., & Russell, M. J. (2008). Hydrothermal vents and the origin of life. In *Nature Reviews Microbiology* (Vol. 6, Issue 11, pp. 805–814). <https://doi.org/10.1038/nrmicro1991>
- ⁸¹ Herschy, B., Chang, S. J., Blake, R., Lepland, A., Abbott-Lyon, H., Sampson, J., Atlas, Z., Kee, T. P., & Pasek, M. A. (2018). Archean phosphorus liberation induced by iron redox geochemistry. *Nature Communications*, 9(1). <https://doi.org/10.1038/s41467-018-03835-3>
- ⁸² Kelley, D. S., Karson, J. A., Früh-Green, G. L., Yoerger, D. R., Shank, T. M., Butterfield, D. A., Hayes, J. M., Schrenk, M. O., Olson, E. J., Proskurowski, G., Jakuba, M., Bradley, A., Larson, B., Ludwig, K., Glickson, D., Buckman, K., Bradley, A. S., Brazelton, W. J., Roe, K., Sylva, S. P. (2005). A Serpentinite-Hosted Ecosystem: The Lost City Hydrothermal Field. *Science*, 307(5714), 1428–1434. <https://doi.org/10.1126/science.1102556>
- ⁸³ Baross, J. A., & Hoffman, S. E. (1985). Submarine hydrothermal vents and associated gradient environments as sites for the origin and evolution of life. *Origins Life Evol Biosphere*, 15, 327–345. <https://doi.org/10.1007/BF01808177>
- ⁸⁴ Honda, H., Hatori, K., & Matsuno, K. (2004). Phosphorylation of Nucleotide Molecules in Hydrothermal Environments. *Orig Life Evol Biosph.*, 34, 465–471. <https://doi.org/10.1023/B:ORIG.0000043121.65714.05>
- ⁸⁵ Lang, S. Q., Butterfield, D. A., Schulte, M., Kelley, D. S., & Lilley, M. D. (2010). Elevated concentrations of formate, acetate and dissolved organic carbon found at the Lost City hydrothermal field. *Geochimica et Cosmochimica Acta*, 74(3), 941–952. <https://doi.org/10.1016/j.gca.2009.10.045>
- ⁸⁶ Russell, M. J., & Hall, A. J. (1997). The emergence of life from iron monosulphide bubbles at a submarine hydrothermal redox and pH front. *Journal of the Geological Society*, 154, 377–402. <https://doi.org/10.1144/gsjgs.154.3.0377>
- ⁸⁷ Shock, E., & Canovas, P. (2010). The potential for abiotic organic synthesis and biosynthesis at seafloor hydrothermal systems. *Geofluids*, 10(1–2), 161–192. <https://doi.org/10.1111/j.1468-8123.2010.00277.x>
- ⁸⁸ McCollom, T. M. (2013). Miller-Urey and Beyond: What Have We Learned About Prebiotic Organic Synthesis Reactions in the Past 60 Years? *Annual Review of Earth and Planetary Sciences*, 41(1), 207–229. <https://doi.org/10.1146/annurev-earth-040610-133457>

-
- ⁸⁹ Yadav, M., Kumar, R., & Krishnamurthy, R. (2020). Chemistry of Abiotic Nucleotide Synthesis. *Chemical Reviews*, 120(11), 4766–4805. <https://doi.org/10.1021/acs.chemrev.9b00546>
- ⁹⁰ Oró J. (1960). Synthesis of adenine from ammonium cyanide. *Biochemical and Biophysical Research Communications*, 2(6), 407–412. [https://doi.org/10.1016/0006-291X\(60\)90138-8](https://doi.org/10.1016/0006-291X(60)90138-8)
- ⁹¹ Yamada, Y., Kumashiro, I., & Takenishi, T. (1968). Synthesis of adenine and 4,5-dicyanoimidazole from. *The Journal of Organic Chemistry*, 33(2), 642–647. <https://doi.org/10.1021/jo01266a036>
- ⁹² Ferris, J. P., & Orgel, L. E. (1958). Studies in Prebiotic Synthesis. I. Aminomalononitrile and 4-Amino-5-cyanoimidazole1,2. *J. Org. Chem*, 91(8), 729. <https://doi.org/10.1021/ja00968a028>
- ⁹³ Shapiro, R. (1995). The prebiotic role of adenine: A critical analysis. *Origins of Life and Evolution of the Biosphere*, 25, 83–98. <https://doi.org/10.1007/BF01581575>
- ⁹⁴ Sanchez R, Ferris J, & Orgel L. (1966). Conditions for Purine Synthesis: Did Prebiotic Synthesis Occur at Low Temperatures? *Science*, 153(3731), 72–73. <https://doi.org/10.1126/science.153.3731.72>
- ⁹⁵ Miyakawa, S., Cleaves, H. J., & Miller, S. L. (2002). The Cold Origin of Life: A. Implications Based On The Hydrolytic Stabilities Of Hydrogen Cyanide And Formamide. *Origins of Life and Evolution of the Biosphere Volume 32*, 195–208. <https://doi.org/10.1023/A:1016514305984>
- ⁹⁶ Miyakawa, S., Cleaves, H. J., & Miller, S. L. (2002). The Cold Origin of Life: B. Implications Based on Pyrimidines and Purines Produced From Frozen Ammonium Cyanide Solutions. *Orig Life Evol Biosph*, 32, 209–218. <https://doi.org/10.1023/A:1019514022822>
- ⁹⁷ Studier, M. H., Hayatsu, R., & Anders, E. (1965). Origin of organic matter in early solar system—I. Hydrocarbons. *Geochimica et Cosmochimica Acta*, 32(2), 151–173. [https://doi.org/10.1016/S0016-7037\(68\)80002-X](https://doi.org/10.1016/S0016-7037(68)80002-X)
- ⁹⁸ Ponnampersumat, C., Lemmon, R. M., Mariner, R., & Calvin, M. (1963). Formation of adenine by electron irradiation of methane, ammonia, and water. *PNAS*, 49(5), 737–740. <https://doi.org/10.1073/pnas.49.5.737>
- ⁹⁹ Kobayashi, K., & Tsuji, T. (1997). Abiotic Synthesis of Uracil from Carbon Monoxide. *Chem. Lett.*, 26, 903–904. <https://doi.org/10.1246/cl.1997.903>
- ¹⁰⁰ Sanchez J P Ferris L E Orgel, R. A. (1961). Cyanoacetylene in Prebiotic Synthesis. *Arch. Biochem. Biophys.*, 94, 579. <https://doi.org/10.1126/science.154.3750.784>
- ¹⁰¹ Okamura, H., Becker, S., Tiede, N., Wiedemann, S., Feldmann, J., & Carell, T. (2019). A one-pot, water compatible synthesis of pyrimidine nucleobases under plausible prebiotic conditions. *Chemical Communications*, 55(13), 1939–1942. <https://doi.org/10.1039/C8CC09435G>
- ¹⁰² Yamada H, & Okamoto T. (1972). A One-step Synthesis of Purine Ring from Formamide. *Chemical and Pharmaceutical Bulletin*, 20(3), 623–624. <https://doi.org/10.1248/cpb.20.623>
- ¹⁰³ Saladino, R., Crestini, C., Costanzo, G., Negri, R., di Mauro, E., & Abac, D. (2001). A Possible Prebiotic Synthesis of Purine, Adenine, Cytosine, and 4(3H)-Pyrimidinone from Formamide: Implications for the Origin of Life. *Bioorganic & Medicinal Chemistry*, 9(5), 1249–1253. [https://doi.org/10.1016/S0968-0896\(00\)00340-0](https://doi.org/10.1016/S0968-0896(00)00340-0)
- ¹⁰⁴ Saladino, R., Ciambecchini, U., Crestini, C., Costanzo, G., Negri, R., & di Mauro, E. (2003). One-pot TiO₂-catalyzed synthesis of nucleic bases and acyclonucleosides from formamide: Implications for the origin of life. *ChemBioChem*, 4(6), 514–521. <https://doi.org/10.1002/cbic.200300567>
- ¹⁰⁵ Saladino, R., Crestini, C., Ciambecchini, U., Ciciriello, F., Costanzo, G., & di Mauro, E. (2004). Synthesis and degradation of nucleobases and nucleic acids by formamide in the presence of montmorillonites. *ChemBioChem*, 5(11), 1558–1566. <https://doi.org/10.1002/cbic.200400119>
- ¹⁰⁶ Saladino, R., Crestini, C., Neri, V., Ciciriello, F., Costanzo, G., & di Mauro, E. (2006). Origin of informational polymers: The concurrent roles of formamide and phosphates. *ChemBioChem*, 7(11), 1707–1714. <https://doi.org/10.1002/cbic.200600139>

-
- ¹⁰⁷ Saladino, R., Neri, V., Crestini, C., Costanzo, G., Graciotti, M., & di Mauro, E. (2008). Synthesis and degradation of nucleic acid components by formamide and iron sulfur minerals. *Journal of the American Chemical Society*, *130*(46), 15512–15518. <https://doi.org/10.1021/ja804782e>
- ¹⁰⁸ Saladino, R., Carota, E., Botta, G., Kapralov, M., Timoshenko, G. N., Rozanov, A. Y., Krasavin, E., & di Mauro, E. (2015). Meteorite-catalyzed syntheses of nucleosides and of other prebiotic compounds from formamide under proton irradiation. *Proceedings of the National Academy of Sciences of the United States of America*, *112*(21), E2746–E2755. <https://doi.org/10.1073/pnas.1422225112>
- ¹⁰⁹ Barks, H. L., Buckley, R., Grieves, G. A., di Mauro, E., Hud, N. v., & Orlando, T. M. (2010). Guanine, adenine, and hypoxanthine production in UV-irradiated formamide solutions: Relaxation of the requirements for prebiotic purine nucleobase formation. *ChemBioChem*, *11*(9). <https://doi.org/10.1002/cbic.201000074>
- ¹¹⁰ Niether, D., Afanasenkau, D., Dhont, J. K. G., & Wiegand, S. (2016). Accumulation of Formamide in hydrothermal pores to Form prebiotic nucleobases. *Proceedings of the National Academy of Sciences of the United States of America*, *113*(16), 4272–4277. <https://doi.org/10.1073/pnas.1600275113>
- ¹¹¹ Schwartz Alan, & Chittenden G J F. (1976). Possible pathway for prebiotic uracil synthesis by photodehydrogenation. *Nature*, *263*, 350–351. <https://doi.org/10.1038/263350a0>
- ¹¹² Schwartz, A. W., & Chittenden, G. J. F. (1977). Synthesis of uracil and thymine under simulated prebiotic conditions. *BioSystems*, *9*, 87–92. [https://doi.org/10.1016/0303-2647\(77\)90016-8](https://doi.org/10.1016/0303-2647(77)90016-8)
- ¹¹³ Menor-Salván, C., Ruiz-Bermejo, D. M., Guzmán, M. I., Osuna-Esteban, S., & Veintemillas-Verdaguer, S. (2009). Synthesis of pyrimidines and triazines in ice: Implications for the prebiotic chemistry of nucleobases. *Chemistry - A European Journal*, *15*(17), 4411–4418. <https://doi.org/10.1002/chem.200802656>
- ¹¹⁴ Oba, Y., Takano, Y., Naraoka, H., Watanabe, N., & Kouchi, A. (2019). Nucleobase synthesis in interstellar ices. *Nature Communications*, *10*(1). <https://doi.org/10.1038/s41467-019-12404-1>
- ¹¹⁵ Butlerow, A. (1861). Formation Synthétique D'une Substance Sucreé. *CR Acad. Sci.* *53*, 145–147. <https://doi.org/10.1002/jlac.18611200308>
- ¹¹⁶ Breslow, R. (1959). *On the Mechanism of the Formose Reaction*. *Tetrahedron Lett.*, *1*, 22 –26. [https://doi.org/10.1016/S0040-4039\(01\)99487-0](https://doi.org/10.1016/S0040-4039(01)99487-0)
- ¹¹⁷ Shapiro, R. (1988). Prebiotic ribose synthesis: a critical analysis. *Orig Life Evol Biosph*, *18*(1–2), 71–85. <https://doi.org/10.1007/BF01808782>.
- ¹¹⁸ Schwartz, A. W., & de Graaf, R. M. (1993). The Prebiotic Synthesis of Carbohydrates: A Reassessment. In *J Mol Evol* (Vol. 36). <https://doi.org/10.1007/BF00166245>
- ¹¹⁹ Decker, P. (1982). Bioids : X. Identification of formose sugars, presumable prebiotic metabolites, using capillary gas chromatography/gas chromatography—massspectrometry of n-butoxime trifluoroacetates on OV-225. *Journal of Chromatography A*, *244*(2), 1–29. [https://doi.org/10.1016/S0021-9673\(00\)85692-7](https://doi.org/10.1016/S0021-9673(00)85692-7)
- ¹²⁰ Zubay, G. (1998). Studies on the Lead-Catalyzed Synthesis of Aldopentoses. *Origins of Life and Evolution of the Biosphere Volume*, *28*, 13–26. <https://doi.org/10.1023/A:1006551410542>
- ¹²¹ Prieur, B. E. (2001). Étude de l'activité prébiotique potentielle de l'acide borique. *Comptes Rendus de l'Académie Des Sciences - Series IIC*, *4*(8–9), 667–670. [https://doi.org/10.1016/S1387-1609\(01\)01266-X](https://doi.org/10.1016/S1387-1609(01)01266-X)
- ¹²² Ricardo, A., Carrigan, M. A., Olcott, A. N., & Benner, S. A. (2004). Borate Minerals Stabilize Ribose. *Science*, *303*(5655), 196. <https://doi.org/10.1126/science.1092464>
- ¹²³ Lambert, J. B., Lu, G., Singer, S. R., & Kolb, V. M. (2004). Silicate complexes of sugars in aqueous solution. *Journal of the American Chemical Society*, *126*(31), 9611–9625. <https://doi.org/10.1021/ja031748v>
- ¹²⁴ Vázquez-Mayagoitia, Á., Horton, S. R., Sumpter, B. G., Šponer, J., Šponer, J. E., & Fuentes-Cabrera, M. (2011). On the stabilization of ribose by silicate minerals. *Astrobiology*, *11*(2), 115–121. <https://doi.org/10.1089/ast.2010.0508>

-
- ¹²⁵ Pallmann, S., Šteflová, J., Haas, M., Lamour, S., Henß, A., & Trapp, O. (2018). Schreibersite: An effective catalyst in the formose reaction network. *New Journal of Physics*, *20*(5). <https://doi.org/10.1088/1367-2630/aabb99>
- ¹²⁶ Usami, K., & Okamoto, A. (2017). Hydroxyapatite: Catalyst for a one-pot pentose formation. *Organic and Biomolecular Chemistry*, *15*(42), 8888–8893. <https://doi.org/10.1039/c7ob02051a>
- ¹²⁷ Zhao, Z.-R., & Wang, X. (2021). A plausible prebiotic selection of ribose for RNA - formation, dynamic isolation, and nucleotide synthesis based on metal-doped-clays. *Chem*, *7*(12), 3292–3308. <https://doi.org/10.1016/j.chempr.2021.09.002>
- ¹²⁸ Kopetzki, D., & Antonietti, M. (2011). Hydrothermal formose reaction. *New Journal of Chemistry*, *35*(9), 1787–1794. <https://doi.org/10.1039/c1nj20191c>
- ¹²⁹ Islam, S., Bučar, D. K., & Powner, M. W. (2017). Prebiotic selection and assembly of proteinogenic amino acids and natural nucleotides from complex mixtures. *Nature Chemistry*, *9*(6), 584–589. <https://doi.org/10.1038/nchem.2703>
- ¹³⁰ Müller Daniel, Pitsch Stefan, Kittaka Atsushi, Wagner Ernst, Wintner Claude E., Eschenmoser Albert, & Ohlofjgewidmet Güntner. (1990). Chemie von a-Aminonitrilen. *Helv. Chim. Acta*, *73*, 1410–1468. <https://doi.org/10.1002/hlca.19900730526>
- ¹³¹ Krishnamurthy, R., Arrhenius, G., & Eschenmoser, A. (1999). Formation of Glycolaldehyde Phosphate from Glycolaldehyde in Aqueous Solution. *Origins of Life and Evolution of the Biosphere Volume*, *29*, 333–354. <https://doi.org/10.1023/A:1006698208873>
- ¹³² Sagi, V. N., Punna, V., Hu, F., Meher, G., & Krishnamurthy, R. (2012). Exploratory experiments on the chemistry of the “glyoxylate scenario”: Formation of ketosugars from dihydroxyfumarate. *Journal of the American Chemical Society*, *134*(7), 3577–3589. <https://doi.org/10.1021/ja211383c>
- ¹³³ Oró, J., & Cox, A. C. (1962). Non-enzymic synthesis of 2-deoxyribose. *Federation Proceedings*, *21*(3), 439–444.
- ¹³⁴ Steer, A. M., Bia, N., Smith, D. K., & Clarke, P. A. (2017). Prebiotic synthesis of 2-deoxy-d-ribose from interstellar building blocks promoted by amino esters or amino nitriles. *Chemical Communications*, *53*(75), 10362–10365. <https://doi.org/10.1039/c7cc06083a>
- ¹³⁵ Ritson, D. J., & Sutherland, J. D. (2014). Conversion of biosynthetic precursors of RNA to those of DNA by photoredox chemistry. *Journal of Molecular Evolution*, *78*(5), 245–250. <https://doi.org/10.1007/s00239-014-9617-0>
- ¹³⁶ Xu, J., Green, N. J., Gibard, C., Krishnamurthy, R., & Sutherland, J. D. (2019). Prebiotic phosphorylation of 2-thiouridine provides either nucleotides or DNA building blocks via photoreduction. *Nature Chemistry*, *11*(5), 457–462. <https://doi.org/10.1038/s41557-019-0225-x>
- ¹³⁷ Sutherland, J. D. (2010). Ribonucleotides. In *Cold Spring Harbor perspectives in biology* (Vol. 2, Issue 4). <https://doi.org/10.1101/cshperspect.a005439>
- ¹³⁸ Fuller, W. D., Sanchez, R. A., & Orgel, L. E. (1972). Studies in Prebiotic Synthesis: VI. Synthesis of Purine Nucleosides. *J. Mol. Biol.*, *67*(1), 25–33. [https://doi.org/10.1016/0022-2836\(72\)90383-X](https://doi.org/10.1016/0022-2836(72)90383-X)
- ¹³⁹ Fuller, W. D., Sanchez, R. A., & Orgel, L. E. (1972). Studies in prebiotic synthesis. VII. Solid-State Synthesis of Purine Nucleosides. *J. Molec. Evolution*, *1*, 249–257. <https://doi.org/10.1007/BF01660244>
- ¹⁴⁰ Ingar, A. A., Luke, R. W. A., Hayter, B. R., & Sutherland, J. D. (2003). Synthesis of cytidine ribonucleotides by stepwise assembly of the heterocycle on a sugar phosphate. *ChemBioChem*, *4*(6), 504–507. <https://doi.org/10.1002/cbic.200300554>
- ¹⁴¹ Kolb, V. M., Dworkin, J. P., & Miller, S. L. (1994). Alternative Bases in the RNA World: The Prebiotic Synthesis of Urazole and Its Ribosides. *J Mol Evol*, *38*, 549–557. <https://doi.org/10.1007/BF00175873>

-
- ¹⁴² Bean, H. D., Sheng, Y., Collins, J. P., Anet, F. A. L., Leszczynski, J., & Hud, N. v. (2007). Formation of a β -pyrimidine nucleoside by a free pyrimidine base and ribose in a plausible prebiotic reaction. *Journal of the American Chemical Society*, *129*(31), 9556–9557. <https://doi.org/10.1021/ja072781a>
- ¹⁴³ Kim, H. J., & Benner, S. A. (2017). Prebiotic stereoselective synthesis of purine and noncanonical pyrimidine nucleotide from nucleobases and phosphorylated carbohydrates. *Proceedings of the National Academy of Sciences of the United States of America*, *114*(43), 11315–11320. <https://doi.org/10.1073/pnas.1710778114>
- ¹⁴⁴ Kim, H. J., & Kim, J. (2019). A Prebiotic Synthesis of Canonical Pyrimidine and Purine Ribonucleotides. *Astrobiology*, *19*(5), 669–674. <https://doi.org/10.1089/ast.2018.1935>
- ¹⁴⁵ Becker, S., Thoma, I., Deutsch, A., Gehrke, T., Mayer, P., Zipse, H., & Carell, T. A. (2016). A high-yielding, strictly regioselective prebiotic purine nucleoside formation pathway. *Science*, *352*(6287), 833–836. <https://doi.org/10.1126/science.aad2808>
- ¹⁴⁶ Trinks, U. P.; Eschenmoser, A. Zur Chemie der Aminopyrimidine, Thesis, ETH Zurich (1987), ETH 2-collection; <http://dx.doi.org/10.3929/ethz-a-000413538>.
- ¹⁴⁷ Becker, S., Schneider, C., Okamura, H., Crisp, A., Amatov, T., Dejmek, M., & Carell, T. (2018). Wet-dry cycles enable the parallel origin of canonical and non-canonical nucleosides by continuous synthesis. *Nature Communications*, *9*(1). <https://doi.org/10.1038/s41467-017-02639-1>
- ¹⁴⁸ Becker, S., Feldmann, J., Wiedemann, S., Okamura, H., Schneider, C., Iwan, K., Crisp, A., Rossa, M., Amatov, T., & Carell, T. (2019). Unified prebiotically plausible synthesis of pyrimidine and purine RNA ribonucleotides. *Science*, *366*(6461), 76–82. <https://doi.org/10.1126/science.aax2747>
- ¹⁴⁹ Chen, Q.-Q., Zhao, Z.-R., & Wang, X. (2021). A Prebiotic Ribosylation of Pyrimidine Nucleobases Enabled by Metal Cations and Clay Minerals. *Life*, *11*(12), 1381. <https://doi.org/10.3390/life11121381>
- ¹⁵⁰ Chen, Q.-Q., Zhao, Z.-R., Patehebieke, Y., & Wang, X. (2023). Regioselective ribonucleoside synthesis through Ti-catalysed ribosylation of nucleobases. *Nature Synthesis*, *2*(4), 348–356. <https://doi.org/10.1038/s44160-022-00206-1>
- ¹⁵¹ Sanchez, R. A., & Orgel, L. E. (1970). Studies in prebiotic synthesis. *Journal of Molecular Biology*, *47*(3), 531–543. [https://doi.org/10.1016/0022-2836\(70\)90320-7](https://doi.org/10.1016/0022-2836(70)90320-7)
- ¹⁵² Stairs, S., Nikmal, A., B ur, D. K., Zheng, S. L., Szostak, J. W., & Powner, M. W. (2017). Divergent prebiotic synthesis of pyrimidine and 8-oxo-purine ribonucleotides. *Nature Communications*, *8*. <https://doi.org/10.1038/ncomms15270>
- ¹⁵³ Patel, B. H., Percivalle, C., Ritson, D. J., Duffy, C. D., & Sutherland, J. D. (2015). Common origins of RNA, protein and lipid precursors in a cyanosulfidic protometabolism. *Nature Chemistry*, *7*(4), 301–307. <https://doi.org/10.1038/nchem.2202>
- ¹⁵⁴ Ponnamperna, C., & Kirk, P. (1964). Synthesis of Deoxyadenosine under Simulated Primitive Earth Conditions. *Nature*, *203*, 400–401. <https://doi.org/10.1038/203400a0>
- ¹⁵⁵ Xu, J., Chmela, V., Green, N. J., Russell, D. A., Janicki, M. J., G ra, R. W., Szabla, R., Bond, A. D., & Sutherland, J. D. (2020). Selective prebiotic formation of RNA pyrimidine and DNA purine nucleosides. *Nature*, *582*(7810), 60–66. <https://doi.org/10.1038/s41586-020-2330-9>
- ¹⁵⁶ Gull, M., & Pasek, M. A. (2021). The Role of Glycerol and Its Derivatives in the Biochemistry of Living Organisms, and Their Prebiotic Origin and Significance in the Evolution of Life. *Catalysts*, *11*(1), 86. <https://doi.org/10.3390/catal11010086>
- ¹⁵⁷ Shigemasa, Y., Matsuda, Y., Sakazawa, C., & Matsuura, T. (1977). Formose Reactions. II. The Photochemical Formose Reaction. *Bull. Chem. Soc. Jpn.*, *50*, 222–226. <https://doi.org/10.1246/bcsj.50.222>
- ¹⁵⁸ Briggs, R., Ertem, G., Ferris, J. P., Greenberg, J. M., McCain, P. J., Mendoza-Gomez, C. X., & Schutte, W. (1992). Comet Halley as an aggregate of interstellar dust and f. *Orig. Life Evol. Biosph.*, *22*, 287–307.

-
- ¹⁵⁹ Bernstein, M. P., Dworkin, J. P., Sandford, S. A., Cooper, G. W., & Allamandola, L. J. (2002). Racemic amino acids from the ultraviolet photolysis of interstellar ice analogues. *Nature*, *416*, 401–403. <https://doi.org/10.1038/416401a>
- ¹⁶⁰ Agarwal, V. K., Schutte, W., Greenberg, J. M., Ferris, J. P., Briggs, R., Connor, S., vande Bult, C. P. E. M., & Baas, F. (1985). Photochemical reactions in interstellar grains photolysis of co, NH₃, and H₂O. *Origins of Life and Evolution of the Biosphere Volume 16*, 21–40. <https://doi.org/10.1007/BF01808047>
- ¹⁶¹ Meinert, C., Myrgorodska, I., de Marcellus, P., Buhse, T., Nahon, L., Hoffmann, S. v., d’Hendecourt, L. L. S., & Meierhenrich, U. J. (2016). Ribose and related sugars from ultraviolet irradiation of interstellar ice analogs. *Science*, *352*(6282), 208–212. <https://doi.org/10.1126/science.aad8137>
- ¹⁶² McCollom, T. M., Ritter, G., & Simoneit, B. R. T. (1999). Lipid Synthesis Under Hydrothermal Conditions by Fischer-Tropsch-Type Reactions. *Origins of Life and Evolution of the Biosphere*, *29*(2), 153–166. <https://doi.org/10.1023/A:1006592502746>
- ¹⁶³ McCollom, T. M., & Simoneit, B. R. T. (1999). Abiotic Formation of Hydrocarbons and Oxygenated Compounds During Thermal Decomposition of Iron Oxalate. *Origins of Life and Evolution of the Biosphere*, *29*(2), 167–186. <https://doi.org/10.1023/A:1006556315895>
- ¹⁶⁴ Rushdi, A. I., & Simoneit, B. R. T. (2001). Lipid formation by aqueous Fischer-Tropsch-type synthesis over a temperature range of 100 to 400 degrees C. *Origins of Life and Evolution of the Biosphere*, *31*(1/2), 103–118. <https://doi.org/10.1023/A:1006702503954>
- ¹⁶⁵ Klein, A. E., & Pilpel, N. (1973). Oxidation of n-alkanes photosensitized by 1-naphthol. *Journal of the Chemical Society, Faraday Transactions 1: Physical Chemistry in Condensed Phases*, *69*(0), 1729. <https://doi.org/10.1039/f19736901729>
- ¹⁶⁶ Yuen, G. U., Lawless, J. G., & Edelson, E. H. (1981). Quantification of monocarboxylic acids from a spark discharge synthesis. *Journal of Molecular Evolution*, *17*(1), 43–47. <https://doi.org/10.1007/BF01792423>
- ¹⁶⁷ Allen, W. v., & Ponnampereuma, C. (1967). A possible prebiotic synthesis of monocarboxylic acids. *Biosystems*, *1*(1), 24–28. [https://doi.org/10.1016/0303-2647\(67\)90017-2](https://doi.org/10.1016/0303-2647(67)90017-2)
- ¹⁶⁸ Noonan, D. W., Gibert, J. M., Gelpi, E., & Oró, J. (1976). Closed system Fischer-Tropsch synthesis over meteoritic iron, iron ore and nickel-iron alloy. *Geochimica et Cosmochimica Acta*, *40*(8), 915–924. [https://doi.org/10.1016/0016-7037\(76\)90140-X](https://doi.org/10.1016/0016-7037(76)90140-X)
- ¹⁶⁹ Eichberg, J., Sherwood, E., Epps, D. E., & Oró, J. (1977). Cyanamide mediated syntheses under plausible primitive earth conditions. *Journal of Molecular Evolution*, *10*(3), 221–230. <https://doi.org/10.1007/BF01764597>
- ¹⁷⁰ Rushdi, A. I., & Simoneit, B. R. T. (2006). Abiotic Condensation Synthesis of Glyceride Lipids and Wax Esters Under Simulated Hydrothermal Conditions. *Origins of Life and Evolution of Biospheres*, *36*(2), 93–108. <https://doi.org/10.1007/s11084-005-9001-6>
- ¹⁷¹ Simoneit, B. R. T., Rushdi, A. I., & Deamer, D. W. (2007). Abiotic formation of acylglycerols under simulated hydrothermal conditions and self-assembly properties of such lipid products. *Advances in Space Research*, *40*(11), 1649–1656. <https://doi.org/10.1016/j.asr.2007.07.034>
- ¹⁷² Hargreaves, W. R., Mulvihill, S. J., & Deamer, D. W. (1977). Synthesis of phospholipids and membranes in prebiotic conditions. *Nature*, *266*(5597), 78–80. <https://doi.org/10.1038/266078a0>
- ¹⁷³ Ourisson, G., & Nakatani, Y. (1994). The terpenoid theory of the origin of cellular life: the evolution of terpenoids to cholesterol. *Chemistry & Biology*, *1*(1), 11–23. [https://doi.org/10.1016/1074-5521\(94\)90036-1](https://doi.org/10.1016/1074-5521(94)90036-1)
- ¹⁷⁴ Désaubry, L., Nakatani, Y., & Ourisson, G. (2003). Toward higher polyprenols under ‘prebiotic’ conditions. *Tetrahedron Letters*, *44*(36), 6959–6961. [https://doi.org/10.1016/S0040-4039\(03\)01624-1](https://doi.org/10.1016/S0040-4039(03)01624-1)
- ¹⁷⁵ Teller, G., Nakatani, Y., Ourisson, G., Keller, M., Hafenbradl, D., & Stetter, K. O. (1995). A One-Step Synthesis of Squalene from Farnesol under Prebiotic Conditions. *Angewandte Chemie International Edition in English*, *34*(17), 1898–1900. <https://doi.org/10.1002/anie.199518981>

-
- ¹⁷⁶ Veselovsky, V. V., Grigorieva, N. Ya., & Moiseenkov, A. M. (1989). Synthesis of compounds relating to polyprenols. *Chemistry and Physics of Lipids*, *51*(3–4), 147–157. [https://doi.org/10.1016/0009-3084\(89\)90002-9](https://doi.org/10.1016/0009-3084(89)90002-9)
- ¹⁷⁷ Potter, S., & Fothergill-Gilmore, L. A. (1993). Molecular evolution: The origin of glycolysis. *Biochemical Education*, *21*(1), 45–48. [https://doi.org/10.1016/0307-4412\(93\)90018-U](https://doi.org/10.1016/0307-4412(93)90018-U)
- ¹⁷⁸ Clay, A. P., Cooke, R. E., Kumar, R., Yadav, M., Krishnamurthy, R., & Springsteen, G. (2022). A Plausible Prebiotic One-Pot Synthesis of Orotate and Pyruvate Suggestive of Common Protometabolic Pathways. *Angewandte Chemie International Edition*, *61*(11). <https://doi.org/10.1002/anie.202112572>
- ¹⁷⁹ Varma, S. J., Muchowska, K. B., Chatelain, P., & Moran, J. (2018). Native iron reduces CO₂ to intermediates and end-products of the acetyl-CoA pathway. *Nature Ecology & Evolution*, *2*(6), 1019–1024. <https://doi.org/10.1038/s41559-018-0542-2>
- ¹⁸⁰ Beyazay, T., Ochoa-Hernández, C., Song, Y., Belthle, K. S., Martin, W. F., & Tüysüz, H. (2023). Influence of Composition of Nickel-Iron Nanoparticles for Abiotic CO₂ Conversion to Early Prebiotic Organics. *Angewandte Chemie International Edition*, *62*(22). <https://doi.org/10.1002/anie.202218189>
- ¹⁸¹ Weber, A. L. (2001). The sugar model: catalysis by amines and amino acid products. *Origins of Life and Evolution of the Biosphere*, *31*(1/2), 71–86. <https://doi.org/10.1023/A:1006750423942>
- ¹⁸² Guzman, M. I., & Martin, S. T. (2009). Prebiotic metabolism: production by mineral photoelectrochemistry of alpha-ketocarboxylic acids in the reductive tricarboxylic acid cycle. *Astrobiology*, *9*(9), 833–842. <https://doi.org/10.1089/ast.2009.0356>
- ¹⁸³ Wang, W., Yang, B., Qu, Y., Liu, X., & Su, W. (2011). FeS/S/FeS(2) redox system and its oxidoreductase-like chemistry in the iron-sulfur world. *Astrobiology*, *11*(5), 471–476. <https://doi.org/10.1089/ast.2011.0624>
- ¹⁸⁴ Cody, G. D., Boctor, N. Z., Filley, T. R., Hazen, R. M., Scott, J. H., Sharma, A., & Yoder, H. S. (2000). Primordial Carbonylated Iron-Sulfur Compounds and the Synthesis of Pyruvate. *Science*, *289*(5483), 1337–1340. <https://doi.org/10.1126/science.289.5483.1337>
- ¹⁸⁵ Cooper, G., Reed, C., Nguyen, D., Carter, M., & Wang, Y. (2011). Detection and formation scenario of citric acid, pyruvic acid, and other possible metabolism precursors in carbonaceous meteorites. *Proceedings of the National Academy of Sciences*, *108*(34), 14015–14020. <https://doi.org/10.1073/pnas.1105715108>
- ¹⁸⁶ Pasek, M. A. (2019). Phosphorus volatility in the early solar nebula. *Icarus*, *317*, 59–65. <https://doi.org/10.1016/j.icarus.2018.07.011>
- ¹⁸⁷ Pirim, C., Pasek, M. A., Sokolov, D. A., Sidorov, A. N., Gann, R. D., & Orlando, T. M. (2014). Investigation of schreibersite and intrinsic oxidation products from Sikhote-Alin, Semychan, and Odessa meteorites and Fe₃P and Fe₂NiP synthetic surrogates. *Geochimica et Cosmochimica Acta*, *140*, 259–274. <https://doi.org/10.1016/j.gca.2014.05.027>
- ¹⁸⁸ Zanda, B., Bourot-Denise, M., Perron, C., & Hewins, R. H. (1994). Origin and Metamorphic Redistribution of Silicon, Chromium, and Phosphorus in the Metal of Chondrites. *Science*, *265*(5180), 1846–1849. <https://doi.org/10.1126/science.265.5180.1846>
- ¹⁸⁹ Mittlefehldt, D. W., McCoy T.J., Goodrich, C. A., & Kracher, A. (1998). Non-chondritic meteorites from asteroidal bodies. *Reviews in Mineralogy & Geochemistry*1998, *36*(4), 1–194. (
- ¹⁹⁰ Sugiura, N., & Hoshino, H. (2003). Mn-Cr chronology of five IIIAB iron meteorites. *Meteoritics & Planetary Science*, *38*(1), 117–143. <https://doi.org/10.1111/j.1945-5100.2003.tb01050.x>
- ¹⁹¹ Gull, M., Mojica, M. A., Fernández, F. M., Gaul, D. A., Orlando, T. M., Liotta, C. L., & Pasek, M. A. (2015). Nucleoside phosphorylation by the mineral schreibersite. *Scientific Reports*, *5*(1), 17198. <https://doi.org/10.1038/srep17198>
- ¹⁹² Pasek, M. A., Harnmeijer, J. P., Buick, R., Gull, M., & Atlas, Z. (2013). Evidence for reactive reduced phosphorus species in the early Archean ocean. *Proceedings of the National Academy of Sciences*, *110*(25), 10089–10094. <https://doi.org/10.1073/pnas.1303904110>

-
- ¹⁹³ Pasek, M. (2019). A role for phosphorus redox in emerging and modern biochemistry. *Current Opinion in Chemical Biology*, 49, 53–58. <https://doi.org/10.1016/j.cbpa.2018.09.018>
- ¹⁹⁴ Hazen, R. M. (2013). Paleomineralogy of the Hadean Eon: A preliminary species list. *American Journal of Science*, 313(9), 807–843. <https://doi.org/10.2475/09.2013.01>
- ¹⁹⁵ Watson, E. B. (1980). Apatite and phosphorus in mantle source regions: An experimental study of apatite/melt equilibria at pressures to 25 kbar. *Earth and Planetary Science Letters*, 51(2), 322–335. [https://doi.org/10.1016/0012-821X\(80\)90214-9](https://doi.org/10.1016/0012-821X(80)90214-9)
- ¹⁹⁶ Pasek, M. A. (2020). Thermodynamics of Prebiotic Phosphorylation. *Chemical Reviews*, 120(11), 4690–4706. <https://doi.org/10.1021/acs.chemrev.9b00492>
- ¹⁹⁷ Toner, J. D., & Catling, D. C. (2020). A carbonate-rich lake solution to the phosphate problem of the origin of life. *Proceedings of the National Academy of Sciences*, 117(2), 883–888. <https://doi.org/10.1073/pnas.1916109117>
- ¹⁹⁸ Burcar, B., Pasek, M., Gull, M., Cafferty, B. J., Velasco, F., Hud, N. v., & Menor-Salván, C. (2016). Darwin’s Warm Little Pond: A One-Pot Reaction for Prebiotic Phosphorylation and the Mobilization of Phosphate from Minerals in a Urea-Based Solvent. *Angewandte Chemie International Edition*, 55(42), 13249–13253. <https://doi.org/10.1002/anie.201606239>
- ¹⁹⁹ Burcar, B., Castañeda, A., Lago, J., Daniel, M., Pasek, M. A., Hud, N. v., Orlando, T. M., & Menor-Salván, C. (2019). A Stark Contrast to Modern Earth: Phosphate Mineral Transformation and Nucleoside Phosphorylation in an Iron- and Cyanide-Rich Early Earth Scenario. *Angewandte Chemie International Edition*, 58(47), 16981–16987. <https://doi.org/10.1002/anie.201908272>
- ²⁰⁰ Emerson, S., & Widmer, G. (1978). Early diagenesis in anaerobic lake sediments—II. Thermodynamic and kinetic factors controlling the formation of iron phosphate. *Geochimica et Cosmochimica Acta*, 42(9), 1307–1316. [https://doi.org/10.1016/0016-7037\(78\)90035-2](https://doi.org/10.1016/0016-7037(78)90035-2)
- ²⁰¹ Bjerrum, C. J., & Canfield, D. E. (2002). Ocean productivity before about 1.9 Gyr ago limited by phosphorus adsorption onto iron oxides. *Nature*, 417(6885), 159–162. <https://doi.org/10.1038/417159a>
- ²⁰² Arrhenius, G., Sales, B., Mojzsis, S., & Lee, T. (1997). Entropy and Charge in Molecular Evolution—the Case of Phosphate. *Journal of Theoretical Biology*, 187(4), 503–522. <https://doi.org/10.1006/jtbi.1996.0385>
- ²⁰³ Rasmussen, B., Muhling, J. R., Suvorova, A., & Fischer, W. W. (2021). Apatite nanoparticles in 3.46–2.46 Ga iron formations: Evidence for phosphorus-rich hydrothermal plumes on early Earth. *Geology*, 49(6), 647–651. <https://doi.org/10.1130/G48374.1>
- ²⁰⁴ Martin, W., & Russell, M. J. (2007). On the origin of biochemistry at an alkaline hydrothermal vent. *Philosophical Transactions of the Royal Society B: Biological Sciences*, 362(1486), 1887–1926. <https://doi.org/10.1098/rstb.2006.1881>
- ²⁰⁵ Russell, M. J., Hall, A. J., & Turner, D. (1989). In vitro growth of iron sulphide chimneys: possible culture chambers for origin-of-life experiments. *Terra Nova*, 1(3), 238–241. <https://doi.org/10.1111/j.1365-3121.1989.tb00364.x>
- ²⁰⁶ Barge, L. M., Doloboff, I. J., Russell, M. J., VanderVelde, D., White, L. M., Stucky, G. D., Baum, M. M., Zeytounian, J., Kidd, R., & Kanik, I. (2014). Pyrophosphate synthesis in iron mineral films and membranes simulating prebiotic submarine hydrothermal precipitates. *Geochimica et Cosmochimica Acta*, 128, 1–12. <https://doi.org/10.1016/j.gca.2013.12.006>
- ²⁰⁷ de Zwart, I. I., Meade, S. J., & Pratt, A. J. (2004). Biomimetic phosphoryl transfer catalysed by iron(II)-mineral precipitates. *Geochimica et Cosmochimica Acta*, 68(20), 4093–4098. <https://doi.org/10.1016/j.gca.2004.01.028>
- ²⁰⁸ Yamagata, Y., Watanabe, H., Saitoh, M., & Namba, T. (1991). Volcanic production of polyphosphates and its relevance to prebiotic evolution. *Nature*, 352(6335), 516–519. <https://doi.org/10.1038/352516a0>
- ²⁰⁹ Keefe, A. D., & Miller, S. L. (1996). Potentially prebiotic syntheses of condensed phosphates. *Origins of Life and Evolution of the Biosphere*, 26(1), 15–25. <https://doi.org/10.1007/BF01808157>

-
- ²¹⁰ Rabinowitz, J., Chang, S., & Ponnampereuma, C. (1968). Phosphorylation on the Primitive Earth: Phosphorylation by way of Inorganic Phosphate as a Potential Prebiotic Process. *Nature*, *218*(5140), 442–443. <https://doi.org/10.1038/218442a0>
- ²¹¹ Osterberg, R., & Orgel, L. E. (1972). Polyphosphate and trimetaphosphate formation under potentially prebiotic conditions. *Journal of Molecular Evolution*, *1*(3), 241–248. <https://doi.org/10.1007/BF01660243>
- ²¹² Hermes-Lima, M. (1990). Model for prebiotic pyrophosphate formation: Condensation of precipitated orthophosphate at low temperature in the absence of condensing or phosphorylating agents. *Journal of Molecular Evolution*, *31*(5), 353–358. <https://doi.org/10.1007/BF02106049>
- ²¹³ Miller, S., & Parris, M. (1964). Synthesis of Pyrophosphate Under Primitive Earth Conditions. *Nature*, *204*(4965), 1248–1250. <https://doi.org/10.1038/2041248a0>
- ²¹⁴ Hagan, W. J., Parker, A., Steuerwald, A., & Hathaway, M. (2007). Phosphate Solubility and the Cyanate-Mediated Synthesis of Pyrophosphate. *Origins of Life and Evolution of Biospheres*, *37*(2), 113–122. <https://doi.org/10.1007/s11084-006-9020-y>
- ²¹⁵ Weber, A. L. (1982). Formation of pyrophosphate on hydroxyapatite with thioesters as condensing agents. *Biosystems*, *15*(3), 183–189. [https://doi.org/10.1016/0303-2647\(82\)90002-8](https://doi.org/10.1016/0303-2647(82)90002-8)
- ²¹⁶ Weber, A. L. (1981). Formation of pyrophosphate, tripolyphosphate, and phosphorylimidazole with the thioester, N, S-diacetylcysteamine, as the condensing agent. *Journal of Molecular Evolution*, *18*(1), 24–29. <https://doi.org/10.1007/BF01733208>
- ²¹⁷ Pasek, M. A., Kee, T. P., Bryant, D. E., Pavlov, A. A., & Lunine, J. I. (2008). Production of Potentially Prebiotic Condensed Phosphates by Phosphorus Redox Chemistry. *Angewandte Chemie International Edition*, *47*(41), 7918–7920. <https://doi.org/10.1002/anie.200802145>
- ²¹⁸ Wang, L., Chen, S., Xu, T., Taghizadeh, K., Wishnok, J. S., Zhou, X., You, D., Deng, Z., & Dedon, P. C. (2007). Phosphorothioation of DNA in bacteria by dnd genes. *Nature Chemical Biology*, *3*(11), 709–710. <https://doi.org/10.1038/nchembio.2007.39>
- ²¹⁹ Britvin, S. N., Murashko, M. N., Vapnik, Y., Polekhovskiy, Y. S., & Krivovichev, S. v. (2015). Earth's Phosphides in Levant and insights into the source of Archean prebiotic phosphorus. *Scientific Reports*, *5*(1), 8355. <https://doi.org/10.1038/srep08355>
- ²²⁰ Ritson, D., Xu, J., & Sutherland, J. (2016). Thiophosphate – A Versatile Prebiotic Reagent? *Synlett*, *28*(01), 64–67. <https://doi.org/10.1055/s-0036-1589414>
- ²²¹ Ritson, D. J., Mojzsis, S. J., & Sutherland, John. D. (2020). Supply of phosphate to early Earth by photogeochemistry after meteoritic weathering. *Nature Geoscience*, *13*(5), 344–348. <https://doi.org/10.1038/s41561-020-0556-7>
- ²²² Nazarov, M. A., Kurat, G., Brandstaetter, F., Ntaflos, T., Chaussidon, M., & Hoppe, P. (2009). Phosphorus-bearing sulfides and their associations in CM chondrites. *Petrology*, *17*(2), 101–123. <https://doi.org/10.1134/S0869591109020015>
- ²²³ Walton, C. R., Ewens, S., Coates, J. D., Blake, R. E., Planavsky, N. J., Reinhard, C., Ju, P., Hao, J., & Pasek, M. A. (2023). Phosphorus availability on the early Earth and the impacts of life. *Nature Geoscience*, *16*(5), 399–409. <https://doi.org/10.1038/s41561-023-01167-6>
- ²²⁴ Fiore, M., & Strazewski, P. (2016). Prebiotic Lipidic Amphiphiles and Condensing Agents on the Early Earth. *Life*, *6*(2), 17. <https://doi.org/10.3390/life6020017>
- ²²⁵ Ponnampereuma, C., Sagan, C., & Mariner, R. (1963). Synthesis of Adenosine Triphosphate Under Possible Primitive Earth Conditions. *Nature*, *199*(4890), 222–226. <https://doi.org/10.1038/199222a0>
- ²²⁶ Ponnampereuma, C., & Mack, R. (1965). Nucleotide Synthesis under Possible Primitive Earth Conditions. *Science*, *148*(3674), 1221–1223. <https://doi.org/10.1126/science.148.3674.1221>

- ²²⁷ Beck, A., Lohrmann, R., & Orgel, L. E. (1967). Phosphorylation with Inorganic Phosphates at Moderate Temperatures. *Science*, *157*(3791), 952–952. <https://doi.org/10.1126/science.157.3791.952>
- ²²⁸ Gibard, C., Bhowmik, S., Karki, M., Kim, E.-K., & Krishnamurthy, R. (2018). Phosphorylation, oligomerization and self-assembly in water under potential prebiotic conditions. *Nature Chemistry*, *10*(2), 212–217. <https://doi.org/10.1038/nchem.2878>
- ²²⁹ Krishnamurthy, R., Guntha, S., & Eschenmoser, A. (2000). Regioselective α -Phosphorylation of Aldoses in Aqueous Solution. *Angewandte Chemie International Edition*, *39*(13), 2281–2285. [https://doi.org/10.1002/1521-3773\(20000703\)39:13<2281::AID-ANIE2281>3.0.CO;2-2](https://doi.org/10.1002/1521-3773(20000703)39:13<2281::AID-ANIE2281>3.0.CO;2-2)
- ²³⁰ Osumah, A., & Krishnamurthy, R. (2021). Diamidophosphate (DAP): A Plausible Prebiotic Phosphorylating Reagent with a Chem to BioChem Potential? *ChemBioChem*, *22*(21), 3001–3009. <https://doi.org/10.1002/cbic.202100274>
- ²³¹ Schwartz, A., & Ponnamperna, C. (1968). Phosphorylation on the Primitive Earth: Phosphorylation of Adenosine with Linear Polyphosphate Salts in Aqueous Solution. *Nature*, *218*(5140), 443–443. <https://doi.org/10.1038/218443a0>
- ²³² Schwartz, A. W. (1969). Specific phosphorylation of the 2'- and 3'- positions in ribonucleosides. *J. Chem. Soc. D*, *0*(23), 1393a–1393a. <https://doi.org/10.1039/C2969001393A>
- ²³³ Yamagata, Y., Inoue, H., & Inomata, K. (1995). Specific effect of magnesium ion on 2', 3'-cyclic amp synthesis from adenosine and trimeta phosphate in aqueous solution. *Origins of Life and Evolution of the Biosphere*, *25*(1–3), 47–52. <https://doi.org/10.1007/BF01581572>
- ²³⁴ Nam, I., Lee, J. K., Nam, H. G., & Zare, R. N. (2017). Abiotic production of sugar phosphates and uridine ribonucleoside in aqueous microdroplets. *Proceedings of the National Academy of Sciences*, *114*(47), 12396–12400. <https://doi.org/10.1073/pnas.1714896114>
- ²³⁵ Hu, J., Lei, W., Wang, J., Chen, H.-Y., & Xu, J.-J. (2019). Regioselective 5'-position phosphorylation of ribose and ribonucleosides: phosphate transfer in the activated pyrophosphate complex in the gas phase. *Chemical Communications*, *55*(3), 310–313. <https://doi.org/10.1039/C8CC08510B>
- ²³⁶ Schimpl, A., Lemmon, R. M., & Calvin, M. (1965). Cyanamide Formation under Primitive Earth Conditions. *Science*, *147*(3654), 149–150. <https://doi.org/10.1126/science.147.3654.149>
- ²³⁷ Steinman, G., Lemmon, R. M., & Calvin, M. (1964). Cyanamide: A Possible Key Compound In Chemical Evolution. *Proceedings of the National Academy of Sciences*, *52*(1), 27–30. <https://doi.org/10.1073/pnas.52.1.27>
- ²³⁸ Yamagata, Y. (1999). Prebiotic Formation of ADP and ATP from AMP, Calcium Phosphates and Cyanate in Aqueous Solution. *Origins of Life and Evolution of the Biosphere*, *29*(5), 511–520. <https://doi.org/10.1023/A:1006672232730>
- ²³⁹ Halmann, M., Sanchez, R. A., & Orgel, L. E. (1969). Phosphorylation of D-ribose in aqueous solution. *The Journal of Organic Chemistry*, *34*(11), 3702–3703. <https://doi.org/10.1021/jo01263a132>
- ²⁴⁰ Tsanakopoulou, M., & Sutherland, J. D. (2017). Cyanamide as a prebiotic phosphate activating agent – catalysis by simple 2-oxoacid salts. *Chemical Communications*, *53*(87), 11893–11896. <https://doi.org/10.1039/C7CC07517K>
- ²⁴¹ Lohrmann, R. (1972). Formation of urea and guanidine by irradiation of ammonium cyanide. *Journal of Molecular Evolution*, *1*(3), 263–269. <https://doi.org/10.1007/BF01660246>
- ²⁴² Förstel, M., Maksyutenko, P., Jones, B. M., Sun, B.-J., Chang, A. H. H., & Kaiser, R. I. (2016). Synthesis of urea in cometary model ices and implications for Comet 67P/Churyumov–Gerasimenko. *Chemical Communications*, *52*(4), 741–744. <https://doi.org/10.1039/C5CC07635H>
- ²⁴³ Slate, E. C. S., Barker, R., Euesden, R. T., Revels, M. R., & Meijer, A. J. H. M. (2020). Computational studies into urea formation in the interstellar medium. *Monthly Notices of the Royal Astronomical Society*, *497*(4), 5413–5420. <https://doi.org/10.1093/mnras/staa2436>

-
- ²⁴⁴ Lohrmann, R., & Orgel, L. E. (1971). Urea-Inorganic Phosphate Mixtures as Prebiotic Phosphorylating Agents. *Science*, 171(3970), 490–494. <https://doi.org/10.1126/science.171.3970.490>
- ²⁴⁵ Bishop, M. J., Lohrmann, R., & Orgel, L. E. (1972). Prebiotic Phosphorylation of Thymidine at 65° C in Simulated Desert Conditions. *Nature*, 237(5351), 162–164. <https://doi.org/10.1038/237162a0>
- ²⁴⁶ Handschuh, G. J., Lohrmann, R., & Orgel, L. E. (1973). The effect of Mg²⁺ and Ca²⁺ on urea-catalyzed phosphorylation reactions. *Journal of Molecular Evolution*, 2(4), 251–262. <https://doi.org/10.1007/BF01654094>
- ²⁴⁷ Österberg, R., Orgel, L. E., & Lohrmann, R. (1973). Further studies of urea-catalyzed phosphorylation reactions. *Journal of Molecular Evolution*, 2(2–3), 231–234. <https://doi.org/10.1007/BF01654004>
- ²⁴⁸ Reimann, R., & Zubay, G. (1999). Nucleoside Phosphorylation: A Feasible Step in the Prebiotic Pathway to RNA. *Origins of Life and Evolution of the Biosphere*, 29(3), 229–247. <https://doi.org/10.1023/A:1006580009791>
- ²⁴⁹ Schwartz, A. W. (1972). Prebiotic phosphorylation-nucleotide synthesis with apatite. *Biochimica et Biophysica Acta (BBA) - Nucleic Acids and Protein Synthesis*, 281(4), 477–480. [https://doi.org/10.1016/0005-2787\(72\)90147-5](https://doi.org/10.1016/0005-2787(72)90147-5)
- ²⁵⁰ Schwartz, A. W., Veen, M., Bisseling, T., & Chittenden, G. J. F. (1975). Prebiotic nucleotide synthesis-demonstration of a geologically plausible pathway. *Origins of Life*, 6(1–2), 163–168. <https://doi.org/10.1007/BF01372401>
- ²⁵¹ Gull, M., Zhou, M., Fernández, F. M., & Pasek, M. A. (2014). Prebiotic Phosphate Ester Syntheses in a Deep Eutectic Solvent. *Journal of Molecular Evolution*, 78(2), 109–117. <https://doi.org/10.1007/s00239-013-9605-9>
- ²⁵² Orgel, L. E., & Lohrmann, R. (1974). Prebiotic chemistry and nucleic acid replication. *Accounts of Chemical Research*, 7(11), 368–377. <https://doi.org/10.1021/ar50083a002>
- ²⁵³ Shaw, W. H. R., & Bordeaux, J. J. (1955). The Decomposition of Urea in Aqueous Media. *Journal of the American Chemical Society*, 77(18), 4729–4733. <https://doi.org/10.1021/ja01623a011>
- ²⁵⁴ Callahan, B. P., Yuan, Y., & Wolfenden, R. (2005). The Burden Borne by Urease. *Journal of the American Chemical Society*, 127(31), 10828–10829. <https://doi.org/10.1021/ja0525399>
- ²⁵⁵ Seel, F., & Schinnerling, F. (1978). Darstellung und thermische Zersetzung von Erdalkalimetall-Carbamoylphosphaten / Preparation and Thermal Decomposition of Carbamoylphosphates of Alkaline-earth Metals. *Zeitschrift Für Naturforschung B*, 33(4), 374–381. <https://doi.org/10.1515/znb-1978-0405>
- ²⁵⁶ Schoffstall, A. M. (1976). Prebiotic phosphorylation of nucleosides in formamide. *Origins of Life*, 7(4), 399–412. <https://doi.org/10.1007/BF00927935>
- ²⁵⁷ Xu, J., Tsanakopoulou, M., Magnani, C. J., Szabla, R., Šponer, J. E., Šponer, J., Góra, R. W., & Sutherland, J. D. (2017). A prebiotically plausible synthesis of pyrimidine β-ribonucleosides and their phosphate derivatives involving photoanomerization. *Nature Chemistry*, 9(4), 303–309. <https://doi.org/10.1038/nchem.2664>
- ²⁵⁸ Furukawa, Y., Kim, H.-J., Hutter, D., & Benner, S. A. (2015). Abiotic Regioselective Phosphorylation of Adenosine with Borate in Formamide. *Astrobiology*, 15(4), 259–267. <https://doi.org/10.1089/ast.2014.1209>
- ²⁵⁹ Costanzo, G., Saladino, R., Crestini, C., Ciciriello, F., & di Mauro, E. (2007). Nucleoside Phosphorylation by Phosphate Minerals. *Journal of Biological Chemistry*, 282(23), 16729–16735. <https://doi.org/10.1074/jbc.M611346200>
- ²⁶⁰ Gull, M., & Pasek, M. (2013). Is Struvite a Prebiotic Mineral? *Life*, 3(2), 321–330. <https://doi.org/10.3390/life3020321>
- ²⁶¹ Ritson, D. J., & Sutherland, J. D. (2023). Thiophosphate photochemistry enables prebiotic access to sugars and terpenoid precursors. *Nature Chemistry*. <https://doi.org/10.1038/s41557-023-01251-9>
- ²⁶² Epps, D. E., Nooner, D. W., Eichberg, J., Sherwood, E., & Or6, J. (1979). Journal of Molecular Evolution Cyanamide Mediated Synthesis Under Plausible Primitive Earth Conditions VI. The Synthesis of Glycerol and Glycerophosphates. *J. Mol. Evol.*, 14, 235–241.

-
- ²⁶³ Gull, M., Cafferty, B., Hud, N., & Pasek, M. (2017). Silicate-Promoted Phosphorylation of Glycerol in Non-Aqueous Solvents: A Prebiotically Plausible Route to Organophosphates. *Life*, 7(3), 29. <https://doi.org/10.3390/life7030029>
- ²⁶⁴ Albertsen, A. N., Duffy, C. D., Sutherland, J. D., & Monnard, P.-A. (2014). Self-Assembly of Phosphate Amphiphiles in Mixtures of Prebiotically Plausible Surfactants. *Astrobiology*, 14(6), 462–472. <https://doi.org/10.1089/ast.2013.1111>
- ²⁶⁵ Walde, P., Wessicken, M., Rädler, U., Berclaz, N., Conde-Frieboes, K., & Luisi, P. L. (1997). Preparation and Characterization of Vesicles from Mono- *n* -alkyl Phosphates and Phosphonates. *The Journal of Physical Chemistry B*, 101(38), 7390–7397. <https://doi.org/10.1021/jp970898n>
- ²⁶⁶ Powner, M. W., & Sutherland, J. D. (2011). Prebiotic chemistry: a new *modus operandi*. *Philosophical Transactions of the Royal Society B: Biological Sciences*, 366(1580), 2870–2877. <https://doi.org/10.1098/rstb.2011.0134>
- ²⁶⁷ Ourisson, G., & Nakatani, Y. (1999). Addendum: Origins of cellular life: Molecular foundations and new approaches. *Tetrahedron*, 55(11), 3183–3190. [https://doi.org/10.1016/S0040-4020\(99\)00116-7](https://doi.org/10.1016/S0040-4020(99)00116-7)
- ²⁶⁸ Lira, L. M., Vasilev, D., Pilli, R. A., & Wessjohann, L. A. (2013). One-pot synthesis of organophosphate monoesters from alcohols. *Tetrahedron Letters*, 54(13), 1690–1692. <https://doi.org/10.1016/j.tetlet.2013.01.059>
- ²⁶⁹ Pozzi, G., Birault, V., Werner, B., Dannemuller, O., Nakatani, Y., Ourisson, G., & Terakawa, S. (1996). Single-Chain Polypropenyl Phosphates Form “Primitive” Membranes. *Angewandte Chemie International Edition in English*, 35(2), 177–180. <https://doi.org/10.1002/anie.199601771>
- ²⁷⁰ Danilov, L. L., Druzhinina, T. N., Kalinchuk, N. A., Maltsev, S. D., & Shibaev, V. N. (1989). Polypropenyl phosphates: synthesis and structure-activity relationship for a biosynthetic system of *Salmonella anatum* O-specific polysaccharide. *Chemistry and Physics of Lipids*, 51(3–4), 191–203. [https://doi.org/10.1016/0009-3084\(89\)90006-6](https://doi.org/10.1016/0009-3084(89)90006-6)
- ²⁷¹ Keller, R. K., & Thompson, R. (1993). Rapid synthesis of isoprenoid diphosphates and their isolation in one step using either thin layer or flash chromatography. *Journal of Chromatography A*, 645(1), 161–167. [https://doi.org/10.1016/0021-9673\(93\)80630-Q](https://doi.org/10.1016/0021-9673(93)80630-Q)
- ²⁷² Nakatani, Y., Ribeiro, N., Streiff, S., Gotoh, M., Pozzi, G., Désaubry, L., & Milon, A. (2014). Search for the Most ‘primitive’ Membranes and Their Reinforcers: A Review of the Polypropenyl Phosphates Theory. *Origins of Life and Evolution of Biospheres*, 44(3), 197–208. <https://doi.org/10.1007/s11084-014-9365-6>
- ²⁷³ Fayolle, D., Altamura, E., D’Onofrio, A., Madanamothoo, W., Fenet, B., Mavelli, F., Buchet, R., Stano, P., Fiore, M., & Strazewski, P. (2017). Crude phosphorylation mixtures containing racemic lipid amphiphiles self-assemble to give stable primitive compartments. *Scientific Reports*, 7(1), 18106. <https://doi.org/10.1038/s41598-017-18053-y>
- ²⁷⁴ Epps, D. E., Sherwood, E., Eichberg, J., & Oró, J. (1978). Cyanamide mediated syntheses under plausible primitive earth conditions. V. The Synthesis of Phosphatidic Acids. *Journal of Molecular Evolution*, 11(4), 279–292. <https://doi.org/10.1007/BF01733838>
- ²⁷⁵ Bonfio, C., Caumes, C., Duffy, C. D., Patel, B. H., Percivalle, C., Tsanakopoulou, M., & Sutherland, J. D. (2019). Length-Selective Synthesis of Acylglycerol-Phosphates through Energy-Dissipative Cycling. *Journal of the American Chemical Society*, 141(9), 3934–3939. <https://doi.org/10.1021/jacs.8b12331>
- ²⁷⁶ Coggins, A. J., & Powner, M. W. (2017). Prebiotic synthesis of phosphoenol pyruvate by α -phosphorylation-controlled triose glycolysis. *Nature Chemistry*, 9(4), 310–317. <https://doi.org/10.1038/nchem.2624>
- ²⁷⁷ Gull M., Tian, G., Wang, Y., He, C., Shi, Z., Yuan, H., & Feng, S. (2010). Resolving the enigma of prebiotic C–O–P bond formation: Prebiotic hydrothermal synthesis of important biological phosphate esters. *Heteroatom Chemistry*, 21(3), 161–167. <https://doi.org/10.1002/hc.20591>

-
- ²⁷⁸ Gull M., Wang, Y., Wang, Y., Shi, Z., Tian, G., & Feng, S. (2011). Mimicking the prebiotic acidic hydrothermal environment: One-pot prebiotic hydrothermal synthesis of glucose phosphates. *Heteroatom Chemistry*, 22(2), 186–191. <https://doi.org/10.1002/hc.20675>
- ²⁷⁹ Ozawa, K., Nemoto, A., Imai, E., Honda, H., Hatori, K., & Matsuno, K. (2004). Phosphorylation of Nucleotide Molecules in Hydrothermal Environments. *Origins of Life and Evolution of the Biosphere*, 34(5), 465–471. <https://doi.org/10.1023/B:ORIG.0000043121.65714.05>
- ²⁸⁰ Altamura E, Comte A, D’Onofrio A, Roussillon C, Fayolle D, Buchet R, Mavelli F, Stano P, Fiore M, Strazewski P. Racemic Phospholipids for Origin of Life Studies. *Symmetry* **2020**; *12*, 1108. <https://doi.org/10.3390/sym12071108>
- ²⁸¹ Fayolle, D., Altamura, E., D’Onofrio, A. et al. Crude phosphorylation mixtures containing racemic lipid amphiphiles self-assemble to give stable primitive compartments. *Sci Rep* 7, 18106 (2017). <https://doi.org/10.1038/s41598-017-18053-y>
- ²⁸² Datchi, F., LeToullec, R., & Loubeyre, P. (1997). Improved calibration of the SrB4O7:Sm²⁺ optical pressure gauge: Advantages at very high pressures and high temperatures. *Journal of Applied Physics*, 81(8), 3333–3339. <https://doi.org/10.1063/1.365025>
- ²⁸³ Mao, H. K., Xu, J., & Bell, P. M. (1986). Calibration of the ruby pressure gauge to 800 kbar under quasi-hydrostatic conditions. *Journal of Geophysical Research*, 91(B5), 4673. <https://doi.org/10.1029/jb091ib05p04673>
- ²⁸⁴ Le Godec, Y., & Le Floch, S. (2023). Recent Developments of High-Pressure Spark Plasma Sintering: An Overview of Current Applications, Challenges and Future Directions. In *Materials* (Vol. 16, Issue 3). MDPI. <https://doi.org/10.3390/ma16030997>
- ²⁸⁵ Ter-Ovanesian, L.M.P., Rigaud, B., Mezzetti, A. et al. Carbamoyl phosphate and its substitutes for the uracil synthesis in origins of life scenarios. *Sci Rep* **11**, 19356 (2021). <https://doi.org/10.1038/s41598-021-98747-6>
- ²⁸⁶ Maguire, O.R., Smokers, I.B.A. & Huck, W.T.S. A physicochemical orthophosphate cycle via a kinetically stable thermodynamically activated intermediate enables mild prebiotic phosphorylations. *Nat Commun* **12**, 5517 (2021). <https://doi.org/10.1038/s41467-021-25555-x>
- ²⁸⁷ X. Huang, F. M. Raushel. Restricted passage of reaction intermediates through the ammonia tunnel of carbamoyl phosphate synthetase. *J. Biol. Chem.* **2000**, 275, 26233–26240. <https://doi.org/10.1074/jbc.M004521200>
- ²⁸⁸ H. Zhou, Signal-to-Noise (SNR) and Uncertainty Estimates. NMR Protocols - Data Processing (MNOVA) of the University of California. Updated in 2019. <https://nmr.chem.ucsb.edu/protocols/SNR.html>
- ²⁸⁹ Cohn, M., Hu, A. Isotopic (¹⁸O) shift in ³¹P nuclear magnetic resonance applied to a study of enzyme-catalyzed phosphate—phosphate exchange and phosphate (oxygen)—water exchange reactions scrambling. *Biochemistry*. **1978**, Vol. 75, Issue 1. <https://doi.org/https://doi.org/10.1073/pnas.75.1.200>
- ²⁹⁰ Lopalco, A., Douglas, J., Denora, N., & Stella, V. J. Determination of pKa and Hydration Constants for a Series of α -Keto-Carboxylic Acids Using Nuclear Magnetic Resonance Spectrometry. *Journal of Pharmaceutical Sciences*. **2016**. 105(2), 664–672. <https://doi.org/10.1002/jps.24539>
- ²⁹¹ Kibbe WA. 'OligoCalc: an online oligonucleotide properties calculator'. (2007) *Nucleic Acids Res.* 35(webserver issue): May 25, accessed 27 July 2020, <http://biotools.nubic.northwestern.edu/OligoCalc.html#helpIUPAC>
- ²⁹² P. E. Nielsen, Peptide Nucleic Acids - Protocols and Applications, Horizon Bio- science, Norfolk, 2004.
- ²⁹³ Mudalige, A., & Pemberton, J. E. (2007). Raman spectroscopy of glycerol/D₂O solutions. *Vibrational Spectroscopy*, 45(1), 27–35. <https://doi.org/10.1016/j.vibspec.2007.04.002>
- ²⁹⁴ Gryniewicz-Ruzicka, C. M., Arzhantsev, S., Pelster, L. N., Westenberger, B. J., Buhse, L. F., & Kauffman, J. F. (2011). Multivariate Calibration and Instrument Standardization for the Rapid Detection of Diethylene Glycol in Glycerin by Raman Spectroscopy. *Applied Spectroscopy*, 65(3), 334–341. <https://doi.org/10.1366/10-05976>

- ²⁹⁵ Mendelovici, E., Frost, R. L., & Kloprogge, T. (2000). Cryogenic Raman spectroscopy of glycerol. *Journal of Raman Spectroscopy*, 31(12), 1121–1126. [https://doi.org/10.1002/1097-4555\(200012\)31:12<1121::AID-JRS654>3.0.CO;2-G](https://doi.org/10.1002/1097-4555(200012)31:12<1121::AID-JRS654>3.0.CO;2-G)
- ²⁹⁶ Lamelas, F. J., Dreger, Z. A., & Gupta, Y. M. (2005). Raman and X-Ray Scattering Studies of High-Pressure Phases of Urea. *The Journal of Physical Chemistry B*, 109(16), 8206–8215. <https://doi.org/10.1021/jp040760m>
- ²⁹⁷ Rousseau, B., van Alsenoy, C., Keuleers, R., & Desseyn, H. O. (1998). Solids Modeled by Ab-Initio Crystal Field Methods. Part 17. Study of the Structure and Vibrational Spectrum of Urea in the Gas Phase and in Its $P 4_2 1 m$ Crystal Phase. *The Journal of Physical Chemistry A*, 102(32), 6540–6548. <https://doi.org/10.1021/jp981008m>
- ²⁹⁸ Ghule, A., Murugan, R., & Chang, H. (2001). Thermo-Raman Studies on $\text{NaH}_2\text{PO}_4 \cdot 2\text{H}_2\text{O}$ for Dehydration, Condensation, and Phase Transformation. *Inorganic Chemistry*, 40(23), 5917–5923. <https://doi.org/10.1021/ic010043w>
- ²⁹⁹ Choi, B. K., Lee, M. N., & Kim, J. J. (1989). Raman spectra of the NaH_2PO_4 crystal. *Journal of Raman Spectroscopy*, 20(1), 11–15. <https://doi.org/10.1002/jrs.1250200103>
- ³⁰⁰ Zhu, C., Turner, A. M., Abplanalp, M. J., Kaiser, R. I., Webb, B., Siuzdak, G., & Fortenberry, R. C. (2020). An Interstellar Synthesis of Glycerol Phosphates. *The Astrophysical Journal*, 899(1), L3. <https://doi.org/10.3847/2041-8213/aba744>
- ³⁰¹ Hejna, A., Kosmela, P., Klein, M., Formela, K., Kopczyńska, M., Haponiuk, J., & Piszczyk, Ł. (2018). Two-step Conversion of Crude Glycerol Generated by Biodiesel Production into Biopolyols: Synthesis, Structural and Physical Chemical Characterization. *Journal of Polymers and the Environment*, 26(8), 3334–3344. <https://doi.org/10.1007/s10924-018-1217-4>
- ³⁰² Goyal, S., Hernández, N. B., & Cochran, E. W. (2021). An update on the future prospects of glycerol polymers. *Polymer International*, 70(7), 911–917. <https://doi.org/10.1002/pi.6209>
- ³⁰³ Tran, N. H., & Kannangara, G. S. K. (2013). Conversion of glycerol to hydrogen rich gas. *Chemical Society Reviews*, 42(24), 9454. <https://doi.org/10.1039/c3cs60227c>
- ³⁰⁴ Steinman, G., Lemmon, R. M., & Calvin, M. (1964). Cyanamide Formation under Primitive Earth Conditions. *Arch. Biochem. Biophys*, 147(6), 149–150.
- ³⁰⁵ Tordini, F., Bencini, A., Bruschi, M., de Gioia, L., Zampella, G., & Fantucci, P. (2003). Theoretical study of hydration of cyanamide and carbodiimide. *Journal of Physical Chemistry A*, 107(8), 1188–1196. <https://doi.org/10.1021/jp026535r>
- ³⁰⁶ Hill, S. v., Williams, A., & Longridge, J. L. (1984). Acid-catalysed Hydrolysis of Cyanamides: Estimates of Carbodi-imide Basicity and Tautomeric Equilibrium Constant between Carbodi-imide and Cyanamide. *About Journal of the Chemical Society, Perkin Transactions 2*, 6, 1009–1013. <https://doi.org/https://doi.org/10.1039/P29840001009>
- ³⁰⁷ Powner, M. W., Gerland, B., & Sutherland, J. D. (2009). Synthesis of activated pyrimidine ribonucleotides in prebiotically plausible conditions. *Nature*, 459(7244), 239–242. <https://doi.org/10.1038/nature08013>
- ³⁰⁸ Bonfio C., Russell D., Green N., Mariani A., & Sutherland J. D. (2020). Activation chemistry drives the emergence of functionalised protocells. *Chemical Science*, 11, 10688–10697. <https://doi.org/10.1039/d0sc04506c>
- ³⁰⁹ Bonfio, C., Caumes, C., Duffy, C. D., Patel, B. H., Percivalle, C., Tsanakopoulou, M., & Sutherland, J. D. (2019). Length-Selective Synthesis of Acylglycerol-Phosphates through Energy-Dissipative Cycling. *Journal of the American Chemical Society*, 141(9), 3934–3939. <https://doi.org/10.1021/jacs.8b12331>
- ³¹⁰ Koskinen, A. M. P., & Kataja, A. O. (2015). The Tishchenko Reaction. In *Organic Reactions* (pp. 105–410). Wiley. <https://doi.org/10.1002/0471264180.or086.02>
- ³¹¹ GÜthner T., Gehrman H., Eberl M., & Ramos J.-M. (2021). *Use of acylcyanamides or salts thereof for regulating plant growth* (Patent No. WO 2021/089601 A1). Alzchem Trostberg GMBH.

-
- ³¹² Brand, H., Martens, J., Mayer, P., Schulz, A., Seibald, M., & Soller, T. (2009). Salts and ionic liquids of resonance stabilized amides. *Chemistry - An Asian Journal*, 4(10), 1588–1603. <https://doi.org/10.1002/asia.200900181>
- ³¹³ Liu, Z., Wu, L.-F., Xu, J., Bonfio, C., Russell, D. A., & Sutherland, J. D. (2020). Harnessing chemical energy for the activation and joining of prebiotic building blocks. *Nature Chemistry*, 12(11), 1023–1028. <https://doi.org/10.1038/s41557-020-00564-3>
- ³¹⁴ Sattler, A., Pagano, S., Zeuner, M., Zurawski, A., Gunzelmann, D., Senker, J., Müller-Buschbaum, K., & Schnick, W. (2009). Melamine–Melem Adduct Phases: Investigating the Thermal Condensation of Melamine. *Chemistry - A European Journal*, 15(47), 13161–13170. <https://doi.org/10.1002/chem.200901518>
- ³¹⁵ Bojdys, M. J., Müller, J.-O., Antonietti, M., & Thomas, A. (2008). Ionothermal Synthesis of Crystalline, Condensed, Graphitic Carbon Nitride. *Chemistry - A European Journal*, 14(27), 8177–8182. <https://doi.org/10.1002/chem.200800190>
- ³¹⁶ Sanchez, R. A., Ferbis, J. P., & Orgel, L. E. (1967). Studies in Prebiotic Synthesis n. t Synthesis of Purine Precursors and Amino Acids from Aqueous Hydrogen Cyanide. In *J. Mol. Biol* (Vol. 80).
- ³¹⁷ Winnewisser, M., Medvedev, I. R., de Lucia, F. C., Herbst, E., Koput, J., Sastry, K. V. L. N., & Butler, R. A. H. (2005). The millimeter-and submillimeter-wave spectrum of cyanofornamide. *The Astrophysical Journal Supplement Series*, 159, 189–195. <https://doi.org/10.1086/430470>
- ³¹⁸ Dai, Y., Wang, K., Yuan, H., Meng, X., Luo, K., Yu, D., Liu, J., Zhang, X., Ma, Y., Tian, Y., & Zou, B. (2015). Selected reactive sites tuned by high pressure: Oligomerization of solid-state cyanamide. *Journal of Physical Chemistry C*, 119(23), 12801–12807. <https://doi.org/10.1021/acs.jpcc.5b01105>
- ³¹⁹ Kanesaka, I., & Mitsuhashi, E. (2008). A damped oscillator model for infrared spectra of formamide in the liquid state. *Bulletin of the Chemical Society of Japan*, 81(2), 248–253. <https://doi.org/10.1246/bcsj.81.248>
- ³²⁰ Smith, C. H., & Robinson, J. D. (1957). Spectra of Formamide-N-d2 and of Formamide Raman Spectra of Formamide-N-c/2 and of Formamide in Concentrated Hydrochloric Acid. *Journal of the American Chemical Society*, 79(6), 1349–1351. <https://doi.org/10.1021/ja01563a025>
- ³²¹ Cunningham, I. D., Blanden, J. S., Llor, J., Muñoz, L., & Sharratt, A. P. (1991). Chemistry of amidines. Part 1. Determination of the site of initial protonation in N'-pyridylformamidines. *J. Chem. Soc., Perkin Trans. 2*, 11, 1747–1750. <https://doi.org/10.1039/P29910001747>
- ³²² Komber, H., Limbach, H.-H., Böhme, F., & Kunert, C. (2002). NMR Studies of the Tautomerism of Cyclo-tris(4-R-2,6-pyridylformamidine) in Solution and in the Solid State. *Journal of the American Chemical Society*, 124(40), 11955–11963. <https://doi.org/10.1021/ja0202762>